HORT PAPERS IN—

nalytical methods
conomic geology
ngineering geology
eochemistry
eochronology
eomorphology
eophysics
round water
imnology
Marine geology
aleontology
etrology
Quality of water
Quaternary geology
adiohydrology
ock mechanics
edimentation
tratigraphy
tructural geology
est-well construction
Water analysis

GEOLOGICAL SURVEY RESEARCH 1966

Chapter D

GEOLOGICAL SURVEY PROFESSIONAL PAPER 550-D

GEOLOGICAL SURVEY RESEARCH 1966

Chapter D

GEOLOGICAL SURVEY PROFESSIONAL PAPER 550–D

Scientific notes and summaries of investigations in geology, hydrology, and related fields

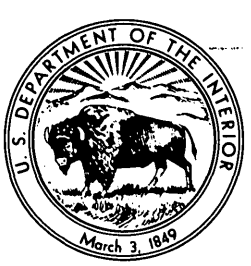

UNITED STATES GOVERNMENT PRINTING OFFICE, WASHINGTON: 1966

UNITED STATES DEPARTMENT OF THE INTERIOR

STEWART L. UDALL, Secretary

GEOLOGICAL SURVEY

William T. Pecora, Director

For sale by the Superintendent of Documents, U.S. Government Printing Office
Washington, D.C. 20402 – Price $2.25

CONTENTS

GEOLOGIC STUDIES

GEOLOGICAL SURVEY RESEARCH 1966

This collection of 44 short papers is the third published chapter of "Geological Survey Research 1966." The papers report on scientific and economic results of current work by members of the Conservation, Geologic, and Water Resources Divisions of the U.S. Geological Survey.

Chapter A, to be published later in the year, will present a summary of significant results of work done during fiscal year 1966, together with lists of investigations in progress, reports published, cooperating agencies, and Geological Survey offices.

"Geological Survey Research 1966" is the seventh volume of the annual series Geological Survey Research. The six volumes already published are listed below, with their series designations.

Geological Survey Research 1960—Prof. Paper 400
Geological Survey Research 1961—Prof. Paper 424
Geological Survey Research 1962—Prof. Paper 450
Geological Survey Research 1963—Prof. Paper 475
Geological Survey Research 1964—Prof. Paper 501
Geological Survey Research 1965—Prof. Paper 525

POSSIBLE WINDOW IN THE ELK RANGE THRUST SHEET NEAR ASPEN, COLORADO

By BRUCE BRYANT, Denver, Colo.

Abstract.—Structurally complex rocks underlie structurally simple rocks of Permian and Pennsylvanian age in the Conundrum Creek valley. Both the overthrust sheet and the underlying rocks, as well as the boundary between them, have been intruded by Tertiary granodiorite and subjected to hornblende hornfels facies metamorphism. Seven miles to the southwest a section of Maroon Formation 10,000 feet thick has been carried over a section of Maroon Formation only 1,000 feet thick along the Elk Range fault. The Conundrum Creek area may be a window in the Elk Range thrust sheet, which was derived by the sliding off the Sawatch Range uplift of a thick section of rock from the interior of the central Colorado trough.

In the Elk Mountains, on Conundrum Creek, 9 miles south of Aspen, Colo. (fig. 1), a block of structurally complex rocks underlies one of structurally simple rocks (fig. 3). The rock types and the structural features indicate that the structurally complex rocks may be in a window in the Elk Range thrust sheet. Both blocks and the boundary between them have been intruded by Tertiary granodiorite of the White Rock pluton and subjected to hornblende hornfels facies metamorphism.

CONUNDRUM CREEK AREA

In the Conundrum Creek area the structurally complex rocks lie in the lower 1,000 feet of a valley about 3,000 feet deep and are mostly covered by colluvium, moraine, talus, and alluvium so that details of the structure and stratigraphy are obscure. The simplest interpretation of the rock relations is shown on the geologic map (fig. 2). These rock units and those in the structurally more simple upper block probably are part of the Pennsylvanian and Permian Systems.

Stratigraphy

The Pennsylvanian and Permian rocks in the region are a thick sequence of dominantly clastic rocks and evaporites, which compose the Belden Shale, Minturn Formation, and Maroon Formation (table 1) and were deposited in a narrow basin known as the central Colorado trough (fig. 1). The trough had a northwest trend in central and northwestern Colorado and a north trend in New Mexico. The deposits are well over 2 miles thick in the deepest parts of the trough, and they thin in relatively short distances at the basin margins (Brill, 1952; Murray, 1958; Mallory, 1958, 1960; De Voto, 1965). Thick sequences of clastic rocks derived from adjacent highlands are found on either side of the trough north and west of the Sawatch Range. These interfinger with evaporites in the center of the trough. Lovering and Mallory (1962) report 4,700 feet of evaporite-bearing beds in a well at Eagle, just north of the area of figure 1. Evaporites occupy more than one belt in the interior of the basin (Mallory, 1960, fig. 5), but lack of data at present prevents delineation of the evaporites in detail. The Aspen area lies southwest of the center of the trough. There the

TABLE 1.—*Formations deposited in the central Colorado trough in late Paleozoic time*

Maroon Formation (Permian and Pennsylvanian)	Thin- to thick-bedded maroon and brick-red sandstone, conglomerate, and mudstone containing a few beds of gray limestone in the lower part. Evaporites well developed near the center of the basin (Lovering and Mallory, 1962); at least one bed south of Aspen.
Minturn Formation (Pennsylvanian)	Thick- to thin-bedded gray sandstone, shale, and limestone. Evaporites near the center of the basin; local lenses south of Aspen.
Belden Shale (Pennsylvanian)	Thin-bedded dark-gray shale and limestone containing a few beds of siltstone, sandstone, and carbonaceous shale. Evaporites generally not recognized, but 100 feet of gypsum is reported in the Hope tunnel 5 miles south of Aspen (Knopf, 1926). Evaporites in small fragments and bedded deposits lacking stratigraphic continuity occur along a fault zone in nearby Highland tunnel.

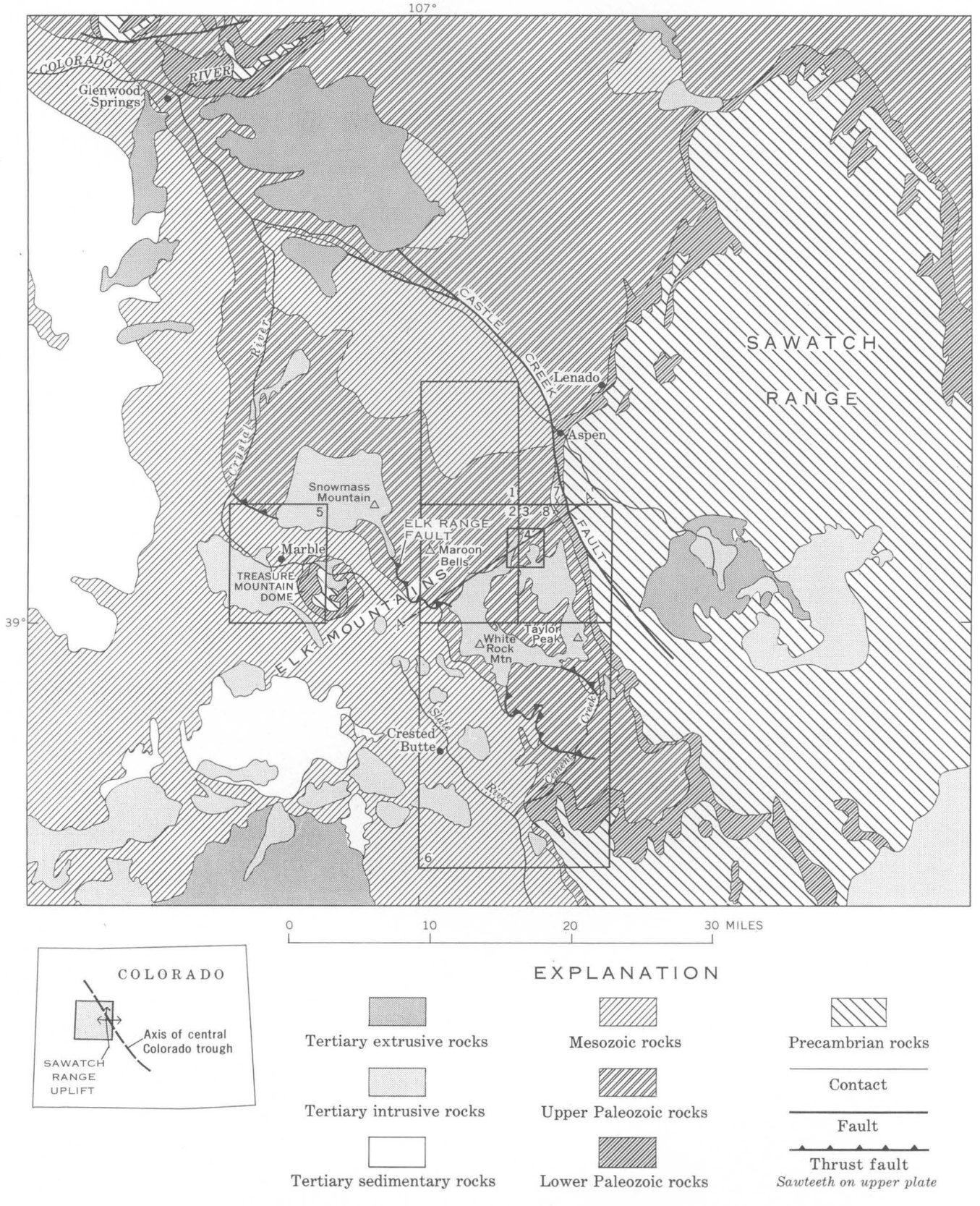

FIGURE 1.—Geologic map of part of west-central Colorado. *1*, Highland Peak quadrangle; *2*, Maroon Bells quadrangle; *3*, Hayden Peak quadrangle; *4*, Conundrum Creek area (fig. 2); *5*, Marble quadrangle; *6*, Crested Butte 15-minute quadrangle; *7*, Highland tunnel; and *8*, Hope tunnel. Section *A–A'*, shown on figure 4. Modified from geologic map of Colorado (Burbank and others, 1935).

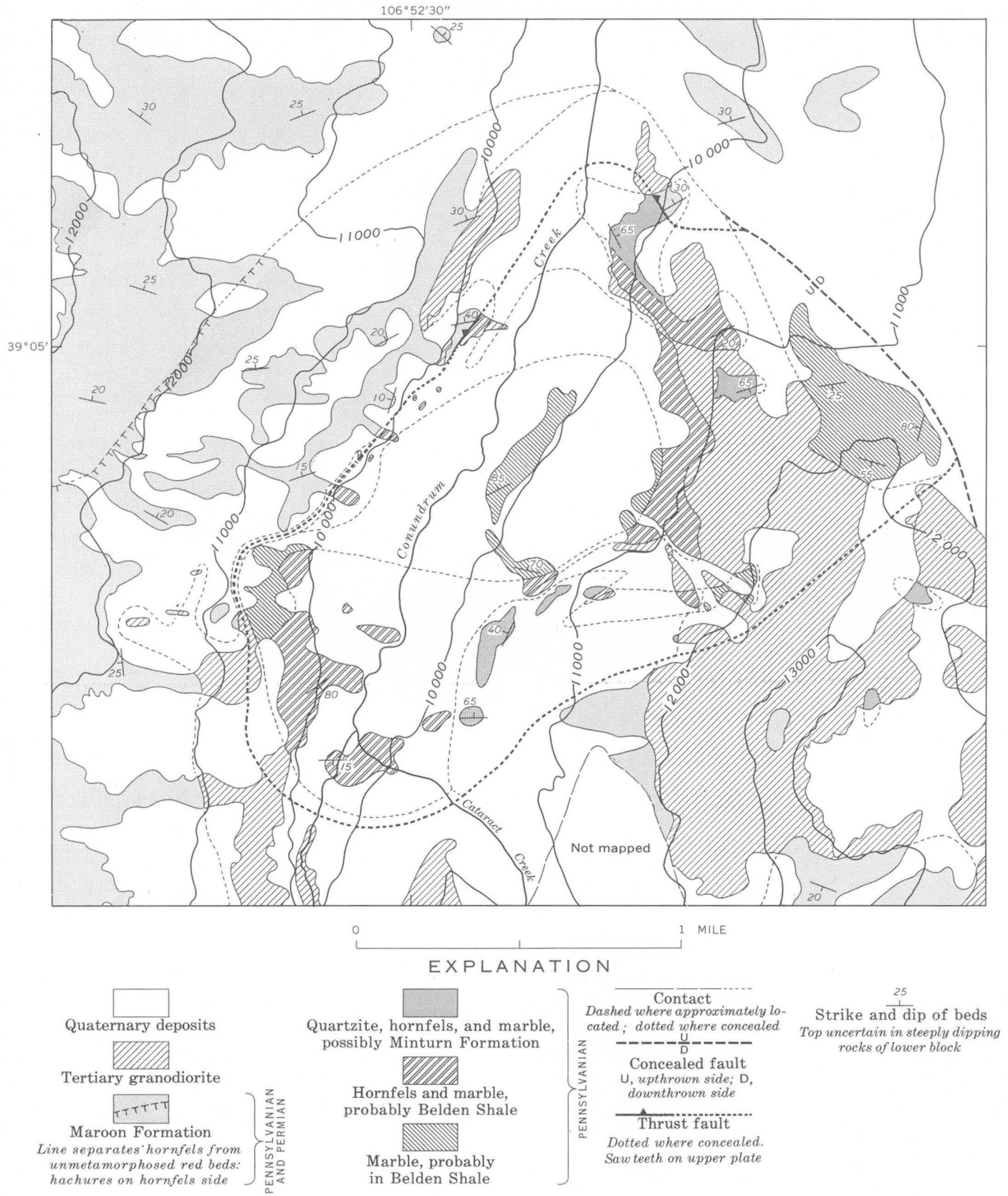

FIGURE 2.—Geologic map of the area of a possible window through the Elk Range thrust sheet on Conundrum Creek. Base from the Maroon Bells and Hayden Peak USGS 7½-minute topographic maps.

rocks are predominantly clastic, and evaporites occur only as local lenses.

The rocks of the lower block along Conundrum Creek appear to be correlative with the Belden Shale and Minturn Formation. A unit of hornfels and marble consists of thinly interbedded dark-gray diopside-scapolite and tremolite marble, pyrite-bearing hornfels, and a few beds of carbonaceous shale, and probably represents metamorphosed rocks of the Belden Shale. Lying either underneath or in the unit of hornfels and marble is a coarse-grained thick- to thin-bedded gray to white marble containing a few beds of hornfels and quartzite. Lenticular beds of this marble are as much as 30 feet thick. The area underlain by the marble is shown as undivided Devonian and Mississippian on the State geologic map (Burbank and others, 1935), but the marble does not resemble the Chaffee Formation of Devonian age, which is composed of dolomite, quartzite, and siltstone. The marble lacks the characteristic chert and is too thin bedded and variable in thickness and lithology to be the Leadville Limestone of Mississippian age. Rocks of the hornfels-marble unit that apparently underlie the marble unit in places do not resemble rocks underlying the Leadville Limestone. The number and thickness of marble beds, which would correspond to limestone beds in the Belden Shale, are not typical of carbonate units in the Belden nearby, but similar lithologies are reported by Vanderwilt (1937) in equivalent rocks mapped as Hermosa(?) Formation cropping out on the Treasure Mountain dome southeast of Marble (fig. 1). West and south of the Conundrum Creek area, stratigraphic units in the Minturn Formation (called Gothic Formation by Langenheim, 1952) have lithologies similar to those represented in the unit of hornfels and marble in the Conundrum Creek area but are associated with more numerous and thicker beds of coarse-grained sandstone (Langenheim, 1952, p. 555, 558, 562).

In the eastern part of the lower block, scattered outcrops of white to light-green quartzite, arkose, hornfels, and marble in beds ¼ inch to 10 feet thick may be metamorphosed rocks of the Minturn Formation. Minor folds are so numerous and irregular in pattern and outcrops so discontinuous that stratigraphic relations between units are uncertain.

Rocks overlying the thrust fault are gray and greenish-gray calc-silicate hornfels typical of the Maroon Formation where it is metamorphosed, but they also resemble parts of the Minturn Formation where it is metamorphosed. Detailed cross sections to points where the top or bottom of the Maroon Formation is exposed, however, suggest that most of these rocks are part of the Maroon Formation. Unmetamorphosed Maroon Formation occupies the northern and northwestern parts of the Conundrum Creek area (fig. 2).

Structural features

The structural pattern of the rocks above the fault contrasts strongly with that of the rocks below the fault (fig. 3). The overlying rocks are less deformed, and generally dip gently to moderately northward (fig. 3*A*). The underlying rocks are highly contorted (fig. 3*B*). Subdividing the underlying rocks into small areas did not produce diagrams with markedly clearer structural patterns. Some of the folds are just a foot or two in wave length; others are large enough to affect the map pattern. The small-scale folds lack a coherent pattern, and the bedding attitudes summarized in figure 3 indicate a lack of pattern in the large-scale folds. The structure evidently is more complex than is indicated by the map pattern deduced from unevenly distributed exposures (fig. 2), and faults as well as folds could be present in the underlying rocks.

Discordance between the overlying rocks and the underlying rocks is most obvious on the southwest side of the Conundrum Creek area where the marble unit is well exposed in two gullies and is truncated at a low angle by granodiorite that occupies the position of the fault. Just to the north, beds in the overlying rocks are cut by the fault occupied by granodiorite (fig. 2).

The fault between the two blocks and the bedding just below in the underlying rocks are concordant over a distance of a few hundred feet on the north and northeast sides of the area. In places, Tertiary granodiorite has invaded the fault between the blocks and the rocks above and below the fault (fig. 2).

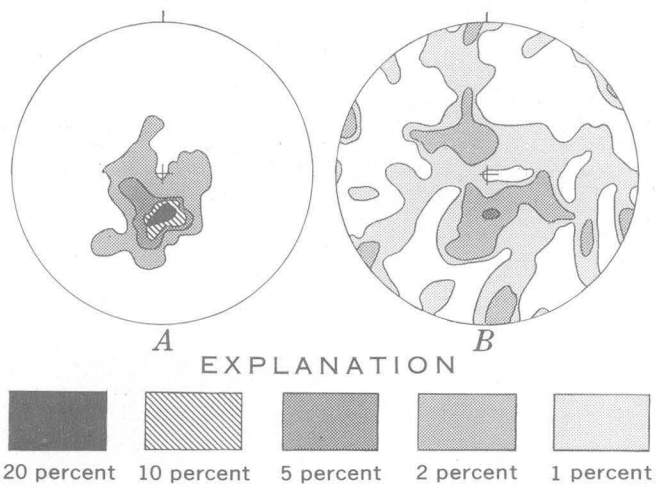

FIGURE 3.—Orientation of bedding above and below the Elk Range fault. Diagrams are equal-area projections on the lower hemisphere; north at top. Diagrams contoured in percentage of points per 1 percent of the area. *A*, 51 poles of bedding above fault; *B*, 90 poles of bedding below fault.

ELK RANGE FAULT

Regional considerations

The Elk Range fault crops out 7 miles southwest of the Conundrum Creek area and extends northwest-southeast for at least 25 miles (fig. 1). This fault was discovered in 1873 by the Hayden Survey (Hayden, 1874, p. 65–68), and reported on in more detail by Holmes (1876, p. 67–71) in the following year. He described the feature as "the great fault fold of the Elk Range," but it has received relatively little attention in recent years. Vanderwilt (1937) described the Elk Range fault and reviewed the literature on it. He did not show all of it on his detailed map and sections, but did include it on small-scale sketch maps (1935, 1937). Part of it is shown on the State geologic map (Burbank and others, 1935). Part of the fault also is shown on a sketch map of the Crested Butte 15-minute quadrangle by Langenheim (1952), and most of its known extent is shown by Godwin and Gaskill (1964).

The Elk Range fault has been described as a fold which has broken so that the northeast limb has overridden the southwest limb with a displacement of 1 to 2 miles (Holmes, 1876) or more than 2 miles (Vanderwilt, 1937).

The rocks above the Elk Range fault are generally less deformed than the rocks below the fault. The overridden rocks are in tight folds overturned to the southwest in the area between the fault and the Treasure Mountain dome (Vanderwilt, 1937). Folds in the overridden rocks extend southeast into the corner of the Maroon Bells quadrangle, where they die out or are obliterated by the White Rock pluton. In the line of the cross section in figure 4*B* the northeast limb of the fold in the overridden block at the southwest margin of the White Rock pluton has been steepened by intrusion of the pluton so that the fold is now asymmetric; the northeast limb has a steeper dip than the southwest one. Folds in the overridden block die out to the northwest in the Marble quadrangle (Gaskill and Godwin, 1966). Detailed information on the folds is lacking to the southeast.

Gaskill and Godwin (1963; 1966; oral commun., 1965,) show that apparent movement on the Elk Range fault dies out abruptly to the northwest, especially between the Snowmass pluton and the Crystal River, where it may indeed be considered a faulted fold with minor horizontal displacement. Relations to the southeast are more obscure; the fault may bifurcate into two thrust faults and be lost where it becomes parallel with bedding. Langenheim (1952) shows Minturn Formation (his Gothic Formation) carried over Mesozoic rocks on both branches of the fault. Consequently, it seems reasonable to assume considerable transport of the Elk Range thrust sheet in that area. No detailed published geologic maps are available at the intersection of the northwest-trending Elk Range fault and the north-trending Sawatch Range.

In the southwestern part of the Maroon Bells quadrangle (fig. 1), the upper part of the Minturn Formation overrides Mesozoic rocks along the Elk Range fault (fig. 4). The Maroon Formation is about 10,000 feet thick in the thrust plate in the western part of this quadrangle and in the southwestern part of the Highland Peak quadrangle. Sections measured by Langenheim (1952, 1954) just to the south beneath the fault show only about 1,000 feet of Maroon Formation.

The Maroon Formation characteristically changes thickness and lithology over short distances. For example, in the thrust plate above the Elk Range fault its thickness changes from 10,000 feet in the Maroon Bells quadrangle to 2,500 feet in the northwestern part of the Marble quadrangle in a distance of 15 miles oblique to the trend of the central Colorado trough (Langenheim, 1954; Gaskill and Godwin, 1966). The thickness of the Maroon may change more rapidly perpendicular to the trend of the trough, and as little as 6 miles of tectonic transport of a thick section southwest toward the margin of the trough could account for the present juxtaposition of a section of Maroon Formation 10,000 feet thick over one only 1,000 feet thick (fig. 4*A*).

The Elk Range fault probably was for the most part a bedding-plane fault on the Belden Shale or perhaps partly on a shaly or evaporitic interval in the Minturn Formation so that in the Conundrum Creek area younger rocks were carried over older ones. Some or possibly most of the Minturn Formation was cut out in the lower block. Deformation of rocks in the overridden block may be due to rumpling of the incompetent shales and thin-bedded limestones below the thick section of more competent sandstones of the thrust sheet. Farther east, along the flank of the Sawatch Range, the fault also may be parallel with bedding in the Belden Shale but with few or no beds missing. Consequently, the fault may be difficult to recognize where it should be along the flank of the Sawatch Range east of the Conundrum Creek area. Southwest of the Conundrum Creek area the fault has cut upward in the section of the overridden block but has remained at approximately the same stratigraphic horizon in the overriding block.

Whether the lower Paleozic rocks below the Belden Shale are as complex structurally as the units of the overridden block exposed in the Conundrum Creek area is unknown. Where the Belden Shale is brought

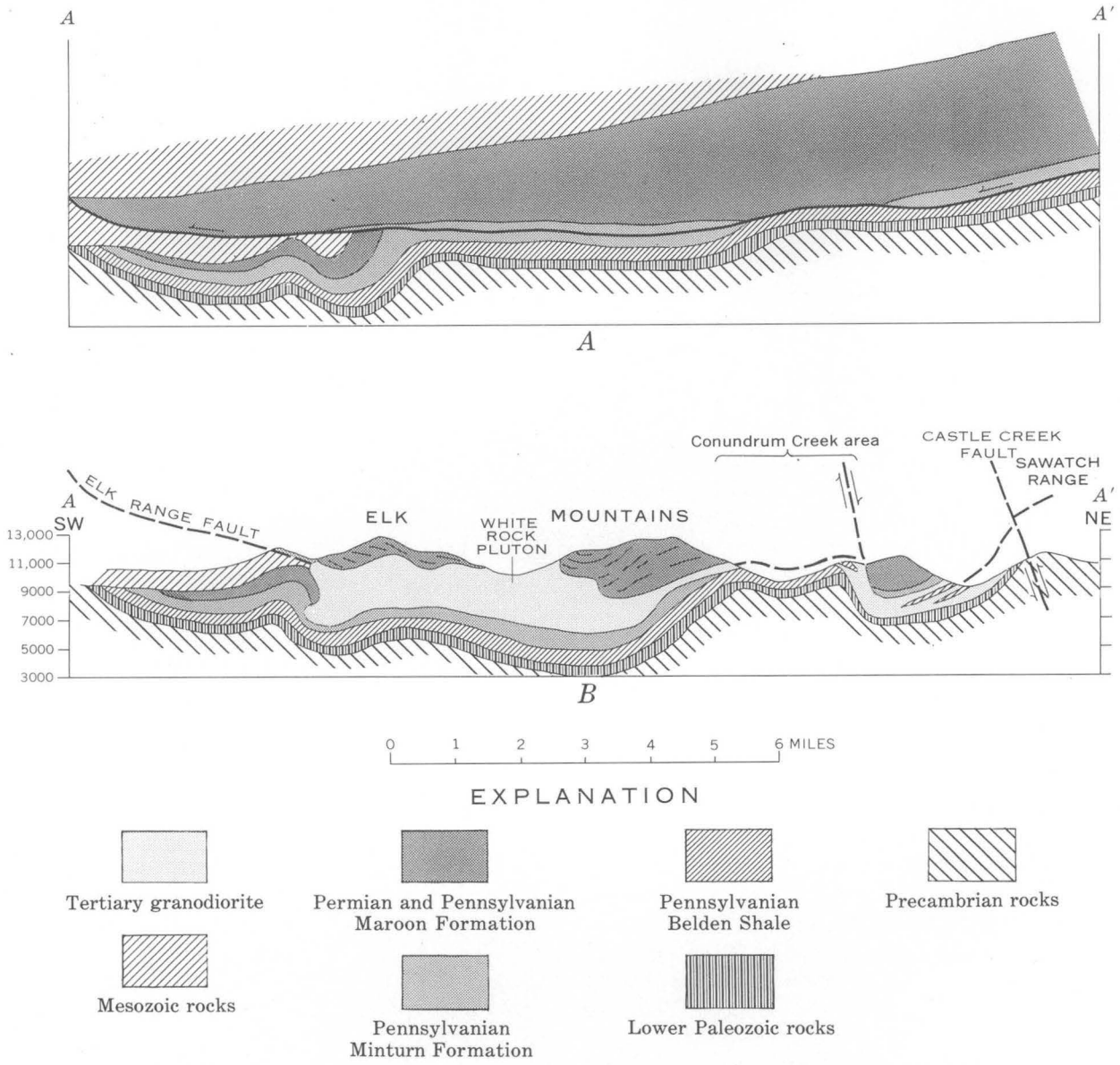

FIGURE 4.—Diagrammatic geologic sections from the flank of the Sawatch Range through the Conundrum Creek area and across the outcrop of the Elk Range fault in the southwest corner of the Maroon Bells quadrangle. Line of section is shown on figure 1, but section is based on more detailed information than shown on small scale of figure 1. *A*, after movement of the Elk Range thrust sheet but before intrusion of Tertiary granodiorite; *B*, at present.

up along the west flank of the Sawatch Range it is highly contorted in many places, and the massive underlying rocks do not have the same contortions. The structural pattern of the overridden rocks between the Conundrum Creek area and the outcrop of the Elk Range fault is not known, and the simplest interpretation is used in the diagrammatic section (fig. 4*B*).

Previous maps and my reconnaissance east of Conundrum Creek suggest that the Castle Creek fault, which apparently has a small displacement in the line of the section (fig. 4*B*), but a much larger one at Aspen, cuts the Elk Range fault. Rocks of the window have been brought to an altitude of more than 12,000 feet and against the Maroon Formation along a fault in the northeast part of the Conundrum Creek area (figs. 2 and 4*B*). This later faulting and the intrusion have obscured the relations between the overridden and overriding rocks on the east side of the window.

Detailed mapping by Gaskill and Godwin (1966) in the Marble quadrangle and by me in the Maroon Bells quadrangle confirms the suggestion provided by earlier mapping (Holmes, 1876; Vanderwilt, 1937, p. 91) that the Elk Range fault exerted a considerable degree of structural control on the subsequent emplacement of

the Snowmass and White Rock plutons. The trace of the fault is now discontinuous as a result of intrusion of the granodiorite (fig. 1), just as the relations between the structurally complex overridden and structurally simple overriding blocks in the Conundrum Creek area are obscured as a result of emplacement of the granodiorite of the White Rock pluton (fig. 2). The pluton does not intrude rocks below the Belden Shale where they are exposed along the west flank of the Sawatch Range (fig. 1), which indicates that it may have had its floor in or above the Belden Shale, near or along the Elk Range fault as shown on figure 4. Map relations show that in the southwestern corner of the Maroon Bells quadrangle and in the Conundrum Creek area the granodiorite at least locally cuts into the overridden block of the Elk Range fault. Detailed mapping of the rocks in the thrust plate shows that the granodiorite is concordant with bedding along well over half its contact length and is sharply discordant elsewhere to produce the highly irregular outcrop pattern of the pluton as a whole (fig. 1).

Origin and age

The position of the Elk Range thrust sheet appears to be related to the steep southwest flank of the Sawatch Range (fig. 1). Folds in the overridden block and the stratigraphic relations in the Maroon Formation indicate that the sheet travelled southwestward out of the northwest-trending central Colorado trough; it could have been derived by gravity sliding off the Sawatch range uplift of a section of rocks from the thick interior part of the trough. Evaporite beds near the center of the trough may have facilitated movement of the sheet (Zen and Hanshaw, 1964).

The age of the Elk Range fault is not clearly established. The fault cuts the Mesaverde Formation of Late Cretaceous age in the Marble quadrangle (Gaskill and Godwin, 1966), and it is cut by Tertiary intrusives, which are of post-early Eocene age in the West Elk Mountains (Godwin and Gaskill, 1964). West of Crested Butte, conglomerate and sandstone of the Ohio Creek Formation of Paleocene age contain pebbles of quartzite, shale, and silty clay (Gaskill and Godwin, 1963), many of which are rock types of the Mesaverde Formation or the Mancos Shale of Cretaceous age, and probably reflect the earliest uplift of the Sawatch Range. By the time the basal part of the Wasatch Formation was deposited, Precambrian rocks were probably exposed in the Sawatch Range, unless the pebbles of plutonic rock (Gaskill and Godwin, 1963, p. C36) in the Wasatch were derived by reworking of conglomerates in the Maroon Formation rather than from the Precambrian. Thus, uplift of the Sawatch Range and consequent movement of the Elk Mountain sheet probably began in Paleocene time.

Along the margin of the Sawatch Range the rocks are broken by many faults. This is the area where the Elk Range fault should crop out if the eastern Elk Mountains consist of a large gravity sheet. Until detailed mapping is done over a large stretch of the outcrop belt of the Belden, Minturn, and Leadville Formations along the west side of the Sawatch Range the presence of the Elk Range fault in that area cannot be proved or disproved. At Lenado, north of Aspen; in the Hope and Highland tunnels 5 miles south of Aspen; and on the northeast side of Taylor Peak south of the Hayden Peak quadrangle; the Belden Shale is broken by numerous faults, many of which are parallel with bedding. Gouge and breccia along them range in thickness from a quarter of an inch to more than 100 feet. Whether some or most of these faults are the Elk Range fault is not yet demonstrable because it is difficult to separate older, originally low-angle bedding faults which have been subsequently steepened by later deformation, from younger high-angle faults along the margin of the Sawatch Range uplift. The geologic relations as now known seem permissive for the hypothesis of a thrust sheet in the eastern Elk Mountains.

The possibility of a window in the Conundrum Creek area and the juxtaposition of stratigraphic sections of the Maroon Formation of vastly different thickness along the Elk Range fault in and south of the Maroon Bells quadrangle require us to consider the Elk Range thrust-sheet hypothesis.

REFERENCES

Brill, K. G., Jr., 1952, Stratigraphy in the Permo-Pennsylvanian zeugogeosyncline of Colorado and northern New Mexico: Geol. Soc. America Bull., v. 63, p. 809–880.

Burbank, W. S., Lovering, T. S., Goddard, E. N., and Eckel, E. B., compilers, 1935, Geologic map of Colorado: U.S. Geol. Survey in coop. with Colorado State Geol. Survey and Colorado State Metal Mining Fund Board.

De Voto, R. H., 1965, Pennsylvanian and Permian stratigraphy of central Colorado: The Mountain Geologist, v. 2, p. 209–228.

Gaskill, D. L., and Godwin, L. H., 1963, Redefinition and correlation of the Ohio Creek Formation (Paleocene) in west-central Colorado: Art. 69 *in* U.S. Geol. Survey Prof. Paper 475–C, p. C35–C38.

——— 1966, Geologic map of the Marble quadrangle, Gunnison and Pitkin Counties, Colorado: U.S. Geol. Survey Geol. Quad. Map GQ–512.

Godwin, L. H., and Gaskill, D. L., 1964, Post-Paleocene West Elk laccolithic cluster, west-central Colorado *in* Geol. Survey Research 1964: U.S. Geol. Survey Prof. Paper 501–C, p. C66–C68.

Hayden, F. V., 1874, Sawatch Range—morainal deposits of Taylors Creek—Elk Mountains, etc., chap. 3 *of* Report of F. V. Hayden, U.S. geologist, *in* Hayden, F. V., Seventh Annual Report of the U.S. Geological and Geographical Survey of the Territories * * * for the year 1873: Washington, U.S. Gov't. Printing Office, p. 53–69.

Holmes, W. H., 1876, Report on the geology of the northwestern portion of the Elk Range, chap. 6 *of* Report of F. V. Hayden, U.S. geologist, *in* Hayden, F. V., Eighth Annual Report of the U.S. Geological and Geographical Survey of the Territories * * * for the year 1874: Washington, U.S. Govt. Printing Office, p. 59–71.

Knopf, Adolph, 1926, Recent developments in the Aspen district, Colorado: U.S. Geol. Survey Bull. 785, p. 1–28.

Langenheim, R. L., Jr., 1952, Pennsylvanian and Permian stratigraphy in Crested Butte quadrangle, Gunnison County, Colorado: Am. Assoc. Petroleum Geologists Bull., v. 36, p. 543–574.

——— 1954, Correlation of Maroon Formation in Crystal River valley, Gunnison, Pitkin, and Garfield Counties, Colorado: Am. Assoc. Petroleum Geologists Bull., v. 38, p. 1748–1779.

Lovering, T. S., and Mallory, W. W., 1962, The Eagle Valley Evaporite and its relation to the Minturn and Maroon Formations, northwest Colorado: Art. 132 *in* U.S. Geol. Survey Prof. Paper 450–D, p. D45–D48.

Mallory, W. W., 1958, Pennsylvanian coarse arkosic redbeds and associated mountains in Colorado *in* Symposium on Pennsylvanian rocks of Colorado: Rocky Mtn. Assoc. Geologists, p. 17–20.

——— 1960, Outline of Pennsylvanian stratigraphy of Colorado, *in* Guide to the geology of Colorado: Geol. Soc. America jointly with Rocky Mtn. Assoc. Geologists and Colorado Sci. Soc., p. 23–33.

Murray, H. F., 1958, Pennsylvanian stratigraphy of the Maroon trough *in* Symposium on Pennsylvanian rocks of Colorado: Rocky Mtn. Assoc. Geologists, p. 47–57.

Vanderwilt, J. W., 1935, Revision of the structure and stratigraphy of the Aspen district, Colorado, and its bearing on the ore deposits: Econ. Geology, v. 30, p. 223–241.

——— 1937, Geology and mineral resources of the Snowmass area, Gunnison County, Colorado: U.S. Geol. Survey Bull. 884, 184 p.

Zen, E-an, and Hanshaw, B. B., 1964, Osmotic equilibrium and mechanics of overthrust faulting [abs.]: Geol. Soc. America Spec. Paper 82, p. 232–233.

STREAM ANTICLINES IN CENTRAL KENTUCKY

By GEORGE C. SIMMONS, Berea, Ky.

Work done in cooperation with the Kentucky Geological Survey

Abstract.—Small nontectonic folds called stream anticlines occur in interbedded limestone and shale of the Upper Ordovician in central Kentucky. Although their amplitude commonly is only a few feet, some anticlines are more than half a mile long; most are fractured along their crests. Stream anticlines are unrelated to tectonic features, and their coincidence with valley bottoms suggests a Recent origin. This origin is substantiated at one place by an eyewitness account near Stanford, Ky.

Small nontectonic anticlines are common in Upper Ordovician limestone and shale in central Kentucky. The anticlines occur along valley floors, and their axes coincide with the trends of the valleys. About 50 of these folds were recently mapped in the Kirksville, Valley View, Richmond North, and Union City quadrangles by the author and by R. C. Greene (1965, 1966) near Richmond, Ky. (fig. 1), and the description to follow is based on observations in that vicinity. These geologic structures are shown as minor anticlines on the quadrangle maps. The term "stream anticline" which describes these folds was suggested by Charles H. Maxwell, of the U.S. Geological Survey (oral commun., 1962) because the folds trend along stream courses and are well exposed where streams flow on bedrock.

Stream anticlines are simple upward flexures without complementary synclines. The beds on the flanks of the folds commonly dip less than 5°, although dips of more than 20° have been recorded. The width of the folds, that is, the distance between unflexed beds on the opposite sides of the folds, is from a few feet to several tens of feet. The amplitude is from a few inches to 5 feet. Despite their small amplitude, some anticlines have a length of more than half a mile; however, lengths of several tens to hundreds of feet are more common.

The stream anticlines are commonly fractured along their crests. The fractures occur singly or in sets with individual fractures spaced a few inches to several feet apart and are either open an inch or two or tightly closed. Most anticlines have a relatively large open fracture along the crestline and parallel, more weakly developed fractures on the flanks. Locally, beds are buckled and have steep dips between fractures or are offset several inches across a fracture.

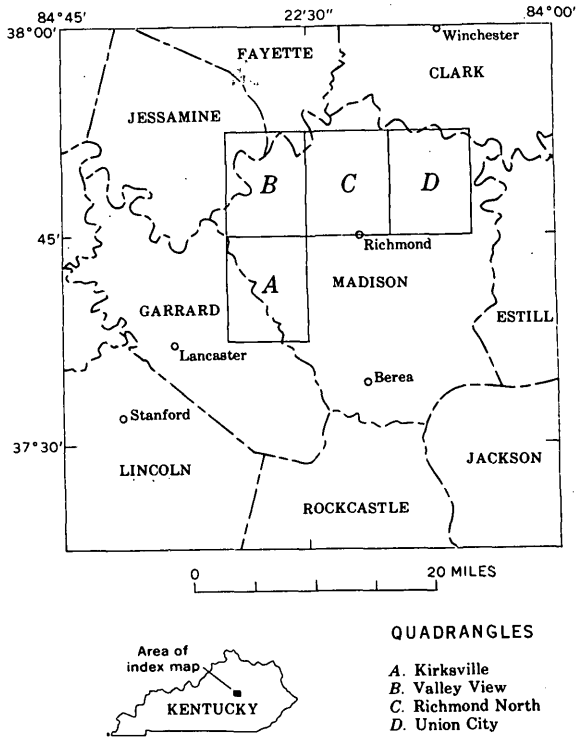

FIGURE 1.—Index map showing quadrangles in central Kentucky where stream anticlines have been mapped.

FIGURE 2.—Stream anticline in interbedded limestone and shale (Grant Lake Member of the Ashlock Formation) on West Fork Otter Creek, Richmond North quadrangle, Kentucky.

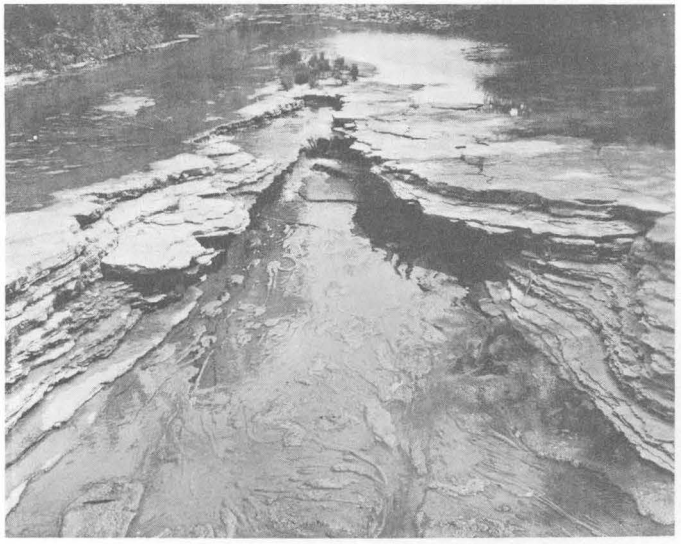

FIGURE 3.—Stream anticline in interbedded limestone and shale (Tate Member of the Ashlock Formation) on West Fork Otter Creek, Richmond North quadrangle, Kentucky. The dip is only 1° on each flank of the fold, but uplift raised the axial region of the anticline high enough to divide the streamflow into two channels during stages of low water. (Maximum width of stream near top of picture is about 40 feet.)

Stream anticlines involve alternating beds of limestone and shale at places where the ratio of limestone to shale is between 3:2 and 3:1. The limestone generally occurs in beds ranging from less than 1 inch to 6 inches in thickness separated by laminae and beds of shale as much as 1 inch thick. The stratigraphic units containing this lithology in the area are the Ashlock Formation, Calloway Creek Limestone, and parts of

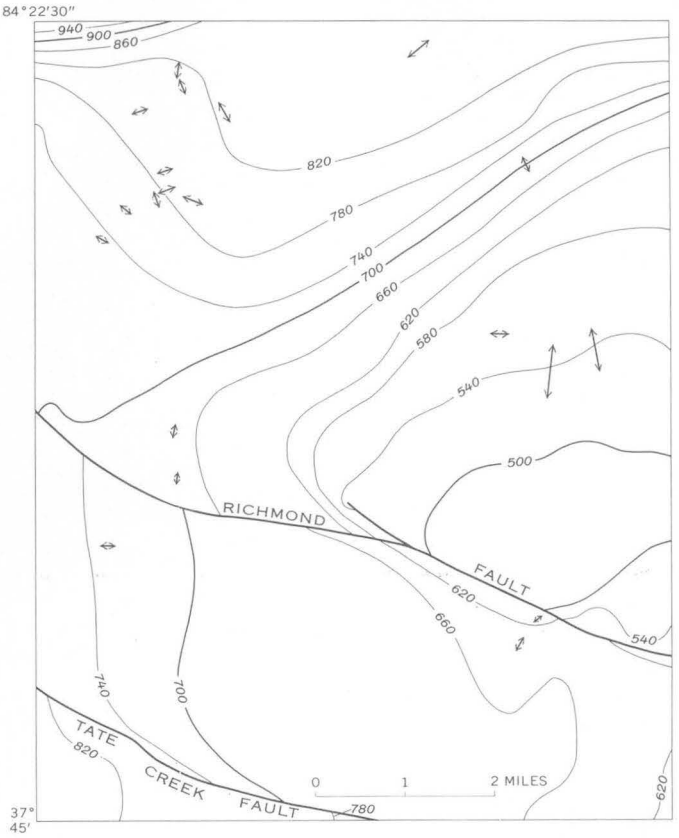

FIGURE 4.—Map of the Richmond North quadrangle, Kentucky, showing the relation of stream anticlines (arrows) to structural features. Structure contours, in feet above sea level, are drawn on the base of the Garrard Siltstone. See figure 1 for location of quadrangle.

the Clays Ferry Formation; thus the stream anticlines are chiefly confined to these formations (figs. 2 and 3).

Stream anticlines are unrelated to structural features of tectonic origin. The folds strike parallel, oblique, and perpendicular to local and regional bedding trends. Only a few anticlines were found near faults, and no evidence was found suggesting a causal relation between the two (fig. 4).

The origin of stream anticlines is not known. One hypothesis is that the absorption of water by clay minerals caused an increase in volume of the shale beds. This in turn produced stresses that were most easily relieved by upward bending of strata in the stream bottoms where little or no overburden was present. Another hypothesis is that "unloading" of bedrock by stream erosion resulted in a reduction of pressure on beds at stream level compared to the pressure on the same beds under adjacent hills. This differential pressure caused a slight plastic flow in the shale toward the streams, and a volume increase in the shale lifted the overlying limestone. Shaler (1877, p. 49) considered that the folding and fracturing resulted from

contraction of limestone caused by solution of various soluble salts—similar to the drying of wood or the shrinkage of brick clay during burning.

Although the genesis of the anticlines is uncertain, their time of origin is undoubtedly Recent. This conclusion is indicated by the coincidence of stream anticlines and drainage (fig. 5), and is confirmed by the report by Shaler (1877, p. 48–49) of an eyewitness account near Stanford, Ky.:

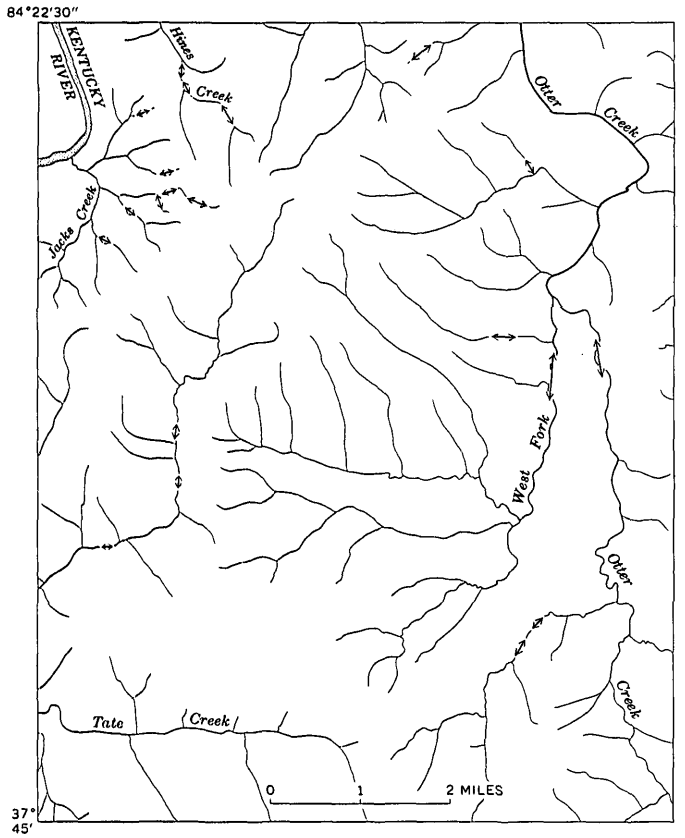

FIGURE 5.—Map of the Richmond North quadrangle, Kentucky, showing the relation of stream anticlines (arrows) to drainage. See figure 1 for location of quadrangle.

The bed of the creek lies in the upper part of the Cincinnati Group, or Blue Limestone series; but at this point the series is much less calcareous than in the region to the northward. The rock lies rather in thin beds, but very compact and dense —rather arenaceous and calcareous—showing a remarkable want of the open joints so common in many of our limestones of this series. Below the level of these hard beds are limestones which show the ordinary jointed beds. The rocks in the bed of the creek are exposed in very broad tables, the one where the disturbance occurred being over two hundred feet long and perhaps twenty feet wide. Above and below this point, the stream had slight falls over the edges of similar beds. Just at this point its bed was upon this broad sheet of rock, all of one layer. The disturbance which was very conspicuous, consisted of a low ridge, about three feet wide and about ten inches high in the middle, which extended obliquely across the stream for a distance of one hundred and fifty feet, either end disappearing beneath the bank of alluvium that bordered the stream. The top of the ridge was shattered into fragments by the process of upheaval, spalls of rock to the number of hundreds having been thrown from its surface by the movement. The top of the ridge was seamed by a fissure about an inch wide, which was irregular in its direction and width.

Fortunately, the formation of this curious ridge was intelligently observed by the son of Mr. Cornelius Trailer, on whose farm the disturbance occurred. At early day, coming with a horse to a wateringplace near the stream, he heard the roaring sound beneath the earth, which was so violent as to cause his horse to break away from him. In a moment he saw the stones begin to fly from the rock in the bed of the creek, near the bank, and directly saw that the disturbance advanced upstream. Following the movement, which went on at the rate of a slow walk, he saw it finally disappear beneath the opposite bank. During the rest of the day there were frequent sounds as of further rending of the rocks at depths beneath the upheaved surface; but by nightfall the sounds had all ceased, and had not been renewed up to the time of my inspection.

REFERENCES

Greene, R. C., 1965, Geologic map of the Kirkville quadrangle, Garrard and Madison Counties, Kentucky: U.S. Geol. Survey Geol. Quad. Map GQ–452.

——— 1966, Geologic map of the Valley View quadrangle, central Kentucky: U.S. Geol. Survey Geol. Quad. Map GQ–470.

Shaler, N. S., 1877, Scientific problems: Kentucky Geol. Survey Rept. Prog., v. 3, pt. 7, new ser. (2d), p. 43–50 (407–414).

224-352 O—66——2

EXOTIC BLOCKS AND COARSE BRECCIAS IN MESOZOIC VOLCANIC ROCKS OF SOUTHEASTERN ARIZONA

By FRANK S. SIMONS, ROBERT B. RAUP, PHILIP T. HAYES, and HARALD DREWES, Denver, Colo.

Abstract.—In the Canelo Hills and the Huachuca, Patagonia, and Santa Rita Mountains of southeastern Arizona, thick sequences of Mesozoic volcanic and volcanic-sedimentary rocks contain sizable exotic blocks or coarse sedimentary breccias of older rocks. The large blocks were emplaced by dragging or rafting by lava flows, by gravity sliding, or possibly by transport in ash flows. These exotic blocks and coarse breccias, together with conglomerate at several horizons, indicate widespread tectonic activity in southeastern Arizona during Mesozoic time.

Several mountain ranges in Santa Cruz and Cochise Counties, southeastern Arizona, contain thick volcanic and volcanic-sedimentary sequences of Triassic to Cretaceous age (fig. 1). In many places these volcanic-sedimentary sequences contain sizable blocks or coarse sedimentary breccias of older rocks. Maximum dimensions of some of the larger blocks are locally measurable in thousands of feet. The volcanic rocks are mainly rhyolite, quartz latite, and dacite, but some are trachyte and trachyandesite. The geologic age of some of the volcanic sequences has been determined by their relation to fossiliferous rocks or by isotopic age determinations, but the age of others is known only within broad limits.

The exotic blocks in the Mesozoic rocks commonly are of upper Paleozoic sedimentary strata but also include lower Paleozoic sedimentary rocks and Precambrian metamorphic rocks as well as Mesozoic volcanic material. The large blocks were emplaced in several ways; some were picked up and dragged by flowing lava or appear to have been rafted on or in lava flows, whereas others are interpreted as gravity slide blocks, some of which may have glided along muddy layers in the host rock. The sedimentary breccias are thick and very coarse but otherwise are lenticular stratigraphic units that were deposited near a rugged source area.

Exotic blocks or breccias from four ranges are described briefly, and some ideas on Mesozoic paleogeography of southeastern Arizona are presented. The Canelo Hills have been studied by Raup, Simons, and Hayes, the Huachuca Mountains by Hayes, the Patagonia Mountains by Simons, and the Santa Rita Mountains by Drewes.

CANELO HILLS

The Canelo Hills comprise a group of low narrow ridges lying between the Huachuca Mountains to the east and the Patagonia and Santa Rita Mountains to the west (fig. 1). They extend from about 6 miles north-northeast of Patagonia southeastward for 22 miles. The northern half of the Canelo Hills is underlain by sedimentary rocks of Paleozoic and Mesozoic age and volcanic rocks of Mesozoic and Tertiary age, whereas the southern half consists largely of silicic and intermediate volcanic rocks of Mesozoic and Tertiary age.

Northern Canelo Hills

The northern part of the Canelo Hills consists mainly of Paleozoic sedimentary rocks, mostly limestone, overlain by Canelo Hills Volcanics of Triassic and Jurassic age (Hayes and others, 1965). The basal unit of the volcanic rocks is as much as 2,000 feet thick and is made up of red beds, tuff, tuffaceous sandstone, conglomerate, and thin silicic lava flows. At most places it rests on Permian Concha Limestone and was deposited on a surface of moderately high relief marked locally by a zone suggestive of a poorly developed regolith. Exotic blocks, probably emplaced by gravity sliding, are abundant in sedimentary rocks near the base of this unit.

U.S. GEOL. SURVEY PROF. PAPER 550-D, PAGES D12-D22

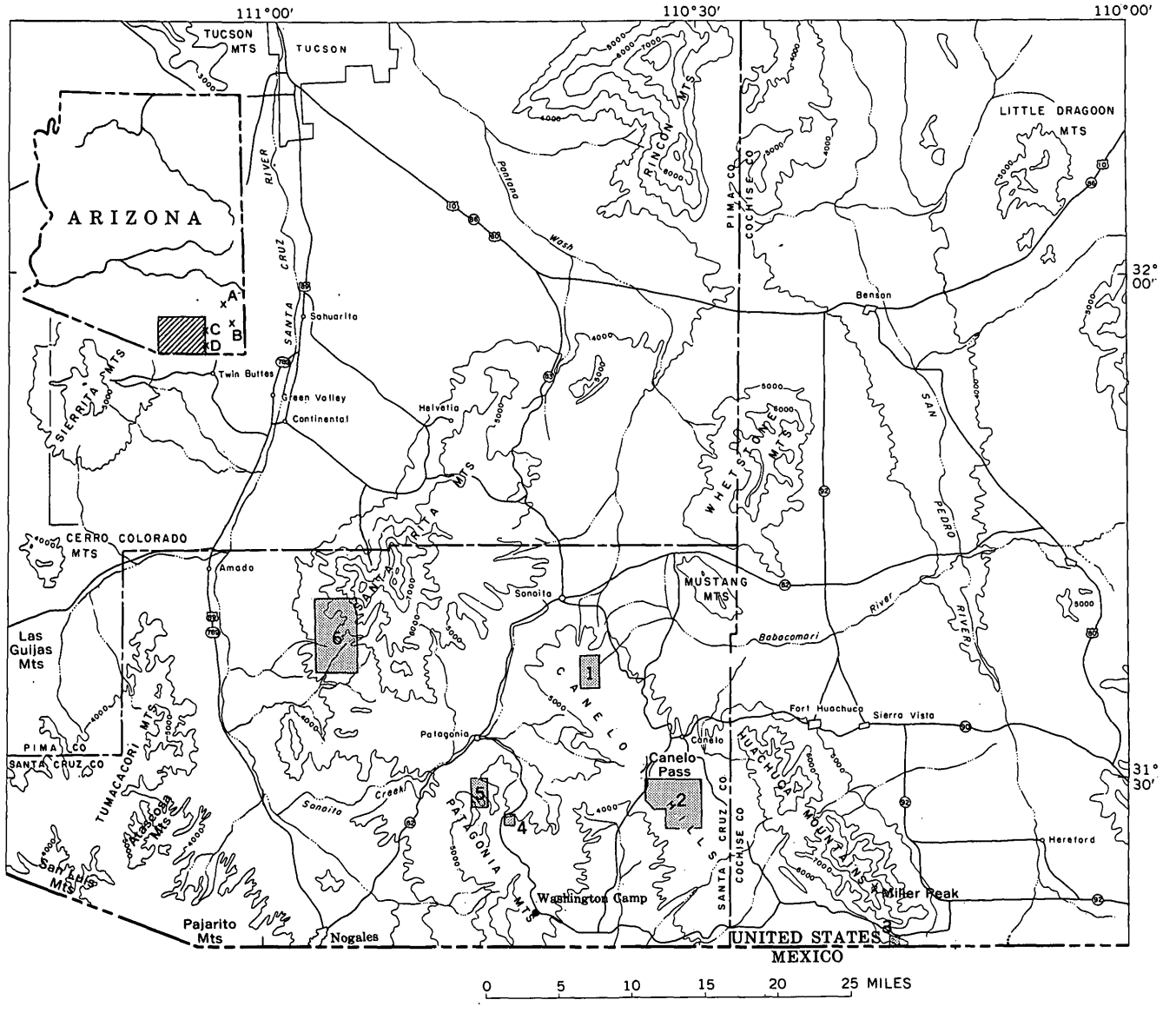

FIGURE 1.—Index map of a part of southeastern Arizona, showing location of areas described in the text. *1*, northern Canelo Hills; *2*, southern Canelo Hills; *3*, Coronado National Memorial, Huachuca Mountains; *4*, American mine area, Patagonia Mountains; *5*, Flux mine area, Patagonia Mountains; and *6*, Josephine Canyon–Montosa Canyon area, Santa Rita Mountains. Index map: *A*, Dos Cabezas Mountains; *B*, Chiricahua Mountains; *C*, Dragoon Mountains; and *D*, Mule Mountains.

Host rocks for the exotic blocks are mainly conglomerate and red beds. The conglomerate is largely massive limestone conglomerate but locally is composed principally of clasts of volcanic rock in a tuffaceous matrix. Interbedded with the conglomerate are thin-bedded tuff and tuffaceous sandstone. The red beds comprise red mudstone with a few thin and discontinuous limy layers and brown medium-grained sandstone. Volcanic flows and tuff occur locally in the red-bed sequence, indicating that the red beds were deposited during a period of volcanic activity in the region.

A typical exotic block is a bedding-plane slab lying generally parallel to the layering in the host rocks. Such blocks range in length from a few tens of feet to at least 4,000 feet and in thickness from a few feet to more than 150 feet. Most blocks are limestone or dolomite of Permian age, from either the Concha Limestone or the Scherrer Formation; some are quartzite or feldspathic sandstone, also of the Scherrer.

All the blocks are brecciated, but the degree of brecciation is not uniform. Distance from possible source rocks, where any estimate can be made, or type of host rock seem to have little influence on the inten-

sity of brecciation; in general, however, brecciation diminishes toward the centers of blocks, so that thick blocks are less brecciated than thin ones.

Breccia fragments of limestone are not everywhere easily recognized owing to subsequent healing of fractures. In some places, original fragments show up because of slight color differences between them and the healing material. The effect of brecciation on chert and fossils is more evident. Chert nodules, so abundant in the Concha Limestone, are thoroughly shattered and their distinctive shapes are destroyed, although the general distribution of chert is little changed. Silicified brachiopods are common in chert nodules of the Concha, and in places the only recognizable fossils remaining in exotic blocks are in fragmented nodules; unsilicified fossils have been obliterated.

Fragments in exotic blocks have been rotated, at least locally. Evidence of rotation can be seen only in fragments of quartzite, which is laminated, and not in fragments of the unlaminated carbonate rocks. Parting planes generally are intact. Near the base of one block, fragments in a thin unit of distinctly laminated quartzite are oriented at random, indicating considerable rotation on a small scale, but the contact between quartzite and the overlying fragmented carbonate rock is practically undisturbed. Apparently the blocks moved as bodies that were sufficiently competent to preserve gross stratigraphic features, even though beds between parting planes were disturbed locally to a greater extent.

All the exotic blocks whose stratigraphic position relative to the underlying Paleozoic bedrock is known are within 300 feet of the Paleozoic rocks, and most are within 100 feet or less. Although blocks occur throughout this interval, within a given area they tend to be concentrated at a particular horizon. Field evidence shows clearly that at least some of the blocks could not have reached their present stratigraphic position as a result of faulting, and it seems likely that all were emplaced by gravity sliding.

Examples of exotic blocks in conglomerate may be seen north of the Canelo Pass road just east of the pass. Here, large blocks, mainly of Concha Limestone, are enclosed in a unit of massive limestone conglomerate and volcanic sedimentary rocks. The conglomerate unit thins abruptly toward the north, suggesting that it was deposited in a local basin. The blocks appear to be ordinary components of the conglomerate, but one exposure suggests that they may have slid on muddy layers within the conglomerate. At this place, the basal few feet of an exotic block of Concha Limestone is typically brecciated, and the healing material is red limy mudstone with only sparse rounded granules and small pebbles of limestone. The mudstone may represent the surface material on which the block slid.

Examples of exotic blocks in red beds are common along both flanks of a faulted syncline on the east side of the northern Canelo Hills. Along the east flank, part of which is shown on figure 2*A*, the relation of exotic blocks to source rocks is particularly well displayed; the exposed source rocks are the lower part of the Concha Limestone, and the blocks too are derived from the lower part of that formation. The surface on which the red beds were deposited is fairly irregular, with local relief of at least 400 feet. Depressions in the older terrane were filled in by red beds with a thin basal conglomerate and abundant exotic blocks. After the depressions were filled, more blocks were emplaced sporadically within a narrow stratigraphic interval.

Southern Canelo Hills

The southern part of the Canelo Hills is made up mainly of rhyolite lava flows more than 1,000 feet thick, overlain by rhyolite welded tuff more than 6,000 feet thick (fig. 2*B*). These rocks have a general northwest strike, and dip moderately southwest.

Several lenses of upper Paleozoic sedimentary rocks, largely of Permian age, are enclosed in or underlain by rhyolite lava, and other lenses have similar, but not entirely clear, field relations. Two are overlain directly by welded tuff. The lenses range in length from 200 to 3,500 feet and are as much as 750 feet in outcrop width. Two lenses are at or near the top of the lavas, two others are probably near the same stratigraphic position, and another seems to be several hundred feet below the top of the lavas. The stratigraphic location of other lenses is uncertain. Carbonate rocks, mostly limestone, are dominant in the lenses, but quartzite is present in four of them.

The lenses have several features in common. All are brecciated; indeed some are so thoroughly fractured that over sizable outcrop areas no fragments more than a few inches across remain unbroken. In some lenses brecciation is most intense near contacts. In general the lenses are little recrystallized, silicified, or otherwise altered, although the limestone of some lenses is slightly reddened near contacts. The lenses are cut by numerous veinlets of white calcite; and dolomitic limestone may be divided into various-sized blocks by irregular septa of lighter colored carbonate which is dedolomitized rock. The lenses seem for the most part to be bedding-plane slabs whose bedding is

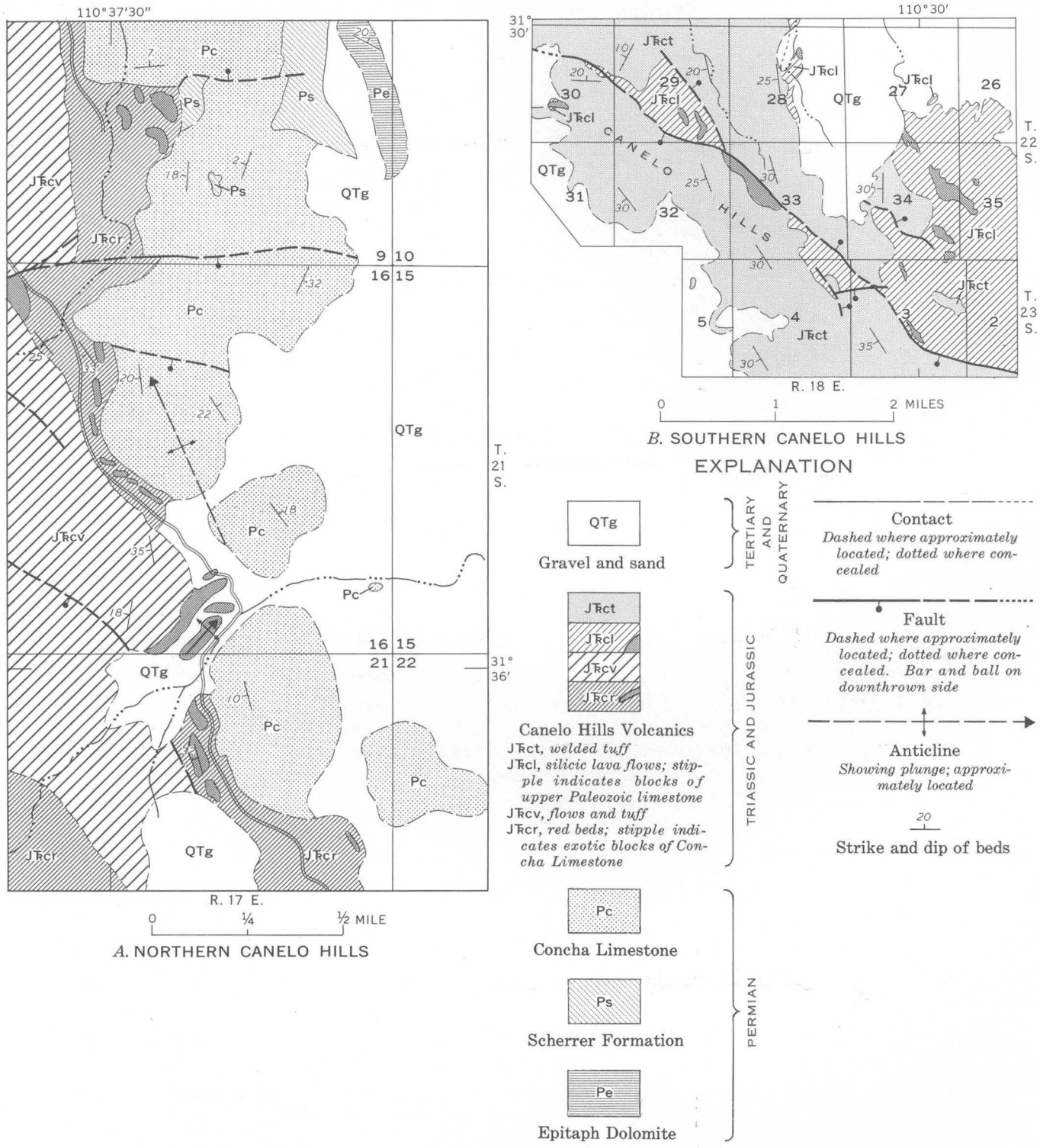

FIGURE 2.—Generalized geologic maps of parts of the northern (*A*) and southern (*B*) Canelo Hills, Santa Cruz County, Ariz.

roughly parallel to the enclosing lavas or to nearby welded tuff. No exposure of a contact between a lens and volcanic rock was found.

In most places, the only rocks associated with the lenses are volcanic. However, one composite block about 1,300 feet long consists of two lenses that are in contact at their north ends; south of the juncture they are separated by as much as 50 feet of conglomerate composed of partly rounded fragments of limestone and volcanic rock in a matrix of calcarenite.

These exotic lenses in volcanic rocks may be interpreted as hills of bedrock protruding through the volcanic material, as slivers along faults, as landslide blocks, or as slabs transported on or within lava flows. Some may indeed be bedrock hills, but such an explanation seems unlikely for long and narrow lenses that crop out on ridgetops and have steep contacts with the lavas. No evidence was found that any of the lenses is a fault sliver, although at least one is bounded by a fault along one side. All the lenses are a mile or more horizontally from the nearest outcrop of what is undoubted prevolcanic bedrock, and several apparently are separated by hundreds of feet of lavas from any underlying prevolcanic rock. The lenses could have been emplaced by landsliding, but some are long thin slabs that might have been noticeably disrupted during landsliding rather than merely brecciated. Two of these thin slabs are underlain by an appreciable thickness of lava and must have travelled a considerable distance.

It seems most likely that the lenses were transported on or in lava flows. At present the nearest outcrops of Paleozoic source rocks are 10 miles west or southwest in the Patagonia Mountains, 5 miles or more northwest in the Canelo Hills, and 8 miles northeast in the Huachuca Mountains. The direction from which the volcanic rocks came is unknown, so no logical choice can be made among these possible source areas. It is possible, of course, that Paleozoic rocks may have been exposed somewhere nearby at the time of extrusion of the lavas; in that event such extensive transport would not need to be invoked.

Transportation by lava, although producing considerable brecciation, has resulted in little or no alteration of the slabs, presumably either because the lava was already rather cool at the time the blocks were entrained, or because the length of time between picking up of the slabs and cooling of the lava was very short.

HUACHUCA MOUNTAINS

The Huachuca Mountains are a northwest-trending range about 20 miles long in the southwest part of Cochise County (fig. 1). The mountains are made up of Precambrian granitic rocks, Paleozoic sedimentary rocks, a wide variety of Mesozoic sedimentary, volcanic, and intrusive rocks, and subordinate Cenozoic igneous rocks.

In the southern part of the Huachucas, numerous exotic blocks of Paleozoic sedimentary rocks are enclosed in volcanic rocks of Mesozoic age. Some of the most instructive examples are in the extreme southern part of the range in Coronado National Memorial between Joe's Canyon Trail and the Mexican border (fig. 3). Here there is a well-exposed body of grayish-red trachytic lava, containing large exotic blocks. It is conformably underlain and overlain by thick units of very poorly sorted volcanic cobble- to boulder-conglomerate that is assigned to the Glance Conglom-

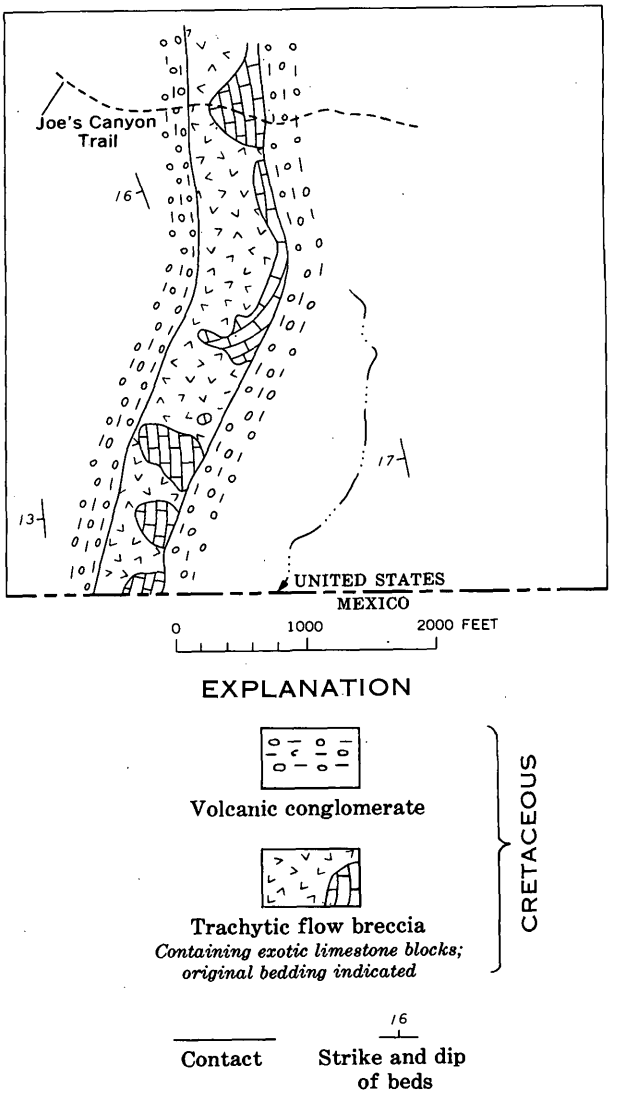

FIGURE 3.—Geologic sketch map of lava flow containing exotic blocks, in Coronado National Memorial, Huachuca Mountains, Cochise County, Ariz. (fig. 1, loc. 3).

erate of the Bisbee Group of Early Cretaceous age. The upper conglomerate unit contains sparse limestone clasts as well as volcanic detritus.

The trachyte seems to be a single lava flow about 200 feet thick. In most places it is a flow breccia, but breccia is much more apparent in the upper part, some of which is vesicular. The rock contains as much as 20 percent phenocrysts of plagioclase up to 5 mm in length.

The exotic blocks are as much as 1,500 feet long and 200 feet high. All the larger blocks are at or very near the base of the trachyte (fig. 3). The blocks readily identifiable as to origin were derived from the Permian Concha Limestone, the youngest Paleozoic formation recognized in the Huachuca Mountains. Bedding in most of the limestone blocks is readily apparent, even though the blocks are highly brecciated, and most bedding is subparallel to the containing lava flow.

Brecciation in the central parts of the larger blocks is not everywhere easily recognized, but close examination generally reveals the limestone to be brecciated and recemented. Brecciation is most intense near the outer edges of the blocks, where in many places lava fills spaces between breccia fragments. Furthermore, the lava near the blocks contains numerous smaller blocks and fragments of limestone, presumably derived from the larger blocks.

These blocks of Concha Limestone undoubtedly were shoved or carried along at or near the base of the trachyte flow and were brecciated during transport. Fragments of limestone that were broken off edges of the blocks were set adrift in the flowing lava. Whether the larger limestone blocks were plucked from bedrock or were landslide blocks picked up by the flow is conjectural.

Elsewhere in the southern Huachuca Mountains, exotic blocks of upper Paleozoic rocks are abundant in a thick and widespread sequence of intermediate volcanic rocks that are considerably older than the trachyte flow described above. The older volcanic rocks are dominantly nonwelded lithic tuffs, but some possible welded tuff and lava have been noted.

Few if any single blocks exceed 1,500 feet in length and 300 feet in thickness, but on the steep slopes east of Miller Peak (fig. 1) the blocks in places are so abundant and so closely spaced as to form masses of brecciated limestone, virtually free of volcanic material, that range from about half a mile to more than 1 mile in length along strike. The enclosing tuffs are generally so poorly exposed and badly weathered that their origin is doubtful. Therefore it is uncertain whether the exotic blocks were transported by ash flows or lahars, or both.

PATAGONIA MOUNTAINS

The Patagonia Mountains (fig. 1) extend from near the village of Patagonia south-southeastward about 14 miles to the Mexican border and beyond for several miles into Mexico. They consist of Precambrian, Mesozoic, and Cenozoic igneous rocks and subordinate amounts of Paleozoic and Cretaceous sedimentary rocks. Exotic lenses and blocks of Paleozoic limestone in younger volcanic terrane crop out in several areas; the most extensive are near the American mine near Harshaw Creek (fig. 4*A*) and in upper Flux Canyon, 4–5 miles south of Patagonia (fig. 4*B*).

American mine area

The area around the American mine (fig. 4*A*) is underlain by rhyolite lava and flow breccia that rest on Concha Limestone and the underlying Scherrer Formation, both of Permian age. The rhyolite is correlated tentatively with pre-Lower Cretaceous silicic volcanic rocks of the central Patagonia Mountains northwest of Washington Camp, which in turn may be equivalent in part to the lower Mesozoic Canelo Hills Volcanics (Hayes and others, 1965).

The largest limestone occurrence is along and at the west end of the east-trending ridge north of the American mine. This ridge consists of blocks of brecciated limestone and some quartzite enclosed in rhyolite. East of Harshaw Creek this limestone-rhyolite complex crops out over an area about 1,500 feet long and 700 feet in maximum width; west of the creek it is very poorly exposed but may extend a distance of 1,000 feet or more. Eastward the complex thins abruptly and passes into limestone conglomerate that in turn lenses out near the Bender mine about 3,500 feet east of Harshaw Creek. The limestone blocks are derived from the Concha Limestone and the quartzite from the Scherrer Formation. Most of the blocks are a few feet across but some are much larger; the largest, at the base of the ridge just east of Harshaw Creek, is a highly brecciated mass of dark-gray limestone possibly 100 feet or more across. The limestone-rhyolite breccia and conglomerate lie as much as 1,000 feet stratigraphically above the base of the volcanic section, and the nearest outcrops of possible source rocks for the limestone fragments are about 1,000 feet south.

A large block of coarse-grained white limestone is exposed in a small gully west of Harshaw Creek and along the westward prolongation of the breccia north of the American mine. It is about 300 feet long and

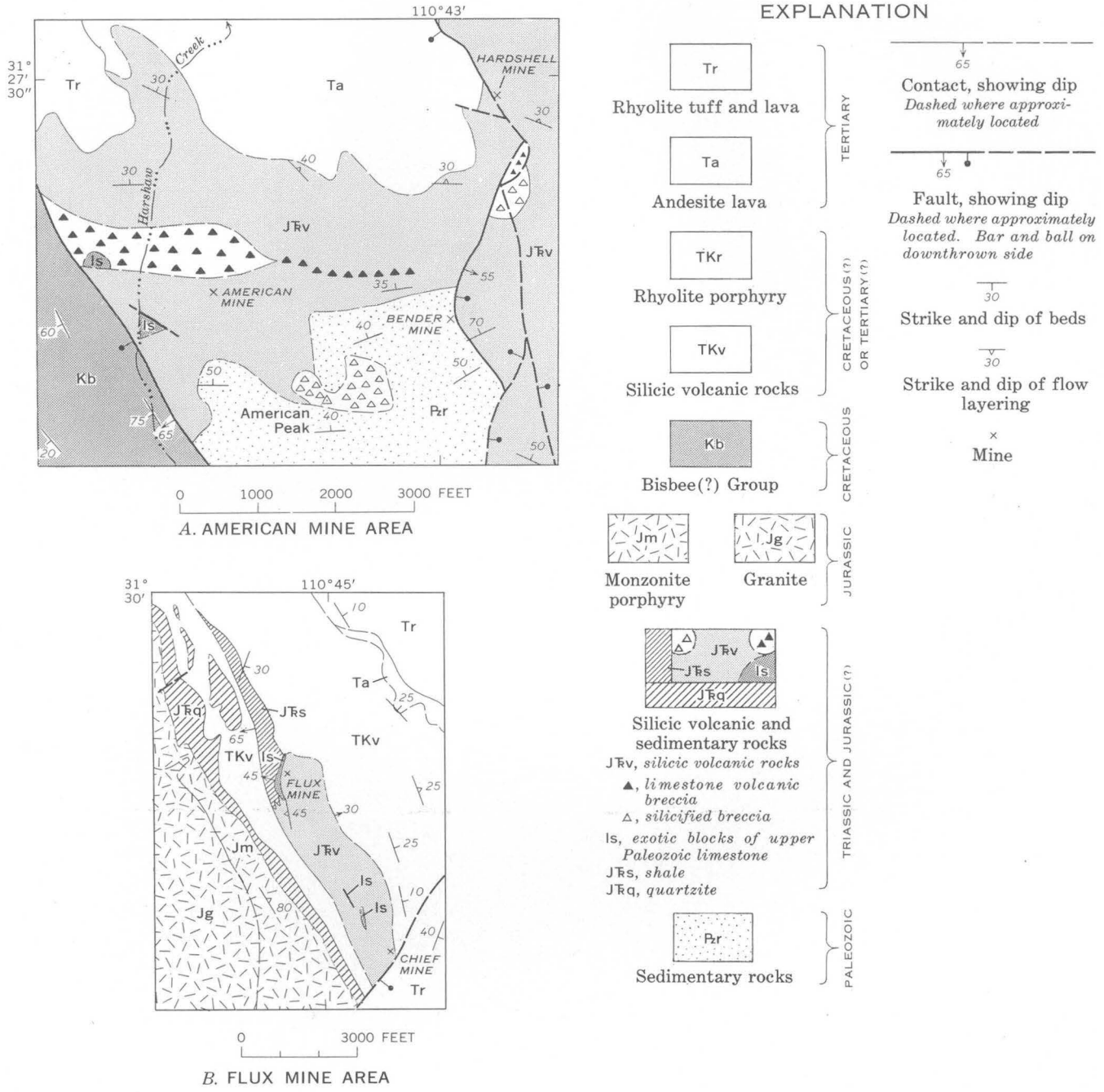

FIGURE 4.—Generalized geologic maps of the American mine area (*A*) and the Flux mine area (*B*), Patagonia Mountains, Santa Cruz County, Ariz. (fig. 1, locs. 4 and 5).

is surrounded by rhyolitic volcanic rock. The ridge to the north offers few exposures, but scattered outcrops of limestone indicate that it probably consists of limestone breccias similar to those north of the American mine.

A limestone block 1,000 feet southwest of the American mine is roughly triangular in outline and is entirely surrounded by rhyolite lava and flow breccia. The northeast contact is a fault dipping southwestward. The limestone block is thoroughly brecciated and bleached, and its identification is uncertain but it is probably Scherrer Formation or Concha Limestone; Permian Concha Limestone crops out 1,500 feet southeast of it.

A small area of limestone breccia crops out 2,000 feet south of the Hardshell mine, 0.8 mile northeast of the American mine (fig. 4*A*). Here a knoll 500 feet long and as much as 200 feet wide is underlain by a

coarse limestone breccia resting on rhyolite tuff. The breccia-tuff block is bounded by faults against silicic volcanic rocks. The limestone fragments are as much as several tens of feet across and are mostly if not entirely of Permian Concha Limestone; the enclosing volcanic rocks are the same as those in the American mine area.

Flux mine area

Rocks at and southwest of the Flux mine, 4 miles south of Patagonia (fig. 4*B*), are mainly silicic volcanic rocks interlayered with a little coarse sandstone, quartzite and shale and intruded by a large sill(?) of rhyolite porphyry. This volcanic-sedimentary sequence trends north-northwest, dips steeply, and is correlated tentatively with silicic volcanic rocks of pre-Early Cretaceous age in the central Patagonia Mountains. It is overlain unconformably by silicic volcanic rocks of Cretaceous(?) or Tertiary(?) age. Limestone slabs, probably all of late Paleozoic age, and associated limestone conglomerate are enclosed in the volcanic-sedimentary sequence at the Flux mine and northwest of the Chief mine.

Many of the workings of the Flux mine are in a lens of highly brecciated limestone with an outcrop length of about 1,000 feet and a maximum width of 75 feet. This lens strikes north and dips steeply west. To the south it tapers out and becomes a thin layer of limestone conglomerate. At the mine road and for some distance uphill to the north, the rocks immediately to the east are much-altered green andesite lava and tuff 40–50 feet thick containing scattered fragments of limestone; farther east are rhyolite lavas. Overlying the limestone to the west is an uncertain thickness, perhaps 40–50 feet, of coarse sandstone and arkose. Apparently these clastic rocks interfinger to the south with silicic volcanic rocks, and to the west they are intruded by rhyolite porphyry. Contacts between limestone and other rocks are rarely exposed but seem to be somewhat sheared and brecciated.

The limestone is a massive gray to dark-gray somewhat cherty rock of uncertain age; it might be from the upper part of the Permian Concha Limestone or, less likely, could be Escabrosa Limestone (Mississippian).

A limestone lens 1,000 feet northwest of the Chief mine is about 600 feet long and as much as 100 feet wide. It consists of jumbled blocks of fossiliferous limestone and silty and sandy limestone, either Horquilla Limestone (Pennsylvanian) or Earp Formation (Pennsylvanian and Permian). The enclosing rocks are mainly rhyolite lavas and tuff, with some shale and sandstone.

Another smaller lens 2,000 feet northwest of the Chief mine is similar in all respects.

The nearest outcrops of Paleozoic source rocks are more than 3 miles to the southeast, around American Peak (fig. 4*A*), but what the relationship may have been at the time the limestone masses of Flux Canyon were emplaced has not yet been determined because of structural complications and uncertain correlations among the volcanic rock units.

SANTA RITA MOUNTAINS

The Santa Rita Mountains (fig. 1) are underlain by abundant volcanic, sedimentary and plutonic rocks of Mesozoic and Cenozoic age, and by small amounts of sedimentary rocks of Paleozoic age and metamorphic and plutonic rocks of Precambrian age. The Mesozoic rocks include Triassic silicic and intermediate volcanic rocks and intercalated sedimentary rocks, Upper(?) Triassic monzonite, Middle(?) Jurassic granite, and a very thick section of Upper Cretaceous sedimentary and silicic to intermediate volcanic rocks. The Mesozoic complex is intruded by many Paleocene (Laramide) granitoid bodies.

On the west side of the mountains, between Josephine and Montosa Canyons (fig. 5), is a thick sequence of Upper Cretaceous silicic volcanic rocks that dips gently southward. This sequence comprises basal dacitic tuff breccia and lava flows, dacitic breccia enclosing many exotic blocks, and latitic welded tuff. Each unit is commonly several hundred feet thick and in places may be as much as 1,000 feet thick. These rocks rest unconformably on a surface of considerable relief carved across Jurassic granite. Unconformities and the distribution of coarse conglomerate indicate that during Cretaceous time this surface sloped westward from a rugged mountain range that lay about along the present crest of the Santa Rita Mountains.

Dacite breccia forms small bluish-gray or greenish-gray outcrops over about 4 square miles. It consists of fragments commonly 3–6 inches in diameter, set in a friable matrix of similar appearance. Phenocrysts in a finely crystalline to glassy highly altered groundmass make up 20–40 percent of the rock. The feldspar phenocrysts are now clay pseudomorphs after hornblende, biotite, probably a little augite, and perhaps an orthopyroxene. Some of the rocks contain finely disseminated silica and a little calcite. The origin of the breccia is uncertain, but most likely it is a flow breccia.

Scattered widely through much of the flow breccia are hundreds of exotic blocks of pre-Cretaceous rocks as large as 1,000 feet across. Only those most conspicuous for their size, or representing some of the less

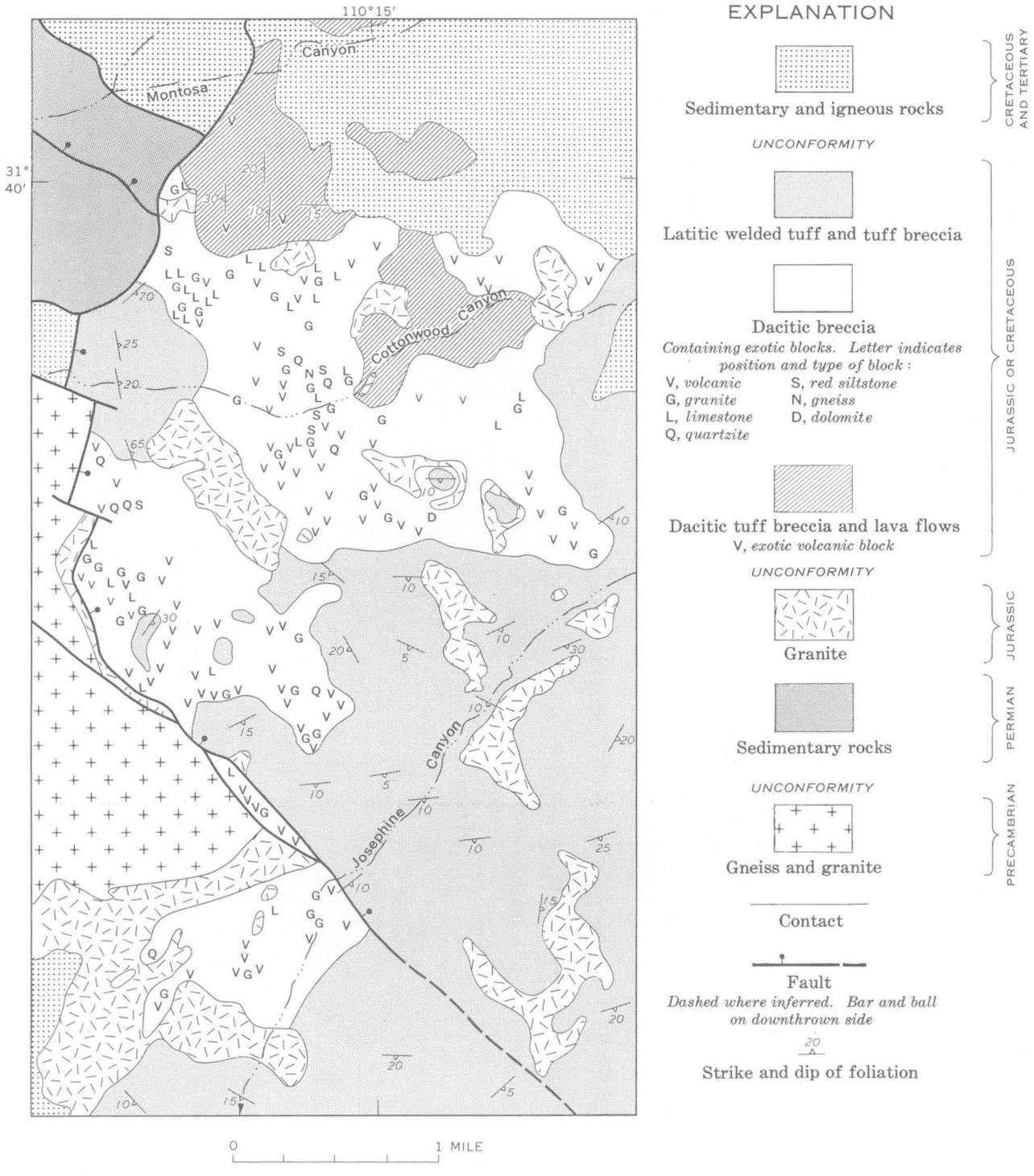

FIGURE 5.—Geologic map showing distribution of volcanic breccia containing exotic blocks, Santa Rita Mountains, Santa Cruz County, Ariz. (fig. 1, loc. 6).

abundant lithologies, are shown by letters on figure 5. The most abundant and generally the largest of the exotic blocks are assorted latite to andesite volcanic rocks derived from Triassic rocks that now crop out only along the crest of the mountains, at least 3 miles to the east. Blocks of Jurassic granite are next in size and abundance, and blocks of Paleozoic rocks, including Permian Concha Limestone, Cambrian Bolsa Quartzite, and possibly also Permian red siltstone and Devonian dolomite, are scarcer and smaller. Permian rocks are exposed immediately north of the breccia area, but the older Paleozoic rocks appear no closer

than 5 miles to the northeast. A few large blocks of Triassic monzonite and some very small blocks of Precambrian gneiss were also identified. The blocks are internally unshattered, are unoriented, and show no spatial variation in type or size, except that where the basal unit of the volcanic sequence is absent and the breccia rests directly on Jurassic granite, abundant small granite chips, apparently weathered debris from the Early Cretaceous(?) land surface, are incorporated in the breccia.

In a few places along the bottoms of canyons the contacts between exotic blocks and breccia matrix are well exposed, and where the blocks are limestone the contacts provide considerable information about geologic conditions prevailing during emplacement of the blocks. One of several limestone blocks, located in Josephine Canyon just southwest of the fault (between the 3 "G" symbols in fig. 5) is shown in figure 6. The volcanic matrix contains abundant chips of disintegrated Jurassic granite and some fragments of other exotic material. The contact between block and host shows many irregularities, and many tongues of volcanic material penetrate the limestone for a foot or more. It seems that when the exotic blocks were emplaced some of the limestone was dissolved along cracks and the spaces were filled by the volcanic material suggesting at least a highly fluid and perhaps warm environment.

Emplacement of the blocks by some sort of flowage is indicated by the widespread distribution of the blocks and the nature of their contacts with the host breccia. Movement on or in a volcanic flow is the favored explanation, but movement in hot mud flows is also a possibility. Possible source areas of most of the exotic blocks lie to the northeast, suggesting that a volcanic source also lay in that direction, conceivably in the area now occupied by a Paleocene (Laramide) dioritic pluton. As already mentioned, the Cretaceous land surface sloped westward, so that the requisite gradient was available for westward movement of the flow breccia. Some of the little exotic blocks may have been ejected from a vent, some larger exotic blocks may have been incorporated into the base of the breccia during flow, and possibly still others fell into the breccia from adjacent steep slopes.

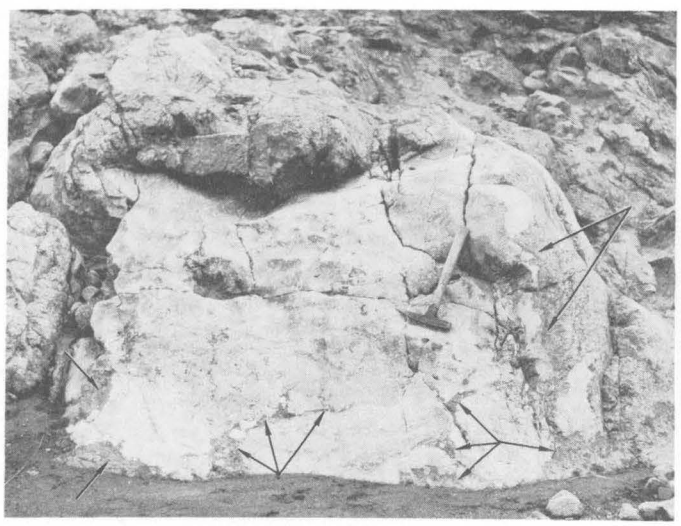

FIGURE 6.—Block of light-gray Paleozoic limestone in dark-gray dacitic breccia, Santa Rita Mountains, Santa Cruz County, Ariz. (fig. 1, loc. 6). Arrows indicate cracks in limestone from which limestone has been dissolved and which are filled with a fine-grained volcanic matrix.

PALEOGEOGRAPHY

During the past few years, extensive fieldwork and radiometric age determinations by members of the U.S. Geological Survey have revealed a tectonically eventful early Mesozoic history in much of southeastern Arizona. Little information had been available for the interval between the Early Permian and Late Cretaceous, although previous workers recognized that both plutonic and volcanic rocks had been emplaced in that interval (Ransome, 1904, p. 84; Schrader, 1915, p. 54, 57–60; Gilluly, 1956, p. 53–70; Sabins, 1957, p. 506; Cooper and Silver, 1964, p. 71–73).

The data at hand suggest at least 2 periods of widespread volcanism, one of Late Permian or Early Triassic age and one of Late Triassic or Early Jurassic age, as well as 2 periods of plutonism of Late Triassic and Middle Jurassic age, respectively. The products of the volcanic episodes have been recognized over an area of 3,000 square miles, including in addition to the mountain ranges discussed herein, the Little Dragoon and probably the Dragoon Mountains. These volcanic rocks are separated by regional unconformities from the underlying Paleozoic sedimentary rocks and the overlying Lower Cretaceous rocks. No volcanic rocks of Triassic or Jurassic age have been identified farther east, in the Mule, Chiricahua, or Dos Cabezas Mountains, and in view of the considerable amount of work that has been done in these ranges it is unlikely that any are present. We do not know whether their absence is due to erosion or to nondeposition. Little detailed geologic mapping has been done immediately west of the Santa Rita and Patagonia Mountains, but it will not be surprising if lower Mesozoic volcanic rocks eventually are identified in the Pajarito, Atascosa, Tumacacori, San Luis, Las Guijas, or Cerro Colorado Mountains.

The many exotic blocks, some of which probably are far travelled, as well as conglomerate at several horizons in the volcanic sequences, attest to widespread

tectonic activity during the early Mesozoic, and the region may well have been the source of volcanic ash and other volcanic debris in the Triassic and Jurassic rocks of northeastern Arizona.

REFERENCES

Cooper, J. R., and Silver, L. T., 1964, Geology and ore deposits of the Dragoon quadrangle, Cochise County, Arizona: U.S. Geol. Survey Prof. Paper 416, 196 p.

Gilluly, James, 1956, General geology of central Cochise County, Arizona: U.S. Geol. Survey Prof. Paper 281, 169 p.

Hayes, P. T., Simons, F. S., and Raup, R. B., 1965, Lower Mesozoic extrusive rocks in southeastern Arizona—the Canelo Hills Volcanics: U.S. Geol. Survey Bulletin 1194–M, 9 p.

Ransome, F. L., 1904, The geology and ore deposits of the Bisbee quadrangle, Arizona: U.S. Geol. Survey Prof. Paper 21, 168 p.

Sabins, F. F., Jr., 1957, Stratigraphic relations in Chiricahua and Dos Cabezas Mountains, Arizona: Am. Assoc. Petroleum Geologists Bulletin, v. 41, no. 3, p. 466–510.

Schrader, F. C., 1915, Mineral deposits of the Santa Rita and Patagonia Mountains, Arizona: U.S. Geol. Survey Bulletin 582, 373 p.

LAST CHANCE THRUST—A MAJOR FAULT IN THE EASTERN PART OF INYO COUNTY, CALIFORNIA

By JOHN H. STEWART, DONALD C. ROSS, C. A. NELSON[1], and B. C. BURCHFIEL,[2]
Menlo Park, Calif.; Los Angeles, Calif.; Houston, Tex.

Work done in cooperation with the California Division of Mines and Geology

Abstract.—The Last Chance thrust has been traced throughout an area of over 400 square miles in the eastern part of Inyo County, Calif., and probably extends in the subsurface under most of the northern Inyo Mountains and southern White Mountains. Late Precambrian, Cambrian, or Ordovician strata form the sole of the upper plate and are thrust over shaly Mississippian strata, and locally carbonate rocks of Silurian age. The strata in the upper plate generally dip eastward into the fault surface, exposing successively younger strata above the fault to the east. These spatial relations show that the upper plate moved east relative to the lower plate for a minimum distance of 20 miles.

A major fault, here called the Last Chance thrust, has been mapped in the eastern part of Inyo County, Calif. (fig. 1). This report describes the extent and the structural characteristics of the fault, and its relationship to other faults in the southern Great Basin. The report is based on detailed mapping in the Inyo Mountains, Dry Mountain area, and part of the Saline Range, and reconnaissance mapping elsewhere. Part of the area included in the study has been mapped by E. H. McKee, U.S. Geological Survey, and B. W. Troxel, California Division of Mines and Geology; permission to use their unpublished information is greatly appreciated.

The region in which the thrust fault occurs is characterized by high mountains and deep intermontane basins. The mountain areas are composed of sedimentary rocks of late Precambrian to Triassic age, granitic rocks of Mesozoic age, and sedimentary and volcanic rocks of Cenozoic age (Burchfiel, in press; McAllister, 1952, 1956; Nelson, 1962, 1963; Ross, 1965, and unpublished compilation of the Inyo Mountains region; and Stewart, 1965). The pre-Tertiary stratigraphic sequence is more than 40,000 feet thick (table 1). The rocks in some parts of the stratigraphic section change facies from the eastern to the western part of the region, and different stratigraphic names have been applied to correlative rocks in these two areas. These facies changes occur mostly within the rocks of the upper plate of the Last Chance thrust, and are not caused by telescoping of the stratigraphic section along the thrust.

The region is characterized by moderately to steeply dipping strata cut by many high-angle faults and a few low-angle thrust faults. Locally the rocks are closely folded, and some folds are overturned. Near intrusive contacts the sedimentary rocks are metamorphosed, sheared, and attenuated. The Death Valley–Furnace Creek fault zone, a major right-lateral strike-slip fault on which displacement may range from 30 to 50 miles (Stewart, in press), passes through the northeast part of the area.

DESCRIPTION OF THE THRUST

The Last Chance thrust underlies a large portion of the Inyo Mountains—Last Chance Range region (fig. 2), and has been traced throughout an area of more than 400 square miles. It crops out in the southern part of the Last Chance Range and in the Dry Mountain area, and in three windows to the west (Saline Range, Jackass Flats, and Eureka Valley windows). Although the thrust cannot be mapped continuously throughout the region, the stratigraphic and structural uniformity in the upper and lower plates suggests that

[1] University of California, Los Angeles.
[2] Rice University.

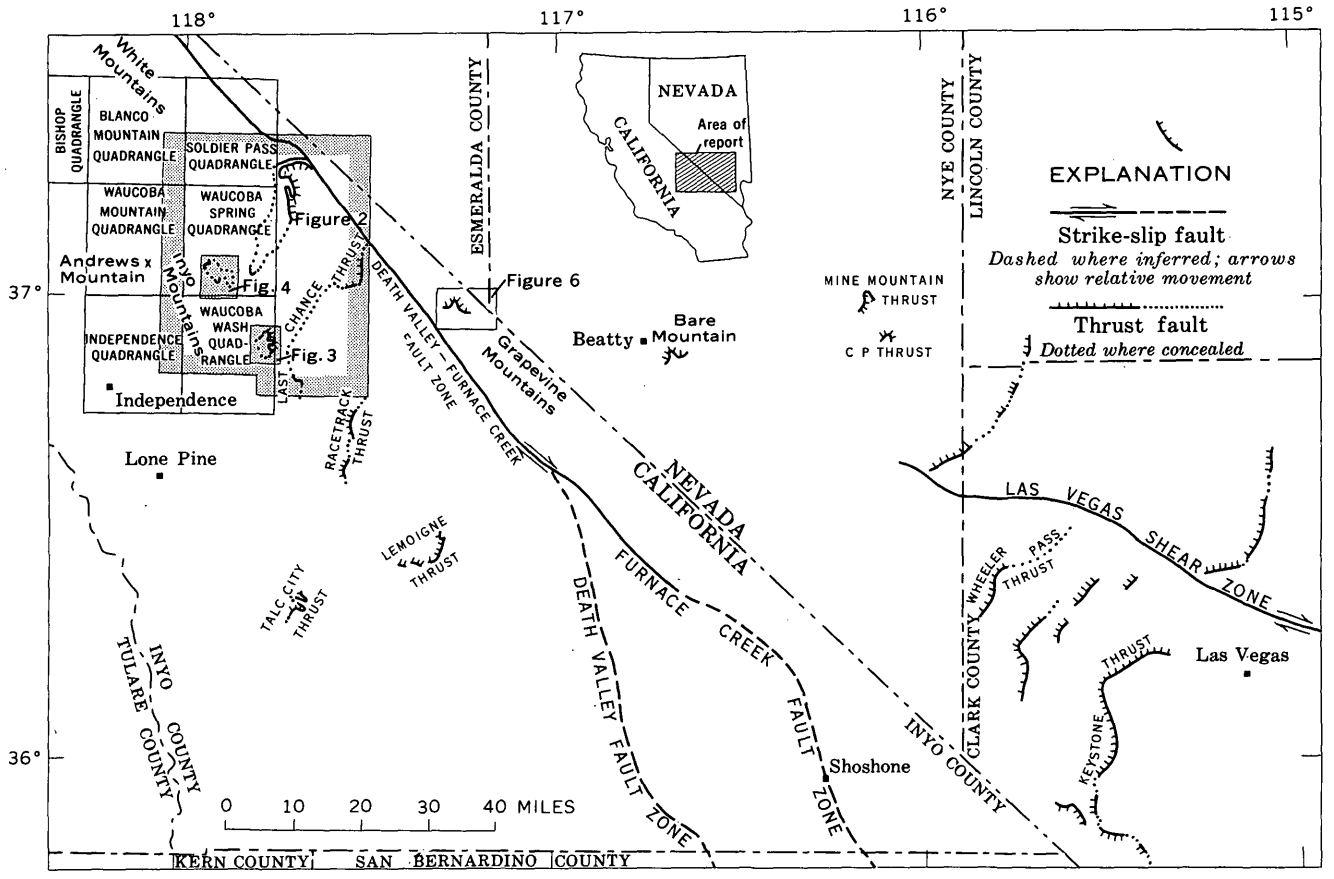

FIGURE 1.—Index map showing location of Last Chance thrust and related structures.

only a single thrust is involved, rather than two or more separate or imbricate thrusts.

Southern part of Last Chance Range, and Dry Mountain area

The trace of the thrust in the southern part of the Last Chance Range (near lat 37°03′ N.) marks a noticeable structural break. Rocks south of the thrust, in the Dry Mountain area, generally consist of west-dipping strata ranging in age from Cambrian to Permian. Those north of the thrust, in the Last Chance Range, generally consist of gently east-dipping Cambrian and Ordovician strata. The thrust can be easily traced at the southeast end of the Last Chance Range. Here it dips gently or is flat and occurs above dark shale and siltstone assigned to the Rest Spring Shale of Late Mississippian age. Rocks above the fault are light to varicolored strata of the Zabriskie Quartzite and Carrara Formation, of Early Cambrian and Early and Middle Cambrian age, respectively. Elsewhere in the southern part of the Last Chance Range the trace of the fault has been studied only briefly, and many of the details of the structural relations are not known.

About 7 miles southwest of Dry Mountain a low-angle fault separates the Eureka Quartzite (Ordovician) above from metamorphosed Rest Spring Shale below. This fault is considered to be a continuation of the Last Chance thrust. The upper plate here consists for the most part of homoclinal rocks of Ordovician and Silurian age that dip generally 30° east. The lower-plate rocks are structurally complex. Metamorphosed Rest Spring Shale has ridden over a syncline of Mississippian and Pennsylvanian rocks, and has overturned the syncline to the east, forming a recumbent fold more than a mile long. In the same area, a thrust slice of Devonian rocks lies between the recumbent syncline and the Rest Spring Shale.

At two other localities in the Dry Mountain area (not shown on fig. 2), the Eureka Quartzite lies with a gently dipping to horizontal fault contact on younger Paleozoic rocks. At one of these localities, 6 miles south of Dry Mountain, several small, strongly brecciated masses of Eureka Quartzite rest on Mississippian

TABLE 1.—*Pre-Tertiary rocks in the Inyo Mountains–Last Chance Range region*

Age	Western part	Thickness (Feet)	Eastern part	Thickness (Feet)
TRIASSIC AND JURASSIC(?)	Volcanic rocks	2200	(Top not exposed)	
	Marine rocks	1800		
	UNCONFORMITY			
TRIASSIC	Owens Valley Formation	1800	Owens Valley Formation	3000±
PERMIAN	Keeler Canyon Formation	2200±	Keeler Canyon Formation	3900
PENNSYLVANIAN	Rest Spring Shale	2500	Rest Spring Shale	300?
MISSISSIPPIAN	Perdido Formation	300-600	Perdido Formation	610
	UNCONFORMITY		Tin Mountain Limestone	475
DEVONIAN			Lost Burro Formation	1525
SILURIAN	Vaughn Gulch Limestone and Sunday Canyon Formation	700-1500	Hidden Valley Dolomite	1365
ORDOVICIAN	Ely Springs Dolomite	200-500	Ely Springs Dolomite	940
	Johnson Spring Formation	100-400	Eureka Quartzite	400
	Barrel Spring Formation	100-200		
	Mazourka Group	1000	Pogonip Group	1440
CAMBRIAN	Tamarack Canyon Dolomite	900	Nopah Formation	1600
	Lead Gulch Formation	300		
	Bonanza King Dolomite	2800	Bonanza King Dolomite	3300
	Monola Formation	1250	Carrara Formation	1640
	Mule Spring Limestone	1000		
	Saline Valley Formation	850		
	Harkless Formation	2000	Zabriskie Quartzite	1360±
	Poleta Formation	1200	Wood Canyon Formation	1300+
PRECAMBRIAN	Campito Formation	3500	(Base not exposed)	
	Deep Spring Formation	1500		
	Reed Dolomite	2000		
	Wyman Formation (Base not exposed)	9000		

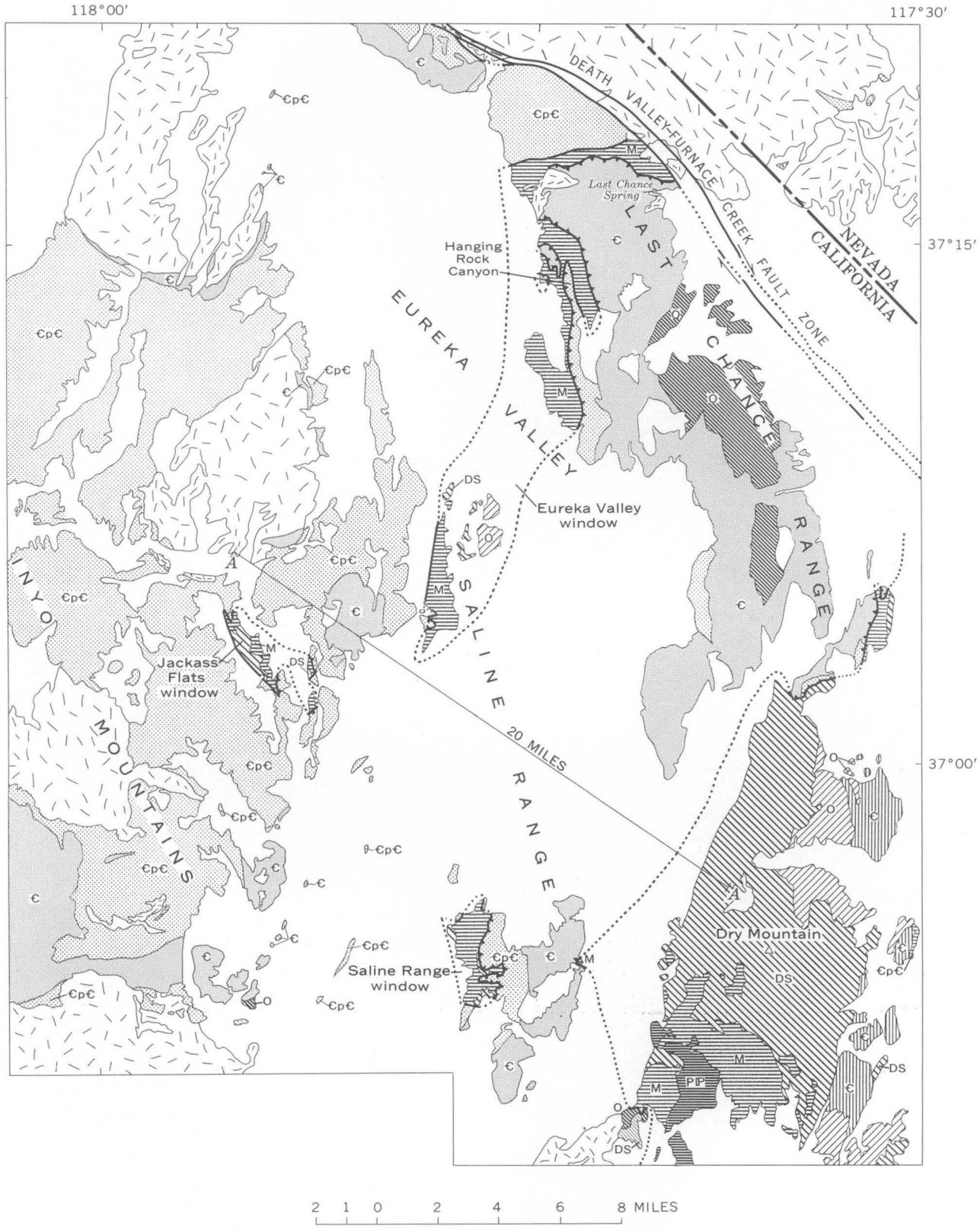

FIGURE 2.—Simplified geologic map of pre-Tertiary rocks, showing Last Chance thrust in Inyo Mountains–Last Chance Range region. Line *A–A* represents the minimum displacement along the Last Chance thrust.

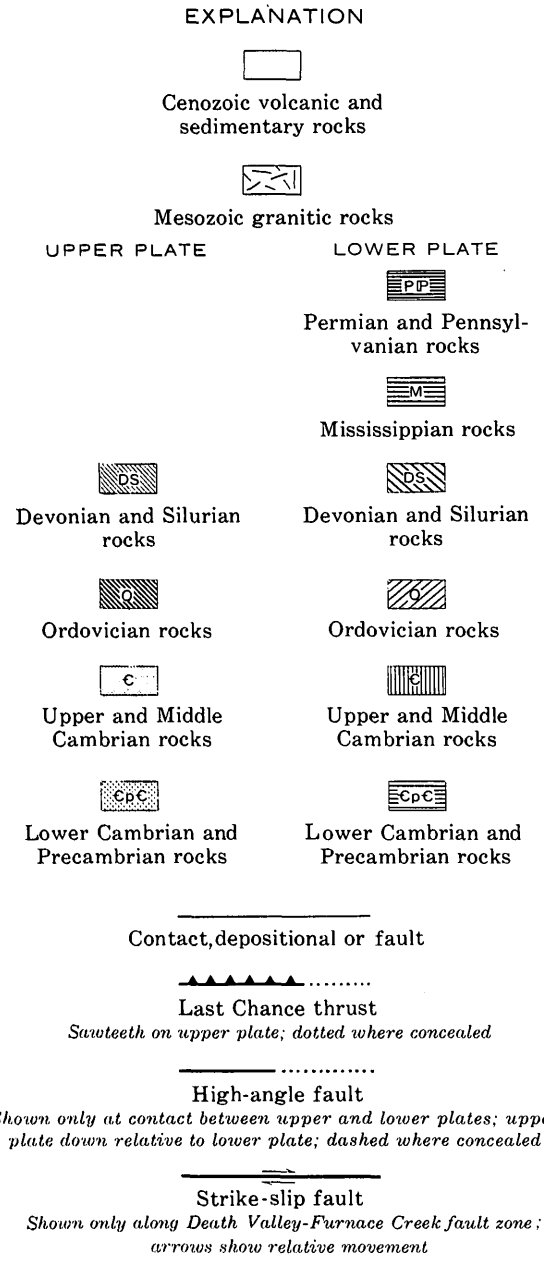

rocks. The brecciated Eureka Quartzite is interpreted as landslide material that may have come either from the Last Chance thrust or from Ordovician rocks that crop out 1 to 2 miles to the east. The other locality is 4 miles north-northwest of Dry Mountain. Here a small mass of Eureka rests on the Lost Burro Formation of Devonian age. The quartzite here is not strongly brecciated except near the base, and the underlying Lost Burro Formation shows considerable evidence of flow by the development of a weak foliation and stretched stromatoporoid corals. The Eureka here is probably a klippe of the Last Chance thrust.

Eureka Valley window.—The Last Chance thrust is considered to extend under the main part of the Last Chance Range; it reappears in a window (the Eureka Valley window) along the northwest and northern part of the range. Rocks on the west side of Eureka Valley, separated from the Last Chance Range by 3 miles of alluvial cover, are also included in the Eureka Valley window.

Lower-plate rocks also crop out in a very small window, not shown on figure 2, at Last Chance Spring, on the east side of the Last Chance Range. The spring is along the thrust fault.

The lower-plate rocks in the northwestern and northern parts of the Last Chance Range consist mostly of gray and greenish-gray shale and locally contain chert-pebble conglomerate, limestone, dolomite, and stratified chert. Crinoidal debris is common in the limestone layers, and at a locality about 1 mile southeast of Hanging Rock Canyon crinoidal debris as well as indeterminate shell fragments, and the bryozoans *Fenestella*, probable *Polypora* or *Polyporella*, and indeterminate scraps of trepostomatous forms, and possibly crushed rhomboporoids, have been identified. These fossils are late Paleozoic in age and, based on occurrences in other parts of the Western United States, may be Mississippian or Early Pennsylvanian (Helen Duncan, written commun., 1964). On a lithologic basis, these rocks can be assigned at least in part to the Rest Spring Shale. In places, strata lithologically similar and perhaps correlative with the Perdido Formation of Mississippian age are also exposed.

The lower-plate rocks in the northwestern and northern parts of the range are commonly highly contorted, and little is known of their detailed structure. The strata in the upper plate, which are dominantly Early and Middle Cambrian in age, are relatively undisturbed and generally dip gently to moderately east.

Along the west side of the Last Chance Range, extending from about 1 mile north of Hanging Rock Canyon to about 2 miles to the south of it, a part of the upper plate, consisting of the Zabriskie Quartzite and Carrara Formation (both Cambrian), appears to have been broken from the main plate, rolled into a tight nearly recumbent syncline that is overturned to the east, and overridden by slices of lower-plate rocks. This complex structure is well exposed at Hanging Rock Canyon, where the fault between the Zabriskie and the lower-plate Mississippian rocks dips steeply eastward. A short distance north of the canyon this fault locally is overturned and dips west, and about 1

224-352 O—66——3

mile north of the canyon, the Mississippian strata appear to have overridden the Zabriskie. To the south of Hanging Rock Canyon the overturned fold persists for about 2 miles and gradually gives way to a structure with east-dipping strata similar to that in the upper plate elsewhere.

Outcrops of lower-plate rocks are bounded on the north in the Last Chance Range by an east-trending high-angle fault dipping 40°–60° N. The upper-plate strata north of this east-trending fault are of late Precambrian age, whereas those to the south are Early and Middle Cambrian in age. The relationship of this fault to the Last Chance thrust is poorly understood, although the structure is more complex than simply a faulted or folded thrust fault. As will be discussed later, the fault may be a tear separating structurally unlike parts of the upper plate.

The part of the Eureka Valley window that lies in the northern part of the Saline Range on the west side of Eureka Valley consists of outcrops largely obscured by high-level gravel and wind-blown sand; nevertheless, it appears that a nearly complete succession from the Pogonip Group of Ordovician age to the Rest Spring Shale of Mississippian age is exposed. Although detailed mapping has not been completed in this area, the strata appear to be a part of a west-dipping homoclinal sequence broken by relatively few normal faults. Over the major part of the window, no exposures of the Last Chance thrust have been found, although Lower Cambrian upper-plate strata occur immediately to the west across a basin-and-range fault and alluvial valley. At the southernmost end of the window, however, Lower Cambrian rocks are thrust over Mississippian.

Saline Range window and vicinity.—In the southern part of the Saline Range, which is an eastern appendage of the Inyo Mountains, outcrops of Paleozoic sedimentary rocks expose (fig. 3) the Last Chance thrust, along which Lower to Upper Cambrian rocks lie on Silurian and Mississippian strata. The thrust dips westerly to southwesterly at 10°–20°.

The structure in the upper plate is rather simple (fig. 3), with the Harkless Formation of Early Cambrian age everywhere resting on the sole. Folding and abundant brecciation near the thrust give way eastward to a somewhat faulted, but remarkably continuous section of Lower to Upper Cambrian beds dipping to the east.

In the lower plate, however, the structure and stratigraphy are less obvious. The gray, cherty dolomite of the lower plate contains corals (a *Palaeophyllum*-like form, and *Cladopora*), a brachiopod (*Coelospira*), and an algae (*?Verticillopora*). Presumably the strata yielding these fossils are in the lower part of the Hidden Valley Dolomite and are Silurian (C. W. Merriam, written commun., 1965). The clastic section called Perdido Formation is lithologically similar to parts of the Perdido in the Independence quadrangle (Ross, 1965, p. O30) to the southwest (fig. 1); the belt of Perdido nearest the thrust (fig. 3) is overturned, as indicated by abundant graded beds. Shale and siltstone (which underlie a large area) are assigned to the Rest Spring Shale, but the structure in this terrane is not well known. Most of the area is characterized by rubbly slopes strewn with chips and pencil-shaped pieces of shale, and bedding is rarely evident.

Other aspects of the stratigraphy of the lower plate and much of its structure are less clear. West of the westernmost Perdido belt is a section of cherty dolomite that has been tentatively assigned to the Devonian Lost Burro Formation. It might, however, be the Mississippian Tin Mountain Limestone or Perdido Formation; but it is quite unlike either of these units exposed elsewhere in the region. Although the stratigraphy of the lower plate presents some problems, its structure is the major enigma. The simplest interpretation is that the Rest Spring Shale forms the core of a nearly recumbent syncline overturned to the west. The overturned Perdido of the eastern belt fits this picture. An alternate interpretation is that the structure is an anticline overturned to the east, with beds in the overturned limb rotated as much as 270°. This latter interpretation fits better with the picture developed from study of other areas that the upper plate has moved eastward relative to the lower plate. A marked discordance between the Silurian dolomite and the eastern belt of Perdido in one well-exposed slope suggests that the dolomite may be an intermediate thrust slice between the two major plates; similar structures have been mapped in the Dry Mountain area.

Two miles east of the Saline Range window, the thrust is again exposed by uplift along a steeply dipping north-trending fault. Here strata of the Lower and Middle Cambrian Carrara Formation lie on cleaved and folded Mississippian shale that contains a large tectonic inclusion of deformed Devonian limestone. The sole of the upper plate is approximately 1,000 feet higher stratigraphically here than it is along the east side of the Saline Range window.

Jackass Flats window.—The principal exposures of lower-plate rocks occur along the east side of Jackass Flats (fig. 4), where dolomite of the Lost Burro Formation of Devonian age is overlain by chert, limestone,

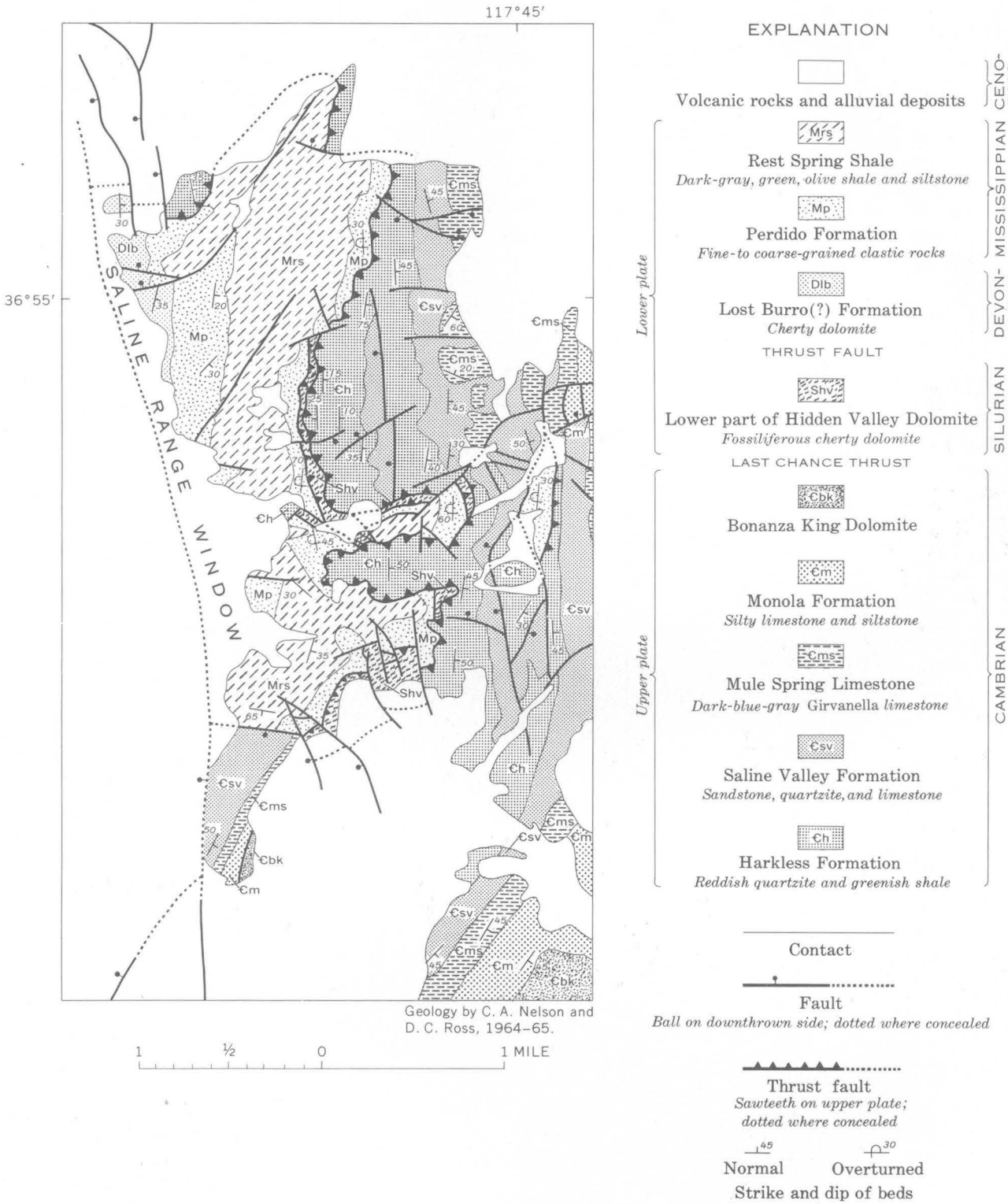

FIGURE 3.—Simplified geologic map of Saline Range window.

EXPLANATION

Volcanic rocks and alluvial deposits — CENOZOIC

Lower plate

Mp — Perdido Formation — MISSISSIPPIAN

Dlb — Lost Burro Formation — DEVONIAN

LAST CHANCE THRUST

Upper plate

€bk — Bonanza King Dolomite

€m — Monola Formation

€ms — Mule Spring Limestone

€sv — Saline Valley Formation

€h — Harkless Formation — CAMBRIAN

€p — Poleta Formation

€p€c — Campito Formation

p€d — Deep Spring Formation

p€r — Reed Dolomite

p€w — Wyman Formation — PRECAMBRIAN

Contact
Dashed where approximately located

Fault
Dashed where approximately located; dotted where concealed; bar and ball on downthrown side

Thrust fault
Sawteeth on upper plate; dotted where concealed

Normal (30) Overturned (60) Vertical
Strike and dip of beds

FIGURE 4.—Simplified geologic map of the Jackass Flats window.

sandstone, and conglomerate of the Perdido Formation of Mississippian age. This succession has been overridden, along the sole of the Last Chance thrust, at the north end of Jackass Flats by quartzite and dolomite of the Reed Dolomite of Precambrian age; near the southern end of Jackass Flats, the upper plate of the thrust includes sandstone, shale, and limestone of the Campito Formation of Precambrian and Early Cambrian age and of the Poleta Formation of Early Cambrian age. At both localities, the thrust surface dips 20°–45° W.

Structure within the lower plate is simple—the plate consists of an east-dipping homocline cut by normal faults of small displacement. However, structure within the upper plate is complex. Near the south end of Jackass Flats, upper-plate rocks are cut by a prethrust normal fault of large displacement, and they are steep to overturned (easterly), and apparently abut the thrust surface at a high angle. Further complexity is indicated (fig. 4) by the presence of considerably older upper-plate strata, on the west side of Jackass Flats, opposite each exposure of the thrust. Rocks as old as the Wyman Formation of Precambrian age are exposed widely on the west side of Jackass Flats. A thrust at the southwestern corner of the Flats, in which strata of the Deep Spring and Campito Formations have ridden over the Wyman Formation, is probably a minor imbricate slice within the upper plate of the Last Chance thrust.

Approximately 2 miles east of Jackass Flats, lower-plate strata, again represented by east-dipping Lost Burro and Perdido Formations, occur in an upfaulted block. Here, rocks directly above the thrust are black sandstone of the Campito Formation and quartzite and shale of the Harkless Formation. Although exposures are limited, upper-plate structures are less complex than those to the west; they comprise simple east-dipping successions cut by normal faults of small displacement. Internal complexity within the upper plate is again suggested by the contrast between this simple homocline and the overturned sequence to the west across the alluvial valley.

RELATION OF THRUST TO WHITE AND INYO MOUNTAINS

Although exposures of lower-plate rocks in the Inyo Mountains are confined to the Saline Range window, the Jackass Flats window, and the southwestern portion of the Eureka Valley window, structural and stratigraphic continuity within the upper plate appear to demand a very extensive thrust underlying much of the region to the north and northwest of the exposures of the lower-plate rocks.

Much of the region of the Inyo Mountains and the southern part of the White Mountains contains large-scale Mesozoic intrusive bodies which may have obliterated much of the evidence critical to the problem of the regional extent of the thrust. However, detailed quadrangle mapping of the Waucoba Wash, Independence, Waucoba Spring, Waucoba Mountain, Soldier Pass, Blanco Mountain, and Bishop 15-minute quadrangles (fig. 1) suggests strongly that the Precambrian and Paleozoic strata of the range from the Jackass Flats window westward to Owens Valley and northward to at least lat 37°30′ N. (southern White Mountains) make up a single complex block lying above the Last Chance thrust. Mississippian to Permian strata exposed along the western face of the Inyo Mountains in the Independence and Waucoba Mountain quadrangles are a part of this upper-plate block.

Although the suggestion that most if not all of the White and Inyo Mountains lie above a thrust is an extreme one, that conclusion seems inescapable on the basis of the detailed and reconnaissance mapping completed to date.

ATTITUDE OF ROCKS IN LOWER AND UPPER PLATES

Although the rocks directly below the thrust are locally highly contorted and overturned, the highest stratigraphic unit exposed in the lower plate throughout much of the region is either the Perdido Formation or Rest Spring Shale of Mississippian age. Only in the Dry Mountain area are younger strata exposed in the lower plate. These relationships suggest that the position of the thrust surface was determined by the incompetent shaly strata in the Mississippian System, and also, in general, that the lower-plate rocks may be subparallel to the thrust surface.

The strata exposed at the sole of the upper plate range through successively higher formations from west to east, starting with the Reed Dolomite of late Precambrian age on the west and ending with the Eureka Quartzite of Ordovician age on the east, a transgression of 20,000 feet of stratigraphic section in 20 miles (fig. 5). This regular succession is broken only at Jackass Flats and near Hanging Rock Canyon, where the Poleta Formation and the Bonanza King Dolomite are, respectively, out of sequence. At both these localities, the rock units that are out of sequence could be interpreted as detached blocks that were left behind as the upper plate moved east. This interpretation fits with evidence (discussed below) that the upper plate moved eastward relative to the lower plate.

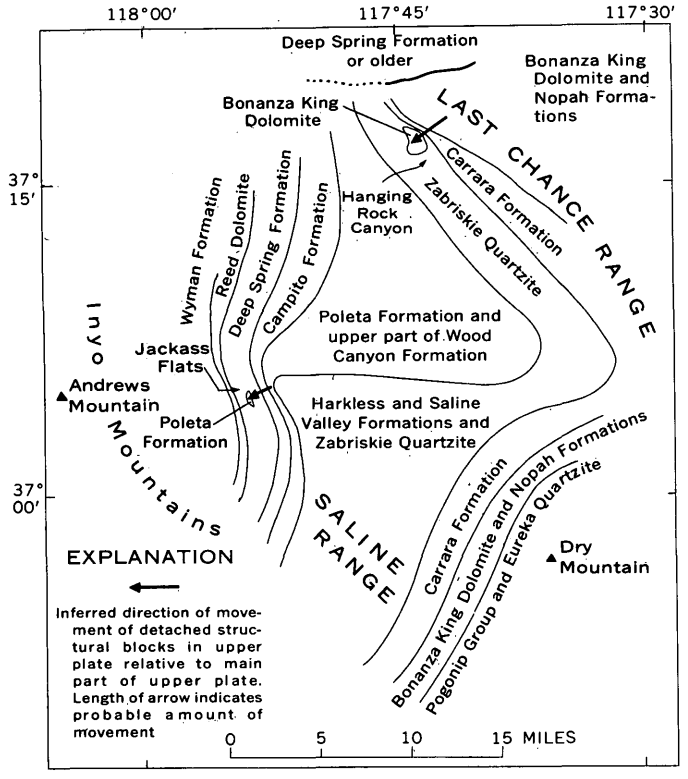

FIGURE 5.—Distribution of stratigraphic units along sole of upper plate of Last Chance thrust.

The regular pattern of units at the base of the upper plate is also broken in the northern part of the Last Chance Range where the Deep Spring or older formations are interpreted to lie above the thrust. This anomalous occurrence is not easily explained, but possibly the east-west high-angle fault that separates the Mississippian strata from the Precambrian in that area is a tear fault that separates structurally unlike parts of the upper plate.

Combining the relationship of progressively higher stratigraphic units at the base of the upper plate with the general easterly dip of upper-plate rocks in the region leads to the interpretation that the upper-plate rocks dip into the fault surface and are cut off at an angle.

AMOUNT, DIRECTION, AND TIME OF MOVEMENT

A displacement of at least 20 miles on the Last Chance thrust is established by the map distance over which Precambrian and lower Paleozoic rocks of the upper plate overlie Mississippian rocks of the lower plate (fig. 2). This is the minimum distance that the upper-plate rocks would have to travel from their original position to give the present map pattern. The total movement could be greater than this, but apparently cannot be estimated with available evidence.

Both structural and stratigraphic evidence indicate that the upper plate of the thrust moved eastward relative to the lower plate. This direction of movement is strongly suggested by the conspicuous recumbent syncline overturned to the east in lower-plate rocks along the west side of the Dry Mountain area, by the syncline overturned to the east at Hanging Rock Canyon in the Last Chance Range, and by the eastward overturn of beds in the upper plate in the Jackass Flats window. This direction of transport is further suggested, although not proved, by the fact that the thrust fault is cutting upward in the stratigraphic sequence from west to east.

Regional stratigraphic relationships also seem to favor an eastward movement. The upper-plate rocks of the Saline Range contain Lower Cambrian rocks identical with the stratigraphic units exposed to the west in the Inyo Mountains. Only 10 miles east of the Saline Range, the Lower Cambrian is represented by different formations characteristic of stratigraphic units to the east and south.

The thrust fault probably is of Mesozoic age. Rocks as young as Permian have been overridden by the thrust, and Triassic rocks in the Inyo Mountains may have been deposited before the thrusting. These Triassic rocks are too far away from the exposures of the Last Chance thrust to definitely determine whether they were involved in the movement, but a regional unconformity with only a slight angular discordance separates the Permian and the Triassic rocks, indicating that little tectonic activity occurred between Permian and Triassic time.

A Mesozoic age for the thrusting is also suggested by the occurrence of granitic intrusives (diorite and quartz monzonite) along and near the Last Chance thrust in the northern part of the Last Chance Range. These intrusives may have been emplaced in a zone of weakness along the thrust, and thus are probably post-thrust features. Biotite and zircon mineral ages (Ross, 1965, p. O46–O48) for similar intrusives in the White-Inyo Mountains range from 75 to 210 million years, and, if the intrusives are the same age in the Last Chance Range, a Mesozoic age of thrusting is indicated.

REGIONAL RELATIONSHIPS

The Last Chance thrust is one of several thrust faults in the southern Great Basin involving the transport of Precambrian or lower Paleozoic strata over upper Paleozoic strata. Most of these appear to be separate faults, although one thrust, in the northern part of the Grapevine Mountains, could be a continuation of the Last Chance thrust. Here, the Bonanza King Dolomite and Nopah Formation of Ordovician

age are thrust over shaly Mississippian strata (fig. 6). Fossil collections from the northernmost exposures of the Mississippian strata in the Grapevine Mountains area contain crinoid columnals, brachiopods, and the ammonite *Goniatites* cf. *G. granosus* Portlock, dated as Late Mississippian (Mackenzie Gordon, Jr., written commun., 1962). This thrust seemingly must pass under much or all of the Grapevine Mountains to the south, although where it reappears is not known. If the interpretation of 30–50 miles of right-lateral offset on the Death Valley–Furnace Creek fault zone (fig. 1) is correct (Stewart, in press), the original position of the rocks in the Grapevine Mountains might have been opposite those in the Last Chance Range. In this case, the close juxtaposition of the thrust in the Grapevine Mountains with the thrust in the Last Chance Range would support the interpretation that they are the same fault. At this time, however, it is impossible to definitely rule out the alternate possibilities that the thrust in the Grapevine Mountains is a continuation of the Racetrack, Lemoigne (fig. 1), or some other thrust.

The Racetrack thrust (McAllister, 1952, 1956) occurs about 15 miles southeast of the Last Chance thrust (fig. 1); it too consists of Cambrian and Ordovician strata thrust over shaly Mississippian strata. Although this thrust involves the same stratigraphic units as the Last Chance thrust, it is not considered to be the same fault because the strata between the Racetrack thrust on the south and the Last Chance thrust on the north seem to be part of one structural plate or block (Dry Mountain structural block). This block consists of Cambrian through Permian rocks that dip generally west, are broken by many high-angle faults, and locally are tightly folded. If the rocks exposed between the Racetrack and Last Chance thrusts belong to one plate, as seems likely, then the lower plate of the Last Chance thrust is the upper plate of the Racetrack thrust, and the two faults are imbricate and separate. Similar and possibly tectonically related imbricate thrusts occur in southern Clark County, Nev. (fig. 1 and Burchfiel, 1965, fig. 4).

A thrust fault on Bare Mountain (Cornwall and Kleinhampl, 1961), and the C P thrust (Harley Barnes and others, written commun., 1966) farther east, in Nevada (fig. 1), also consist of Cambrian strata thrust over shaly Mississippian strata. The relationships of these faults to the Last Chance or Racetrack thrusts or the thrust in the Grapevine Mountains are not known.

The Last Chance thrust is one of many in the southern Great Basin (fig. 1) in which Precambrian or lower Paleozoic strata are thrust over upper Paleozoic or lower Mesozoic strata. The similarity of many of these faults is indicated by their north-trending trace, by the occurrence of the upper plate on the west side, and by the movement of the upper plate eastward or southeastward relative to the lower plate (Hall and MacKevett, 1962, p. 42; Hall and Stephens, 1963, p. 20; and Burchfiel, 1965, fig. 4). These thrusts all appear to be Mesozoic in age; some may be as old as Late Triassic or Early Jurassic (Hall and Stephens, 1963, p. 20), and others may be as young as the middle of the Cretaceous (Longwell, 1960, p. 193).

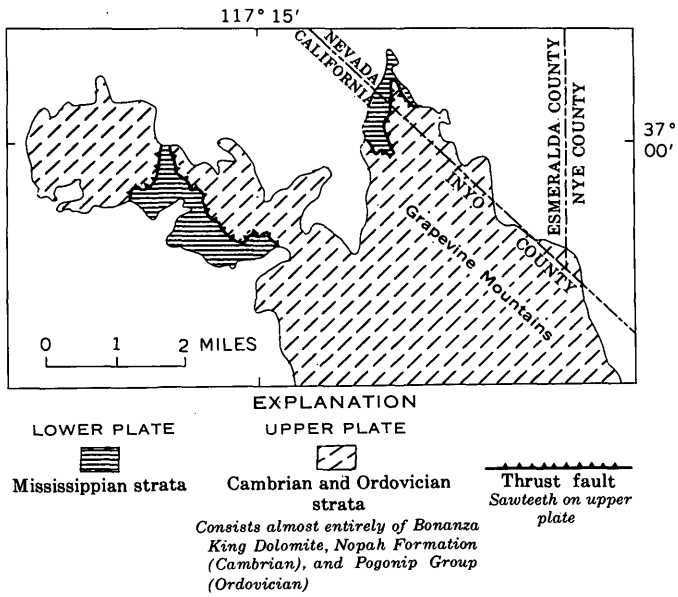

FIGURE 6.—Sketch map of northern part of Grapevine Mountains, showing thrust of Cambrian and Ordovician strata over Mississippian strata. Compiled in part from Albers and Stewart (1965).

REFERENCES

Albers, J. P., and Stewart, J. H., 1965, Preliminary geologic map of Esmeralda County, Nevada: U.S. Geol. Survey Mineral Inv. Map MF–298.

Burchfiel, B. C., 1965, Structural geology of the Specter Range quadrangle, Nevada, and its regional significance: Geol. Soc. America Bull., v. 76, no. 2, p. 175–192.

——— in press, The geology of the Dry Mountain quadrangle: California Div. Mines and Geology Map Sheet Series.

Cornwall, H. R., and Kleinhampl, F. J., 1961, Geology of the Bare Mountain quadrangle, Nevada: U.S. Geol. Survey Geol. Quad. Map GQ–157, scale 1:62,500.

Hall, W. E., and MacKevett, E. M., Jr., 1962, Geology and ore deposits of the Darwin quadrangle, Inyo County, California: U.S. Geol. Survey Prof. Paper 368, 87 p.

Hall, W. E., and Stephens, H. G., 1963, Economic geology of the Panamint Butte quadrangle and Modoc District, Inyo County, California: California Div. Mines Spec. Rept. 73, 39 p.

Longwell, C. R., 1960, Diverse structural patterns in southern Nevada: Am. Jour. Sci., Bradley volume, p. 192–203.

McAllister, J. F., 1952, Rocks and structure of the Quartz Spring area, northern Panamint Range, California: California Div. Mines Spec. Rept. 25, 38 p.

——— 1956, Geology of the Ubehebe Peak quadrangle, California: U.S. Geol. Survey Geol. Quad. Map GQ–95, scale 1:62,500.

Nelson, C. A., 1962, Lower Cambrian-Precambrian succession, White-Inyo Mountains, California: Geol. Soc. America Bull., v. 73, no. 1, p. 139–144.

——— 1963, Preliminary geologic map of the Blanco Mountain quadrangle, Inyo and Mono Counties, California: U.S. Geol. Survey Mineral Inv. Field Studies Map MF–256.

Ross, D. C., 1965, Geology of the Independence quadrangle, Inyo County, California: U.S. Geol. Survey Bull. 1181–O, p. O1–O64.

Stewart, J. H., 1965, Precambrian and Lower Cambrian strata in the Last Chance Range area, Inyo County, California: *in* Cohee, G. V., and West, W. S., Changes in stratigraphic nomenclature by the U.S. Geological Survey, 1964: U.S. Geol. Survey Bull. 1224–A, p. A60–A70.

——— in press, Possible large right-lateral displacement along fault and shear zones in the Death Valley–Las Vegas area, California and Nevada: Geol. Soc. America Bull.

THE BEDROCK STRUCTURE OF COVEY HILL AND VICINITY, NORTHERN NEW YORK AND SOUTHERN QUEBEC

By DONALD R. WIESNET and THOMAS H. CLARK,[1]
Boston, Mass., Montreal, Canada

Abstract.—Covey Hill, which lies on the international border between Quebec and New York, is bordered on the east by the north-trending Havelock fault and on the north by the east-trending Stockwell fault. The Havelock, a rotational, or pivotal fault has its hinge point at or very near the international border. Southward from the hinge point the fault plane presumably dips west, and the upthrown side is on the east; northward from the hinge point the fault plane presumably dips east, and the upthrown side is on the west. A buried ridge of Precambrian rock may account for localization of the faulting, which probably is Taconic in age.

Covey Hill is a pronounced physiographic feature that lies on the border of New York State and Quebec Province, about 27 miles northwest of Plattsburgh, N. Y. Until recently, the bedrock geology of the Covey Hill area had been mapped only in reconnaissance studies in New York by Cushing (1897), and in Quebec by Dresser and Denis (1944) and Houde and Clark (1961); each of these geologists ended their mapping at the New York–Quebec border. This paper results from independent but contemporaneous field-mapping projects by Thomas H. Clark of the Quebec Department of Natural Resources, Geological Exploration Service, and Donald R. Wiesnet of the U.S. Geological Survey. During a field conference in 1964, the writers found that they had independently recognized previously unmapped geologic structures that extend across the international boundary. The Havelock fault was first shown on the Adirondack sheet (Fisher and others, 1962) of the New York State geologic map and was based on unpublished maps by Wiesnet. The detailed geology of southern Quebec was worked out by Clark.[2]

[1] Quebec Department of Natural Resources. Published by permission of the Deputy Minister.

[2] T. H. Clark, 1964, Chateauguay area—Chateauguay, Huntingdon, Beauharnois, Napierville, and St. Jean Counties [Que.]: Quebec Dept. Nat. Resources unpub. geol. rept., 89 p. [duplicated]

REGIONAL SETTING

The summit of Covey Hill lies about 10 miles north-northeast of the nearest outcrop of Precambrian rock in the Adirondack Mountains (fig. 1). Lapping onto the Adirondack massif is the Potsdam Sandstone, which crops out along the periphery of the Adirondack massif and is the initial sedimentary deposit on the uneven surface of the Precambrian rocks of the Adirondack dome. The Potsdam increases in thickness away from the Adirondack Mountains and is presumed to be as much as 1,750 feet thick in the area of Covey Hill. It is diverse lithologically and contains beds that range from red shale and siltstone to conglomerate. The fact that the siltstone and conglomerate in the upper part of the formation are commonly orthoquartzite has added to the difficulty of interpreting the structure because the Potsdam is overlain by an alternating series of orthoquartzite and dolomite beds which, in the United States, are known as the Theresa Dolomite. The similarity between the beds of orthoquartzite of the Potsdam and those in the Theresa makes it difficult to map the boundary between the two formations where outcrops are small and infrequent.

Clark [2] has proposed a revision of the stratigraphy of the Potsdam in southern Quebec, but the applicability of his terms has not yet been determined for northern New York.

COVEY HILL

The eastern slope of Covey Hill is a resequent fault-line scarp that defines the Havelock fault, a rotational, or pivotal, fault, the downthrown side of which lies east of the fault in Quebec but west of the fault in New York (fig. 1). The direction of dip of the fault plane is inferred to change from easterly at the north-

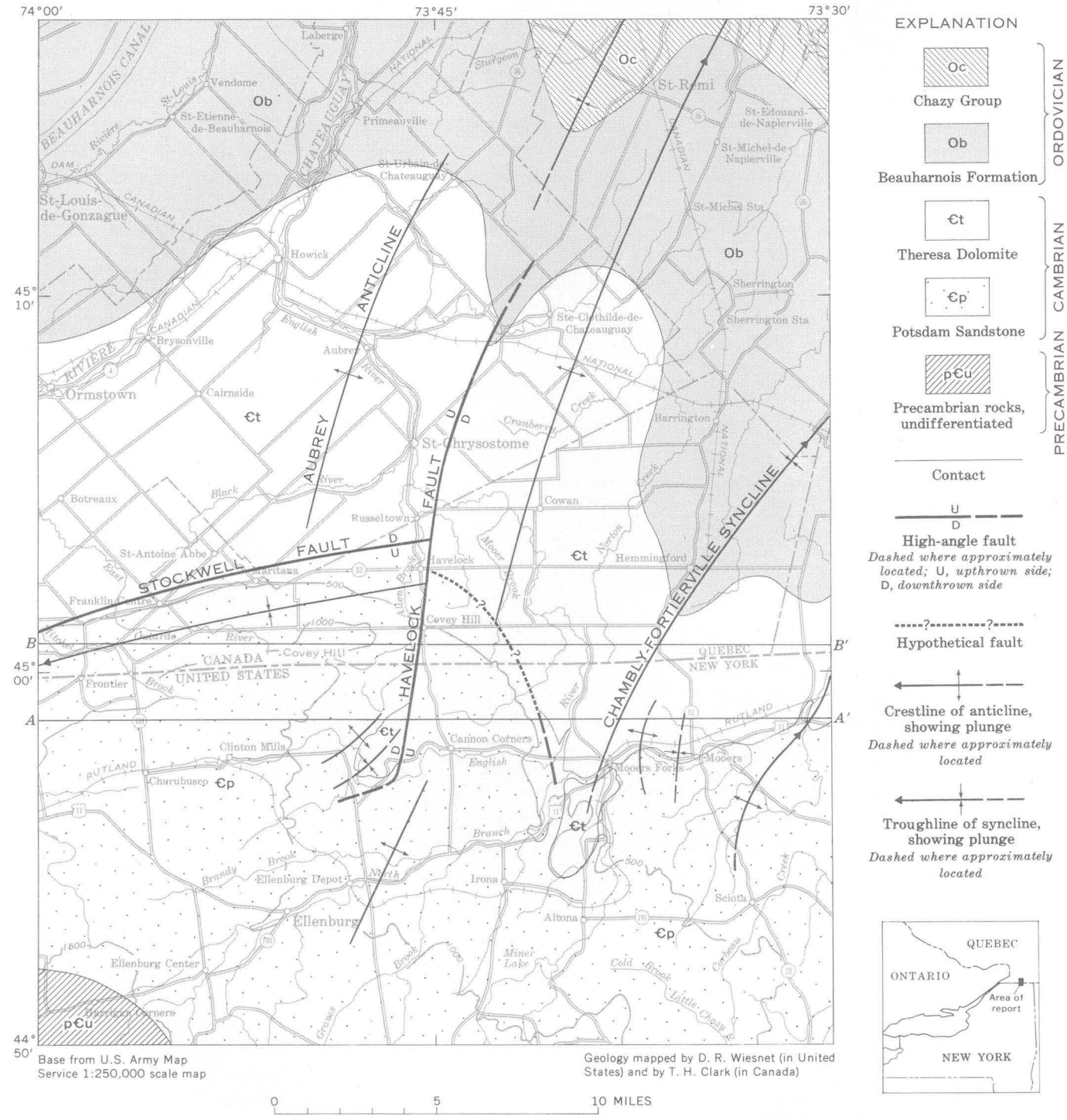

FIGURE 1.—Generalized geologic map of the Covey Hill area, New York–Quebec.

ern end of the fault to westerly at the southern end. To the south of Covey Hill, the fault dies out; in Canada it is traceable for about 12 miles, and then it becomes a syncline (fig. 1).

Covey Hill is bounded on the north by the Stockwell fault, which was mapped by Clark. It strikes east-northeast and ends abruptly against the Havelock fault at Russeltown, Quebec. Covey Hill is then, in essence, a fault block bounded on the north and east by high-angle normal faults.

Three to four miles east of the Havelock fault in New York is a zone of shearing and probable faulting

that trends northerly. On the New York State geologic map (Fisher and others, 1962) the trend of that zone is shown as a fault that curves to the northwest and terminates against the Havelock fault at Havelock, Quebec. The authors accept this interpretation but recognize that evidence in Canada on the exact nature and location of this fault is sparse (fig. 1). This assumed fault is regarded as subsidiary to the Havelock fault.

Other small faults (on the order of 6–24 inches of movement) have been detected in both Quebec and New York, and doubtless many more are hidden beneath the glacial deposits.

Owing to the pivotal nature of the Havelock fault, an east-west section (about 3 miles south of the border in the United States) shows a horst structure (fig. 2, sec. *A–A′*), yet an east-west section about a mile north of the border shows a step-fault structure (fig. 2, sec. *B–B′*). Clark estimates the maximum vertical displacement of the Havelock fault in Canada at well over 1,275 feet and maybe as much as 1,500 feet.

Logan and others (1863) reported large blocks of brecciated Trenton limestone east of Covey Hill. Some of these blocks, as well as brecciated fragments of other carbonate rocks are still there, but the largest block of Trenton has been quarried away. These blocks and outcrops of tectonic breccia are alined with the Havelock fault. Clark believes that the breccias are related to diatremes, but Wiesnet thinks that they are fault breccias and that the large blocks of Trenton have migrated down the fault plane.

The faulting in the vicinity of Covey Hill is related to folding (fig. 1). The most obvious fold is the Chambly-Fortierville syncline, which affects the outcrop pattern as far south as Irona, N.Y. The axial traces of the folds, where unaffected by faulting, are roughly parallel and are oriented northeast. The folds within the Covey Hill fault block—that is, those between the Stockwell and Havelock faults—are oriented east-northeast.

The relation of the thrust faults, normal faults, and folds of the Champlain region has been investigated by Hudson (1931), Quinn (1935), Cady (1945), and Stone (1957). They found that as most of the tectonic elements trend northerly, east-west regional compression is indicated. However, some high-angle faults trend eastward and thus divide the area into faulted blocks. Cady (written commun., 1960) described the area west of the Champlain thrust zone as "just part of the rack and collapse characteristic of craton areas, regardless of the stage of the orogenic cycle in adjacent geosynclinal belts." This is true as a general statement, but the faulting and folding in the Covey Hill area are pronounced and extensive, and most of the fold axes and faults are oriented parallel to the thrust zone in the Champlain Valley.

Stone (1957) concluded that northeast-trending high-angle wrench faulting took place during elevation of the Adirondack arch and before Taconic overthrusting. However, if high-angle faulting took place before the thrusting, it must have been minor because the fact that high-angle faults cut the thrust plates indicates that they formed as tensional features after the thrusting (Cady, 1945, p. 565–567, 577–578).

Wiesnet (1961) pointed out that the progressively greater abundance of feldspar in the Potsdam toward

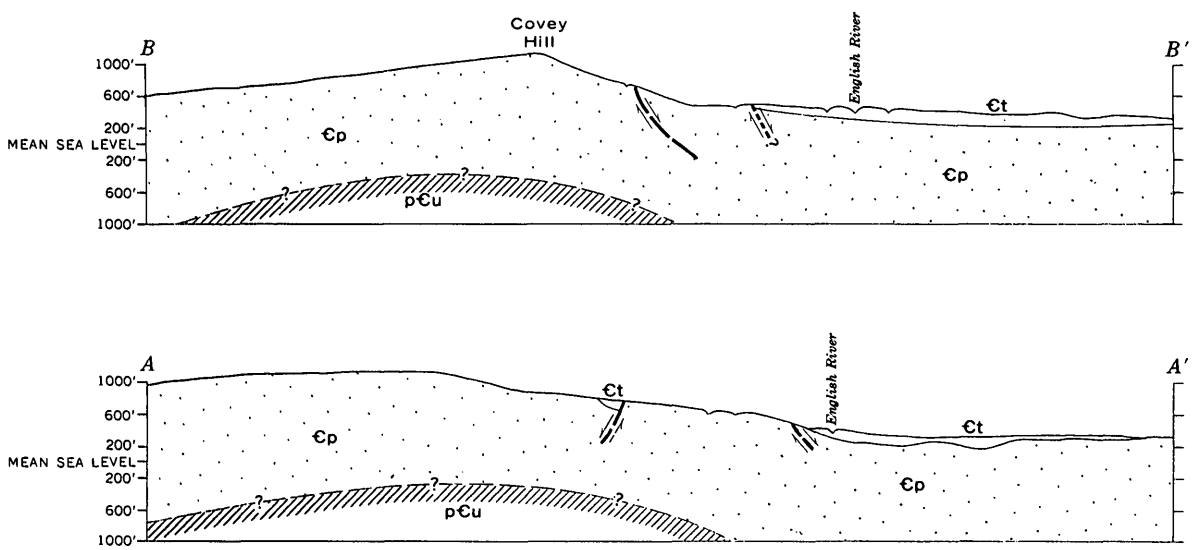

FIGURE 2.—Generalized geologic sections *A–A′* and *B–B′*. Lines of sections are shown on figure 1.

the eastern edge of the Adirondack massif may indicate pre-Potsdam normal faulting in the Precambrian basement. He also suggested that the high-angle faults in the Champlain region may be related to movements along buried pre-Potsdam faults.

The writers believe the Taconic orogeny to be responsible for the regional folding in the Covey Hill area because that orogeny is the only one recorded in the rocks of the St. Lawrence lowlands province. However, in the Sherbrooke area of Quebec two orogenies are definitely recorded. After the compression that produced the gentle folds was relieved by the overthrusting in the Champlain lowlands (or perhaps along with the compression) the Havelock and Stockwell faults—and associated faults—were formed. It is quite possible that a buried ridge of Precambrian rock underlies Covey Hill and not only led to a localization of the rupture but also acted as the pivot for the Havelock fault.

The axes of the folds are parallel to those in the inner folded division of the Appalachian orogenic belt; the north-trending faults are also alined with the faults and fold axes of the Champlain Valley.

It is not surprising that the tectonic effects of the Taconic orogeny extended to Covey Hill and into the St. Lawrence lowland, but prior to the work done by the authors very little evidence had been mapped north of the Adirondacks. The key to the Covey Hill structure was the recognition of the Havelock fault and the working out of the detailed stratigraphy in southern Quebec.

REFERENCES

Cady, W. M., 1945, Stratigraphy and structure of west-central Vermont: Geol. Soc. America Bull., v. 56, no. 5, p. 515–587.

Cushing, H. P., 1897, Report on the geology of Clinton County [New York]: New York State Geologist 15th Ann. Rept., v. 1, p. 503–574.

Dresser, J. A., and Denis, T. C., 1944, Descriptive geology, v. 2 *of* Geology of Quebec: Quebec Dept. Mines Geol. Rept. 20, v. 2, 544 p.

Fisher, D. W., and others, 1962, Adirondack sheet, Geologic map of New York: New York State Geol. Survey Map and Chart Ser., no. 5.

Houde, M., and Clark, T. H., 1961 [no title]: Quebec Dept. Nat. Resources Map 1407.

Hudson, G. H., 1931, The fault systems of the northern Champlain Valley [New York]: New York State Mus. Bull. 286, p. 5–59.

Logan, W. E., and others, 1863, Report on the geology of Canada: Canada Geol. Survey Rept. Prog. to 1863, 983 p.

Quinn, A. W., 1935, Normal faults of the Lake Champlain region: Jour. Geology, v. 41, no. 2, p. 113–143.

Stone, D. S., 1957, Origin and significance of breccias along the northwestern side of Lake Champlain: Jour. Geology, v. 65, no. 1, p. 85–97.

Wiesnet, D. R., 1961, Composition, grain size, roundness, and sphericity of the Potsdam Sandstone (Cambrian) in northeastern New York: Jour. Sed. Petrology, v. 31, no. 1, p. 5–14.

A POSSIBLE BRECCIA IN SOUTHWESTERN MASSACHUSETTS AND ADJOINING AREAS, AND ITS BEARING ON THE EXISTENCE OF THE TACONIC ALLOCHTHON

By E-AN ZEN and NICHOLAS M. RATCLIFFE,[1]
Washington, D.C., New York, N.Y.

Abstract.—The Everett Formation of the Taconic Range in western Massachusetts and adjacent areas overlies the autochthonous Lower Cambrian to Middle Ordovician Stockbridge and the Middle Ordovician Walloomsac Formations; the structural nature of this contact is debatable. A discontinuous zone of carbonate rocks occurs between the Everett and the Walloomsac. The carbonate rocks, locally a breccia, are assigned lithically to the Stockbridge Formation. They are discordant with the surrounding rocks and are interpreted as tectonic slivers, thereby implying that the Everett Formation is allochthonous. Local structural relations indicate that the emplacement of the allochthon preceded both the formation of the earliest cleavage in the rocks and the metamorphism; the emplacement is pre-Acadian and may be the terminal episode of the Ordovician Taconic gravity sliding.

The Taconic sequence of rocks occurs as the geometrically highest stratigraphic units of the Middlebury synclinorium and its southward continuation in western Vermont, western Massachusetts, western Connecticut, and eastern New York. Except for these Taconic rocks, the synclinorium consists of metamorphosed Cambrian and Ordovician carbonate units, with subsidiary quartzite, which are unconformably overlain by a shale unit of Middle Ordovician (Trenton and younger) age, bearing many local names, which will be called in this paper the Walloomsac Formation (Zen and Hartshorn, 1966). These carbonate and quartzite units, as well as the Walloomsac Formation, as a whole are autochthonous.

In contrast, the Taconic sequence consists largely of shale (metamorphosed to slate, phyllite, schist, or gneiss), with subsidiary graywacke and quartzite beds. These rocks can be divided broadly into two sub-belts: a western belt occupying the area between the Taconic Range and the Hudson River or Lake Champlain, and an eastern belt occupying the Taconic Range from Dorset Mountain, Vt., to Sharon, Conn. (see, for example, Doll and others, 1961). Because of their distinct topographic expressions, the western belt will be referred to as the "low Taconic belt" and the eastern one as the "high Taconic belt."

The low Taconic belt has yielded fossils of all ages from Early Cambrian to Middle Ordovician; these rocks are therefore synchronous with rocks of the synclinorium sequence (Zen, 1961, p. 296) and with the Walloomsac Formation. Recent detailed studies revealed a persistent stratigraphy that can be mapped throughout the length of the belt; moreover, these rocks can be assigned to as many as five distinct thrust slices nested within one another. The contacts between thrust slices are locally marked by an intermittent zone of outcrops of dolostone and marble. These carbonate rocks can be matched lithically, and in several instances faunally, with rocks of the synclinorium sequence; they have been interpreted by most of the recent workers as slivers that were dragged to the present sites along the soles of the moving fault slices. These slices have been interpreted by Zen (1961) as gigantic submarine slides of sedimentary deposits that occurred in late Trenton time (*Orthograptus truncatus* var. *intermedius* zone of Berry, 1960). Since the initial episode of intense deformation, involving gravity sliding, faulting, folding, and cleavage formation, the low Taconic rocks were folded at least once more, when they were also metamorphosed (Zen, 1960).

The high Taconic sequence consists of a rather monotonous sequence of green, gray, and gray-green pelitic

[1] City University of New York.

U.S. GEOL. SURVEY PROF. PAPER 550-D, PAGES D39-D46

rocks, with local graywacke and quartzite beds which have not proven to be useful as marker beds. The rocks have produced no fossils to date and, except locally, the stratigraphy characteristic of the low Taconic sequence has not been recognized in detail. Like the low Taconic sequence, the high Taconic sequence rests either on the carbonate units of the synclinorium sequence or on the younger Walloomsac. Because the Taconic Range locally has 3,000 feet of relief, the three-dimensional configuration of the high Taconic sequence is known to be synclinal.

The geologic problem of the high Taconic sequence is thus one of known geometry but unknown age. Because of the absence of internal evidence, all previous suggestions on the structural relations of these rocks have been based on circumstantial evidence. Recently, however, a zone of carbonate rocks has been discovered at or near the contact between the high Taconic sequence and the underlying Walloomsac Formation that is pertinent to the structural origin of the high Taconic rocks. This zone of carbonate rocks, occurring in southwestern Massachusetts and adjoining areas in New York and Connecticut, can be interpreted best as a tectonic breccia similar to the carbonate slivers that mark the soles of slices within and underlying the low Taconic sequence. Before describing these rocks, however, the extant hypotheses on the structural origin of the high Taconic sequence will be briefly summarized.

HYPOTHESES ON THE ORIGIN OF THE HIGH TACONIC SEQUENCE

Two contrasting types of hypotheses have been offered to explain the present position of the high Taconic sequence: the allochthonous and the autochthonous. The autochthonous hypothess maintains that these rocks are in normal sedimentary sequence above the Walloomsac Formation, and emphasizes the local gradational contact between them as supporting evidence (see McFayden, 1956, p. 28 for this interpretation); in addition, a post-Walloomsac unconformity has been invoked to explain the local absence of the Walloomsac (MacFayden, 1956, p. 29; Hewitt, 1961, p. 77). In the context of the local stratigraphic and structural evidence adduced by these workers, the autochthonous hypothesis is indeed the most obvious and simplest explanation for the high Taconic sequence.

Those who advocate an allochthonous hypothesis for the high Taconic sequence point out that the view of a simple sedimentary succession is beset with difficulties. Upper Ordovician (or slightly younger) rocks that are lithically like the high Taconic sequence are not known elsewhere in New England or adjoining New York; the Upper Ordovician rocks of the Mohawk and Champlain valleys do not resemble the high Taconic rocks. If the high Taconic rocks are autochthonous, special local conditions must be invoked for their deposition. Moreover, in the Becraft Mountain area near Hudson, N.Y., Silurian and Devonian rocks rest unconformably on the low Taconic rocks and on the Walloomsac equivalent (Zen and Bird, 1963, p. 52), so that if the high Taconic rocks once covered these areas they must have been stripped completely by erosion by Late Silurian time. On the other hand, supporters of the allochthonous hypothesis point out that rocks lithically and stratigraphically similar to the high Taconic sequence are found (1) within the low Taconic sequence in thrust slices, where they are of Cambrian (?) or Early Cambrian age (see Potter, 1966); (2) within the eugeosynclinal sequence of east Vermont and its continuation in Massachusetts, where they are also of Cambrian (?) or Early Cambrian age; and (3) within the Cavendish Formation (used by Doll and others, 1961) in southern Vermont, where the rocks are of Cambrian (?) and Early Cambrian age. Largely on the basis of regional correlations, these geologists consider the high Taconic sequence to be allochthonous. (For summary, see Zen, 1964, p. 11, 18, 36, 41, 50, 68.)

The allochthonists explain the gradational contact locally found between the high Taconic sequence and the Walloomsac Formation by the intimate comingling of soft sediments during the submarine sliding, by tectonic mixing, and by the effect of super-imposed metamorphism; Zen (1961) reported such gradational contacts in the northern Taconic region between the Walloomsac-equivalent units and rocks of the low Taconic sequence, now generally accepted as allochthonous. Because the gradation is generally one of color, which expresses the nature of the metamorphic mineral assemblages, and because the Walloomsac and the Everett are compositionally locally alike and have been deformed and metamorphosed as a unit, the usefulness of color as a tool of structural geology in this area is questioned.

STRATIGRAPHY IN SOUTHWESTERN MASSACHUSETTS AND ADJOINING CONNECTICUT AND NEW YORK

Recent detailed stratigraphic mapping in the State Line, Egremont, Bashbish Falls, and Sharon 7½-minute quadrangles and adjacent areas (fig. 1) has revealed a mappable stratigraphy within the Cambrian and Ordovician Stockbridge Formation (Ratcliffe, 1965; Zen and Hartshorn, 1966). This formation, as redefined by Zen (Zen and Hartshorn, 1966), consists of

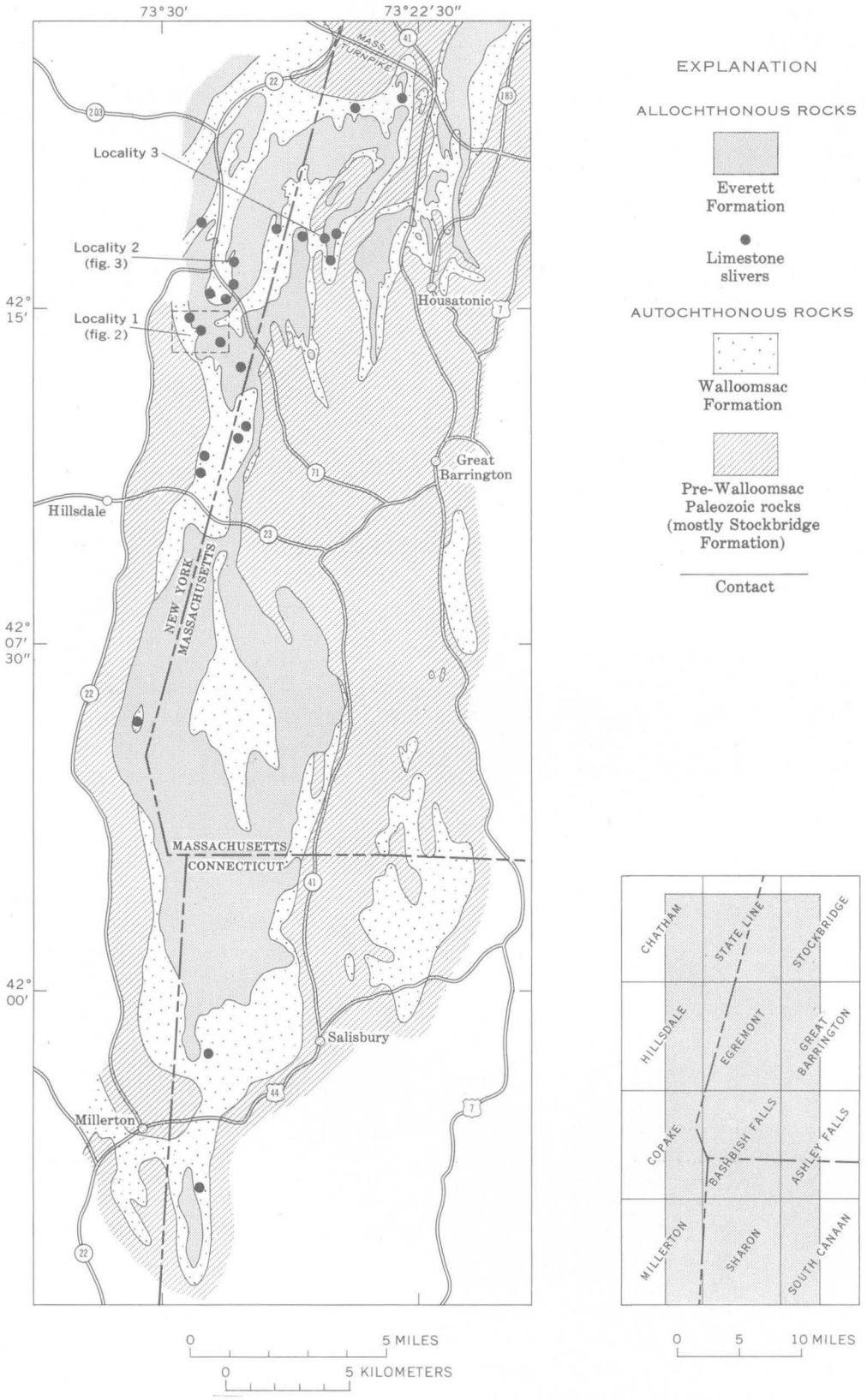

FIGURE 1.—Generalized geologic map of parts of southwestern Massachusetts, northwestern Connecticut, and eastern New York. Localities 1 and 2 are shown in detail in figures 2 and 3, respectively. Locality 3 is referred to in the text. In general, the Everett Formation occupies a highland area and the Stockbridge Formation occurs in the lowland. Normal and fault contacts are not distinguished. Index map shows 7½-minute quadrangles in the report area (shaded).

seven lithostratigraphic members; it is of pre-Trenton, Paleozoic age and probably spans the entire time from Early Cambrian to the Trenton. The lower three units, designated A, B, and C, are dolostones. Units D and F are much alike, being heterogeneous but distinctive calcareous sandstone, siltstone, and dolostone and marble in beds a few feet thick each; they have proved useful as marker units. Units E and G, also mutually similar, are massive marble. The rocks are overlain with an angular unconformity by the Walloomsac Formation, which locally rests on rocks as old as unit B. The Walloomsac is locally calcareous near its base, containing either abundant calcite in the pelite, or silty marble beds as much as 50–70 meters thick. As a rule, these marble beds can be distinguished from those of the Stockbridge. The bulk of the Walloomsac is a gray silty to black carbonaceous pelite; it has been metamorphosed, and ranges from muscovite-chlorite phyllite to staurolite-almandine schist. Greenish-gray schists are locally found at or near the base of the Walloomsac in areas of medium to high grades of metamorphism; this color may reflect the effect of metamorphism.

The high Taconic sequence overlies the Walloomsac Formation; where the Walloomsac is absent, the sequence rests directly on the Stockbridge Formation, although such a contact is nowhere exposed. These high Taconic rocks have been mapped as the Everett Formation (Zen and Hartshorn, 1966; also unpub. data) in the Bashbish Falls and Egremont quadrangles; and have been traced into the State Line and Stockbridge quadrangles (Ratcliffe, 1965). They are green, gray-green to silvery green pelitic rocks, now ranging from phyllite to almandine-staurolite schist. Pebbly graywacke and quartzite beds, calcareous sandstone, and grayish interbeds resembling the Walloomsac are locally present; these beds are subordinate and have not proved to be traceable. Because of the lack of traceable units in the Everett, its internal structure is not known despite detailed mapping; in areas of good outcrop, however, the rocks clearly show at least two episodes of noncoaxial deformation involving isoclinical recumbent folding and small-scale imbrication.

The contact between the Everett and the underlying Walloomsac varies in nature: It is sharp at some outcrops, and gradual, through intercalation of distinct rock types or through color similarities, at others. Where gradational, the contact zone may be from a few meters to tens of meters thick. Where sharp, the rocks on the two sides of the contact may also differ in aspects other than the color. Thus, the Walloomsac tends to be calcareous to feldspathic and is soft, whereas the Everett is noncalcareous and tends to be hard, owing to the high quartz content.

Lenses of carbonate rocks occur sporadically at or very near the zone of contact between the two formations; these lenses individually cannot be traced for any great distance. Because these rocks can be lithically matched with those in the Stockbridge Formation, they require explanation. The lenses vary in size from single blocks a few meters across to tracts nearly 1 kilometer across. The exposed contact between these rocks and the surrounding schists and phyllites is everywhere sharp; the lenses occur on both the east and west sides of belts of the Everett Formation (loc. 3, fig 1). The zones of carbonate lenses commonly dip conformably with the contact between the Walloomsac and the Everett, and define geometric shapes that are overall synclinal.

At most outcrops, the carbonate lenses can be explained by assuming that they are either slivers dragged along the base of thrust slices of the Everett, or local beds in normal sedimentary contact with the rocks above and below. However, two particular outcrops show sufficient details to establish the tectonic origin of this carbonate rock, and, by analogy, the tectonic origin of the other carbonate patches in similar structural positions. For this reason, the two outcrops will be described in detail.

DETAILS OF CARBONATE LENSES

Carbonate rocks crop out on the steep west scarp of a 430-meter (1,410-foot) knob southeast of a sharp turn in the road near a prominent television tower, 2 km N. 30° W. of White Hill (northwest ninth of Egremont quadrangle) in New York (loc. 1, fig. 1; fig. 2). The top of the hill is underlain by a noncalcareous quartzose green phyllite typical of the Everett; these green phyllite outcrops are part of the continuous belt of the high Taconic sequence that makes up the Taconic Range. At about 411 m (1,350 feet) elevation on the northwest and west sides of the hill, the phyllite is underlain with abrupt contact by a zone of carbonate ranging from about 2 to 10 m thick. The carbonate is underlain, again sharply, by a jet-black to dark-gray, noncalcareous phyllite characteristic of the Walloomsac. This phyllite is part of a zone, about 10 m thick, of intimate intercalation between black phyllite similar to the Walloomsac and green phyllite resembling the Everett; within this zone both types of phyllite are strongly sheared while each maintains its lithic identity. To the west of this zone and structurally below it, the area is underlain by the Walloomsac Formation that is part of the autochthon.

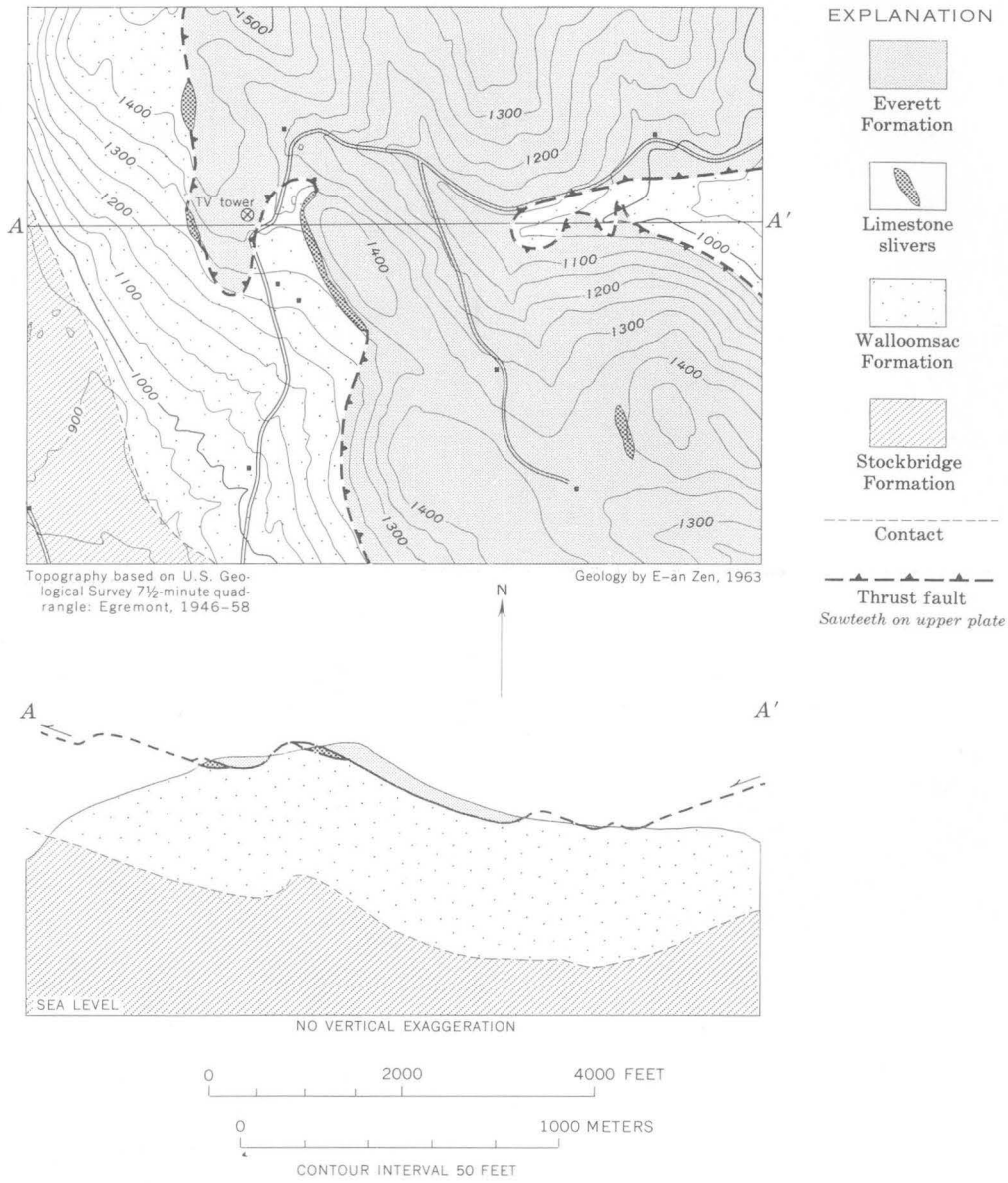

FIGURE 2.—Geologic details of locality 1 of figure 1.

The carbonate zone consists of jumbled blocks of carbonate rocks ranging from a few centimeters to several meters across. The blocks are angular to subrounded, and consist of massive marble, quartzose marble and dolostone, in no apparent order; lithically these rocks can be easily matched with the various units of the Stockbridge Formation. Rare angular blocks of a green phyllite also occur; these phyllite blocks can be matched lithically with the Everett Formation but are now entirely within the carbonate zone. A three-dimensional view of the carbonate blocks is afforded by numerous caverns in the zone; differential solution has generally followed the contacts among the larger blocks.

This carbonate zone clearly is not the result of normal sedimentation; it is interpreted as a tectonic breccia that is a sliver dragged to its present position during the emplacement of the allochthonous Everett Formation. The zone of alternating phyllites under the carbonate zone is regarded as an imbricate zone immediately below the main movement surface.

Another excellent exposure of this possible tectonic breccia occurs in the northwest ninth of the State Line quadrangle (fig. 1), at the contact between the Everett Formation and the underlying Walloomsac Formation along the west limb of a major syncline. This exposure (loc. 2, fig. 1) is approximately 1,000 m N. 40° E. of the intersection of State Routes 71 and 22 in the town

224-352 O—66——4

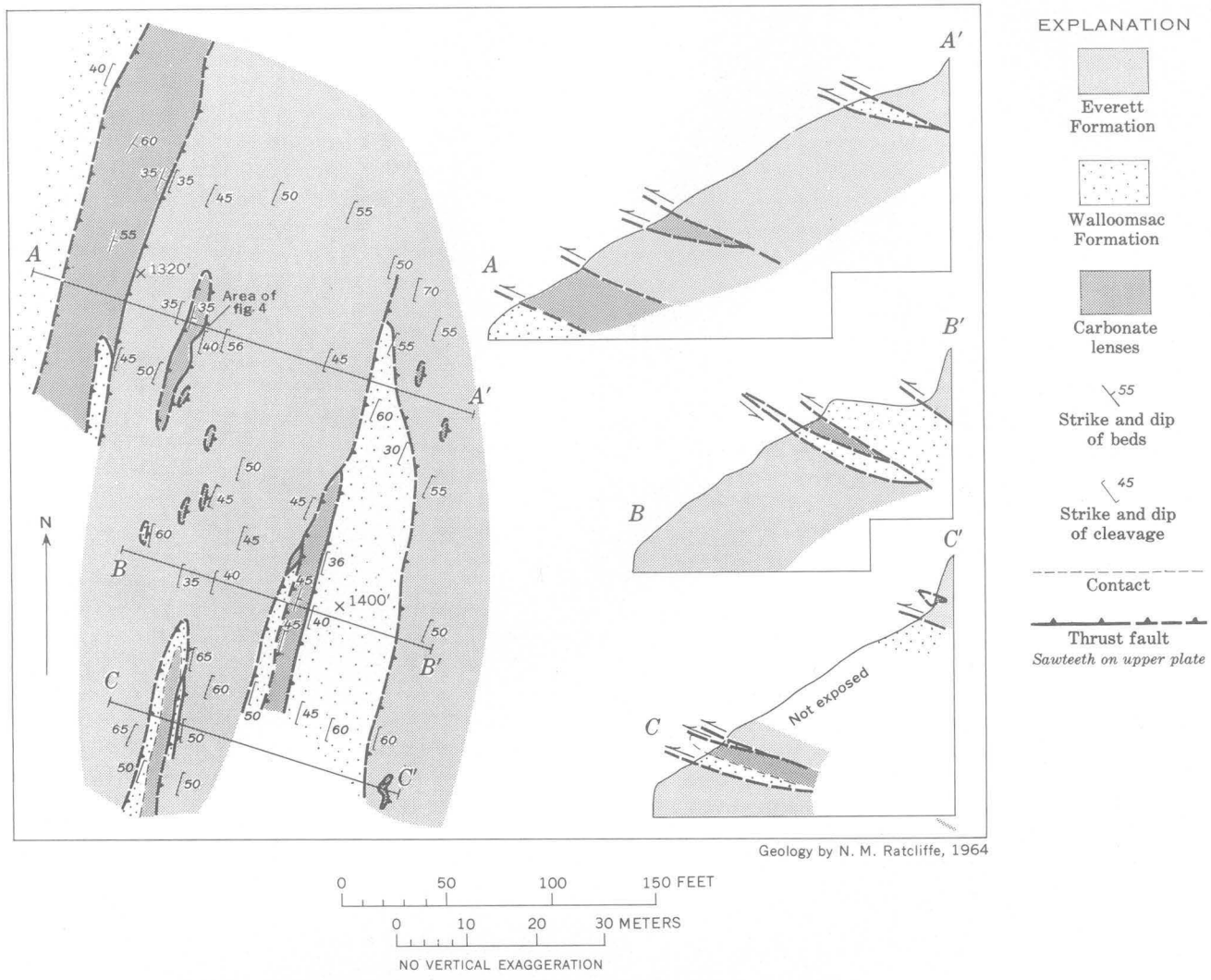

FIGURE 3.—Geologic details of locality 2 of figure 1. Location of the outcrop shown in figure 4 is indicated.

of Green River, N.Y. The carbonate zone, shown in figure 3, is exposed for 120 m along strike, is about 50 m thick, and occurs between the altitudes of approximately 396 m (1,300 feet) to 442 m (1,450 feet). It dips east approximately 40° into the upland underlain by the structurally higher Everett Formation; this general dip is taken as the probable dip of the Everett-Walloomsac contact at this locality. The individual carbonate rocks in the zone terminate along strike as well as down the dip, and thus are lenticular in shape. They commonly are elongate parallel to the strike of the regional cleavage.

Lentils of white calcite marble, gray layered calcite marble, yellow-weathering sandy dolostone, black compact dolostone, graphitic marble, and black graphitic phyllite are present in the outcrop; these rocks lithically resemble rocks of the autochthonous Stockbridge and Walloomsac Formations. The wide assortment of rock types in the carbonate zone, as well as the geometric relationships of these lenses, show that the repetition of carbonate rocks on the hillside cannot be explained by the folding of a normal stratigraphic sequence.

A discordant contact between the upper surface of a lens of calcite marble having sandy dolostone interbeds and the Everett Formation is shown in figure 4. The carbonate lentil is about 5 m thick and 20 m long, and is penetraated by an east-dipping cleavage, parallel to the regional north-northeast-trending axial-plane cleavage found in the surrounding Everett Formation. Minor folds along the contact have this cleavage as their axial plane, and the lineation in the outcrops is parallel to the fold axis. The lower contact of this carbonate lentil is conformable with the Everett Formation. These relations, taken together, indicate that this lens was tectonically enclosed in the Everett prior

A

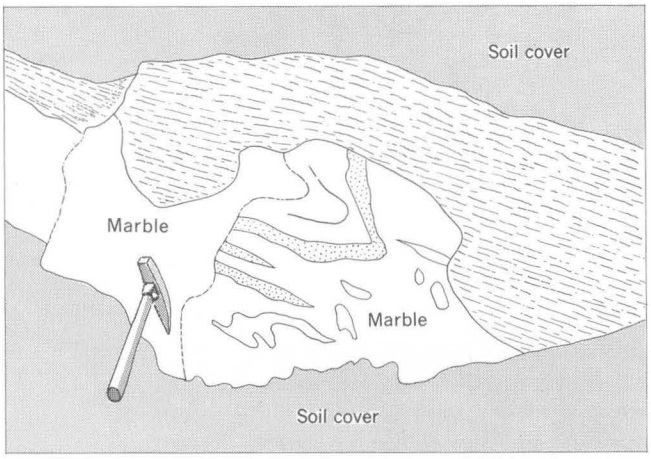

B

FIGURE 4.—Details of the upper contact of a marble lens against the Everett Formation, exposed in an overhanging ledge at locality 2, figure 1 (see also fig. 3). *A*, photograph of outcrop; *B*, simplified sketch of photograph. Bedding in the marble is defined by thin, quartzose dolostone beds (stippled pattern in *B*). The Everett Formation is marked by long-dashed lines in *B*; these lines, as shown, are parallel to the traces of the early cleavage. This cleavage is the axial surface of isoclinal folds that have warped the contact of the two rock units. The Everett immediately next to the contact is peppered with small carbonate chips that weather out to yield the pitted surface. All parts of the outcrop are marble unless otherwise indicated. View is to the north.

to the development of the major northeast-trending structure. The majority of the observed contacts of marble lentils with the surrounding phyllite at locality 2, however, are parallel to the regional cleavage and show no discordance; this conformity is most probably the result of subsequent structural deformation.

The occurrence of the large body of the Walloomsac Formation at locality 2, at approximately 427 m (1,400 feet) elevation, requires a thrust along its geometrically lower contact against the Everett Formation. The Everett-Walloomsac contact here is a zone of imbrication about 50 m thick, much like the relations observed at locality 1. Within this zone, lenticular bodies of carbonate rocks of different lithic types occur as slivers; their lenticular shape and the large number of apparently concordant contacts are the result of subsequent deformation.

CONCLUSIONS

The detailed relations at localities 1 and 2 (fig. 1) rule out the possibility that the carbonate rocks are part of a normal sedimentary sequence, and show that the Everett-Walloomsac contact is a zone of movement and intense deformation. This deformation preceded the development of the earliest cleavage and the metamorphism of the rocks and thus is probably pre-Late Silurian because at Becraft Mountain, near Hudson, N.Y., Silurian and Devonian rocks truncate the beveled edges of folded and well-foliated Middle Ordovician rocks. The emplacement of the carbonate zone could well be an Ordovician event. Moreover, at locality 3 (fig. 1), the carbonate rocks occur in both the west and east limbs as well as near the nose of a narrow north-plunging syncline, between the Walloomsac Formation and the overlying Everett Formation. This zone of movement, therefore, projects both to the east and to the west of the Taconic Range, so that the Everett must be part of a completely detached thrust sheet or sheets, and is allochthonous; this conclusion is not contradicted by the contact relation of the Walloomsac, the carbonate lenses, and the Everett, observed in outcrops whose interpreation is generally equivocal.

The carbonate slivers thus constitute the first local structural evidence, independent of regional correlations, pointing to an allochthonous origin for the high Taconic sequence; the emplacement of the high Taconic sequence may well be mechanically associated with, and chronologically only slightly later than, the emplacement of the low Taconic sequence. The synclines in which the Everett Formation now rests are later structures, perhaps formed during Acadian time; they have no direct bearing on the tectonic origin of the high Taconic sequence.

ACKNOWLEDGMENT

We thank J. M. Bird, of the New York State University, and colleagues of the U.S. Geological Survey for reviewing the manuscript and making many helpful suggestions.

REFERENCES

Berry, W. B. N., 1960, Graptolite faunas of the Marathon region, west Texas: Texas Univ. Pub. 6005, 179 p.

Doll, C. G., Cady, W. M., Thompson, J. B., Jr., and Billings, M. P., 1961, Centennial geologic map of Vermont: Vermont Geol. Survey.

Hewitt, P. C., 1961, The geology of the Equinox quadrangle and vicinity, Vermont: Vermont Geol. Survey Bull. 18, 83 p.

MacFadyen, J. A., Jr., 1956, The geology of the Bennington area, Vermont: Vermont Geol. Survey Bull. 7, 72 p.

Potter, D. B., 1966, Evidence for major thrust sheets in the east-central Taconic Mountains [abs.]: Geol. Soc. America, Northeastern Sec., 1st ann. mtg., Philadelphia, Pa., Program, p. 37.

Ratcliffe, N. M., 1965, Bedrock geology of the Great Barrington area, Massachusetts: The Pennsylvania State Univ., Ph.D. thesis, 213 p.

Zen, E-an, 1960, Metamorphism of Lower Paleozoic rocks in the vicinity of the Taconic Range in west-central Vermont: Am. Mineralogist, v. 45, p. 129–175.

——— 1961, Stratigraphy and structure at the north end of the Taconic Range in west-central Vermont: Geol. Soc. America Bull., v. 72, p. 293–338.

——— 1964, Taconic stratigraphic names—definitions and synonymies: U.S. Geol. Survey Bull. 1174, 95 p.

Zen, E-an, and Bird, J. M., 1963, Roadlog for field trip, *in* Stratigraphy, structure, sedimentation, and paleontology of the southern Taconic region, eastern New York: Geol. Soc. America ann. mtg., New York, Guidebook for field trip 3, 67 p.

Zen, E-an, and Hartshorn, J. H., 1966, Geology of the Bashbish Falls quadrangle, Massachusetts, Connecticut, and New York: U.S. Geol. Survey Geol. Quad. Map GQ–507.

INTERTONGUING RELATIONS OF THE LEE FORMATION IN SOUTHWESTERN VIRGINIA

By KENNETH J. ENGLUND and A. OTIS DeLANEY, Washington, D.C.

Abstract.—Upper Mississippian and Lower Pennsylvanian rocks exposed along the margin of the Southwest Virginia coal field include a cliff-forming sequence of quartzose conglomeratic sandstone beds in the Lee Formation. These clean, coarse clastic rocks terminate northeastward by intertonguing and lateral gradation with relatively less quartzose and finer textured sediments of the Pennington, Pocahontas, and New River Formations.

The Lee Formation of the type area, Lee County, Va., and of adjoining parts of Virginia, Kentucky, and Tennessee is composed largely of quartzose conglomeratic sandstone in tongues and lentils, some of which are as thick as 300 feet. The sandstone in the Lee is thick- to massively bedded and forms an exceptionally rugged terrain of precipitous cliffs and hogbacks that is in contrast to the relatively subdued topography underlain by adjacent formations. Ridges of Lee sandstone are notable historically as natural barriers, and favorable access is confined to a few water or wind gaps such as Cumberland Gap at the southwestern tip of Virginia. In addition to the beds of distinctively quartzose sandstone, the Lee Formation includes lesser amounts of shale, siltstone, coal, underclay, and thin-bedded relatively less quartzose sandstone that are poorly exposed. The Lee Formation is Early Pennsylvanian in age except for its lowermost part, which intertongues with the Upper Mississippian Pennington Formation (Englund, 1964, p. B33).

In Virginia the Lee Formation crops out in a narrow belt that strikes northeastward from Lee County in the southwestern corner of the State. From this outcrop belt, where the beds are steeply inclined and in some places overturned, the Lee dips northwestward beneath the Southwest Virginia coal field (fig. 1). The formation is also exposed locally at the west edge of the State.

Following the naming of the Lee Formation by Campbell (1893, p. 36), usage of the term was extended by subsequent workers along the entire outcrop belt from Lee County to the West Virginia State line. In Scott, Wise, and Russell Counties (fig. 1) the Lee Formation includes quartzose conglomeratic sandstone that is typical of the formation in the type area. However, in Tazewell County, at the northeast end of the outcrop area, the sandstone included in the Lee Formation is predominantly feldspathic, low in quartz content, and relatively nonresistant. Harnsberger (1919, p. 16) reported in Tazewell County: "The rocks of the Lee (Formation) differ very little from those of higher Pennsylvanian formations and cannot be distinguished from them on lithologic grounds." Arkosic sandstone was also noted in the Lee Formation of Tazewell County by Cooper (1944, p. 189–190).

The purpose of this study of Upper Mississippian and Lower Pennsylvanian rocks in southwestern Virginia was to determine (1) the character of facies changes in these rocks, and (2) the stratigraphic position of the Pocahontas Formation, which includes economically important coal beds. For this study closely spaced sections were measured along the outcrop belt that fringes the Southwest Virginia coal field. These surface sections were supplemented by the examination of cuttings from drill holes and wells located immediately northwest of the outcrop area. The principal sections were assembled (fig. 2) to show correlations and thicknesses, as well as the stratigraphic distribution of quartzose sandstone that is commonly composed of more than 90 percent quartz. Other sandstone beds in these sections generally contain less than 70 percent quartz. Sections 1 through 5 (fig. 2) are in areas of detailed mapping, and the indicated lateral extension of units was observed in the field. Units in the remainder of the sections were extended laterally by reconnaissance mapping, by the use of aerial photographs, and by the correlation of key beds. However,

U.S. GEOL. SURVEY PROF. PAPER 550-D, PAGES D47-D52

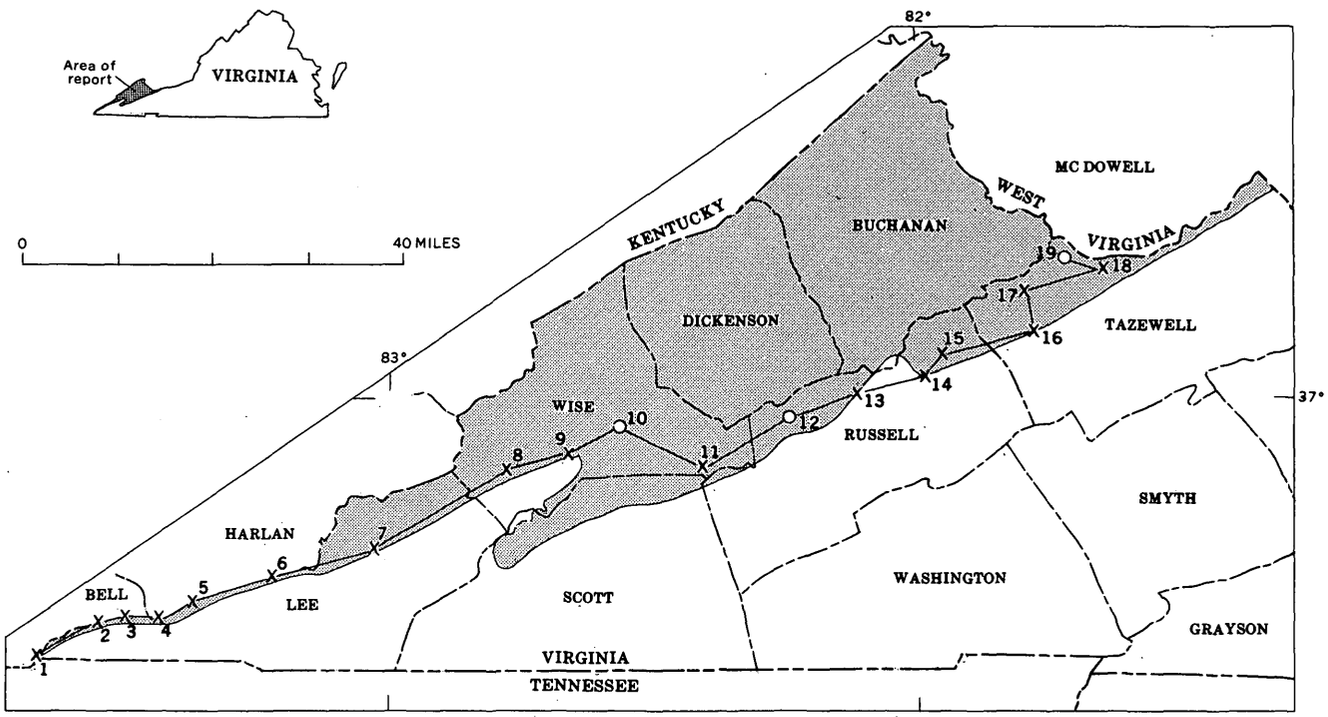

1. Cumberland Gap section, Lee County, Va., and Bell County, Ky.
2. Butcher Knob section, Lee County, Va.
3. Chadwell Gap section, Lee County, Va., and Bell County, Ky.
4. White Rocks section, Lee County, Va., and Harlan County, Ky.
5. Falling Water Gap section, Lee County, Va., and Harlan County, Ky.
6. Wagonroad Tunnel section, Lee County, Va., and Harlan County, Ky.
7. Pennington Gap section, Lee County, Va.
8. Big Stone Gap section, Wise County, Va.
9. Little Stone Gap section, Wise County, Va.
10. Clinchfield Coal Corp. well 187, Wise Development Co., Wise County, Va.
11. Bond Gap, Miller Yard, and Little Stony Creek composite section, Wise and Scott Counties, Va.
12. Clinchfield Coal Corp. well 189, John F. McElhenney, Russell County, Va.
13. Hart and Alvy Creeks composite section, Russell County, Va.
14. Lewis Creek section, Russell County, Va.
15. Swords Creek section, Russell County, Va.
16. Middle Creek section, Tazewell County, Va.
17. Big Creek section, Tazewell County, Va.
18. Beech Fork section, Tazewell County, Va., and McDowell County, W. Va.
19. United Fuel Gas well 9050, New River and Pocahontas Consolidated Coal Co., Tazewell County, Va.

FIGURE 1.—Index map showing the location of outcrop (×) and subsurface (○) sections (fig. 2) at the fringe of the Southwest Virginia coal field (shaded).

critical relations, such as the tonguing out of the Bee Rock Sandstone Member of the Lee Formation, were mapped in detail in the field.

LEE FORMATION

In Lee County, at the southwest end of its outcrop belt, the Lee Formation has been divided on the basis of lithology into seven members which are, in ascending order, as follows: the Pinnacle Overlook, Chadwell, White Rock Sandstone, Dark Ridge, Middlesboro, Hensley, and Bee Rock Sandstone Members.

In the lower part of the Lee Formation the Pinnacle Overlook, Chadwell, and White Rocks Sandstone Members are northwestward-extending quartzose sandstone lobes that intertongue with the Pennington Formation (Englund, 1964). Intertonguing also occurs at the northeast edges of these lobes as shown in figure 2. Nonresistant beds that overlie the White Rocks Sandstone Member and locally the Chadwell Member are included in the Dark Ridge Member. These beds consist mostly of fine-grained, thin-bedded sandstone, shale, coal, and underclay.

The Middlesboro Member is the most prominent part of the Lee Formation at the southwestern end of the outcrop belt, as it consists of four coalescing conglomeratic sandstone units. A northeastward increase in the proportion of nonresistant strata in the member is accompanied by divergence and splitting of the conglomeratic sandstone units. Farther to the northeast the conglomeratic sandstone units tongue out completely and, at their extremities, grade into nonresist-

ant feldspathic micaceous sandstone that has a relatively low quartz content of about 50 to 65 percent. Quartz pebbles and granules are rare in the feldspathic sandstone.

The Hensley Member is a sequence of nonresistant sandstone, siltstone, shale, coal, and underclay in the upper part of the Lee Formation at the southwestern end of the outcrop belt. Northeastward from central Wise County, where the overlying Bee Rock Sandstone Member tongues out, strata equivalent to the Hensley Member have been included in the Norton Formation (Eby, 1923).

The Bee Rock Sandstone Member is a northwestward-protruding lobe of quartzose conglomerate sandstone (Englund, 1964) that grades at its northeastern fringe into a thin, nonresistant feldspathic sandstone. Strata overlying the Bee Rock Sandstone Member consist of siltstone, shale, coal, underclay, and relatively dirty sandstone that commonly contains 50 to 70 percent quartz. These rocks are assigned to the Hance Formation in Bell and Harlan Counties, Ky., and to the Norton Formation in Lee and Wise Counties, Va. Where the Bee Rock Sandstone Member tongues out in Wise County, the top of the Lee Formation was mapped by early workers (Eby, 1923) at the top of the next lower quartzose sandstone, which is stratigraphically about 500 feet lower. This downward placement of the Lee-Norton contact was pointed out by Gathright (1964). The placing of the top contact of the Lee Formation at the top of the uppermost quartzose sandstone is also done commonly in other areas (Englund, 1962). Therefore, the Lee Formation is recognized regionally as a rock-stratigraphic unit with lower and upper contacts defined by quartzose sandstone.

PENNINGTON GROUP OR FORMATION

Only the Little Stone Gap Member (Miller, 1964) of the Hinton Formation, its correlatives, and overlying beds of the Pennington Group or Formation are shown in figure 2. The Little Stone Gap Member, a medium-gray calcareous shale with thin interbeds of argillaceous limestone, contains abundant marine fossils including brachiopods and bryozoans. Because of its extensive occurrence and distinctive marine lithology, the Little Stone Gap Member is useful as a key bed for correlation purposes. Overlying beds of the Pennington consist mostly of light-olive-gray to greenish-gray sandstone and medium-gray, greenish-gray, and grayish-red shale and siltstone. Except for quartzose conglomeratic sandstone that in many places overlies the Little Stone Gap Member, the Pennington sandstone beds are mostly fine grained, nonresistant, and have a relatively low quartz content of about 40 to 65 percent. Shale in the upper part of the Pennington Formation, including widespread grayish-red beds, thins southwestward and intertongues with the lower part of the Lee Formation (fig. 2).

POCAHONTAS FORMATION

The recently redefined Pocahontas Formation (Read and Mamay, 1964) is a sequence of sandstone, siltstone, shale, coal, and underclay that overlies the Pennington Group. The Pocahontas Formation contains a Lower Pennsylvanian flora including *Neuropteris pocahontas* which was identified by S. H. Mamay (written commun., 1965) in fossil plant collections from sections 13 and 18 (fig. 2). Other than sandstone that crops out in cliffs locally, the rocks of the formation are nonresistant. The sandstone is mostly light gray, fine to medium grained, and thin to thick bedded. It is feldspathic and contains finely dispersed carbonaceous fragments and mica flakes. The amount of quartz in the sandstone is similar to that of Pennington sandstone and averages about 60 percent. In contrast, shale and siltstone are varicolored in the Pennington Formation and medium gray to black in the Pocahontas Formation. The Pocahontas Formation thins southwestward, probably by truncation, and may be partly equivalent to the Dark Ridge Member of the Lee Formation. Both units contain mined coal beds that are as much as 7 feet thick in the Dark Ridge Member in Lee County and as much as 10 feet thick in the Pocahontas Formation in Tazewell County.

NEW RIVER FORMATION

The recently redefined New River Formation (Read and Mamay, 1964) overlies the Pocahontas Formation in southwestern Virginia and southern West Virginia. In Tazewell County the New River Formation consists of interbedded sandstone, siltstone, shale, coal, and underclay that are lithologically similar to the Pocahontas Formation except that some sandstone beds in the New River include a few pebbles and granules of quartz. The sandstone is light gray, fine to coarse grained, thin to thick bedded, and locally massive. In addition to quartz, which ranges mostly from 40 to 65 percent, the sandstone contains abundant feldspar, mica, and carbonaceous fragments. Much of the feldspar weathers white or is completely altered to clay; the feldspar, disseminated dark heavy minerals, and

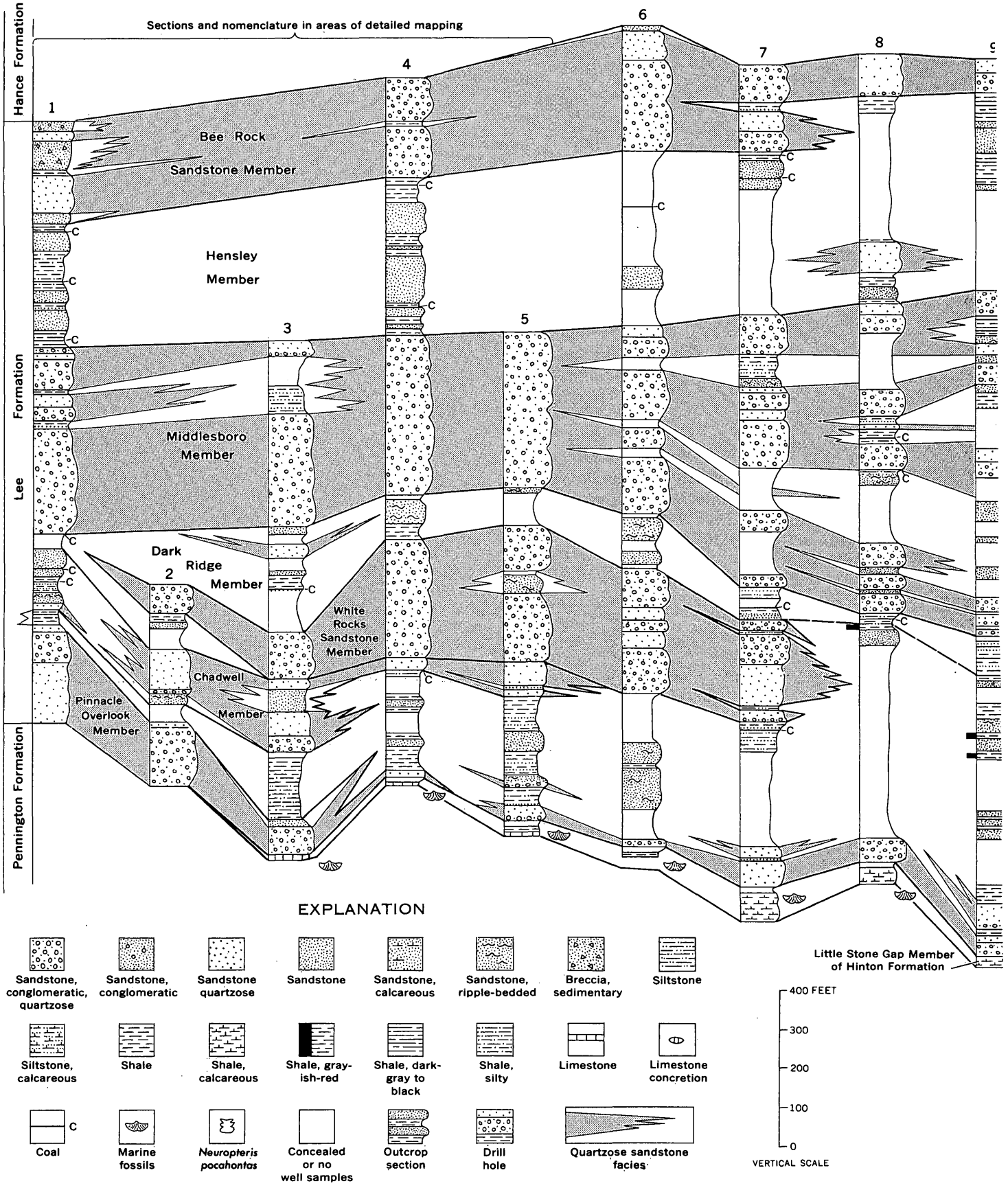

FIGURE 2.—Correlation of the Lee Formation, and the stratigraphic relation of the Lee Formation to equivalent rocks along the southeast fringe of the Southwest Virginia coal field. Location of stratigraphic sections shown on figure 1.

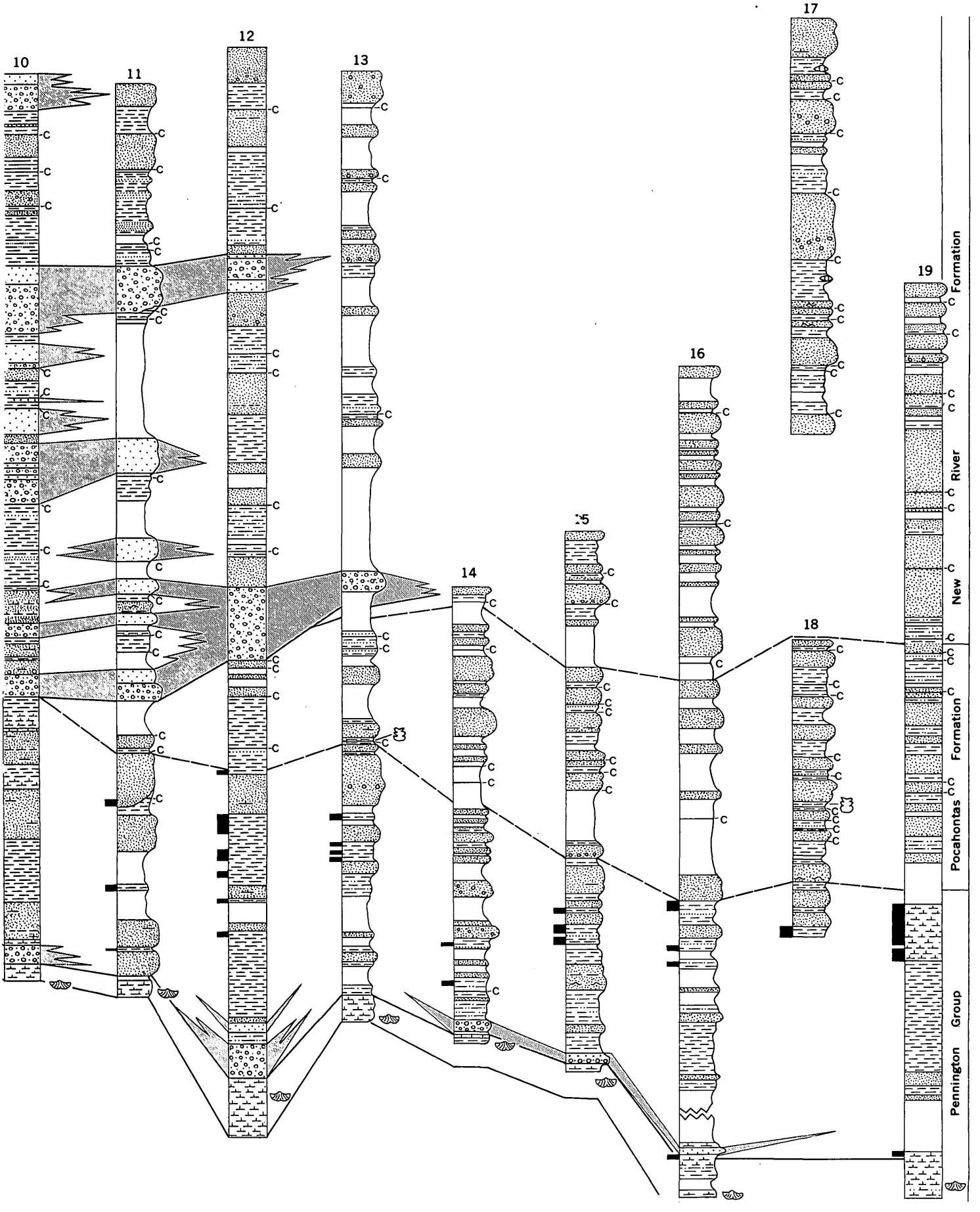
10
11
12
13
14
15
16
17
18
19
Formation
River
New
Formation
Pocahontas
Group
Pennington

carbonaceous fragments give a "salt and pepper" appearance to the sandstone.

RELATION OF THE LEE FORMATION TO EQUIVALENT ROCKS

A comparison of measured sections alined northeastward through southwestern Virginia shows that the quartzose conglomeratic sandstone beds of the Lee terminate northeastward by intertonguing and lateral gradation with equivalent rocks. Regional evidence indicates that these clean, coarse quartzose sandstones are near-shore deposits that were winnowed by shore currents and waves. At the extremities of the sandstone tongues of the Lee, the clean, coarse sediments grade into relatively less quartzose and finer textured sediments that are atypical of the Lee Formation. Sandstone in the lower part of the Lee Formation tongues out in the predominantly marine Pennington Formation, whereas sandstones in the middle and upper parts tongue out in a sequence of mostly continental beds, many of which are coal. Rocks that are laterally equivalent to much of the Lee Formation have been assigned to the Pocahontas and New River Formations in southwestern Virginia and southern West Virginia (Read and Mamay, 1964). This assignment will conform with usage elsewhere which restricts the name Lee to rocks consisting predominantly of quartzose sandstone.

REFERENCES

Campbell, M. R., 1893, Geology of the Big Stone Gap coal field of Virginia and Kentucky: U.S. Geol. Survey Bull. 111, 106 p.

Cooper, B. N., 1944, Geology and mineral resources of the Burkes Garden quadrangle, Virginia: Virginia Geol. Survey Bull. 60, 229 p.

Eby, J. B., 1923, The geology and mineral resources of Wise County and the coal-bearing portion of Scott County, Virginia: Virginia Geol. Survey Bull. 24, 617 p.

Englund, K. J., 1962, Regional relation of the Lee Formation to overlying formations in southeastern Kentucky and adjacent areas of Tennessee [abs.]: Geol. Soc. America Spec. Paper 68, p. 69–70.

——— 1964, In the Cumberland Mountains of southeastern Kentucky, stratigraphy of the Lee Formation, *in* Geological Survey Research 1964: U.S. Geol. Survey Prof. Paper 501–B, p. B30–B38.

Gathright, T. M., 2d., 1964, Revision of the Lower Pennsylvanian correlations in Wise County, Virginia [abs.]: Virginia Jour. Sci., v. 15, new ser., no. 4, p. 331–332.

Harnsberger, T. K., 1919, The geology and coal resources of the coal-bearing portion of Tazewell County, Virginia: Virginia Geol. Survey Bull. 19, 195 p.

Miller, R. L., 1964, The Little Stone Gap Member of the Hinton Formation (Mississippian) in southwest Virginia, *in* Geological Survey Research 1964: U.S. Geol. Survey Prof. Paper 501–B, p. B39–B42.

Read, C. B., and Mamay, S. H., 1964, Upper Paleozoic floral zones and floral provinces of the United States: U.S. Geol. Survey Prof. Paper 454–K, 35 p.

CRETACEOUS STRATIGRAPHY OF THE KAMISHAK HILLS, ALASKA PENINSULA

By DAVID L. JONES and ROBERT L. DETTERMAN, Menlo Park, Calif.

Abstract.—Cretaceous rocks of the Kamishak Hills area, Alaska Peninsula, rest conformably on Upper Jurassic strata and are subdivided into two formations. The lowermost formation, of Early Cretaceous age, is unnamed and comprises two units. The lower unit consists of 200 feet or more of gray shaly siltstone with numerous 1-foot-thick beds of *Inoceramus*-prism calcarenite of late Hauterivian to early Barremian age. The upper unit consists of 200–300 feet of rusty brownish-gray siltstone of Barremian age. This is the first known occurrence of strata of these ages on the Alaska Peninsula. The uppermost Cretaceous Kaguyak Formation overlies the Lower Cretaceous beds with slight angular unconformity and is of Maestrichtian age.

Upper Cretaceous sedimentary rocks are widespread on the Alaska Peninsula, but Lower Cretaceous rocks are scarce and are well known only in the Port Moller area in the western part of the Peninsula. Parkinson's brief report (1960) citing the presence of Lower Cretaceous strata in the Kamishak Hills near Cape Douglas at the eastern end of the Peninsula encouraged us to visit that area to establish a more definitive age for these strata and to further extend our scanty knowledge of the Early Cretaceous history of this important petroliferous region.

The weather was poor during the time in which a helicopter was available to carry us into the relatively inaccessible Kamishak Hills, and we were able to study only hurriedly two partial stratigraphic sections. Time did not permit thorough fossil collecting or tracing out of the beds, but the few fossils found are sufficient to date most of the rocks and to establish correlations with stratigraphic sequences elsewhere in southern Alaska. Consequently, these data are published even though a more thorough study of the area is warranted and more accurate stratigraphic measurements are needed.

Two partial stratigraphic sections were examined in the Kamishak Hills east of the South Fork of the Kamishak River in the Mt. Katmai (D–1) quadrangle (fig. 1). Section 1 is on the headwaters of an unnamed tributary of the South Fork Kamishak River, and section 2 is on the headwaters of an unnamed western tributary of the Douglas River.

STRATIGRAPHY

Lower Cretaceous rocks

Very gently dipping Lower Cretaceous strata rest with apparent conformity on sandstone and siltstone of the Upper Jurassic Naknek Formation (for a

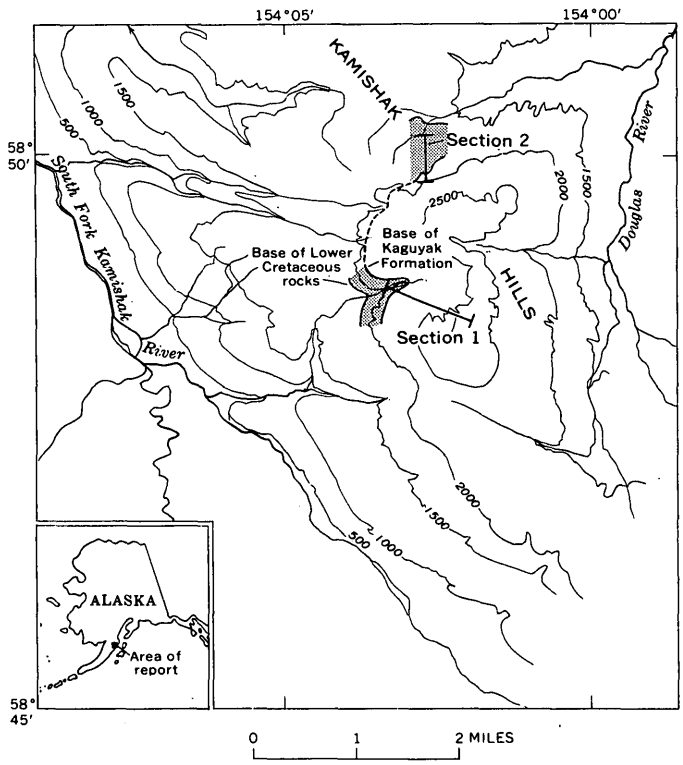

FIGURE 1.—Index map of southern part of the Kamishak Hills, showing location of the two stratigraphic sections studied.

description of this unit, see Keller and Reiser, 1959, p. 269–273) and are overlain with very slight angular unconformity by Upper Cretaceous strata (Parkinson, 1960).

In the Kamishak Hills, the Lower Cretaceous rocks are subdivided into two informal units (fig. 2). The upper unit in section 1 consists of 200–300 feet of rusty-weathering, brownish-gray, bentonitic shale and siltstone that bears fossiliferous calcareous concretions. Belemnites and ammonites were found in it at several places in section 1, but no fossils were observed in section 2. Owing to lack of time, the base of this unit was not studied at section 1. In section 2, however, the rusty-weathering, brownish-gray shale unit is thinner than in section 1 and grades downward into slabby-bedded, light-gray sandstone about 20 feet thick that contains grit beds near the base. The upper contact of the upper unit is placed below massive, cliff-forming, dark-greenish-gray sandstone of the Kaguyak Formation that contains abundant ammonites of Late Cretaceous (Maestrichtian) age. Fossils (figs. 3 and 4) collected from 1 to 3 feet below this contact at section 1 consist of the ammonite *Acrioceras* cf. *A. starrkingi* Anderson (1938) and a belemnite, *Acroteuthis* sp., with a long and deep ventral furrow similar to, but more slender than, a new but unnamed species figured by Jeletzky (1964, pl. 19, fig. 1a–c).

These fossils indicate a late Neocomian (Barremian) age, and their position just below Upper Cretaceous (Maestrichtian) rocks shows that beds of Aptian through Campanian ages are missing.

About 100 feet below the top of the upper unit in section 1 robust specimens of *Acroteuthis* sp. were found, as well as a fragment of an heteromorphic ammonite perhaps related to *Hoplocrioceras remondi* (Gabb). These fossils are probably Hauterivian or Barremian in age.

The lower unit of the Lower Cretaceous rocks consists of 200 feet or more of gray shale and siltstone with many calcarenite interbeds as much as 1 foot thick containing abundant, mostly fragmented, valves of *Inoceramus* (fig. 4*e*, *f*). The calcarenite itself consists mainly of *Inoceramus* prisms and a little terrigenous clastic material. The gray shale and siltstone contain abundant thin layers of broken *Inoceramus* shell debris that probably makes up from 5 to 10 percent of the section.

Because the lower 100 feet or so of the lower unit was not studied, its total thickness and details of the contact with the Naknek Formation of Late Jurassic age are unknown.

Fossils from the lower unit in section 2 consist of an unidentified belemnite and numerous specimens of *Inoceramus ovatoides* Anderson. In California this pelecypod is most abundant in the late Hauterivian zone of *Hertleinites aquila* and ranges up into the early

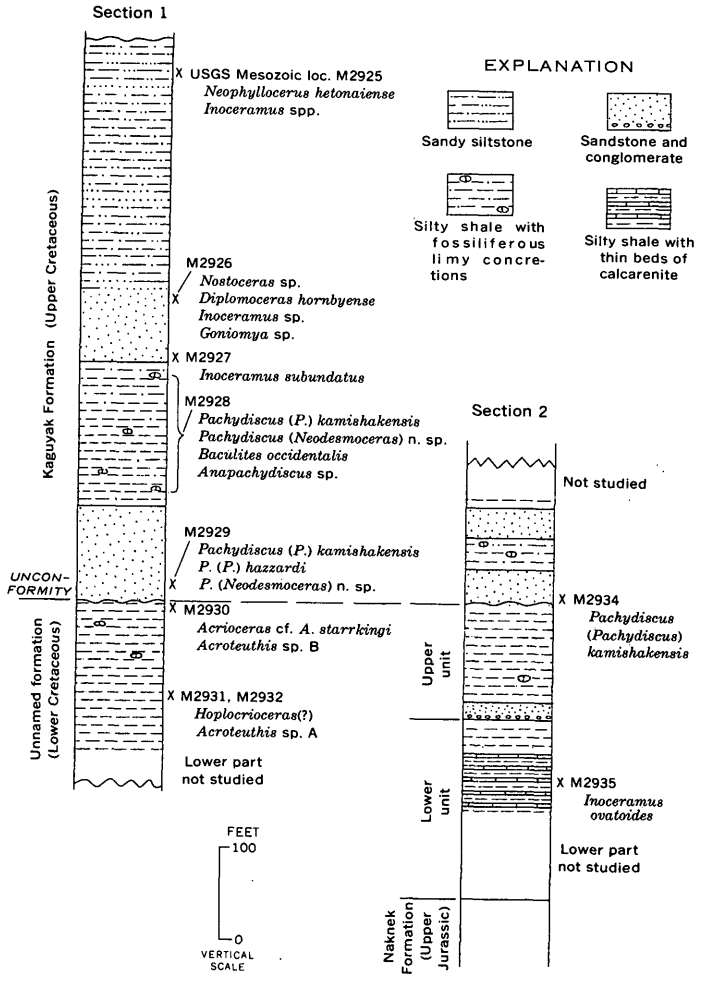

FIGURE 2.—Schematic generalized columnar sections of Cretaceous rocks in the southern part of the Kamishak Hills.

FIGURE 3.—Specimens of *Acrioceras*, *Hoplocrioceras*(?), and *Acroteuthis* collected from USGS Mesozoic localities M2930 and M2931. All specimens natural size.

a–d. *Acrioceras* cf. *A. starrkingi* Anderson.
a, *d*. Lateral views.
b, *c*. Dorsal and ventral views.
Specimen from USGS Mesozoic loc. M2930, in the uppermost part of Lower Cretaceous strata in the Kamishak Hills. USNM 153996.

e–f. *Hoplocrioceras*(?) sp., perhaps related to *H. remondi* (Gabb). Lateral and ventral views. From USGS Mesozoic loc. M2931, about 100 feet below top of the Lower Cretaceous strata. USNM 153997.

g–i. *Acroteuthis* sp. *A*.
g, *i*. Ventral and lateral views; note very shallow depression on flattened ventral side.
h. End view; note alveolus displaced toward flattened ventral side.
From USGS Mesozoic loc. M2931, about 100 feet below top of Lower Cretaceous strata. USNM 153998.

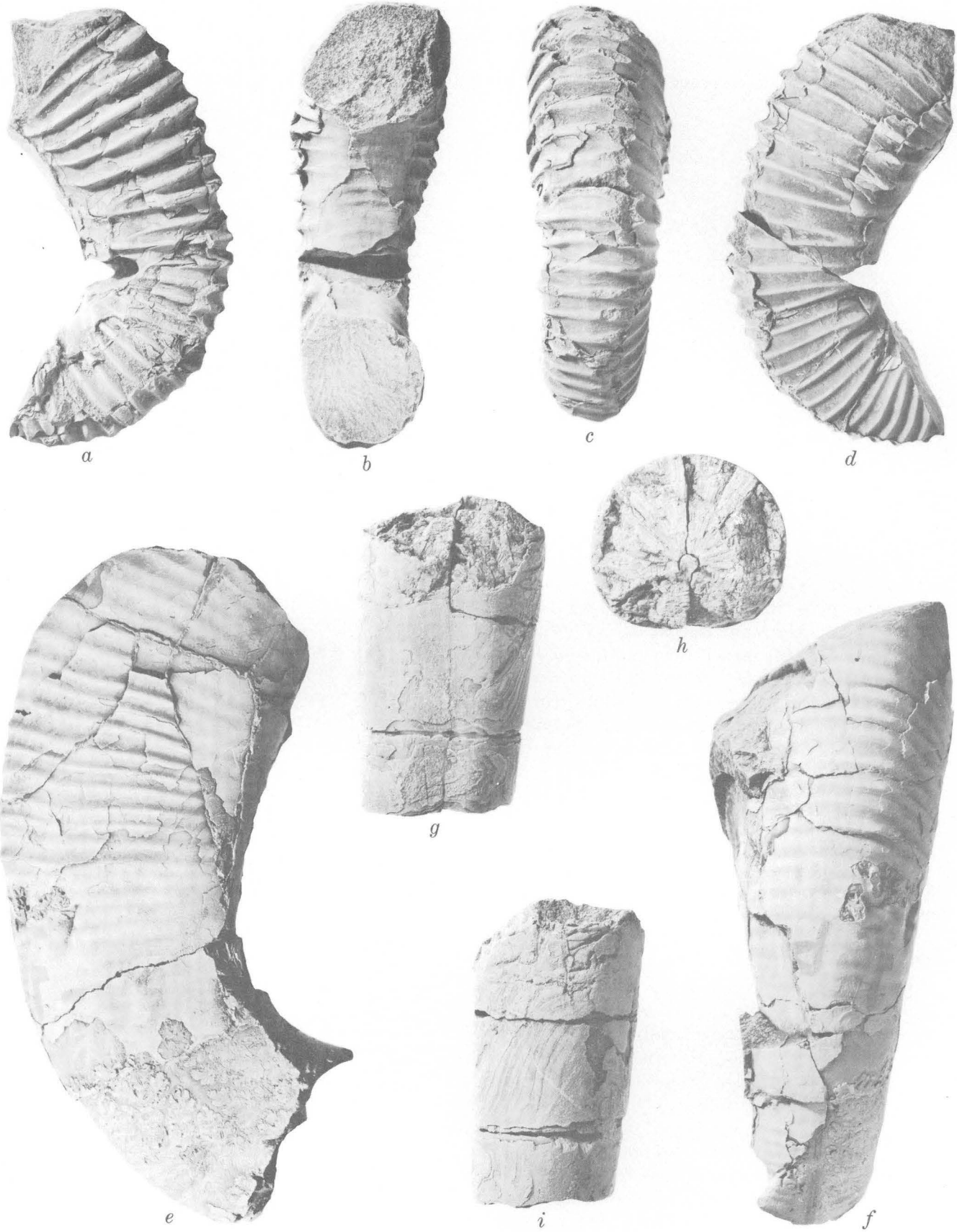

a

b

c

d

e

g

h

i

f

Barremian zone of *Shasticrioceras poniente* (Imlay, 1960, p. 179–180).

Correlation of Lower Cretaceous rocks in the Kamishak Hills

The rocks of the upper unit are the first of definite Barremian age to be recognized anywhere in Alaska and are possibly the only deposits of that age present in the State.

The lower unit is similar lithologically and faunally to the Nelchina Limestone and the Herendeen Limestone, although it contains a greater percentage of shale and siltstone than is typical for those units. The Nelchina Limestone in the Kotsina-Kuskulana area of the lower Chitina Valley, over 400 miles to the northeast, consists of a massive *Inoceramus*-prism calcarenite that contains well-preserved specimens of *I. ovatoides* and overlies sandstone and siltstone of Hauterivian age (Grantz and others, 1966). The Nelchina Limestone at its type locality in the Nelchina area is likewise an *Inoceramus*-prism calcarenite and has yielded Foraminifera of Hauterivian age (Bergquist, 1961, p. D236).

The Herendeen Limestone of the Port Moller area (Atwood, 1911, p. 39) also consists of an *Inoceramus*-prism calcarenite similar to the Nelchina Limestone and to the thin calcarenite beds of the Kamishak Hills. Atwood (1911, p. 40) reports that the Herendeen Limestone contains *Buchia* (=*Aucella*) *crassicollis* of Valanginian age, but according to Burk (in press) these fossils came from the underlying Staniukovich Shale, and only fragments of *Inoceramus* are known from the Herendeen. Burk believes that this formation can be only slightly younger than the Staniukovich and suggests a latest Valanginian or younger age. The Herendeen Limestone and the lower unit in the Kamishak Hills are probably equivalent in age, with the latter representing a finer grained, less calcareous correlative of the former.

Upper Cretaceous rocks

Upper Cretaceous rocks in the Cape Douglas area were named the Kaguyak Formation by Keller and Reiser (1959), with the type locality designated as the rocks exposed along the northern shore of Kaguyak Bay. On the basis of photogeologic interpretation, these rocks were traced inland to the Kamishak Hills and are shown on their geologic map (pl. 29) in approximately their correct position. Fossils in the U.S. Geological Survey collections from the Kaguyak Formation of the Kamishak Hills were collected some years ago by oil company geologists before accurate maps of the area were available. Some of these fossils were described and illustrated by Jones (1963), and the position of the fossil localities, as nearly as could be reconstructed, was shown on his plate 3 (Jones, 1963). During our brief visit to the Kamishak Hills, it was apparent that a few localities had been incorrectly located and that no Cretaceous rocks are present in the indicated places. In particular, USGS Mesozoic localities 25855 and 25856 are misplaced, and the fossils undoubtedly came from a patch of fossiliferous Kaguyak Formation lying a few miles to the east.

In the type section of the Kaguyak Formation, Keller and Reiser (1959, p. 275–276) report 4,550 feet of interbedded sandstone, siltstone, and siltshale. In section 1 in the Kamishak Hills, only about 600 feet of strata representing the lower part of the formation is preserved. These beds dip about 5° to the east and locally overlie the Lower Cretaceous beds with very slight angular unconformity. The uppermost part of the Kaguyak Formation consists of a basal massive sandstone that grades up into thin-bedded fine-grained sandstone and sandy siltstone, contains abundant fossiliferous calcareous concretions, and is estimated to be about 300 feet thick. Siltstone and shale, about 150 feet thick, appear to underlie the upper unit, but the contact is obscured by minor faulting. The upper 60–80 feet of this siltstone and shale unit consists of gray siltstone that has fossiliferous sandy calcareous concretions. This siltstone grades down into rusty-weathering brownish-gray siltstone that also contains abundant fossiliferous concretions. The base of the Kaguyak Formation consists of massive silty sandstone that contains abundant specimens of ammonites and *Inoceramus*. In section 1 this basal unit is estimated to be about 100 feet thick. In section 2, the basal unit, also about 100 feet thick, is tripartite. It has a massive basal sandstone that is overlain by gray siltstone containing many large calcareous concretions. This siltstone is, in turn, overlain by rubbly-bedded sandstone. Ammonites are very abundant and well preserved in the lower third of the basal unit and are present, but poorly preserved, in its upper third.

FIGURE 4.—Specimens of *Acroteuthis* and *Inoceramus* collected from USGS Mesozoic localities M2930, M2932, and M2935. All specimens natural size.

a, b. Acroteuthis sp. *B.* Ventral and lateral views of poorly preserved and distorted specimens from USGS Mesozoic loc. M2930, about 3 feet below top of the Lower Cretaceous strata. USNM 153999.

c, d. Acroteuthis sp. *A* . Ventral and lateral views of a poorly preserved specimen from USGS Mesozoic loc. M2932, about 100 feet below top of the Lower Cretaceous strata. USNM 154000.

e, f. Inoceramus ovatoides Anderson.

e. Left valve. USNM 154001.

f. Slab of calcarenite with abundant shell fragments. Both from USGS Mesozoic loc. M2935, lower member of the Lower Cretaceous strata. USNM 154002.

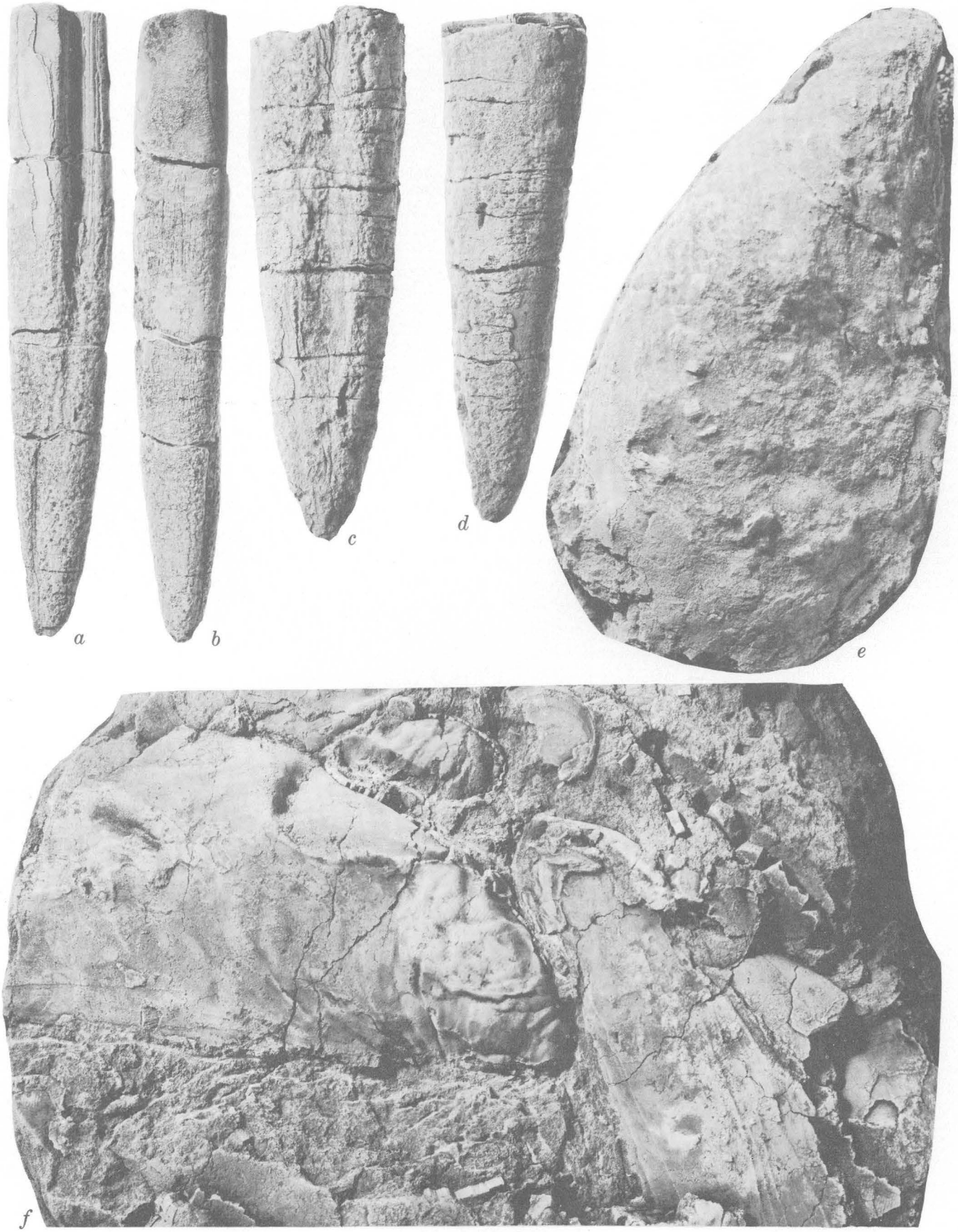
a
b
c
d
e
f

The fossils found throughout the Kaguyak Formation are listed in section 1 of figure 2. *Pachydiscus* (*Pachydiscus*) *kamishakensis* Jones is abundant in the basal sandstone and overlying siltstone unit; this fossil is of probable early Maestrichtian age and is the index to the ammonite zone bearing its name in southern Alaska (Jones, 1963).

SUMMARY OF GEOLOGIC HISTORY

Following deposition of the Naknek Formation of Oxfordian and Kimmeridgian age, marine deposition was apparently interrupted until late Neocomian time, on the basis of the apparent absence in the Kamishak Hills of *Buchia*-bearing beds of latest Jurassic and early Neocomian ages. Only minor uplift is indicated by this break. This contrasts with many other places in southern Alaska where Upper Jurassic and Cretaceous beds are discordant. Marine deposition occurred throughout the latest Neocomian (late Hauterivian and Barremian), but the absence of any depositional record between the late Barremian and early Maestrichtian precludes an understanding of the intervening history. The near concordance in attitude of the Lower Cretaceous and Upper Cretaceous beds suggests a period of structural stability in this area throughout Cretaceous time. Since the end of the Cretaceous, these beds have been uplifted a minimum of 3,000 to 4,000 feet and have undergone only very minor tilting and faulting.

REFERENCES

Anderson, F. M., 1938, Lower Cretaceous deposits in California and Oregon: Geol. Soc. America Spec. Paper 16, 339 p., 85 plates, 6 figs.

Atwood, W. W., 1911, Geology and mineral resources of parts of the Alaska Peninsula: U.S. Geol. Survey Bull. 467, 137 p., 14 plates, 18 figs.

microfossils in south-central Alaska: Art 374 *in* U.S. Geol. microfossilsin south-central Alaska: Art 374 *in* U.S. Geol. Survey Prof. Paper 424–D, p. D236–D237.

Burk, C. A., in press, Geology of the Alaska Peninsula, island arc and continental margin: Geol. Soc. America Spec. Paper.

Grantz, Arthur, Jones, D. L., and Lanphere, M. A., 1966, Stratigraphy, paleontology, and isotopic ages of upper Mesozoic rocks in the southwestern Wrangell Mountains, Alaska *in* Geological Survey Research 1966: U.S. Geol. Survey Prof. Paper 550–C, p. C39–C47.

Imlay, R. W., 1960, Ammonites of Early Cretaceous Age (Valanginian and Hauterivian) from the Pacific Coast states: U.S. Geol. Survey Prof. Paper 334–F, p. 167–228, plates 24–43.

Jeletzky, J. A., 1964, Illustrations of Canadian fossils—Lower Cretaceous marine index fossils of the sedimentary basins of western and arctic Canada: Canada Geol. Survey Paper 64–11, 101 p., 36 plates, 1 table.

Jones, D. L., 1963, Upper Cretaceous (Campanian and Maestrichtian) ammonites from southern Alaska: U.S. Geol. Survey Prof. Paper 432, 53 p., 41 plates.

Keller, A. S., and Reiser, H. N., 1959, Geology of the Mount Katmai area, Alaska: U.S. Geol. Survey Bull. 1058–G, p. 261–298, pl. 29–32, figs. 44–46.

Parkinson, L. J., Jr., 1960, Cretaceous strata of the Cape Douglas area, Alaska Peninsula, Alaska [abs.]: Geol. Soc. America Bull., v. 71, no. 12, pt. 2, p. 2087.

LITHOLOGY AND EASTWARD EXTENSION OF THE DALLES FORMATION, OREGON AND WASHINGTON

By R. C. NEWCOMB, Portland, Oreg.

Abstract.—The Dalles Formation consists of the uneroded part of a low cone of volcanic agglomerate deposited northward and northeastward and an interfingering sedimentary facies of tuff, siltstone, and conglomerate deposited by westward-flowing rivers. The sedimentary facies was mapped eastward to Rufus, Oreg., and similar deposits bearing other names were seen in an eastward reconnaissance as far as the vicinity of McKay Reservoir, Oreg., about 120 miles east of The Dalles. Name and age changes may be necessary as this Pliocene stratigraphy becomes clarified.

The Dalles Formation was described by Condon (1902) as the horizontal strata of "gray sandstone" overlying the Columbia River Basalt at The Dalles. Subsequently, Buwalda and Moore (1930), Piper (1932), and Chaney (1944) have described parts of the formation; Piper and Chaney both noted that only a slight erosional unconformity characterizes the top of the underlying Columbia River Basalt beneath the otherwise conformable Dalles Formation. Piper (1932, p. 120–127) gave a comparatively full account of the volcanic-sedimentary nature of the main body of the formation near The Dalles. His sections (Piper, 1932, p. 121–124) contain much the same observations as the writer's but give the name of "sandstone" to more of the water-laid sandy tuffs.

Some basic aspects of the Dalles Formation were observed in recent years during structural and hydrologic mapping by the writer in the area covered by the White Salmon, The Dalles, and Wishram 15-minute quadrangles, west of Rufus, and during reconnaissance eastward to the Umatilla River (fig. 1). This paper describes generally the two facies of the Dalles Formation, indicates the continuation of one of these facies eastward to Rufus, Oreg., and points out a possible discrepancy between the early Pliocene age assigned to the Dalles Formation and the middle Pliocene age assigned to sedimentary deposits in a similar position farther east, to where the Dalles Formation may extend.

LOCATION AND COMPOSITION OF THE DALLES FORMATION

Within the mapped area to the west, the Dalles Formation was conformably deposited as thickly bedded units in a shallow (upland?) basin and on slopes leading into it. The formation was deformed in two uplifts of the Cascade Range and in the broad folds which curve away from the east side of the range. The formation has been eroded from the crests of some of the anticlines and, in places, has been covered by later volcanic materials in the Cascade Range and by volcanic and sedimentary materials in lower areas like the Hood River Valley. As a result of the second and principal deformation and of the subsequent canyon cutting, most of the Dalles Formation now lies beneath plateaus. The bulk of the formation occurs west, south, and east of The Dalles—in the Dalles and Mosier synclines. The formation is about 1,800 feet thick in the Mill Creek valley, but thins eastward and northward so that it is only 500 feet thick near The Dalles, near Mosier Creek valley, and in the lower valley of Fifteenmile Creek. The thickness is 400 feet northwest of Lyle, 250 feet at the east side of the Deschutes River canyon, and only 160 feet at a locality farther east, near Rufus.

The formation consists of two deposits, or facies, which interfinger: the volcanic-debris facies, a large, low cone of volcanic tuff and agglomerate, much of which was water deposited as debris flows moving north and east; and the sedimentary facies, a train of clastic sedimentary materials deposited by westward-flowing rivers. One lava flow was interlayered high in the sedimentary facies.

The most common rock of the volcanic-debris facies is a gray agglomerate composed of a matrix of shards of pumiceous, partly altered, volcanic glass and mineral grains, with included pieces of dark and light scoria, pumice, and andesite. About 20 percent of the

U.S. GEOL. SURVEY PROF. PAPER 550-D, PAGES D59-D63

224-352 O—66——5

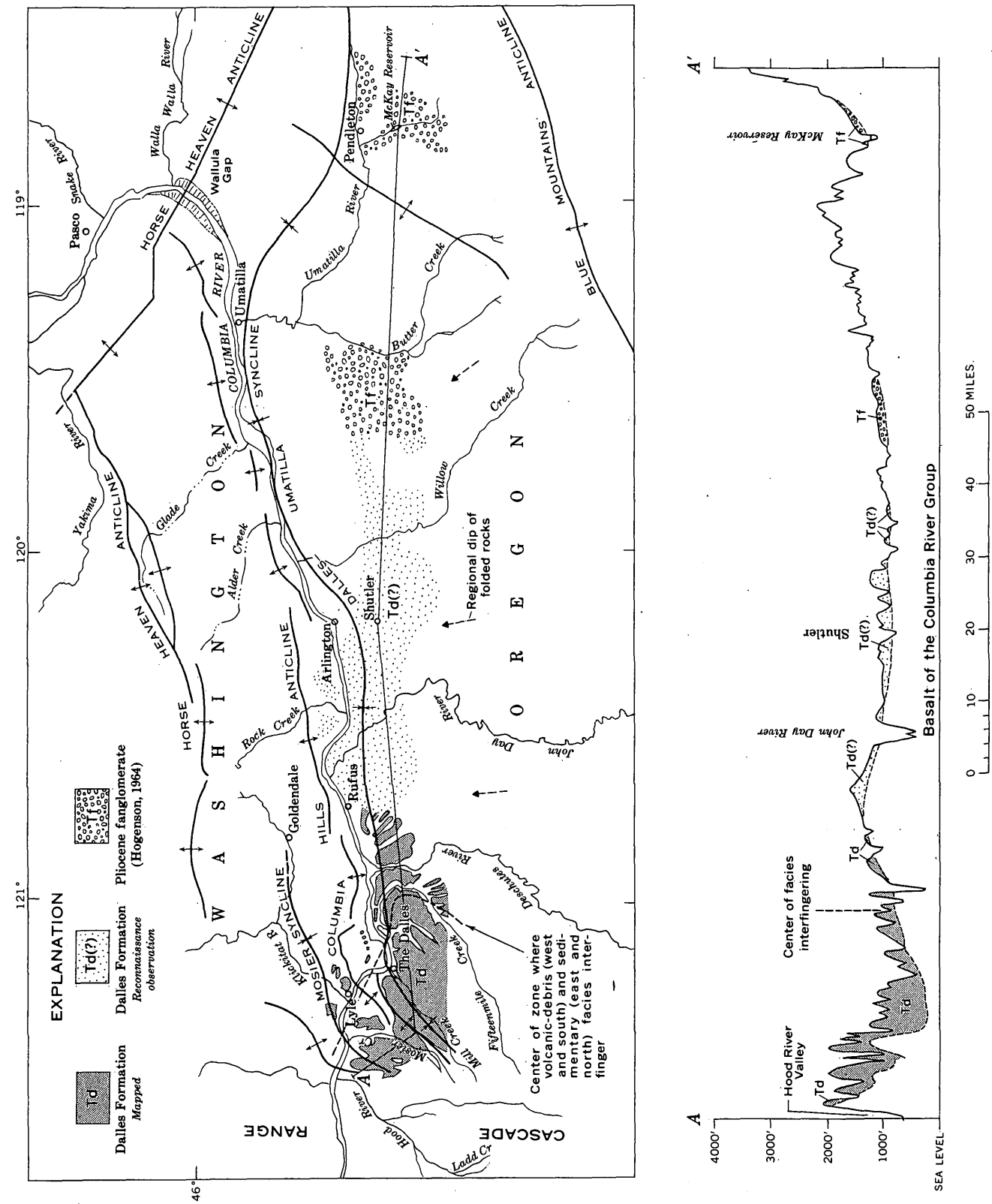

FIGURE 1.—Tentative extension of the Dalles Formation and its relation to Pliocene fanglomerate.

mass is made up of andesite clasts, which range in size from pebbles to boulders. They consist largely of one type of andesite. The coarseness of the fragments decreases northward and eastward. The size of the largest andesite clasts ranges from great angular blocks 5 to 10 feet across, in the upper parts of the Mill Creek and Mosier Creek areas, to cobble and pebble sizes at the Columbia River on the north and at lower Fifteenmile Creek on the east. Minor amounts of coarse sandstone, siltstone, and conglomerate occur sporadically.

The most common rock of the volcanic-debris facies is moderately strong, but the degree of consolidation and induration varies considerably from layer to layer and from place to place. The agglomerate stands in steep walls of young canyons, but sloughs and slides to gentler slopes beneath the older surfaces. It has much nonconnected pore space and is a comparatively lightweight rock.

A representative section of the volcanic-debris facies, 1,100 feet thick, is exposed in the north side of the canyon at the junction of the North and South Forks of Mill Creek. Near this section, wells were drilled about 700 feet through additional and similar strata, below the creek level, before reaching the underlying basalt. The exposed strata of the volcanic-debris facies consist of tuffaceous agglomerate, tuffaceous sandstone, tuff breccia, and tuff. The bedding dips 1° to 2° northeast. The master layers are rather uniformly and conformably bedded, but subunits contain irregular and even crossbedded strata and lenticular segregations of coarse rock clasts and smaller grains. No significant change in coarseness of the debris from top to bottom is evident in either the exposed or subsurface sections. During deposition, much of the tuffaceous agglomerate must have been moved as sheets of thick slurry, in mudflow or debris-flow manner. Materials in the coarse agglomerate layers are similar in grain size and size distribution to the material in the debris flow which moved 4 miles down Ladd Creek from the slopes of Mount Hood on September 1, 1961 (Birch, 1963).

East from The Dalles and north of the Columbia River, the material of the Dalles Formation is finer; fine-grained tuff, along with fine sand and silt, are progressively more common, and the sedimentary facies interfingers in the distal end of the fan of volcanic debris. East and north of lower Fifteenmile Creek, fine-grained tuff is the predominant representative of the volcanic-debris facies; it contains diatomite, sand, and silt. Of the materials of the volcanic-debris facies, only the impure fine-grained tuff, derived from airborne ash, was seen east of the Deschutes River.

In the sedimentary facies the strata of fine-grained tuff, silt, and sand are interbedded with layers of river-laid conglomerate. Individual conglomerate layers are generally 10 to 50 feet thick, broadly lenticular in transverse section, and, apparently, many miles in length. Collectively, the conglomerate layers form about half the deposit. The conglomerate is composed of rounded pebbles and cobbles with some small boulders, and has interstices partly filled by a loosely consolidated matrix of earthy sand and granular gravel. The particles are entirely different from those of the volcanic conglomerate in the volcanic-debris facies to the southwest; they consist of dense andesitic lavas, silicified tuff, basalt (all three types generally associated with the Clarno and John Day Formations), much cryptocrystalline silica, and basalt of the Columbia River Group. These rocks are similar to those occurring in much of the present John Day River basin. Most of the cobbles from the basalt of the Columbia River Group have thick decomposition rinds; some crumbly rinds are as much as ⅛ inch thick. No quartzite or other rocks indicative of origin in the northern Rocky Mountains were observed.

The sedimentary facies, consisting of conglomerate and fine-grained sediments, prevails east of lower Fifteenmile Creek and north of the lowest parts of that creek. It forms the remnants of the Dalles Formation north of the Columbia River (fig. 1) and in the Mosier syncline west of Lyle. A 55-foot thick flow of porphyritic andesitic basalt is interlayered in the upper part and forms the rimrock of the ridge between Fifteenmile Creek and the Deschutes River. At several places east of the Deschutes River, the fine-grained earthy tuffs and tuffaceous siltstones, which are typical of the Dalles Formation east of The Dalles, form the top part of the sedimentary facies. The ash content of these siltstones indicates that the effusion of volcanic dust from eruptive centers, like those that were feeding materials to the volcanic-debris facies, probably continued to the end of the deposition of the sedimentary facies.

An example of the eastward change in lithology is obtained by comparing the 1,100-foot section at the forks of Mill Creek (where the formation is all agglomerate, tuff, and tuffaceous sandstone) with the section (table 1) on Fifteenmile Creek, near where the volcanic-debris and sedimentary facies interfinger.

East of the Deschutes River, full sections of the Dalles Formation and other materials are difficult to find. A part of the existing section, usually a few tens of feet at the most, is all that can be examined at one place, without extensive excavations.

TABLE 1.—*Section measured in Fifteenmile Creek valley southwestward down ravine in northern part of sec. 33, T. 2 N., R. 15 E., above Petroff farmhouse*

[Hand-level control based on contour altitude of road at farmhouse]

Material	Thickness (feet)	Altitude (feet)
Covered; loess soil. (Several miles to the south this zone consists of finely bedded soft buff tuffaceous siltstone.)	0–150	1,230–1,080
Basalt, andesitic, porphyritic; a single flow.	150–205	1,080–1,025
Conglomerate, semicompact, weakly cemented; cobbles at top grade to pebbles near base; 2-foot thick lenticular bed of tuffaceous sand in top part. Pebbles and cobbles are mostly hard felsite porphyries, basalt, hardened tuffs, and cryptocrystalline silica. Particles are well rounded and polished, but those of basalt have crumbly rinds.	205–240	1,025–990
Covered (deep slough over zone indicates a weak layer.)	240–275	990–955
Conglomerate; pebble and granular gravel in tuffaceous matrix, whitish-tan. Has cemented stratum at the top.	275–285	955–945
Covered, probably conglomeratic.	285–300	945–930
Conglomerate; much like 275–285-foot zone.	300–335	930–895
Tuff, sandy, buff-pink; compact but clayey content causes it to loosen and slough on outer surfaces.	335–370	895–860
Covered (tuffaceous breccia rubble).	370–400	860–830
Conglomerate; pebble and granular gravel with sandy tuffaceous matrix.	400–405	830–825
Covered. Soil and extent of sloughing indicate that this zone contains tuff or siltstone.	405–445	825–785
Top of Columbia River Group, pillow lava.	-------	785

EXTENSION OF THE DALLES FORMATION TO THE EAST

The sedimentary facies of the Dalles Formation was mapped as far east as Rufus by the writer (fig. 1). By reconnaissance inspection, similar materials were found for 28 miles to the east from Rufus, on the plateau top, to where they are part of the deposits that Hodge called "Arlington Lake beds" (Hodge, 1932, map) and "Shutler Formation" (Hodge, 1932, p. 6), and to the fossil locality of Shotwell's Arlington beds (Shotwell, 1956, p. 717). The horizontal continuation of this material is shown on figure 1.

Thirty-two miles east of Shutler, similar but more basaltic conglomerate and interbedded sandy siltstone in the same stratigraphic position were mapped as "Pliocene fanglomerate" by Hogenson (1964, pl. 1), who said (p. 24 and 31) that it contained the gravels in the vicinity of McKay Reservoir. These beds at the reservoir are informally called the "McKay beds," but they have not been formally designated except by inclusion in Hogenson's "Pliocene fanglomerate." Siltstone and weak sandstone below a conglomerate yielded the fossils described by Shotwell (1956, p. 717) as coming from the "sediments * * * on the east bank of McKay Reservoir." Hogenson (1964, p. 24) also said that his Pliocene fanglomerate included the deposit that had been designated as the lower Shutler Formation by Hodge (1942, p. 19).

Hodge (1942, p. 19) had noted that the "Shutler Formation interfringes [sic] to the west with the Dalles Formation. " Hodge (1942, map) used the Deschutes River canyon as an arbitrary boundary between the Dalles Formation and his Shutler Formation.

A reconnaissance of the tuffaceous siltstone and volcanic-ash beds high in the section just west of Shutler indicates that some have originated from sources other than the eruptive centers of the volcanic-debris facies of the Dalles Formation. For example, the clean, glassy volcanic ash that is being quarried for pozzuolana in the northwest corner of sec. 31, T. 2 N., R. 21 E. (4 miles southwest of Shutler), is cleaner, less pumiceous, and less altered than the tuffs typical of the Dalles Formation. In addition to small amounts of sediments of probable post-Dalles age, the "Arlington Lake beds" are overlain to an altitude of about 1,100 feet by proglacial lacustrine and fluvial materials, partly described by Allison (1933, p. 690–701). These Pleistocene materials are thin and spotty at places, especially at altitudes above 900 feet, but are as much as 150 feet thick and are extensive in the Umatilla River basin, where Hogenson (1964) mapped them as "glacial-lake sediments" and "glaciofluvial deposits."

AGE DETERMINATIONS REPORTED FOR THE DALLES FORMATION AND OTHER DEPOSITS

On the basis of the ages assigned to two vertebrate fossils collected southeast of The Dalles from the eastern part of the volcanic-debris facies, and to one collected west of Lyle from the sedimentary facies, Buwalda and Moore (1930, p. 17) determined a late Miocene or early Pliocene age for the Dalles Formation. By fossil leaves from two localities, a few hundred feet apart stratigraphically in the outer part of the volcanic-debris facies, Chaney (1944, p. 307) determined an early Pliocene age. From a few vertebrates collected near the lower of the two leaf localities of Chaney (a locality that is near the base of the formation), an early Pliocene age has been determined (A. J. Shotwell, written commun., 1965).

From vertebrate collections, Shotwell (1958, p. 276) determined the beds about 3 miles southeast of Arlington and the "McKay beds" (1956, p. 717) to be of Hemphillian, middle Pliocene, age.

The Pliocene age of Hogenson's fanglomerate (Hogenson, 1964, p. 25) was determined on the basis of two vertebrate fossils. Hogenson (1964, p. 34) also found that the deposition of the conglomerate took place between the initial and the main uplifts of the basalt of the Columbia River Group in the Blue Mountains anticline.

Two potassium-argon age determinations on the lava flow in the sedimentary facies of the Dalles Formation between Fifteenmile Creek and the Deschutes River gave 10.6 million years (Geochron R0420) and 15.2 m.y. (Geochron R0419), a spread that, alone, renders the effort indeterminate.

CONCLUSIONS

The Dalles Formation is a composite of two facies, at least partly contemporaneous. The volcanic-debris facies forms the southwestern and thicker part of the formation, and the sedimentary facies forms the eastern and northern thinner part. The sedimentary facies represents a true part of the Dalles Formation east to Rufus, Oreg. It is believed to continue several tens of miles farther east. If these reconnaissance continuations are correct, either the middle Pliocene strata to the east overlap the Dalles Formation, or the assigned early Pliocene age of the Dalles Formation is too old. Lithologic similarity, stratigraphic position, and paleontologic data now indicate an early and middle(?) Pliocene age for the Dalles Formation.

The apparent continuation eastward of the sedimentary facies of the Dalles Formation may necessitate some restriction of that name or a revision of the present names Arlington Lake beds, Arlington beds, lower Shutler Formation, and Pliocene fanglomerate, as well as a definition of "McKay beds."

No materials from the northern Rocky Mountains are known to have been laid down in the ancestral drainageway now forming part of the present Dalles-Umatilla syncline during the time of the deposition of the sedimentary deposits that have been determined as of middle Pliocene age.

REFERENCES

Allison, I. S., 1933, New version of the Spokane flood: Geol. Soc. America Bull., v. 44, p. 675–722, 24 illus.

Birch, D. C., 1963, Ladd Creek mudflow: Geol. Soc. of the Oregon Country Geol. News Letter, v. 29, no. 4, p. 27, April.

Buwalda, J. P., and Moore, B. N., 1930, The Dalles and Hood River Formations and the Columbia River Gorge: Carnegie Inst. Washington Pub. 404, p. 11–26, 1 fig.

Chaney, R. W., 1944, The Dalles flora (Oregon), chap. 11 *of* Pliocene floras of California and Oregon: Carnegie Inst. Washington Pub. 553, Contr. Paleontology, p. 1–19, 285–322, illus. incl. index map.

Condon, Thomas, 1902, The two islands and what came of them: Portland, Oreg., J. K. Gill Co., 221 p.

Hodge, E. T., 1932, Geological map of north central Oregon: Oregon Univ. Pub. Supp. to Geology Series, v. 1, no. 5, 7 p., scale 1:250,000.

——— 1942, Geology of north central Oregon: Oregon State College Mon., Studies in Geology, no. 3, 76 p.

Hogenson, G. M., 1964, Geology and ground water of the Umatilla River basin, Oregon: U.S. Geol. Survey Water-Supply Paper 1620, 162 p., 16 illus.

Piper, A. M., 1932, Geology and ground-water resources of The Dalles region, Oregon: U.S. Geol. Survey Water-Supply Paper 659–B, p. 107–189, 12 illus., map.

Shotwell, J. A., 1956, Hemphillian mammalian assemblage from northeastern Oregon: Geol. Soc. America Bull., v. 67, p. 717–738, 7 figs.

——— 1958, Inter-community relationships in Hemphillian (mid-Pliocene) mammals [Oregon and Texas]: Ecology, v. 39, no. 2, p. 271–282, 13 figs.

PERMIAN-TRIASSIC BOUNDARY IN EASTERN UINTAH COUNTY, UTAH, AND WESTERN MOFFAT COUNTY, COLORADO

By ELMER M. SCHELL and ELLIS L. YOCHELSON,
Denver, Colo., Washington, D.C.

Abstract.—The Permian Park City Formation exposed along the south flank of the Uinta Mountains near the Utah-Colorado State line is redefined to include 25 to 67 feet of tawny beds at the top. Previously, these beds were included in the overlying Triassic Moenkopi Formation. The tawny beds consist mainly of silty limestone and dolomite but contain a cherty zone and a phosphatic-dolomite marker bed near the top. A limestone containing a Permian fauna underlies the marker bed. The tawny beds are correlated with the upper unit of the Franson Member of the Park City Formation in the Ashley Creek–Brush Creek area, north of Vernal, Utah.

The separation of the Permian Park City Formation and the Triassic Moenkopi Formation is difficult in northeastern Utah and northwestern Colorado owing to facies change. Kinney (1955, p. 53), in the Ashley Creek–Brush Creek area (figs. 1 and 2) and westward, used the top of the highest slabby, light-gray, cherty limestone or limy sandstone as the top bed of the Park City. In the Ashley Creek–Brush Creek area, the cherty limestone is overlain by as much as 25 feet of tawny beds that Kinney placed in the Moenkopi Formation of Triassic age. Between Brush Creek and the Colorado border as much as 67 feet of tawny beds overlying the cherty limestone was included in the Moenkopi Formation (Thomas and others, 1945; Untermann and Untermann, 1954, p. 101–102). The tawny beds include soft, light-gray, sparsely phosphatic limestone, dolomite, mudstone, chert, and a dolomite marker bed. Fossils collected from 5 to 10 feet below the marker bed by Schell and identified by Yochelson are indicative of Permian age. Therefore, the Park City is here redefined to include the tawny beds (fig. 3).

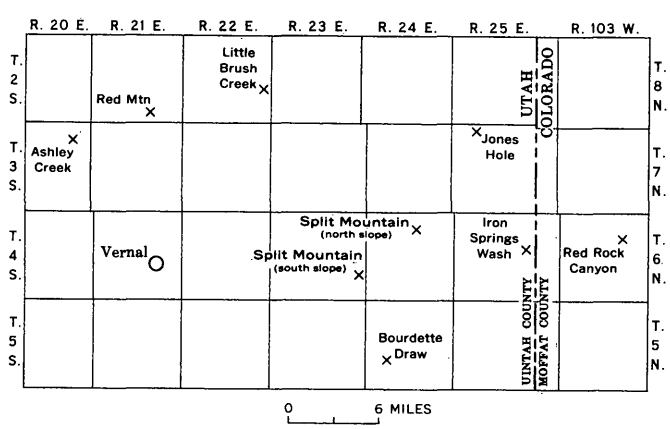

FIGURE 1.—Location of measured sections (×) of the Park City Formation in parts of Uintah County, Utah, and Moffat County, Colo.

CHARACTER AND AGE OF THE TAWNY BEDS

During 1964 and 1965 the redefined Park City Formation was mapped from Ashley Creek to the Split Mountain and Jones Hole areas, a linear distance of about 40 miles. Sections measured at several other localities in the eastern part of the Uinta Mountains in Colorado indicate that this is a mappable unit as far east as Cross Mountain in Colorado, 30 miles east of the Red Rock Canyon section.

The tawny beds of the Park City are 35 to 67 feet thick, east and southeast of Little Brush Creek in northeastern Utah and northwestern Colorado. Generally, these beds are poorly exposed. In the Split Mountain–Jones Hole area and eastward, the tawny beds are predominantly carbonate rocks—silty limestone and dolomite—and for the most part are only slightly argillaceous. A soft unit of argillaceous limestone interbedded with calcareous mudstone and siltstone, about 13 feet thick, is near the middle of the tawny beds. This unit at Split Mountain may be correlative with a zone about 25 feet thick in the Franson Member at Little Brush Creek. A zone of carbonate

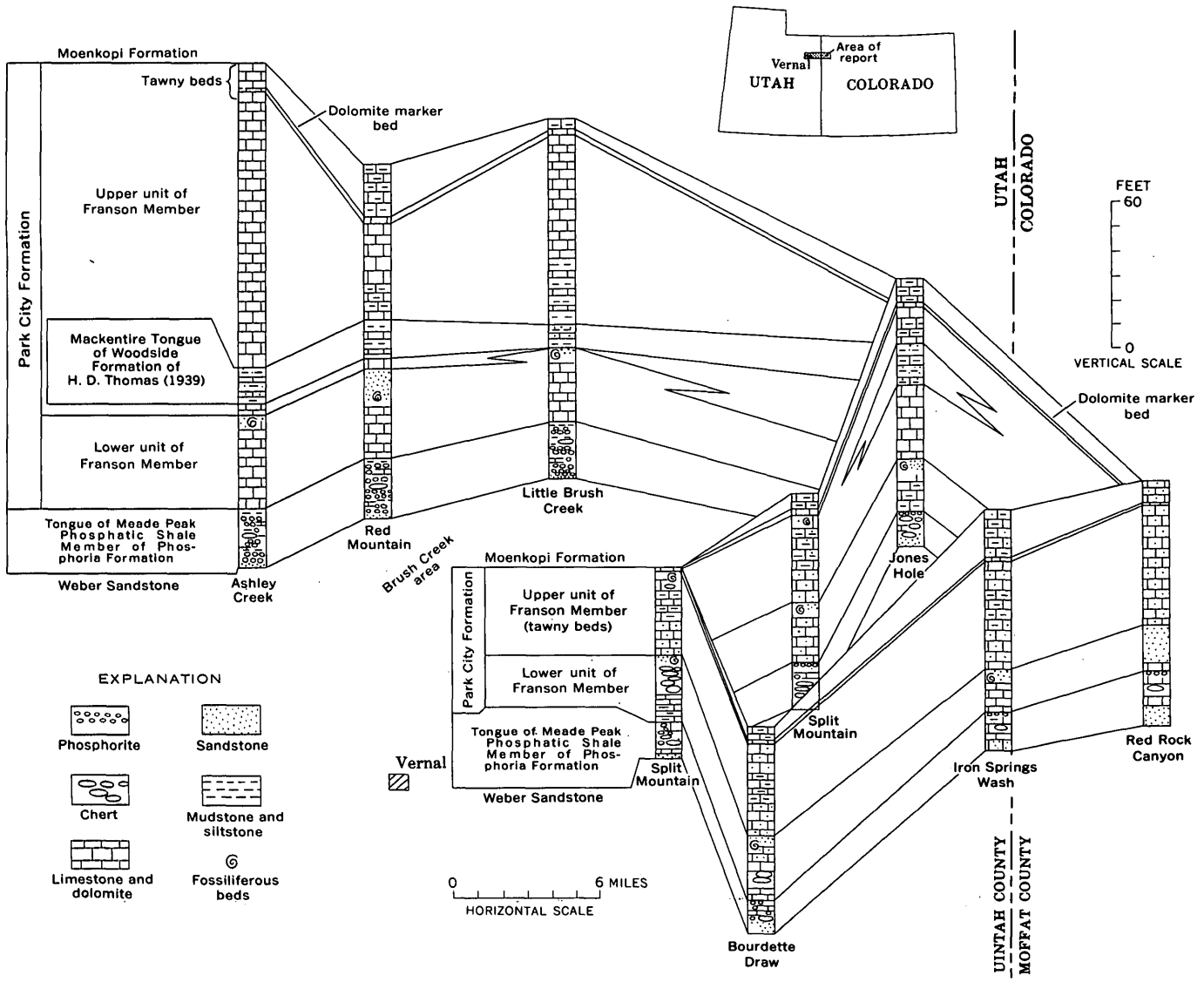

FIGURE 2.—Correlation diagram of the Park City Formation in eastern Uintah County, Utah, and western Moffat County, Colo.

rock about 4 feet thick, that contains thin chert beds, occurs in the upper part of the tawny beds in the Split Mountain area.

A marker bed as much as 4 feet thick overlies the cherty carbonate-rock zone; it consists of very fine grained hard ledge-forming dolomite or limestone. It is from 10 to 30 feet below the top of the tawny beds. This bed is shown on figure 2 as the dolomite marker bed. It contains phosphatic bioclastic debris, abundant fine to very coarse phosphorite pellets, glauconite, sand, silt, and sparse chert beds less than 1 inch thick. The marker bed has been traced as far west as about 1½ miles west of Ashley Creek; east of Red Rock Canyon it was noted in measured sections in the Skull Creek anticline, Section Ridge anticline, Cross Mountain, and Vermilion Creek areas. In western Colorado this marker bed is within 10 feet of the top of the tawny beds; at Red Mountain it is 23 feet below the top.

On the north and west slopes of Split Mountain the tawny beds contain a fossiliferous limestone unit that is 0.5 to 3.5 feet thick and 5 to 10 feet stratigraphically below the dolomite marker bed. A collection of silicified fossils (U.S. Geol. Survey collection 21603–PC) from this unit in the NW¼ sec. 11, T. 4 S., R. 23 E., Salt Lake meridian, was identified by Yochelson. The faunal list includes the following:

small ramose bryozoans (abundant), undet.
fenestrate bryozoans, undet.
Composita sp.
Beecheria cf. *B. bovidens* (Morton)
Spiriferina cf. *S. pulchra* (Meek) (abundant)
Polidevcia sp. indet.

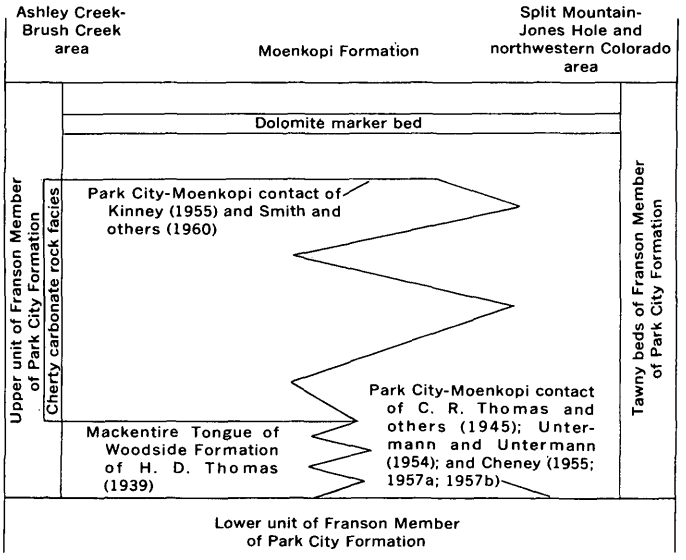

FIGURE 3.—Gereralized section of rocks in the upper part of the Park City Formation in eastern Uintah County, Utah, and western Moffat County, Colo.

?Permophorous sp. indet.
?parallelodont pelecypod, indet.
Myalina (*Myalinella*) cf. *M.* (*M.*) *meeki* Dunbar
Schizodus sp. indet.
Aviculopecten sp. indet.
bellerophontacean gastropod, indet.
?pleurotomariacean gastropod, indet.
Naticopsis (*Naticopsis*) sp. indet.
murchisoniid gastropod, indet.
nautiloid cephalopod, undet.
ammonoid cephalopod, undet.
ammonoid fragment cf. *Pseudogastrioceras*
spindle-shaped borings in shells, undet.

Yochelson believes that this collection indicates a Permian age. In the abundance of bryozoans and *Spiriferina* the collection is similar to collections from near the top of Permian rocks at Tosi Creek, Wyo.

DISCUSSION OF THE PARK CITY FORMATION

In the Ashley Creek–Brush Creek area, the Park City Formation as now defined consists of three mappable units (fig. 2). In ascending order these units are: (1) about 25 feet of phosphorite, phosphatic mudstone, carbonate rock, and chert; (2) 30 to 35 feet of light-gray cherty limestone, sandstone, and dolomite; and (3) 85 to 145 feet of light-gray phosphatic cherty limestone, dolomite, mudstone, and chert, and reddish-brown and grayish-orange limestone, siltstone, and sandstone. The upper 25 feet of unit 3 comprises the tawny beds. Following the nomenclature proposed by McKelvey and others (1959, p. 9), unit 1 should be termed a tongue of the Meade Peak Phosphatic Shale Member of the Phosphoria Formation. Unit 2 forms the lower part of the Franson Member of the Park City Formation, and unit 3, including the tawny beds, forms the upper part of the Franson Member.

J. Stewart Williams (1939, p. 91–93, 98) proposed the name "Mackentire 'red beds' tongue" of the Phosphoria Formation for rocks included in unit 3 and an overlying 75 feet of siltstone. McKelvey and others (1959) assigned these light-gray carbonate rocks of unit 3 to the Franson Member of the Park City Formation and the tawny beds and the upper 75 feet of siltstone to the lower part of the Woodside Formation (now known as the Moenkopi Formation) in the Ashley Creek area. H. D. Thomas (1939) and Thomas and Krueger (1946, p. 1263–1270) considered the reddish-brown and grayish-orange rocks to be the Mackentire Tongue of the Woodside Formation (fig. 3). Kinney (1955, p. 170) and Smith and others (1960) divided the Park City Formation into 3 units but included the upper 25 feet of the tawny beds (here redefined as part of the upper unit of the Franson Member) in the Moenkopi Formation (fig. 3).

The Park City Formation is concealed by Tertiary deposits for about 10 miles east and southeast of Little Brush Creek. Where it is exposed in the Split Mountain–Jones Hole area (fig. 2) the Park City Formation differs considerably from its western counterpart. The rocks immediately above the Permian and Pennsylvanian Weber Sandstone are light-gray, cherty, sandy, partly phosphatic carbonate rock, sandstone, chert, mudstone, and thin phosphorite beds. These rocks are 33 to 46 feet thick and are equivalent to the tongue of the Meade Peak Phosphatic Shale Member of the Phosphoria Formation and the lower unit of the Franson Member of the Park City Formation. Eastward from Little Brush Creek, the Meade Peak changes laterally into a predominantly cherty carbonate-rock facies containing a few thin phosphorite beds in the Split Mountain–Jones Hole area. McKelvey and others (1959, p. 23) found a similar west-to-east change in equivalent strata in central Wyoming.

The top of the lower unit of the Franson Member in the Ashley Creek–Brush Creek area is well marked by a sandstone, conglomeratic and fossiliferous in places, which is underlain by fossiliferous sandy limestone beds. These beds are recognizable in the Split Mountain–Jones Hole area and as far east as Cross Mountain in northwestern Colorado.

In the Split Mountain–Jones Hole area, and eastward, the lower unit of the Franson Member is overlain by the tawny beds, which are 35 to 67 feet thick

and consist chiefly of argillaceous silty limestone and dolomite with sparse thinly bedded chert layers; these are equivalent to the upper unit of the Franson Member. The tawny beds also include the reddish-brown beds of the Mackentire Tongue in the Jones Hole area, but these reddish-brown beds are absent at Split Mountain and farther to the east. The contact with the overlying Moenkopi Formation is placed at the top of these tawny beds.

The basal beds of the overlying Moenkopi Formation generally are interbedded reddish-brown and yellowish-gray calcareous siltstones which, because of the distinctive lithologic break and their mappable boundary, are distinct from the underlying tawny beds. Ripple marks and gypsum veinlets are common in the Moenkopi but are absent in the tawny beds of the Park City Formation. The contact of the Park City and Moenkopi Formations appears to be conformable, and fossils have not been found in the basal Moenkopi beds Therefore, it is possible that part of the basal Moenkopi as here redefined is also Permian in age.

In the Split Mountain area, the top of the Park City Formation has been picked at various places by previous workers (fig. 3). Schultz (1918, p. 47–54) measured the Park City Formation near Red Mountain and placed the boundary between the Park City and the Triassic rocks at the base of the continuous red-shale series. He included about 350 feet that he called tawny beds in the Park City Formation. This boundary is seemingly not mappable, as the red color is not persistent and rises stratigraphically eastward. Also, most of these tawny beds are lithologically more similar to the Moenkopi than to the Park City Formation. Thomas and others (1945) measured 69 feet of Park City at Split Mountain, but they did not include the tawny beds referred by Schultz to the Park City. Thomas and Krueger (1946, p. 1268–1269) suggested that the lower part of the tawny beds is Permian in age, but they did not state the evidence for this conclusion. Untermann and Untermann (1954, p. 101–102, 117, 125; oral commun., 1964) measured several Park City sections in the Split Mountain–Jones Hole area and included the tawny beds with the overlying Moenkopi Formation. Cheney (1955, fig. 3; 1957a, fig. 1; 1957b, p. 24) measured 39 feet of the lower unit of the Franson Member of the Park City Formation at Split Mountain and stated that the upper unit of the Franson Member in the Little Brush Creek area presumably grades into the lower beds of the Moenkopi Formation at Split Mountain. J. Steele Williams (*in* McKelvey and others, 1959, p. 39) stated that the lower part of the overlying formation at the east end of the Uinta Mountains is of Permian age; however, McKelvey and others (1959) included the tawny beds in the Woodside Formation of H. D. Thomas (1939) (now considered part of the Moenkopi Formation).

CONCLUSIONS

We conclude that the tawny beds of westernmost Colorado and easternmost Utah are correlatives of the upper unit of the Franson Member farther to the west in the Uinta region (figs. 2 and 3). In western Wyoming, Sheldon (1963, p. 124) informally divided the Franson Member into a lower and an upper cycle; these are not to be equated with the informal lower and upper units used here. In many parts of the western phosphate field, the younger Retort Phosphatic Shale Member of the Phosphoria Formation is overlain by the Ervay Carbonate Rock Member of the Park City Formation (McKelvey and others, 1959). In the Uinta Mountains and eastward, the Retort Member is absent and the Franson Member includes all limestone of Permian age above the tongue of the Meade Peak Phosphatic Shale Member of the Phosphoria Formation. It is possible, though not yet conclusively demonstrable from the available stratigraphic and fossil evidence, that the upper unit of the Franson Member as used here may be partly or entirely equivalent to the Ervay Member occurring to the northwest.

REFERENCES

Cheney, T. M., 1955, Facies and oil possibilities of the Phosphoria formation and equivalent strata in eastern Utah and southwestern Wyoming, *in* Wyoming Geol. Assoc. Guidebook 10th Ann. Field Conf., Green River basin, 1955: p. 65–67.

——— 1957a, Phosphate deposits in the Uinta Mountains, Utah, *in* Intermountain Assoc. Petroleum Geologists Guidebook 8th Ann. Field Conf., Uinta Basin, 1957: p. 144–148.

——— 1957b, Phosphate in Utah and an analysis of the stratigraphy of the Park City and the Phosphoria Formations, Utah—a preliminary report: Utah Geol. and Mineralog. Survey Bull. 59, 54 p.

Kinney, D. M., 1955, Geology of the Uinta River–Brush Creek area, Duchesne and Uintah Counties, Utah: U.S. Geol. Survey Bull. 1007, 185 p.

McKelvey, V. E., and others, 1959, The Phosphoria, Park City, and Shedhorn Formations in the western phosphate field: U.S. Geol. Survey Prof. Paper 313–A, p. 1–47.

Schultz, A. R., 1918, A geologic reconnaissance of the Uinta Mountains, northern Utah, with special reference to phosphate: U.S. Geol. Survey Bull. 690–C, p. 31–94.

Sheldon, R. P., 1963, Physical stratigraphy and mineral resources of Permian rocks in western Wyoming: U.S. Geol. Survey Prof. Paper 313–B, p. 49–273.

Smith, Larry, Kinney, D. M., and Rominger, J. F., 1960, Geology of the Park City formation in the Ashley Creek–Brush Creek area, Uintah County, Utah: U.S. Geol. Survey open-file report, 1 map.

Thomas, C. R., McCann, F. T., and Raman, N. D., 1945, Mesozoic

and Paleozoic stratigraphy of northwestern Colorado and northeastern Utah: U.S. Geol. Survey Oil and Gas Inv. (Prelim.) Chart 16.

Thomas, H. D., 1939, Comment on "Park City" beds on southwest flank of Uinta Mountains: Am. Assoc. Petroleum Geologists Bull., v. 23, no. 8, p. 1249–1250.

Thomas, H. D., and Krueger, M. L., 1946, Late Paleozoic and early Mesozoic stratigraphy of the Uinta Mountains, Utah: Am. Assoc. Petroleum Geologists Bull., v. 30, no. 8, pt. 1, p. 1255–1293.

Untermann, G. E., and Untermann, B. R., 1954, Geology of Dinosaur National Monument and vicinity, Utah-Colorado: Utah Geol. and Mineralog. Survey Bull. 42, 228 p.

Williams, J. Stewart, 1939, "Park City" beds on southwest flank of Uinta Mountains, Utah: Am. Assoc. Petroleum Geologists Bull., v. 23, no. 1, p. 82–100.

ERECT PLANTS IN THE EARLY SILURIAN OF MAINE

By JAMES M. SCHOPF, ELY MENCHER,[1] ARTHUR J. BOUCOT,[2] and HENRY N. ANDREWS,[3]
Columbus, Ohio, Cambridge, Mass., Pasadena, Calif., Storrs, Conn.

Abstract.—Small, erect plant axes, referred to *Eohostimella* Schopf, n. gen., occur in a Lower Silurian deposit in northern Maine. Surfaces are spinulate, and the cortical outer layer is persistent and generally coalified. This outer layer evidently consists of mechanical tissue to account for the erect posture of the axes. No trace of vascular tissue has been observed in a large suite of material, suggesting that any possible conducting strand was delicate and simple. These fossils may represent a primitive type of land vegetation in which the mechanical function of cortical tissue was more advanced than the conductive, or vascular, specialization. Other plant remains in the deposit are not erect and probably represent foliose algae.

In recent years a persistent search has been carried on for pre-Devonian plants that represent ancestral vascular plants or plants from which vascular plants may have arisen (see Obrhel, 1959, 1962; Roselt, 1962; Leclercq, 1956; Senkevich, 1959, 1963). At the same time, further investigation has shown that fairly advanced types of vascular plants, formerly regarded as Late Silurian (Lang and Cookson, 1930, 1935; Cookson, 1935), probably are in reality assignable to the Early Devonian (Jaeger, 1962, 1964; Berry, 1964). The diversity of the Early Devonian flora has emphasized the possibility that psilophytes, commonly regarded as representing primitive land plants, may not be truly primitive. Their simple structures can also be explained as a result of reduction and swamp xerophytism or, at most, simply as persistent little-changed derivatives from those of considerably earlier forms that first lived on land. This latter alternative was discussed by Scott (1924, p. 192, 206–207, 223), Eames (1936, p. 327–329), Berry (1945, p. 46), and, more recently, by Leclercq (1954). A truly primitive land flora is not well known, but it seems to be clearly established that the best known examples of psilophytes occur too late in the geologic record to have been in direct ancestral alinement with any vascular groups other than modern Psilotales.

Along with these considerations of phyletic botany are those regarding the more accurate and effective use of early plant fossils as indexes to geologic time and theoretical discussion concerning the monophyletic or the polyphyletic origin of vascular plants. Vascular plants are generally presumed to be members of the primitive terrestrial flora, but detailed information is lacking. Possibly one should inquire whether primitive transmigrants were actually vascular, or whether xylem originated as a conductive specialization that developed a little later. Regardless of the answer to this question, there is considerable probability that a transitional series of transmigrant forms will eventually be discovered. One possible representative of an early transmigrant form is described in this paper.

Field work for this study has been supported by National Science Foundation research grant GP–1547 to Massachusetts Institute of Technology under direction of Ely Mencher, and by N.S.F. research grant B–16793 to Henry N. Andrews of the University of Connecticut. New taxa are ascribed solely to J. M. Schopf in order to assign his primary responsibility for laboratory study of the plant material. A. J. Boucot is principally responsible for age determination.

GEOLOGIC OCCURRENCE

In August 1964, Stanley A. Heath and William A. Brown, students at the Massachusetts Institute of Technology, mapping in northern Maine under the direction of Mencher, discovered carbonaceous plant remains in thin, laminated, coarse siltstone beds, interbedded with thicker bedded coarse and conglomeratic sandstones containing marine invertebrate fossils. These original plant collections were submitted to the

[1] Massachusetts Institute of Technology.
[2] California Institute of Technology.
[3] University of Connecticut.

senior author for examination, and at the same time examples of the invertebrates were examined by Boucot. Lithologically the coarse sandstones are typical of the Frenchville Formation (Boucot and others, 1964, p. 31–33) of northern Aroostook County, Maine, and appear to bear the same Early Silurian (late Llandovery, Zone C_4–C_5) fauna as found in the type area at the Frenchville Church (now destroyed) 5 miles northeast of the town of Ashland.

The fossil locality is in a railroad cut on the main line of the Bangor and Aroostook Railroad 2.1 miles north of the station at Stockholm, Aroostook County, Maine (fig. 1). Both the plant and invertebrate fossils come from the east side of the cut. At this place the Frenchville beds are exposed in a low anticlinal flexure, the axis of which strikes N. 30° to N. 35° E.

The plant fossils (fig. 2) have been found near the axis of the fold. Two distinct plant-bearing beds are present, separated from each other by about 1.5 feet of sandstone. The lower bed, 2 to 6 inches thick, has yielded the majority of the specimens described below as *Eohostimella*; the upper bed, which varies from a thin parting at the fold axis to a layer about 7 inches thick on the south flank, contains the foliose algal(?) material, although *Eohostimella* cross sections are also present. The invertebrate-bearing conglomeratic sandstone is seen best near the south end of the cut and lies approximately 15 feet stratigraphically above the upper plant layer.

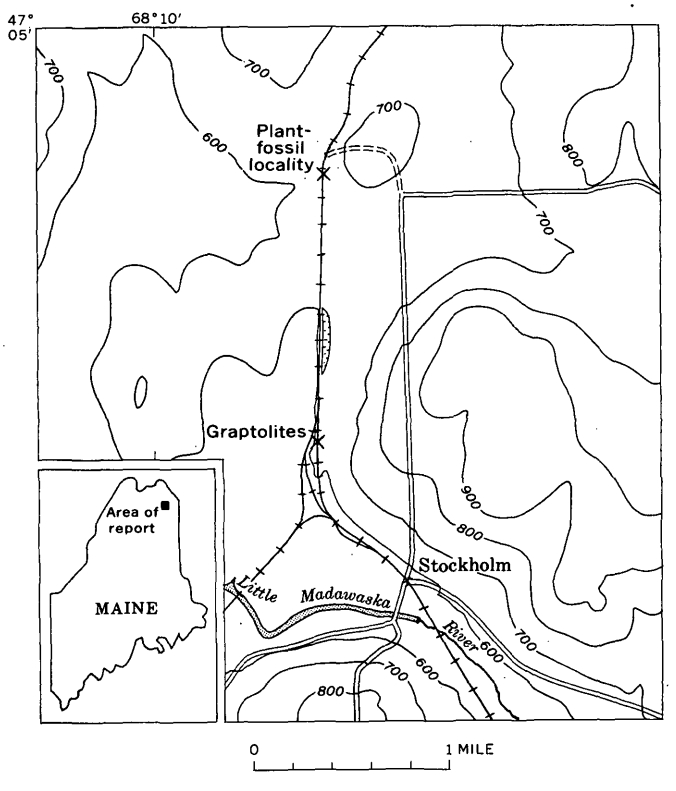

FIGURE 1.—Map showing location of plant fossils in the report area (from USGS 15-minute Stockholm quadrangle, Maine).

The following invertebrate fossils have been identified by Boucot from the conglomeratic sandstone: orthotetacids, *Atrypa?* sp., *Pentamerus?* sp., rostrospiroid, *Eocoelia* sp. (coarse-ribbed), "*Dolerorthis*" *flabellites*, rhynchonellids, *Stricklandia lens* cf. *ultima*, *Cyrtia* sp., *Plectodonta* sp., *Resserella* sp., *Leptaena* "*rhomboidalis*", *Paleocyclus?* sp., *Favosites*, unidentified brachiopods, and a poleumitid gastropod. This fauna suggests an age of about C_3 to C_5 in the upper Llandovery Stage of the Early Silurian.

The occurrence of a coarse-ribbed form of *Eocoelia* is of primary importance. This form cannot be identified specifically, owing to the fragmentary nature of the material, but it is certainly a more advanced type than *Eocoelia hemisphaerica* and has not nearly reached the stage of development of *Eocoelia sulcata*. The latter two forms occur respectively in the C_1–C_2 and C_6–Wenlock portions of the Llandovery and Wenlock.

The occurrence of *Stricklandia lens* cf. *ultima* is consistent with a C_4–C_5 age or possibly even a C_3 age. However, it should be pointed out that all these specimens are relatively fragmentary and were badly broken up prior to final deposition. Fragmentary specimens of *Costistricklandia* can easily be confused with *Stricklandia lens* cf. *ultima*. If the coral listed as *Paleocyclus?* is, indeed, truly a *Paleocyclus*, it could be taken to suggest that this collection contains specimens that were derived partly by reworking from beds of C_3 to C_6 to early Wenlock age, since true *Paleocyclus*, as well as *Costistricklandia*, is restricted to beds of C_6 to early Wenlock age in this part of North America. However, at the present time, it seems most likely that the beds belong in the C_3 to C_5 range of age in the Early Silurian and, in any event, cannot be much younger.

Further confirmation of the Llandovery age of the strata is found in beds carrying *Monograptus marri* Perner, as determined by W. B. N. Berry (written commun. to Mencher Dec. 22, 1964), which occur in another railroad cut 1.4 miles to the south of the plant-fossil locality (see fig. 1). Dr. Berry states that *M. marri* is restricted in its range to the interval of Elles and Wood's Zones 22 to 25 of the late Llandovery, which correspond to the interval C_3–C_6 in terms of brachiopod stages. As all outcrops between Stockholm, Maine, and the plant locality dip steeply to the southeast, the graptolite beds are estimated to overlie the plant beds by about 3,000 feet.

The known distribution of the Frenchville Formation, a near-shore deposit, has been summarized by

Boucot and others (1964, p. 70–72), and the present locality falls within that area. Since it is inferred that a major landmass lay immediately to the west of this region, the occurrence of interbedded plant-bearing layers is consistent with the regional setting.

COLLECTIONS

In June 1965, a more thorough search for better preserved plant material was carried out by Schopf and Andrews and members of the M.I.T. group, with the assistance and very generous cooperation of the employees and administration of the Bangor and Aroostook Railroad Co., Mr. W. Jerome Strout, President, and Mr. Palmer H. Swales, Chief Engineer. At that time, overburden and covering rock were removed by bulldozer from an area sufficient to provide more than 200 specimens. Results, therefore, are based on a reasonable sampling of the material provided by this locality.

Scattered examples of similar fossils (fig. 2, *l*) also have been recently discovered in the Frenchville Formation at a new locality about a mile east of Ashland Maine, by David C. Roy, also engaged in the M.I.T. project in northern Maine. This locality is about 30 miles southwest of the Stockholm occurrence and suggests that the plant-bearing facies, although probably intermittent, may still have been persistent.

Some of the fossils appear to be advanced algal types, but others have an erect habit, are dichotomously branching, and have a minutely spiny cortex very suggestive of subaerial types of plants. It is tempting to think of the erect plant fossils as representatives of a primitively emergent vegetation. The erect mode of growth and general habit of these forms is suggestive of the Psilophytes. Whether or not the erect forms belong to the Psilopsida must remain undecided until some fertile structures are discovered. There is no evidence that vascular tissues were differentiated; if present, the conductive tissues certainly were impersistent.

The plants are described as a new genus for which the reference name of *Eohostimella* is proposed. For the most part, the plants seem to be erect. They consist of tubular axes 1 to 2 millimeters in diameter with a thin, coaly, cortical zone bearing minute spinules, and internal sedimentary filling. Axes of otherwise similar appearance are associated in the deposit parallel or inclined to the bedding and show regular dichotomy at a narrow angle. If these remains had been present in Devonian or Upper Silurian, rather than in Lower Silurian deposits, they would probably have been assigned without hesitation to a spinose small species of *Hostimella*. Their unusual stratigraphic position seems to preclude this determination and has prompted more critical study. In any event, these plants show a vegetative habit that seems to correspond with that of psilophytes, and they probably are old enough geologically that they could represent ancestors of the different phyla of land plants (see recent discussion by Banks, 1965).

The siltstone in which these forms occur lacks other recognizable fossils and is thinly laminated and carbonaceous (fig. 2, *a* and *b*). Larger carbonaceous fragments are hard and fragile and have yielded no histologic information by maceration. The coaly fragments appear to be anthracitic. The finer texture of the siltstone matrix contrasts with that of the normal Frenchville lithology. The lithology and fossil axes in the parting are suggestive of original deposition in a near-shore environment that was temporarily sheltered from the wave action and admixture with coarser sediment. The erect plant axes penetrate bedding planes and seem to be in situ. A temporarily sheltered flooded coastal flat which was slowly accumulating winnowed sediment would seem a plausible site for preservation of traces of incipient land vegetation.

DESCRIPTION OF FOSSILS

Eohostimella Schopf, n. gen.

Description.—Small plants, axes 1–2mm in diameter, of creeping and ascendant or erect habit, horizontal axes dichotomously branching at an angle less than 45°. Outer cortex persistent, stereomic, commonly represented by a coalified crust 100–300 microns thick; dermal surfaces roughened by minute and spinose appendages irregularly arranged. Mode of reproduction and internal anatomy unknown.

Eohostimella heathana Schopf, n. sp.

Figure 2, *c–r*

Description as given for the genus. Holotype specimen illustrated in figure 2, *p–r*. The species is named for Stanley A. Heath of the Geology Department, Massachusetts Institute of Technology, who made the initial discovery of fossil plants at this locality.

Discussion.—The suggestion that *Eohostimella* may represent an incipient type of land plant depends on the nature of the persistent outer cortex and on its erect habit. Both features are uncommon for even higher algae. General agreement with *Hostimella*-type of axes, commonly noted in Devonian terrigenous deposits and also regarded as a generalized representative of primitive land plants, is noteworthy. *Hostimella* axes, however, generally are larger, have a

smoother surface and probably are vascular. The occurrence of *E. heathana* in Lower Silurian deposits, before vascular plants are known to have been present, suggests that the lack of vascular preservation in *Eohostimella* may not be wholly accidental.

Except for lack of evidence of vascular tissues, axes of *Eohostimella* correspond fairly well with some of the minute shoots sometimes associated with *Psilophyton*. *Psilophyton* represents a relatively primitive type of vascular plant, although not all fossils referred to the genus bear any more evidence of vascular tissue than these of *Eohostimella* in which no trace is preserved. One might suggest a close alliance between *Eohostimella* and some of the *Psilophyton* varieties, particularly with *P. (?) hedei* Halle from the Late Silurian (Ludlow) on the island of Gotland (see Halle, 1920). The original specimen on which this species is based was reexamined by Andrews in 1964. As Halle points out, one cannot be absolutely sure that *P. (?) hedei* was a vascular plant. Halle's species is no larger than *E. heathana*, but it has longer, more regular, spiny emergences, and some of the emergences can be followed within the axis for 2 or 3 mm. Although the spinules and spines of *Eohostimella* invite comparison with longer and more prominent glandular spines of *Psilophyton*, they are sporadic and many are much shorter. Few of the spinules are as long as 0.3 mm (fig. 2, *d*, *i*, and *r*, and other photographs). The axes of *Eohostimella* show much less regularity of outer surfaces than one associates with either *Hostimella* or *Psilophyton*.

If *Eohostimella* from the Stockholm, Maine, locality actually represents a group of incipient land plants, the age relationship of primitive land plants would assume more logical order. Possibly *Eohostimella* is old enough to occupy an ancestral position for both *Baragwanathia* and *Psilophyton*, both of which should now be regarded as contemporary members of Early Devonian assemblages.[4] Although *Baragwanathia* is much larger and has a central woody cylinder, like *Psilophyton* and *Eohostimella*, it depended on its thick specialized outer cortex for mechanical support.

In view of the consistent coaly preservation of the outer cortex in *Eohostimella*, we may at least conclude that any central conductive strand was less durable than cortical tissues. The likelihood is that a stereomic outer layer represents a more primitive (and more efficient) type of mechanical support than any vascular strand whose initial function was specifically related to diffusion control and conduction. The functions of support and of conduction probably were served by

[4] The best known psilophytes from Rhynie, Aberdeenshire, Scotland, also are now regarded as probably Early Devonian (Westoll, 1951). The Rhynie Chert beds are strongly inclined and evidently were affected by Caledonian (? = Acadian) folding. Although some Middle Devonian plant beds are affected by similar folding—the "flat-lying" beds with Givetian-age plant fossils near Presque Isle, Maine (Schopf, 1964), are "flat" only because they are so near the center of a structural basin (see map by Boucot and others, 1964)—the deformation in different places no doubt extended over a considerable interval. Lacking other significant evidence, beds that are folded, as at Rhynie, are more likely to be somewhat older.

FIGURE 2.—Fossils of erect plants from the Lower Silurian of Maine. All specimens, except that shown in *l*, are from the Frenchville Formation at a rock cut 2.1 miles north of Stockholm, Aroostook County, Maine, along the Bangor and Aroostook Railroad. Massachusetts Institute of Technology locality SH–124.

a. Thinly laminated, carbonaceous coarse siltstone (× 1). Surface prepared by smoothing and etching in HF. [negative 2475 b]

b. Surface section, HF etched, showing texture of sediment enclosing a compressed carbonaceous structure indicative of an unidentified plant fossil (× 50). Ultropak photo (incident light) corresponding to one of the larger black specks on the surface illustrated at natural size in *a*. [neg. 2475–32]

c. Cross section of erect axis (× 5) with fine-textured sedimentary filling. Surrounding fracture surface is nearly horizontal, but it crosses a bedding plane and shows both coarse and fine texture of adjacent beds. Coarse dark granules are carbonaceous. Specimen cleaned with hot HCl, surface etched in HF. [neg. 2309]

d. Cross section of erect axis (× 5) showing three spinose appendages. The black circle represents coalified cortical tissues; sediment occurs inside. Natural horizontal fracture surface cleaned with hot HCl. [neg. 2311]

e. Cross section of erect axis (× 5), coaly cortex fragmented. Specimen cleaned with hot HCl, surface etched in HF. [neg. 2308]

f, *g*. Cross sections of erect axes (× 5) showing variation in cortical preservation. Preparation as above. [negs. 2305, 2301]

h. Oblique cross section of an erect axis (× 5) that intersects bedding at a steep angle. Preparation as above. [neg. 2304]

i. Cross section of erect axis (× 5) showing coalified cortical structures, bottom coarser part of bedding shown on the right. Specimen cleaned with hot HCl, surface etched in HF. [neg. 2302]

j, *k*. Cross sections of erect axes (× 5) as exposed on bedding planes, showing varying degrees of preservation of coalified cortex. Preparation as above. [neg. 2307, 2303]

l. Obliquely vertical axis (× 4) in fine sandy matrix. Specimen obtained from a different locality (DR 815, about 1 mile east of Ashland). Note rugose outer surface of thin coaly layer and the fine silt filling inside. Cleaned with hot HCl. [neg. 2488]

m. Oblique cross section of erect axis (× 5) which intersects bedding at an angle. Preparation as above. [neg. 2310]

n, *o*. As above, but showing cortical thickenings (× 5) which may be related to branching. [negs. 2306, 2300]

p. Counterpart of specimen (× 1.8) shown in *q* photographed without chemical treatment; surfaces dark brown. [neg. 2267]

q, *r*. Segment of subhorizontal axis (× 1.8; × 5) showing branching, exposed along a bedding plane. Note small spinose appendages and rugose surface best shown in *r*. Axis "plunges" below the exposed surface at the bottom of the pictures. Surface cleaned with hot HCl and etched in HF. Note that texture of matrix appears much finer than in *p* [negs. 2267, 2312]

s. Coherent film of carbonaceous material (× 4); granulose texture probably induced by compression in silty matrix. Similar flakes are common along some bedding planes and suggest debris from thallose algae. [neg. 2487]

t, *u*. Part and counterpart of a curved "frondose" algal tip (× 1.5) from which the axis appears to be lacking. Surface cleaned with hot HCl. [neg. 2541]

v. Association of laminar fragments with thick axes of *Taeniocrada* type (× 0.8). Thin carbonaceous films are detectable on most fragments, but no suggestion of cuticle or vascular tissues has been noted. [neg. 2266]

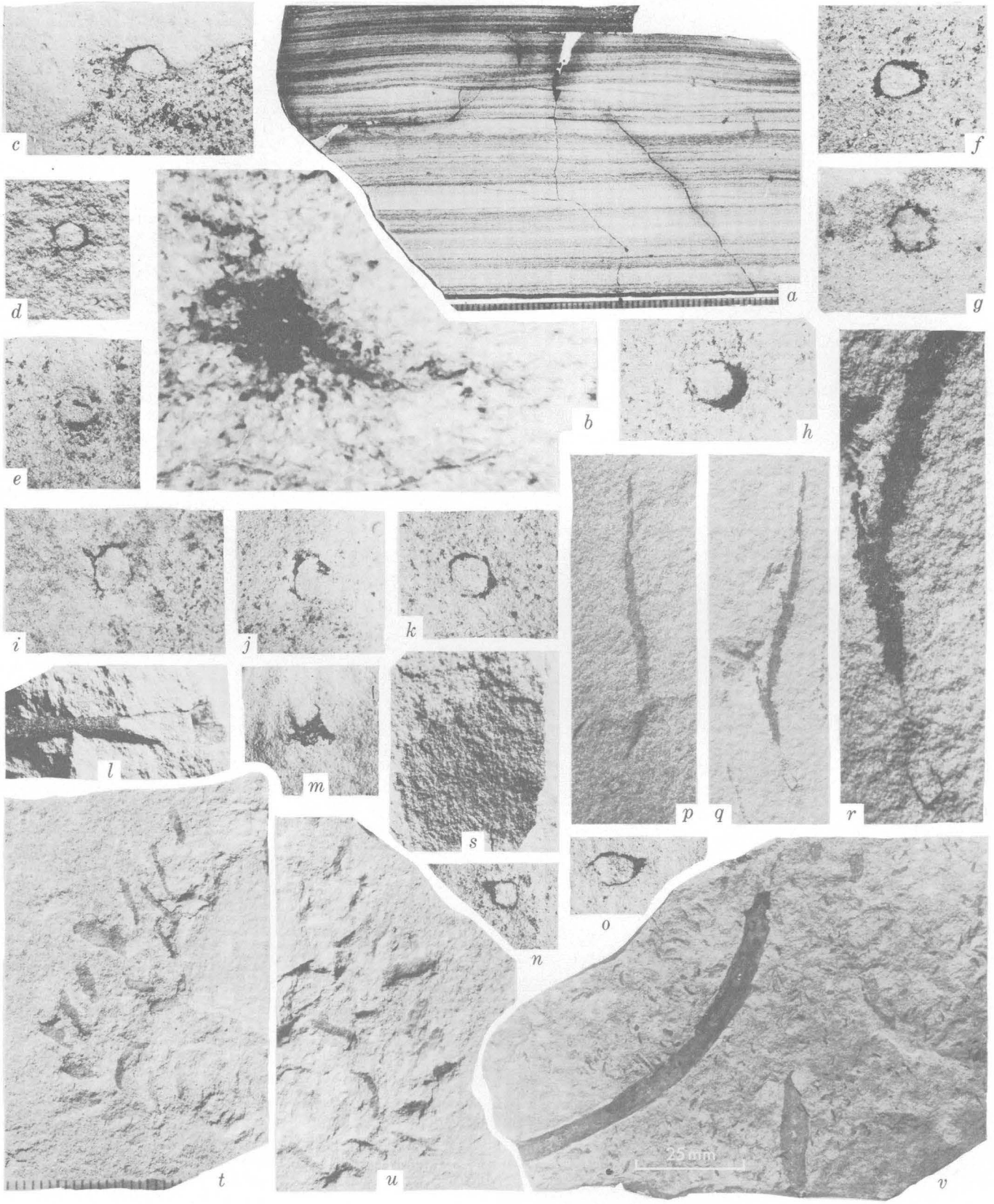
c
a
f
d
g
b
h
e
i
j
k
p
q
r
l
m
s
o
n
t
u
25 mm
v

entirely different tissue systems and adaptations in the really primitive transmigrants to the land.

Foliose(?) algae

Figure 2, *s–v*

Larger and more obviously plantlike fossils occur in the upper of the two silty, carbonaceous layers. They are normally arranged parallel to the bedding and show axes as much as 8 cm long and 8 mm wide, with laminar appendages 1 to 2 mm wide and as much as 8 mm long, spaced every 3 or 4 mm in either a pinnate or possibly lax spiral arrangement (see fig. 2, *t* and *u*). Coarser axes show fewer and less regular appendages. The best arrangements of appendages occur on smaller specimens in which axes are less evident or wanting. Yet the association is convincingly intimate so that we suspect that all represent the same type of plant, probably the same species.

When collected, the specimens were generally brown as a result of limonitic iron stain. After treatment with hot dilute HCl to remove the iron, surfaces of fossils commonly show a tenuous and sometimes perforate or exfoliated carbonaceous film. Occasionally a faint trace of striation may appear in the coaly film, but the matrix is silty and irregular enough to render questionable any detailed botanical interpretation. The coarse axes shown in figure 2, *v* resemble some of the smooth ambiguous Devonian forms which have commonly been assigned to *Taeniocrada*, but we are not aware of species of that genus which show small laminate appendages. Pinnate trace fossils, probably the tracks of ancient invertebrates, are fairly common (see Häntzschel, 1962, p. W177–W222), but the "pinnation" of trace fossils, is usually more closely spaced, and they lack the carbonaceous films. The carbonaceous films remaining on the surfaces of the Maine material indicate that these probably do represent remains of plants. Something of the nature of algae assigned to *Letterstedtia* (as illustrated by Fritsch, 1935) is suggested. They probably represent a relatively advanced foliose or possibly tubular parenchymatous type of alga which grew in shallow water along the seashore. It is very likely that the siltstone represents a slack-water estuarine deposit in which algal debris was occasionally preserved.

SUMMARY

Two plant types are represented in finer textured layers intercalated in marine sandstone of the Frenchville Formation assigned to the Llandovery Stage of the Early Silurian. Both layers with plant fossils appear to represent shallow-water, local deposits. The larger fossils may represent debris from parenchymatous algae deposited in near-shore beds during periods of fairly quiet, slack water. The smaller and more obscure type includes many axes which are erect and probably in the position in which they grew, possibly as land plants when temporary nonmarine conditions prevailed. They resemble some of the primitive types of land plants chiefly known from Devonian deposits. However, no trace of a conducting strand characteristic of Devonian land plants is preserved. Whether or not these plants had advanced to an evolutionary stage beyond range of permissible reference to algae, they apparently possessed a stereomic outer cortex which supported them in an erect position. In these respects, at least, the fossils resemble land plants more than they do algae. Development of erect axes with cortical stereomic tissue suggests a type of organization essential to growth in a subaerial environment.

REFERENCES

Banks, H. J., 1965, Some recent additions to the knowledge of the early land flora: Phytomorphology, v. 15, no. 3, p. 235–245, 1 table.

Berry, E. W., 1945, The beginnings and history of land plants: Johns Hopkins Univ. Studies in Geology, no. 14, p. 9–91, 12 figs.

Berry, W. B. N., 1964, Siluro-Devonian graptolites from Eildon, Victoria: Australian Jour. Sci., v. 26, no. 7, p. 223–224.

Boucot, A. J., Field, M. T., Fletcher, Raymond, Forbes, W. H., Naylor, R. S., and Pavlides, Louis, 1964, Reconnaissance bedrock geology of the Presque Isle quadrangle, Maine: Maine Geol. Survey Quad. Mapping Ser., no. 2, 123 p.

Cookson, I. C., 1935, On plant remains from the Silurian of Victoria, Australia, that extend and connect floras hitherto described: Royal Soc. London, Philos. Trans., ser. B, v. 225, p. 127–148.

Eames, A. J., 1936, Morphology of vascular plants: New York, McGraw Hill, 433 p.

Fritsch, F. E., 1935 (reprinted 1961), The structure and reproduction of the algae: New York, Cambridge Univ. Press, v. 1.

Halle, T. G., 1920, *Psilophyton (?) hedei* n. sp., probably a landplant, from the Silurian of Gotland: Svensk Bot. Tidsk., v. 14, no. 203, p. 258–260, 1 pl.

Häntzschel, Walter, 1962, Trace fossils and problematica, *in* Moore, R. C., and others, eds., Treatise on invertebrate paleontology, Pt. W. Miscellanea: Geol. Soc. America, Univ. Kansas Press, p. W177–W245, figs. 109–149.

Jaeger, Hermann, 1962, Das Alter der ältesten bekannten Landflanzen (*Baragwanathia*-Flora) in Australien auf Grund der begleitenden Graptolithen [The age of the oldest land plants (*Baragwanathia* flora) in Australia, based on associated graptolites]: Paläont. Zeitschr., v. 36, no. 1/2, p. 7.

——— 1964, *Monograptus hercynicus* in den Westsudeten und das Alter der Westsudeten-Hauptfaltung [*Monograptus hercynicus* in West Sudetenland and the age of the principal West Sudeten folding], pts. 1 and 2: Geologie, v. 13, no. 3, p. 249–277, 2 pls., 1 chart; v. 13, no. 4, p. 377–394.

Lang, W. H., and Cookson, I. C., 1930, Some fossil plants of Early Devonian type from the Walhalla Series, Victoria, Australia: Royal Soc. London, Philos. Trans., ser. B, v. 219, p. 133–163.

——— 1935, On a flora, including vascular land plants, associated with *Monograptus*, in rocks of Silurian age from Victoria, Australia: Royal Soc. London, Philos. Trans., ser. B, v. 224, p. 421–449.

Leclerq, Suzanne, 1954, Are the Psilophytales a starting or a resulting point?: Svensk Bot. Tidskr., v. 48, no. 2, p. 301–315, 6 figs.

——— 1956, Evidence of vascular plants in the Cambrian: Evolution, v. 10, no. 2, p. 109–114.

Obrhel, Jiri, 1959, Ein Landpflanzenfund im mittelböhmischen Ordovizium [A discovery of land plants in the Ordovician of central Bohemia]: Geologie, v. 8, no. 5, p. 535–541.

——— 1962, Die Flora der Pridoli-Schichten (Budnany-Stufe) des mittelböhmischen Silurs [The flora of the Pridoli beds (Budnany stage) of the Silurian in central Bohemia]: Geologie, v. 11, no. 1, p. 83–97, 2 pls., 1 fig., 5 charts.

Roselt, Gerhard, 1962, Über die ältesten Landpflanzen und eine mögliche Landpflanze aus dem Ludlow Sachsens [The oldest land plants and a possible land plant from the Ludlow of Saxony]: Geologie, v. 11, p. 320–333, 4 pls.

Schopf, J. M., 1964, Middle Devonian plant fossils from northern Maine, *in* Geological Survey Research 1964: U.S. Geol. Survey Prof. Paper 501–D, p. D43–D49, 2 figs.

Scott, D. H., 1924, Extinct plants and problems of evolution: London, MacMillan and Co., Ltd., 240 p., 63 figs.

Senkevich, M. A., 1959, Nakhoda primitivnogo plaunovogo v Silure Kazakhstana [Finding of primitive lycopod of Silurian of Kazakhstan]: Dokl. Akad. Nauk SSSR, v. 129, no. 1 [in Russian].

——— 1963, New finding of Upper Ordovician flora in Kazakhstan: Translation in Internat. Geol. Rev., v. 7, no. 3, p. 476–485, 2 pls., 3 figs.

Westoll, T. S., 1951, The vertebrate-bearing strata of Scotland: Internat. Geol. Congress, 18th, London, 1948, Proc. Sect. K, pt. 11, p. 5–21.

224-352 O—66——6

ASSOCIATED MEGASPORES AND MICROSPORES OF THE CRETACEOUS GENUS *ARIADNAESPORITES* POTONIÉ, 1956, EMEND.

By ROBERT H. TSCHUDY, Denver, Colo.

Abstract.—A sample from the Tuscaloosa Formation of Alabama yielded many specimens of a new species of *Ariadnaesporites* Potonié, 1956. Morphologically similar large and small spores, found in masses, were joined by intertwined long distal hairlike appendages. As these two spore types probably represent megaspores and microspores of the same species, they are both described under the name *Ariadnaesporites cristatus*, n. sp. The presence of leaflike extensions (here named acrolamellae) of the lips of the laesurae on the first-described member of the genus, *Ariadnaesporites ariadnae*, had not been noted previously. Emendation of the genus is presented.

Several hundred specimens of a distinctive megaspore, accompanied by thousands of microspores, have been recovered from a sample of dark-gray-brown organic clay from the Upper Cretaceous Tuscaloosa Formation. The sample is from an outcrop at an altitude of 510 feet, on the south side of U.S. Highway 78, NW¼ sec. 34 , T. 3 S., R. 15 W., Colbert County, Ala. The sample was collected by W. W. Olive, of the U.S. Geological Survey (his sample Ala–2), who stated (written commun., 1964) that it probably is from unit 4 described by Stephenson and Monroe (1940, p. 46). The locality of the sample has been designated as USGS paleobotanical loc. D3415.

The spores are characterized by three prominent leaflike outgrowths of the lips of the trilete suture, hereafter referred to as acrolamellae,[1] and by many long hairlike appendages, which are primarily confined to the distal part of the spore body. These spores represent a new species of the genus *Ariadnaesporites* Potonié, 1956.

The association of abundant disseminated large and small spores joined by intertwined distal hairlike appendages is unique. Such intimate association and the morphological similarity of the two spore types indicate that both belong to the same species.

Miner (1932) described and illustrated six specimens of an Upper Cretaceous megaspore from the east coast of Disko Island, Greenland, under the name *Selaginellites ariadnae*. He failed, however, to designate a holotype. Potonié (1956) recognized that the spores described by Miner were distinctly different from any known *Selaginella* spores and believed that the name *Selaginellites* should be used only for compressed plant remains; he therefore erected the new genus *Ariadnaesporites* to accommodate the distinctive spores. He chose as the lectotype the specimen shown on figure 1, *b* (from Miner, 1932, fig. 28). Neither Miner nor Potonié noted the leaflike extensions of the lips of the trilete suture, although this feature is visible on at least one of Miner's original photomicrographs (fig. 1, *f*, of this report). Because of this oversight, emendation of the genus is desirable.

Acknowledgments.—I thank Professor C. A. Arnold of the University of Michigan for making available Miner's original slides, and Helen Pakiser for assistance in isolation and photography of specimens.

MORPHOLOGY OF *ARIADNAESPORITES*

All specimens of *Ariadnaesporites* used by Miner (1932) to represent the species *Selaginellites ariadnae* possess long, contorted, hairlike outgrowths of the outer wall layer. These are chiefly confined to the distal hemispheres of the megaspores. A simple trilete suture is present on the inner layer of the spore wall. A trilete suture, located just above that of the inner wall layer, is also present on the outer layer of the spore wall. The lips of this suture are greatly modified to form, at the proximal pole, prominent leaflike structures, the acrolamellae. The height of most acrolamellae is at least equal to the axial diameter of the

[1] For the leaflike extensions of the leasurae, I am proposing the term "acrolamella," taken from the Greek *akros*, pertaining to the tip, and the Latin *lamella*, a plate, leaf, or layer. This term is intended to distinguish these structures from gula and "apical prominences" found in some Paleozoic spores.

spore. Most of Miner's specimens possess at least torn remnants of these membranous structures. All specimens of the new species described in this paper also possess the above characteristics.

OTHER GENERA OF SOMEWHAT SIMILAR MORPHOLOGY

In the palynological literature, comparatively few genera are described that possess distinctive, enlarged, proximal leaflike extensions of the lips of the trilete sutures. Only six Mesozoic genera are known to possess this type of proximal structure. These include *Arcellites* (Miner) Ellis and Tschudy, 1964, with six large twisted acrolamellae; *Molaspora* Schemel, 1950, with very short leaflike segments; and *Balmeisporites* Cookson and Dettman, 1958, with three large acrolamellae. Systematic relationship of these 3 genera has been expressed by the suggestion that all 3 are representatives of the Hydropteridae (Cookson and Dettmann, 1958; Hall, 1963). Other less well defined genera possessing possible acrolamellae are *Glomerisporites* Potonié, 1956; *Capulisporites* Potonié, 1956; and *Rugotriletes* (van der Hammen) ex Potonié, 1956. These three genera originally were described by Dijkstra (1949; 1951) under *Triletes*.

Several Paleozoic spore genera possess somewhat similar leaflike structures; a few of the better examples are mentioned here. *Triletes globosus* Arnold, var. C, a Pennsylvanian lycopsid megaspore, was reported by Winslow (1959) to possess an "apical prominence" with a height of 115 to 165 microns. This type of prominence is distinctly different from that in the lageniculate types of megaspores in which the apical prominences are enlargements of the pyramic areas (gula). The prominence in *Triletes globosus* is proportionately of significant size, inasmuch as the spore diameters range from 480μ to 770μ, and the apical prominences are about a fourth the axial length of the spore body.

Apical prominences are present in some other Pennsylvanian members of the genus *Triletes*, notably *Triletes indianensis* Chaloner, and *Triletes splendidus* (Zerndt) Schopf, Wilson, and Bentall. Winslow (1959, p. 26) noted that

> the three segments of the prominence, probably a hyperdevelopment of the lip at the proximal pole, show a fan-like grain radiating from the center of each apical segment. The segments are joined only along the outer edges, forming a hollow central cavity which is enclosed at its base by an inner membrane. Therefore, the apical prominence is identical in its morphology to that on spores of *Triletes splendidus* (Zerndt) Schopf, Wilson, and Bentall as originally described by Zerndt. He postulated that this upper, completely enclosed cavity was not a microspore receptacle but rather served as a float mechanism aiding in the dispersal of the megaspores.

Although the apical prominences described by Winslow are superficially similar to those found in *Ariadnaesporites*, they are extensions of only the apical portions of the lips, whereas in *Ariadnaesporites* the lips are extended into a leaflike membrane around the entire periphery of the laesurae.

Felix and Burbridge (1961) described a Mississippian spore having six prominent membranous "wings." These structures, however, are expansions of the perisporial membrane and are not extensions of the lips of the trilete suture.

In the Lower Mississippian and the Devonian of Ohio, Winslow (1962) described *Dicrospora porcata* as having membranous lips 30μ–55μ in height on spores 125μ–250μ in axial length. These spores also possess coarse distal spines terminated by bifurcate, grapnel-like tips with recurved hooks. Chaloner (1959) described a similar spore from the Devonian of Canada (*Nikitinsporites canadensis*) with "triradiate lips greatly extended to form an apical prominence up to 195μ high . . . ," on spores ranging from 390μ to 710μ in axial length. These spores also possess grapnellike hooks on the coarse distal projections which are about 200μ long and 30μ in diameter.

Thus it is seen that the development of membranous extensions of the lips of the laesurae is rare in Paleozoic genera, and it is present in only a few Mesozoic genera. Extreme development is observed only in the Mesozoic genera *Ariadnaesporites*, *Arcellites*, and *Balmeisporites*.

Long, hairlike, distal extensions of the outer wall layer are known in no genus other than *Ariadnaesporites*. The Devonian and Mississippian spores mentioned above, *Capulisporites*, and some species belonging to the genus Arcellites, do possess distal extensions, but none of these types of extensions are hairlike or filamentous. In this respect the genus *Ariadnaesporites* is unique.

ASSOCIATION OF MEGASPORES AND MICROSPORES

Relationship between megaspores and microspores can be established in several ways. These include the isolation of megaspores and microspores from within a single strobilus; the constant association of the two types of spores either stratigraphically or within the micropylar areas of seeds; and the morphologic similarity of the two spore types. The intimate association of fossil megaspores and microspores described by Sahni (1941) is outstanding. Megaspores and microspores of *Azolla intertrappea* Sahni and Rao, 1941,

were found in thin sections of chert. The microspore-bearing massulae were attached to the megaspore by means of specialized hooked structures known as glochidia. *Azolla* is an extant genus of water ferns and is known to possess reproductive structures that are almost identical with those found in the silicified Tertiary material. Such union, although not within a fructification, is convincing evidence that both the megaspore and the massulae (bearing the microspores) belong to the same species of fossil *Azolla*.

In *Ariadnaesporites cristatus*, n. sp., there are two spore types, differing in size and in some other features. Although it has not been demonstrated that the large and small spores were derived from a single plant species, and in spite of the fact that no sporocarp or other evidence of the morphology or structure of the parent plant or plants was seen, I believe, principally on the basis of their morphologic similarity, that the two types of spores are megaspores and microspores of the same plant species. They both possess prominent acrolamellae (an uncommon feature) which have similar surface ornamentation, and they both have long hairlike distal extensions of the outer wall (known only in this genus).

The intimate association of these two spore types also implies that they are of the same species. Not only were they found in the same preparation, but also the distal hairs of the two types were so intertwined that separation of individual spores from the tangled mass was difficult or impossible to accomplish without breaking some of the hairs. Such intimate association is similar to that in the fossil *Azolla intertrappea* in which the microspores in massulae are attached to the megaspore by hooked glochidia. Intertwining of distal hairs, I believe, is but a step removed from organic union—the development of long, contorted distal hairs on both the large and small spores is an adaptation to promote the entanglement of the two types of spores, thus providing greater probability of insuring the fertilization of the female gametophyte in the developing megaspore.

AFFINITY

The morphology of *Ariadnaesporites* is somewhat similar to that of a few other Mesozoic spores, and it is strikingly similar to the morphology of some species of *Arcellites*. For example, both *Arcellites disciformis* and *Ariadnaesporites* possess unusual lip extensions, distal ornamentation in the form of clavate or threadlike appendages, and an inner and an outer wall layer. These spores with "delicate and elaborate appendages" have been attributed to the Hydropteridae or water ferns by Dijkstra (1951) and by Hughes (1955). I believe that in all likelihood *Ariadnaesporites* also is an extinct member of the Hydropteridae.

SYSTEMATIC DESCRIPTIONS

Miner's (1932) specimens figured in this report were all seen on his original slide, No. 15498. This slide is deposited in the collections of the Museum of Paleontology, University of Michigan.

All photographed specimens of the new species described herein are on slides deposited in the U.S. National Museum, Washington, D. C. All illustrated specimens of the new species have been circled on the slides in black ink; mechanical-stage coordinates for each of these specimens are also given. In order that others may correlate their mechanical-stage coordinates with those given here, our coordinates of the center point of a 1 × 3-inch standard microscope slide are given, as follows: 108.0 mm and 12.3 mm.[1]

Color photographs of Miner's specimens and of the new species described in this paper are available from the U.S. Geological Survey pollen laboratory, Denver, Colo., on a limited loan basis.

Genus *Ariadnaesporites* Potonié, 1956, emend.

Figure 1, *a–i*; 2, *a–j*

Ariadnaesporites Potonié, 1956, Beih. zum Geol. Jahrb., v. 23, p. 37.

Emended diagnosis.—Megapores or microspores, outline circular, spore body originally spherical or nearly so; triradiate laesurae extending more than half the

[1] The center of a 1 × 3-inch microscope slide may be obtained by drawing diagonal lines on the slide. To test the accuracy of the diagonal lines locating the center point, the intersection of the lines is placed in the center of a microscope field, then the slide is reversed. If the lines are accurately drawn, the intersection will still be in the center of the field.

FIGURE 1.—*Ariadnaesporites ariadnae* and *A. cristatus*. Parts *a*, *c*, *d*, *e*, and *f* are shown at about × 100; part *b* at about × 200, and parts *g–i* at about × 1,000.

a–f. Ariadnaesporites ariadnae, rephotographed from Miner's (1932) original slide 15498, Museum of Paleontology, University of Michigan.
- *a*. Coordinates 106.4 × 8.9, 220 microns.
- *b*. Lectotype, coord. 95.2 × 13.7, 290μ (Miner's fig. 28).
- *c*. Coord. 105.0 × 5.7, 240μ; this specimen clearly shows the acrolamellae.
- *d*. Coord. 98.9 × 11.0, 270μ.
- *e*. Coord. 95.4 × 12.3, 240μ (Miner's fig. 27).
- *f*. Coord. 92.8 × 15.9, 316μ (Miner's fig. 31).

g–i. Ariadnaesporites cristatus, USGS paleobot. loc. D3415.
- *g*. Base of hollow hairlike extension (mega 12), coord. 96.4 × 5.8. USNM 42570.
- *h*. Section of inner and outer wall layers, and vesicles and fine surface ornamentation of outer wall (mega 10), coord. 92.6 × 17.0. USNM 42571.
- *i*. Base of acrolamellae (mega 12), coord. 97.9 × 10.6. USNM 42572.

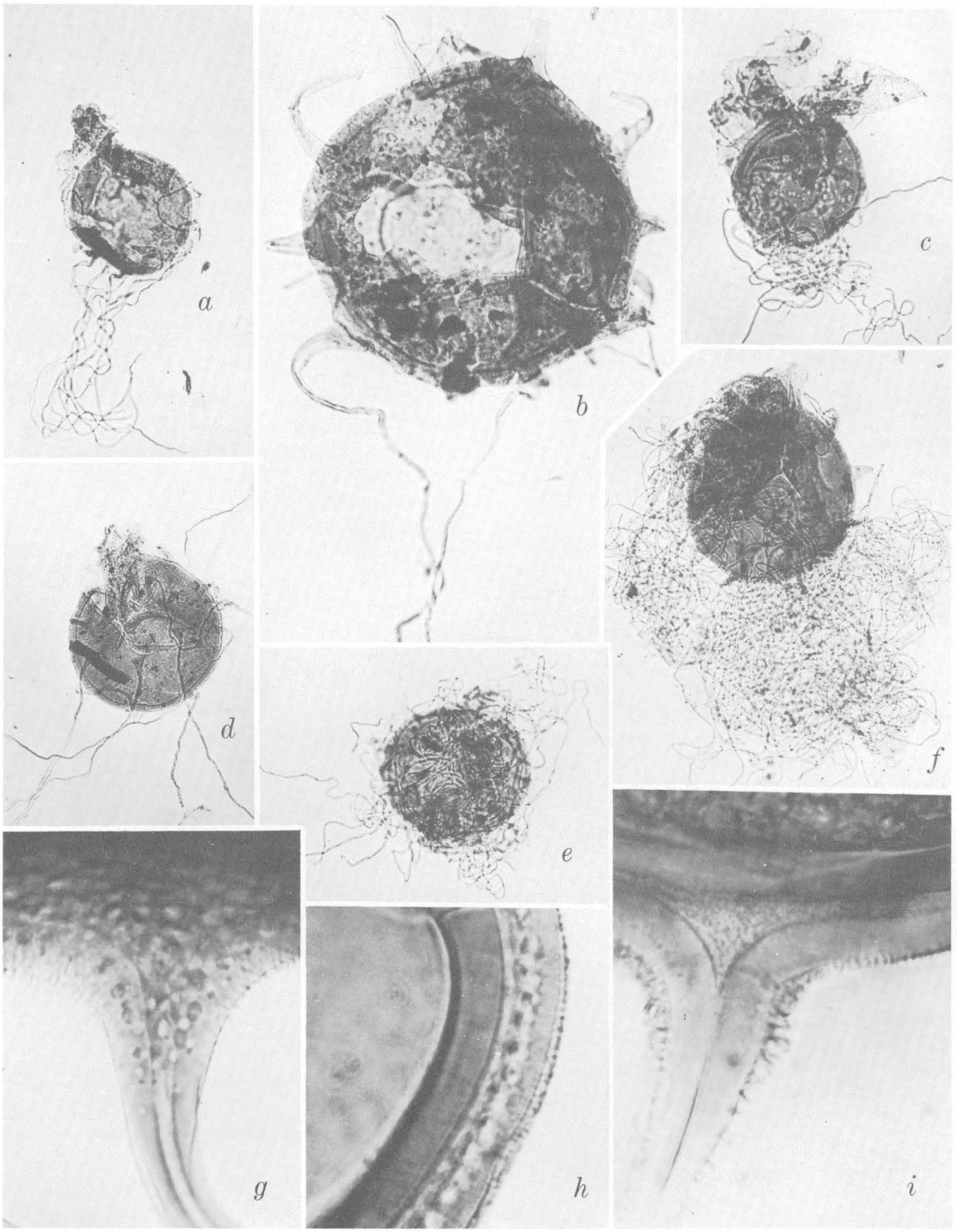
a
b
c
d
e
f
g
h
i

distance to the equator; lips of laesurae provided with prominent acrolamellae; wall at least two layered, the outer layer provided with long, primarily distal, threadlike extensions, few to many times as long as the diameter of the spore.

Type species.—*Ariadnaesporites ariadnae* (Miner) Potonié 1956.

Discussion.—The acrolamellae, although visible, are not clearly evident in Miner's (1932) original photomicrographs. The lectotype chosen by Potonié, Miner's figure 28, here reproduced as figure 2*b*, possesses only remnants of the acrolamellae. The acrolamellae probably were torn during deposition or during preparation of the slides.

Figure 1, *c* shows a specimen with acrolamellae from the same slide that provided the lectotype.

Ariadnaesporites ariadnae (Miner) Potonié, 1956, emend.

Figure 1, *a–f*

Selaginellites ariadnae Miner, 1932, Washington Acad. Sci. Jour., v. 22, nos. 18, 19, p. 505.

Ariadnaesporites ariadnae (Miner) Potonié, 1956, Beih. zum Geol. Jahrb. v. 23, p. 37.

Emended description.—The megaspores possess a nearly spherical spore body. The diameter ranges from 150μ to 316μ, the mean being 233μ. The triradiate laesurae extend over half the distance to the equator. and are characterized by prominent, nearly smooth, membranous leaflike extensions from the margins of the laesurae. These acrolamellae are usually more than 200μ high. The spore wall is two layered, the inner layer about 1μ thick, and the outer layer 8μ–10μ thick. The outer wall layer possesses 8–15 long threadlike extensions, about 3μ–8μ in diameter and a few to several times the diameter of the spore in length. The threadlike extensions are tubular, funnelform at their bases, and narrowing toward their tips. They are more numerous on the distal face of the spore than on the proximal face.

Lectotype (selected by Potonié, 1956).—Miner's figure 28, slide 15498, Museum of Paleontology, University of Michigan. Microscope coordinates 95.2 × 13.7. Rephotographed as figure 1, *b*.

Discussion.—In most of the specimens photographed by Miner (1932) the acrolamellae are partly or almost completely torn off. However, remnants of acrolamellae can be seen, in the original slide material, on all but one of the specimens he photographed (Miner 1932, fig. 29).

Additional specimens from Miner's original slide, which show acrolamellae but which were not figured or discussed by him, are photographed here on figure 1, *a*, *c*, and *d*. Figure 1, *a* and *d* show torn acrolamellae, and figure 1, *c* shows almost entire folded membranous acrolamellae. These additional specimens are from the same slide as the lectotype.

Miner stated that "the spores are usually entangled by the threadlike appendages, which sometimes completely hide the spore." This condition is shown on figure 1, *e* and *f*. (These are the same specimens photographed by Miner, 1932, figs. 27 and 31, respectively.)

At the present time the species *Ariadnaesporites ariadnae* is limited to megaspores.

Occurrence.—Western Greenland. Age, Late Cretaceous.

Ariadnaesporites cristatus, n. sp.

Figures 1, *g–i*; 2, *a–j*

Holotype.—USNM 42449, slide D3415 (mega 13), coordinates 99.6 × 5.5, figure 2, *a*.

Paratype.—USNM 42453, slide D3415 (mega 8), coordinates 90.8 × 7.3, figure 2, *d*.

Paratype.—USNM 42569, slide D3415 (mega 5), coordinates 91.6 × 21.0, figure 2, *j*.

Species description, megaspores.—The megaspores possess nearly spherical spore bodies with diameters ranging from 180μ to more than 300μ. The triradiate laesurae extend over half the distance to the equator and are bordered by prominent acrolamellae approximately equal in height to the diameter of the spore. The outer surfaces of the acrolamellae are densely verrucate. The projections are commonly fused at their bases, forming a finely rugulate surface ornamentation. The spore wall is made up of 2 layers, each about 10μ thick. In some specimens the outer wall layer is separated from the inner wall layer. The outer layer characteristically possesses many small vesicles which

FIGURE 2.—*Ariadnaesporites cristatus* megaspores and microspores. Parts *a–e* are shown at about × 200; parts *f*, *g*, and *j* at about × 500; and parts *h* and *i* at about × 100.

a, *d–f*, *h–i*. *Ariadnaesporites cristatus* megaspores, USGS paleobot. loc. D3415.

a. Holotype (mega 13), coord. 99.6 × 5.5. USNM 42449.

d. Paratype (mega 8), coord. 90.8 × 7.3. USNM 42453.

e. (Mega 7), coord. 83.9 × 17.3; remnants of intine and protoplasm are present in lower part of spore body. USNM 42454.

f. (Mega 9), coord. 85.9 × 18.2; shows separation of inner and outer wall layers. USNM 42455.

h. (Mega 12), coord. 99.0 × 8.9; shows the common condition of microspores entangled in the hairs of a megaspore. USNM 42451.

i. (Mega 2), coord. 92.8 × 10.8. USNM 42568.

b, *c*, *g*, *j*. *Ariadnaesporites cristatus* microspores, USGS paleobot. loc. D3415.

b. (Mega 6), coord. 87.2 × 15.6. USNM 42450.

c. (Mega 12), coord. 99.0 × 8.9; shows trilete suture. This is the same microspore as uppermost specimen of figure 17. USNM 42452.

g. (Mega 1), coord. 88.5 × 17.3; shows reticulation and baculae ornamenting the outer wall. USNM 45267.

j. Paratype (mega 5), coord. 9.6 × 21. USNM 42569.

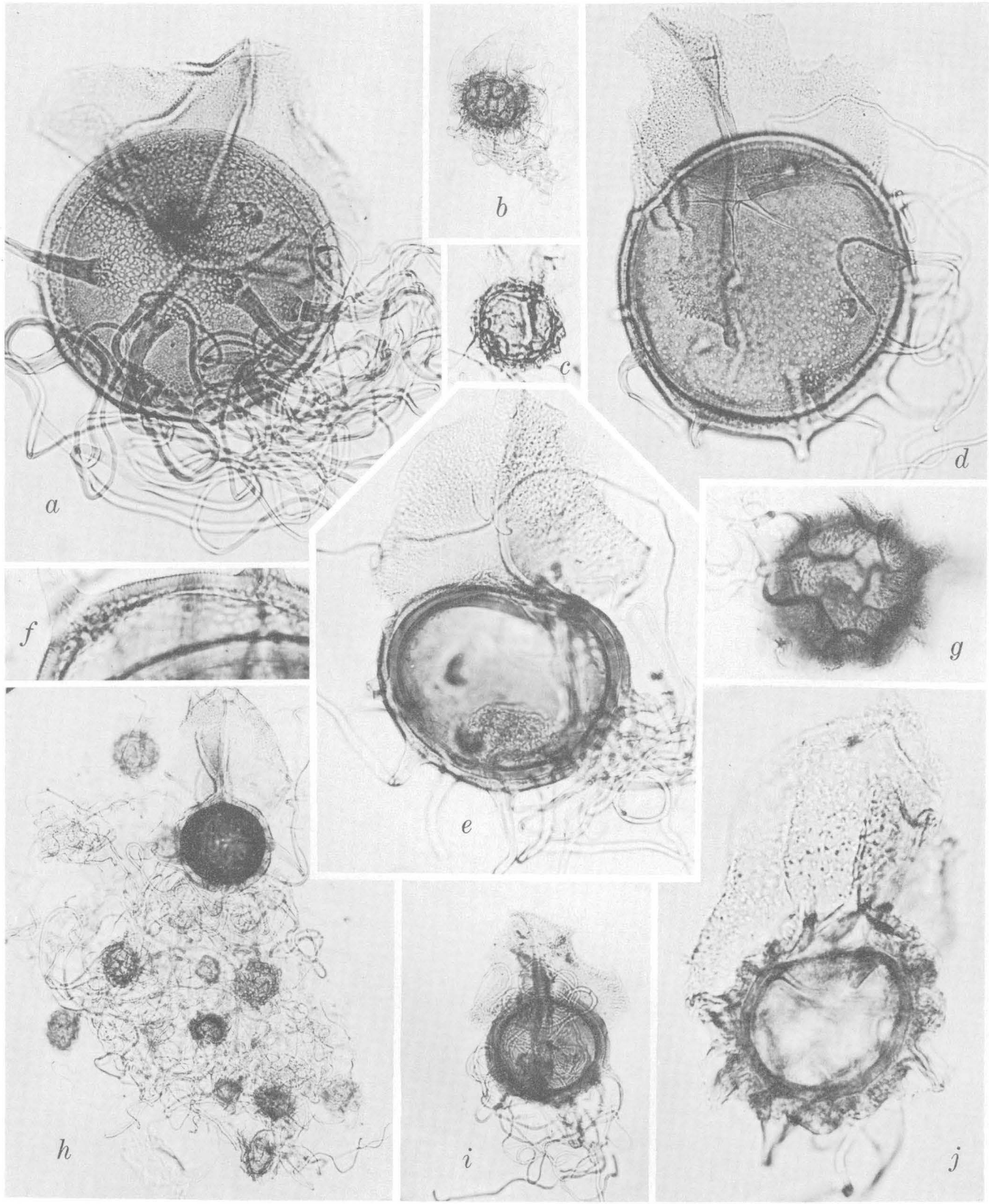
a
b
c
d
e
f
g
h
i
j

give it the appearance of being foveolate; a section of the wall clearly shows the vesicles within, although some extend to the surface, forming true foveolae. The outer wall layers possess about 12 long, intertwining, threadlike extensions, more numerous on the distal surfaces of the spores. The threadlike extensions are about 4μ to 8μ in diameter, and are several times as long as the diameter of the spore; they are smooth, hollow, funnelform at their bases, and narrow toward their tips. The outer wall layer and bases of "threads" are densely covered with short baculae. The inner wall layer is smooth, and it possesses simple laesurae immediately below the outer wall laesurae that possess acrolamellae. The ornamentation of the spore surface and the acrolamellae, the presence of vesicles in the outer wall layer, and the thickness of the inner wall layer distinguish the megaspores of this species from the megaspores of *Ariadnaesporites ariadnae*.

Microspores.—The microspores possess nearly spherical bodies which range in diameter from 50μ to 90μ. The triradiate laesurae extend more than half the distance to the equator and are bordered by acrolamellae approximately equal in height to the diameter of the spores. The outer surfaces of the acrolamellae possess short baculate, clavate, or verrucate projections. The spore wall is made up of two layers. The inner layer is about 4μ thick and of fairly uniform diameter. The outer wall layer, which is about 3μ thick, is coarsely rugulate to reticulate, apparently owing to the fact that it was too large to fit around the inner wall layer. The outer layer possesses baculate projections similar to those found on the acrolamellae. It possesses two to several long threadlike extensions, 2μ to 5μ in diameter and several times as long as the diameter of the spore; they are smooth, tubular, funnelform at their bases, and narrow toward their tips. The smaller size and the coarsely rugulate outer wall distinguish the microspores from the megaspores of *A. cristatus*.

Discussion.—The threadlike megaspore hairs are hollow extensions of the outer wall, as shown on figure 1 *g*. The hairs on megaspores and microspores are structurally the same with the exception of minor differences. The microspore hairs are smaller in diameter; they are shorter, and they lack vesicles such as are present at the bases of most megaspore hairs.

Vesicles are also present in the outer wall layer, as shown on figures 2, *a* and *d*. The vesicles, when seen in surface view, may be large and somewhat irregular in shape or they may be smaller and more evenly distributed. In some specimens the vesicles are sparse and may be confined to only one part of the spore. The thick solid inner wall layer, the vesicles within the outer wall layer, and the dense surface ornamentation are shown in detail on figure 1, *h*.

The basal parts of the two appressed membranes surrounding the laesurae, which are in fact the basal parts of megaspore acrolamellae, are shown on figure 1, *i*. A simple trilete laesura on the inner wall is shown on figure 2, *d*. In some megaspores the inner and outer wall layers are partially separated as shown on figure 2, *d*, and to a greater degree on figure 2, *f*. In the microspores, however, the inner and outer wall layers are in contact, and the outer layer is strongly folded or wrinkled. The surface ornamentation of the microspore body and acrolamellae (baculae or verrucae) is shown on figures 2 *g* and *j*, respectively.

Occurrence.—Tuscaloosa Formation of Alabama. Age, Late Cretaceous.

REFERENCES

Chaloner, W. G., 1959, Devonian megaspores from Arctic Canada: Paleontology, v. 1, pt. 4, p. 321–332.

Cookson, I. C., and Dettman, M. E., 1958, Cretaceous "megaspores" and a closely related microspore from the Australian region: Micropaleontology, v. 4, no. 1, p. 39–49.

Dijkstra, S. J., 1949, Megaspores and some other fossils from the Aachenian (Senonian) in South Limburg, Netherlands: Geol. Stichting, Meded., n. ser., no. 3, p. 19–32.

——— 1951, Wealden megaspores and their stratigraphical value: Geol. Stitching, Meded., n. ser., no. 5, p. 7–22.

Ellis, C. H., and Tschudy, R. H., 1964, The Cretaceous megaspore genus *Arcellites* Miner: Micropaleontology, v. 10, no. 1, p. 73–79.

Felix, C. J., and Burbridge, P. P., 1961, *Pteroretis* a new Mississippian spore genus: Micropaleontology, v. 7, no. 4, p. 421–425.

Hall, J. W., 1963, Megaspores and other fossils in the Dakota Formation (Cenomanian) of Iowa (U.S.A.): Pollen et Spores, v. 5, no. 2, p. 425–443.

Hughes, N. F., 1955, Wealden plant microfossils: Geol. Mag., v. 92, no. 3, p. 201–217.

Miner, E. L., 1932, Megaspores ascribed to *Selaginellites*, from the Upper Cretaceous coals of western Greenland: Washington Acad. Sci. Jour., v. 22, nos. 18, 19, p. 397–506.

Potonié, Robert, Synopsis der Gattungen der Sporae dispersae; I. Sporites: Beih. zum. Geol. Jahrb., v. 23, 103 p.

Sahni, Birbal, 1941, Indian silicified plants; I. *Azolla intertrappea* Sah. and H. S. Rao: Indian Acad. Sci. Proc., v. 14, p. 489–501.

Schemel, M. P., 1950, Cretaceous plant microfossils from Iowa: Am. Jour. Botany, v. 37, p. 750–754.

Stephenson, L. W., and Monroe, W. H., 1940, The Upper Cretaceous deposits: Mississippi Geol. Survey Bull. 40, 296 p.

Winslow, M. R., 1959, Upper Mississippian and Pennsylvanian megaspores and other plant microfossils from Illinois: Illinois Geol. Survey Bull. 86, 135 p.

——— 1962, Plant spores and other microfossils from Upper Devonian and Lower Mississippian rocks of Ohio: U.S. Geol. Survey Prof. Paper 364, 93 p.

AN 800-YEAR HISTORY OF STREAM EROSION AS INDICATED BY BOTANICAL EVIDENCE

By VALMORE C. LaMARCHE, JR., Menlo Park, Calif.

Abstract.—Under certain conditions recent erosional events on small streams are recorded in the histories of adjacent trees—exposed roots can indicate higher past levels of a streambed, and rapid uncovering of a tree's root system may result in growth suppression. According to this interpretation of external form and internal growth features of two trees, degradation by an ephemeral stream in southwestern Utah has totaled 10 feet since 1150 A.D. Erosion was apparently accelerated about 1700. Features of the nearby flood plain suggest that downcutting of this ephemeral tributary was triggered by a lateral shift of the channel of the master stream. Thus, the downcutting may not be related to an erosional cycle of regional extent.

The timing of epicycles of erosion and deposition on larger streams in the southwestern United States has been established from archaeological and paleontological evidence, from radiometric age determinations, and from historical documentation. The erosional histories of small tributaries are not so well known, and conflicting views have been held on the relation of upland erosion to the behavior of the main stream channels (Schumm, 1965, p. 792; Antevs, 1955, p. 318; Leopold and Miller, 1954, p. 83). As illustrated here with an example from southwestern Utah, botanical evidence may be uniquely suited to the study of recent erosional events on small streams.

The stream investigated is a very small ephemeral tributary of Red Creek, located about 2.5 miles above the junction of Red Creek with the Sevier River, on Utah Route 12, about 10 miles southeast of Panquitch (fig. 1). In this reach, the course of Red Creek is an arroyo 10 feet deep cut into the alluvium along the southern edge of the floor of Red Canyon. Steep, rocky slopes underlain by marly limestone of the Eocene Wasatch Formation (Gregory, 1951) rise abruptly from the alluvial plain. They are barren except for widely scattered trees of several coniferous species.

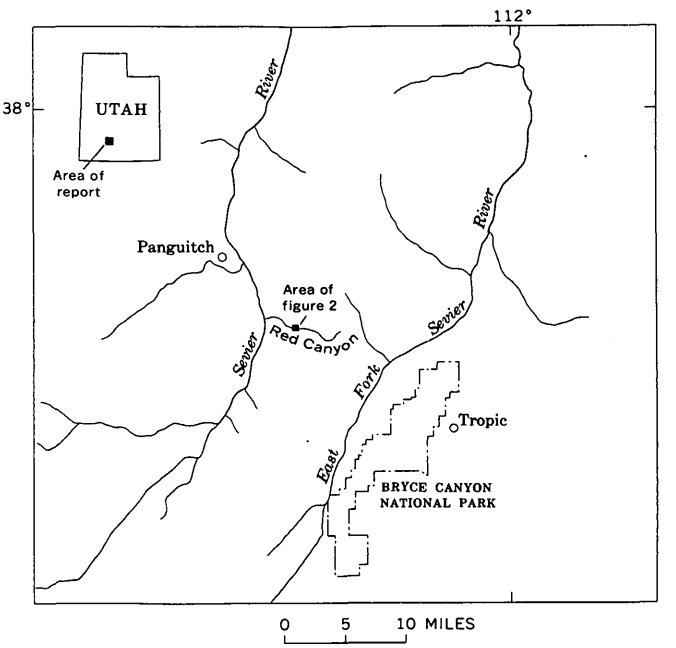

FIGURE 1.—Location map of area studied in southwestern Utah.

The small, amphitheaterlike basin of the stream, carved into the north slope of the canyon (fig. 2), is similar to many in the highly dissected Red Canyon area but differs from all but a few nearby basins in having a deeply entrenched axial gully system. The channel gradients are steep, ranging from about 0.4 foot per foot near the basin mouth to 0.6 ft per ft at the heads of the smallest tributary channels near the drainage divide. The depth of entrenchment also varies with distance along the channel, increasing progressively downstream to the mouth of the basin. Here, the main channel is flanked by steep cut-banks that rise 15 feet above the streambed. The banks are at an angle of 35° to 40°, whereas the slopes above have a relatively gentle angle of 25°. This "V-in-V"

U.S. GEOL. SURVEY PROF. PAPER 550-D, PAGES D83-D86

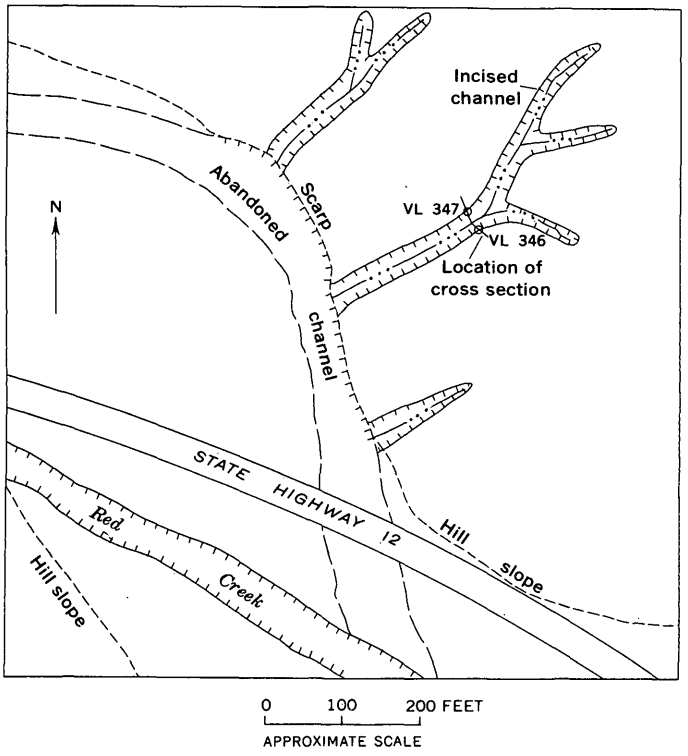

FIGURE 2.—Sketch map of part of Red Canyon. Location shown on figure 1.

cross profile is clearly due to accelerated downcutting of the stream channel.

The progressive downcutting can be traced through the external growth characteristics of two trees flanking the incised channel. The developing root system of a typical young pine tree in this region is at shallow depth, and conforms closely to the shape of the contemporary ground surface. Where erosion later exposes these roots, the form of the original surface is preserved in the exposed root system.

The younger of the trees (VL 346) is a limber pine (*Pinus flexilis* James) that, according to the record of annual growth rings studied in cores taken with an increment borer, was established about 1550 A.D. The gully must have existed at that time because the exposed roots on the channel side of the tree slope steeply downward, parallel to the present cut-bank. However, as shown by the position of these roots, 3 feet above the present surface (fig. 3*C*), the gully was neither as wide nor as deep as now (fig. 3*B*). The local erosional history can be extended to even earlier times from the evidence provided by a dead tree (VL 347) on the opposite bank. This tree, probably a limber pine, began growing about 1150 and died in 1700. These dates are based on cross-dating of the growth record with those of nearby trees and with a

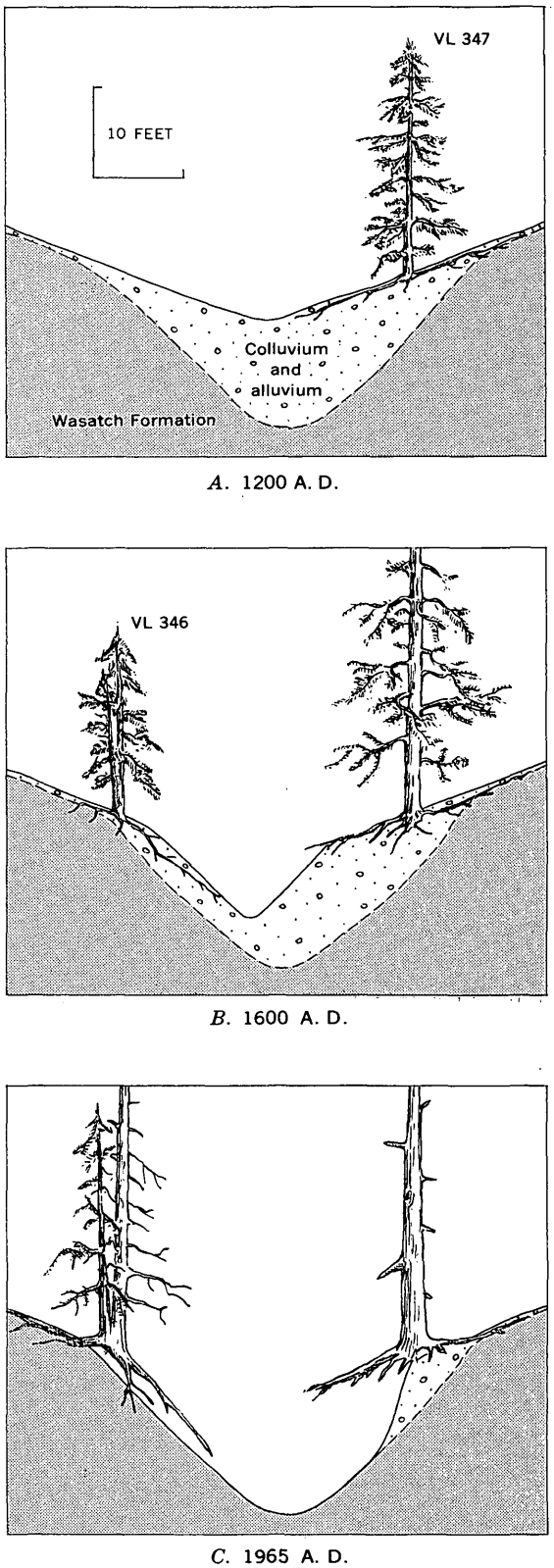

FIGURE 3.—Diagram showing stages of gully erosion; view is downstream.

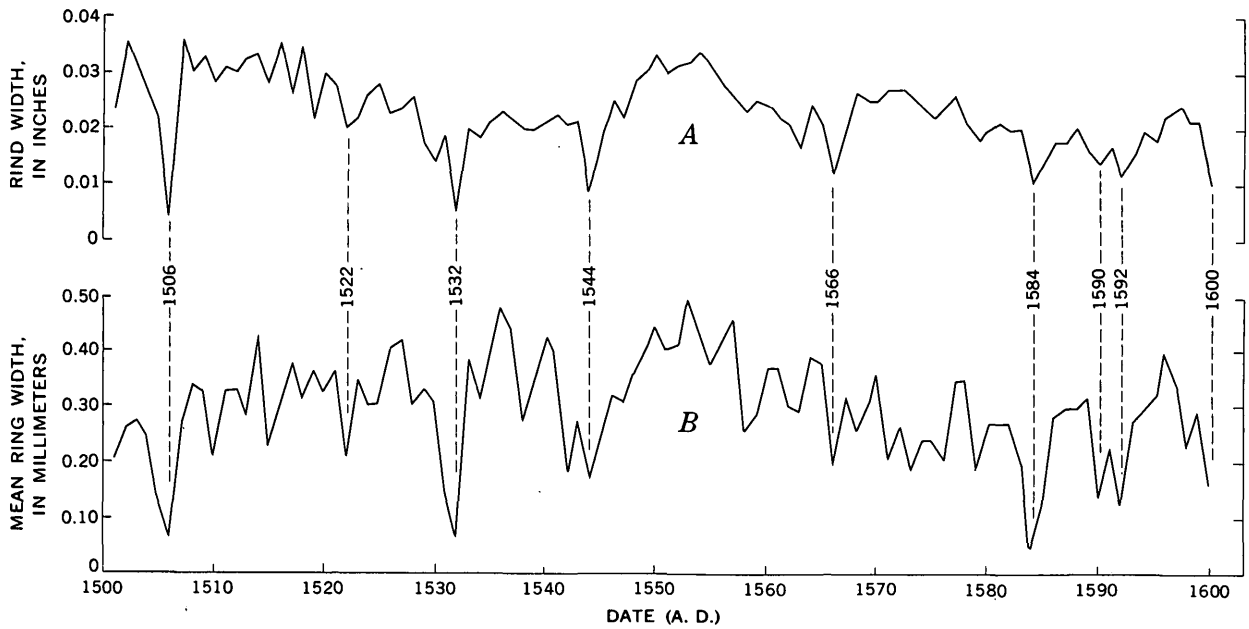

FIGURE 4.—Graph illustrating cross-dating between part of the growth record of tree VL 347 (curve *A*) and part of the composite record of 23 trees at 5 localities in the region (curve *B*) given by Schulman (1956, p. 104, table 53). Dotted lines correlate important index rings.

published chronology for the region (fig. 4). The deeply exposed roots of the older tree are parallel to the upper slope and project nearly to the center of the incised channel, but are 13 feet above the streambed. When the root system developed, about 800 years ago, the gentle upper slope continued smoothly to the center of the valley (fig. 3*A*). At this time, the valley apparently contained an alluvial-colluvial deposit, a remnant of which is still preserved on the gully wall (fig. 3*C*). The gully and deposit, together, must represent an episode of channel incision followed by deposition at some time prior to 1150.

A record of past erosional events may also be preserved in the growth histories of the trees. The root system of VL 346 is exposed around half the perimeter of the tree. That of VL 347 is about three-quarters exposed. Suppression of growth would be an expected result of rapid exposure of a large portion of a tree's root system. Therefore, the permanent decrease in the growth rate of VL 346 to a third of its former value in the period 1690–1700 (fig. 5) and the death of VL 347 in 1700 (± 5 years) strongly suggest that rapid channel downcutting and bank retreat occurred at this time. A bristlecone pine (*Pinus aristata* Eng.) 100 feet downstream has a position, age, and appearance similar to that of VL 346; it also shows a marked decrease in growth rate about 1700. The growth records of nearby trees that are outside the gullied area do not show this effect, however. Local erosion, rather than general climatic or other factors, is therefore probably responsible for this correlative growth suppression.

The erosional history of this small ephemeral stream can be outlined from botanical evidence cited above. Prior to 1150, the shallow channel was on alluvial fill that was continuous between the gentle valley sideslopes. Downcutting began, probably after 1200, and by 1550 the bed had been incised about 5 feet below its original level. Rapid enlargement of this gully took place about 1700, exposing the weak, friable bedrock that now forms the streambed. There is nothing to indicate that the erosion was interrupted by a period of deposition. In the southwest, periods of widespread arroyo cutting have been recognized in the 1200's and from the late 1800's to the present, but the intervening time was characterized by aggradation or comparative stability. Thus, there seems to be no direct relation between this record of progressive erosion and the general alluvial sequence common to many of the larger

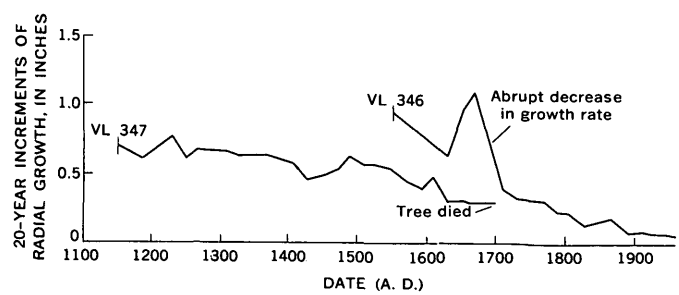

FIGURE 5.—Graph representing change in rate of tree growth.

streams in the southwest (Miller and Wendorf, 1958). Local hydrologic events rather than cyclic episodes of regional extent best explain the behavior of this upland stream.

The immediate cause of the channel degradation is the low local base level of erosion. Incised channels and gully systems are common to the basin studied and to the adjacent small tributaries of Red Creek. These streams are "hanging" with respect to the master stream—their courses pass through notches that have been cut into the upper part of a 10-foot bedrock scarp at the edge of the valley. At the base of the scarp is an old, abandoned channel of Red Creek (fig. 2). The early period of deposition in the tributary basins may have coincided with the spread of their alluvial fans upon the flood plain at a time when Red Creek flowed on the opposite side of the canyon. Slow lateral migration or an abrupt shift in the course of the master stream, and the consequent removal of alluvial-fan deposits, could have triggered the downcutting of the tributaries to the new base level. If this interpretation is correct, Red Creek has since reverted to its earlier location, and small alluvial cones are again being formed at the mouths of the tributaries.

REFERENCES

Antevs, Ernst, 1955, Geologic-climatic dating in the West: Am. Antiquity, v. 20, p. 317–335.

Gregory, H. E., 1951, The geology and geography of the Paunsaugunt region, Utah: U.S. Geol. Survey Prof. Paper 226, 116 p.

Leopold, L. B., and Miller, J. P., 1954, A postglacial chronology for some alluvial valleys in Wyoming: U.S. Geol. Survey Water-Supply Paper 1261, 90 p.

Miller, J. P., and Wendorf, Fred, 1958, Alluvial chronology of the Tesuque Valley, New Mexico: Jour. Geology, v. 66, p. 177–194.

Schulman, Edmund, 1956, Dendroclimatic changes in semiarid America: Tucson, Ariz., Univ. of Ariz. Press, 142 p.

Schumm, S. A., 1965, Quaternary paleohydrology, *in* Wright, H. E., and Frey, D. G., eds., The Quaternary of the United States: Princeton, N.J., Princeton Univ. Press, p. 783–794.

LAKE PADUCAH, OF LATE PLEISTOCENE AGE, IN WESTERN KENTUCKY AND SOUTHERN ILLINOIS

By WILDS W. OLIVE, Paducah, Ky.

Work done in cooperation with the Kentucky Geological Survey

Abstract.—A Pleistocene lake in western Kentucky and southern Illinois, herein named Lake Paducah, has been dated by the radiocarbon method as late Pleistocene (Wisconsin). The date, obtained from mollusk shells in a deposit of sandy silt, is 21,080±400 years B. P. (sample W–1353).

Finch, Olive, and Wolfe (1964) present evidence to show that a lake occupied the valleys of the Ohio, Tennessee, and Clarks Rivers in parts of Kentucky and Illinois near Paducah, Ky., during Pleistocene time. The extent of the ancient lake, here named Lake Paducah, is indicated by elongate gravel ridges that were developed along the margins of the lake (Finch and others, 1964, fig. 1). The crests of the ridges are accordant and stand at an altitude of about 355 feet. Absence of loess on the ridges is interpreted by Finch and others (1964, p. C133) as an indication of "a fairly young age, probably late Wisconsin."

Geologic investigations by Olive after 1964 in the Paducah East 7½-minute quadrangle in Kentucky have led to the discovery of a fossiliferous deposit within the area of the lake. Carbon–14 dating of shell material from the deposit confirms the earlier interpretation that Lake Paducah existed during late Pleistocene time. The fossils provide paleontologic evidence which, though not adequate to date the deposit firmly, is consistent with the carbon–14 date. The purpose of this report is to describe the deposit and to present information on the carbon–14 dating and paleontology of the fauna as evidence of the lake's age.

The fossiliferous deposit (fig. 1) is exposed for a distance of a fourth of a mile between altitudes of 320 and 330 feet, in the channel and along the south valley wall of an east-flowing tributary of Garrison Creek, 0.9 to 1.0 mile northeast of Reidland High School. The exposure is near the margin of Lake Paducah and is 25 to 30 feet below the old lake level. The deposit consists of light-gray, slightly sandy and pebbly, argillaceous silt. Near the west end of the exposure the silt intergrades with light-gray to brownish-gray, nonfossiliferous gravelly silt which overlies

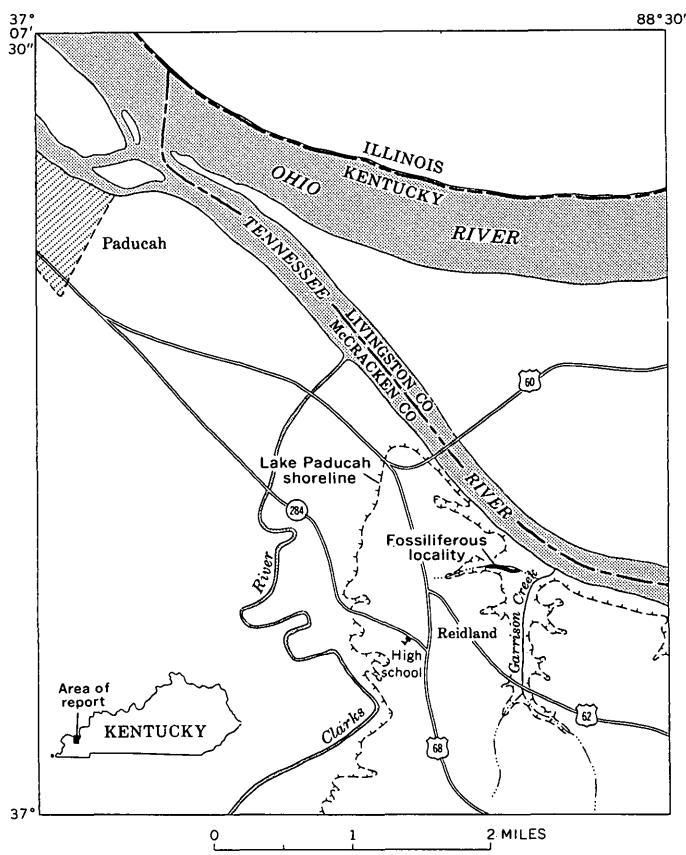

FIGURE 1.—Location of fossiliferous deposit of ancient Lake Paducah, in the Paducah East 7½-minute quadrangle, western Kentucky.

reddish-orange, crossbedded, micaceous argillaceous fine sand of the Clayton and McNairy Formations of Paleocene and Late Cretaceous ages, respectively. At the mouth of the tributary the silt overlies reddish-orange sandy gravel of Pliocene(?) and Pleistocene age. Throughout much of its exposed extent the fossiliferous deposit is overlain by yellowish-brown gravelly silt and silty gravel of alluvial origin.

The fossils at this locality are very small and abundant. They consist predominantly of gastropod shells and a comparatively small number of pelecypod shells, ostracode tests, and fish remains. Most fossils are well preserved except the fish remains, which are fragmentary.

Mollusk shells of the fossil assemblage were identified by J. P. E. Morrison (written commun., 1964) as follows:

High spiral gastropods—
Amnicola lifosa (Say),
Amnicola walkeri Pilsbry(?),
Cincinnatia cincinnatiensis (Anthony), and
Physa species (juvenile).
Planispired gastropods—
Valvata tricarinata Say, and
Gyraulus parvus (Say).
Pelecypods—
Pisidium species cf. *variabile* Prime,
Pisidium compressum Prime, and
Pisidium species.

Morison states that "all identifiable species of mollusks are Recent; not assignable to any particular glacial time."

Ostracodes were examined by I. G. Sohn (written commun., 1963 and 1964), who identified *Limnocythere ornata wabashensis* Staplin, a species of *Cypridopsis*?, and a species of the *Candona* group. According to Sohn, "*Limnocythere* and the *Candona* group live on mud in ponds and slow-moving streams. *Cypridopsis* is a swimmer, and lives on plants. This assemblage could have lived in a lake." With reference to the occurrence of *Limnocythere ornata wabashensis* Staplin in the Wabash-Ohio River watershed, Staplin (1963, p. 1195) states that "It appears to be an inhabitant of cool slightly alkaline lakes in all cases. * * * [This] variety occurred in localities [that are] all Wisconsin in age (Tazewell-Mankato)."

D. H. Dunkle and L. P. Schultz (written commun., 1964) examined fish fragments of the assemblage and report that "Teleostean fish remains are involved, but on the basis of our knowledge and available comparative materials they cannot be precisely identified."

The age of fossil mollusk shells from the deposit, as determined in the radiocarbon laboratory of the U.S. Geological Survey (sample W–1353; Meyer Rubin, written commun., 1964), is 21,080±400 years.

Thus, on the basis of radiocarbon dating the fossil shells correspond to the early Woodfordian (22,000 to 12,500 B.P.) of Frye and others (1962, p. 2) and to the Gardena Intraglacial (Iowan-Tazewell) interval of Leighton (1960, p. 549). This correlation would remain unchanged even if as much as 2,000 years were subtracted from the radiocarbon date of the shell material in order to compensate for probable inert or dead carbonate (containing no carbon–14) in the shells. Inert carbon as a source of error in carbon–14 dating is discussed by Rubin and Taylor (1963).

The absence of loess on the gravel ridges developed along the margins of the lake suggests that the lake existed at least until cessation of loess deposition, which was probably not until late Woodfordian time in the area of Lake Paducah.

REFERENCES

Finch, W. I., Olive, W. W., and Wolfe, E. W., 1964, Ancient lake in western Kentucky and southern Illinois, *in* Geological Survey Research, 1964: U.S. Geol. Survey Prof. Paper 501–C, p. C130–C133.

Frye, J. C., Glass, H. D., and Willman, H. B., 1962, Stratigraphy and mineralogy of the Wisconsinan loesses of Illinois: Illinois Geol. Survey Circ. 334, 55 p.

Leighton, M. M., 1960, The classification of the Wisconsin glacial stage of north central United States: Jour. Geology, v. 68, p. 529–552.

Rubin, Meyer, and Taylor, D. W., 1963, Radiocarbon activity of shells from living clams and snails: Science, v. 141, no. 3581, p. 637.

Staplin, F. L., 1963, Pleistocene Ostracoda of Illinois, pt. II. Subfamilies Cyclocyprinae, Cypridopinae, Ilyocyprinae; Families Darwinulidae and Cytheridae—Stratigraphic ranges and assemblage patterns: Jour. Paleontology, v. 37, no. 6, p. 1164–1203.

A TWO-TILL LOCALITY IN NORTHEASTERN CONNECTICUT

By FRED PESSL, JR., Boston, Mass.

Work done in cooperation with the State of Connecticut Geological and Natural History Survey

Abstract.—Two tills are exposed in the Mashamoquet Brook valley, northeastern Connecticut. The unoxidized, light-gray upper till is crudely stratified and has a loose, sandy matrix. The oxidized, olive-brown lower till is very compact and has a more silty matrix. The two tills are separated by fine-grained, unoxidized, stratified sediments containing fragments of lower till; the stratified sediments are strongly folded and faulted. The oxidation of the lower till, the lack of significant oxidation in the upper till, and the intertill zone of deformed sediments indicate that the tills were deposited by different advances of glacier ice, and that a weathering interval preceded the last glacial advance.

Two superposed tills are exposed in the Mashamoquet Brook valley, in the town of Pomfret, Conn. An unoxidized upper till is separated from an oxidized lower till by a mixed zone of deformed, well-sorted, fine-grained, stratified sediments that contains fragments of the lower till. The degree of oxidation in the lower till indicates that a weathering interval followed deposition of the lower till. The upper till was deposited by a later advance of glacier ice.

The locality is in the southeast corner of the Eastford quadrangle, approximately 1.4 miles northwest of Abington (fig. 1). The exposure in the southwest side of a broad, drumloidal hill shows the stratigraphic relationships described in table 1.

LOWER TILL

The matrix of the lower till is olive brown (2.5*Y*5/4–4/4, moist), very compact, and commonly regular in texture. It consists of 44 percent sand (2–0.062 mm), 43 percent silt (0.062–0.005 mm), and 5 percent clay (<0.005 mm) (fig. 2). Stones larger than $\frac{3}{8}$ inches in diameter constitute 20 percent of the sample by weight. Pebbles and cobbles up to 8 inches in diameter are sparsely scattered throughout the matrix. Boulders are rare and small; the largest observed was 24 inches in diameter. In 1965 the maximum exposed thickness of the lower till was approximately 5 feet. This thickness was observed only in a small pit dug through slumped material at the base of the working face.

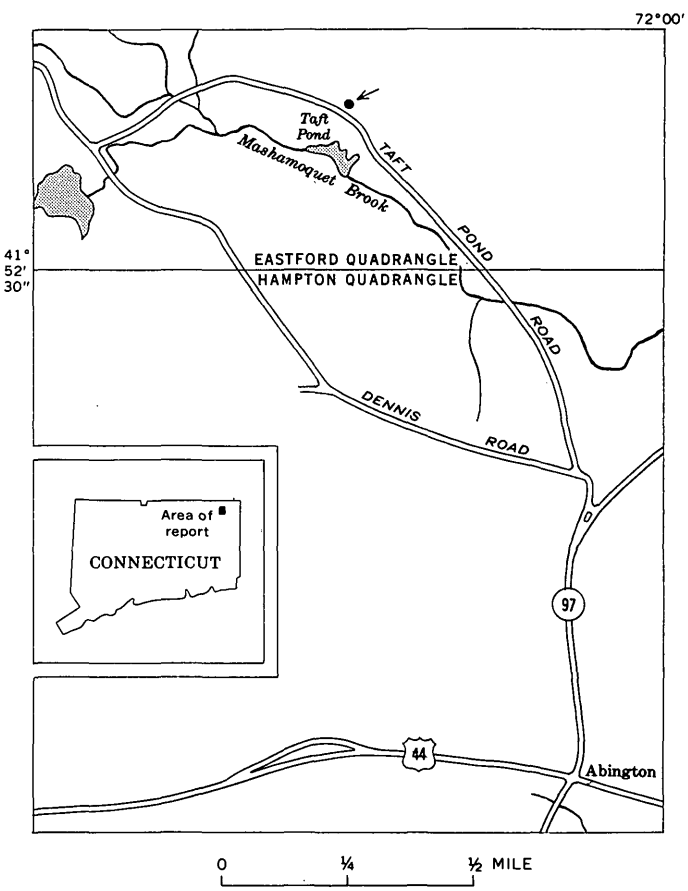

FIGURE 1.—Index map showing till locality (arrow).

TABLE 1.—*Stratigraphic section near northern end of working face of pit 1.4 miles northwest of Abington, Conn.*

[Location shown on fig. 1. Working face trends N. 70° W.]

Unit	Thickness (feet)
Undifferentiated mantle; frost-mixed till, eolian sand and silt	1. 5
Till, sandy, unoxidized, light-gray-olive (5*Y*6/1–5/3); with friable matrix and lenses of stratified sand and gravel	8–10
Mixed zone; stratified, well-sorted, light-gray (5*Y*6/1) to pale-yellow (5*Y*8/4) sand and silt with smears and fragments of till; bedding strongly deformed	15 (approx.)
Till, sandy to silty, oxidized, olive-brown (2.5*Y*5/4–4/4); with compact matrix; interbedded, discontinuous, oxidized sand layers	5 (exposed)

Interbedded, oxidized, medium-grained sand occurs in some parts of the lower till. Fissility is poorly developed at this exposure; however, other nearby exposures of texturally similar till exhibit moderate to strong fissility. The weathered surface is characterized by thin (3–5 mm), irregularly shaped plates, subparallel to the weathered face and bounded by arcuate fractures normal to the weathered face. The lower till is oxidized throughout the exposed thickness; in some portions of the matrix, iron staining is concentrated in small blebs, producing a faintly speckled weathered surface. Manganese staining is common on joint faces and in irregular pods throughout the matrix. The exposed till is noncalcareous and contains rotten gneiss and schist pebbles up to 3 inches in diameter.

MIXED ZONE

Stratified sediments of the mixed zone are chiefly silt and fine- to medium-grained sand. Where undisturbed these sediments have thin, even bedding; small-scale crossbedding is present in a few of the sand layers. The sand and silt are well sorted (So=1.5) and range from light gray (5*Y*/6/1) to pale yellow (5*Y*/8/4). Iron staining, attributed to ground-water circulation, is commonly restricted to coarse sand and along fractures and faults in the finer sand and silt. Laminated clay irregularly interbedded with iron-stained sand is exposed near the base of the mixed zone at one place (sect. *B*, fig. 3). Inclusions of lower till are common in most parts of the mixed zone. These occur both as discrete masses of till, most commonly surrounded by deformed silt beds, and as smears, streaks, and indistinct blebs within the sand and silt layers (fig. 4).

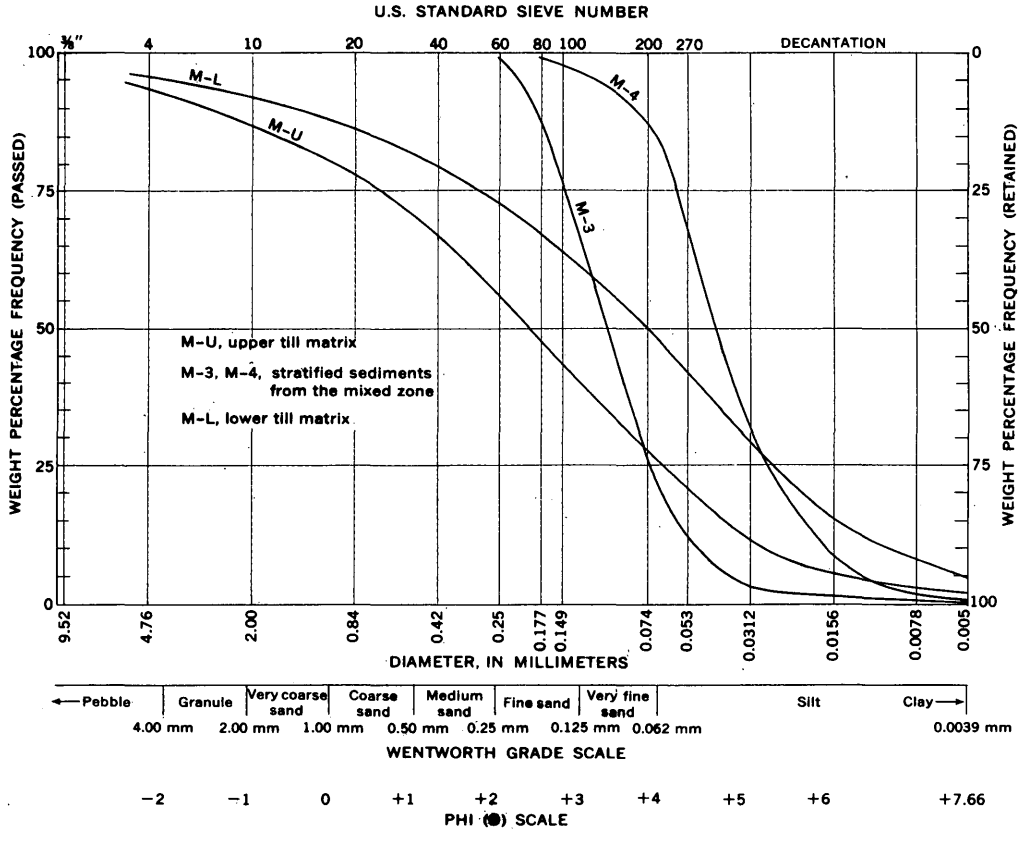

FIGURE 2.—Grain-size data from sediments exposed at the Mashamoquet Brook till locality.

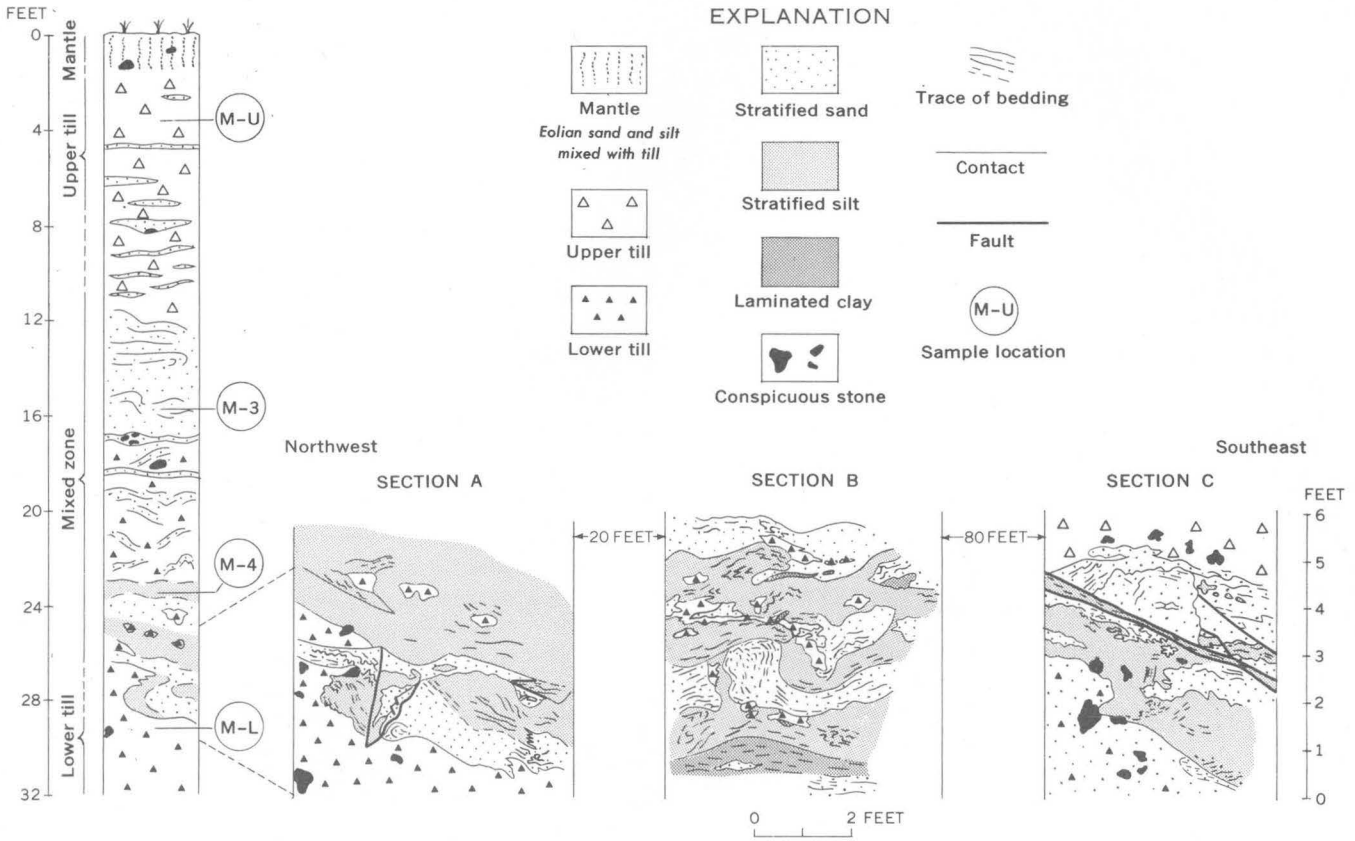

FIGURE 3.—Generalized stratigraphic column and geologic sections, Mashamoquet Brook valley, Pomfret, Conn.

Irregular concentrations of small pebbles generally associated with till fragments are scattered throughout the mixed zone.

Folding is the principal form of deformation in the sediments of the mixed zone, and is most strongly developed in the silt layers (fig. 3, secs. *A* and *B*). Individual beds within the larger silt layers are tightly folded and in many places overturned. Beds of fine- to medium-grained sand are also folded but generally are not as tightly deformed as the silt. Faulting and thrusting are well developed in the southeastern portion of the working face (fig. 3, sec. *C*). Stringers of lower till and clay are smeared along planes extending from some of the larger till inclusions (fig. 3, sec. *B*; fig 4).

UPPER TILL

The matrix of the upper till is light gray to olive (5*Y*6/1–5/3, moist) and has a crude horizontal stratification. It is noncalcareous, very friable, and contains 62 percent sand (2–0.062 mm), 23 percent silt (0.062–0.005 mm), and 2 percent clay (<0.005 mm) (fig. 2). Stones greater than ⅜ inch in diameter constitute 38 percent of the total mass. Angular to subrounded pebbles and cobbles as much as 6 inches in diameter are common. Boulders are widely scattered throughout the upper till; the largest observed has a diameter of 18 inches. Horizontal sandy partings are present in the siltier layers. Thin lenses, ¼ inch to 1 inch thick,

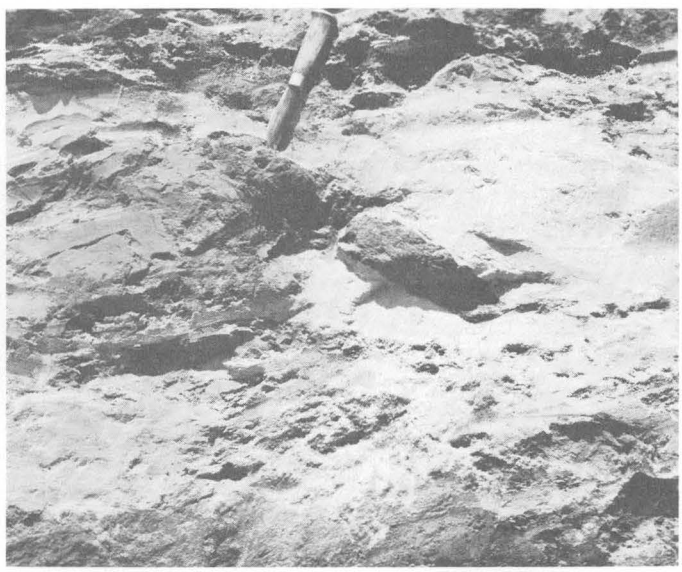

FIGURE 4.—Detail of lower-till fragments in stratified sand and silt. Knife point rests on large till fragment. Note elongate till stringers extending from lower right of till fragment.

224-352 O—66——7

of medium- to coarse-grained sand and granule- to small-pebble-size gravel, are common. Oxidation, attributed to local ground-water circulation, is generally limited to these coarse-grained sand and gravel lenses.

DIRECTIONAL DATA

Till fabric

The orientations of the long axes of pebbles in the tills were measured to determine the direction of ice movement during deposition of the two tills. The fabric of the lower till has a preferred orientation of S. 5°–15° E.; the fabric of the upper till has a preferred orientation of S. 15°–35° W. (fig. 5). These data indicate that the lower till was deposited by ice moving in a south-southeast direction, and the upper till by ice moving in a south-southwest direction.

Deformation of mixed-zone sediments

Neither folds nor faults present clear, consistent evidence for the direction of forces responsible for the deformation of the sediments in the mixed zone. Examples of deformation by forces from both the south and the north can be inferred from the details of the exposed sections. But, in general, the major deformation appears to be the result of forces acting in a southerly direction. This is particularly evident in section *B*, figure 3.

Striations

Till was not observed in contact with striated bedrock at the Mashamoquet Brook till locality. Striations do not, therefore, provide direct evidence for the direction of flow of the glacier ice that deposited the tills. Only a few striation localities are known near the till exposure; at the nearest, in the Hampton quadrangle to the southeast (Dixon and Pessl, 1966), faint striae trend S. 0°–3° E. Striations trending S. 8° E. are reported from the Eastford quadrangle, 8 miles north of the Mashamoquet Brook till locality (M. H. Pease, oral commun., 1966). Uncertainty of the nature of the till associated with these striations and the similarity of trend of the striae prohibit their use as distinctive, independent directional data.

INTERPRETATION

The lower till is oxidized throughout its exposed thickness (5 feet) at the Mashamoquet Brook locality; at other nearby exposures of texturally and structurally similar till, oxidation is observed to a depth of about 10 feet. The base of the oxidized zone was not observed at any exposures in this area; however, the exposed depth and thoroughness of oxidation in the lower till indicate that a period of weathering followed deposition of this till.

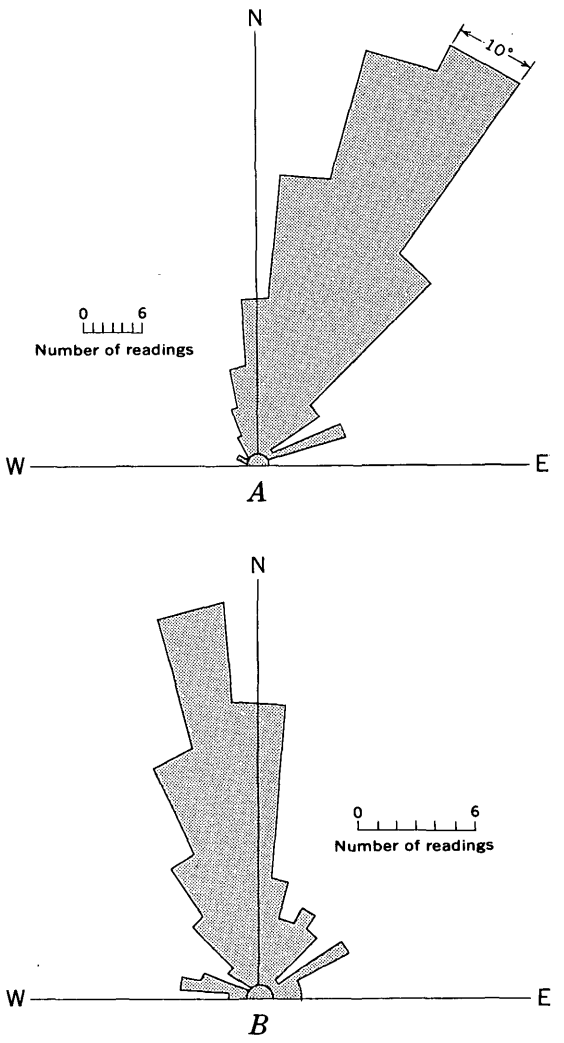

FIGURE 5.—Fabric diagrams from upper and lower tills, Mashamoquet Brook valley, northeastern Connecticut. *A*, fabric diagram from upper till, based on 204 pebbles with long axes ½–4 inches. *B*, fabric diagram from lower till, based on 102 pebbles with long axes ½–4 inches. In diagrams, azimuth data are grouped in 10° classes.

The unoxidized upper till and the deformed, unoxidized, stratified sand and silt of the mixed zone, with inclusions of oxidized lower till, are deposits of a later advance of glacier ice.

The fine texture and thin, even stratification of the sediments in the mixed zone indicate deposition in quiet or slow-moving water. Deposition of these sediments may have occurred as proglacial outwash in front of the advancing ice, before being overridden; or deposition may have occurred subglacially, prior to stagnation of the ice. In either case, deformation of

the fine-grained sediments and mixing of lower till fragments with the stratified sand and silt probably were caused by overriding glacier ice.

The combination of the stratification in the upper till, the occurrence of well-sorted sand and gravel interbedded with the upper till, and the relative thinness of the upper till (8 to 10 feet) suggests that the upper till is an ablation deposit. However, it seems unusual for an ablation till to have such a strongly oriented fabric as indicated in figure 5. More detailed study of numerous exposures in the upper till is necessary to properly determine its precise mode of deposition.

The nature of these tills is in general similar to that shown by other reported observations of two tills in Connecticut. White (1947) reported a sequence of two tills from the Strafford Springs area. A series of exposures there indicated a sequence of thick, compact, fissile, oxidized till overlain by a sandy, friable, unoxidized till. In general this description resembles that of the Mashamoquet Brook sequence. These two localities are less than 20 miles apart and at approximately the same latitude. Correlation of the two tills in the Stafford Springs area with those of the Mashamoquet Brook locality, although based only on reported textural and stratigraphic similarity, seems reasonable.

Flint (1961) described two tills exposed during construction of a dam at Lake Chamberlin, northwest of New Haven, Conn. The lower till matrix (Lake Chamberlin till) is described as unoxidized, very compact and regular in texture, containing 60 percent sand and 40 per cent silt-clay. The upper till matrix (Hamden till) is described as unoxidized and more friable, containing 58 percent sand and 42 percent silt-clay. Directional data from the Lake Chamberlin till indicate deposition by ice moving toward the south or southeast; similar data from the Hamden till indicate deposition by ice moving toward the southwest.

Despite striking similarities in the stratigraphic, textural, and directional data from the Lake Chamberlin and Mashamoquet Brook till localities, the unoxidized nature of the Lake Chamberlin till makes correlation of this till with the lower Mashamoquet Brook till questionable. Flint suggests that perhaps an upper, oxidized portion of the Lake Chamberlin till was eroded by Hamden ice. It is also possible that both the Lake Chamberlin till and the Hamden till are younger than the lower Mashamoquet Brook till, and perhaps are to be correlated with the upper Mashamoquet Brook till.

REFERENCES

Dixon, H. R., and Pessl, Fred, Jr., 1966, Geologic map of the Hampton quadrangle, Windham County, Connecticut: U.S. Geol. Survey Geol. Quad. Map GQ–468.

Flint, R. F., 1961, Two tills in southern Connecticut: Geol. Soc. America Bull., v. 72, no. 11, p. 1687–1692.

White, S. E., 1947, Two tills and the development of glacial drainage in the vicinity of Stafford Springs, Connecticut: Am. Jour. Sci., v. 245, p. 754–778.

SIGNIFICANCE OF CLIMBING-RIPPLE STRUCTURE

By EDWIN D. McKEE, Denver, Colo.

Abstract.—Climbing-ripple lamination (ripple drift structure) forms only under the relatively weak hydrodynamic conditions suitable for the development of a rippled surface and where a very large amount of sand or silt is available for deposition. Probably not all situations have yet been recognized in which these two requirements are met; however, river flood plains and areas of overbank flow are particularly favorable, as illustrated by examples along the Colorado, Mississippi, and Indus Rivers, where climbing-ripple lamination commonly is associated with horizontal lamination, with a limited amount of trough and planar types of cross stratification and with contorted bedding of convolute and recumbent types. Some places where ripple marks are abundantly developed, such as the tidal flats of Cholla Bay, Mexico, and the tidal margins of the Ganges (Hooghly) estuary in India, are largely devoid of climbing-ripple structure because new sand is not being introduced rapidly, whereas that on hand is constantly reworked and ripple marks are destroyed.

The considerable and growing interest in sedimentary structures is reflected in descriptions of structures characteristic of modern environments in numerous parts of the world, in recent experimental work in which structures are being reproduced, and in studies of the hydrodynamics involved in forming such structures. Furthermore, field geologists attempting to describe and interpret the facies in ancient sedimentary rocks are finding an ever-increasing number of features that need explanation.

Observations on the occurrence and distribution of the sedimentary structure known as "climbing-ripple lamination" or "ripple drift structure" have prompted the writer to summarize ideas concerning its significance. Climbing-ripple lamination is a type of stratification in which ripple crests of vertically succeeding ripple laminae, in sections parallel to the direction of current or wave movement, appear to be advancing upslope.

Theoretical and experimental data indicate that its formation and distribution are controlled by two concomitant factors—velocity of water and sediment load. Field observations strongly suggest that it is limited to a few specific environments and is rare or absent in others. Climbing-ripple structure thus seems to be a valuable aid in the interpretation of depositional environments.

Acknowledgments.—The assistance of Dr. B. Raychandhuri and Dr. Pamela Robinson of the Indian Statistical Institute, Calcutta, in arranging for the investigation on the Ganges estuary, and that of Dr. H. Rahman of the Pakistan Geological Survey for similar help on the Indus delta study, is gratefully acknowledged. Discussions of this study with Eleanor Crosby and Henry Berryhill of the U.S. Geological Survey and with James Coleman of the Coastal Studies Institute in Baton Rouge were very helpful. Thanks are extended also to E. Tad Nichols of Tucson, Ariz., who made nearly all the photographic illustrations.

FACTORS RESPONSIBLE FOR CLIMBING-RIPPLE STRUCTURE

In the investigation of depositional environments, a distinction between the significance of ripple marks and that of climbing-ripple laminae (ripple drift) should be recognized. Ripple marks develop on a sand or silt surface whenever and wherever a particular stage of the lower flow regime, as described by Simons and Richardson (1961, p. 87), is attained by currents; likewise, ripple marks form under certain comparable conditions resulting from oscillatory wave movement. Climbing-ripple lamination (fig. 1*D*), in contrast, although formed from superposed ripple marks, involves sand accretion as well as migration and does not necessarily develop each time ripple marks form. In a laboratory tank or flume, ripple marks that form and migrate downstream for hours may never develop the characteristic structure of climbing ripples (ripple drift).

An essential element in the genesis of climbing-ripple lamination is the introduction of an abundance of sand or silt, so that the processes of sedimentation and ripple

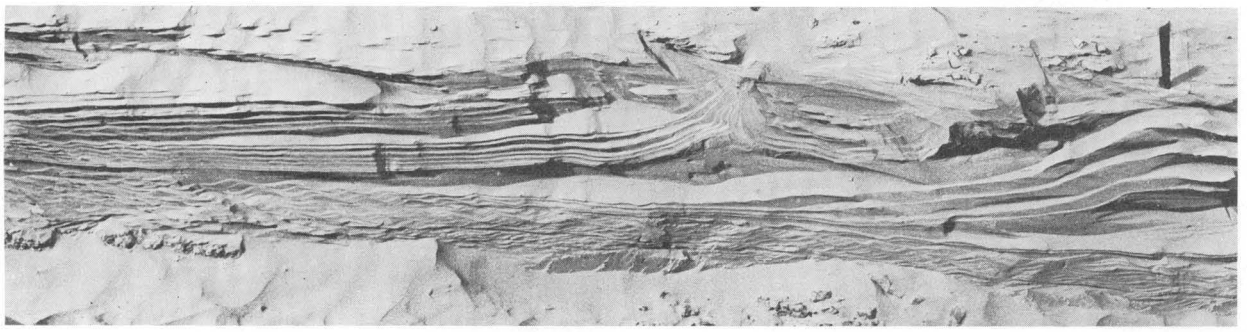

A

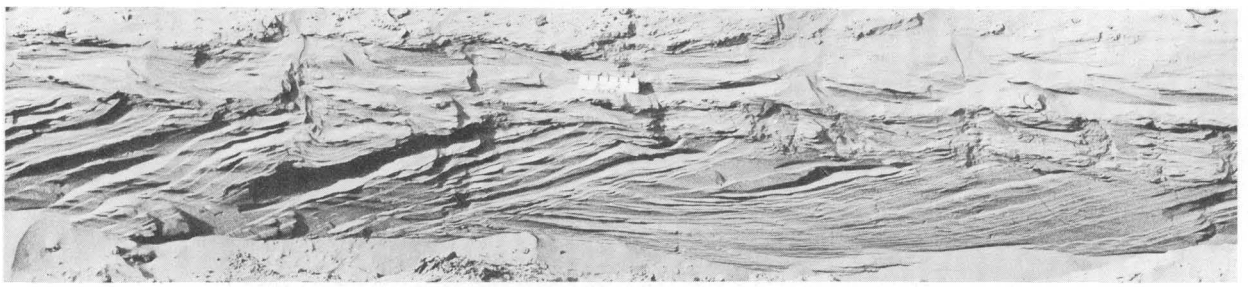

B

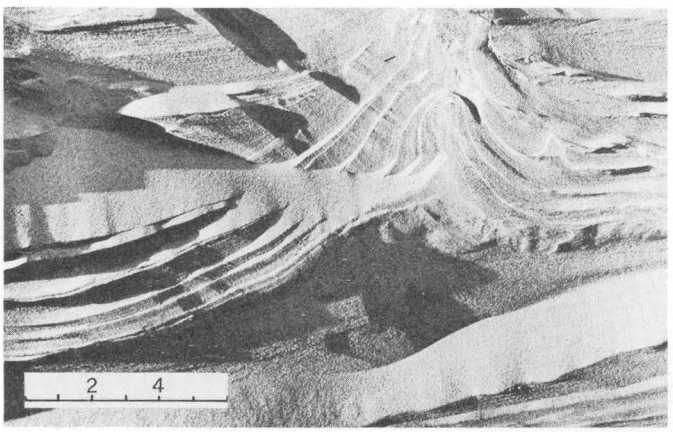

C

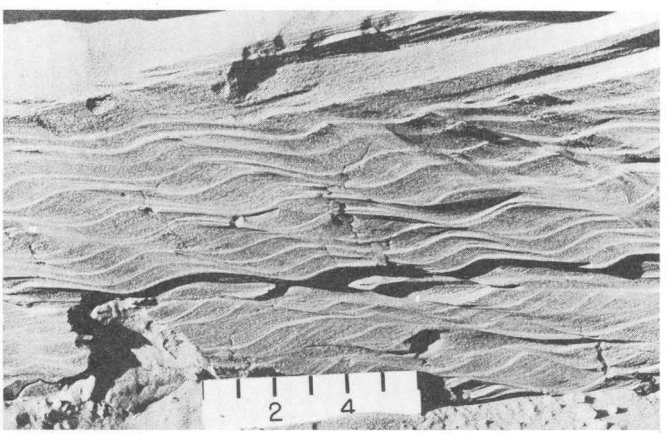

D

FIGURE 1.—Recent deposits of fine sand on flood plain, west side of Indus River at Kotri, West Pakistan. Climbing-ripple laminae are in lower half of *A* and in *D;* convolute structure is in upper half of *A* and in *C;* tabular planar structure (foresets) are in *A* and *B;* and horizontal laminae in *A*. Photographs by E. Tad Nichols. (4-inch knife handle in upper right of *A* gives the scale; scales in *B*, *C*, and *D*, are in inches.)

migration can proceed simultaneously. This fact was recognized as long ago as 1859 when Sorby (1859, p. 143) described "ripple drift" as developing where water was carrying heavy loads of sediment. It was referred to by Bucher (1919, p. 155) and more recently has been stressed by Reineck (1961), Allen (1963, p. 220) and Walker (1963). As expressed by Allen, "... the rate a moving rippled surface builds up is directly proportional to the rate at which sediment is deposited on it from an external source, thought to be the load of sediment in suspension." On the other hand, where sand is relatively sparse and is carried forward as fast as it is introduced, the only traces of ripple marks to be preserved as laminae are solitary profiles of individual ripple layers (McKee, 1957, fig. 7), and the structures referred to as both lenticular bedding (lenses of ripples) and flaser bedding (incomplete ripple lenses) (Reineck, 1962, p. 155). The latter types are recorded from the German tidal flats.

Because a considerable supply of sediment is necessary for the development of climbing ripples from ripple marks, the resulting structure can be expected in some sedimentary environments but not in others. Flood plains of rivers seem to be especially favorable sites for the forming of climbing ripples, as large quantities of sand and silt commonly are deposited by floods that overflow banks and spread rapidly across adjacent flats. Beaches and tidal flats, on the other hand, are not favorable for the development of climbing-ripple structure, even though ripple marks commonly develop on their surfaces; new sand is introduced sparingly and unevenly, and deposits are constantly reworked by waves and tidal currents.

ENVIRONMENT CONTAINING ABUNDANT CLIMBING-RIPPLE LAMINAE

Flood plains of the Colorado delta, Arizona

Prior to construction of Hoover Dam the Colorado River delta extended from a little north of the international boundary between the United States and Mexico southward to the Gulf of California. Usually twice each year (Sykes, 1937, p. 151) the overflow of the Colorado River covered extensive flood plains of the delta. Mostly sand and a little mud were deposited to the north, but proportionately less sand and more mud downstream. Stratification in the fine sand of this flood plain consists largely of climbing-ripple laminae and other small-scale structures (McKee, 1939, p. 71, pl.1*c–e*); locally medium-scale, moderately high angled foresets of small deltas are numerous (1939, p. 77, 78; pl. 1*f*).

Since construction of Hoover Dam, a new delta of the Colorado River has developed at the head of Mead Lake, largely within the Grand Canyon of Arizona. This new delta has much more restricted flood plains than those of the older delta. This restriction makes relatively easy the examination and recording of deposits from individual floods. Each deposit consists of a layer of cross-stratified sand from one to several feet thick, overlain by a layer of mud of comparable magnitude. As on the older delta, the relative thickness of sand layers, in proportion to their companion mud layers, becomes progressively less in a downstream direction.

In an area near Columbine Falls, from 10 to 20 miles below the head of the delta, studies of primary structures in various parts of the flood plain were made during the spring of 1961 and of 1962, after the water level had dropped following floods (McKee, 1965). Exposures along freshly cut banks were numerous, and cross-stratification patterns were well displayed. Estimates made at that time indicate that climbing-ripple laminae formed about 75 or 80 percent of the structures in the sand layers of the area. Other structures included flat or horizontal laminae, medium-scale "delta forsets" or tabular planar cross beds, and cross laminae of the scour-and-fill or trough type.

Flood plain of the Indus River, West Pakistan

A brief examination of sedimentary structures in the flood plain of the Indus River in southern West Pakistan was made in November of 1964. This study, supported by the Pakistan Geological Survey and made with the assistance of Farhat Husein, was centered at two localities—at Kotri near Hyderabad, and near Tatta Ferry, about 50 miles downstream. At each place trenches were dug, at distances ranging from a few feet to several hundred feet back from the present river banks, in fine sand and silt deposits of the flood plain or surface of overflow. The trenches were oriented both parallel to and normal to the river course, and were made at several different flood levels.

On a flood plain west of the Indus at Kotri the uppermost sedimentary unit across a wide area consists of fine to very fine sand (table 1) ranging in thickness from 18 to 24 inches and resting on beds of clay. In a trench that extended 280 feet normal to the river, climbing-ripple lamination in numerous independent cosets (fig. 1*A*, *D*) was the dominant structure. It was associated with sets of tabular planar cross strata, groups of horizontal or nearly horizontal laminae, and trough-type structures. In some places, cosets of climbing-ripple laminae formed discrete units,

TABLE 1.—*Grade-size distribution, in percent, in detrital sediment from Indus River flood plain, at Kotri, West Pakistan*

[Samples were collected 15 feet above river surface]

Location	Very coarse sand	Coarse sand	Medium sand	Fine sand	Very fine sand	Silt and clay
15 ft from river bank	0.0	0.1	0.1	51.9	38.0	9.2
85 ft from river bank	.0	.1	.2	29.4	48.3	22.0
150 ft from river bank	.0	.0	.5	47.9	43.0	8.6

TABLE 2.—*Grade-size distribution, in percent, of detrital sediment from Indus River flood plain at Tatta Ferry, West Pakistan*

[Upper sand-silt bed is 15 feet above river level; middle sand-silt bed is 9 feet above]

Horizon	Very coarse sand	Coarse sand	Medium sand	Fine sand	Very fine sand	Silt	Clay
Middle sand-silt bed	0.0	0.1	0.2	1.2	15.2	77.8	5.3
Upper sand-silt bed	.0	.0	.0	4.7	39.9	52.3	2.9
	.2	.6	.7	18.6	56.4	22.3	1.2

separated by horizontal parting planes from other types of cross strata above or below; elsewhere they graded laterally into other types.

In an 18-foot section exposed in the Indus River banks near Tatta Ferry, pairs of sandy silt beds (table 2) and clay layers are repeated five times (fig. 2). The beds of sandy silt are mostly ripple laminated, with a characteristic "climbing" structure; the clay beds are thin and flat but locally show much contortion. Each pair of silt and clay layers, ranging from 1 foot to several feet in thickness, is believed to be the product of a single flood, with the finest sediment settling last.

Natural levees on the delta of the Mississippi River

Detailed studies of sedimentary structures on the Mississippi delta by Coleman and others (1964) have indicated the principal types of structures developed there and the combinations of these structures that are representative of various depositional environments. For example, at the mouth of Johnson's Pass, which is a prograding distributary within the delta, climbing-ripple laminae are abundant in the natural levees, rare in stream-channel deposits, and unrecorded in four other sedimentary environments that do not involve overbank flow (Coleman and others, 1964, fig. 5). Samples more widely distributed across the delta, including some from the upper reaches where typical meanders and point bars occur, likewise indicate a restriction of these structures largely to natural levees and, locally, to channel deposits (Coleman and Gagliano, 1965, p. 145).

Throughout the Mississippi delta complex, as in the other regions described, the abundance of climbing-ripple laminae in areas of overbank flow, including both subaerial and submarine levees, shows that the development of climbing ripples is favored by rapid deposition from heavily laden floodwaters. In contrast, these structures do not characterize the sand and silt that were less rapidly accumulated or that were reworked by tides as illustrated by the deposits of bars, interdistributary bays, and various other environments (Coleman and Gagliano, 1965, table 1).

Subaerial levees of the Mississippi are ". . . usually covered with a dense growth of woody plants" (Coleman and Gagliano, 1965, p. 146), the roots of which tend to obscure and commonly to interfere with the development of ripple laminae, the result being many irregular or wavy laminae associated with the climbing-ripple lamination. Such structures ". . . appear to be a marker of this and subaqueous levee environments within the delta" (Coleman and Gagliano, 1965, p. 146). In contrast, flood-plain deposits bordering the Colorado and Indus Rivers, developing in arid regions

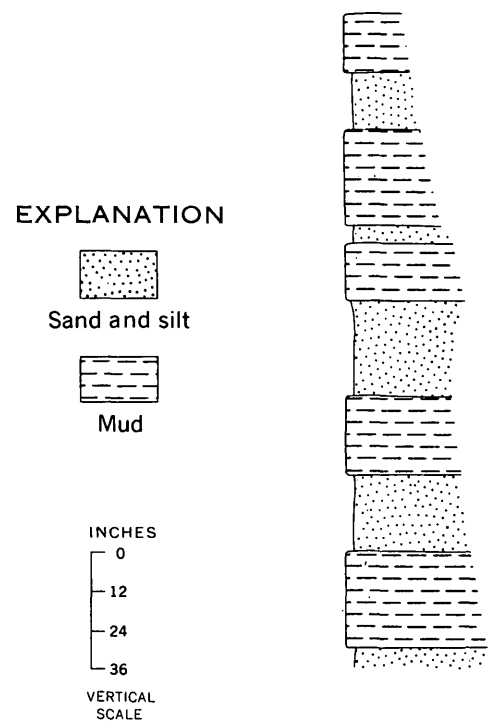

FIGURE 2.—Section in upper part of flood plain at Tatta Ferry, on Indus River, West Pakistan, showing alternating units of sand and mud. Sand units are largely ripple laminated but include convolute structures and local foresets. Mud units are thin horizontal beds with local convolute folds.

where dense vegetation is less common, probably contain relatively more undisturbed climbing-ripple structure. Relatively few irregular or wavy laminae were noted in the deposits of those rivers.

SEDIMENTARY STRUCTURES COMMONLY ASSOCIATED WITH CLIMBING-RIPPLE LAMINATION

Structure assemblages

Environments of deposition may be distinguished by definite and distinctive assemblages or suites of sedimentary structures, as has been well demonstrated for the Mississippi River by Coleman and Gagliano (1965, p. 133). Each type of structure is the product of one or more hydrodynamic or other factors, and its distribution is therefore restricted to the particular environments in which these factors are operative.

Climbing ripples, as described earlier, develop only where a heavy feeding of sediment occurs. Moreover, as has been shown experimentally (McKee, 1965, p. 79), much of the sand must come from above by a settling of suspended load. The deposition of sediment from suspension may result in several types of structure, depending largely on the form of base upon which accumulation takes place but probably also on the amount of sediment being dropped, on the velocity of the transporting agent, and on other factors. In addition to forming a climbing-ripple structure, sediment dropping from suspension also commonly forms horizontal (parallel) bedding, and may be responsible for further development into convolute lamination.

Convolute structure

A type of contorted bedding commonly referred to as convolute structure, and described (Ten Haaf, 1956) as ". . . sets of wavy or contorted laminae whose deformation characteristically dies out both upward and downward within a given sedimentation unit," is associated with climbing ripples in numerous places. It is represented by a variety of morphological forms, all of which consist basically of relatively thin, pointed anticlines separated by more rounded and wider synclines (fig. 1*A*, *C*; 3*A*, *B*); and it occurs in fine sands, silts, and muds. Analyses shown in tables 1 and 2 are typical of sediments that contain convolute lamination. Furthermore, these structures may occur within a sand unit that grades laterally into climbing-ripple laminae, in sand or silt layers immediately above a sequence of climbing ripples, or in mud layers overlying a climbing-ripple silt unit.

The origin of convolute bedding has been much debated within recent years. The two principal theories attribute this structure to a lateral "gliding" or "laminar flow of liquefied, confined beds under the influence of gravity" (Rich, 1950; Williams, 1960) and to hydraulically induced deformation during deposition of fine sediment (Kuenen, 1953; Ten Haaf, 1956; Sanders, 1960). The structure may be formed in more than one way (Dzulynski and Smith, 1963), and very likely results from a combination of two or more processes as suggested by Dott and Howard (1962, p. 120). It is a common feature of both river flood-plain and point-bar environments, and has been formed (fig. 3*C*) in laboratory experiments (McKee and others, 1962a, p. D152) as a result of sand dropping out of suspension from above.

Numerous illustrations of convolute structure were recorded during recent examination of overbank or flood-plain deposits along the Indus River. Scattered and isolated "anticlines" in otherwise nearly horizontal sandbeds overlying climbing-ripple structures were observed at Kotri (fig. 1*A*, *C*) and in horizontal mud beds within a mud-silt sequence at Tatta (fig. 3*B*, upper part). Groups of very irregular, tonguelike "anticlines" also are present in silt beds of the same sequence (fig. 3*A*, *B*); these silt beds elsewhere contain either ripple lamination or foresets of compound cross bedding.

On the delta of the Mississippi River also, beds with convolute structure are common, according to Coleman and Gagliano (1965, p. 136). They (1965, fig. 5) illustrate an intimate relationship between some convolute laminations and climbing-ripple structure, with the one grading upward into the other. Convolute structures are recorded by them (1965, table 1) as common to abundant on subaqueous levees and as rare on subaerial levees and in distributary channels.

Horizontal laminae

Stratification that is horizontal or nearly so may be formed in at least two very different ways, and both types of horizontal strata are associated locally with climbing-ripple structures. Horizontal laminae of one type or another occur in nearly all environments, however; so by themselves they are not significant as environmental indicators. On the Mississippi delta, for example, horizontal or "parallel" laminae are recorded as either common or abundant in all 12 environments recognized (Coleman and Gagliano, 1965, table 1).

One type of horizontal lamination is formed under conditions of upper flow regime in which currents are sufficiently strong to move sand in a streaming movement with little turbulence. Evidence that this type of structure is sometimes preserved in association with climbing-ripple structure is furnished by experimental

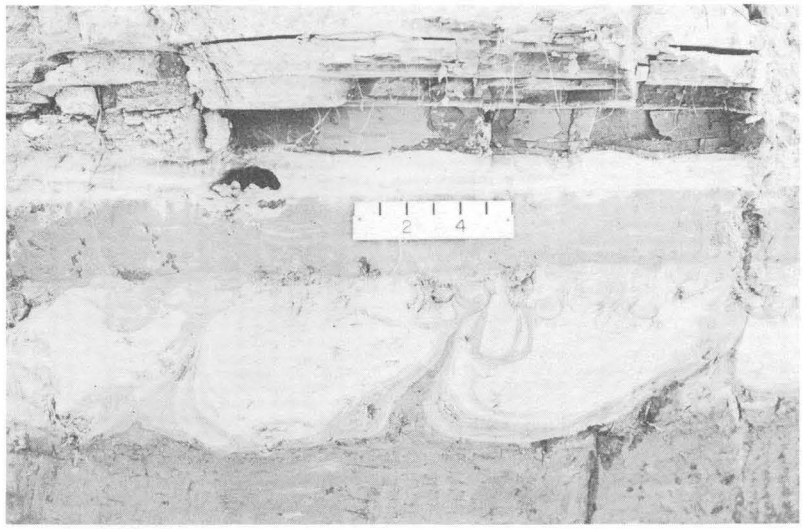

A

B

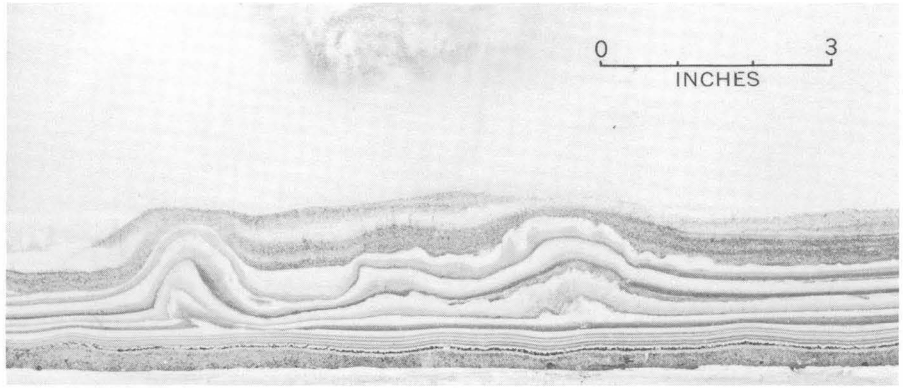

C

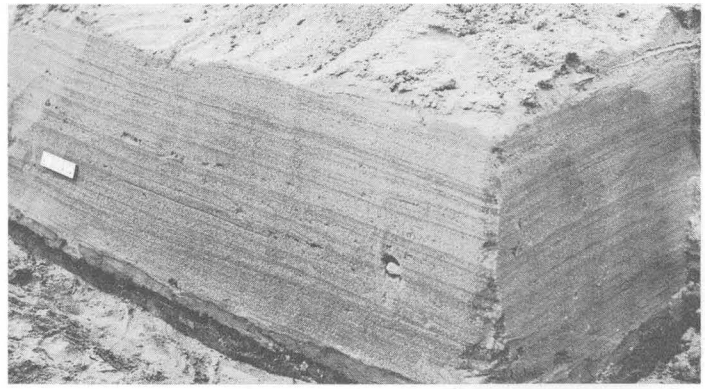

D

FIGURE 3.—Bedding and structure in flood-plain deposits and laboratory model. *A*, *B*, flood-plain deposits, west side of Indus River at Tatta Ferry, West Pakistan, showing thin horizontal beds of mud overlying thick silt layer; an irregular variety of convolute structure occurs in the silt which elsewhere contains climbing-ripple laminae and delta foresets; in *B*, convolute structure also occurs in mud. *C*, convolute structure developed in laboratory from sand falling vertically from suspension to a surface of horizontal laminae in mud. *D*, horizontal laminae of sand and fine gravel deposited by water in upper stream regime overflowing banks of East Bijou Creek, Colo., during flood of 1965. Photographs *A* and *B* by E. Tad Nichols. Scales are in inches.

models (McKee, 1965, figs. 4*a*, *b*) and by samples from the active Mississippi delta (Coleman and Gagliano, 1965, p. 139). In both examples horizontal laminae of sand form the end product of a structure sequence that begins with small climbing-ripple laminae and that is produced by a progressive increase in current velocity. Horizontal laminae caused by currents in the upper flow regime have been described as thin but widespread in channel sands of the Rio Grande (Harms and Fahnestock, 1965, p. 93, 97, 106); they are the dominant structure (fig. 3*D*) in extensive sand deposits that cover the banks to a thickness of several feet along East Bijou Creek, Colo. These deposits were laid down during the major flood of 1965.

The second type of horizontal lamination associated with some climbing ripples is the result of deposition from suspension of detrital particles, especially silt and clay. This process involves very slow movement of water. It is formed on flood plains by the settling of mud or sand in ponded areas and in the bottomset deposits of delta cones. Its association with climbing-ripple structure has been illustrated in laboratory experiments where it commonly accumulates in the relatively quiet water to the lee of a growing mound of climbing ripples in a water tank (McKee, 1965, fig. 4*c*, *d*, 5*d*). This type of horizontal lamination, however, probably is best developed and most representative of lakes and other bodies of quiet water.

Other structures

Certain structures commonly associated with climbing-ripple lamination are not largely dependent for growth upon sediment introduced out of suspension. These structures include various types of medium- to large-scale crossbedding, mostly developed by an increase or decrease from the velocity responsible for forming ripple marks. Thus, increase in velocity may from trough-type cross strata, as when megaripples or aqueous dunes develop. Similarly, an abrupt change in depth or decrease in stream velocity may start deposition of foresets to make wedge or tabular cross strata. Although the trough structure seems to be especially typical of a stream-channel environment (Harms and Fahnestock, 1965, p. 109–110), and the wedge or tabular planar structure is characteristic of delta cones, these structures also form in a number of other environments and were observed in association with climbing-ripple lamination at various places, including the Colorado River (McKee, 1939, p. 78) and the Indus River (fig. 1*B*) flood plains.

Intraformational recumbent folds have been shown (McKee and others, 1962b, p. D155) to develop where sediment of heavily laden currents causes a horizontal drag across the upper ends of foreset beds. They are found among climbing-ripple deposits, and small-scale varieties are reported to be common in bar, channel, and levee sediments of the Mississippi delta (Coleman and Gagliano, 1965, p. 136). They have also been noted among ripple laminae on the flood plain of the Colorado River.

SOME ENVIRONMENTS OF ABUNDANT RIPPLE-MARK DEVELOPMENT LARGELY UNFAVORABLE TO CLIMBING-RIPPLE STRUCTURE

Environments are numerous in which climbing-ripple lamination is scarce or absent. Many of these environments, including swamps, playas, and marshes, need not be considered here as they obviously are not favorable for ripple development. Certain others, particularly tidal flats and some beaches, typically show abundant ripple marks. Despite the ripple-forming tendencies in such environments, only ripple lenses and incomplete ripple structures such as those recorded by Reineck (1962, p. 155), are preserved in appreciable amount in such places.[1] Thus, the conclusion is reached that climbing-ripple structure is inhibited by a limited supply of new sand or silt and by the constant reworking of available sediment.

Tidal flats of Cholla Bay, Mexico

Tidal flats composed entirely of sand form the floor of Cholla Bay bordering the Gulf of California in Sonora, Mexico. During low tide, when these deposits are exposed to view for a distance of several miles along shore and to seaward, they are almost completely covered with parallel-type ripple marks resulting from tidal currents and waves (McKee, 1957, p. 1740). Trenches cut into these deposits with various orientations, however, fail to show any climbing-ripple structure and give very little evidence of ripple form in the lamination. Latex peels of trench walls taken by the writer and X–ray photographs prepared by W. K. Hamblin show laminae that are largely flat lying but generally irregular or uneven, interpreted as the result of constant reworking of the sediment.

Delta tidal areas at mouth of Ganges (Hooghly) River, India

Primary structures of delta beaches and tidal flats at the mouth of the Ganges (Hooghly) River in India were examined early in the winter of 1965. Supriya Sen Gupta, S. K. Baksi, and T. S. Kutty of the Indian

[1] Although climbing-ripple lamination is largely or entirely absent on tidal flats, it has been observed in Queensland, Australia, in tidal channels that drain the low tide flats (J. M. Coleman, written commun., Feb. 1966).

Statistical Institute, and Indranil Banarjee of the University of Calcutta, participated in the work, which was done by landings from a Forestry Service boat furnished for the project.

A considerable amount of sand (table 3), apparently

TABLE 3.—*Grade-size distribution in detrital sediment from beaches and tidal flats at mouth of Ganges (Hooghly) River, in percent*

[Dominant grades in italic]

	Pitts Point, estuary beach crest		Pitts Point, tidal flat, 100 yds in	Fraserganj, Lacams channel, backshore			Fraserganj, Lacams channel, foreshore	New Moore Island, Sager Sand, tidal flat	
Very coarse sand	0.1	0.0	0.0	0.0	0.0	0.0	0.0	0.0	0.0
Coarse sand	.1	.1	.1	.1	1.1	.1	.0	.1	.1
Medium sand	.6	.4	.5	1.4	15.8	.5	.4	.6	.6
Fine sand	*72.2*	46.6	22.8	27.5	40.8	35.7	*50.9*	*67.6*	*78.2*
Very fine sand	26.3	*50.0*	*72.7*	*66.5*	*41.1*	*61.7*	47.8	31.5	21.0
Clay and silt	.7	2.8	3.9	4.3	1.2	2.0	.9	.3	.1

introduced by marine longshore currents from the southwest and not from the river, has accumulated in lower parts of the estuary. Farther upstream toward Calcutta only mud is present. A relatively small tide reworks the sand constantly, but apparently does not pile up new sediment at a rapid rate in many places. It maintains beaches and broad tidal flats of sand along the outer delta margins, adjacent to the Bay of Bengal. Although parts of the beaches and all of the adjacent flats are covered with ripple marks (fig. 4*B*, p. D102), few traces of them were seen in exploratory cross sections.

The delta beaches in general contain primary structures much like those of normal beaches elsewhere. Foreshores consist of extensive even laminae in sets that dip seaward at various low angles (2°–8°) (fig. 4*A*). Backshore laminae commonly are disrupted by minor scours, sags, and folds as illustrated at Fraserganj beach (figs. 4*C*, *D*); and they include zones of brecciation and trash. In one backshore section at Fraserganj, however, well-developed climbing-ripple laminae with drift normal to the beach crest are interpreted as the result of rapid deposition in a sheltered area behind the berm. Probably they formed at time of high tide, large waves, or both, when an abundance of sand was introduced over the crest.

Sandy tidal flats extending across wide areas bordering on the Bay of Bengal and at the mouths of distributaries are largely covered with parallel, asymmetrical ripple marks (fig. 4*B*). Trenches dug in these flats, both at Pitts Point and at Sager Sand (New Moore Island), disclosed sections with weakly developed, irregular but nearly flat-lying beds (fig. 4*B*), and with no ripple lamination despite the abundance of ripple marks on the surface above. In contrast to these structures, flood-plain deposits at Halisahar, 30 miles upstream from Calcutta, are reported by Indranil Banerjee (written commun., May 21, 1965) to contain extensive climbing-ripple lamination, horizontal lamination, and also convolute bedding.

CONCLUSIONS

Examination of sedimentary structures in a number of modern environments suggests that climbing-ripple lamination is characteristic of certain fluvial deposits—especially those of flood plains and natural levees—and is less common in river-channel deposits. Climbing-ripple structures are rare in areas where deposition is largely a result of tidal action, despite the common development of surficial ripple marks in such environments.

Factors controlling the development of climbing ripples and, therefore, responsible for their restriction to a relatively few environments are (1) a comparatively weak current, favorable to the forming of ripple marks, and (2) a large supply of sand or silt that will permit an upward as well as a forward growth of the rippled surface.

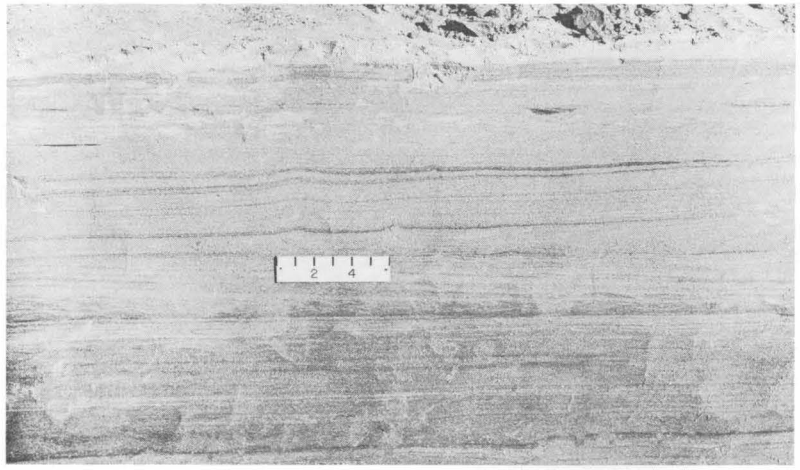

A

B

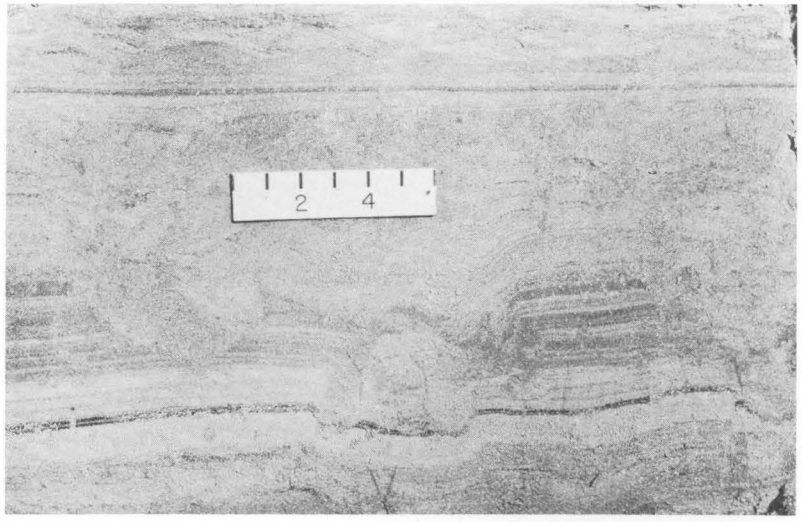

C

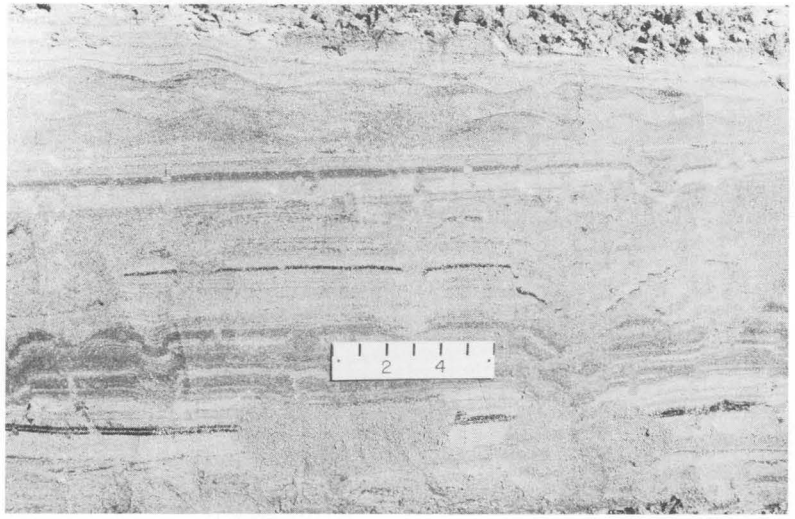

D

FIGURE 4.—Sand deposits of tidal area at front of Ganges (Hooghly) delta, India. *A*, Fraserganj beach, section parallel to crest; *B*, tidal flat at Sager Sand, New Moor Island; *C*, *D*, Fraserganj beach, deformation and scouring in backshore normal to crest (*C*) and parallel to crest (*D*). Photographs by E. Tad Nichols. Scales are in inches.

REFERENCES

Allen, J. R. L., 1963, Asymmetrical ripple marks and the origin of water-laid cosets of cross-strata: Liverpool-Manchester Geol. Jour., v. 3, pt. 2, p. 187–236.

Bucher, W. H., 1919, On ripples and related sedimentary forms and their paleogeographic interpretation: Am. Jour. Sci., v. 47, p. 149–210, 241–269.

Coleman, J. M., and Gagliano, S. M., 1965, Sedimentary structures—Mississippi River deltaic plain, *in* Primary sedimentary structures and their hydrodynamic interpretation: Soc. Econ. Paleontologists and Mineralogists Spec. Pub. 12, p. 133–148.

Coleman, J. M., Gagliano, S. M., and Webb, J. E., 1964, Minor sedimentary structures in a prograding distributary: Marine Geology, v. 1, no. 3, p. 240–258.

Dott, R. H., Jr., and Howard, J. K., 1962, Convolute lamination in non-graded sequences: Jour. Geology, v. 70, no. 1, p. 114–121.

Dzulynski, Stanislaw, and Smith, A. J., 1963, Convolute lamination, its origin, preservation, and directional significance: Jour. Sed. Petrology, v. 33, p. 616–627.

Harms, J. C., and Fahnestock, R. K., 1965, Stratification, bed forms, and flow phenomena (with an example from the Rio Grande), *in* Primary sedimentary structures and their hydrodynamic interpretation: Soc. Econ. Paleontologists and Mineralogists Spec. Pub. 12, p. 84–115.

Kuenen, Ph. H., 1953, Significant features of graded bedding: Am. Assoc. Petroleum Geologists Bull., v. 37, no. 5, p. 1044–1066.

McKee, E. D., 1939, Some types of bedding in the Colorado River delta: Jour. Geology, v. 47, p. 64–81.

McKee, E. D., 1957, Primary structures in some recent sediments: Am. Assoc. Petroleum Geologists Bull., v. 41, no. 8, p. 1704–1747.

McKee, E. D., 1965, Experiments on ripple lamination, *in* Primary sedimentary structures and their hydrodynamic interpretation: Soc. Econ. Paleontologists and Mineralogists Spec. Pub. 12, p. 66–83.

McKee, E. D., Reynolds, M. A., and Baker, C. H., Jr., 1962a, Laboratory studies on deformation in unconsolidation sediment: Art. 1964 *in* U.S. Geol. Survey, Prof. Paper 450–D, p. D151–D155.

——— 1962b, Experiments on intraformational recumbent folds in crossbedded sand: Art. 165 *in* U.S. Geol. Survey Prof. Paper 450–D, p. D155–D160.

Reineck, Hans-Erich, 1961, Sedimentbewegungen an Kleinrippeln im Watt.: Senckenbergiana lethaca, v. 42, no. 1/2, p. 51–67.

——— 1962, Schichtungsarten in Wattenboden: Zeitschrift für Pflanzenernährung, Düngung, Bodenkunde, v. 99 (144), no. 2/3, p. 154–159.

Rich, J. L., 1950, Flow markings, groovings, and intrastratal crumplings as criteria for recognition of slope deposits, with illustrations from Silurian rocks of Wales: Am. Assoc. Petroleum Geologists Bull., v. 34, p. 717–741.

Sanders, J. E., 1960, Origin of convoluted laminae: Geol. Mag., v. 47, no. 5, p. 409–421.

Simons, D. B., and Richardson, E. V., 1961, Forms of bed roughness in alluvial channels: Am. Soc. Civil Eng. Proc., Jour. Hydraulics Div., p. 87–93.

Sorby, H. C., 1859, On the structures produced by the currents present during the deposition of stratified rocks: The Geologist, v. 2, p. 137–147.

Sykes, Godfrey, 1937, The Colorado delta: Carnegie Inst. Washington Pub. 460, 193 p.

Ten Haaf, Ernst, 1956, Significance of convolute lamination: Geol. en Mijnbouw, v. 18, p. 188–194.

Walker, R. G., 1963, Distinctive types of ripple-drift cross laminations: Sedimentology, v. 2, p. 173–188.

Williams, Emyr, 1960, Intra-stratal flow and convolute folding: Geol. Mag., v. 97, p. 208–214.

VOLCANIC ROCKS DREDGED SOUTHWEST OF THE HAWAIIAN ISLANDS

By CELESTE G. ENGEL and A. E. J. ENGEL,[1] La Jolla, Calif.

Abstract.—Dredging in a seamount province southwest of the Hawaiian Islands confirms earlier conclusions concerning the association of tholeiitic and alkalic basalts on the ocean floor. Rocks dredged from a small volcano on a major geomorphic, structural, and magnetic lineament which separates contrasting oceanic provinces, consist of tholeiitic basalt related in composition to the Hawaiian tholeiites. Alkali-rich basalt, and other alkalic rocks, including hornblende-bearing varieties and a rare biotite trachyte, were dredged from adjacent and nearby large submarine volcanoes south of the lineament. Spatial relations of the rocks in this part of the Pacific Ocean substantiate the hypothesis that in the oceans, volcanic rocks of the alkali series are confined to, and are ideally developed on, large volcanoes.

During Expedition Dodo of the Scripps Institution of Oceanography, University of California, under the direction of Victor Vacquier, dredge hauls of volcanic rocks were obtained by the research vessel *Argo* from 7 localities: from the tops and flanks of 6 submarine volcanoes, and from an elongate volcanic ridge in the region southwest of the Hawaiian Islands (fig. 1). Fred Dixon, of the University of California, supervised dredging, and Dallas Peck, of the U.S. Geological Survey, made shipboard petrographic studies of the hauls. The rocks dredged from 6 volcanoes belong to the alkali series; 5 are alkali-rich basalts, 2 of which contain hornblende. The sixth dredge haul from the top of a large volcano is a biotite trachyte of uncommon composition. In contrast to these dredge hauls of alkali-rich volcanic rocks, a tholeiitic basalt (PV 324 B) somewhat similar in composition to Hawaiian tholeiites was dredged from the low volcanic ridge (fig. 1).

REGIONAL SETTING

All the submarine volcanoes in the region are built either south of or along the well-defined geomorphic, structural, and geomagnetic lineament which trends west-southwest from a point south of the island of Molokai (see insert, fig. 1). The lineament probably defines a major fracture zone, and the characteristics of the sea floor differ appreciably on either side of it (U.S. Naval Oceanographic Office, 1962, p. 7). This lineament probably represents a southwestern extension of the great Molokai fracture zone, which has been traced east-northeast of the Hawaiian Islands almost to the mainland of North America. The lineament has been traced as a broad depression southwest of the region shown in figure 1 from long 164° to 167° W. by the Six-Pac Expedition of the Scripps Institution of Oceanography, in April 1966 (Thomas Chase, oral commun., May 1966).

If these alined segments of fracture zones southwest of Hawaii are actually part of the Molokai fracture zone, the Hawaiian Islands are not obviously displaced by it. Hence, either the Hawaiian Islands are younger than the Molokai fracture zone, or there is little geologically recent displacement along it.

Geomorphically, the lineament includes a series of alined, broad depressions with discontinuous, bordering ridges. These features lie along and just south of a well-defined, elongate, negative magnetic anomaly with residual values of about —300 gammas (fig. 1).

Immediately north of the lineament the sea floor is almost featureless and slopes gently west-southwest. But the eastward prolongation of the lineament forms an angle of some 30° with the northwest trend of the great Hawaiian rift. Several smaller, elongate, negative anomalies exist north of the lineament and are parallel to it (U.S. Naval Oceanographic Office, 1962).

The sea floor to the south of the lineament also slopes west-southwest, but more steeply than the sea floor to the north. In this southerly region, a swarm of more irregular, negative magnetic anomalies (not shown on fig. 1) extends southwest in crudely elongate subparallel patterns, at angles of some 25°to 40° to the major anomaly along the lineament. All the submarine volcanoes except one occur within these irregular anomalies, and the largest negative anomalies

[1] University of California, San Diego.

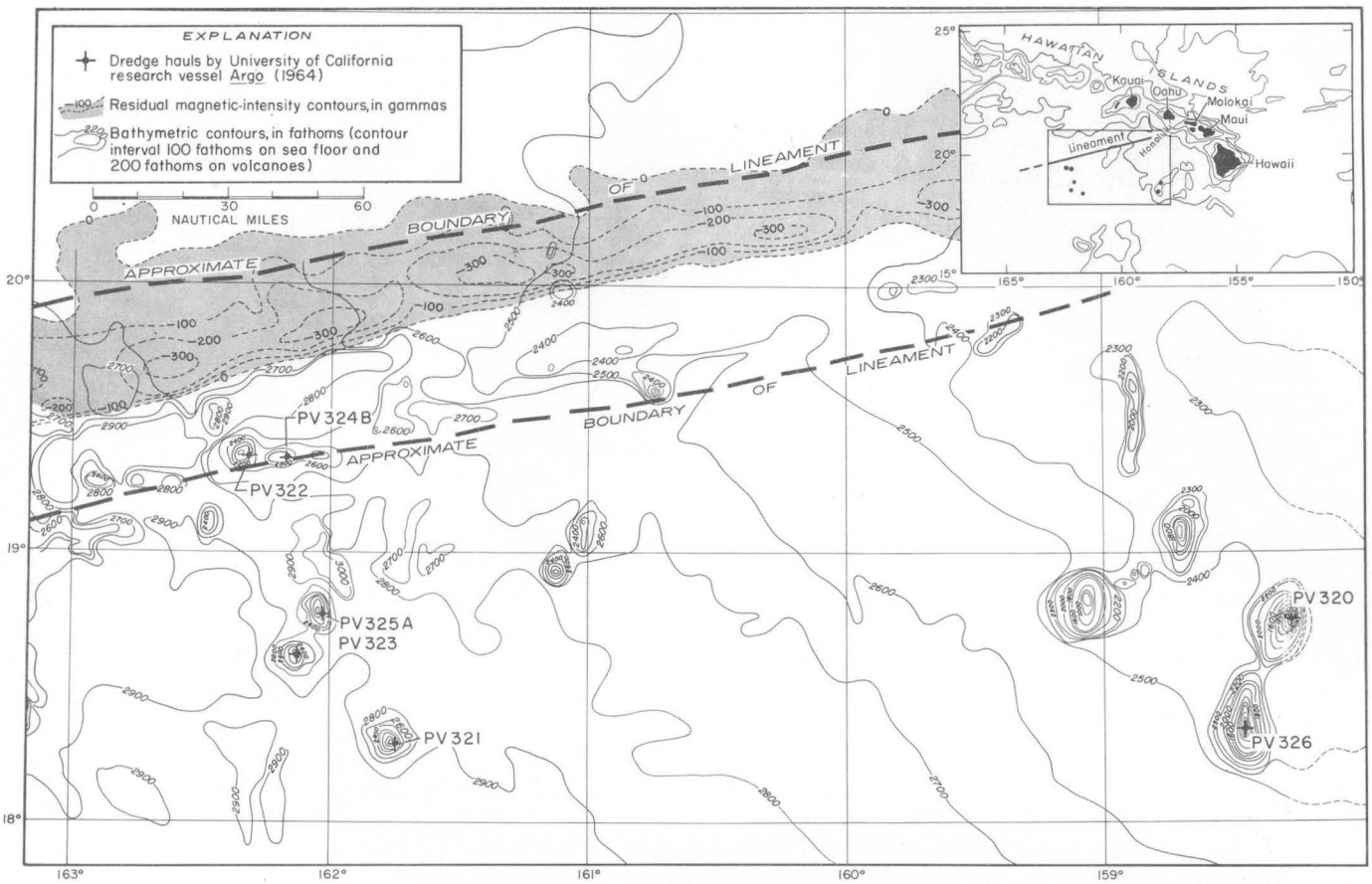

FIGURE 1.—Bathymetric contour map of the region southwest of the Hawaiian Islands. The major geomorphic, structural, and magnetic lineament separates the volcano-studded province to the south from the relatively featureless ocean floor to the north.

coincide with the volcanoes in the eastern part of figure 1.

Several features of the volcanic rocks in this region are noteworthy. The one haul of tholeiitic basalt (PV 324 B, fig. 1) was recovered from a low peak (a small volcanic cone, or deposits from a fissure eruption?) built along one of the volcanic ridges. The dredge haul (PV 322) made immediately to the west on a much larger volcano recovered alkali-rich volcanic rocks. South of the lineament only alkali- and alumina-rich volcanic rocks were obtained from the large single and paired volcanoes. The data from these several hauls are consistent with previous information; in more than 200 dredge hauls from the upper slopes of isolated and paired volcanoes of this type, only alkali-rich basalts have been obtained (Engel and Engel, 1964, p. 480). Yet tholeiitic basalts dominate the rift volcanoes of Hawaii (Macdonald and Katsura, 1964) and appear to the exclusion of alkali basalts on fault scarps, and submarine ridges of the ocean floor (Engel and others, 1965). We have suggested that this correlation of composition with volcanic structure and morphology may be due to differences in the rate and mode of construction of these different features. This interpretation is reviewed after a discussion of the petrologic and chemical features of the rocks from these contrasting, new occurrences.

COMPOSITION OF THE ROCKS

Rocks from 5 of the 7 dredge hauls have been chemically analyzed and studied in detail; those from the other two have not been studied in detail. A rock from one of these two hauls, PV 323, was dredged from the top and upper slopes of a submarine volcano at depths of from 1,800 to 2,500 fathoms (3,300 to 4,500 meters) (fig. 1). It is a vesicular, porphyritic, alkali-rich basalt with approximately 30 percent plagioclase phenocrysts and 5 percent green pyroxene in a fine-grained groundmass. Other rocks in this dredge haul were altered and encrusted with hydrated manganese oxides.

A sample from the other dredge haul, PV 326, was dredged from the top and upper slopes of a volcano at a depth of about 675 fathoms (1,235 m) (fig. 1). It is an amygdaloidal alkali basalt with small phenocrysts

of plagioclase. The vesicles are round and filled with calcite.

Sample PV 320 from the dredge haul of the same number was collected from a submarine mountain approximately 150 nautical miles south of Honolulu (fig. 1). The rock was dredged from the top of the seamount at a depth of about 265 fathoms (500 m). Rocks in the dredge haul consist of numerous boulders and several rounded cobbles. The largest boulder, approximately 80 × 70 × 30 cm is coated with a deep-brown, Mn-rich stain. The rock is unaltered except for minor discoloration and oxidation along platy cleavage surfaces. On broken surfaces, the rock is light gray and contains scattered phenocrysts of plagioclase and biotite in a dense, fine-grained trachytic groundmass. The groundmass consists of an alkali feldspar which exhibits undulatory extinction, a plagioclase (oligoclase?), and minor opaque minerals. The rare andesine phenocrysts are as much as 3 mm in length, and the biotite phenocrysts are smaller, reddish brown, and rimmed with aggregates of magnetite. Apatite is an accessory mineral. The chemical composition of sample PV 320 is listed in table 1, and the modal analysis is given in table 2.

Volcanic rocks of this composition are rare in the oceans. Macdonald and Katsura (1964, p. 117, table 3, column 18), report a similar "trachyte trending toward mugearite," from the Hawi Volcanic Series in an upper member of Kohala volcano, and another rock of approximately the same composition (1964, p. 121, table 6, column 27) from the Honolua Volcanic Series of West Maui volcano. The Hawaiian samples contain about 58 weight percent silica and similar amounts of sodium as sample PV 320. However, PV 320 has more potassium, thus raising its total alkali content ($Na_2O + K_2O$) to 10.6 weight percent, which projects it outside the field of Hawaiian mugearites and trachytes as shown in figure 2.

Le Maitre (1962, p. 1329, table 10, sample G–11) has called a rock similar in composition to PV 320 from Gough Island in the Atlantic Ocean a biotite trachyte. But these are among the very rare analogs of PV 320 in recent analyses of oceanic volcanic rocks.

Sample PV 321 was collected from a depth of about 1,500 fathoms (2,700 m) on the upper slopes of a submarine volcano in the southwest part of the region studied (fig. 1). Rocks collected from this volcano consist of boulders and cobbles of hornblende-bearing basalt. The rocks are gray, porphyritic, and slightly vesicular. The most abundant phenocrysts are plagioclase, zoned from labradorite to andesine. Many of them are of irregular shape and show skeletal and composite growth patterns. Some of the labradorite contains large overgrowths of a feldspar which has a much lower index of refraction and which is probably alkali feldspar. The mafic phenocrysts are hornblende and augite. Some hornblende phenocrysts are as large as 5 mm long, and most are rimmed with a sheath of magnetite. The groundmass has a pronounced trachytic texture, and consists of fine-grained oligoclase(?), clinopyroxene, and minor opaque minerals. Palagonite occurs in irregular patches in the groundmass.

TABLE 1.—*Chemical composition of volcanic rocks dredged south and southwest of the Hawaiian Islands*

[Location of samples shown on figure 1]

	Sample No. (taken from No. of dredge haul)				
	PV 320	PV 321	PV 322	PV 325 A	PV 324 B
Oxides (weight percent) [1]					
SiO_2	56. 12	51. 64	50. 38	47. 71	49. 52
TiO_2	. 82	1. 37	1. 52	1. 55	1. 81
Al_2O_3	18. 55	20. 19	19. 46	20. 36	15. 51
Fe_2O_3	4. 00	4. 99	4. 37	6. 00	4. 49
FeO	. 32	1. 36	1. 77	1. 27	6. 70
MnO	. 16	. 10	. 25	. 08	. 15
MgO	. 71	2. 34	1. 82	2. 05	6. 43
CaO	5. 43	6. 83	5. 71	4. 15	8. 65
Na_2O	6. 00	4. 38	4. 02	3. 32	2. 58
K_2O	4. 63	2. 70	3. 60	1. 26	. 50
H_2O^+	. 72	1. 56	2. 71	5. 02	2. 11
H_2O^-	. 35	1. 63	3. 38	6. 35	1. 05
P_2O_5	1. 83	. 86	. 81	. 69	. 18
Total	99. 64	99. 95	99. 80	99. 81	99. 68
Elements (parts per million) [2]					
B	<30	<30	100	130	<30
Ba	1, 500	400	1, 500	270	13
Co	<3	11	6	9	28
Cr	17	82	5	14	180
Cu	5	32	41	100	97
Ga	21	17	23	19	20
La	120	<80	180	<80	<80
Li	12	22	45	51	15
Nb	130	42	150	52	<30
Ni	16	30	32	25	63
Rb	110	30	90	20	10
Sc	<4	19	<4	20	54
Sr	500	370	1, 800	320	76
V	32	220	88	190	260
Y	60	36	92	40	48
Yb	4	4	6	4	5
Zr	580	240	480	300	96

Ag <3, Be <2, Mo <5.

PV 320 (Dodo dredge haul 7–1, seamount 7–N), lat 18°45′ N., long 158°15′ W.
321 (Dodo dredge haul 9–2, seamount 1), lat 18°18′ N., long 161°46′ W.
322 (Dodo dredge haul 14–2, seamount 5–W), lat 19°22′ N., long 162°19′ W.
325 A (Dodo dredge haul 11, seamount 2–N), lat 18°47′ N., long 162°03′ W.
324 B (Dodo dredge haul 15–2, seamount 5–E), lat 19°23′ N., long 162°10′ W.

[1] Analyses by C. G. Engel, U.S. Geol. Survey.
[2] Quantitative spectrographic analyses (±15 percent) by R. G Havens, U.S. Geol. Survey.

TABLE 2.—*Approximate percentages, in volume percent, of minerals in volcanic rocks dredged south and southwest of the Hawaiian Islands*

[Chemical composition of samples given in table 1, and location on figure 1. Tr., trace]

	Sample No. (taken from No. of dredge haul)				
	PV 320	PV 321	PV 322	PV 325 A	PV 324 B
Groundmass [1]	93	70	75	[2] 69	------
Plagioclase	1	16	11	22	46
Pyroxene	------	2	2	4	43
Olivine	------	------	------	?	------
Hornblende	------	2	------	?	------
Biotite	2	------	------	------	------
Vesicles	2	6	3	2	1
Opaque minerals	Tr.	1	3	1	5
Alteration [3]	2	3	4	2	5
Nepheline	------	------	2	Tr.	------
Apatite	Tr.	Tr.	Tr.	Tr.	------

[1] Includes crystallites of plagioclase and opaque minerals.
[2] Glass with crystallites of plagioclase and opaque minerals.
[3] Includes palagonite, calcite, chlorite, and rare zeolites.

Apatite is an abundant accessory mineral. Vesicles are irregular in shape.

Sample PV 325 A was dredged from the upper slopes and crest of a volcano at depths of 1,700 to 2,500 fathoms (3,170 to 4,700 m). The dredge haul consisted of extremely heavily weathered boulders and cobbles coated with manganese oxide. The freshest sample, PV 325 A (table 1), is a buff, porphyritic basalt with phenocrysts of labradorite and minor clinopyroxene. Other samples of what is probably the same rock type in the dredge haul are altered to clay with a few fresh remnant plagioclase phenocrysts. The phenocrysts in PV 325 A are of labradorite, pale-green pyroxene, magnetite, altered hornblende or olivine, and rare nepheline. The groundmass consists of hydrated glass containing abundant feldspar crystallites in subparallel alinement. Apatite is an accessory mineral. Vesicles are rare, but are round or almond shaped and filled with aggregates of a silica mineral which is probably chalcedony. The chemical analysis of this alkali basalt is given in table 1. A characteristic of this, and the other alkali-rich volcanic rocks from volcanoes south of the lineament, is their extremely high alumina content, which ranges from 18.5 to 20.3 weight percent Al_2O_3.

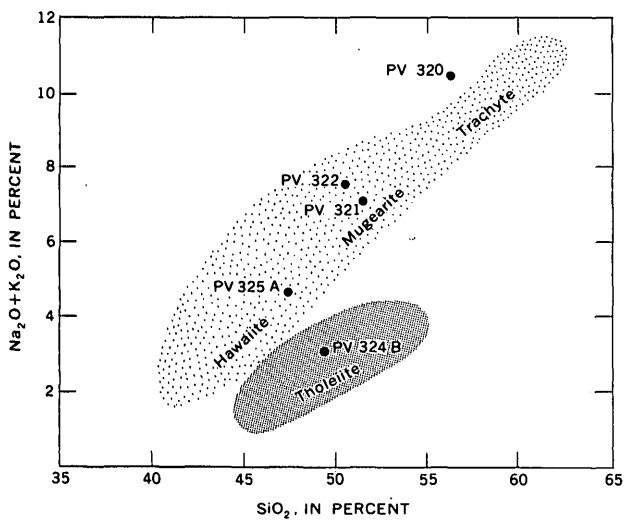

FIGURE 2.—Plot of total Na_2O+K_2O against SiO_2, showing named fields of occurrence of the Hawaiian rock series (Macdonald and Katsura, 1962), and the position (filled circles) of rocks analyzed from the region southwest of Hawaii.

Sample PV 322 is representative of the rocks collected from the upper slopes of the largest volcano along the lineament. The haul was obtained at depths of 1,890 to 2,160 fathoms (3,400 to 3,900 m). The rock is a fine-grained, gray, vesicular and slightly porphyritic alkali basalt. It contains phenocrysts of andesine, light-tan clinopyroxene, nepheline, and magnetite set in a fine-grained trachytic groundmass of plagioclase and pyroxenes. Most vesicles are elongated and alined along the flow surfaces in the basalt. Zeolites occur in some of these vesicles.

Sample PV 324 B was dredged from a point 12 miles east of PV 322 (fig. 1), but on a much smaller submarine peak, and at greater depths, 2,150 to 2,400 fathoms (3,900 to 4,400 m). The rock fragments are pale-gray, fine-grained basalt. In thin section, subradiating and randomly oriented laths of plagioclase, prismatic augite, and opaque oxides are scattered through a microcrystalline groundmass composed largely of these same minerals.

The chemical composition of sample PV 324 B is given in table 1. The analysis, coupled with the mineralogical data (table 2), indicates that PV 324 B is a tholeiitic basalt similar in most respects to the average of Hawaiian tholeiitic basalt, but in other respects it is intermediate in composition between the alkali-rich basalts which cap the adjacent higher volcanoes and the typical tholeiites of the ocean floor. Hawaiian tholeiites contain more Ti, Fe, and K and less Al and Na than oceanic tholeiites. PV 324 B shows values of Al and Na intermediate between the average Hawaiian and oceanic tholeiites, but it contains more ferric iron, K, and less Mg and Ca. In these respects it has affinities with the alkali-rich basalts. The tholeiitic basalt (PV 324 B) contains less Ba, Nb, Rb, and Zr, and more Co, Cr, Ni, and Sc than do the alkali-rich basalts in table 1. These are characteristic differences between the tholeiitic basalts of the oceans and the alkali-rich varieties (Engel and others, 1965, table 2).

224-352 O—66——8

RELATION OF ROCK TYPE TO TYPE OF VOLCANO

Volcanoes south of the lineament (fig. 1) have probably evolved much like those in the eastern Pacific Ocean (Baja Seamount province) in a manner that may be contrasted with the Hawaiian chain. The volcanoes of figure 1 are of moderate size and occur singly and in pairs, but without marked connecting ridges, or large, fringing "archipelagic aprons" of lava. In these respects, the volcanoes appear to have been built over relatively confined, localized conduits, supplying limited volumes of lava, possibly at moderate rates of extrusion. Under these circumstances, ideal conditions may exist for gravitative differentiation, especially the aqueous transfer of alkalis upward in the elevated volcanic conduits (Engel and others, 1965, p. 726–727).

In contrast, the Hawaiian chain is constructed from extremely voluminous lava flows which emanated from a great rift zone in a relatively short period; the exposed parts of the Hawaiian chain have been built in less than 2 million years (McDougall, 1964, p. 107).

Along the great Hawaiian rift the large volume and rapid extrusion of lava would have prevented appreciable gravity differentiation and aqueous transfer of alkalis from occurring except during lulls and waning stages of the eruptive cycles (Macdonald and Katsura, 1964, p. 82–92). It is largely during these lulls and late stages that the subordinate alkali-rich lavas appear in the Hawaiian Islands.

The proximity of alkali-rich basalt PV 322 on the upper flanks of an elevated volcano and tholeiitic basalt PV 324 B on the smaller volcanic peak immediately to the east also suggests that many of the large volcanoes have been built upon tholeiitic roots.

This suggestion also is implicit in the results of Moore's (1965) study of material dredged immediately to the northeast. He has dredged basalts from the submarine extension of the east rift zone of Kilauea volcano, and from the tops and upper slopes of seamounts southwest of Hawaii. All the basalts from the rift zone are tholeiitic; but the single alkali-basalt described by Moore is from the top of the McCall seamount, a volcano which rises about 3,000 m above the surrounding sea floor. It contains, in weight percent, 4.08 percent Na_2O, 2.11 percent K_2O, and has an Fe_2O_3/FeO ratio of 0.32.

One other contrast between alkali-rich and tholeitic basalts is apparent from recent dredging work. Alkali basalts appear to vesiculate at higher hydrostatic pressures than tholeiitic basalts. This was suggested by earlier dredging and seems to be confirmed in our studies in the vicinity of Hawaii. The alkali-rich basalts that mantle the upper slopes of seamounts built upon the abyssal sea floor southwest of Hawaii are far more vesicular, and contain larger vesicles than tholeiitic basalts extruded at equivalent and much shallower depths along the Hawaiian rift. The close proximity of the contrasting lava types, and crude equivalence in age seems to preclude the possibility that the vesiculated, alkali-rich basalts also were extruded much nearer the surface and subsequently depressed by warping of the sea floor. Very possibly the difference in vesicularity is due to a greater volatile content, including some sea and meteoric water, in alkali basalt magmas.

REFERENCES

Engel, A. E. J., and Engel, C. G., 1964, Igneous rocks of the East Pacific Rise: Science, v. 146, p. 477–485.

Engel, A. E. J., Engel, C. G., and Havens, R. G., 1965, Chemical characteristics of oceanic basalts and the upper mantle: Geol. Soc. America Bull., v. 76, p. 719–734.

Le Maitre, R. W., 1962, Petrology of volcanic rocks, Gough Island, South Atlantic: Geol. Soc. America Bull., v. 73, p. 1309–1340.

Macdonald, G. A., and Katsura, T., 1962, Relationship of petrographic suites in Hawaii; The Crust of the Pacific Basin: Am. Geophys. Union Mon. 6, p. 187–195.

——— 1964, Chemical composition of Hawaiian lavas: Jour. Petrology, v. 5, p. 82–133.

McDougall, Ian, 1964, Potassium-argon ages from lavas of the Hawaiian Islands: Geol. Soc. America Bull., v. 75, p. 107–128.

Moore, J. G., 1965, Petrology of deep-sea basalt near Hawaii: Am. Jour. Science, v. 263, p. 40–52.

U.S. Naval Oceanographic Office, 1962, A marine magnetic survey south of the Hawaiian Islands: Tech. Rept. TR–137, 47 p.

THE EFFECT OF MAGMATIC DIFFERENTIATION ON THE MAGNETIC PROPERTIES OF DIABASE SHEETS OF SOUTHEASTERN PENNSYLVANIA

By MYRL E. BECK, JR., Silver Spring, Md.

Abstract.—Specimens from 6 differentiated sheets of Triassic diabase from southeastern Pennsylvania show a marked increase in remanent and induced magnetic intensity accompanying crystal fractionation. This increase in magnetic moment probably reflects absolute enrichment in total iron, accompanied by a rise in the relative importance of ferric iron, in passing from mafic to felsic differentiates. In gently dipping sheets there is a tendency for residual fluids to concentrate near the top of the sheet, and this process may produce marked asymmetry in aeromagnetic profiles across such sheets. Especially high stability of remanent magnetization seems to be associated with the mafic fraction.

Differentiated sheets of tholeiitic diabase have been subject to intensive study by petrologists and mineralogists for many years, and as a result their fractionation trends are comparatively well known. In recent years they have also claimed the attention of geophysicists because they are excellent subjects for paleomagnetic investigations. Much of this work has tended to show that there is a strong correlation between the magnetic properties of a particular specimen of diabase and its state of differentiation (see, for instance, Bull and others, 1962; Jaeger and Joplin, 1955; Jaeger and Green, 1958). In view of this interest in diabase intrusions, it was decided to examine the relationship between lithology and certain magnetic properties in several thick sheets from the Triassic of southeastern Pennsylvania. The average direction of remanent magnetization for these bodies has been determined previously (Beck, 1965), and aeromagnetic mapping shows that strong internal magnetic contrasts are present (Bromery and Griscom, in press). The present paper attempts to account for some of these contrasts in terms of magmatic differentiation.

VARIATIONS IN TOTAL MAGNETIZATION AND LITHOLOGY

A total of 219 specimens were collected from 6 highway and railroad cuts (fig. 1) which offered substantially continuous sections through major portions of thick diabase sheets. The following properties were determined for each specimen: natural remanent magnetization (J_n); remanent magnetization after demagnetization in an alternating field of 150 oersteds (J_{150}); apparent magnetic susceptibility (k); and density (ρ). In addition, 32 thin section were scanned to determine the following: color index and grain size; presence or absence of olivine and orthopyroxene; amount of micropegmatite; amount, grain size, and apparent mode of occurrence of opaque grains; and degree of alteration of primary ferromagnesian minerals.

Figure 2 shows variations in magnetization in 210 of these specimens — the remaining 9 are very strongly magnetized and fall outside the diagram.

The total intensity of magnetization of a volume of rock in situ ($\vec{J}$) is given by

$$\vec{J} = \vec{J}_n + k\vec{T},$$

where $\vec{T}$ is the total intensity of the earth's magnetic field and $\vec{J}_n$, the remanent intensity, can have any orientation, depending on: (1) the direction and polarity of the earth's magnetic field at the time the remanence was acquired, (2) the degree to which this remanence originally paralleled the paleogeomagnetic field, (3) the degree to which it retained its original direction (with respect to coordinates fixed in the rock), and (4) the tectonic history of the rock after it became magnetized. However, $\vec{T}$ is not a rock property, and neither are the more important factors (numbers 1 and

U.S. GEOL. SURVEY PROF. PAPER 550-D, PAGES D109-D116

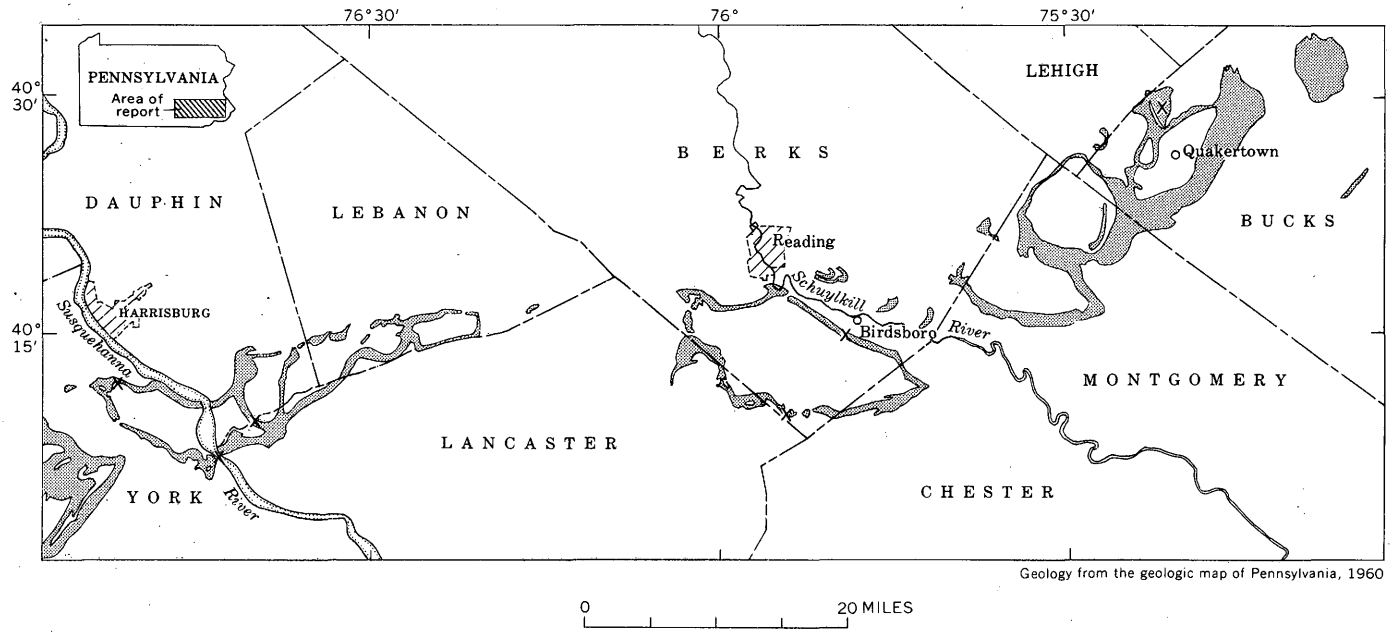

FIGURE 1.—Index map of southeastern Pennsylvania showing areas of outcrop of Triassic diabase (shaded) and sampled localities (×)

4) controlling the direction of $\vec{J}_n$. A relationship of greater interest here is

$$J = J_n + K,$$

where $K = 1 \cdot k$, (defining a standard induced intensity of magnetization as that induced in a unit magnetic field, and numerically equal to the apparent susceptibility). This function defines a magnetization which is independent of direction and of the inducing field. The remaining factors controlling the direction of $\vec{J}_n$ are related to lithology and must be included in a complete investigation of the effect of differentiation on rock magnetic properties. However, factor 2, magnetic anisotropy, probably is insignificant in homogeneous rocks containing unoriented grains of magnetic oxide. Factor 3, magnetic stability, is dealt with in a later section.

The relationship $J = J_n + K$ is implicit in figure 2, in which remanent intensity is plotted against standard induced intensity. In this plot, specimens of equal magnetization lie on straight lines with a slope of minus one. The loci of points $J = 1.12 \times 10^{-3}$ and $J = 2.52 \times 10^{-3}$ electromagnetic units per cubic centimeter are indicated. The median intensity for these 219 specimens is approximately 1.75×10^{-3} emu cm^{-3}, and 95 percent are included in the range $2.52 > J_n/K > 0.37$, which for southeastern Pennsylvania is equivalent to a range in the ratio for remanent to induced magnetization of $4.4 > Q > 0.64$, where Q, the Koenigsberger ratio, represents the quantity J_n/KT (Koenigsberger, 1938).

The three regions of figure 2 defined by the lines $J = 1.12 \times 10^{-3}$ and $J = 2.52 \times 10^{-3}$ emu cm^{-3} are used below to describe variations in lithology.

(1) Specimens for which $J \leq 1.12 \times 10^{-3}$ emu cm^{-3} tend to be conspicuously mafic, with color indices averaging about 55. Most contain orthopyroxene, in many cases as phenocrysts, and very few contain large opaque grains. Interstitial micropegmatite is very rare in these specimens, and pyroxene grains tend to be little altered.

(2) Specimens with magnetization in the range $1.12 \times 10^{-3} < J \leq 2.52 \times 10^{-3}$ emu cm^{-3} contain very little orthopyroxene (none was observed in the upper part of the range). Color indices average less than 50, and micropegmatite is present in most slides, ranging up to about 8 percent. Large opaque grains are rare, but they are slightly more common than in the weakly magnetized group, especially in the upper half of the range. Most pyroxene grains are not badly altered, but there is a definite increase in the number of grains surrounded and partially replaced by hydrous minerals (mainly chlorite and biotite) and by opaque material.

(3) In thin sections representative of the strongly magnetized specimens, in which $J > 2.52 \times 10^{-3}$ emu cm^{-3}, the proportion of micropegmatite shows a sharp increase, to a maximum observed abundance of 30 percent. Largely as a result of this increase, the color index declines. No orthopyroxene was observed in this group, and clinopyroxene grains tend to be moderately to strongly altered to hydrous silicates and

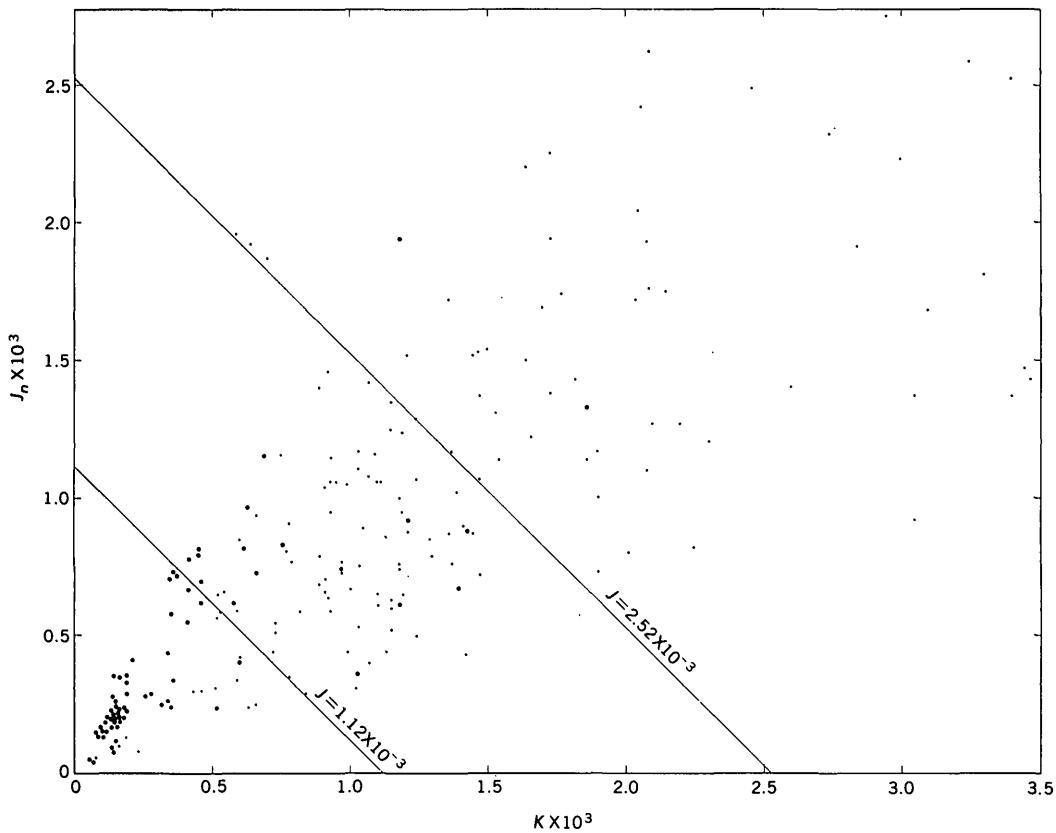

FIGURE 2.—Intensity of natural remanent magnetization (J_n) and intensity of induced magnetization for a field of 1 oersted (K), for 210 specimens of differentiated diabase. Large dots indicate specimens for which $J_{150}/J_n \geq 0.70$.

opaque material. Large opaque grains are possibly a little more abundant than in the preceding groups but still are not common; their maximum dimensions, on the other hand, are slightly increased. There is a marked increase in the amount of opaque material associated with alteration of ferromagnesian minerals. In overall appearance even the most felsic specimens in this group are "normal" diabase, although several approach the "schlieren" or "patch" varieties of diabase pegmatite described by Walker (1953). No attempt was made to include pegmatitic or granophyric differentiates in figure 2.

To summarize, increase in magnetization is accompanied by a growth in the proportion of late-stage, interstitial micropegmatite and by a general increase in the content of felsic material. Pyroxene alteration increases with magnetization, and orthopyroxene, probably an indicator of relatively early, high-temperature crystallization (Poldervaart and Hess, 1951), is found only in weakly magnetized specimens. On the average there is an increase in grain size with increasing magnetization, but the range in grain size for the three groups is nearly identical. Also, there is little evidence of a strong correlation between the average opaque grain size and total magnetization, although specimens in the group $J > 2.52 \times 10^{-3}$ emu cm^{-3} have more large (> 0.5mm) opaque grains than do the other specimens. As might be expected, there is a strong correlation between J and the percentage of opaque grains in a given specimen. Olivine is almost entirely absent from these rocks.

An attempt was made to detect systematic petrographic differences in samples with similar magnetization, but strong differences in the relative values of the remanent and induced components (the J_n/K ratio). If such differences exist they are too subtle to be detected by reconnaissance petrography. However, among weakly magnetized specimens there seems to be a slight tendency for relatively high values of J_n/K to be confined to particularly mafic, micropegmatite-free material.

MAGNETIC STABILITY

Figure 2 also has been used to indicate variations in coercive force, an intrinsic property closely related to stability of remanent magnetization (see, for instance,

Irving, 1964, p. 21-22). For all specimens the ratio J_{150}/J_n was determined; large values of this ratio show that the bulk of J_n was unaffected by alternating magnetic fields of 150 oersteds and thus is relatively "hard" and presumably stable. Values of $J_{150}/J_n \geq 0.70$ are shown as large dots on figure 2. There is a clear tendency for specimens with high coercivity ratios to be concentrated in regions of low magnetization, and a less obvious preference on the part of such specimens for the "high J_n" side of the plot. All but a few specimens with coercivity ratios of 0.70 or more are clustered near the line $J_n = 1.55K$. The significance of this alinement is not clearly understood.

The relationship between magnetization and magnetic stability is indicated more clearly in figure 3 (A) and (B), in which the 219 diabase specimens have been placed in 10 groups of approximately equal magnetization. The limits of these groups are indicated in table 1. From figure 3A it is apparent that the

TABLE 1.—*Upper and lower limits of magnetization for the 10 groups of figure 3*

Group	Interval J×10³ emu cm⁻³	Group	Interval J×10³ emu cm⁻³
1	≤0.34	6	1.79–2.12
2	0.35–.59	7	2.13–2.52
3	.60–1.12	8	2.53–3.11
4	1.13–1.55	9	3.12–4.48
5	1.56–1.78	10	>4.48

coercivity ratio, and presumably the stability, of these rocks declines steadily with increasing magnetization.

For this suite of specimens it is also possible to test for magnetic stability directly, because the mean direction of remanent magnetization of Triassic diabase in Pennsylvania is known with considerable precision from previous studies (Opdyke, 1961; Beck, 1965). Figure 3B provides such a test in the form of a tabulation of the percentage of specimens in each group which differ by more than 36° from the true mean direction. The angle 36° was selected because it represents approximately twice the angular dispersion (δ) shown by Creer (1962) to be inherent in modern geomagnetic secular variation at a latitude equal to the paleomagnetic latitude of the Pennsylvania diabase intrusions. For certain distributions, δ is the best estimate of standard deviation, and by analogy with planar distributions 2δ may be expected to include approximately 95 percent of the population. Since geomagnetic secular variation may have been less in the Triassic than at present (Beck, 1965, p. 2850–2851), individual specimens which deviate by more than 2δ (36°) from the mean clearly may be classed as aberrant, and probably are unstable. Figure 3B shows that the frequency of such specimens generally increases with increasing magnetization from group 1 through

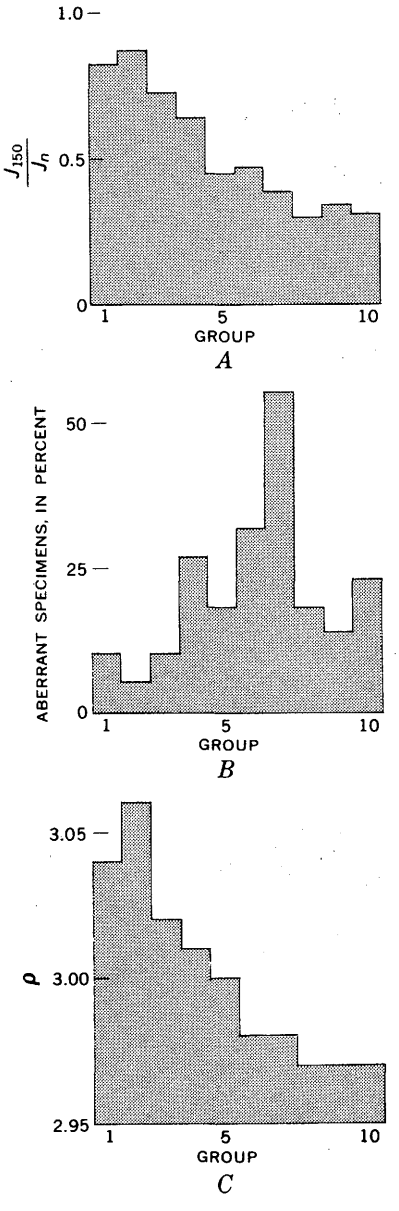

FIGURE 3.—Average values of the coercivity ratio (A) and density (C), with the proportion of specimens with strongly deviating directions of remanent magnetization (B), for groups of specimens of nearly equal magnetization. Average magnetization increases from group 1 through 10 (see table 1 and text).

group 7, but drops to moderately low levels in groups 8 through 10. Evidently specimens with magnetization greater than about 2.50×10^{-3} emu cm^{-3} have fairly high stability of remanent directions even though a large fraction of their remanent moments are concentrated in domains of low coercivity. For reasons that are not clear, disturbing magnetic fields have been relatively ineffective in producing a realinement of low-

coercivity domains in these highly magnetized specimens. Extreme stability, however, seems to be a property of weakly magnetized diabase.

Average densities for the 10 groups are shown in figure 3*C*. The inverse correlation between density and magnetization is striking.

DISCUSSION

Origin of magnetic variations

According to Everitt (1961, p. 692), magnetic variations in differentiated diabase sheets may arise from differences in, (1) total iron content; (2) proportion of total iron occurring as magnetic oxides; and (3) kind of magnetic oxide, taking into consideration mineralogical factors which might affect saturation magnetization, such as crystal structure and chemical composition. Everitt was concerned with remanent magnetic intensities only, and for these he suggested that differences in the amount of natural remanence acquired by a uniform magnetic mineral fraction also could be significant. The latter explanation could account for some of the variation of J_n observed in the present study, but it does not explain differences in magnetic susceptibility. However, the strong correlation between J_n and K in these rocks suggests that processes which effect one without the other probably are of secondary importance.

An important chemical trend in many differentiated basalt sequences is toward enrichment in total iron until late in the magmatic history of the rock, followed by an abrupt decrease in iron in the final stages of crystallization. This differentiation sequence is best exemplified by layered plutonic bodies, but it also is recognizable in some thick diabase sills. The chemical data presented by Hotz (1953) and Walker (1940) show that this trend has been followed by representatives of the family of diabase intrusions studied in this report.

If a constant proportion of total iron in rocks of basaltic composition were to occur as magnetic oxides, iron enrichment would produce an increase in magnetization. However, for the diabase bodies examined in this report this process alone is quantitatively inadequate. As a first approximation, magnetization should be roughly proportional to content of magnetic oxide, if all mineralogical factors are constant, and under these circumstances total iron content and total magnetization should show a similar range of variation. The ratio of the average magnetization of group 1, figure 3, to that of group 10 can be used as an index of the increase in magnetization accompanying the differentiation process in these diabase sheets; this ratio is 17/1 and is somewhat conservative because of the exclusion of diabase pegmatites. This is in distinct contrast to the ratio of maximum to minimum total iron in most suites of differentiated diabase, which rarely exceeds 3/1. Evidently other processes also contribute to the observed differences in magnetization.

Besides producing an increase in total iron, differentiation of diabase magma also might cause a systematic change in the proportion of total iron crystallizing as magnetic oxides. Chemical analyses suggest that this is the case, since many suites of analyses indicate that the ratio of ferric to total iron increases with increased differentiation. Analyses listed by Walker (1953, p. 50–51) for diabase pegmatities and associated nonpegmatitic diabase show the pegmatites with higher ratios of ferric to total iron in 7 of 9 cases; one pair, from the Karoo dolerites, shows a sixfold increase, and a search of the literature indicates that this value is not uncommon. This figure also may serve as a rough upper limit of the variation in the percentage of total iron crystallizing as magnetic oxides within a suite of differentiated diabase. Ferric iron is found in silicates as well as oxides, and further complications are introduced by the fact that there are wide variations in the ferric iron content of the several iron oxide minerals which may contribute to the magnetization of a rock. However, it seems safe to assume that rarely does the proportion of total iron crystallizing as magnetic oxides increase within a single differentiated diabase suite by a ratio of more than 6/1. This, combined with a 3/1 increase in total iron, shows that the 17-fold increase in magnetization of figure 2 could be brought about by ordinary differentiation processes, without the aid of changes in mineralogy of the magnetic grains.

No adequate study of the opaque minerals in these rocks has been attempted to date. Nevertheless, on theoretical grounds and by analogy with other bodies it seems safe to predict that systematic changes in opaque mineralogy are present. These changes might be of two types: (1) variations in the amount of titanium, or other metallic ions, substituting for iron in the oxide lattice; (2) oxidation effects, involving crystallization of magnetic oxides as cubic minerals with lattice vacancies (titanomaghemite and transitional types), as members of the hexagonal hematite-ilmenite series, or, in the case of very strong oxidation, as members of the paramagnetic pseudobrookite series.

The effect of mineralogical changes on total magnetization is not easy to predict. In the magnetite-ulvospinel solid-solution series there is a steady decrease in saturation magnetization with increasing titanium content, and titanium content in turn is con-

trolled to a great extent by temperature and oxygen pressure (Buddington and Lindsley, 1964). By this reasoning, magnetite with relatively low saturation magnetization should be found in mafic material, and such a correlation has been observed in volcanic rocks (Nagata, 1961, p. 92). High oxygen pressure also can bring about the crystallization of oxidized iron-titanium spinels intermediate in composition between magnetite-ulvospinel and hematite-ilmenite, and in extreme cases titanomaghemite or minerals within the hematite-ilmenite-psuedobrookite field can develop (Katsura and Kushiro, 1961). Progressive oxidation of these spinel phases involves an increase in the number of vacancies in cation lattice sites, and this in turn seems certain to have an important effect on magnetite properties. Akimoto and others (1957, p. 177) have traced the change in saturation magnetization with oxidation over part of the compositional field lying between the magnetite-ulvospinel and the hematite-ilmenite joins, and their data suggest that, depending on titanium content, moderate oxidation can either raise or lower saturation magnetization to a slight extent. Data for strongly oxidized spinels are lacking. However, extreme oxidation, resulting in the crystallization of hematite-ilmenite or pseudobrookite at the expense of a spinel phase, might be expected to lower total magnetization, if no other changes take place. In view of these uncertainties it seems unprofitable to speculate on the magnetic effects of changes in opaque mineralogy which may accompany the differentiation process in diabase sheets. Mineralogical changes undoubtedly occur, and study of such changes should contribute to an understanding of basaltic differentiation, especially as regards the role of oxygen pressure. However, changes in opaque mineralogy are not necessary to explain the pattern of magnetic variation observed in differentiated diabase.

Stability of remanent magnetization is another physical property of diabase which clearly relates to differentiation, and here it is likely that changes in opaque mineralogy play a dominant role. Figures 2 and 3 show that high magnetic stability is an attribute of weakly magnetized material probably formed early in the cooling history of the diabase sheets, and figure 3 *A* and *C* indicates that as the rock varies from mafic to felsic, coercivity decreases. This probably reflects systematic changes in the mineralogy of the magnetic oxides brought on by falling temperature and increasing volatile content; in particular, oxidation probably plays an important role. For instance, Akimoto and Kushiro (1960) have shown that instability of remanent magnetization in a Miocene diabase is related to the presence of titanomaghemite, apparently formed at the expense of titanomagnetite. Watkins and Haggerty (1965), in a detailed study of a single thin basalt flow, demonstrated a marked correlation between magnetic stability and oxidation state; in their specimens instability also correlated with the presence of maghemite, as an alteration product of magnetite and ilmenite. However, in Watkins and Haggerty's study, the maghemite zone constituted the least oxidized part of the flow; as maghemite gave way to hematite and pseudobrookite, magnetic stability rose. This change was accompanied by an increase in the intensity of remanent magnetization, which might have been caused by the effect of increasing oxidation on the proportion of total iron in the rock existing as magnetic oxides. In view of these observations it is tempting to suggest that the changes in magnetic stability observed in the present study also reflect the influence of oxidation. Thus, the steady decline in magnetic stability from group 1 to group 7 (figure 3 *B*) could represent a gradual oxidation of titanomagnetite toward titanomaghemite, while the sudden rise in stability in group 8 might reflect the appearance of members of the hematite-ilmenite series. However, this would not seem to explain the continued decline in coercivities.

Variation in grain size of magnetic oxides also may contribute to differences in magnetic stability through the well-known inverse relationship between particle diameter and coercive force (Nagata, 1961, p. 27–29; 99). Coercivity changes related to grain size also might be expected to influence magnetic susceptibility. A general tendency for grain size to increase with total magnetization was noted above, and it is possible that this increase contributes to the gradual decline in coercivity shown in figure 3*A*. However, it seems unlikely that grain-size effects in the present study are significant, for the following reasons: (1) Above 100 to 200 microns, particle size apparently has little effect on coercivity, and the bulk of the opaque grains in these rocks are considerably larger than this. (2) Within each group of figure 3 there is a considerable range in grain size, but no within-group correlation between grain size and either susceptibility or coercivity could be detected. (3) High coercivity caused by very small magnetic particles might be expected to produce a noticeable increase in the ration J_n/K, but no such increase was observed.

Summary of the effects of magmatic differentiation on magnetic properties in diabase

The following is a simple working hypothesis based on widely recognized chemical and petrological trends.

It can easily be tested against other examples of differentiated tholeiitic basalt. In principle it is applicable to large intrusive bodies of any shape, but the following sketch is aimed specifically at diabase sheets which were substantially horizontal during crystallization.

(1) Fractional crystallization progressively enriches the melt in iron, as well as in water and other volatiles. Total iron enrichment may be of the order of threefold. Cooling proceeds from both top and bottom of the sheet, but gravity causes the residual liquid to accumulate substantially above the center (Hess, 1960 p. 187–190). This final liquid is very fluid and may be injected along fractures or migrate upward through cracks developed during cooling.

(2) Concentration of volatile material causes progressive oxidation. The ratio of ferric to total iron can increase by as much as sixfold.

(3) Primary magnetite, probably rich in titanium and similar cations suitable as substitutes for iron, begins to form early and continues to form throughout much of the cycle. This high-temperature spinel is responsible for the high magnetic stability of groups 1–3. Specimens with only primary magnetite tend to be weakly magnetized because: (1) they crystallize early, thus are low in iron, especially ferric iron, and hence contain little magnetic oxide; (2) their magnetic oxides may contain comparatively large amounts of cation "impurities" and thus have low values of saturation magnetization.

(4) As the temperature falls and iron and volatile material accumulate, the quantity of primary magnetite increases. These later spinels may have less titanium and other "impurities" in solid solution, but they also may tend to crystallize with lattice vacancies and so approach maghemite in composition.

(5) Deuteric alteration produces a later generation of magnetic oxide at the expense of primary ferromagnesian grains, and iron oxide minerals formed earlier are partially or completely recrystallized. The amount of alteration in any one sample is proportional to its content of interstital volatile material. These deuteric oxides probably are highly oxidized forms and may consist of titanomaghemite, members of the hematite-ilmenite solid solution series, or even pseudobrookite.

Application to magnetic surveys and paleomagnetism

Figure 2 suggests that a common assumption of magnetic interpretation, uniform magnetization, is valid only for very small bodies of rock. For instance, magnetization contrasts of more than 3.50×10^{-3} emu cm^{-3} are present within 6 closely related diabase sheets of figure 2, and a large part of that contrast is present within several individual sheets, none of which attains an unusually high degree of differentiation. If, as is to be expected, the highly magnetic fraction accumulates near the top of the sheet, there would be more magnetization contrast between the upper third and lower third of the sheet than between the lower third and the underlying "nonmagnetic" country rock. This explanation may account for the pattern observed in the Triassic of Pennsylvania (Bromery and Griscom, in press), where the peaks of aeromagnetic anomalies associated with gently dipping diabase sills almost invariably are located near the upper contact, regardless of the direction of dip. This may reflect the tendency for highly magnetic, relatively felsic residual material to accumulate near the top of the sheet, possibly even penetrating the overlying solid diabase and baked country rock along joints or cooling fractures. By a similar process the peak magnetic anomaly over a thick differentiated dike should occur near its center.

The amplitude of internal aeromagnetic anomalies which might be expected over differentiated diabase sheets can be estimated from the magnetic contrast between group 10 and the average magnetization of the 6 diabase sheets. For $T = 0.6$ oersted this can range from 0.15 to 2.35×10^{-3} cgs emu cm^{-3}, depending on the direction of remanence. A semi-infinite slab of material with this magnetization, 100 feet thick, would produce anomalies of up to 100 gammas at a distance of 500 feet. Differentiation may produce rare accumulations of highly magnetic material somewhat thicker than this, but only in structurally favorable portions of extremely thick sheets. For comparison, the magnetic anomalies over commercial magnetite deposits associated with diabase in southeastern Pennsylvania range from several hundred to more than 1,000 gammas at a flight elevation of 500 feet.

The indication that high magnetic stability is associated with mafic differentiates of diabase sheets may be useful in paleomagnetism since it should enable investigators to attain maximum precision with a minimum number of samples. In extreme cases, limited collections of mafic samples may give reliable paleomagnetic poles even without extensive magnetic "cleaning". For instance, the data presented below contrast the precision obtained with samples from groups 1–3 (table 1) with results for the entire collection. Increasing the number of samples by a factor of more than three has greatly lowered overall precision, as indicated by δ, and has tightened the circle of confidence by an insignificant margin. Neither direction differs significantly

from the direction reported previously (Beck, 1965) after magnetic "cleaning".

Group	N	D	I	δ	α_{95}
1–3	65	356°	+23°	19°	4½°
1–10	219	1°	+21°	31°	3½°

N, number of samples.
D, mean declination of remanent magnetization.
I, mean inclination of remanent magnetization.
δ, angular standard deviation.
α_{95}, semi-apical angle of the cone of confidence at the 95-percent confidence level.

REFERENCES

Akimoto, Syun-iti, Katsura, Takashi, and Yoshida, Minoru, 1957, Magnetic properties of $TiFeO_4$–Fe_3O_4 system and their change with oxidation: Jour. Geomagnetism Geoelectricity, v. 9, p. 165–178.

Akimoto, Syun-iti, and Kushiro, Ikuo, 1960, Natural occurrence of titanomaghemite and its relevance to the unstable magnetization of rocks: Jour. Geomagnetism Geoelectricity, v. 11, p. 94–110.

Beck, M. E., Jr., 1965, Paleomagnetic and geological implications of magnetic properties of the Triassic diabase of southeastern Pennsylvania: Jour. Geophys. Research, v. 70, p. 2845–2856.

Bromery, R. W., and Griscom, Andrew, in press, Aeromagnetic and generalized geologic map of southeastern Pennsylvania: U.S. Geol. Survey Geophys. Inv. Map, GP–577.

Buddington, A. F., and Lindsley, D. H., 1964, Iron-titanium oxide minerals and synthetic equivalents: Jour. Petrology, v. 5, p. 310–357.

Bull, C., Irving, E., and Willis, I., 1962, Further paleomagnetic results from South Victoria Land, Antarctica: Geophys. Jour., v. 6, p. 320–336.

Creer, K. M., 1962, The dispersion of the geomagnetic field due to secular variation and its determination for remote times from paleomagnetic data: Jour. Geophys. Research, v. 67, p. 3461–3476.

Everitt, C. W. F., 1961, The magnetic properties of three Carboniferous sills: Philos. Mag., v. 6, p. 689–699.

Hess, H. H., 1960, Stillwater igneous complex, Montana: Geol. Soc. America Mem. 80, 230 p.

Hotz, P. E., 1953, Petrology of granophyre in diabase near Dillsburg, Pennsylvania: Geol. Soc. America Bull., v. 64, p. 675–704.

Irving, E., 1964, Paleomagnetism and its application to geological and geophysical problems: New York, John Wiley & Sons, Inc., 399 p.

Jaeger, J. C., and Green, Ronald, 1958, A cross-section of a tholeiite sill, *in* Dolerite, a symposium: Hobart, Univ. Tasmania, p. 26–37.

Jaeger, J. C., and Joplin, Germaine, 1955, Rock magnetism and the differentiation of dolerite sill: Jour. Geol. Soc. Australia, v. 2, p. 1–19.

Katsura, Takashi, and Kushiro, Ikuo, 1961, Titanomaghemite in igneous rocks: Am. Mineralogist, v. 46, p. 134–145.

Koenigsberger, J. G., 1938, Natural residual magnetism of eruptive rocks: Terrestrial Magnetism Atmospheric Electricity, v. 43, p. 119–130, 299–320.

Nagata, Takesi, 1961, Rock magnetism, revised ed.: Tokyo, Maruzen Co., Ltd., 350 p.

Opdyke, N. D., 1961, The paleomagnetism of the New Jersey Triassic—A field study of the inclination error in red sediments: Jour. Geophys. Research, v. 66, p. 1941–1949.

Poldervaart, Arie, and Hess, H. H., 1951, Pyroxenes in the crystallization of basaltic magmas: Jour. Geology, v. 59, p. 472–489.

Walker, Frederick, 1940, Differentiation of the Palisade diabase, New Jersey: Geol. Soc. America Bull., v. 51, p. 1059–1106.

——— 1953, The pegmatitic differentiates of basic sheets: Am. Jour. Sci., v. 251, p. 41–60.

Watkins, N. D., and Haggerty, S. E., 1965, Some magnetic properties and the possible petrogenetic significance of oxidized zones in an Icelandic olivine basalt: Nature, v. 206, no. 4986, p. 797–800.

MAGNETIZATION OF KEWEENAWAN GABBRO IN NORTHERN WISCONSIN AND ITS RELATION TO TIME OF INTRUSION

By KENNETH G. BOOKS,[1] WALTER S. WHITE,[2] and MYRL E. BECK, JR.,[1]

[1] Silver Spring, Md., [2] Beltsville, Md.

Abstract.—The average direction of remanent magnetization for gabbro that is intrusive into steeply dipping middle Keweenawan lavas in northern Wisconsin is similar to directions measured by P. M. DuBois, of the Canada Geological Survey, for the Portage Lake Lava Series, the Copper Harbor Conglomerate, and the Duluth Gabbro Complex in the Lake Superior region. If the direction of remanent magnetization for the gabbro in Wisconsin is rotated to eliminate the effect of tilt in the enclosing lavas, the similarity is destroyed. This suggests that the gabbro intrusion occurred after tilting. Further analysis of all significant paleomagnetic data for the region appears to limit intrusion of the gabbro in northern Wisconsin to the late Keweenawan.

Directions of remanent magnetization have been applied by a number of investigators to problems of geologic structure and correlation (Blundell, 1961; Blundell and Read, 1958; and Tarling, 1962). Recently P. M. DuBois (1962), of the Canada Geological Survey, has had some success in applying remanent magnetization to the stratigraphic correlation of Keweenawan rocks exposed in the Lake Superior area. In view of the encouraging results obtained by DuBois it was decided to apply paleomagnetic techniques to the question of the age, correlation, and structural history of a Keweenawan gabbro-granophyre complex located west of Mellen, in northern Wisconsin.

Many of the available paleomagnetic data, however, have many uncertainties and low precision. The following data establish limits as to the possible intrusion times for the gabbro near Mellen and demonstrate the potential use of detailed paleomagnetic analysis in stratigraphic and structural studies.

GEOLOGIC SETTING

The gabbro-granophyre complex near Mellen was studied in considerable detail by Leighton (1954). In the area of the present work (figs. 1 and 2) it consists of at least two distinct bands of gabbro and granophyre that are intrusive into basaltic lava flows of middle Keweenawan age. The gabbro and granophyre probably are correlative with the Portage Lake Lava Series of the Keweenaw Peninsula in Michigan and the North Shore Volcanic Group of Gehman (1958) in the Duluth area, Minnesota. The Duluth Gabbro Complex and the gabbro-granophyre complex west of Mellen exhibit many similar petrologic and structural features, and are intrusive into middle Keweenawan basalt exposed on opposite flanks of the Lake Superior geosyncline (fig. 1). Because of these similarities, they have been considered by some investigators as being of the same age (Grout, 1918, p. 445, 446). The Duluth Gabbro Complex has been called middle Keweenawan in age (Grout and others, 1951), whereas Leighton (1954, p. 406) concludes that the gabbro in northern Wisconsin "cannot be dated more accurately than post-lower Keweenawan".

The stratified rocks of Keweenawan age in the vicinity of Mellen have steep dips to the north; the average attitude of lava flows in the area is N 70° E., 63° N. (Leighton, 1954, p. 405). Bands of gabbro and granophyre trend roughly parallel to the strike of the flows (fig. 2).

Internal structures of two types are fairly common within the gabbro of the complex near Mellen. The more prevalent is a fluxion structure, defined by parallelism of platy feldspar grains, that have an average attitude nearly parallel to the layering of the flows, along which the gabbro was injected. Leighton (1954, p. 410) attributes fluxion structure in the gabbro to "orientation produced by friction during magmatic movement". Banding, consisting of parallel layers of contrasting mineral proportions, was observed in only three gabbro outcrops. Leighton (1954) states that this banding, which he interprets as being due to originally

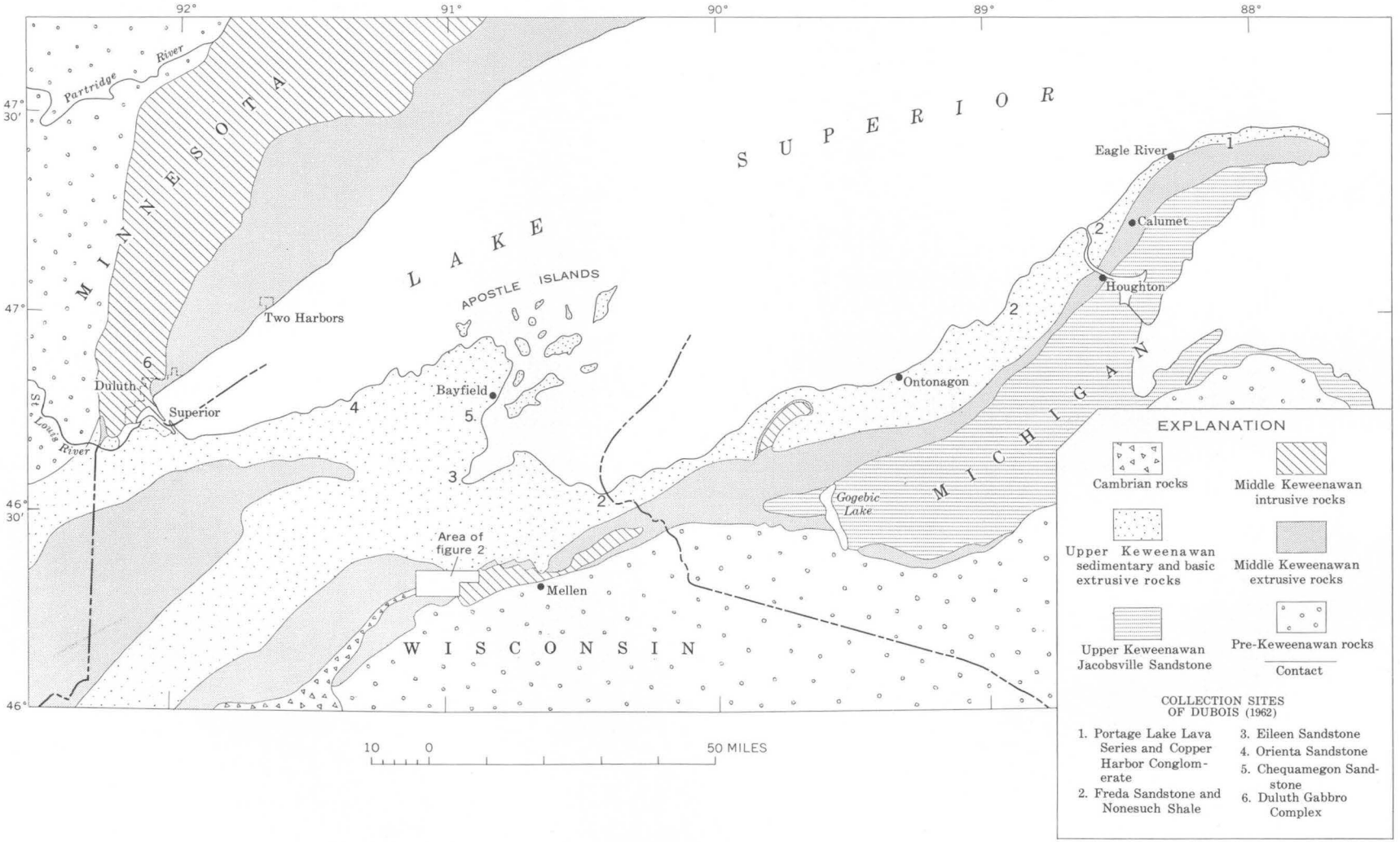

FIGURE 1.—Generalized geologic map of part of the Lake Superior area. Modified from Leith and others (1935, pl. 1).

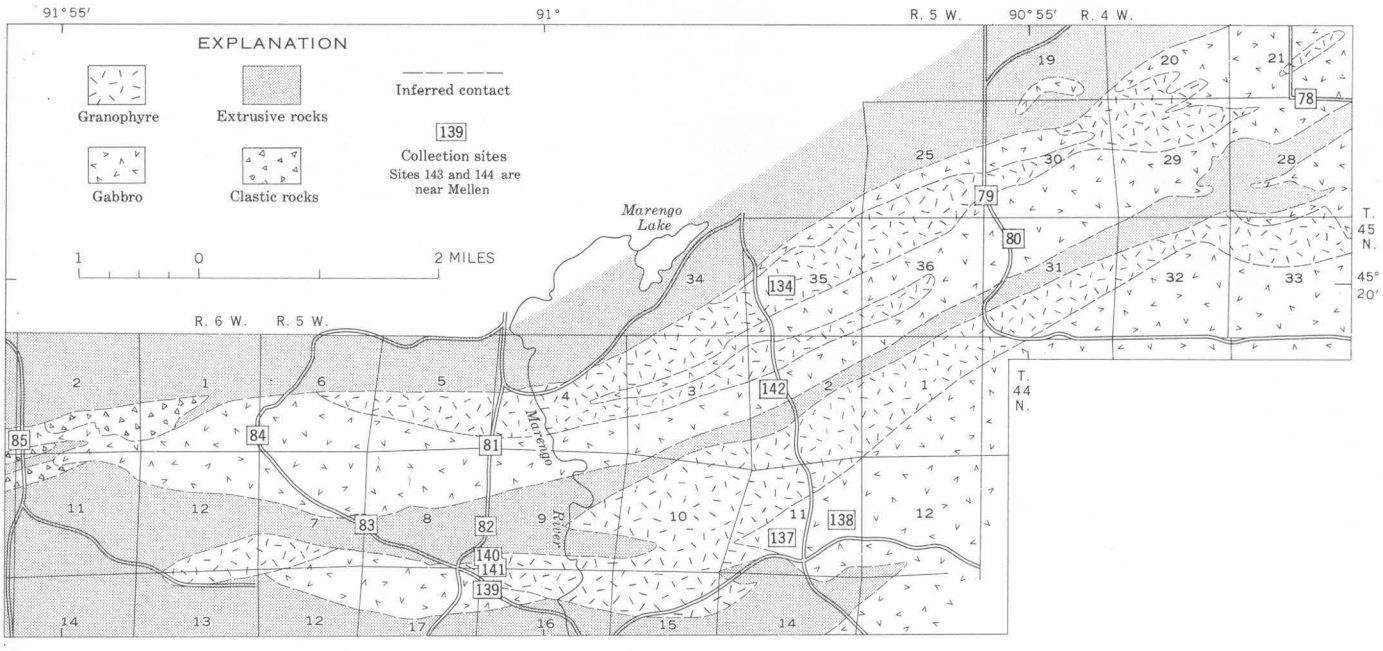

FIGURE 2.—Geologic map of the area west of Mellen, Wis. Modified from Leighton (1954).

subhorizontal crystal settling, has a dip that averages 15° – 20° less than the fluxion structure, that is, about 45° NW. He cites this difference in dip as evidence for folding of the Lake Superior geosyncline prior to intrusion of the gabbro (Leighton, 1954, p. 410, 411); according to this interpretation the volcanic rocks had acquired dips averaging 15° – 20° at the time the gabbro was intruded.

The paleomagnetic geochronology developed by DuBois (1962) for the Keweenawan of the Lake Superior region provides background for an independent solution of the problem of the time relation between intrusion and tilting. Providing that the rocks acquired their magnetization during or immediately after their initial cooling, the mean directions of remanent magnetism for various Keweenawan formations given by DuBois (1962, table XVIII) can be used to help define the time of intrusion of specific Keweenawan rocks. As part of a broader program of geophysical studies in the area, therefore, we have measured the direction of remanent magnetization of the gabbro west of Mellen, in the hope of determining (1) the amount of tilt in the lavas at the time of intrusion of the gabbro-granophyre complex and (2) the time of intrusion of the gabbro relative to the time of intrusion of other Keweenawan formations.

FIELD AND LABORATORY METHODS

A total of 80 drill-core samples were collected from 12 sites in the gabbro, 3 sites in the granophyre, and 2 sites in adjacent Keweenawan lava flows. The cores were drilled in situ using a water-cooled diamond-impregnated bit powered by a modified chain-saw motor. Local declination anomalies required the use of a sun compass for orientation.

Remanent magnetic moments were measured on a motor-driven "spinner" magnetometer (Doell and Cox, 1965). To eliminate the effects of unstable magnetic moments, all samples were magnetically "washed" in alternating fields in steps up to 500 oersteds. Conventional Fisher (1953) statistical analyses were applied to the directions of magnetization derived from these procedures; mean directions were computed for individual sampling sites, and an overall site mean for the gabbro was calculated using means from 14 sites. Three site means (localities 137, 140, and 141) which included 13 samples were discarded from the final calculations because the circle of confidence (α_{95}) exceeded 25° and thus did not meet Irving's (1964, p. 102) minimum criteria of reliability. Data from two sites located in extrusive rock between the two main gabbro sheets (localities 82 and 83, fig. 2) were included in these calculations because: (1) the hornfelsic textures of the rocks indicate that they were recrystallized and possibly reheated above their Curie temperature at the time of gabbro intrusion; (2) the direction of magnetization of these extrusive rocks is typical of the gabbro and is at least 50° different from any direction which might be expected from a middle Keweenawan lava flow after the effect of postmag-

netization tilting is removed; and (3) the remanant magnetization directions show a relatively high within-site scatter, which is more typical of the slowly cooled gabbro than of unmetamorphosed middle Keweenawan lava flows measured by the authors elsewhere in the Lake Superior area. If the two sites from these extrusive rocks were to be discarded, the average direction for the gabbro west of Mellen would be shifted an insignificant amount, but the statistical precision of the results would be decreased.

Mean directions of magnetization for the 14 sites (fig. 2) and for the entire gabbro body, together with pertinent statistical data, are presented in table 1. These directions have been recomputed to an equivalent direction at lat. 45° N., long. 90° W., in conformity with the practice used by DuBois (1962, p. 56) to permit direct comparison of directions of magnetization from sampling sites located at great distances from one another. The recomputed data are shown in figure 3 together with mean directions calculated by DuBois (1962, p. 57) for the Duluth Gabbro Complex, the Portage Lake Lava Series, and the Copper Harbor Conglomerate. The data for the Duluth Gabbro Complex are uncorrected for geologic dip, the Portage Lake data are corrected for dips of 39° NW. to 57° NW., and the Copper Harbor data are corrected for dips of 29° NW. to 31° NW.

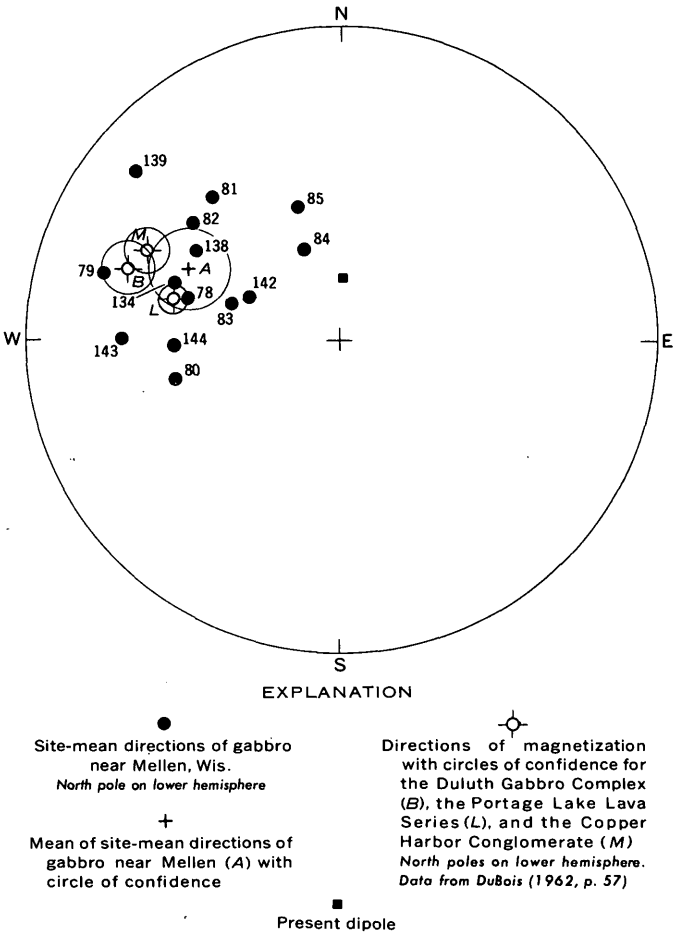

FIGURE 3.—Mean directions of magnetization for the gabbro near Mellen, Wis., the Duluth Gabbro Complex, the Portage Lake Lava Series, and the Copper Harbor Conglomerate. Directions are recalculated to values that the equivalent dipole would produce at lat 45° N., long 90° W. Numbers apply to corresponding sites in table 1. Equal-area projection.

DISCUSSION

A summary of the paleomagnetic results of DuBois (1962, table XVIII) for the Keweenawan stratigraphic units of the region around Mellen is given in table 2 and figure 4. The mean directions for individ-

TABLE 1.—*Summary of paleomagnetic data for gabbro and intercalated lavas near Mellen, Wis.*

Site No. (fig. 1)	Location of collecting site		Mean direction of magnetization at collecting site		Radius of confidence circle α_{95}	Precision parameter (K)	Number of samples (N)	Mean direction at lat 45° N., long 90° W.	
	N. lat (degrees)	W. long (degrees)	Azimuth (D) (degrees)	Inclination (I) (degrees)				Azimuth (D') (degrees)	Inclination (I') (degrees)
78	46.4	90.9	283.0	48.5	19.3	16.6	5	284.0	48.5
79	46.3	90.9	283.5	23.5	19.9	15.7	5	285.0	23.5
80	46.3	90.9	255.0	46.5	8.1	128.2	4	255.5	45.5
81	46.3	91.0	316.5	41.0	23.5	11.5	5	317.0	39.5
82	46.3	91.0	307.0	42.0	21.4	7.6	4	307.5	40.5
83	46.3	91.0	286.0	61.5	20.3	15.1	5	287.5	60.5
84	46.3	91.0	338.5	67.0	19.2	13.1	5	338.5	65.5
85	46.3	91.1	341.0	55.5	5.0	339.9	4	341.0	54.0
134	46.3	91.0	287.0	45.5	20.3	9.4	4	288.0	44.0
138	46.3	91.0	300.5	47.5	10.9	50.6	4	301.0	46.0
139	46.3	91.0	308.5	19.0	15.7	18.5	5	309.0	17.5
142	46.3	90.9	293.0	65.5	21.5	13.6	5	294.0	64.5
143	46.3	90.7	268.5	31.5	7.6	78.5	6	269.0	31.0
144	46.4	90.6	265.5	39.5	23.9	8.8	6	266.5	39.0
Mean of site means at A [1]			293.5	47.5	11.2	13.5	14	294.0	46.5

[1] Mean of site means on figure 2.

TABLE 2.—*Summary of paleomagnetic data for some Keweenawan formations of the Lake Superior region*

[Modified from DuBois (1962, table XVIII)]

Stratigraphic sequence (letters in parentheses refer to points in fig. 4.)	Mean direction at lat 45° N., long 90° W.		Radius of confidence circle α_{95}	Precision parameter (K')	Number of samples (N')
	Azimuth (D') (degrees)	Inclination (I') (degrees)			
Upper Keweenawan					
Bayfield Group: Chequamegon Sandstone (S)	228.5	73.5	5.5	46.5	15
Devils Island Sandstone					
Orienta Sandstone (R)	273.0	−6.0	22.0	6.5	8
Eileen Sandstone (P)	300.5	−20.5	6.5	18.5	28
Oronto Group: Freda Sandstone, Nonesuch Shale (O)	283.5	0.0	3.5	25.8	68
Copper Harbor Conglomerate (M)	293.5	33.0	6.5	20.2	25
Middle Keweenawan					
Duluth Gabbro Complex (B)	287.5	30.0	8.5	17.0	18
Portage Lake Lava Series (L)	282.5	45.0	4.0	47.2	31

ual formations have been connected by solid lines for great-circle paths on the lower hemisphere and dashed lines for paths on the upper. Arrows indicate the progression from older to younger formations. Although the true course and nature of the path connecting these points are highly speculative, the diagram does suggest a fairly orderly shift in direction of remanent magnetism from the Portage Lake Lava Series to the Eileen Sandstone, possibly followed by a change in the opposite direction back to the Orienta Sandstone.

Duluth Gabbro Complex

The implications of the available paleomagnetic data for the gabbros near Duluth, Minn., and Mellen, Wis., respectively, are summarized in figure 4. Point B represents the present direction of remanent magnetism in the gabbro at Duluth, and point B' represents what the direction would be if the gabbro were tilted 15° toward the west to make the underlying lavas horizontal; B', in other words, represents the direction of the earth's magnetic field at the time of intrusion of the gabbro, provided that the lavas were horizontal at that time. Because the actual attitude of the lavas at the time of intrusion is unknown, all that can be said is that within the limits of error of the actual measurements, the direction of remanent magnetization at the time of intrusion apparently lies somewhere on the dotted line B–B'.

If all the data in figure 4 were precise, including the path along which the direction of remanent magnetism changed between Portage Lake (L) and Copper Harbor (M) time, the intersection of B–B' and L–M' would represent the direction of remanent magnetism during intrusion and would suggest intrusion during the interval between Portage Lake and Copper Harbor

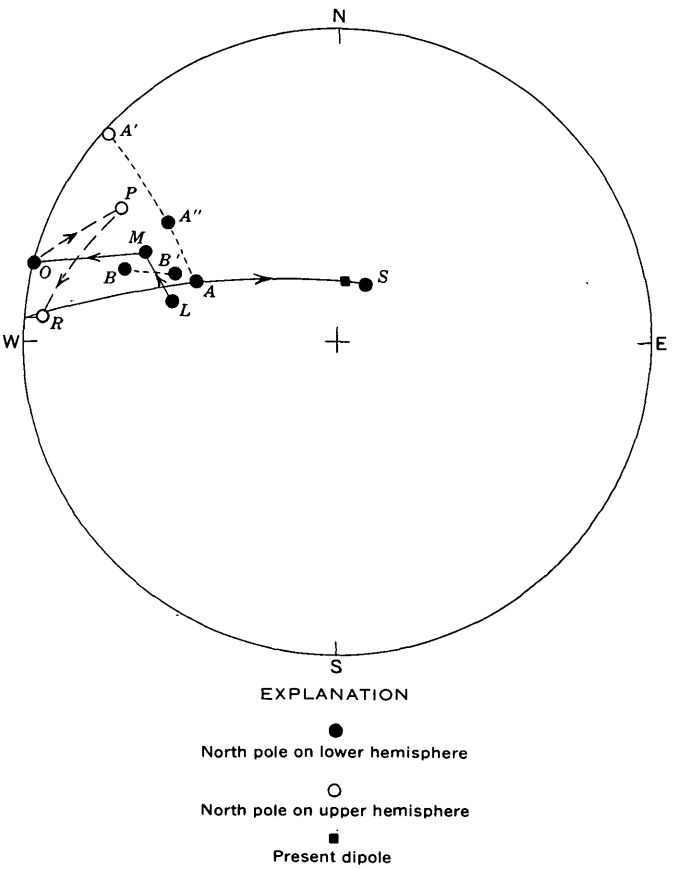

FIGURE 4.—Synoptic diagram of mean directions of remanens magnetization, Keweenawan rocks, western Lake Superiot region, recomputed to lat 45° N., long 90° W. Geologic unitr are A, gabbro near Mellen, Wis., and B gabbro near Duluth, Minn., uncorrected for dip; A' and B' are, respectively, the same gabbros but corrected for dip of the underlying lava flows; A'' represents a 20° dip correction from A; L, Portage Lake Lava Series; M, Copper Harbor Conglomerate; O, Freda Sandstone and Nonesuch Shale; P, Eileen Sandstone, R, Orienta Sandstone; and S, Chequamegon Sandstone. Data from the gabbro near Mellen are new, the remainder are from DuBois (1962, table XVIII). Equal-area projection.

times. Considering all the uncertainties, however, it is probably safe to conclude only that the Duluth Gabbro Complex was intruded when the underlying rocks were somewhat flatter than they are now, and during the general interval that includes Portage Lake and Copper Harbor time.

Gabbro intrusion near Mellen

There is a general agreement between the paleomagnetic field directions for the Portage Lake Lava Series (*L*) and the Copper Harbor Conglomerate (*M*), both corrected for geologic dip, and the two gabbros (*A* and *B*), both uncorrected for dip (fig. 4). In addition, the field directions for collection sites 82 and 83 agree (fig. 3). These are from steeply dipping lava flows probably altered during the gabbro intrusion near Mellen.

The grouping of all paleomagnetic field directions suggests emplacement during the same general time interval and seems to imply that the gabbros were intruded subsequent to Copper Harbor time after most of the tilting had been completed. Such a conclusion, however, ignores the fact that upper Keweenawan sedimentary rocks overlying the Copper Harbor have been tilted along with the lavas and conglomerate but do not have similar paleomagnetic field directions. DuBois (1962) has calculated mean directions of magnetization for these sedimentary rocks which, after correction for dip, are significantly different from the means for the three igneous units (fig. 4 and table 2). Thus, an apparent paradox exists, and alternative explanations must be considered.

Three alternative possibilities are discussed below.

(1) It is possible that directions of magnetization are here unreliable as stratigraphic indicators. This would occur, for instance, if the measured directions of magnetization for the various rock units did not reflect the ambient geomagnetic field at the time these rock units were formed. Alternatively, a rapidly fluctuating, nonsystematic geomagnetic field would introduce much scatter in remanence directions and lead to confusion in attempts to interpret the paleomagnetic data. However, a preliminary compilation indicates great consistency in direction of magnetization for the Portage Lake Lava Series and Copper Harbor Conglomerate throughout nearly 20,000 feet of stratigraphic, and 130 miles of horizontal, extent, which strongly suggests a stable field (Books, unpub. data). DuBois (1962, p. 25) also cites evidence for magnetic stability in the Portage Lake Lava Series, and our results for the gabbro near Mellen are based on directions of magnetization freed of the effects of magnetic instability by careful alternating-field "washing". As the igneous units in question are largely unaltered and effectively isotropic, there is little doubt that their directions of magnetization reflect the ambient magnetic field at the time of their formation.

The origin of the directions of magnetization of the sedimentary units, however, is less certain. Irving (1964, p. 30–32, 96–99) has summarized the special problems involved in the interpretation of direction of magnetization of sedimentary rocks, and an analysis of the problem is beyond the scope of this paper. It may be noted, however, that two commonly occurring interpretative problems involve (a) an inclination of remanent magnetization shallower than that of the paleomagnetic field, and (b) a direction of remanent magnetization acquired at some time later than the time of accumulation of the clastic fraction of the rock, as, for example, during diagenesis. A direction of remanent magnetization that differs from that of the ambient field at the time of sedimentation, nevertheless, could be highly stable and might well be accepted as a reliable indicator of paleomagnetic direction in the absence of careful analysis. It is noteworthy that 3 of DuBois' 5 directions of magnetization for upper Keweenawan sedimentary units (fig. 4, table 2) have inclinations markedly flatter than the inclinations of the middle Keweenawan igneous rocks. Of the two remaining sedimentary units, the Copper Harbor field direction is based in large part on data from intercalated lava flows, while the Chequamegon Sandstone has a direction of magnetization not much different from that of the present dipole field. DuBois (1962, p. 11) believes that the magnetization of the Chequamegon is stable, but reports (1962, p. 39) sample collections from this unit as being too small in vertical extent and too restricted in areal extent to be completely satisfactory. In effect, the sampling may be from too small a thickness to completely average out secular fluctuations. Thus, sedimentary rocks may exhibit directions of remanent magnetization which are misleading as a record of the ambient field during sedimentation, and are utilized with reservation in a later section of the present report.

(2) The effect of postintrusion tilt on the paleomagnetic field direction is potentially much greater for the gabbro near Mellen than for the Duluth Gabbro Complex, depending on the dip of underlying lava flows at the time of intrusion. The effect of postintrusion tilt can be studied by reference to dotted line *A*–*A*′ (fig. 4). Point *A* represents the direction of magnetization if there has been no tilt of the underlying

lavas since intrusion, and point A' the direction of magnetization if the lavas were horizontal at the time of intrusion. The only part of the line A–A' that is close to the directions of magnetization represented by the Portage Lake (L) and Copper Harbor (M) rocks is the part within 20° of point A (A'–A''). Providing that the separations of points A, L, and M of figure 4 are within the error due to all geologic and paleomagnetic uncertainties, their similar orientation suggests (a) that the gabbro was intruded in Portage Lake or Copper Harbor time, and (b) that there has been relatively little tilting (perhaps up to 10° to 20°) since intrusion of the gabbro. Inasmuch as the Copper Harbor Conglomerate, wherever observed, is practically conformable with the Portage Lake Lava Series, and has shared in the same tilting, the observed relationships are best explained by intrusion of the gabbro late in Copper Harbor time, when the underlying lavas were already dipping nearly 50°. This is geologically plausible, but does imply the existence of an angular unconformity between the Copper Harbor Conglomerate and the overlying Nonesuch Shale of a magnitude that is not suggested by any other evidence presently available.

(3) Assuming that the mean directions for upper Keweenawan sedimentary rock units, represented by O, P, and R on figure 4, are not misleading as previously discussed, one other possibility remains to be considered. If the gabbro near Mellen had been intruded during some episode of post-Orienta time, during which the geomagnetic field, quite fortuitously, had returned to the same direction and polarity as it had exhibited during Portage Lake time, the observed relationship would have resulted. This can be represented either by path R–S, which is defined by DuBois' average directions for the Orienta and Chequamegon Sandstones, or by a path R–A if the Chequamegon is suspect as a paleomagnetic indicator. The two paths would imply from nearly 40° (path R–A) to more than 70° (path R–S) of polar wandering during the interval between the middle Keweenawan and deposition of the upper Keweenawan Chequamegon Sandstone. In addition, path R–A would imply a reversal in the orderly movement of the late Precambrian pole position shown by DuBois (1962, fig. 31, p. 69). Thus, although the Orienta-Chequamegon time interval cannot be eliminated on this evidence alone it is nonetheless discounted as a plausible time of intrusion for the gabbro near Mellen. Irving (1964, p. 123–125) in his review of available paleomagnetic data, shows no pole position for the lower Paleozoic of North America having his minimum reliability criteria and lying within 30° of the mean pole position for Portage Lake time.

Paleomagnetic evidence, then, does not favor intrusion of the gabbro near Mellen in very late Keweenawan or later time. In this it concurs with the geologic evidence: volcanic and intrusive rocks younger than the Copper Harbor Conglomerate are rare, and none are known to cut rocks of the Bayfield Group.

CONCLUSIONS

It is probable that the gabbro near Mellen was intruded after much, if not all, of the tilting of the invaded flows had been completed. The close agreement between paleomagnetic field directions for the gabbro and adjacent steeply dipping altered lava flows (both uncorrected for tilt), and the Portage Lake Lava Series and Copper Harbor Conglomerate (both corrected for tilt), supports such a conclusion. Two possibilities as to the time of intrusion exist: (1) intrusion in late Copper Harbor time, in which case a considerable angular unconformity must exist closely overlying the Copper Harbor Conglomerate; or (2) intrusion during the late Keweenawan after Copper Harbor time, indicating that the average directions given by DuBois (1962) for rocks of the Oronto and Bayfield Groups are not valid measurements of geomagnetic field directions during that time interval.

Analysis of paleomagnetic data for the Lake Superior region apparently leads to equivocal results. It does, however, significantly restrict the span of time during which the intrusion near Mellen might conceivably have occurred, and indicates how additional paleomagnetic data, of increased precision, can be used to test explanations of regional geologic structure and history.

REFERENCES

Blundell, D. J., 1961, Rock magnetism applied to some geologic problems: Geol. Mag., v. 98, p. 301–312.

Blundell, D. J., and Read, H. H., 1958, Paleomagnetism of the younger gabbros of Aberdeenshire and its bearing on their deformation: Geol. Assoc. Proc., v. 69, p. 191–204.

Doell, R. R., and Cox, Allan, 1965, Measurement of the remanent magnetization of igneous rocks: U.S. Geol. Survey Bull., 1203–A, 32 p.

DuBois, P. M., 1962, Paleomagnetism and correlation of Keweenawan rocks: Canada Geol. Survey Bull. 71, 75 p.

Fisher, R. A., 1953, Dispersion on a sphere: Royal Soc. London Proc., ser. A, v. 217, p. 295–305.

Gehman, H. M., Jr., 1958, The petrology of the Beaver Bay com-

plex [abs.], *in* Institute on Lake Superior geology, April 21–22, 1958: Univ. Minnesota Center for Continuation Studies, p. 1.

Grout, F. F., 1918, Internal structures of igneous rocks: Jour. Geology, v. 26, p. 437–458.

Grout, F. F., Gruner, J. W., Schwartz, G. M., and Thiel, G. A., 1951, Precambrian stratigraphy of Minnesota: Geol. Soc. America Bull., v. 62, p. 1017–1078.

Irving, E., 1964, Paleomagnetism and its application to geological and geophysical problems: New York, John Wiley & Sons, Inc., 399 p.

Leighton, M. W., 1954, Petrogenesis of a gabbro-granophyre complex in northern Wisconsin: Geol. Soc. America Bull., v. 65, p. 401–442.

Leith, C. K., Lund, R. J., and Leith, Andrew, 1935, Precambrian rocks of the Lake Superior Region: U.S. Geol. Survey Prof. Paper 184, 34 p.

Tarling, D. H., 1962, Tentative correlation of Samoan and Hawaiian Islands, using "reversals" of magnetization: Nature, v. 196, no. 4857, p. 882–883.

CRUSTAL STRUCTURE DETERMINED BY SEISMIC-REFRACTION MEASUREMENTS BETWEEN THE NEVADA TEST SITE AND LUDLOW, CALIFORNIA [1]

By J. F. GIBBS and J. C. ROLLER, Denver, Colo.

Abstract.—Seismic-refraction measurements from nuclear and chemical explosions were made to determine the crustal structure along a line from the Nevada Test Site (NTS) to Ludlow, Calif. Additional recordings from nuclear explosions were made southward toward Calexico, Calif. The thicknesses of the successive crustal layers at NTS are h_0=1.0 km (v_0=2.5 km/sec), h_1=13 km (v_1=6.1 km/sec), and h_2=20 km (v_2=6.8 km/sec); the total crustal thickness is 34 km. The successive crustal layers at Ludlow have thicknesses of h_0=1.4 km, h_1=13 km, and h_2=13 km; the total crustal thickness is 27 km.

The U. S. Geological Survey recorded a reversed seismic-refraction profile between the Nevada Test Site (NTS) and Ludlow, Calif., in August 1962 (fig. 1). Recordings from the Ludlow shotpoint were made at 26 locations from 3 chemical explosions of 4,000, 8,000, and 12,000 pounds. The first charge was in a single drill hole; the two larger charges were distributed, respectively, in 3 and 4 drill holes 50 feet apart. The Ludlow shotpoint was located at lat 34°49.36′ N. and long 116°11.02′ W. The reverse of this profile was obtained by recording seismic waves generated by five underground nuclear explosions at the Nevada Test Site. Recordings were made at 14 locations between NTS and Ludlow, plus 12 locations beyond Ludlow southward towards Calexico, Calif. Ten seismic-recording units (Warrick and others, 1961) were used to make the recordings. Jackson and others (1963) have described the field procedures used in this study.

GEOLOGY AND PHYSIOGRAPHY

The seismic-refraction profile lies entirely within the Basin and Range province, starting at the south end of the Great Basin and terminating in the Sonoran Desert (Fenneman, 1946). The region is characterized by a series of basins, ranges, and faults that generally strike northwest. All the major divisions of geologic time are represented by the rocks exposed in this region (Nolan, 1943). The Precambrian rocks have been studied little, but several unconformable sequences have been distinguished. The Paleozoic and lower Mesozoic deposits suggest a persistent geosyncline, in which many thousands of feet of sediments were deposited. In mid-Mesozoic time, marine sedimentation ceased; later Mesozoic and Cenozoic deposits are composed of widely distributed local accumulations of nonmarine sedimentary beds and intrusive and igneous rocks (Nolan, 1943). The seismic profile traverses many of the northwestward-striking ranges. Some of the major topographic features include the Spectre Range, Spring Mountains, Pahrump Valley, Nopah Range, Silurian Hills, Shadow Range, Soda Mountains, Bristol Range, and the Cody Mountains. The average altitude of the recording locations is 671 meters, with the highest station at 1,524 m in the San Jacinto Mountains, and the lowest 67 m below sea level near the Salton Sea.

CHARACTERISTICS OF SEISMOGRAMS

Ludlow

The Ludlow shotpoint proved to be relatively efficient in converting explosive energy to seismic energy. Seismograms recorded from Ludlow are of good quality out to a distance of about 175 kilometers; beyond 175 km they are generally usable, although they have higher background noise, and the first upward compressional motion cannot be observed on all seismograms.

First arrivals for 11 seismograms recorded from Ludlow to a distance of 94 km are identified as P_g, a wave that travels in the upper crust. The first upward compressional motion can be observed on most of these recordings (fig. 2). First arrivals on 5 seismograms

[1] Work performed under Advanced Research Project Agency Order No. 193–64.

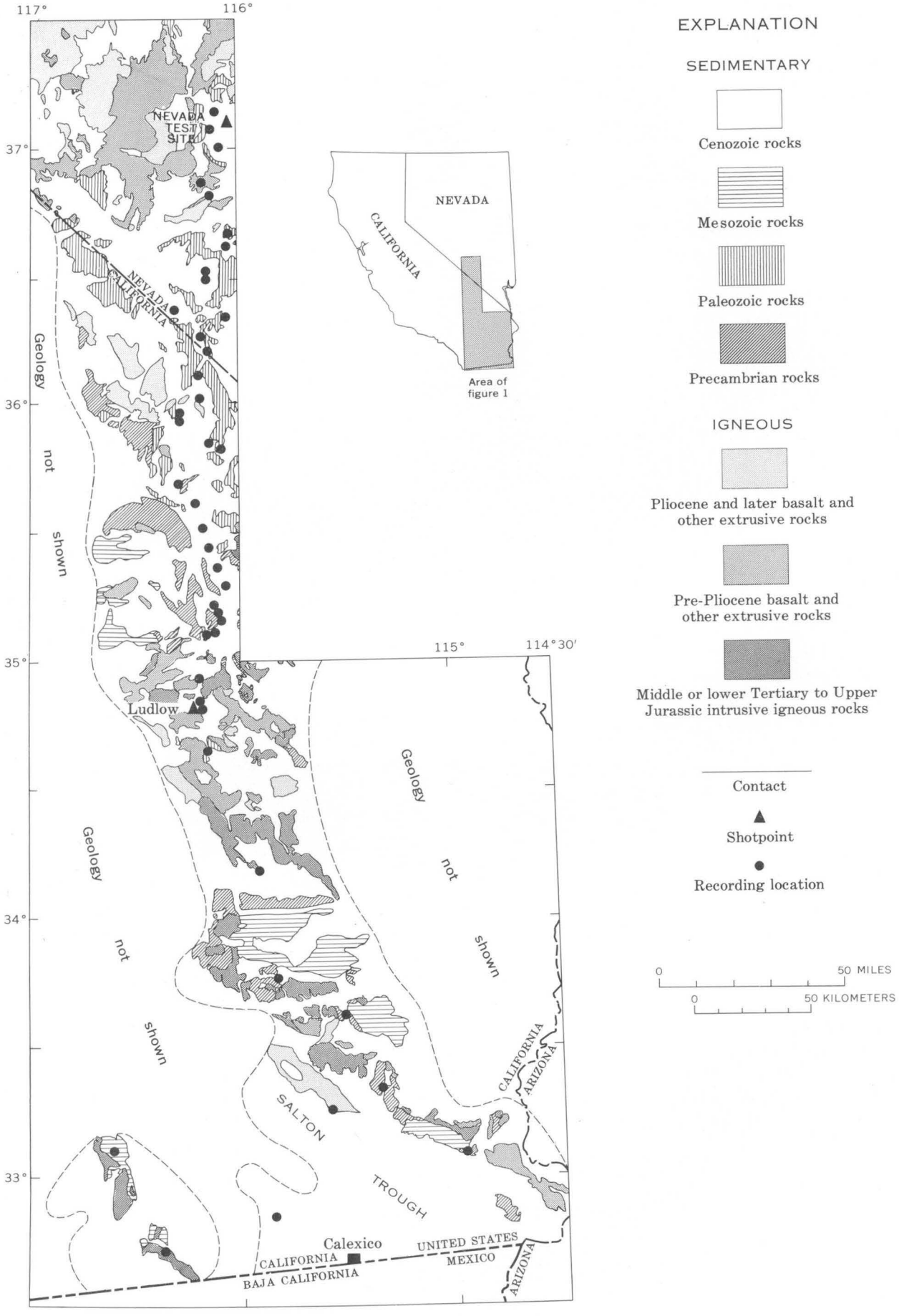

FIGURE 1.—Index maps showing shotpoints, seismic-recording locations, and generalized geology of the area of report.

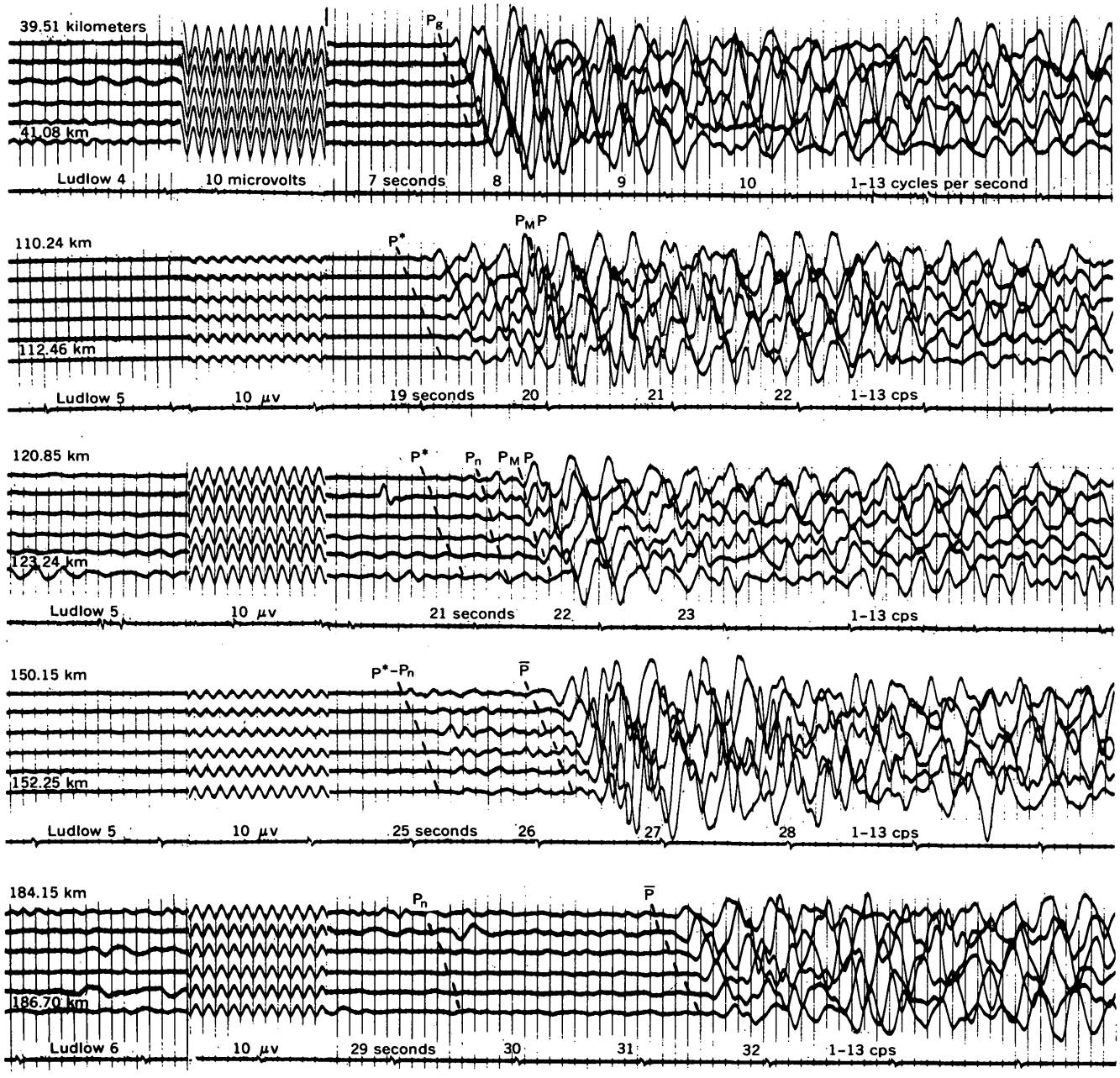

FIGURE 2.—Selected seismograms from chemical explosions, illustrating phases used in interpretation. Amplitudes are in microvolts; P_g, direct crustal wave; P*, wave critically refracted from an intermediate layer in the crust; P_n, mantle-refracted wave; P_MP reflection from the Mohorovicic discontinuity, $\bar{P}$, a guided wave in the crust. The exact nature of $\bar{P}$ is not known (Ryall and Stuart, 1963).

recorded at distances ranging from 106 to 150 km are tentatively identified as P*, a wave that is critically refracted from an intermediate layer in the crust. First arrivals on 8 seismograms recorded in the distance range from 150 to 203 km are identified as P_n, a wave that is critically refracted from the upper mantle below the Mohorovicic discontinuity. A large-amplitude wave train that follows P_n by several seconds is identified as $\bar{P}$ (fig. 2). This event has an apparent velocity of 6.1 km/sec. The nature of $\bar{P}$ has been discussed by Ryall and Stuart (1963), Roller and Healy (1963), and others.

Six seismograms in the distance range 67 to 112 km show a group of strong secondary arrivals which are tentatively identified as reflections from the Mohorovicic discontinuity. This event, P_MP, is shown on the reduced traveltime curve (fig. 3) between P* and the backward extension of P_n. It is not observed beyond the crossover point of P_g and P*. These events occur earlier than the backward extension of the P_n line,

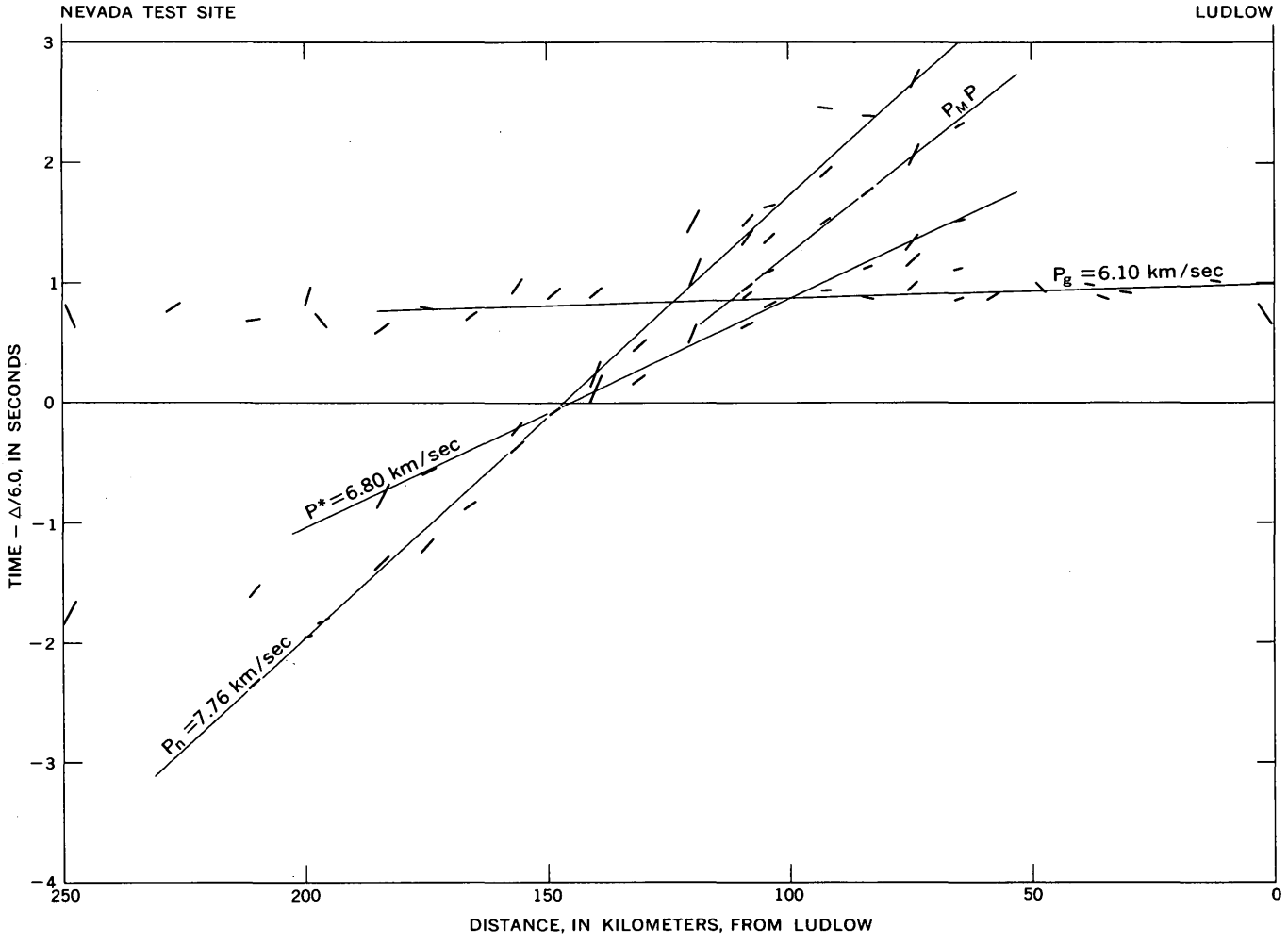

FIGURE 3.—Reduced traveltime-distance graph, Ludlow to the Nevada Test Site. Dashes of different lengths are the time-distance plots for individual recorders of the various seismic waves. P*, wave critically refracted from an intermediate layer in the crust; P_n, mantle-refracted wave; P_MP, reflection from the Mohorovicic discontinuity; P_g, direct crustal wave.

which suggests that the Mohorovicic discontinuity is not a flat surface but changes dip along the profile.

Nevada Test Site (NTS)

The reverse of this profile was made by recording seismic waves generated by five underground nuclear explosions at the Nevada Test Site. The maximum distance between shotpoints at the Test Site was 9.7 km between shots 3 and 4. Shots 1, 2, 4, and 5 are all within a radius of less than 1 km. Despite the scatter of shotpoints, the traveltimes show a systematic agreement. Seismograms from the nuclear explosions are of good quality with a high signal-to-noise ratio.

The phase P_g can be identified on 3 seismograms at distances less than 105 km. Beyond 105 km, P_g was not observed as a distinguishable arrival. The phase P_n is observed as a first arrival on 21 seismograms in the distance range from 140 to 490 km.

The phase P_MP was tentatively identified on 6 seismograms in the distance range from 100 to 175 km. A very large amplitude event which follows an extension of the P_g traveltime line (fig. 4) by approximately 2 seconds was observed and tentatively identified as $\overline{P}$.

TIME OF FIRST ARRIVALS

The first waves from NTS to reach recording locations to a distance of 155 km are P_g and fit the line which can be expressed mathematically as $t_1 = 0.74 + \Delta/6.10$ where t is the arrival time and Δ the distance from the shot point (fig. 4). From 135 km to the P_g–P_n crossover, at 155 km, the true first arrivals on 3 recordings are not distinguishable from the noise. In the range 155 to 265 km from NTS, first arrivals fit the line $t_3 = 6.70 + \Delta/8.04(P_n)$. With the exception of the arrivals on one seismogram, they all are within 0.1 sec of this line. The exception deviates from the line by less than 0.3 sec. In the distance range 315 km

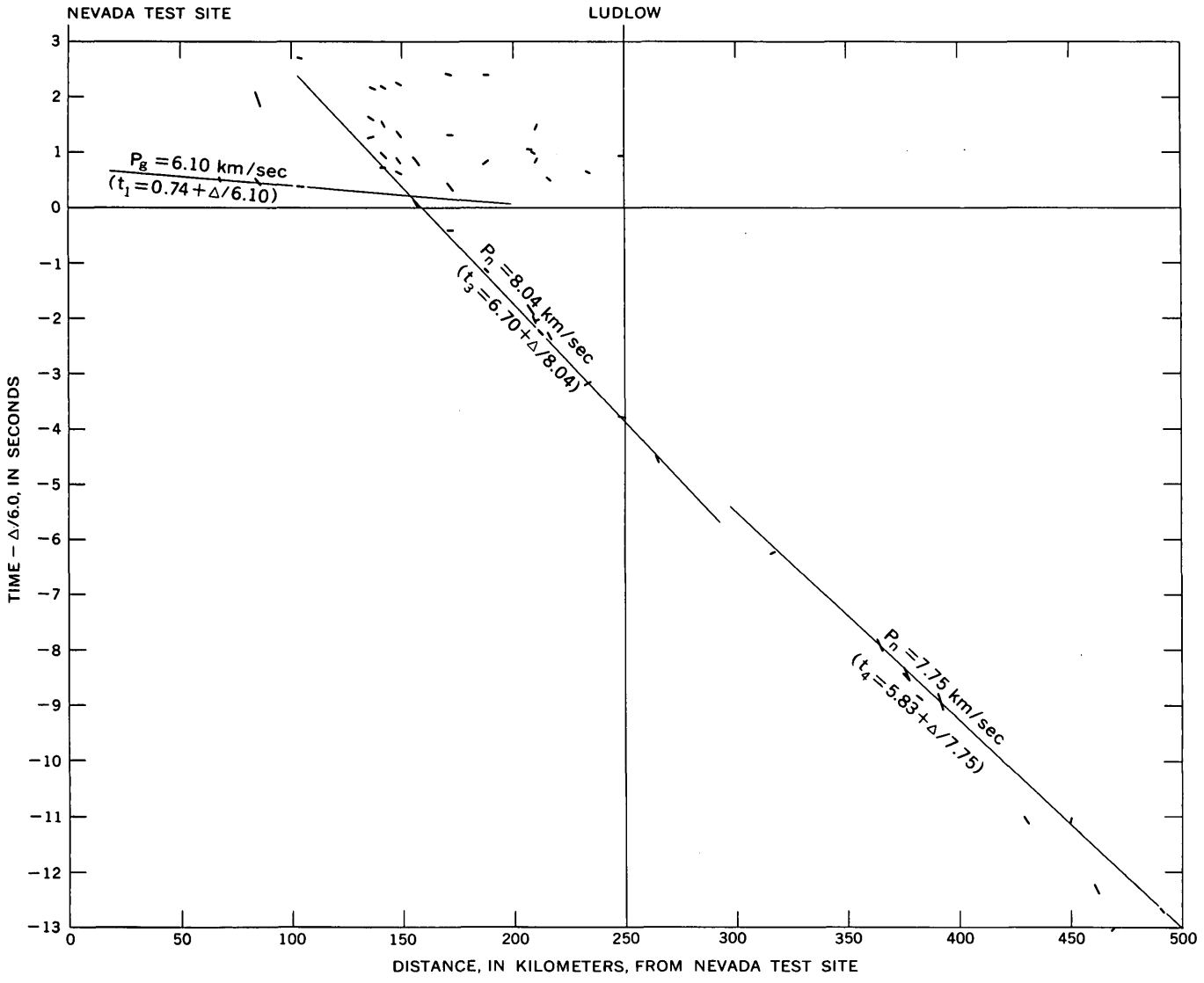

FIGURE 4.—Reduced traveltime-distance graph, Nevada Test Site to Ludlow. Dashes of different lengths show the position of the individual seismic detectors and the arrival time of various wave groups. P_g, direct crustal wave; P_n, mantle-refracted wave. Equations for first arrivals in certain distance ranges are indicated within parentheses: Δ=67 to 155 km; Δ=155 to 265 km; Δ=315 to 490 km.

to 490 km, the first arrivals from 8 seismograms fit the line $t_4 = 5.83 + \Delta/7.75$ (P_n). The group of secondary arrivals shown between 125 and 250 km could not be identified with any particular wave group. They are shown only to indicate that the records do contain secondary arrivals.

The first waves from Ludlow shotpoint to reach recording locations to a distance of 95 km fit the line $t_1 = 1.00 + \Delta/6.10$ (P_g) with a maximum deviation of 0.1 seconds. The first arrivals in the distance range 103 to 152 km fit the line $t_2 = 2.81 + \Delta/6.80$ (P^*). Again in this range, all the first arrivals fit this line within 0.1 sec. The first arrivals in the distance range 152 to 215 km fit the line $t_3 = 5.48 + \Delta/7.76$ (P_n). The largest deviation from this line is less than 0.2 sec.

DEPTH CALCULATIONS

Using the zero-intercept times and the apparent velocities of only the first arrivals (Mota, 1954) depth calculations were made for two crustal models (table 1). Disregarding the evidence for an intermediate layer, the depth to the crust-mantle interface was calculated to be 30 km at NTS and 22 km at Ludlow (table 1, model I). The depth of 30 km in the area of the Nevada Test Site agrees well with other authors. Diment and others (1961) report a depth, using a one-layer crustal model, of 28 km to the Mohorovicic discontinuity from recordings southeast of the Nevada Test Site. Pakiser and Hill (1963) report a one-layer crustal thickness of 28 km along an unreversed profile

TABLE 1.—*Computed crustal models*

Layer	From Ludlow, Calif.		From Nevada Test Site	
	Velocity (km/sec)	Thickness (km)	Velocity (km/sec)	Thickness (km)
Model I				
h_0	2. 50	1. 4	2. 50	1. 0
h_1	6. 10	21	6. 10	29
h_2	7. 76	--------	8. 04	--------
Total depth to Mohorovicic discontinuity.	22 km		30 km	
Model II				
h_0	2. 50	1. 4	2. 50	1. 0
h_1	6. 10	13	6. 10	[1] 13
h_2	6. 80	13	[1] 6. 80	20
h_3	7. 76	--------	8. 04	--------
Total depth to Mohorovicic discontinuity.	27 km		34 km	

[1] Assumed.

north of the Nevada Test Site. However, it is somewhat deeper than the 24.3 km reported by Ryall and Stuart (1963) from an unreversed profile extending eastward from the Nevada Test Site, using a one-layer crust.

Model I was computed only to show the extent of agreement. The preferred model using the strong evidence for an intermediate layer is shown in model II (table 1). A depth to the Mohorovicic discontinuity of 27 km was calculated at Ludlow by using a two-layer crust and assuming that the apparent velocity of 6.8 km/sec recorded from Ludlow is the true velocity of the intermediate layer. If we assume that the thickness of the upper layer in the crust is the same at NTS as it is at Ludlow, a depth to the Mohorovicic discontinuity of 34 km can be calculated at NTS. This would make the thickness of the intermediate layer 13 km at Ludlow and 20 km at NTS. The crustal thickness at NTS was calculated on the assumption of constant dip on the upper-mantle surface.

By using the reflected events identified as P_MP, the depth of the reflecting surface was computed to be approximately 23 km immediately north of Ludlow. Three seismograms recorded in the Imperial Valley area have P_n arrivals which are 1.1 sec, 0.6 sec, and 0.6 sec earlier than an extension of the P_n line. These stations have altitudes of —67 m, 335 m, and 366 m, and are located on alluvium, Tertiary volcanic rock, and a Precambrian outcrop, respectively. These early arrivals do not seem to be caused entirely by local geology or altitude and may suggest a thinning of the crust in the area of the Salton Trough. If we assume that all of this time difference is due to thinning of the crust and not to velocity changes, the depth to the Mohorovicic discontinuity would be 7 km shallower near the Salton Sea than at Ludlow, or about 20 km.

AMPLITUDES

Because of the difficulty of observing the first upward compressional motion on seismograms at large distances, amplitudes were scaled from the first trough to the second peak (fig. 5). A charge size of 4,000 pounds

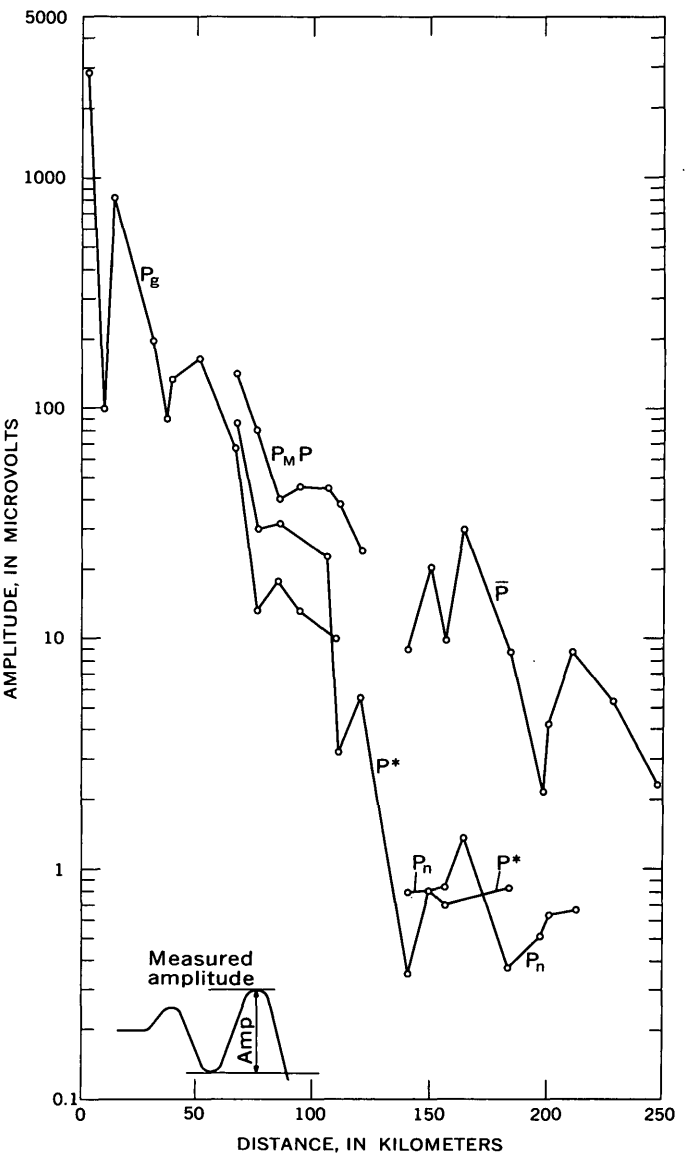

FIGURE 5.—Graph showing phase amplitude versus distance, from Ludlow chemical explosions.

was used to normalize the amplitudes, on the assumption that a linear function exists between charge size and amplitude. The amplitudes of the reverse profile from NTS are not plotted. Only relative amplitudes will be discussed for this half of the profile. The phase P_g attenuates very rapidly to a distance of 110 km from the Ludlow shotpoint. Beyond this distance P_g arrivals cannot be positively identified. On 7 seismograms large-amplitude events identified as reflections from the Mohorovicic discontinuity occur as secondary arrivals in the distance range 67 to 121 km.

The phase P* appears as a secondary arrival from 65 to 105 km and as a first arrival from 110 to 155 km; it has approximately the same attenuation with distance as P_g (fig. 5).

The phase P_n is weak; it appears as a first arrival at 150 km and disappears into the noise at 215 km. The largest amplitude arrivals in the distance range 140 to 250 km are identified as $\overline{P}$.

Amplitudes from the nuclear explosions are very much like those observed from the Ludlow shotpoint. The phase P_g drops off very rapidly with distance and is not distinguishable from the noise at 135 km. Large-amplitude events arriving at a time appropriate for reflections from the Mohorovicic discontinuity are observed on 6 recordings in the distance range 105 to 170 km. A very large amplitude event is observed on 5 seismograms in the distance range 135 to 190 km. This event has approximately three times the amplitude of P_MP and has the largest amplitude on the seismogram. It has not yet been identified.

CONCLUSIONS

A P_g velocity of 6.10 km/sec was recorded from both directions. The velocity of P_n from Ludlow to NTS is 7.76 km/sec and from NTS to Ludlow is 8.04 km/sec. A dip of 1.7° in the Mohorovicic discontinuity would account for this difference in the apparent velocities.

Using a one-way refraction profile from Ludlow southward the velocity of P_n decreases to 7.75 km/sec. This would indicate that the Mohorovicic discontinuity begins to flatten out at a distance of 315 km south of NTS. An intermediate-layer velocity of 6.80 km/sec was determined from first arrivals from the Ludlow shotpoint. No evidence for an intermediate layer was observed from the NTS; however, the separation between recording locations from NTS may have been too great to establish the presence of an intermediate layer.

The thickness of the crust was computed to be 27 km at Ludlow and 34 km at NTS. Evidence was found that indicates the crust may be as thin as 20 km in the Salton Sea area.

REFERENCES

Diment, W. H., Stewart, S. W. and Roller, J. C., 1961 Crystal structure from the Nevada Test Site to Kingman, Arizona, from seismic and gravity observations: Jour. Geophys. Research, v. 66, no. 1, p. 201–214.

Fenneman, N. M., 1946, Physical divisions of the United States: U.S. Geol. Survey map.

Jackson, W. H., Stewart, S. W., and Pakiser, L. C., 1963, Crustal structure in eastern Colorado from seismic-refraction measurements: Jour. Geophys. Research, v. 68, no. 20, p. 5767–5776.

Mota, Lindonor, 1954, Determination of dips and depths of geological layers by the seismic-refraction method: Geophysics, v. 19, no. 2, p. 242–254.

Nolan, T. B., 1943, The Basin and Range province in Utah, Nevada, and California, *in* Shorter contributions to general geology: U.S. Geol. Survey Prof. Paper 197–D, p. 141–196.

Pakiser, L. C., and Hill, D. P., 1963, Crustal structure in Nevada and southern Idaho from nuclear explosions: Jour. Geophys. Research, v. 68, no. 20, p. 5757–5766.

Roller, J. C., and Healy, J. H., 1963, Seismic-refraction measure- Lake Mead: Jour. Geophys. Research, v. 68, no. 20, p. 5837–ments of crustal structure between Santa Monica Bay and Lake Mead: Jour. Geophys. Research, v. 68 no. 20, p. 5837–5849.

Ryall, Alan, and Stuart, D. J., 1963, Travel times and amplitudes from nuclear explosions, Nevada Test Site to Ordway, Colorado: Jour. Geophys. Research, v. 68, no. 20, p. 5821–5835.

Warrick, R. E., Hoover, D. B., Jackson, W. H., Pakiser, L. C., and Roller, J. C., 1961, The specification and testing of a seismic-refraction system for crustal studies: Geophysics, v. 26, p. 820–824.

SEISMIC-REFRACTION MEASUREMENTS AT SUNNYSIDE, UTAH

By BENTON L. TIBBETTS, C. RICHARD DUNRUD,
and FRANK W. OSTERWALD, Denver, Colo.

Abstract.—Three reversed seismic-refraction profiles were recorded in the Sunnyside, Utah, area in August 1965. The average velocity of the seismic waves is 4.3 km/sec through the Mesozoic and lower Tertiary sedimentary rocks and an average of 6.0 km/sec along the upper portion of the Paleozoic carbonate rocks. The thickness of sediments that overlie the upper Paleozoic carbonate refractor horizon ranges from 1.2 km in Clark Valley to 3.7 km in Range Creek.

In August 1965, the U.S. Geological Survey conducted a seismic-refraction study in the Sunnyside, Utah, district to determine the velocity of seismic waves traveling through the sedimentary rocks, and to delineate the gross subsurface structure. This information will be used to study the relationship between earth tremors and dangerous coal mine "bumps" (rock bursts) that occur frequently in the mines of the district.

GEOLOGY AND PHYSIOGRAPHY

The Sunnyside district is near the northwestern corner of the Colorado Plateaus province about 25 miles east of Price, Utah (fig. 1). The major structural features of the region are the north-northeast-trending San Rafael swell to the south, and the generally west-trending Uinta basin to the north. Structural relief between the highest part of the San Rafael swell and the lowest part of the Uinta basin, a distance of approximately 160 km, is about 6.7 km (measured on top of the Chinle Formation of Late Triassic age) and has a generally constant gradient from 2.2 km above sea level to 4.6 km below sea level, respectively (U.S. Geol. Survey and Am. Assoc. Petroleum Geologists, 1961). Rocks as old as late Paleozoic (Baars, 1962) are exposed in the San Rafael swell; rocks as young as middle Tertiary crop out in the Uinta basin (William B. Cashion, oral commun., 1966).

Along the seismic profile, rocks that range in age from Early Cretaceous to Eocene(?) (Fisher, and others, 1960, p. 21–22) are exposed or are covered by a thin veneer of Quaternary surficial material. The thickness and lithology of these rocks are known locally from a geologic study of the Sunnyside mining district (C. R. Dunrud and F. W. Osterwald, unpub. data). Local drill-hole logs reveal approximately 0.06 km of Upper Cretaceous sandstone and claystone and

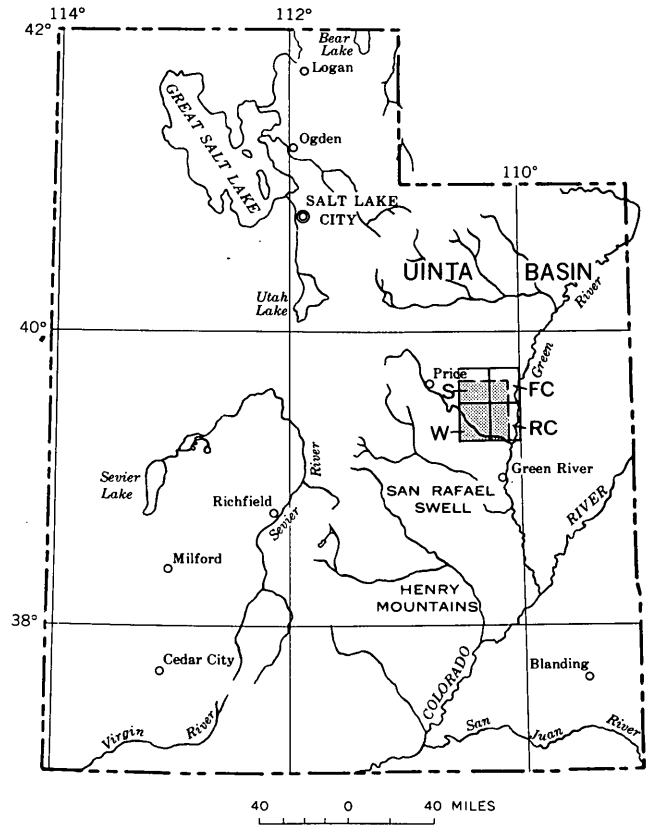

FIGURE 1.—Index map of Utah, showing area covered by figure 2 (stippled) and location of Sunnyside (S), Flat Canyon (FC), Range Creek (RC), and Woodside (W) 15-minute quadrangles.

an overlying 0.91 to 1.07 km of Upper Cretaceous Mancos Shale. Next, the thick sandstone and interbedded shale and siltstone of the Upper Cretaceous Mesaverde Group have a total thickness of about 0.37 km. Paleocene and Eocene(?) sedimentary rocks that are considered fluviatile and lacustrine (Fisher and others, 1960, p. 21–22) overlie the Mesaverde Group. These rocks include approximately 1 km of variegated claystone, siltstone, and lenticular sandstone.

The subsurface stratigraphy along the refraction profile is known in a general way from the local and regional geologic mapping. The Paleozoic rocks are composed of at least 1.2 km and perhaps as much as 1.5 km of thick-bedded limestone and dolomite with some interbedded shale, sandstone, and local evaporites. At the top of the Paleozoic section is a Permian sandstone that is approximately 0.15 km thick. The overlying Triassic and Jurassic sedimentary rocks have an aggregate thickness of about 1.0 km and comprise thick sandstone and locally thick shale and siltstone with thin interbedded layers of limestone, marlstone, and one rather thick layer of anhydrite.

Erosion has sculptured bold cliffs 0.5 to 0.8 km high from the predominantly resistant rocks of the Mesaverde Group. These are the Book Cliffs, which face westward and southward and are generally parallel to the regional strike (fig. 1). Topographically, the Book Cliffs divide the lowlands of Clark Valley, which is underlain by the weakly resistant Mancos Shale, from the highlands, which are underlain by erosion-resistant Mesaverde and younger rocks. Streams have incised steep-walled canyons in these resistant rocks, making the topography of the Book Cliffs extremely rugged.

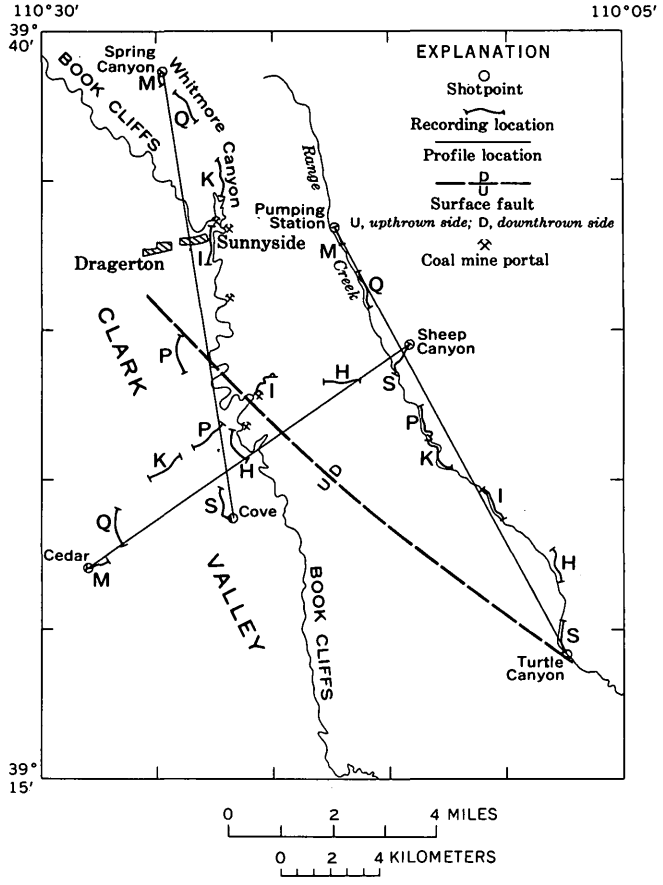

FIGURE 2.—Sketch map of the Sunnyside, Utah, area, showing recording locations, shotpoints, and general direction of the three reversed seismic-refraction profiles that were measured. Base from portions of the Woodside, Sunnyside, and Range Creek 15-minute topographic quadrangles.

FIELD PROCEDURES

Seismic-refraction measurements were made along 3 reversed profiles that were 24 to 30 km in length (fig. 2). Seven seismic-refraction recording units (Warrick and others, 1961) were used to record the seismic waves generated by the detonation of 1,000-pound chemical charges that were loaded in drill holes at both ends of each profile. Each unit recorded the output of 6 vertical seismometers and 2 horizontal seismometers on photographic paper and on magnetic tape. The vertical seismometers were spaced 0.5 km apart and were positioned along secondary roads that generally parallel the profile. The two horizontal seismometers were placed at one of the vertical sites and were oriented parallel and transverse to the profile.

The Pumping Station–Turtle Canyon profile is along Range Creek east of and about parallel to the Book Cliffs (fig. 2). The Spring Canyon-Cove line is oriented in the same general direction at the base of the Book Cliffs. These two profiles generally parallel the strike of the regional structure. The Cedar–Sheep Canyon profile is approximately transverse to the Book Cliffs and the other two profiles. The change in elevation along the Cedar–Sheep Canyon profile is approximately 0.7 km, and the east end of the profile is stratigraphically higher than the west end by about 2.2 km of Cretaceous and lower Tertiary rocks. The change in elevation along the Pumping Station–Turtle Canyon and the Spring Canyon–Cove profiles is about 1 km, and the north end of each profile is stratigraphically higher than the south end by nearly the same amount.

RESULTS

The locations of the recording units and shotpoints were plotted on 15-minute topographic maps (scale 1:62,500). The distances from the shotpoints to each seismometer were scaled to within 0.05 km, and the

FIGURE 3.—Seismogram recorded by unit P from the Cove shotpoint. The first compressional-wave arrival and the shear-wave arrival are identified as P and S, respectively. V and H refer to channels recording seismic impulses from vertical and horizontal seismometers, respectively. Tc indicates time correction.

traveltimes of the seismic waves to each seismometer were determined to within 0.01 second.

The relative efficiency of the shotpoints, with the exception of the Turtle Canyon one, in converting explosive energy into seismic energy was good. The quality of most of the seismograms is very good; the first upward (compressive) motion (P, fig. 3) can be identified on most of the seismograms.

A traveltime curve was constructed for each of the three reversed profiles. The apparent velocities were determined by visually fitting straight lines to the traveltime data. The plots of the traveltimes of first arrivals on all three profiles define a two-segment time-distance curve.

No corrections for elevation differences between shotpoints or between recording locations were made on the traveltime curves of the three profiles. First-arrival plots of the direct compressional wave on the traveltime curves for the 3 profiles show a time intercept ranging from 0.02 second to a maximum of 0.06 second (figs. 4, 5, and 6). These small time intercepts indicate a generally thin layer of surficial material and weathered bedrock throughout much of the area. Alluvial deposits are thicker and could locally be relatively thick in Range Creek (Pumping Station-Turtle Canyon profile) and in Whitmore Canyon (Spring Canyon–Cove profile). This could partially account for the local deviations from a linear plot of the first arrivals in these areas. Shallow seismic profiles along the three refraction lines would be necessary to make delay-time corrections for alluvium in the valleys.

In determining depths to, and dips of, the high-velocity refracting horizon beneath the various shotpoints, conventional intercept-time computing methods were used (Heiland, 1940, p. 521–529; Mota, 1954). Corrections were made for the thin, low-velocity layer and applied to the depth calculations.

Pumping Station to Turtle Canyon profile

The curve representing the apparent velocity of the direct compressional wave through the near-surface sediments from the Pumping Station shotpoint is poorly defined because of a "missed" record (Q) at a key position (5 to 10 km) on the line (fig. 4). However, the apparent velocity of 4.4 km/sec corresponds with that from the Turtle Canyon shotpoint. The apparent velocity of 6.2 km/sec is defined by the second segment of the traveltime curve. The physical mechanism by which energy is transmitted along the upper portion of the high-velocity Paleozoic refractor is treated in detail by Dobrin (1960, p. 70–71). The depth to this 6.2-km/sec refractor beneath the Pumping Station shotpoint was calculated to be 3.7 km. This depth correlates very well with the position of the top of the Paleozoic carbonates, projected on the basis of available surface and subsurface stratigraphic control.

Seismic waves generated at the Turtle Canyon shotpoint were very weak. Because the recording units that were positioned near the source were operated at low gains to prevent overdriving of the instruments by the anticipated large signals, amplitudes on all the seismograms were small. Identification of the first arrivals beyond the crossover distance at 12 km was very difficult. Signals interpreted to be first arrivals

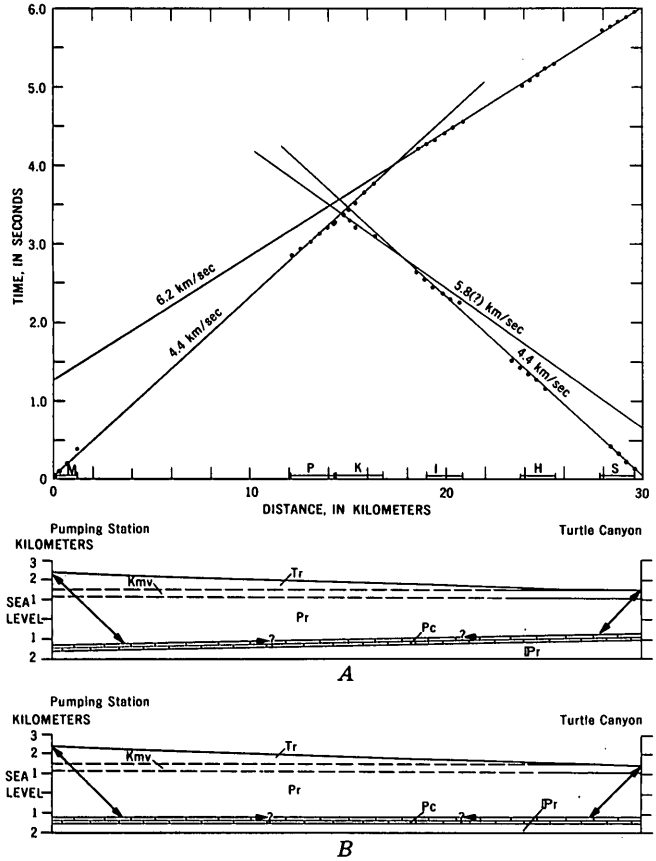

FIGURE 4.—Traveltime curves (above) of first arrivals, and interpretive cross sections (below, *A*, *B*) along the Pumping Station–Turtle Canyon seismic-refraction profile. *A*, seismically determined position of rocks transected and the ray path of least time; *B*, geologically determined position of rocks transected and the implied ray path of least time. M, P, K, I, H, and S are recording-location lines (see fig. 2). Rocks are: Tr, Tertiary; Kmv, Late Cretaceous (Mesaverde); Pr, Early Permian (Leonard) and younger; Pc, Early Permian (Wolfcamp); PPr, Pennsylvanian and older.

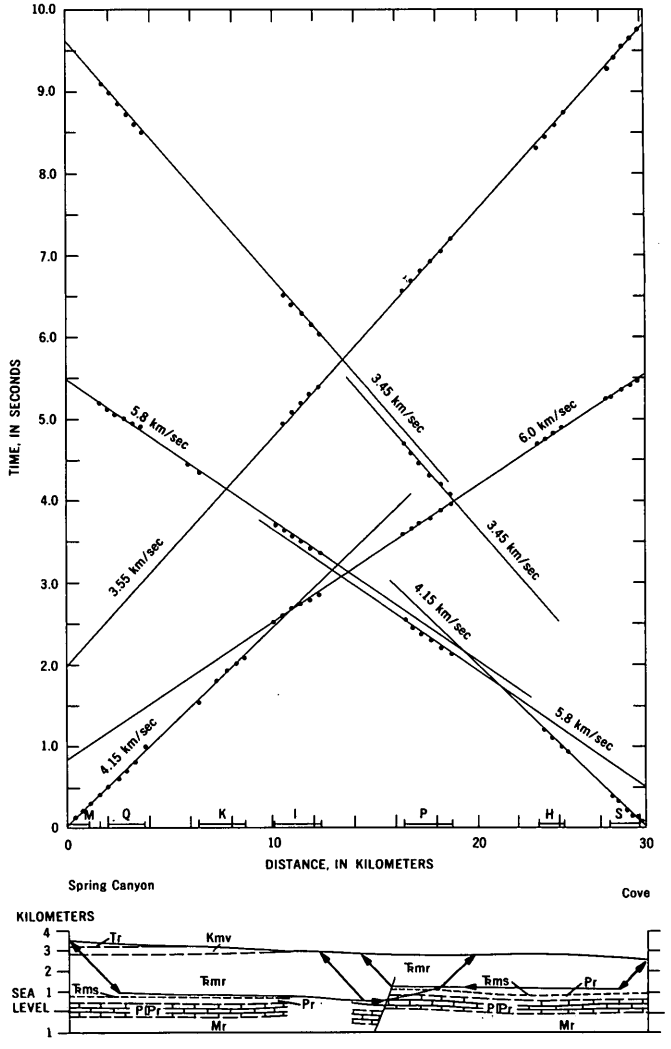

FIGURE 5.—Traveltime curves (above) of first and secondary arrivals, and interpretive cross section (below), along the Spring-Canyon–Cove seismic-refraction profile, showing the geologically determined positions of rocks transected and the seismically determined ray path of least time. M, Q, K, I, P, H, and S are recording-location lines (see fig. 2). Rocks are: Tr, Tertiary; Kmv, Late Cretaceous (Mesaverde); Tmr, Triassic (Moenkopi) and younger; Tms, Triassic (Sinbad [limestone]); Pr, Early Permian (Leonard) and younger; PPr, Early Permian (Wolfcamp) and Pennsylvanian; Mr, Mississippian and older.

could be identified on only three traces. The plots of these three traveltimes are insufficient data for determining an accurate apparent velocity. The 5.8-km/sec apparent-velocity line was assumed from the velocities obtained from the other two profiles together with the reliable updip apparent velocity of 6.2 km/sec observed from the Pumping Station shot. The calculated depth beneath the Turtle Canyon shotpoint is 2.2 km.

Another possible interpretation of the traveltime data received from this profile is based upon the orientation of the profile, which appears to approximately parallel the regional strike (fig. 2). This interpretation asserts that the apparent velocity, 6.2 km/sec, observed from the Pumping Station data is the true velocity of the Paleozoic refractor. This anomalously high velocity, compared to the true velocities for the same refractor obtained from the other two profiles (5.9 and 6.0 km/sec), would have to result from a lateral change in velocity along that refractor. This could conceivably be caused by a change in bulk composition or a change in crystallinity of the layer. Asuming that the arrivals recorded on the three profiles are from the same refractor, it appears unlikely that the dissimilar velocities would be caused by the effects of porosity and composition because of the similar depth and geologic age of the unit. For these reasons, the first interpretation (fig. 4*A*), as stated above is taken as the most reasonable. The true velocity computed from the two apparent velocities mentioned earlier (6.2 and 5.8 km/sec) is 6.0 km/sec.

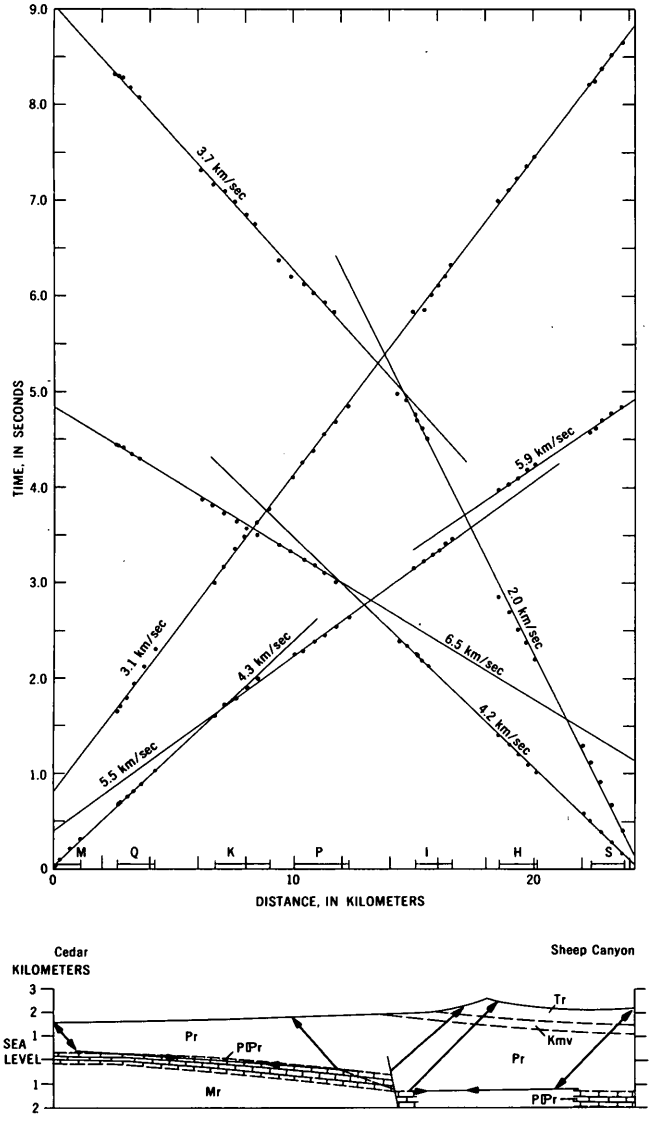

FIGURE 6.—Traveltime curves (above) of first and secondary arrivals, and interpretive cross section (below), along the Cedar–Sheep Canyon seismic-refraction profile, showing the geologically determined positions of rocks transected and the seismically determined ray path of least time. M, Q, K, P, I, H, and S are recording-location lines (see fig. 2). Rocks are: Tr, Tertiary; Kmv, Late Cretaceous (Mesaverde); Pr, Early Permian (Leonard) and younger; PPr, Early Permian (Wolfcamp and Pennsylvanian); Mr, Mississippian and older.

Spring Canyon to Cove profile

Apparent velocities of 4.15 km/sec and 6.0 km/sec are well defined by the first arrivals from the Spring Canyon shotpoint for the compressional waves through the near-surface sediments and from the Paleozoic refractor, respectively (fig. 5). Signals from the Cove shotpoint received beyond the crossover describe two parallel and displaced linear segments, indicating a possible fault. The stratigraphic separation, calculated from the difference between the intercept times of the two linear segments of the traveltime curve, is 0.8 km. Although no fault of this magnitude has been observed on the surface, well logs in the area indicate its position, attitude and displacement. There is no evidence of the fault from the Spring Canyon arrivals.

The relatively small difference between the reversed apparent velocities (6.0 and 5.8 km/sec) of the Paleozoic refractor suggests that the orientation of the profile nearly parallels the strike of the structure along the Paleozoic strata. This is borne out by available geologic information. These apparent velocities yield a true velocity of 5.9 km/sec.

The cross-section illustration in figure 5 indicates the trace of the average elevation of the ground surface and the Paleozoic refractor. The fault is included, showing the amount of throw. The cross section reveals that the true dip on the refracting horizon is gently toward the Cove shotpoint. However, the relative difference in elevation between the ground surface and refractor increases toward the Spring Canyon shotpoint, which explains the downdip relative apparent velocity depicted by the first-arrival plots in that direction. The depth to the refractor was calculated to be 1.4 km beneath the Cove shotpoint, and 2.5 km beneath the Spring Canyon shotpoint.

The depths to the refractor, as calculated from the traveltime curves, do not agree with the projected depths to the top of the carbonates of Early Permian age along this profile, as determined from available geologic information. The depths do agree in the first two profiles discussed, but in this profile the refractor is about 0.5 km stratigraphically higher (fig. 5). In drill logs a limestone layer about 100 feet thick was noted at the top of the Sinbad Limestone Member of the Moenkopi Formation of Early Triassic age, which is close enough in stratigraphic position to be the refractor horizon.

Cedar to Sheep Canyon profile

All units recorded good arrivals from the Cedar and Sheep Canyon shotpoints. This profile nearly parallels the true dip direction of the sediments, which is to the northeast into the Uinta basin. An average velocity of 4.25 km/sec was recorded on the first segment of the traveltime curves (fig. 6). Plots from the seismograms recorded from the Cedar shot beyond the crossover define a downdip velocity of 5.5 km/sec. The updip velocity observed from the opposite direction from the same layer is 6.5 km/sec. The resulting true velocity is calculated by standard formulas (Mota, 1954) to be 5.9 km/sec. This is consistent with the 6.0–km/sec true velocity determined for the same refractor from the Spring Canyon–Cove profile travel-

time curves, and the assumed true velocity of 6.0 km/sec calculated from the Pumping Station–Turtle Canyon profile data.

The dip of this layer is about 4° to the northeast. This dip agrees with the average plotted dip of corresponding beds from surface geology and well-log control in this area. The calculated depth at the Cedar shotpoint is 1.2 km; at Sheep Canyon it is 3.3 km.

The first arrivals from the Cedar shotpoint beyond the crossover necessitated two parallel and displaced lines similar to those from the Cove shotpoint, again suggesting a fault. The observed difference in intercept times was used to calculate the stratigraphic separation of the fault of 0.8 km, assuming that the refractor horizon is the same lithologic unit on either side of the fault. This value is the same as that determined on the Spring Canyon–Cove profile. This similarity in magnitude and direction of separation, together with the location of the separation on the profiles, indicates that this fault is the same one shown on the Spring Canyon–Cove profile. When extended to the southeast the trace of this fault passes near the Turtle Canyon shotpoint, where there is subsurface evidence of major faulting.

Secondary arrivals

A group of secondary arrivals of strong amplitude was observed on most of the seismograms beyond the crossover distance and was interpreted to be shear waves refracted from the Paleozoic carbonates (S, fig. 3). Correlation of these arrivals between records is predictably difficult because the shear phase is hard to consistently delineate from other body-wave phases, particularly from reflected phases. However, traveltimes of these arrivals can be fitted with apparent-velocity lines on two of the profiles (figs. 4 and 5). From the Sheep Canyon shot, a direct shear velocity of 2.0 km/sec is suggested. This phase could not be delineated on any of the other seismograms. Traveltimes of shear arrivals presumed to be refracted from the surface of the Paleozoic carbonates make up the second segment of the traveltime curve, which defines an apparent velocity of 3.7 km/sec. The same curve from the Cedar shot reveals an apparent velocity of 3.1 km/sec. The apparent velocities for the corresponding phase observed from the Cove and Spring Canyon shots were 3.4 and 3.5 km/sec, respectively.

The offset of the second segment of the traveltime curve representing the compressional wave from the Cove shotpoint that was attributed to faulting is also indicated by plots of the shear arrivals.

CONCLUSIONS

The velocities of the direct and refracted compressional waves were accurately determined from 2 of the 3 reversed refraction profiles. This more complete and accurate knowledge of velocities has aided in more precisely locating epicenters and foci of tremors originating in and near coal mines in the area (Dunrud and Osterwald, 1965; Osterwald and Dunrud, 1965).

The average velocity of the direct compressional wave is 4.3 km/sec. The velocities measured on all 3 profiles varied by only 0.2 km/sec, which is a remarkably consistent value considering that these velocities were measured through sections of rock composed predominantly of shale and siltstone as well as through sections composed of thick sandstone and interbedded siltstone and shale. The average refracted compressional-wave velocity is 6.0 km/sec and ranged from 5.9 km/sec to 6.0 km/sec. These refracted-wave velocities and range (0.10 km/sec) are in good agreement with published velocities for dolomite and limestone (Birch's "Handbook of physical constants" *in* Dobrin, 1960, p. 22). First arrivals from basement rocks were not seen in even the longest profile (30 km) because of the high-velocity carbonate rocks that are closer to the surface.

REFERENCES

Baars, D. L., 1962, Permian system of Colorado Plateau: Am. Assoc. Petroleum Geologists Bull., v. 46, no. 2, p. 149–218.

Dobrin, M. B., 1960, Introduction to geophysical prospecting: New York, McGraw-Hill, 446 p.

Dunrud, C. R., and Osterwald, F. W., 1965, Seismic study of coal mine bumps, Carbon and Emery Counties, Utah: New York, Am. Inst. Mining Metall. Engineers Trans., v. 232, p. 174–182.

Fisher, D. J., Erdmann, C. E., and Reeside, J. B., Jr., 1960, Cretaceous and Tertiary formations of the Book Cliffs, Carbon, Emery, and Grand Counties, Utah, and Garfield and Mesa Counties, Colorado: U.S. Geol. Survey Prof. Paper 332, 80 p.

Heiland, C. A., 1940, Geophysical exploration: New York, Prentice-Hall, 1,012 p.

Mota, Lindonor, 1954, Determination of dips and depths of geological layers by the seismic refraction method: Geophysics, v. 19, p. 242–254.

Osterwald, F. W., and Dunrud, C. R., 1965, Geology applied to the study of coal mine bumps at Sunnyside, Utah: New York, Am. Inst. Mining Metall. Engineers Trans., v. 232, p. 168–174.

U.S. Geological Survey and the American Association of Petrolenum Geologists, 1961, Tectonic map of the United States: 2 sheets, scale 1:2,500,000.

Warrick, D. E., Hoover, D. B., Jackson, W. H., Pakiser, L.C., and Roller, J. C., 1961, The specification and testing of a seismic-refraction system for crustal studies: Geophysics, v. 26, no. 6, p. 820–824.

UPHOLE SEISMIC MEASUREMENTS AS AN INDICATION OF STRESS RELIEF IN GRANITIC ROCK TUNNELS

By RODERICK D. CARROLL and JAMES H. SCOTT, Denver, Colo.

Work done in cooperation with the Defense Atomic Support Agency

Abstract.—Seismic velocities obtained in holes drilled into the walls of a tunnel in granitic rock show the presence of a low-velocity zone ranging in thickness from 0 to 8 feet. The low-velocity zone is attributed to the effects of movement of rock into the tunnel. The detection, thickness, and velocity of the zone appear related to the presence of fractures rather than to the size of the tunnel. The seismic velocities measured in this environment appear related to rock competence rather than to the thickness of the low-velocity layer. Research into the quantitative relationship of the velocity differences to actual stress distribution around a tunnel opening is required.

The anomaly of stress around a tunnel due to the disequilibrium of forces arising as a consequence of the opening has been described by numerous investigators. Obert and others (1960) utilized mathematical analyses to describe the state of stress around a tunnel opening. Studies using photoelastic methods have also been used for similar analyses (Frocht, 1941). Both of these methods, however, suffer from the limitation that simplifying assumptions must be made regarding the conditions of analyses. In mathematical analyses, homogeneous elastic media must be assumed, and Hooke's law is assumed to apply; and in photoelastic methods a homogenous material is used in the tests. The addition of inhomogeniety complicates the solution of the problem. These methods do, however, provide a basis for understanding of the problem of support requirements around underground openings.

Depending on the initial distribution of stress in a rock—a distribution related both to geologic environment and tectonic history—the rock will tend to rearrange itself in the vicinity of an opening in such a manner as to recreate equilibrium conditions. Consequently, a stress pattern is created around the tunnel opening. When the magnitude of these stresses becomes sufficiently large, support is required to prevent rock from moving destructively into the tunnel. Consequently the in situ determination of the zone of stress anomaly is of importance in support design, and any measurements which aid in defining its geometry can be of considerable value in tunnel engineering.

One means of observing the variation in stress around a tunnel is to measure the variation of seismic velocity in the rock in the immediate vicinity of the tunnel. Although such measurements must be made after the excavation has been made, the measurements are desirable for two reasons: (1) they contribute to basic data on rock behavior in general, and (2) they may enable support requirements to be predicted, on the basis of the geology over the major portion of a tunnel, from selected measurements obtained during the initial stages of construction.

The velocity-stress dependence of rocks is an observed phenomenon (Wyllie and others, 1958). The tendency of seismic velocities in rock to increase under increasing compressive stress and to decrease under tensile forces due to the changes in transmission characteristics across grain contacts and microfractures suggests an indirect method of measuring stress. Because of the movement of rocks into a tunnel, tensile forces may be expected to produce a low-velocity zone around the tunnel opening. We choose to define this zone as the zone of stress relief. It is realized that this layer possibly includes some effects due to blast damage. It is felt, however, that the magnitude of the velocity layering obtained at many of our stations is not compatible with blast damage.

Some indirect evidence that the low-velocity zone is not a function of blasting was recently obtained by Scott.

Seismic methods indicated a 16-foot-thick low-velocity zone in a section of tunnel in the Straight Creek pilot bore in Colorado. This section—a granite shear zone—yielded by plastic deformation; the floor moved up by more than 1 foot, necessitating additional support in the section. Because movement was by squeezing, the affect of blasting may be considered nil in opening fractures. Consequently, the low-velocity zone was not a function of blasting in this instance but probably of stress relief. Although this evidence does not eliminate the possibility of a low-velocity layer caused by blasting it does suggest that blasting alone cannot account for the low-velocity layer in all places. We prefer to consider the low-velocity zone noted in our present study as being, in most instances, due to stress relief, but we do not exclude the possibility that blast damage caused some of our shallower anomalies.

Other things being equal (for example, rock composition, degree of weathering, and fracturing), the ability to discriminate velocity changes arising from changes in stress in a rock is strongly dependent on porosity. In general, the incremental velocity change for a rock with high pore porosity is greater for a given incremental stress change than is that for the same rock type with lower porosity. On the other hand, at low pore porosities a great many rock types exhibit little velocity change with increasing compressive stress until failure. In such cases, however, the presence of secondary porosity (fracturing) can greatly decrease velocity. The present investigation deals with rocks of this type.

LOCALE AND METHOD OF MEASUREMENT

The seismic-velocity measurements were made in tunnels located in the Climax stock at the U.S. Atomic Energy Commission Nevada Test Site, Mercury, Nev. The tunnel complex was constructed at a depth of 1,500 feet in quartz monzonite and granodiorite. Primary porosity in these rocks is extremely low, commonly less than 2 percent, and consequently stations for measurement were selected in order to sample both rock types on the basis of the wide range of fracture conditions which existed. The locations ranged from sections in both rock types wherein several tens of feet of unfractured rock were available, to extensively sheared rock sections of similar extent. At the selected stations, 3-inch-diameter holes were drilled normal to the main axis of the tunnel to depths of 20 to 30 feet. In most places holes were drilled in both ribs, the back, and the floor. At 9 stations a total of 36 holes were sampled by measuring uphole traveltimes. Measurements were obtained by detonating a dynamite cap at the hole collar and observing the arrival time at 3 accelerometers located in the hole on 2-foot centers out from the collar. The accelerometers were positioned deeper in the hole on successive shots until a time-distance plot of seismic arrivals was obtained throughout the length of the hole. Details of the instrumentation and of the uphole positioning apparatus have been published elsewhere (Carroll and others, 1966).

The tunnel complex in the Climax stock, in general, was unsupported at the time of measurement, with the exception of a few sections where rock bolts were required.

RESULTS OF MEASUREMENTS

The results of measurements made in a section of moderately to severely fractured quartz monzonite are shown in figure 1. This station, located where two drifts converge, permitted a check on the usefulness of the velocity method to investigate the zone of stress relief. It allowed a two-way check on measurements by penetrating both drifts with a single hole, thus affording the opportunity to record from both ends of the hole. As shown in figure 1, the velocity contrast between rock near the tunnel and that farther away is marked. There is a tendency for the low-velocity zone to increase in thickness as one approaches the intersection of the shop and supply drifts. This seems reasonable in that there is more open tunnel to be supported by the adjacent rock as one moves toward the intersection. Consequently, the measurable zone of stress relief might be expected to increase in thickness.

In other sections of the tunnel however, the thickness of the low-velocity layer was not a noticeable function of the tunnel dimensions. This was true even at stations where the tunnel diameters were 3 to 4 times that of the shop and supply drifts. A summary of the measurements and pertinent data is shown in table 1.

The results of measurements made in holes in the periphery of the tunnel, at the northernmost station in the shop drift (fig. 1), are shown in figure 2. The low-velocity zone indicates that stress relief is sufficient on all sides of the tunnel to yield a noticeable velocity contrast. The two-way observation of the low-velocity zones between the shop and supply drifts is noteworthy.

In contrast to the results obtained in the fractured quartz monzonite section shown in figures 1 and 2, figure 3 shows the results of measurements made in a relatively fracture-free section of quartz monzonite in the main access drift of the complex. Here a low-velocity zone was not detected. In general, similar results were obtained at other locations in the tunnel (table 1), that is, the more pronounced the fractures

224-352 O—66——10

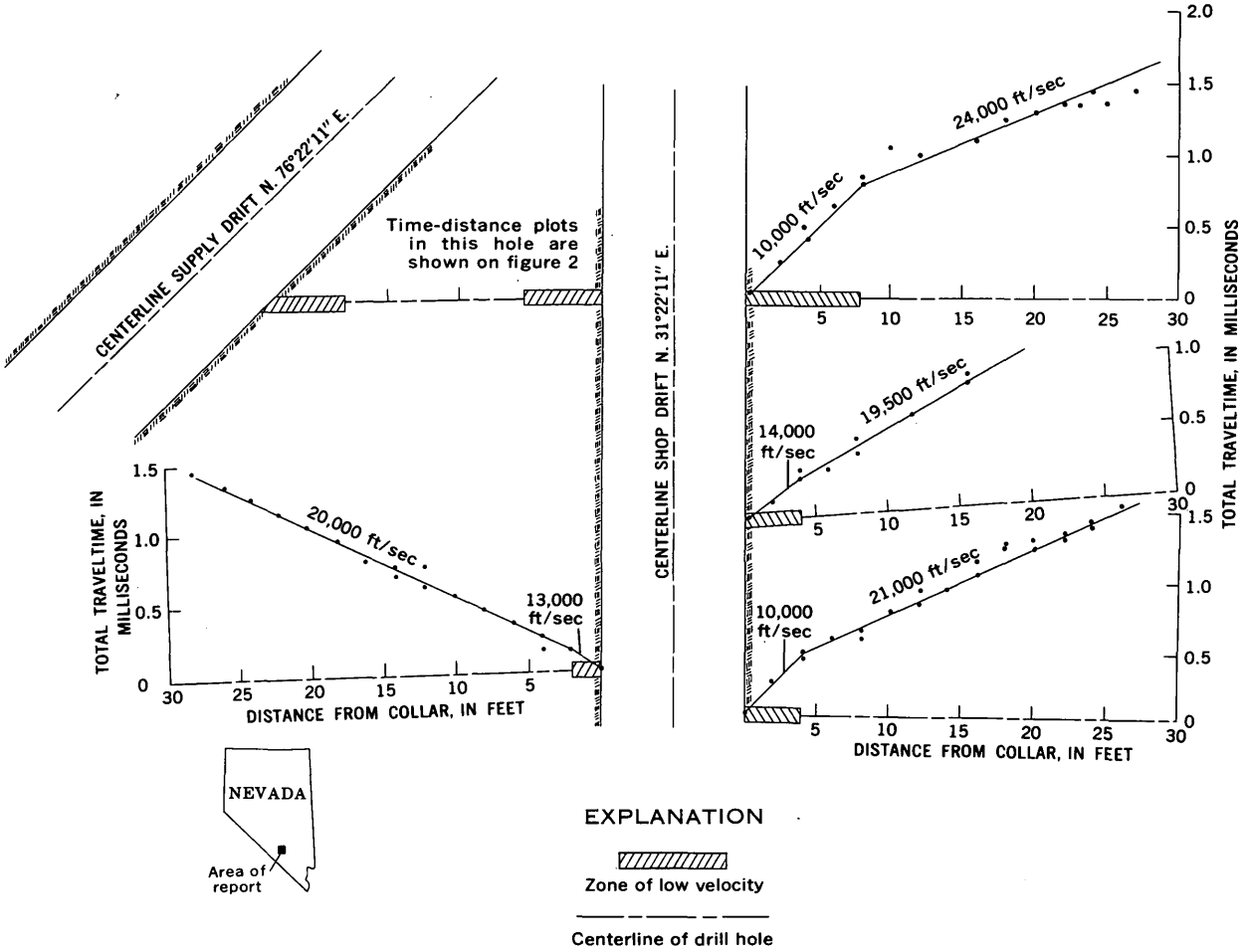

FIGURE 1.—Plan view of horizontal holes in shop and supply drifts within the Climax stock, Nevada, showing results of uphole velocity measurements in fractured quartz monzonite.

the greater likelihood of appearance of the low-velocity layer in the drill holes. Consequently, the presence or absence of a low-velocity zone around the tunnels of the Climax stock, or similar rock, may be expected to be strongly dependent on the fracture patterns in the rock.

SUMMARY AND CONCLUSIONS

Seismic velocities in the low-velocity zone ranged from 5,000 to 14,000 feet per second in tunnels in the Climax stock. No discrimination between granodiorite and quartz monzonite was evident on the basis of velocity. Velocities qualitatively exhibited an inverse relation to the degree of fracturing. Apparent velocities in rock behind the low-velocity zone and in sections where no layer was recorded ranged from 14,000 to 25,000 feet per second, with the higher velocities generally restricted to those sections where a low-velocity layer was recorded. This suggests that the rock behind the low-velocity layer may be under greater compressive stress than is the rock where no layer is present.

The thickness of the low-velocity zone ranged from 0 to 8 feet, and aside from its general association with fracturing, no relationship was found relating it to the size of the tunnel.

The low-velocity layer, where measured, exhibited asymmetry at many locations in that it was not recorded in all holes at a specific location. The layer was absent in no preferential direction—at various stations the layer was absent in either the back, floor, or ribs, while generally it was present in the other directions. The results of reconnaissance mapping showed no obvious correlation of the presence or absence of the low-velocity layer with the trend of any of the three major joint systems present in the tunnel complex. However, extensive studies along these lines were not pursued.

In one highly sheared section which required extensive support (crossdrift AR, section 2) the thickness

TABLE 1.—*Summary of uphole-velocity measurement data*

Station	Location	Rock type	Rock support at time of measurement	Tunnel diameter (feet)	Degree of fracturing	Thickness of destressed zone interpreted from uphole seismic data (feet) [1]	Uphole velocity (ft/sec) in—	
							Low-velocity layer	High-velocity layer
Shop drift	West rib	Quartz monzonite.	None	10	Moderately fractured.	6.0	11,000	19,000
	do	do	do	10	do	2.0	13,000	20,000
	East rib	do	do	10	do	8.0	10,000	24,000
	do	do	do	10	do	4.0	14,000	19,500
	do	do	do	10	do	4.0	10,000	21,000
	Back	do	do	10	do	6.0	14,000	18,500
	Floor	do	do	10	do	6.0	13,500	21,000
Supply drift	East rib	Quartz monzonite.	None	10	Moderately fractured.	5.5	13,000	21,500
Main access drift, 4+25.	West rib	Quartz monzonite.	None	10	Extensively fractured.	5.0	11,000	18,000
	East rib	do	do	10	do	4.0	11,500	25,000
	Back	do	do	10	do	5.5	10,000	19,000
	Floor	do	do	10	do	4.0	11,000	24,000
Main access drift, 7+30.	East rib	Quartz monzonite.	None	10	Relatively free of fractures.	No destressed zone.	----	18,500
	West rib	do	do	10	do	do	----	18,000
	Back	do	do	10	do	do	----	19,000
Main access drift, 9+20.	East rib	Contact between quartz monzonite and granodiorite.	None	10	Extensively fractured.	6.0	6,500	22,000
	West rib	do	do	10	do	6.0	11,500	20,000
	do	do	do	10	do	2.5	10,000	20,000
	Back	do	do	10	do	No destressed zone.	----	18,000
	Floor	do	do	10	do	4.0	11,500	21,000
Main access drift, 11+60.	East rib	Granodiorite	None	10	Extensively fractured.	4.5	12,000	19,000
	West rib	do	do	10	do	4.0	13,500	19,000
	Back	do	do	10	do	5.0	12,000	21,000
	Floor	do	do	10	do	No destressed zone.	----	19,000
Main access drift, 12+60.	East rib	Granodiorite	None	10	Relatively free of fractures.	No destressed zone.	----	17,000
	West rib	do	do	10	do	do	----	18,500
	Back	do	do	10	do	do	----	18,000
Crossdrift AL, test section 6.	North rib	Granodiorite	None	27	Moderately fractured.	No destressed zone.	----	17,000
	South rib	do	do	27	do	8.0	11,500	23,500
	Back	do	Rock bolts	27	do	4.0	11,000	23,000
Crossdrift AR, test section 2.	North rib	Quartz monzonite.	Rock bolts and wire net.	27	Extensively fractured.	6.0	5,000	14,000
	South rib	do	do	27	do	No destressed zone.	----	16,000
	Back	do	Rock bolts	27	do	4.0	12,000	18,500
Crossdrift AR, test section 1.	North rib	Quartz monzonite.	None	44	Moderately fractured.	No destressed zone.	----	19,000
	South rib	do	do	44	do	4.0	10,300	17,500
	Back	do	do	44	do	No destressed zone.	----	18,000
Range of values	----	----	----	----	----	0.0 to 8.0	5,000 to 14,000	14,000 to 25,000
Average values	----	----	----	----	----	3.3	11,200	19,600

[1] Where more than one velocity value is listed, more than one hole was tested.

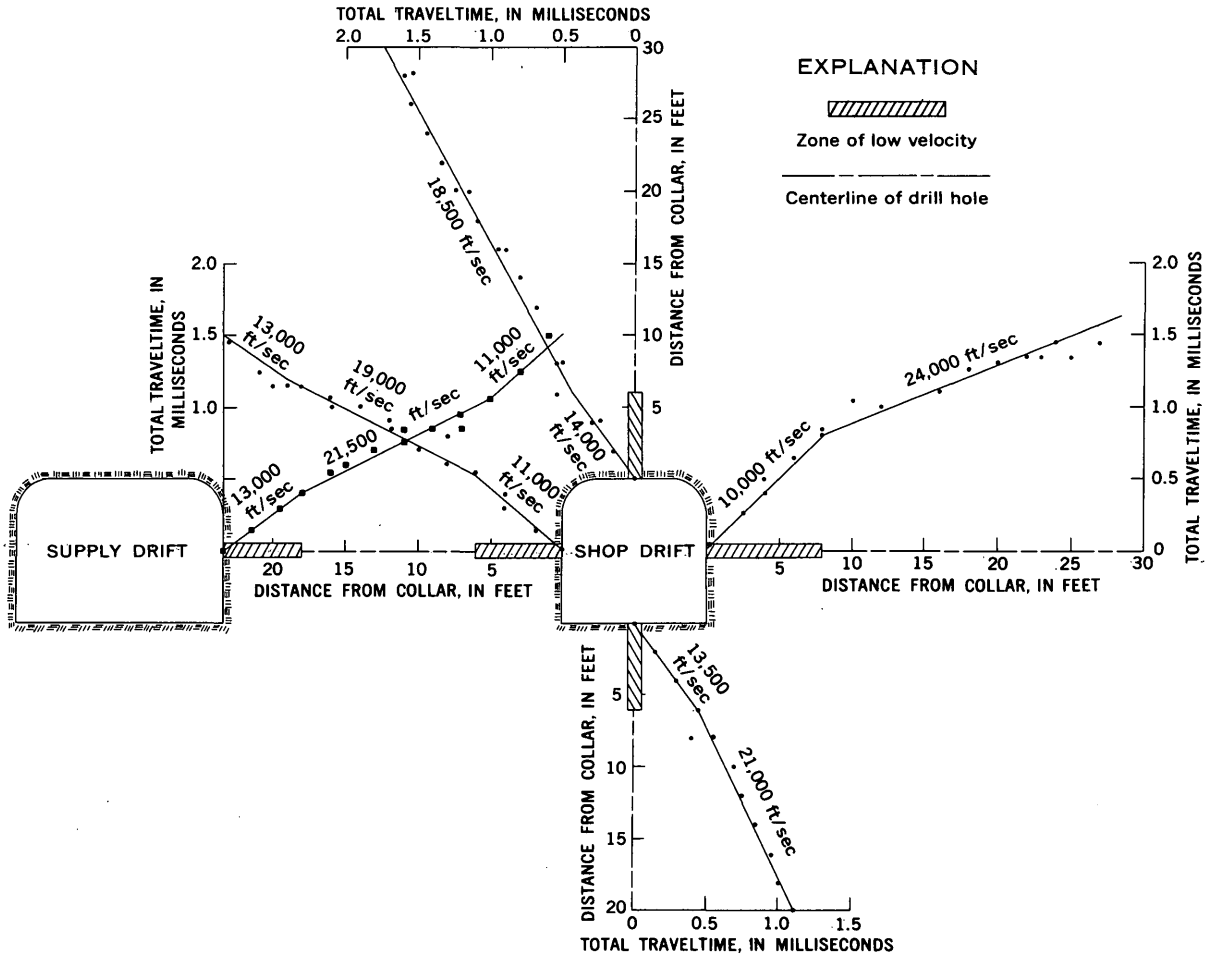

FIGURE 2.—Cross-sectional view of selected holes in shop and supply drifts, showing results of uphole velocity measurements in fractured quartz monzonite.

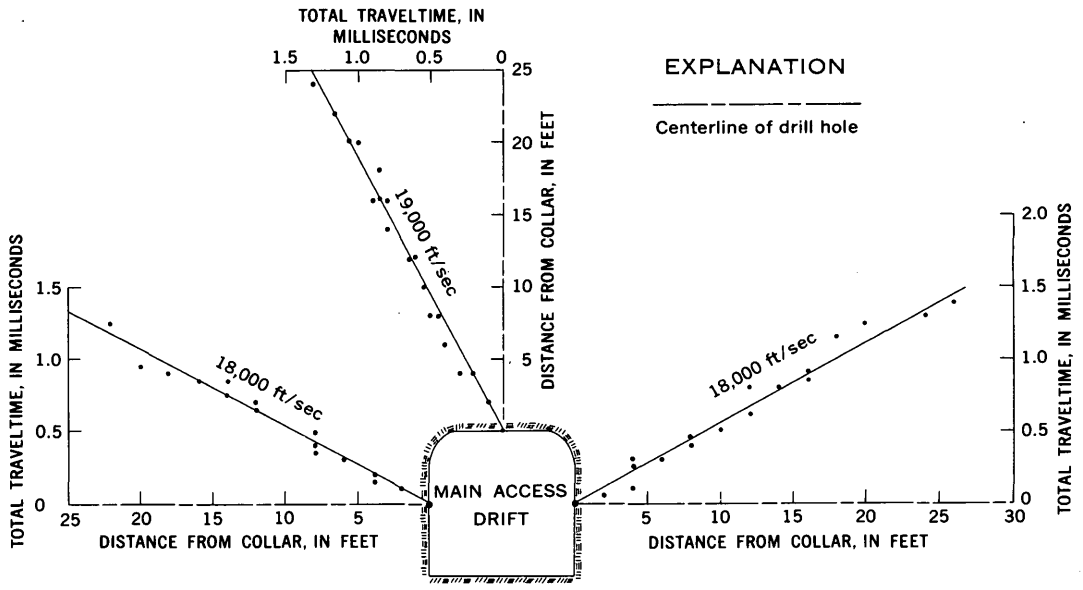

FIGURE 3.—Cross-sectional view in main access drift, station 7+30, showing results of uphole velocity measurements in relatively fracture free quartz monzonite. No low-velocity layer was detected at this station.

of the low-velocity zone was not significantly different from that at other stations, although the velocity was the lowest found throughout the tunnel. The presence of low seismic velocity was found to be more diagnostic of structurally weak sections than was the thickness of the low-velocity layer.

The presence of a low-velocity zone is considered significant because it may provide an estimate of the thickness of rock which may require support in tunnels. Additional research is required to determine the relationship between the low-velocity zone and the actual stress pattern around a tunnel opening. A comparison with uphole dynamic strain measurements which, hopefully, would indicate the extent of arching with time is considered desirable.

REFERENCES

Carroll, R. D., Scott, J. H., and Cunningham, D. R., 1966, Elastic moduli of granitic rock from in situ measurements of seismic velocity *in* Geological Survey Research 1966: U.S. Geol. Survey Prof. Paper 550–C, p. C25–C28.

Frocht, M. M., 1941, Photoelasticity: New York, John Wiley and Sons, 411 p.

Obert, Leonard, Duvall, W. I., and Merrill, R. H., 1960, Design of underground openings in competent rock: U.S. Bur. Mines Bull. 587.

Wyllie, M. J. R., Gregory, A. R., and Gardner, G. H. F., 1958, An experimental investigation of factors affecting elastic wave velocities in porous media: Geophysics, v. 23, no. 3.

FORMATION OF PHYLLONITES IN THE GRANDFATHER MOUNTAIN AREA, NORTHWESTERN NORTH CAROLINA

By BRUCE BRYANT, Denver, Colo.

Abstract.—Field relations, petrographic data, and limited chemical data show that phyllonites derived by Paleozoic low-grade metamorphism of Precambrian granitic rocks and gneisses formed in chemical systems generally open to K, Na, Ca, and H and locally open to a number of other components. Hydrolysis of feldspars was the principal reaction affecting the alkali content of the phyllonites. Changes in chemical and mineral composition of the rock in the phyllonite zones were probably controlled through a combination of intense shearing and type and availability of solution.

In the Grandfather Mountain area of northwestern North Carolina, plutonic rocks were metamorphosed during the Paleozoic to a wide variety of cataclastic rocks of low metamorphic grade. These rocks are exposed in the Grandfather Mountain window and in the structurally lower part of the tectonically overlying Blue Ridge thrust sheet (Bryant, 1962, 1963; Bryant and Reed, 1962; Reed, 1964a, 1964b).

The principal units of plutonic rocks in the Grandfather Mountain window are the Wilson Creek Gneiss and the Blowing Rock Gneiss. The Wilson Creek Gneiss is chiefly a nonlayered plutonic rock ranging from diorite to granite in composition; quartz monzonite and granodiorite are the most common varieties. Small areas in the eastern part of the window are layered gneiss. The Blowing Rock Gneiss is a rather uniform, nonlayered coarse-grained quartz monzonite gneiss to granodiorite augen gneiss. Both units contain scattered dikes, pods, and irregular bodies of pegmatite.

In the lower part of the Blue Ridge thrust sheet adjacent to the Grandfather Mountain window and between it and the Mountain City window, the Cranberry Gneiss is the main unit of plutonic rock. The Cranberry is a layered and nonlayered predominantly granitic gneiss containing many layers and lenses of amphibolite and schist and some lenses, stringers, pods, and, rarely, dikes of pegmatite. The granitic portions range in composition from diorite to granite, but rocks of granodioritic and quartz monzonitic composition dominate.

During Paleozoic time these plutonic rocks were all converted into cataclastic rocks ranging from recrystallized mortar gneiss to blastomylonite and phyllonite. Blastomylonitic and phyllonitic gneiss predominate.[1] The variations in the degree of shearing and recrystallization of the rocks allow interpretation of the more metamorphosed varieties. In least sheared rocks, quartz is strained and plagioclase partly saussuritized (fig. 1*A*). In slightly sheared rocks, rims of recrystallized mortar composed of quartz and feldspar occur between the quartz and feldspar grains of the granitic rock. Feldspar, biotite, and, especially, quartz are strained. Most plagioclase is saussuritized. All gradations occur in typical blastomylonitic gneiss in which much of the original quartz and feldspar have been granulated and recrystallized into a fine-grained mosaic-textured groundmass set with porphyroclasts of microcline, quartz, altered plagioclase, and, less commonly, biotite and amphibole(figs 1*B* and *C*). Microcline porphyroclasts are generally bent and fractured, and the fractures are healed by recrystallized groundmass minerals; otherwise the large microcline grains remaining are unaltered. Plagioclase is saussuritized and granulated to various degrees (fig. 1*C*). Albite and epidote produced by destruction of more calcic plagioclase are recrystallized in the groundmass. Biotite generally is granulated and recrystallized as groundmass biotite, but a few porphyroclasts rimmed by new biotite may remain. Hornblende is partly or

[1] Blastomylonitic gneiss is used here for a plutonic rock in which 10 to 90 percent of the rock has been granulated and recrystallized. It consists of numerous mineral grains derived from the original rock in a matrix of blastomylonite.

Phyllonitic gneiss is used here for a plutonic rock in which 10 to 90 percent of the rock has been granulated and recrystallized with conversion of feldspar to mica so that the rock consists of numerous mineral grains of the original rock in a matrix of phyllonite.

U.S. GEOL. SURVEY PROF. PAPER 550-D, PAGES D144-D150

completely altered to actinolite but tends to remain as porphyroclasts.

In some of the more phyllonitic gneiss the plagioclase is altered to sericite and epidote. The sericite and, where retained in the rock, the epidote are distributed in the groundmass, although in a few less sheared rocks the sericite forms aggregates pseudomorphous after the plagioclase grains (fig. 1*D*). Microcline, also, may be partly altered to sericite, although plagioclase is usually the first feldspar to disappear. Quartz forms a larger proportion of the porphyroclasts than in the blastomylonitic gneiss because the sericitic matrix of the phyllonitic gneiss apparently takes up much of the stress that would be transmitted to the quartz if the feldspars were granulated but not altered.

Zones in the blastomylonitic and phyllonitic gneisses were converted to phyllonite, which is a fine-grained lustrous micaceous rock resembling phyllite but derived through shearing and, in this case, retrogressive metamorphism of a previously coarser grained plutonic rock.

The phyllonites occur in discrete zones a few inches to 20 feet thick that are generally parallel to cataclastic foliation. Locally the phyllonite zones mark mappable faults, as in the Cranberry Gneiss between the Grandfather Mountain and Mountain City windows (Bryant, 1962), but phyllonite also occurs in diffuse discontinuous zones thousands of feet wide that are difficult to map as separate units. Large diffuse zones are best developed in Wilson Creek Gneiss in the central part of the Grandfather Mountain window (Reed, 1964a; Bryant, 1962). All gradations between these types of occurrences can be found.

The phyllonite zones generally grade to blastomylonitic or phyllonitic gneiss at their margins; the proportion of porphyroclasts of minerals of the plutonic generation and of quartz and feldspar in the matrix increase, and the amount of mica in the matrix decreases. Some of the narrower phyllonite zones have sharp contacts. The wider zones commonly contain lenses of pegmatite and less sheared gneiss that have tectonic contacts with the more metamorphosed phyllonite. The pegmatites are coarse grained, mica poor, and rich in potassium feldspar and are therefore resistant to cataclasis.

The phyllonites may be silvery gray, gray, dark gray, light green, green, or blue gray, depending on the proportions of muscovite, biotite, chlorite, and opaque minerals they contain. Lenticular quartz segregations are common. Northwest-trending cataclastic *a* lineation formed by streaked-out micas or porphyroclasts of quartz and feldspar is conspicuous in the phyllonites and is characteristic of most of the cataclastically metamorphosed rocks in the area. Locally the phyllonites display crinkles 1 mm to 2 cm in amplitude with axes perpendicular to the mineral lineation.

In places the phyllonites contain disseminated magnetite, hematite, ilmenite, pyrite, or graphite. Rarely they contain torbernite or sphalerite. Because of these concentrations some phyllonite zones have been prospected for iron, uranium, graphite, and titanium.

A detailed chemical and mineralogical study of the formation of phyllonites from granitic rock was not possible during the study of the Grandfather Mountain area because of deep weathering of the rocks. Some fresh outcrops of phyllonite were found, but nowhere was a complete transition from blastomylonitic granitic gneiss to phyllonite found in an entirely fresh outcrop. The strongly developed foliation of the phyllonite generally allows partial weathering along the foliation planes so that most samples are not suitable for chemical analysis. However, field observations, modal data, and a limited amount of chemical data allow a qualitative estimate of chemical changes during the formation of phyllonites.

The phyllonites exhibit a wide span of modal compositions because of their gradational relations with phyllonitic and blastomylonitic gneiss and their derivation from rocks ranging from granite to diorite. Rocks classified as phyllonite in the Wilson Creek Gneiss contain 30 to 80 percent sericite, 4 to 60 percent quartz, 0 to 30 percent biotite, 0 to 30 percent chlorite, and 0 to 25 percent epidote. A typical phyllonite contains 60 percent sericite and 30 percent quartz; opaque minerals, biotite, chlorite, epidote, and sphene comprise the remaining 10 percent. The content of calcium-bearing minerals in many phyllonites is less than would be obtained by isochemical metamorphism of quartz monzonite or granodiorite and is less than that of adjacent blastomylonitic gneiss derived from those rock types. Of 34 phyllonites derived from the Wilson Creek Gneiss, 21 lack calcium-bearing minerals detectable in thin section. If all the calcium were in clinozoisite, a phyllonite derived from a typical quartz monzonite should have over 5 percent of that mineral and one derived from a granodiorite close to 10 percent. Some phyllonites are composed mostly of sericite and quartz. In places the green color and high index of refraction of the fine-grained mica indicates that it is rich in ferric iron and similar to mica described by Foster and others (1960) from overlying upper Precambrian rocks. Paragonite was not detected in X-ray bulk-rock studies by E. J. Young, of the U.S. Geological Survey, of several phyllonites rich in white mica. The analyzed rocks were judged on the basis of field

relations to have been derived from rocks rich in plagioclase and poor in potassium feldspar. The abundance of sericite and the lack of significant quantities of albite and paragonite in the phyllonites show that they are enriched in K and H and impoverished in Na as compared with the typical granodioritic or quartz monzonitic parent rocks. Their mineralogy commonly also indicates impoverishment in Ca, Fe, or Mg and enrichment in Si or Fe.

Table 1 gives chemical analyses of the Blowing Rock Gneiss and phyllonite derived from it. The Blowing Rock Gneiss has been metamorphosed at low grade, and its composition may be somewhat modified compared to the original plutonic rock from which it formed. The gneiss in table 1, column 1, contains porphyroclasts of saussuritized plagioclase (fig. 1*C*), whereas in the gneiss of column 2 the alteration products of the plagioclase, such as epidote, albite, and sericite have been more thoroughly distributed in the matrix.

The analyzed phyllonites from the Blowing Rock Gneiss (table 1, columns 3 and 4, and figs. 1*D* and *E*) contain porphyroclasts of minerals from the parent rock and therefore do not represent end products of phyllonitization. The phyllonite of column 3, which is from the same outcrop as the gneiss of column 2, has numerous porphyroclasts of potassium feldspar and a few porphyroclasts of saussuritized plagioclase, which are unusual in phyllonites of the Grandfather Mountain area.

TABLE 1.—*Chemical analyses, in weight percent, of Blowing Rock Gneiss and phyllonite derived from it* [1]

	Gneiss		Phyllonite	
	1 [2]	2	3	4
Field No.	GMB-3	GMB4	P1	P3
Laboratory No.	161252	H3264	161253	161254
SiO_2	61.2	63.30	73.6	63.1
Al_2O_3	14.2	14.87	11.6	16.8
Fe_2O_3	1.8	1.15	1.1	2.2
FeO	4.6	3.74	2.1	3.1
MgO	1.6	1.27	.79	1.1
CaO	4.7	3.14	1.7	1.8
Na_2O	3.4	2.18	1.0	.19
K_2O	3.1	4.70	4.0	6.5
H_2O^-	.05	.04	.04	.06
H_2O^+	1.2	1.20	1.4	2.2
TiO_2	1.6	1.12	.72	1.6
P_2O_5	.80	.40	.26	.74
MnO	.14	.09	.04	.04
CO_2	.82	1.09	.94	<.05
F	.22	.20	------	------
Cl	.01	.01	------	------
BaO	------	.16	------	------
S	.03	.06	------	------
Total	99	99.61	99	99

[1] Analysis 2 is standard rock analysis by C. L. Parker. Other analyses by rapid colorimetric methods by Paul Elmore, Samuel Botts, Gillison Chloe, Lowell Artis, and H. Smith.

[2] S determined by induction-furnace method by I. C. Frost. F and Cl determined by V. C. Smith.

1. Gray and white cataclastic nonlayered augen gneiss containing white porphyroclasts of potassium feldspar as much as 3 cm long speckled with inclusions in a green-gray matrix of fine-grained mica. Porphyroclasts of microcline and perthitic microcline broken and healed by recrystallized quartz and calcite, somewhat bent brown biotite as much as 1 mm long, and saussuritized plagioclase as much as 3 mm in diameter in a matrix of quartz, green biotite, sericite, subordinate FeMg chlorite from biotite, epidote, and accessory ilmenite, sphene, apatite, pyrite, allanite, stilpnomelane, and zircon. From road-metal quarry along U.S. Highway 321 just north of the south contact of Blowing Rock Gneiss, Blowing Rock quadrangle.
2. Dark-gray and white cataclastic nonlayered augen gneiss containing white porphyroclasts of potassium feldspar as much as 2 cm long in a green-gray matrix of fine-grained mica. Porphyroclasts of microcline and perthitic microcline as much as 2 cm long filled with inclusions of quartz and plagioclase, and of quartz as much as 1 cm in diameter in a matrix of recrystallized albite, sericite, quartz, and green biotite with accessory sphene, calcite, allanite, zircon, and epidote. From roadcut on U.S. Highway 321 through meander of the South Fork of New River 1.75 miles N. 50° E. of junction between U.S. Highways 321 and 221 in the village of Blowing Rock, Blowing Rock quadrangle.
3. Porphyroclastic phyllonite from Blowing Rock Gneiss. Gray sericitic rock containing numerous quartz and feldspar porphyroclasts as much as 5 mm in diameter. Porphyroclasts of quartz as much as 7 mm, perthitic microcline 5 mm, and plagioclase 2 mm in diameter in a matrix of recrystallized sericite and quartz containing accessory calcite, pyrite, sphene, zircon, and apatite.
4. Phyllonite from Blowing Rock Gneiss. Dark-gray phyllitic rock containing a few quartz porphyroclasts. Quartz porphyroclasts as much as 2 mm in diameter in a groundmass of recrystallized sericite, Fe-Mg chlorite, quartz, and accessory sphene, ilmenite, pyrite, apatite, allanite, and zircon. From roadcut on U.S. Highway 321, 100 yards north of junction with road to Aho, Blowing Rock quadrangle.

FIGURE 1.—Photomicrographs of blastomylonitic gneiss and least sheared granitic rock.

A. Slightly deformed and altered biotite granodiorite. Biotite (b), microcline (m), strained quartz (q), and variously saussuritized plagioclase (p). Least altered plagioclase An_{20-25}.

B. Blastomylonitic augen gneiss, analyzed specimen, table 1, column 2. Large porphyroclasts of microcline (m) and quartz (q), in part granulated and recrystallized to a mosaic-textured aggregate (mq), a few small ones of saussuritized plagioclase (p) in a matrix of recrystallized quartz, sericite, biotite, albite, and epidote.

C. Blastomylonitic augen gneiss, analyzed specimen, table ,1 column 1. Large saussuritized and partly fragmented plagioclase porphyroclast (p). A quartz grain (q) mostly converted to a mosaic-textured aggregate of smaller quartz grains (mq). Matrix of recrystallized biotite, epidote, quartz, and albite.

D. Phyllonite derived from Blowing Rock Gneiss, analyzed specimen, table 1, column 4. Strained and partly granulated and recrystallized quartz porphyroclasts (q) in a groundmass of recrystallized sericite, chlorite, and quartz. Sericite-rich lenses (s) probably represent former large microcline grains.

E. Porphyroclastic phyllonite from Blowing Rock Gneiss, analyzed specimen table 1, column 3. Porphyroclasts of quartz (q), perthitic microcline (m), and plagioclase (p) in a matrix of recrystallized sericite and quartz.

F. Phyllonite (table 4). Strained and broken porphyroclasts of quartz (q) in a matrix of sericite, quartz, and chlorite.

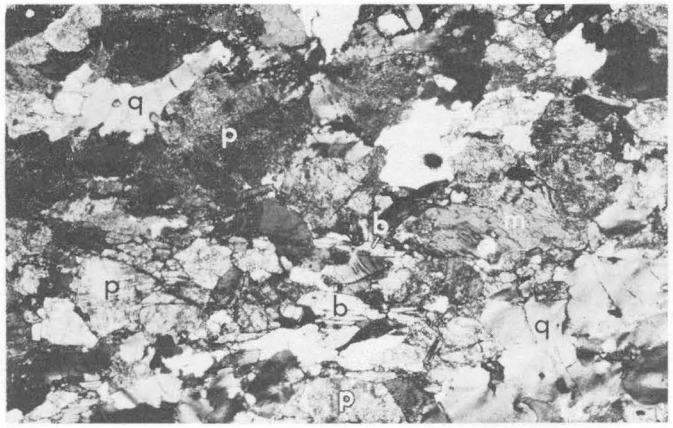

A

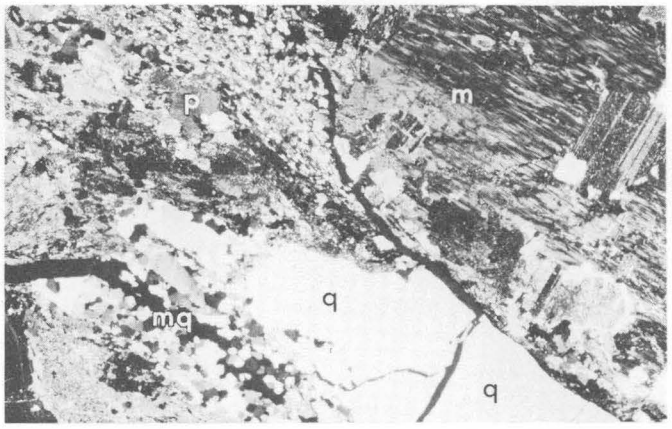

B

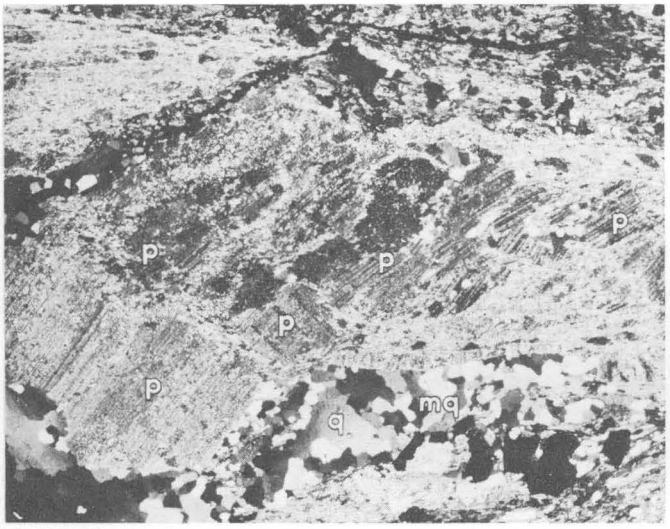

C

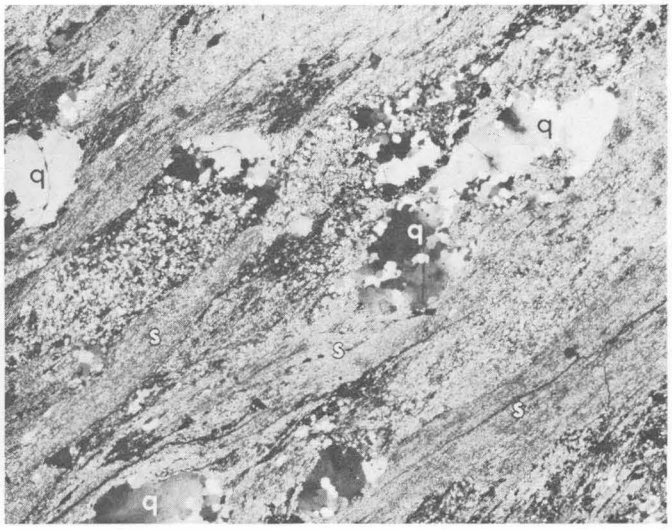

D

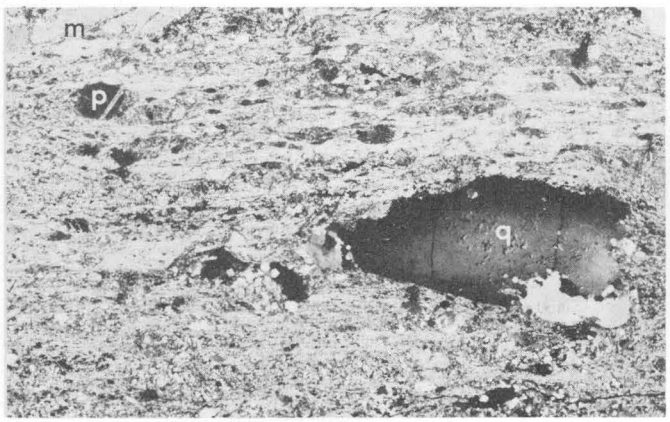

E

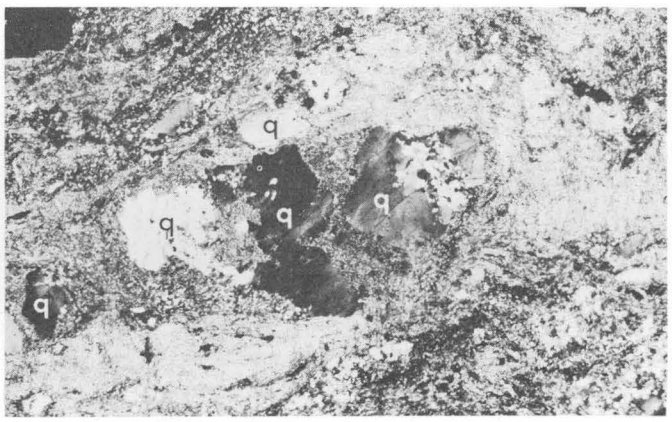

F

0 2 mm

Table 2 shows the weight percent of selected elements in the analyzed samples of Blowing Rock Gneiss and phyllonite. Table 3 compares the compositions of the phyllonites with the compositions of the parent rocks, first on the assumption that the amount of Si has remained constant, and second on the assumption that Al has remained constant. One analyzed phyllonite (sample 3) is compared with gneiss from the same outcrop (sample 2). The other phyllonite (sample 4) is compared with the average of the two analyses of gneiss.

These limited chemical data and the mineralogical data show that the phyllonitization of granitic rocks involves changes in alkali content and H content and may involve subtraction or addition of a number of elements. A precise determination of losses and gains does not seem justified because it is doubtful that these changes took place at constant volume. However, changes relative to constant Al and Si (table 3) show that Na, Ca, Fe and Mg are lost regardless of whether Al or Si is assumed constant. In the transformation of the gneiss (sample 2) to phyllonite (sample 3) the assumption of constant Al seems most reasonable because K and H must be gained to form mica, and it is the greater content of mica that distinguishes the phyllonite from the Blowing Rock Gneiss. In comparing sample 4 with the average of samples 1 and 2, neither assumption appears more favorable. The compositional changes are apparently similar to those involved in hydrothermal alteration, but probably took place at higher pressure and shear stress than prevails during hydrothermal alteration adjacent to a fissure.

TABLE 2.—*Selected elements, in weight percent, in Blowing Rock Gneiss and phyllonite derived from it*

Sample (table 1)	Si	Al	Ca	Na	K	Fe	Mg	H	Ti
1	28.8	7.5	3.4	2.5	2.6	4.9	1.0	0.138	0.96
2	29.8	7.9	2.3	1.6	3.9	3.7	.8	.137	.675
3	34.6	6.1	1.2	.7	3.3	2.4	.5	.160	.43
4	28.6	8.9	1.3	1.5	5.4	3.9	.7	.250	.96

TABLE 3.—*Gains and losses, in weight percent, of selected elements in phyllonite derived from Blowing Rock Gneiss, assuming constant* Si *and* Al

[+, gain; −, loss. Chemical analyses given in table 2]

	Si	Al	Ca	Na	K	Fe	Mg	H	Ti
Gneiss (sample 2) compared with phyllonite (sample 3)									
Si constant	Constant	−2.7	−1.3	−1.0	−1.1	−1.6	−0.4	Constant	−0.305
Al constant	+14.8	Constant	−.8	−.7	+.4	−.6	−.2	+0.069	−.115
Average of gneiss (samples 1 and 2) compared with phyllonite (sample 4)									
Si constant	Constant	+1.4	−1.4	−1.85	+2.2	−0.3	−0.2	+0.113	+0.15
Al constant	−4.5	Constant	−1.6	−1.87	+1.4	−.9	−.3	+.073	Constant

TABLE 4.—*Qualitative changes, in weight percent, of selected elements in Cranberry Gneiss during phyllonitization*

Rock	Ca	Na	K	Fe	Mg
Quartz diorite [1]	2.0–3.9	2.3–3.7	1.0–1.4	1.7–4.8	0.5–1.5
Calculated composition of quartz diorite from which phyllonitic gneiss was derived [2]	1.4	2.7	1.2	2.9	1.3
Phyllonitic biotite quartz diorite gneiss [3 4]	.15	.15	3	7	1
Granodiorite and quartz monzonite [1]	1.1–3.4	2.2–3.0	2.2–3.8	1.7–4.4	.4–1.5
Chlorite-quartz-sericite phyllonite [3 5] derived from granodiorite or quartz monzonite	.5	1	5	5	1

[1] Calculated from range of Nockolds' (1954) averages for rocks of this classification.
[2] Composition calculated assuming sericite derived from plagioclase An_{25}, the composition of plagioclase in nearby rock of similar composition containing a few plagioclase grains which are unaltered, and assuming no magnetite or pyrite. Iron content might have been a percent or two higher.
[3] Spectrographic analysis by J. C. Hamilton. Results are reported in the series 1, 0.7, 0.5, 0.3, 0.2, 0.15, and 0.1, and so forth, which represent approximate midpoints of group data on a geometric scale. The assigned group for semiquantitative results will include the quantitative value about 30 percent of the time.
[4] Sericite in aggregates pseudomorphous after strung-out plagioclase grains. Microcline, which occurs in a very small amount, is not altered. Biotite only slightly altered to muscovite, but it is bent and broken. Quartz is strained and broken down into lenses of smaller grains. Graphite and pyrite and lesser amounts of magnetite constitute several percent of rock.
[5] Quartz as scattered porphyroclasts and recrystallized mortar. Matrix predominately sericite with some chlorite. A few percent of opaque minerals, most of which are pyrite.

Table 4 is a comparison of the proportions of selected elements in phyllonitic gneiss and phyllonite in the Cranberry Gneiss with their proportions in their inferred parent rocks, and it shows similar, although not identical, relations as the more accurate analyses of table 1. The analyses indicate that during phyllonitization these rocks lost Ca and Na and gained K and probably Fe. Mg stayed approximately constant. Petrographic study shows that the principal mineralogical change has been sericitization of the plagioclase in the phyllonitic gneiss and all feldspar in the phyllonite (fig. 1*F*). Consequently the loss of Ca and Na and gain of K took place during that process. Introduced Fe is principally in pyrite in these two rocks. The occurrence of graphite in the phyllonitic gneiss indicates that some carbon must have been introduced, since the less metamorphosed granitic rocks lack carbon and only locally contain accessory carbonate.

The first and most widespread reaction during formation of phyllonite is the sericitization of plagioclase. It may be written as follows:

$$0.5\underset{\text{(oligoclase, An}_{20}\text{)}}{Na_4CaAl_6Si_{14}O_{40}} + 2H^{+1} + K^{+1} \rightleftharpoons \underset{\text{(muscovite)}}{KAl_3Si_3O_{10}(OH)_2} + 2Na^{+1}\uparrow + 0.5Ca^{+2}\uparrow + \underset{\text{(quartz)}}{4SiO_2}. \quad (1)$$

Hydrogen and potassium metasomatism are necessary for the reaction to occur. The reaction explains the loss of Ca and Na and the enrichment in K and H inferred by mineral composition and suggested by the analyses above. It also explains the high content of

quartz in many of the phyllonites compared with the parent rocks. The Na and Ca leave in solution, but we have no geologic record of where they go.

Reaction 1 has been written assuming constant Al. If we assume constant Si, the equation could be written

$$1.5Na_4CaAl_6Si_{14}O_{40}+14H^{+1}+7K^{+1}+24O^{-2}+12Al^{+3} \rightleftharpoons 7KAl_3Si_3O_{10}(OH)_2+6Na^{+1}\uparrow+1.5Ca^{+2}\uparrow. \quad (1a)$$

The reaction as written requires additions of large quantities of O, Al, K, and H and would necessitate a substantial increase in the volume of the rock. It could be simplified by having quartz as one of the products of the reaction, but that would destroy the assumption of constant Si. Consequently, constant Al seems the more reasonable assumption for the reaction.

For some phyllonitic gneisses and a few phyllonites, at least some of the Ca remains in the rock as a component of epidote-group minerals. For rocks in which the Ca is retained, the reaction may be

$$\underset{\text{(oligoclase, An}_{20})}{Na_4CaAl_6Si_{14}O_{40}}+1.5\underset{\text{(potassium feldspar)}}{KAlSi_3O_8}+0.5K^{+1}+0.5H_2O+3.5H^{+1} \rightleftharpoons \underset{\text{(clinozoisite)}}{0.5Ca_2Al_3Si_3O_{12}(OH)}+\underset{\text{(muscovite)}}{2KAl_3Si_3O_{10}(OH)_2}+\underset{\text{(quartz)}}{11SiO_2}+4Na^{+1}\uparrow. \quad (2)$$

This reaction results in loss of Na and increase in the proportions of quartz, muscovite, and epidote. These reactions could occur simultaneously, thus accounting for a partial, but not complete, loss of the Ca of the original plagioclase. The epidote-group mineral may contain ferric iron, in which case the reaction would be more complicated and involve a mafic mineral and probably some oxidation.

The next step is sericitization of potassium feldspar, possibly by the reaction

$$\underset{\text{(potassium feldspar)}}{1.5KAlSi_3O_8}+H^{+1}=\underset{\text{(muscovite)}}{0.5KAl_3Si_3O_{10}(OH)_2}+K^{+1}\uparrow+\underset{\text{(quartz)}}{3SiO_2}. \quad (3)$$

This reaction also results in an increase in the content of quartz and muscovite. The K^{+1} ions released might participate in the sericitization of plagioclase elsewhere. In some cases, such as the rock of column 3, table 1, reactions 1 and 3 may take place simultaneously, but in that rock they did not go to completion. When plagioclase is altered by reaction 1 alone, reaction 3 might proceed simultaneously, resulting in alteration of any potassium feldspar phase in the plagioclase. The end result of reactions 1 and 3 on granitic rocks is a quartz-muscovite (sericite) rock like many phyllonites in the Grandfather Mountain area.

The components lost and gained in the phyllonite zones ideally may be considered as perfectly mobile. As pointed out by Korzhinsky (1936) and Thompson (1959) the number of phases expected in an assemblage is less than or equal to the number of components which define a sequence of metasomatic assemblages minus the number of perfectly mobile components. In the simplest case the sequence might start with a rock of granodioritic composition composed of biotite, plagioclase, potassium feldspar, and quartz and result in a rock composed of muscovite and quartz. This would involve changes in K_2O, Na_2O, CaO, FeO, MgO, and H_2O, which may be considered mobile components. In addition the inert components Al_2O_3 and SiO_2 are needed to define the system. The total number of components is 8: of these, 6 are perfectly mobile and 2 are inert; thus, the rock should have a maximum of 2 phases. The quartz-sericite phyllonite fulfills that requirement.

Phyllonitic gneiss containing porphyroclasts of minerals of the plutonic generation obviously did not achieve equilibrium with conditions of the Paleozoic metamorphism it underwent. Phyllonite having a more complex mineralogy than just quartz and sericite —for instance containing biotite or chlorite—formed in environments in which fewer components were perfectly mobile. Some quartz-sericite rocks could be derived from pegmatite or gneiss lacking mafic minerals, but the amount and field relations of such rock indicate that much of the quartz-sericite phyllonite originated from normal biotite-containing gneiss.

Hemley and Jones (1964) point out, in reference to alteration of granitic rocks, that reactions in the system K_2O–Na_2O–Al_2O_3–SiO_2–H_2O depend on the temperature, pressure, and ratio of the activities of various base cations to the activity of hydrogen ion in the altering solutions. In the rocks under consideration, temperature and perhaps pressure were quite uniform during metamorphism because mineral assemblages formed during the Paleozoic metamorphism are similar in similar rock types over an area of more than 500 square miles. However, in the phyllonite zones those minerals occur in different proportions and various bulk chemical changes have taken place. Since the amount of reaction depends on the absolute concentration or availability of reactants, the concentration of the various ions in the solutions probably differed somewhat from zone to zone or within the zones, causing somewhat different changes in rocks at various places. Hemley shows that at a given temperature an

increase in the H^{+1} ion concentration of an alkaline solution favors hydrolysis. Changes in pressure do not affect the reactions greatly if the solution is relatively dense.

It is difficult to evaluate the relation of the phyllonite zones to intensity of shearing. The sharp local zones along faults suggest that intense shearing favored the formation of the phyllonite. On the other hand, the wide diffuse zones suggest that shearing in those areas was no more intense than that occurring throughout the basement rocks in the window during regional cataclastic metamorphism and formation of blastomylonitic and phyllonitic gneisses. A zone of shearing might have allowed more solution to flow through the rock and in that way facilitate the chemical changes that distinguish the phyllonites from the blastomylonitic gneisses. However, in the wide diffuse zones the availability of such solutions appears to have had some different control, or perhaps in these areas the ratio of the activities of the base cations to the activity of hydrogen controlled the formation of the phyllonites.

The source of the H^{+1} ions may be water from the overlying sedimentary rocks which were being subjected to progressive metamorphism involving dehydration at the same time that the plutonic rocks were being retrogressively metamorphosed.

The source of K^{+1} ions could have been rock that had undergone reaction 3. Other elements such as Fe, Ti, and U were probably derived from the plutonic rocks, especially from the phyllonite zones. They were carried as ions in solution and locally deposited because of changes in solution composition.

The occurrence of graphite in some of the phyllonite zones is an interesting problem and worthy of further study. Whether or not it was deposited through reduction of introduced CO_2 is unknown. It does not seem likely that C was brought in as ions in a solution. The primary source of the introduced C is even more obscure as carbonaceous matter is not found in the less metamorphosed plutonic rocks of the area.

Phyllonite zones in the Grandfather Mountain area can be considered to have formed in chemical systems open to K, Na, Ca, and H and, to a less uniform extent, to a variety of other components. The openness of the chemical systems in these zones was probably controlled through a combination of intense shearing and the chemical nature and availability of solutions.

REFERENCES

Bryant, Bruce, 1962, Geology of the Linville quadrangle, North Carolina-Tennessee—A preliminary report: U.S. Geol. Survey Bull. 1121–D, 30 p.

——— 1963, Geology of the Blowing Rock quadrangle, North Carolina: U.S. Geol. Survey Geol. Quad. Map GQ–243.

Bryant, Bruce, and Reed, J. C., Jr., 1962, Structural and metamorphic history of the Grandfather Mountain area, North Carolina—A preliminary report: Am. Jour Sci., v. 260, p. 161–180.

Foster, M. D., Bryant, Bruce, and Hathaway, J., 1960, Iron-rich muscovitic mica from the Grandfather Mountain area, North Carolina: Am. Mineralogist, v. 45, p. 839–851.

Hemley, J. J., and Jones, W. R., 1964, Chemical aspects of hydrothermal alteration with emphasis on hydrogen metasomatism: Econ. Geology, v. 59, p. 538–569.

Korzhinsky, D. S., 1936, Mobility and inertness of components in metasomatosis: Akad. Nauk SSSR Izvest., Ser. Geol., no. 1, p. 58–60.

Nockolds, S. R., 1954, Average chemical compositions of some igneous rocks: Geol. Soc. America Bull., v. 65, p. 1007–1032.

Reed, J. C., Jr., 1964a, Geology of the Lenoir quadrangle, N. C.: U.S. Geol. Survey Geol. Quad. Map GQ–244.

——— 1964b, Geology of the Linville Falls quadrangle, North Carolina: U.S. Geol. Survey Bull. 1161–B, 53 p.

Thompson, J. B., Jr., 1959; Local equilibrium in metasomatic processes, *in* Abelson, P. H., ed., Researches in geochemistry: New York, John Wiley and Sons, p. 427–457.

"ECLOGITE" IN HAWAIIAN BASALTS

By EVERETT D. JACKSON, Menlo Park, Calif.

Abstract.—Preliminary results of an investigation of xenoliths in Hawaiian basalt include new data on the garnet-clinopyroxene rocks called "eclogite". Garnet-bearing xenoliths, previously known to occur in the Salt Lake Tuff, Oahu, have been found in the Aliamanu and Makalapa Tuffs as well. Xenoliths in these tuffs are of two dominant types—one containing about 75 percent clinopyroxene, 15 percent garnet, and 10 percent olivine; the other about 75 percent olivine, 15 percent orthopyroxene, and 10 percent clinopyroxene. But xenoliths gradational between these two types are found, and the two types are interlayered in some single hand specimens. It seems clear that the "eclogite" xenoliths are members of a very heterogeneous group of deep-seated rocks whose origin cannot be considered separately from each other or from the origin of their host rocks.

Garnet-bearing xenoliths have been known to occur in the bedded tuffs of Salt Lake Crater, Oahu, (fig. 1) for many years (Hitchcock, 1900). Interest in these rocks was recently stimulated in papers by Kuno (1959) and Yoder and Tilley (1962), who reached the conclusion that the xenoliths represent fragments of rocks that formed at considerable depths in the mantle. Since 1962, Salt Lake Crater, as the only known oceanic source of the garnet-clinopyroxene rocks called "eclogite," has been the subject of considerable discussion by O'Hara and Mercy (1963), Kuno (1963), Kushiro and Kuno (1963), Heier (1963), Tilton and Reed (1963), Lovering and Richards (1964), Coleman and others (1965), Forbes (1965), Macdonald (1965), Roedder (1965), Forbes and Kuno (1965), White (1966), and others. The U.S. Geological Survey has recently begun a comprehensive study of the xenoliths in all the basaltic rocks of Hawaii, including those of Salt Lake Crater. Several preliminary results of the field investigations will be of interest to students of the eclogite problem.

OCCURRENCE OF GARNET-BEARING XENOLITHS

Garnet-bearing xenoliths have been found in two previously unreported localities on the island of Oahu —Aliamanu Crater and Makalapa Crater (fig. 1). The xenoliths, like those at Salt Lake Crater, occur as inclusions in bedded tuff. The tuffs that compose these three craters are members of the nepheline-rich Honolulu Volcanic Series (Stearns and Vaksvik, 1935).

The xenoliths of coarse-grained rocks in the tuffs average about 25 mm in diameter and range up to 150 mm. They are larger and more abundant near the centers of the craters, where they are commonly scattered among larger inclusions of tholeiitic basalt and nepheline basalt. The coarse-grained xenoliths are considerably more abundant in the Salt Lake Tuff than in the Aliamanu Tuff, and more abundant in the Aliamanu than in the Makalapa Tuff.

The xenoliths make up an extremely heterogeneous group of rocks. White (1966) has recently pointed out that lherzolite xenoliths, as well as the more publicized garnet-bearing xenoliths, are abundant at Salt Lake Crater. In order to obtain a statistically meaningful sample of the compositional range and abundance of xenoliths, about 750 were broken free from the enclosing tuffs and carefully examined. Triaxial dimensions, shape, structure, texture, estimated mineral proportions, and grain size were recorded for each xenolith.

The estimated mineral proportions of these xenoliths are plotted on the faces of tetrahedra in figures 2 and 3. In addition to the 4 plotted minerals, most xenoliths contain 1 to 5 percent chromite, some contain mica and amphibole, and a few contain plagioclase. Inspection of figures 2 and 3 reveals that about half the xenoliths in the Salt Lake Tuff, and a little less than half of the xenoliths in the Aliamanu Tuff are garnet bearing. In the xenoliths from the Salt Lake Tuff there are two dominant mineral assemblages—one averaging about 75 percent olivine, 15 percent orthopyroxene, and 10 percent clinopyroxene; the other averaging about 75 percent clinopyroxene, 15 percent garnet, and 10 percent olivine. In the Aliamanu Tuff there seems to be less orthopyroxene associated with

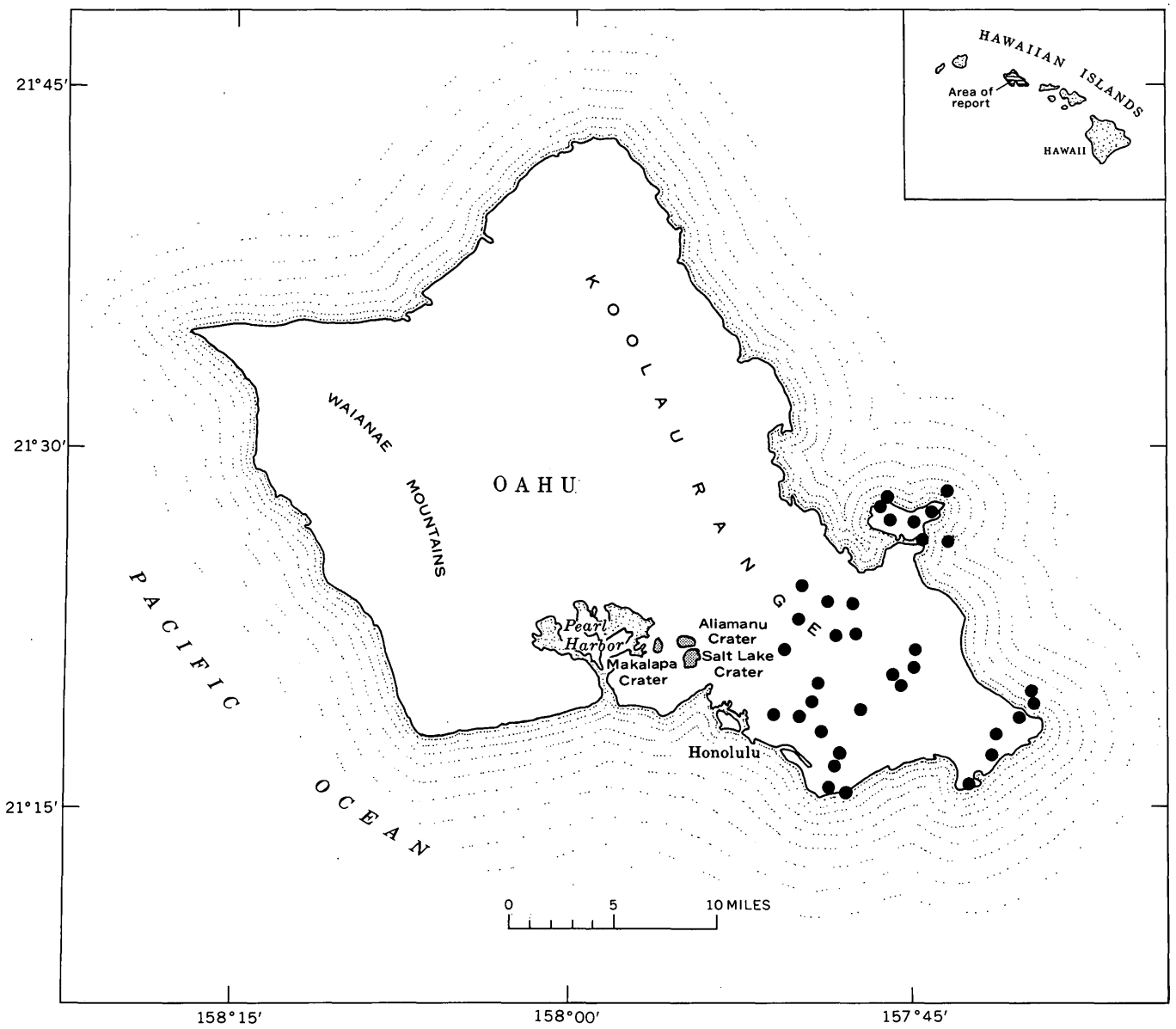

FIGURE 1.—Source vents of the Honolulu Volcanic Series on Oahu, Hawaii. Patterned areas are vents known to contain garnet-bearing xenoliths; solid circles are other known vents.

the olivine-rich rocks. Not enough xenoliths have been counted in the Makalapa Tuff to permit a plot, but they resemble the Aliamanu rather than the Salt Lake suite. It is apparent from figures 2 and 3 that every gradation in mineral assemblage occurs between the olivine maximum and the clinopyroxene-garnet maximum. Garnet occurs in these rocks in amounts ranging from 1 to more than 50 percent.

For the purposes of field classification, I will refer to these rocks as garnet-free peridotites and garnet-bearing peridotites. In the Salt Lake Tuff, the most abundant type of garnet-free peridotite xenoliths would be called lherzolite in most classification systems; in the Aliamanu Tuff the most abundant type would be called wehrlite. In both tuffs, the most abundant type of garnet-bearing peridotite xenoliths might be classed as "eclogite," even though considerable olivine is present. However, I would prefer not to use "eclogite" for any of these garnet-clinopyroxene rocks until the term is better defined, particularly because of the widespread acceptance of chemical equivalence of eclogites and basalts (Yoder and Tilley, 1962; Coleman and others, 1965). If the mode of the most abundant type of garnet-bearing xenoliths is taken at 75 percent clinopyroxene, 15 percent garnet, and 10 percent olivine, and if these percentages are

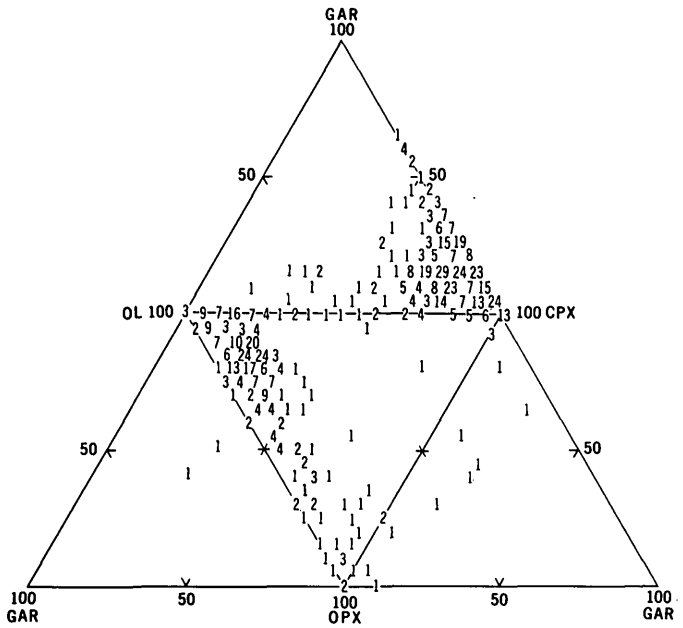

FIGURE 2.—Tetrahedral plot of mineral proportions in 699 xenoliths from the Salt Lake Tuff. Numbers indicate total number of specimens at a single plot point. GAR, garnet; OL, olivine; CPX, clinopyroxene; OPX, orthopyroxene.

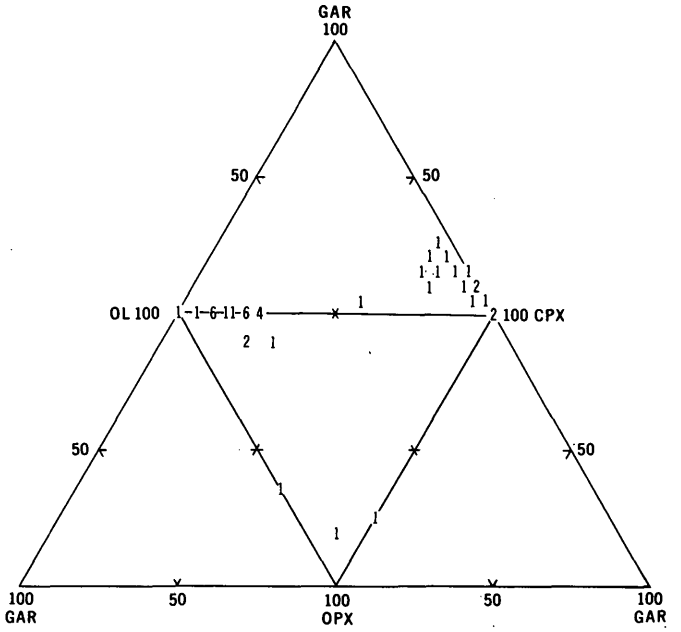

FIGURE 3.—Tetrahedral plot of mineral proportions in 50 xenoliths from the Aliamanu Tuff. Numbers indicate total number of specimens at a single plot point. GAR, garnet; OL, olivine; CPX, clinopyroxene; OPX, orthopyroxene.

multiplied proportionately by the appropriate compositions of Salt Lake minerals published by Yoder and Tilley (1962) and White (1966), the calculated total-rock composition is very similar to previously published Salt Lake "eclogite" whole-rock analyses (table 1, analyses 1–3). Neither the reconstructed analysis nor the two whole-rock analyses are similar to analyses of average nepheline basalts of the Honolulu Volcanic Series (table 1, analysis 4), average alkalic basalts (table 1, analysis 5), or any other Hawaiian extrusive rocks that I know of. The differences in MgO/CaO and MgO/Al_2O_3 ratios and content of total alkalis, TiO_2, and Cr_2O_3 between the "eclogites" and the basalts are particularly noticeable, and, in general, correspond to differences between other eclogites and basalts pointed out by Forbes (1965). Although I do not think that the Salt Lake garnet-bearing peridotites correspond in composition to known natural extrusive liquid melts, they are chemically similar in many ways to mafic gabbros, particularly those of cumulate origin. The Hawaiian "eclogites" may, in fact, be metamorphosed gabbros, troctolites, and feldspathic peridotites. It is hoped that further work will clarify this problem.

Most of the xenoliths in the Salt Lake, Aliamanu, and Makalapa Tuffs have metamorphic textures and structures. Many of the garnet-free peridotites have gneissic structures, and the garnet-bearing peridotites have reaction textures.

EXTRUSIVE HOST ROCKS OF GARNET-BEARING XENOLITHS

The Honolulu Volcanic Series is composed of a group of nepheline basanite, nepheline basalt, and nepheline melilite basalt tuffs and flows that were extruded from about 30 vents in the southeastern part of the Koolau Range on Oahu (Stearns and Vaksvik, 1935; Winchell, 1947). The Honolulu rocks, and the similar nepheline-rich rocks of the Koloa Volcanic Series on Kauai (Macdonald and others, 1960), are considerably more undersaturated (see table 1) and very much younger than the tholeiitic and alkalic basalt shields onto which they have been extruded.

McDougall (1964) reported K/Ar ages in excess of 2 million years for the youngest tholeiites and alkalic basalts of the Koolau Volcanic Series on Oahu, whereas the overlying Honolulu Volcanic Series is late Pleistocene and Recent in age. On Kauai, McDougall (1964) found evidence for a 2-m.y. time interval between the youngest alkalic basalts of the Waimea Canyon Volcanic Series and the still younger undersaturated rocks of the Koloa Volcanic Series. Preliminary results on K/Ar ages on a large number of basaltic rocks from Kauai confirm the existence of this interval (G. B. Dalrymple, oral commun., May 3, 1966).

Macdonald and Katsura (1961) proposed that Hawaiian eruptive rocks be classified into three major groups: a tholeiitic suite, an alkalic suite, and a nephe-

TABLE 1.—*Chemical analyses of Hawaiian "eclogite" and basalt*

	1	2	3	4	5
SiO_2	48. 12	48. 41	49. 26	39. 52	46. 46
Al_2O_3	9. 11	10. 41	8. 63	12. 19	14. 64
Fe_2O_3	1. 89	2. 58	3. 24	4. 91	3. 27
FeO	7. 03	5. 61	5. 09	8. 64	9. 11
MgO	17. 62	17. 78	19. 40	11. 87	8. 19
CaO	13. 83	12. 17	12. 44	12. 47	10. 33
Na_2O	1. 38	1. 24	. 88	4. 11	2. 92
K_2O	. 01	. 11	. 06	1. 06	. 84
H_2O	-------	. 43	. 40	1. 34	-------
TiO_2	. 63	. 62	. 62	2. 65	3. 01
P_2O_5	-------	. 04	. 02	. 90	. 37
MnO	. 17	. 18	. 17	. 14	. 14
CO_2	-------	. 28	-------	. 05	-------
Cr_2O_3	. 29	. 43	. 31	. 02	-------
Total	100. 08	100. 29	100. 52	99. 87	99. 28

1. Calculated "eclogite" based on 75 percent clinopyroxene, 15 percent garnet, 10 percent olivine; analyses of minerals from xenoliths from Yoder and Tilley (1962) and White (1966).
2. "Hypersthene eclogite" (66118) from Salt Lake Crater, from Yoder and Tilley (1962, p. 482).
3. "Eclogite" (62–2) from Salt Lake Crater, from Macdonald and Katsura (1964, p. 123).
4. Average of 12 analyses of extrusive rocks from the Honolulu Volcanic Series, from Winchell (1947); Macdonald and Katsura (1964); Yoder and Tilley (1962); and Forbes and Kuno (1965).
5. Average of 28 analyses of Hawaiian alkalic basalts, from Macdonald and Katsura (1964, p. 124).

linitic suite. It is apparent that they intended the nephelinitic suite to be composed of the rocks of the Honolulu and Koloa Volcanic Series. In subsequent papers, Macdonald and Katsura (1962, p. 190; 1964) abandoned a separate nephelinitic suite, and it has also been the practice of other authors (Tilley, 1950; Yoder and Tilley, 1962) to include nephelinitic basalts among the alkali olivine basalts. Whether or not the rocks of the Honolulu and Koloa Volcanic Series are classified as a separate volcanic suite, it is evident that they are at least as chemically and physically distinct from typical Hawaiian alkalic basalts as the alkalic basalts are from the tholeiitic basalts.

OCCURRENCE OF GARNET-FREE XENOLITHS

White (1966) found a close relation between the mineralogy of garnet-free Hawaiian xenoliths and the chemical composition of their host basalts. On this basis he divided the xenoliths into three groups: (1) small, sparse, inclusions of diverse mineralogy that occur in tholeiite; (2) dunite, wehrlite, feldspathic peridotite, and gabbro inclusions that occur preferentially in alkaline olivine basalt, and (3) lherzolite inclusions that occur preferentially in olivine nephelinite. Thus far in the present investigation, 3,700 xenoliths from Macdonald and Katsura's (1961) alkalic suite (alkalic basalts, hawaiites, and trachytes), and 1,150 xenoliths from the Honolulu and Koloa Volcanic Series (nephelinites) have been tabulated by mineral proportions; White's observations have, in general, been confirmed. In particular, lherzolite xenoliths of the type found in the Salt Lake, Aliamanu, and Makalapa Tuffs are exceedingly rare in alkalic basalt host rocks.

The mineral proportions in 401 xenoliths in nephenite-rich rocks of the Honolulu and Koloa Volcanic Series exclusive of the Salt Lake, Aliamanu, and Makalapa Tuffs, are given in figure 4. Again, the mineral proportions are reduced to the faces of the tetrahedron. In addition to the plotted constituents, most of the xenoliths contain 1–5 percent chromite, and a fair number contain plagioclase. It is apparent that this group of host rocks displays the same general assemblage of garnet-free peridotites as the Salt Lake, Aliamanu, and Makalapa Tuffs, but differs from them in containing no garnet-bearing rocks. The assemblages of xenoliths vary considerably among the individual flows and tuffs of the two volcanic series, and more "boulder counts" will be necessary to assess the significance of different proportions of dunite, wehrlite, and lherzolite inclusions. Additional fieldwork will also be necessary to determine the distribution of those Honolulu and Koloa extrusive rocks that lack xenoliths.

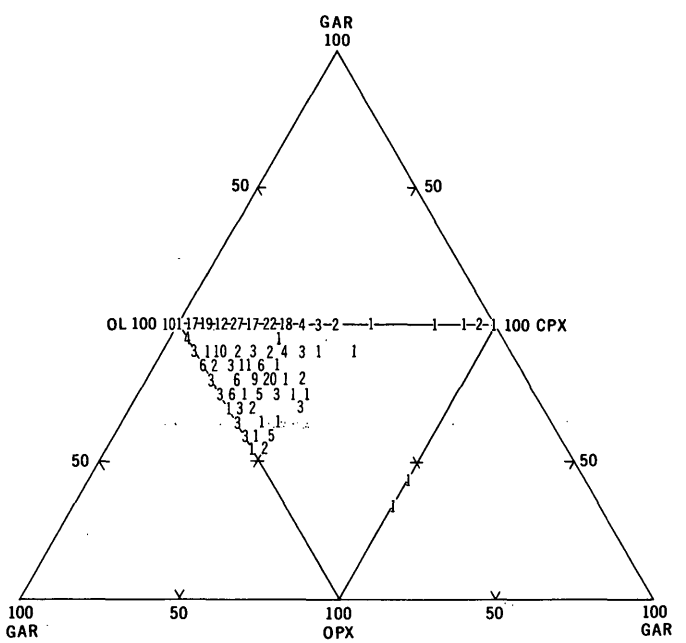

FIGURE 4.—Tetrahedral plot of mineral proportions in 401 xenoliths from flows and tuffs of the Honolulu and Koloa Volcanic Series, exclusive of the Salt Lake, Aliamanu, and Makalapa Tuffs. Numbers indicate total specimens at a single plot point. GAR, garnet; OL, olivine; CPX, clinopyroxene; OPX, orthopyroxene.

ORIGIN OF GARNET-BEARING XENOLITHS

In the past, attempts to explain all the Hawaiian xenoliths as fragments of a common body of deep-seated rock with a common alkali olivine basalt transporting host, have led to sharply conflicting opinions (Ross and others, 1954; Richter and Murata, 1961; Forbes and Kuno, 1965). Nor have attempts to determine crustal or mantle origin on the basis of the properties of selected xenolithic rocks or minerals led to any unanimous body of opinion (Yoder and Tilley, 1962; Heier, 1963; Roedder, 1965). In fact, it is evident that broad generalizations about this extremely diverse group of rocks are premature, and that White (1966), in demonstrating a compositional relation between the xenoliths and their host rocks, and in arguing for multiple origins of the xenoliths, has sharply focused attention on the nature of the problem.

It is apparent from the present investigation that garnet-bearing peridotites transitional between "eclogites"and lherzolites are fairly abundant in certain extrusive rocks of the Honolulu Volcanic Series. In fact, some single xenolith hand specimens consist of alternating layers of these two rock types. It is clear that the two kinds of xenoliths are either intimately mixed at depth, or are transitionally contiguous. The problem of origin of the "eclogites" cannot, therefore, be separated from the origin of the lherzolites and other olivine-rich xenoliths common to the Honolulu nephelinites, nor from the origin of the Honolulu Volcanic Series as a whole.

The problem of why the garnet-bearing peridotite xenoliths are confined to certain vents of the Honolulu Volcanic Series, and are not present in the others, has received surprisingly little attention in the literature. The present investigation, while far from complete, can at least define some possible explanations. These may be divided into four categories: the xenoliths are localized by (1) geographic area, (2) time of eruption, (3) depth of source material, or (4) composition of their host basalts. These categories are not necessarily mutually exclusive.

One possible explanation is that the parent garnet-bearing peridotite body exists in the crust or mantle only under a restricted area of southwest Oahu. The occurrence of garnet-bearing peridotite xenoliths at the Aliamanu and Makalapa centers enlarges the previously known source area to about 6 square miles. The proximity of the new centers to the previously known source at Salt Lake Crater supports a restricted source area, but more localities may very well be discovered in the future.

Another possible explanation is that the distribution of garnet-bearing peridotite xenoliths is due to the eruption sequence within the Honolulu Volcanic Series. The Salt Lake Tuff unconformably overlies the Aliamanu Tuff, and, locally, a soil zone is found at the contact. From this relation and many others, Stearns and Vaksvik (1935) and Winchell (1947) have placed the Aliamanu eruption fairly early in the Honolulu Volcanic Series, and the Salt Lake and Makalapa events fairly late in the series. The presence of garnet-bearing peridotite xenoliths in both the Salt Lake and Aliamanu Tuffs suggests that time of eruption within the Honolulu Volcanic Series is not an important factor in explaining the localization.

A third possible explanation is that the parent garnet-bearing peridotite body lies deeper in the crust or mantle than the garnet-free peridotite body, and that the Salt Lake, Aliamanu, and Makalapa primary magmas were generated deeper than the other magmas of the Honolulu Volcanic Series. If this is the case, one would suppose that the garnet-bearing peridotite xenoliths carried to the surface would typically be smaller in size than garnet-free peridotite xenoliths, having travelled farther up the vent. Figure 5 is a cumulative size-distribution curve of the average diameters of 326 garnet-free peridotite xenoliths and 373 garnet- bearing peridotite xenoliths from the Salt Lake Tuff. Differences in mean size are small and probably not significant, but if anything, the garnet-bearing xenoliths are larger. On the other hand, the garnet-pyroxene association is often considered to be a high-pressure assemblage, and pressure is commonly equated with depth. It is hoped that further study of the mineralogy and texture of the xenoliths will lead to independent criteria for estimating their depth of origin.

A fourth possible explanation is that the distribution of garnet-bearing peridotite xenoliths is related to differences in composition of the magmas of the Salt Lake, Aliamanu, and Makalapa eruptions from those of the rest of the Honolulu Volcanic Series. The chemical composition of the primary material that produced the Salt Lake, Aliamanu, and Makalapa Tuffs is not certainly known (Winchell, 1947), but inclusions of nepheline and melitite in unaltered glass fragments (Wentworth, 1926) suggest that the magmatic material was nepheline melilite basalt. Forbes and Kuno(1965) give an analysis of "nepheline olivine basalt, Salt Lake Crater, Oahu, Hawaii," but I know of no basalt interbedded with the Salt Lake Tuff. Perhaps the material analyzed was collected from the flow described by Stearns (1940), which locally under-

224-352 O—66——11

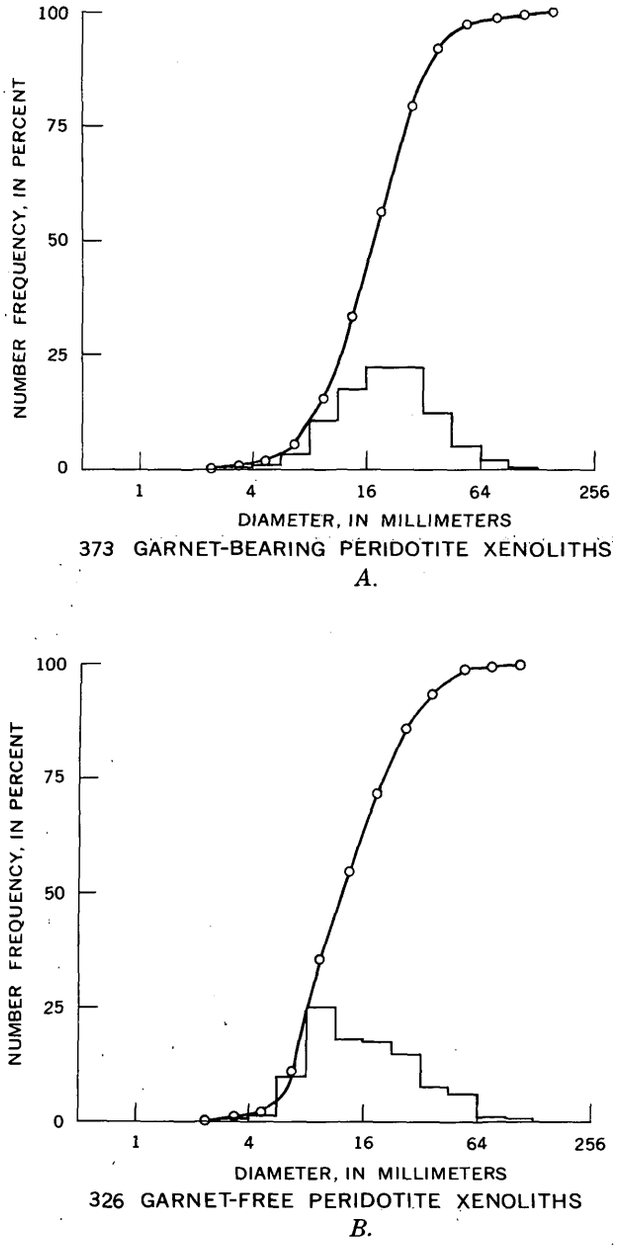

FIGURE 5.—Comparison of size-frequency distributions of xenoliths from the Salt Lake Tuff. *A*, garnet-bearing peridotite xenoliths; arithmetic mean diameter is 24 mm. *B*, garnet-free peridotite xenoliths; arithmetic mean diameter is 20 mm.

lies the Salt Lake Tuff. R. L. Hay (oral commun., May 5, 1966) is currently analyzing fresh glass shards from the Salt Lake Tuff with the electron microprobe.

Although at present the composition of these tuffs cannot be compared with the composition of other Honolulu Series basalts, the constructional forms of the tuffs may provide a clue to their volatile content. All the tuff cones on Oahu have characteristically large ratios of inside crater diameter to total cone width, and their origin has been ascribed to eruption under sea water (Stearns and Vaksvik, 1935; Winchell, 1947). Wentworth (1926) has studied the shapes of the tuff cones, and he notes that the Salt Lake, Aliamanu, and Makalapa cones have characteristically gentler slopes, lower rims, and contain larger ejected blocks than the others. In fact, the shapes are reminiscent of continental maars (Shoemaker and others, 1962). The possibility remains, therefore, that whether erupted under sea water or not, the Salt Lake, Aliamanu, and Makalapa juvenile magmas contained more volatile material than the other Honolulu Series magmas, and that this feature is directly related to the presence of the fragments of garnet-bearing peridotite in their extrusive rocks.

In summary, the preliminary results of this investigation of Hawaiian xenoliths provide some limits within which speculation on the origin of the garnet-bearing peridotites may be confined:

(1) Garnet-bearing peridotite xenoliths have been found in the Salt Lake, Aliamanu, and Makalapa Tuffs.

(2) The garnet-bearing xenoliths occur in about equal numbers with garnet-free peridotite xenoliths typical of the other volcanic rocks of the Honolulu Volcanic Series.

(3) Although two rock types are dominant, every gradation of mineral proportions between them is present among the xenoliths; in addition, the two dominant rock types are interlayered in some single specimens.

(4) Many of the garnet-bearing xenoliths are not compositionally equivalent to basalt, and probably few of them are.

(5) Texturally, most of the garnet-bearing and garnet-free peridotites are metamorphic rocks.

(6) The mean size and size distribution of the two kinds of xenoliths are nearly identical.

(7) The origin of the xenoliths is an integral part of the origin of the nepheline-rich rocks of the Honolulu Volcanic Series.

(8) The data presently available are insufficient to warrant a conclusion as to whether any or all of the xenoliths are fragments of the oceanic mantle; further work may provide a solution to this problem.

REFERENCES

Coleman, R. G., Lee, D. E., Beatty, L. B., and Brannock, W. W., 1965, Eclogites and eclogites—their differences and similarities: Geol. Soc. America Bull., v. 76, p. 483–508.

Forbes, R. B., 1965, The comparative chemical composition of eclogite and basalt: Jour. Geophys. Research, v. 70, p. 1515–1521.

Forbes, R. B., and Kuno, Hisashi, 1965, The regional petrology of peridotite inclusions and basaltic host rocks, *in* Smith, C. H., and Sorgenfrei, Theodor, eds., The upper mantle symposium, New Delhi, 1964: Copenhagen, Det Berlingske, Bogtrykkeri.

Heier, K. S., 1963, Uranium, thorium, and potassium in eclogitic rocks: Geochim. et Cosmochim. Acta, v. 27, p. 849–860.

Hitchcock, C. H., 1900, Geology of Oahu: Geol. Soc. America Bull., v. 11, p. 15–60.

Kuno, Hisashi, 1959, Discussion of a paper by J. F. Lovering, "The nature of the Mohorovicic discontinuity": Jour. Geophys. Research, v. 64, p. 1071–1072.

——— 1963, Crustal and upper mantle rocks beneath Hawaiian volcanoes [abs.]: Upper Mantle Symposium, XIII General Assembly, Internat. Union Geodesy and Geophysics, v. 1, p. 1–35.

Kushiro, Ikuo, and Kuno, Hisashi, 1963, Origin of primary basalt magmas and classification of basaltic rocks: Jour. Petrology, v. 4, p. 75–89.

Lovering, J. F., and Richards, J. R., 1964, Potassium-argon age study of possible lower-crust and upper-mantle inclusions in deep-seated intrusions: Jour. Geophys. Research, v. 69, p. 4895–4901.

Macdonald, G. A., 1965, The lithologic constitution of the crust and mantle in the Hawaiian area: Pacific Science, v. XIX, p. 285–286.

Macdonald, G. A., Davis, D. A., and Cox, D. C., 1960, Geology and ground-water resources of the island of Kauai, Hawaii: Hawaii Div. Hydrography Bull. 13, 212 p.

Macdonald, G. A., and Katsura, Takashi, 1961, Variations in the lava of the 1959 eruption in Kilauea Iki: Pacific Science, v. XV, p. 358–369.

——— 1962, Relationship of petrographic suites in Hawaii: Am. Geophys. Union Mon. 6, p. 187–195.

——— 1964, Chemical composition of Hawaiian lavas: Jour. Petrology, v. 5, p. 82–133.

McDougall, Ian, 1964, Potassium-argon ages from lavas of the Hawaiian Islands: Geol. Soc. America Bull., v. 75, p. 107–128.

O'Hara, M. J., and Mercy, E. L. P., 1963, Petrology and petrogenesis of some garnet peridotites: Royal Soc. Edinburgh Trans., v. XLV, p. 251–314.

Richter, D. H., and Murata, K. J., 1961, Xenolithic nodules in in the 1800–1801 Kaupulehu flow of Hualalai volcano: Art. 89 *in* U.S. Geol. Survey Prof. Paper 424–B, p. B215–B217.

Roedder, Edwin, 1965, Liquid CO_2 inclusions in olivine-bearing nodules and phenocrysts from basalts: Am. Mineralogist, v. 50, p. 1746–1782.

Ross, C. S., Foster, M. D., and Myers, A. T., 1954, Origin of dunites and olivine-rich inclusions in basaltic rocks: Am. Mineralogist, v. 39, p. 693–737.

Shoemaker, E. M., Roach, C. H., and Byers, F. M., 1962, Diatremes and uranium deposits in the Hopi Buttes, Arizona: Geol. Soc. America, Buddington volume, p. 327–355.

Stearns, H. T., 1940, Supplement to the geology and groundwater resources of the island of Oahu, Hawaii: Hawaii Div. Hydrography Bull. 5, 164 p.

Stearns, H. T., and Vaksvik, K. N., 1935, Geology and groundwater resources of the island of Oahu, Hawaii: Hawaii Div. Hydrography Bull. 1, 479 p.

Tilley, C. E., 1950, Some aspects of magmatic evolution: Geol. Soc. London Quart. Jour. v. 106, p. 37–61.

Tilton, G. R., and Reed, G. W., 1963, Radioactive heat production in eclogite and some ultramafic rocks, *in* Earth science and meteoritics: Amsterdam, North-Holland Publishing Co., p. 31–43.

Wentworth, C. K., 1926, Pyroclastic geology of Oahu: Honolulu, Hawaii, B. P. Bishop Museum Bull. 30, 121 p.

White, R. W., 1966, Ultramafic inclusions in basaltic rocks from Hawaii: Beiträge zur Mineralogie und Petrographie, v. 12, p. 275–314.

Winchell, Horace, 1947, Honolulu Series, Oahu, Hawaii: Geol. Soc. America Bull. v. 58, p. 1–48.

Yoder, H. S., and Tilley, C. E., 1962, Origin of basalt magmas—An experimental study of natural and synthetic rock systems: Jour. Petrology, v. 3, p. 342–532.

PRELIMINARY REPORT ON A PLUTONIC BELT IN WEST-CENTRAL ALASKA

By THOMAS P. MILLER, WILLIAM W. PATTON, JR., and MARVIN A. LANPHERE,
Menlo Park, Calif.

Abstract.—Preliminary studies of a belt of plutons in west-central Alaska indicate that the plutons are divisible into an older, 100-m.y-old suite composed chiefly of saturated to undersaturated monzonite and syenite and a younger 81-m.y.-old suite chiefly of granodiorite and quartz monzonite. The older plutons occur in the western half of the plutonic belt and the younger plutons in the eastern half.

Investigations by the U.S. Geological Survey since 1953 along a belt of plutons in west-central Alaska (fig. 1) have resulted in the mapping of nine previously unreported plutons (fig. 2, plutons 1, 3, and 5–11). In addition two other plutons (fig. 2, plutons 2 and 4) along this belt that were previously noted by Smith (1913) and Eakin (1916) have been mapped in greater detail. Potassium-argon age determinations on hornblende and biotite from six of these plutons (fig. 2, plutons 1–6, and table 1) indicate that magma emplacement occurred in two distinct episodes in Cretaceous time. Two of the dated plutons, Indian Mountain and Zane Hills, previously have been reported as Eocene(?) by Eakin (1916) and Tertiary by Dutro and Payne (1957). Preliminary geologic mapping and petrographic studies indicate that the two episodes of magma emplacement may be characterized by granitic-textured suites of different compositions. The older suite, which is exposed in the western part of the pluton belt, is not yet completely mapped; however, results to date indicate that a considerable number of these rocks are saturated to undersaturated in composition. They range in composition from quartz monzonite to feldspathoidal syenite with hornblende-pyroxene syenite and monzonite probably the most common rock types. The younger, more silicic suite, exposed mainly in the eastern part of the pluton belt but possibly present also in the west, is more uniform in composition and consists chiefly of quartz-bearing rocks, mainly hornblende-biotite granodiorite and quartz monzonite with subordinate leucocratic granodiorite and alaskite.

GEOLOGIC SETTING

The plutons discussed here occur as irregular bodies ranging from a few square miles to more than 350 square miles in area in the Selawik, Shungnak, and Hughes 1:250,000 quadrangles (fig. 1). In most places, the plutons form the cores of low mountain ranges and occur along a belt about 25 miles wide and 220 miles long extending from the east end of the Seward Peninsula to just east of the Koyukuk River (figs. 1 and 2). This belt lies about 50 miles south of the Brooks Range and has been named the Hogatza uplift

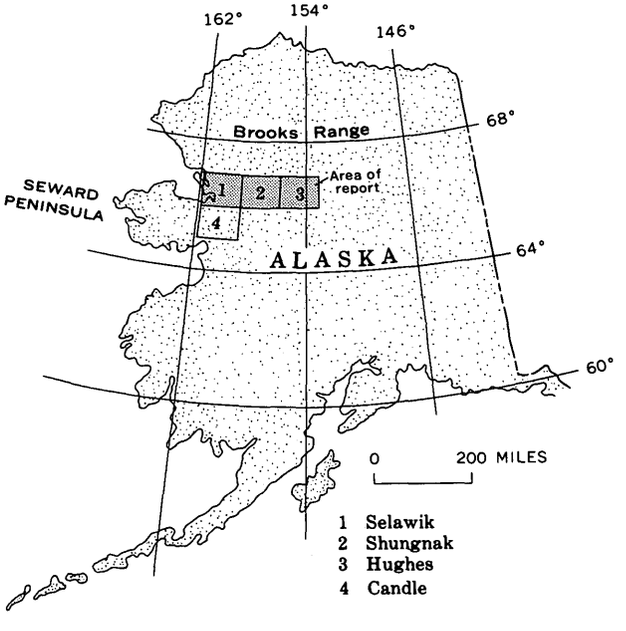

FIGURE 1.—Index map showing location of report area (shaded) and topographic quadrangles (numbered) referred to in text.

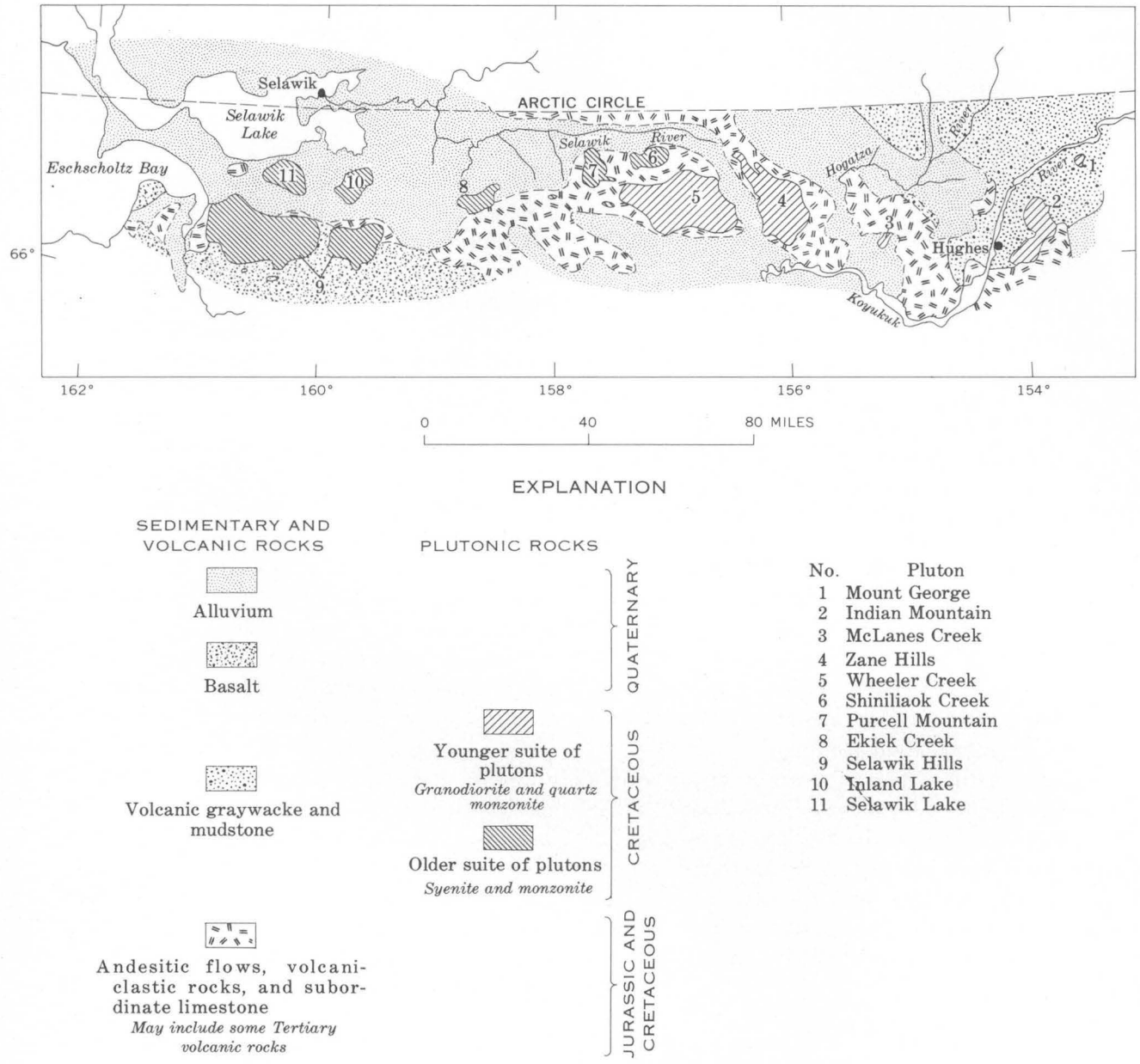

FIGURE 2.—Generalized geologic map of the report area in west-central Alaska, showing location of plutons.

by Payne (1955) and the Hogatza arch by Miller and others (1959).

Stratigraphic and intrusive relations indicate that the plutons of this belt were emplaced at two different times. The plutonic rocks of both ages intrude, and are therefore younger than, a thick sequence of marine andesitic volcanic rocks of earliest Cretaceous and possibly Jurassic age. These volcanic rocks are chiefly pyroxene andesite flows and volcaniclastic rocks with subordinate fossiliferous limestone. This unit occurs over large areas of west-central Alaska and, on the Koyukuk River near Hughes, has been given the name Koyukuk Series by Schrader (1902, p. 246). This unit was renamed the Koyukuk Group by Smith (1913, p. 80). South of the Selawik Hills pluton in the Candle quadrangle, plutonic rocks from the Hunter Creek pluton appear to have supplied detritus to volcanic graywacke and conglomerate of probable mid-Cretaceous age (Patton, in press). These plutonic rocks are correlated with the Selawik Hills pluton and the other older plutons on the basis of petrographic similarity. On the basis of this stratigraphic evidence, the early

plutons are older than the mid-Cretaceous volcanic graywacke and conglomerate. The young Indian Mountain and Mount George plutons at the east end of the area (fig. 2) intrude a volcanic graywacke and mudstone unit (Patton and Miller, 1966) also of mid-Cretaceous age; on this evidence, the later plutons are younger than the mid-Cretaceous volcanic graywacke and mudstone.

The volcanic and sedimentary units are for the most part unaltered except in areas adjacent to the plutons. Here rocks of the hornblende hornfels facies are confined to a narrow zone near the borders of the plutons and grade through a zone of albite-epidote hornfels facies rocks into a zone of propylitically altered rocks. The hornfelsic rocks are commonly more resistant than the plutonic rocks and in places form high ridges of resistant rock rimming parts of the plutons. The contacts between the plutons and the surrounding wall-rock are sharp, relatively straight, and steeply dipping; everywhere the plutons appear to be discordant. Where the Mount George and Indian Mountain plutons intrude the mid-Cretaceous graywacke and mudstone unit, swarms of satellitic hypabyssal quartz latite porphyries are found intruding the sedimentary rocks. These porphyritic intrusive rocks are in locally cross-cutting dikes and sills that range in thickness from a few feet to several hundred feet.

The Selawik Hills pluton is partially overlain by a considerable volume of Quaternary olivine basalt. The Purcell Mountain pluton is overlain by a rhyolite welded tuff of Late Cretaceous or Tertiary age containing granitic rock fragments. Other volcanic rocks ranging in composition from basalt to rhyolite occur in this area and may be correlative with the rhyolitic volcanic rocks.

PETROGRAPHY

Older suite

Preliminary mapping has indicated that the older suite of plutonic rocks (fig. 2, plutons 6–11) consists chiefly of saturated to undersaturated alkaline rocks but also includes some quartz-rich rocks. The following rock types are found: pyroxene-hornblende syenite and monzonite, granodiorite, quartz monzonite, alkali granite, nepheline syenite, biotite-melanite nepheline syenite, and perthosite.

The chief minerals in the syenite and monzonite are perthitic orthoclase, plagioclase, hornblende, pyroxene, and subordinate amounts of biotite. Quartz is present only as an accessory mineral in the syenite and monzonite but occurs interstitially in amounts up to 25 percent in the granodiorite and quartz monzonite. The orthoclase occurs in anhedral to euhedral, tabular to tablet-shaped crystals as much as 4 centimeters long and is perthitic with string-and-braid-type perthite most common; microline is found in some sections. In some specimens, potash feldspar constitutes more than 65 percent of the rock. Plagioclase is usually in small euhedra and ranges in composition from oligoclase to labradorite. The hornblende is strongly pleochroic from yellow brown to dark green. Relict pyroxene cores are common in many crystals. Pyroxene ranges in color from grayish white to pale green to dark bottle green, it is unzoned, and some is pleochroic. Olivine has been found only in a monzonite stock southwest of the Purcell Mountain pluton where it occurs enclosed by pyroxene. Biotite varies from reddish brown to greenish brown and is generally less abundant than the other varietal mafic minerals. The accessory minerals are abundant large sphene euhedra, magnetite-ilmenite intergrowths, apatite, zircon, and, less commonly, allanite; tourmaline is common in the monzonite and syenite of the Shiniliaok Creek pluton.

Perthitic orthoclase, anorthoclase(?), nepheline, zeolite, hornblende, pyroxene, biotite, and melanite garnet occur in the more undersaturated feldspathoidal syenites. At the Ekiek Creek pluton, melanite garnet composes more than 10 percent by volume of some specimens, along with 2 percent biotite, 65 percent soda orthoclase(?), and 23 percent nepheline and zeolite. Sphene, apatite, fluorite, magnetite-ilmenite intergrowths, and zircon are accessory minerals in these rocks. The texture of the older plutonic rocks is chiefly hypidiomorphic granular but includes such textures as porphyritic, trachytoid, and gneissic.

Younger suite

In the younger suite of plutonic rocks (fig. 2, plutons 1–5) the composition ranges from granodiorite to alaskite with minor amounts of monzonite and hybrid diorite, but granodiorite is the most common rock type. The plagioclase occurs as fresh subhedral crystals showing common oscillatory and normal progressive zoning; the range of composition of individual crystals is oligoclase to labradorite. The average composition is andesine. Quartz is commonly interstitial. The potash feldspar is usually perthitic orthoclase, but microcline was observed in about a third of the sections examined; the potash feldspar is commonly anhedral and interstitial. Myrmeketic intergrowths of quartz with feldspar are common. The varietal mafic minerals are

biotite and hornblende; the biotite occurs as medium-dark-brown plates and ragged patches commonly containing halo-surrounded zircon crystals. Hornblende occurs in ragged to euhedral crystals and is typically light green. Magnetite, apatite, sphene, zircon, and allanite are ubiquitous accessory minerals. Alteration products are not abundant in the younger suite. Some of the plagioclase has been subjected to minor sericitization, and some of the biotite shows a little chloritization on crystal borders. These rocks are medium grained and have a hypidiomorphic texture.

The younger plutons are intruded by thin aplite and fine-grained alaskite dikes which in some places follow preexisting joint planes. Tourmaline occurs in a few of these aplites. The aplites are common along the contacts and also cut the intruded wallrock but do not extend for any great distance into it. Quartz veins are not abundant and seem to be most common in the southern and western parts of the Zane Hills pluton where veins composed of milky white quartz with minor chalcopyrite and limonite occur in several places.

A large body of alaskite occurs at the west end of the Wheeler Creek pluton, and consists of rocks as silicic as 32 percent quartz, 47 percent potash feldspar, 20 percent plagioclase, and less than 1 percent mafic minerals. This rock is characterized by large black smoky quartz anhedra as much as 15 millimeters across.

Inclusions are not abundant, but those present are scattered throughout these younger plutons. These inclusions are composed of dark fine-grained granodiorite with the same minerals as the host granodiorite but in different proportions. The inclusions are lenticular to irregularly shaped and sharply bounded.

AGE

Potassium-argon ages of the older suite were measured on biotite from the Purcell Mountain and Shiniliaok Creek plutons and hornblende from the Selawik Hills pluton. The younger-suite ages were measured on hornblende from the Indian Mountain and Zane Hills plutons and biotite from the Wheeler Creek pluton. The mineral separates from all six samples were fresh and unaltered. The plus-or-minus value assigned each age (see table 1) is the estimated standard deviation of analytical precision.

The ages for each suite agree within analytical uncertainty and indicate two distinct periods of pluton emplacement in Cretaceous time. The ages indicate that the intrusion of the older suite occurred about 100 million years ago, in about the middle of the Cretaceous (late Albian according to Folinsbee and others, 1963), and the younger suite was intruded in Late Cretaceous time, about 81 m.y. ago, according to Kulp's (1961) time scale. These results are in good agreement with a potassium-argon age reported by Patton (in press) of 102 m.y. for hornblende from monzonite of the Hunter Creek pluton which is in the northwest corner of the Candle quadrangle southwest of the Selawik Hills pluton.

The close agreement between biotite and hornblende ages for each suite indicates that the measured ages can be considered reliable crystallization ages for the igneous rocks. Thus we conclude that in west-central Alaska two periods of pluton emplacement occurred during the Cretaceous approximately 100 m.y. ago and 81 m.y. ago. The older suite is composed chiefly of saturated monzonite and syenite, and undersaturated feldspathoidal syenite, while the younger suite is

TABLE 1.—*Potassium-argon age determinations for plutonic rocks of west-central Alaska*

[Potassium analyses: 2, 4, 5-7, L. B. Schlocker and H. C. Whitehead. Argon analyses and age calculations: 2, 4-6, M. A. Lanphere; 7, M. A. Lanphere, J. D. Leutscher, and E. H. McKee. Analysis and age calculation: 9, H. H. Thomas, R. F. Marvin, and Paul Elmore]

Pluton	No. (fig. 2)	Location		Field No.	Mineral	K_2O (percent)	Ar^{40}_{rad} (10^{-10} moles/g)	$\frac{Ar^{40}_{rad}}{Ar^{40}_{total}}$	Age (m.y.)
		Lat (N.)	Long (W.)						
Indian Mountain	2	66°01′	154°06′	63APa216	Hornblende	0. 569, 0. 569 (avg 0.569)	0. 7003	0. 46	81. 5±3. 0
Zane Hills	4	66°07′30″	155°55′	63APa229	do	0. 722, 0. 708 (avg 0.715)	. 8360	. 73	81. 9±3. 0
Wheeler Creek	5	66°20′	157°37′30″	64APa96	Biotite	7. 44, 7. 46 (avg 7.45)	9. 065	. 94	80. 6±2. 0
Shiniliaok Creek	6	66°21′	157°16′	64APa92	do	8. 83, 8. 83 (avg 8.83)	13. 32	. 95	99. 4±2. 4
Purcell Mountain	7	66°15′30″	156°30′	64APa95	do	6. 87, 6. 94 (avg 6.90)	10. 33	. 92	98. 6±2. 9
Selawik Hills	9	66°08′	160°09′	61APa118	Hornblende	1. 36	2. 082	. 77	100 ±5

K^{40} decay constants: $\lambda_t = 0.585 \times 10^{-10}$ year^{-1}; $\lambda_\beta = 4.72 \times 10^{-10}$ year^{-1}.
Abundance ratio: $K^{40}/K = 1.19 \times 10^{-4}$ atom percent.

represented by quartz-bearing granodiorite and quartz monzonite.

REFERENCES

Dutro, J. T., Jr., and Payne, T. G., 1957, Geologic map of Alaska: U.S. Geol. Survey, scale 1:2,500,000.

Eakin, H. M., 1916, The Yukon-Koyukuk region, Alaska: U.S. Geol. Survey Bull. 631, 85 p.

Folinsbee, R. E., Baadsgaard, Halfdan, and Cumming, G. L., 1963, Dating of volcanic ash beds (bentonites) by the K–Ar method: Washington, D.C., Natl. Acad. Sci–Natl. Research Council Pub. 1075, p. 70–82.

Kulp, J. L., 1961, Geologic time scale: Science, v. 133, no. 3459, p. 1105–1114.

Miller, D. J., Payne, T. G., and Gryc, George, 1959, Geology of possible petroleum provinces in Alaska: U.S. Geol. Survey Bull. 1094, 131 p.

Patton, W. W., Jr., in press, Regional geologic map of the Candle quadrangle, Alaska: U.S. Geol. Survey Misc. Geol. Inv. Map I–492.

Patton, W. W., Jr., and Miller, T. P., 1966, Regional geologic map of the Hughes quadrangle, Alaska: U.S. Geol. Survey Misc. Geol. Inv. Map I–459.

Payne, T. G., 1955, Mesozoic and Cenozoic tectonic elements of Alaska: U.S. Geol. Survey Misc. Geol. Inv. Map I–84.

Schrader, F. C., 1902, Geological section of the Rocky Mountains in northern Alaska: Geol. Soc. America Bull., v. 13, p. 233–252.

Smith, P. S., 1913, The Noatak-Kobuk region, Alaska: U.S. Geol. Survey Bull. 536, 157 p.

RATE OF PALAGONITIZATION OF SUBMARINE BASALT ADJACENT TO HAWAII

By JAMES G. MOORE, Menlo Park, Calif.

Work done in cooperation with the U.S. Coast and Geodetic Survey

Abstract.—Dredge hauls of pillow basalt from three Hawaiian volcanoes and from a sublake flow in Japan indicate that palagonitization of submarine basaltic glass proceeds faster than that in fresh water, and much faster than hydration of obsidian in a subaerial environment. The thickness of palagonite as a function of time (T) in kiloyears (ky) may be defined by: $S = \sqrt{CT}$, where S is thickness in microns (μ), and C is a constant. The value of C ranges from 480 to 2,000μ^2/ky for Hawaiian submarine basalt glass. During replacement of basaltic glass by palagonite, Na, Ca, and Mn are lost, and K, Ti, and Fe are gained. The resultant chemical zoning of a palagonitized basalt pillow resembles that found in ancient metamorphosed basalt pillows and suggests that their zoning is due to palagonitization which occurred prior to metamorphism.

Many of the lava samples dredged from deep water on the flanks of the Hawaiian volcanoes are fragments of basalt pillows (Moore, 1965). Commonly the outer surface of these pillows shows two thin rinds: an inner, yellow-brown layer of hydrated and altered basalt glass (palagonite), and an outer black layer of a hydrous manganese mineral. The palagonite forms by alteration of a crust of basalt glass on the pillow and increases in thickness by replacing the glass inward from the outer surface and from the walls of cracks and vesicles. The manganese-bearing rind apparently forms by slow accumulation on the exposed basalt surfaces, with the manganese precipitating at a rather constant rate from sea water (Bender and others, 1966).

Characteristically, the submarine basalt from the youngest and most active Hawaiian volcano, Kilauea, has only a very thin rind of palagonite and no recognizable manganese rind. Basalt dredged from the older Mauna Kea volcano, however, has layers approximately 1 millimeter thick of both palagonite and manganese oxide. The difference in thickness of the layers in these two groups of samples is regarded as due to different ages. Both the replacement of basalt glass by palagonite and the accumulation of manganese are processes which proceed at definite rates.

Acknowledgments.—The Hawaiian samples were collected as part of a cooperative program between the U.S. Geological Survey and the U.S. Coast and Geodetic Survey. Dredge hauls from Kilauea Volcano were made aboard the *Pioneer*, Captain H. G. Conerly commanding, in October 1962, and those from Mauna Loa and Mauna Kea volcanoes were made aboard the *Surveyor*, Captain Don A. Jones commanding, in October 1964. The writer is grateful to the officers and crew of these Coast and Geodetic Survey vessels and to Dallas Peck and Robert Koyanagi, of the Geological Survey, who helped with shipboard operations.

Shigeo Aramaki, University of Tokyo, first conducted the writer to the Mount Fuji locality; and collecting there was done by the Tokyo Aqua Divers Club headed by Masao Kudo.

Electron-microprobe analyses were made by Bernard W. Evans, University of California, Berkeley.

LOCATION AND AGE OF SAMPLES

The most important samples have been collected from the submarine parts of 3 of the 5 volcanoes which make up the Island of Hawaii (fig. 1). These include samples from Kilauea, Mauna Loa, and Mauna Kea volcanoes. Samples have also been collected from seamounts adjacents to Hawaii. A final suite of samples was collected from a historic lava flow which flowed into a lake on the east side of Mount Fuji, Japan (fig. 2).

The samples from Kilauea volcano were taken from the submarine extension of the east rift zone and have been described elsewhere (Moore, 1965). These basalts cannot be dated directly, but there is strong evidence that they are very young. The subaerial part of the

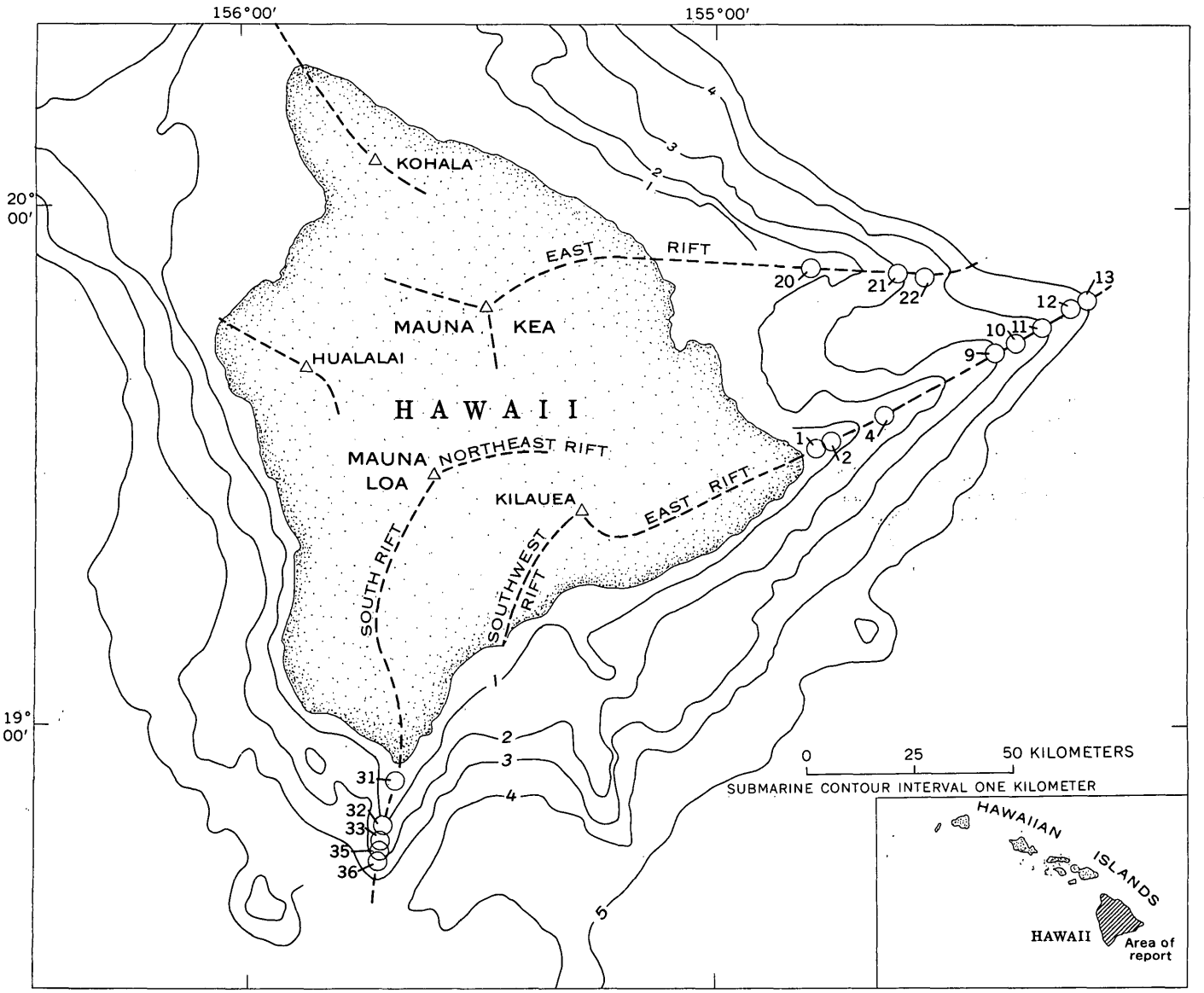

FIGURE 1.—Sample localities (numbered circles) of dredge hauls on the rift zones of Mauna Loa, Mauna Kea, and Kilauea, Hawaii Volcanoes are indicated by triangles.

east rift zone of Kilauea volcano has been very active in historic time. Since 1750, when records of eruptions began, roughly half of the subaerial crest of the rift zone has been mantled by new lava flows. Hence, the mean age of lava from the submerged part of the same rift zone is assumed to be similar, or roughly 200 years before present.

The samples from Mauna Loa volcano were collected from the submarine part of the south rift zone off the south cape of the island (fig. 1). Although Mauna Loa is presently an active volcano, the age of lava flows on its submarine southwest rift zone is difficult to estimate. Where the rift zone goes into the sea, thin and discontinuous lavas of the prehistoric member of the Kau Volcanic Series overlie rocks of the Kahuku Volcanic Series (Stearns and Macdonald, 1946). These two series are separated by the Pahala Ash, a thick widespread ash from Kilauea that has been determined by radiocarbon dating to be from 10,000 to 17,000 years old (Rubin and Berthold, 1961). Since the mantling layers of Pahala Ash and Kau Volcanic Series are concentrated on the upper parts of Mauna Loa (Stearns and Macdonald, 1946), the chances are good that most of the submarine lavas of the rift zone belong to the Kahuku Volcanic Series and are older than 10,000–17,000 years.

On the other hand, the older age limit of these rocks is more difficult to determine. McDougall (1964) has

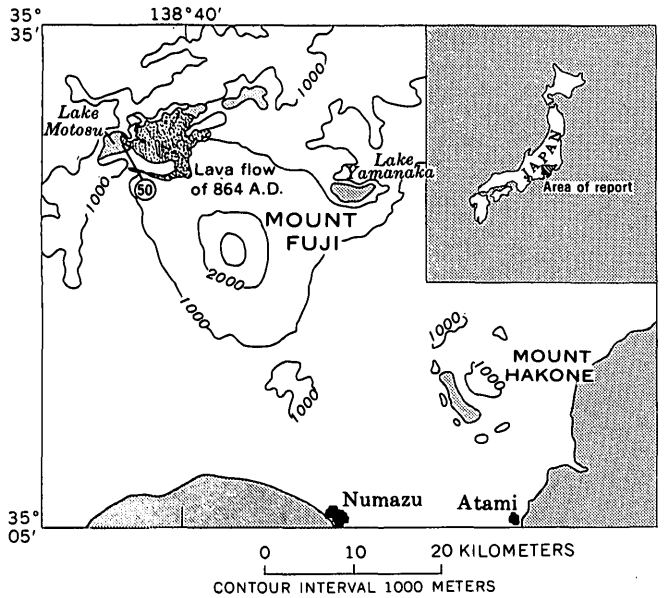

FIGURE 2.—Mount Fuji region in central Japan. Sample 50 was collected below lake level in Lake Motosu from the lava flow of 864 A.D.

determined by the potassium-argon method that lava from the deepest canyons of the oldest volcano (Kohala) on the Island of Hawaii is less than 1 million years old. Moreover, Doell and Cox (1961) have shown that all of 152 lava flows sampled from the Island of Hawaii, including those from the oldest exposed rocks of Kohala, the oldest volcano, show normal magnetic polarity. Assuming that the density of sampling precludes the omission of a polarity epoch, all of the exposed rocks are younger than the last magnetic reversal, which is estimated to have occurred 700,000 years ago (Doell and Dalrymple, 1966).

The lava flows on the east rift zone of Mauna Kea are considered to be much younger than 700,000–1,000,000 years because they occur on the upper surface of the volcano, albeit under water, and because Mauna Kea volcano is much less eroded than Kohala volcano. Likewise, the lavas of the submarine east rift of Mauna Kea volcano are believed to be older than those of the submarine south rift of Mauna Loa, because Mauna Kea is much less active, and more eroded than Mauna Loa.

The chemistry of the Mauna Kea submarine lavas is transitional between that of tholeiitic and alkalic basalt (table 1); one analyzed rock (21, table 1) is tholeiitic in composition, but two (20 and 22, table 1) have enough $K_2O + Na_2O$ to mark them as transitional between tholeiitic and alkalic basalt (Kuno, 1965). Hence, the lava collected on the east rift zone

TABLE 1.—*Standard gravimetric chemical analyses and norms of submarine basalts from Mauna Kea and Mauna Loa volcanoes*

[Analyst: Ellen S. Daniels. Location of samples shown on figure 1, petrology shown in table 2]

U.S. Geol. Survey Lab Nos.	D100696	D100697	D100698	D100694	D100695
Locality Nos.	20	21	22	31	36
Chemical analyses					
SiO_2	47.94	47.28	47.01	52.12	48.50
Al_2O_3	10.43	10.00	12.12	13.41	10.42
Fe_2O_3	2.03	2.30	2.86	2.47	1.69
FeO	9.54	9.05	9.29	9.45	9.41
MgO	17.34	19.82	12.61	5.50	17.83
CaO	7.42	7.55	8.98	8.89	7.72
Na_2O	1.99	1.59	2.36	2.97	1.76
K_2O	.39	.26	.72	.72	.32
H_2O+	.49	.39	.66	.61	.52
H_2O-	.09	.12	.41	.08	.05
TiO_2	1.98	1.46	2.48	3.17	1.59
P_2O_5	.24	.14	.27	.42	.16
MnO	.17	.17	.17	.17	.17
CO_2	.02	.01	.02	.01	.02
Cl	.10	.05	.10	.20	.03
F	.03	.02	.04	.05	.02
Subtotal	100.20	100.21	100.10	100.24	100.21
Less O	.03	.02	.04	.07	.02
Total	100.17	100.19	100.06	100.17	100.19
Norms					
Qz				6.78	
Or	2.30	1.53	4.25	4.25	1.89
Ab	16.07	13.06	19.21	23.64	14.64
An	18.73	19.54	20.72	21.91	19.66
Di Wo	6.75	7.00	9.06	7.58	7.22
Di En	4.76	5.06	6.19	4.15	5.06
Di Fs	1.42	1.30	2.15	3.15	1.55
Hy En	16.76	16.04	8.34	9.54	18.09
Hy Fs	5.00	4.10	2.90	7.24	5.53
Ol	20.10	25.29	16.33		19.82
Il	3.75	2.77	4.71	6.02	3.01
Mt	2.94	3.33	4.14	3.58	2.45
Ap	.57	.33	.64	.99	.38
Rest	.25	.13	.27	.42	.12
Total	99.40	99.48	98.91	99.25	99.42

20. East rift zone of Mauna Kea, depth 1650 m.
21. East rift zone of Mauna Kea, depth 2750 m.
22. East rift zone of Mauna Kea, depth 3200 m.
31. South rift zone of Mauna Loa, depth 550 m.
36. South rift zone of Mauna Loa, depth 2200 m.

of Mauna Kea was erupted when the volcano was changing from the primitive shield-building tholeiitic stage to the late alkalic stage. When this occurred is not known precisely, but it was long before the eruption of the Pahala Ash and occurred during the eruption of the Hamakua Volcanic Series (Stearns and Macdonald, 1946, and Macdonald and Katsura, 1964).

Lava samples were also collected from seamounts adjacent to the Island of Hawaii (Moore, 1965). There is no radiometric dating available on these rocks, but they are all highly altered and appear much

older than those recovered from Kilauea, Mauna Loa, or Mauna Kea.

A suite of samples was collected in September 1965 from a historic lava flow from Mount Fuji, Japan, where the lava poured into Lake Motosu on the northwest side of the volcano. Historic records fix the date of this eruption as 864 A.D. (Tsuya, 1938). Samples down to depths of 15 meters were broken from the flow top by divers with pry bars. According to a long-time resident of the lake area, the lake may rise as much as 3 m above the level at the time the samples were collected, but it never falls more than 1 m below that level. Hence, the samples collected more than a few meters deep had presumably not been subjected to subaerial conditions after the lava had been chilled below lake level 1,101 years before collection.

DESCRIPTION OF SAMPLES

Most of the submarine lava samples show an outer smoothly curved surface, apparently the outer surface of pillows (fig. 3). The outer surface commonly has wrinkles not unlike those of pahoehoe lava. This surface is believed to represent the original lava-flow boundary chilled against sea water. The exterior surface is coated with a rind of yellow-brown palagonite and a black manganese mineral. The manganese layer is commonly minutely botryoidal, and the

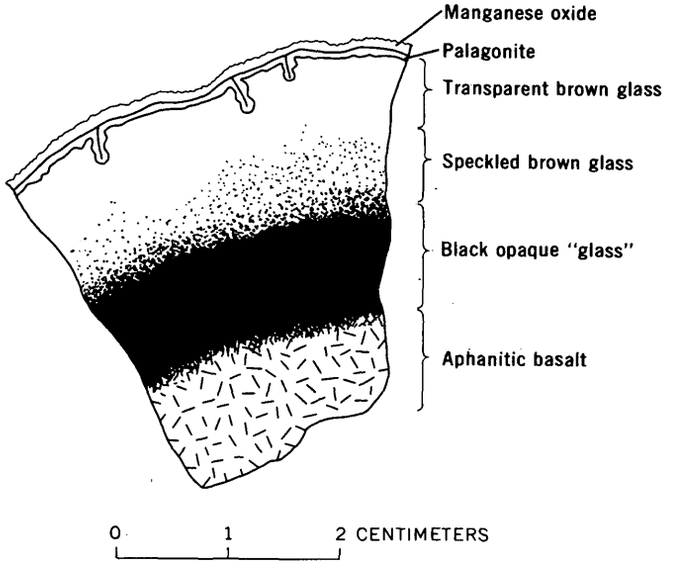

FIGURE 3.—Diagrammatic sketch of fragment of outer part of basalt pillow from the submerged flanks of Hawaiian volcanoes. The layers of transparent brown glass, speckled brown glass, and black opaque "glass" are the result of chilling of basalt against sea water. The outer rinds of palagonite and manganese oxide are the result of alteration of the glass and accumulation on the original pillow surface, respectively, after formation of the pillow. Phenocrysts and vesicles are not shown.

size of the subhemispherical elements of the surface is partly dependent on the thickness of the manganese crust. When the crust is about 1 millimeter thick, the diameter of the individual hemispherical protuberances is about ½ mm.

Most of the fragments of basaltic pillows that have been recovered have poorly developed columnar joints perpendicular to the outer smooth surface, and the joints are 2 to 5 centimeters apart and converge inward.

Thin sections show that the outer surface of the lava has been quenched. The glassy skin is composed of several distinct layers which occur inward from the rinds of palagonite and manganese (fig. 3). The outer layer of the pillows is composed of transparent light-brown basalt glass which commonly contains phenocrysts and a few microlites. The thickness of this layer is variable and no doubt depends on composition, vesicularity, and rate of quenching, but it generally ranges between 2 and 10 mm (table 2). The outer transparent glass layer is transitional to the second layer which is here called the speckled glass layer. It is composed of transparent basalt glass in which scattered black, opaque areas occur, commonly on the margins of phenocrysts and microlites. These opaque spots under high power prove to be fine feathery and dendritic crystallites. The speckled glass layer is usually 4 to 10 mm thick and is gradational to the third layer of black, opaque "glass," which is apparently made up of many tiny interfering crystallites in glass. The black, opaque layer is generally about 10 mm thick and is transitional into the stony or aphanitic material which makes up most of the interior of the pillow. Because of the regularity of these layers, the relationship of a random dredge sample to a pillow or at least its cooling surface can be determined with considerable confidence. If there is no outer transparent glass layer, then the surface in question is probably not the outer quenched layer.

The palagonite rind grows inward by replacement of the outer layer of transparent glass. Given enough time it replaces the speckled glass layer and eventually the black, opaque layer, but because of the different physical properties of these layers, especially the opaque layer, the processes of palagonitization proceed at different rates.

The palagonite layer itself is yellow brown in thin section, and shows a minute botryoidal banding convex in detail toward the inner part of the pillow. The banding may be extremely fine and parallel layers as thin as 1 micron can be identified on the inner part of 1-mm-thick palagonite rinds.

The palagonite is in sharp contact with the glass and near the contact it is generally pale yellowish to almost

TABLE 2.—*Petrology of subaqueous basalts*

Sample No.[1]	Volcano	Depth (meters)	Refractive index of transparent glass	SiO_2 (whole rock)[2]	Thickness of layers			
					Transparent glass (mm)	Speckled glass (mm)	Palagonite (microns)	Manganese oxide (microns)
1	Kilauea	490	----	50. 32	3	6	2	0
2	do	550	----	----	0	4	2	0
4	do	1, 400	1. 595	49. 44	10	9	3	0
9	do	2, 960	----	----	4	7	6	0
10	do	3, 420	----	48. 41	5	8	3	0
12	do	4, 680	1. 600	49. 16	6	6	2	0
13	do	5, 000	----	47. 68	7	10	15	0
20	Mauna Kea	1, 650	1. 600	47. 94	3	5	500	400
21	do	2, 750	1. 599	47. 28	0	1	250	1, 100
22	do	3, 200	1. 601	47. 01	5	8	700	1, 000
31	Mauna Loa	550	1. 600	52. 12	2	10	40	10
32	do	1, 100	----	----	2	8+	200	100
33	do	1, 370	----	----	0	0	0	170
35	do	1, 870	----	----	0	0	0	20
36	do	2, 200	1. 596	48. 50	4	4	180	50
50	Mt. Fuji	3 to 15	1. 596	----	7	8	9	0

[1] Kilauea sample numbers are the same as those in fig. 1 of Moore (1965).
[2] By gravimetric chemical analysis.

white and distinctly lighter in color than the pale-brown glass it replaces. Proceeding outward toward successively older layers, the palagonite becomes darker yellow brown and minutely granular in texture and is darker than the glass it replaces. It is generally isotropic, but the granular material shows faint, incipient birefringence. The index of refraction of the glass is close to 1.60 (table 2); that of the palagonite is variable and generally ranges from less than 1.59 to more than 1.65.

Preliminary electron-microprobe analyses of the transparent glass, palagonite, and manganese rinds on sample 22 from the east rift zone of Mauna Kea (table 3) show that considerable chemical change occurs when the glass is transformed into palagonite. The weight percentage of sodium in palagonite is reduced to about a third of its amount in the glass, and calcium to less than a tenth. On the other hand, potassium is enriched from 2 to 4 times in the palagonite. Apparently, in the process of palagonitization, potassium ions are absorbed from sea water, and sodium and calcium ions are lost. Qualitative electron-microprobe measurements also show that titanium and iron are enriched and manganese depleted in the palagonite relative to the glass which it replaces.

These analyses are of particular interest because of their bearing on the origin of the chemical zoning of ancient basalt pillows. Bailey and others (1964, p. 52) show for the pillow basalts of the Franciscan Formation in California that Na_2O and CaO decrease from core to rim and MgO and K_2O increase. They attribute this change to alkali transfer acting across the thermal gradient from core to rim of a still-hot pillow. The analyses of table 3 suggest that the chemical zonation could be achieved by later palagonitization of the rim of cold pillows with attendant chemical change. Later metamorphism to the greenschist facies would reconstitute the palagonite into silicate minerals and produce the zonation so commonly observed in ancient pillows.

Moreover, the decrease in manganese in the palagonite, as well as the decrease in manganese of more thoroughly altered submarine basalts (Moore, 1965, p. 47), is a potential source for the manganese which is continually accumulating in deep-sea sediments as crusts on exposed rock and as nodules.

TABLE 3.—*Electron-microprobe analyses of transparent glass, palagonite, and manganese oxide layers in sample 22, east rift zone of Mauna Kea*

[Analyst, B. W. Evans, University of California, Berkeley. Location of samples shown on figure 1, description in table 2]

Run No.	Part of sample 22	Weight percent		
		Na	Ca	K
1	Transparent glass	1. 9	7. 4	0. 9
2	do	1. 9	7. 4	. 9
3	Palagonite rind	. 7	. 4	2. 8
4	do	. 8	. 7	1. 3
5	do	. 4	. 5	3. 0
6	do	1. 2	. 3	3. 5
7	do	. 4	. 4	3. 5
8	do	. 9	. 7	1. 7
9	do	. 5	1. 2	2. 7
10	do	. 4	. 5	3. 3
11	Manganese rind	1. 5	3. 4	. 5
12	do	1. 4	3. 3	. 4
13	do	1. 6	3. 5	. 5

The samples from Kilauea volcano are the freshest examined. No manganese rinds were identified from 15 dredge hauls on the east rift zone of Kilauea. The thickest palagonite rind on the Kilauea material is 15 microns (sample 13); all the other samples have thinner layers, the thinnest being about 2 microns thick (table 2). The 15-micron layer is thick enough to impart its light-brown color (5YR5/6; Goddard and others, 1948) to the surface of the pillow. However, when the palagonite is only a few microns thick, the black hue of the glass beneath it shows through, and the surface of the pillow appears dark yellowish brown (10YR4/2) to grayish brown (5YR3/2).

Samples from the south rift of Mauna Loa are coated with 40 to 200 microns of palagonite and clearly show manganese layers from 10 to 170 microns thick.

Samples from the east rift of Mauna Kea have palagonite rinds 250 to 700 microns thick and manganese rinds from 400 to 1,100 microns thick.

Samples from the seamounts adjacent to Hawaii are highly altered and cemented with calcareous and phosphatic material. None of them contains the glassy outer layers, and no rinds of palagonite can be identified as such. Manganese oxide rinds of varying thicknesses are present on most of this material except that which is so unconsolidated that its surface probably flakes off continually. The thickest manganese layers measured are 9 mm (9,000 microns), but commonly fragments are coated with several millimeters of manganese oxide, and breccias have individual fragments coated with manganese before cementation.

Samples from Lake Motosu in Japan are different from the other samples in that the lava-flow surface is not pillowed, but rather is blocky with poorly developed bread-crust texture. The rock below lake level is very glassy with onionskin fracture.

In thin section the difference is also apparent in the minute fractures which extend inward several millimeters from the surface. These fractures are about 0.1 mm apart, and the walls of all are palagonitized, giving the effect in hand specimen that the orange palagonite layer is several millimeters thick. The original cracks are visible as median hairlines in palagonite veins. As the edge of the basalt is approached, the palagonite veins are closer together, slightly thicker, and change from pale yellow to dark orange brown with granular texture. In the interior most of the veins are about 14 microns thick, but toward the outside they attain a thickness of 18 microns. The palagonite layer is half of the vein thickness, or 7 to 9 microns, as the palagonite grew out from each wall of the crack.

RATE OF GROWTH OF PALAGONITE

Recently, Bender and others (1966) have shown by thorium-230 dating of both deep-sea sediments and of manganese nodules that the rate of manganese deposition is nearly constant in the world's oceans. They estimate that the growth rate of manganese nodules is about 3 mm per million years. Hence, by measuring the thickness of the manganese rind on submarine lavas a method of approximating their age is available.

Friedman and Smith (1960) have demonstrated that obsidian (rhyolitic volcanic glass) will take up water from the atmosphere to form a hydrated surface layer. They demonstrated in their work with obsidian artifacts of known age that the hydration process is time dependent and may be used to date artifacts of unknown age. Hydration of obsidian, like palagonitization, is a diffusion process and may be expressed by: $S = \sqrt{CT}$, where S is the thickness of the surface layer produced (either hydrated obsidian or palagonite), C is a constant, and T is the time since the process began. If S is expressed in microns (μ) and T in thousands of years or kiloyears (ky), then C for obsidian ranges from 0.36 to 14 μ^2/ky (Friedman and Smith, 1960, p. 492). The higher values of C occur in warmer climates as shown in figure 4. Other than temperature, factors such as humidity, chemical composition of the obsidian, and erosion of the hydrated layer (as by wind abrasion) can be important in affecting the thickness of the hydrated layer.

The processes involved in palagonitization are not fully understood because they involve not only hydration of the basaltic glass, but exchange of certain elements with sea water and progressive devitrification and crystallization of the resultant product. However, since the palagonitization proceeds inward from the outer surface of pillows and from the walls of cracks as a diffusion process, its thickness is assumed to also be proportional to the square root of time.

The temperature factor is probably not important for samples collected from the top surface of lava flows such as those described in this report. The lavas show evidence of drastic chilling as evidenced by the outer rim of quenched transparent glass. The extremely minute layers of palagonite on the very young Kilauean samples demonstrate that significant amounts of palagonite do not form on the surface of the top pillows during the eruptive episode. The ocean-water temperatures in the environment where the basalt was dredged are known to be low and relatively constant. Reid (1965) reports that water temperature in the Hawaiian region is 1.5°C at 5,000 m, 2°C at 2,500 m, and 6°C at 700 m. It is probable, on the other hand,

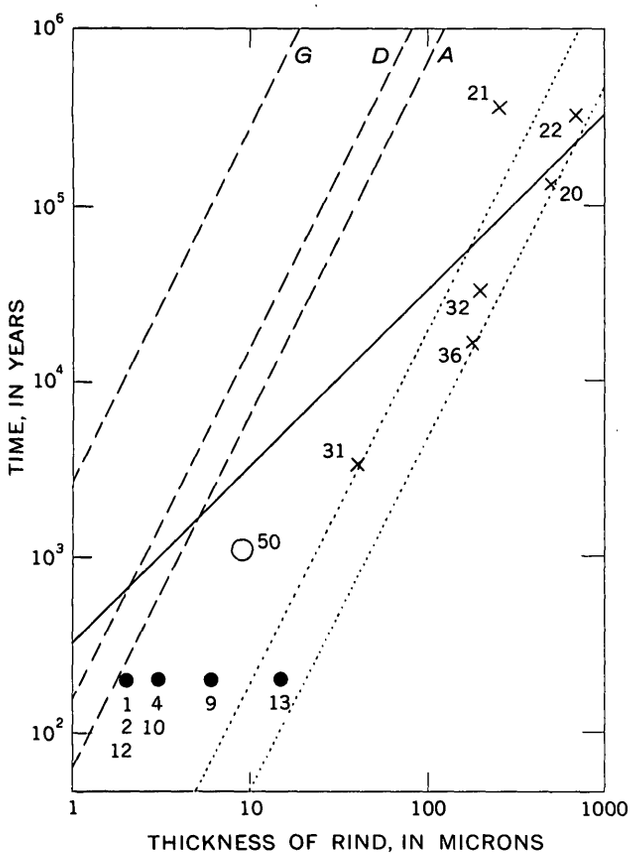

FIGURE 4.—Thickness of palagonite rinds, in microns, of subaqueous basalts. Mauna Kea and Mauna Loa samples (×) are dated by thickness of manganese oxide rind according to the curve of Bender and others (1966) (solid line). Kilauea samples (dots) are assumed to be 200 years old (see text). Mount Fuji sample (No. 50) is shown by circle. Dashed lines are rates of hydration of obsidian, after Friedman and Smith (1960), for dry climate (Egypt, trachyte, *A*), temperate climate (*D*), and arctic climate (*G*). Dotted lines are rates of submarine palagonitization based on Mauna Loa and Mauna Kea samples.

that high temperatures within a thick sequence of submarine lava that erupted during a short time interval might be maintained long enough to cause significant rapid palagonitization, but such material would not be available for collection by conventional dredging techniques.

The chemical composition of the glass controls, to an important degree, the rate of hydration. Many submarine basalts have a restricted composition, and the refractive index of the glass is a guide to significant differences in composition. Likewise, the stage of crystallization of the glass is important in its future alteration history. Transparent glass, rather than speckled or opaque, should be used for measurements of palagonite growth.

The erosion factor, an important consideration in the studies of Friedman and Smith (1960), because of removal of the hydrated layer in their material by wind and other processes of abrasion, no doubt operates also in the deep sea. Ocean currents causing rolling of bottom particles, one against another, may cause significant erosion of either the fragile palagonite or manganese rinds. Such a process would be indicated by reduction in thickness of the transparent glass layer. Material broken from an outcrop during dredging would be less likely to be eroded than loose fragments, but unfortunately most dredge hauls are composed principally of the latter.

Other factors, not applicable in the subaerial hydration of obsidian, are local changes in the chemistry and pH of sea water, perhaps caused by upwelling or descending currents, and the sealing effect of the outer manganese layer on the growing palagonite.

The hydration curves of Friedman and Smith (1960) in terms of the thickness of the hydration rind on obsidian of known age are plotted in figure 4. On the same plot is the tentative curve of manganese nodule growth of Bender and others (1966), which is 3 mm per million years.

The dredge samples from Kilauea volcano have been plotted in figure 4, assuming that the age of all is 200 years, for reasons stated earlier. The Mauna Loa and Mauna Kea samples have been plotted, assuming their age to be proportional to their manganese oxide rind thickness as determined from the curve of Bender. The Mount Fuji sample has been plotted at its known age; because it is in a fresh-water lake, no manganese rind is present.

It is immediately apparent that the rate of palagonitization of basalt is considerably more rapid than hydration of obsidian. Five of the Mauna Kea and Mauna Loa data points (fig. 4) can be included between two rather close lines parallel to the curves of Friedman and Smith (thickness proportional to the square root of time). The sixth point, that of sample 21, is ignored because it has no transparent glass (table 2); it has apparently undergone abrasion, and the palagonite has replaced the speckled glass at a slower rate. These curves indicate that the palagonite forms much faster than does the hydrated rim on obsidian; the constant C ranges from 480 to 2,000 μ^2/ky. C for obsidian ranges from 0.36 to 14μ^2/ky.

The fresh-water palagonitization of the Mount Fuji basalt is slower than that of the submarine basalt, and $C = 81\mu^2$/ky. Perhaps the fresh-water environment is chemically less reactive despite the fact that the water is warmer (17°C in the summer) than water in

the deep marine environment. Van Lier and others (1960) have shown that the solubility of quartz is greatly accelerated by the presence of NaCl.

DISCUSSION AND CONCLUSIONS

Since palagonitization of the top surface of pillow basalt proceeds at a slow and definite rate, it is considered to be a process of submarine weathering[1]; indeed, it is one of the important processes of such weathering. The limited data available on palagonitization in the deep submarine environment make it impossible to define the details of the process precisely, but enough data are available to approximate the rate and chemistry involved.

For the Hawaiian submarine basalts with chilled transparent glass with a refractive index of 1.598± 0.003, palagonitization proceeds faster than for similar basalt in a fresh-water environment and much faster than does the hydration of obsidian in a subaerial environment. The constant C in the equation $S = \sqrt{CT}$ ranges from 480 to 2,000 μ^2/ky.

During replacement of basalt glass by palagonite, sodium, calcium, and manganese are lost, and potassium, titanium, and iron are gained, apparently through exchange with sea water. The resultant chemical zoning of a palagonitized basalt pillow resembles that found in ancient metamorphosed basalt pillows and suggests that their zoning is due to palagonitization which occurred prior to metamorphism.

Thickness of the manganese layers indicates an age (Bender and others, 1966) of 130,000 to 360,000 years for the 3 Mauna Kea samples and 2,300 to 56,000 years for the Mauna Loa samples. These ages are in general agreement with the limitations imposed by available dating and therefore support the concept of Bender and others that manganese is accumulating at a rather constant rate. However, further work will no doubt refine the rate of accumulation of manganese, and consequently the rate of growth of palagonite will have to be modified accordingly.

The lack of manganese on all of the samples of young lava from the active submarine east rift zone of Kilauea volcano suggests that the manganese is not formed by rapid accumulation from submarine volcanic exhalations as suggested by Bonatti and Nayudu (1965). Instead, chemical analyses of layers of palagonite compared to analyses of unaltered basaltic glass suggest that much of the manganese may be released from basaltic glass by the palagonitization process and transferred to sea water, where it is free to later accumulate on the sea floor.

The extreme thinness of the palagonite layers on some of the Kilauea samples is not consistent with their assumed age of 200 years. If the palagonite growth curve is correct, the lava samples with 2 microns of palagonite would be only a few years old, and indeed may actually be submarine equivalents of recent major eruptions of Kilauea volcano, such as those of 1924, 1955, and 1960.

The rapid palagonitization of submarine basalt glass demonstrated here requires an explanation for the rare occurrences of ancient unpalagonitized basalt glass. Brew and Muffler (1965) described an Upper Triassic undevitrified submarine basaltic glass from southeastern Alaska. This material occurs in a bedded aquagene tuff which is tightly cemented by calcite. Brew and Muffler (1965, p. C43) reason that the preservation of this glass may be due to the calcite cementation, which would inhibit the circulation of water through the tuff. In any event, such bedded material was no doubt rapidly deposited and buried, and in that way differs markedly from the pillow basalts collected from ridge crests adjacent to Hawaii which have been exposed directly to sea water continuously since the eruption which produced them.

[1] Submarine weathering is here defined as the group of processes, such as the chemical action of sea water and organisms, and the mechanical action of organisms and of changes in temperature, whereby rocks on exposure to sea water at depth change in character, decay, and finally crumble into loose material.

REFERENCES

Bailey, E. H., Irwin, W. P., and Jones, D. L., 1964, Franciscan and related rocks, and their significance in the geology of western California: California Div. Mines and Geology Bull. 183, 177 p.

Bender, M. L., Teh-Lung Ku, and Broecker, W. S., 1966, Manganese nodules—their evolution: Science, v. 151, p. 325–328.

Bonatti, E., and Nayuda, Y. R., 1965, The origin of manganese nodules on the ocean floor: Am. Jour. Sci., v. 263, p. 17–39.

Brew, D. A., and Muffler, L. J. P., 1965, Upper Triassic undevitrified volcanic glass from Hound Island, Keku Strait, southeastern Alaska, *in* Geological Survey Research 1965: U.S. Geol. Survey Prof. Paper 525–C, p. C38–C43.

Doell, R. R., and Cox, Allan, 1961, Paleomagnetism of Hawaiian lava flows: Nature, v. 192, p. 645–646.

Doel, R. R., and Dalrymple, G. B., 1966, Geomagnetic polarity epochs—a new polarity event and the age of the Brunhes-Matuyama boundary: Science, v. 152, no. 3725, p. 1060–1061.

Friedman, I. I., and Smith, R. L., 1960, A new dating method using obsidian; pt. I, The development of the method: Am. Antiquity, v. 25, p. 476–522.

Goddard, E. N., and others, 1948, Rock-color chart: Rock-color Chart Comm., Natl. Research Council, Washington D.C., 11 p.

Kuno, Hisashi, 1965, Fractionation trends of basalt magmas in lava flows: Jour. Petrology, v. 6, pt. 2, p. 302–321.

van Lier, J. A., de Bruyn, P. L., and Overbeek, J. Th. G., 1960, The solubility of quartz: Jour. Phys. Chemistry, v. 64, p. 1675–1682.

Macdonald, G. A., and Katsura, Takashi, 1964, Chemical composition of Hawaiian lavas: Jour. Petrology, v. 5, p. 82–133.

McDougall, Ian, 1964, Potassium-argon ages from lavas of the Hawaiian Islands: Geol. Soc. America Bull., v. 75, p. 107–128.

Moore, J. G., 1965, Petrology of deep-sea basalt near Hawaii: Am. Jour. Science, v. 263, p. 40–52.

Reid, J. L., Jr., 1965, Intermediate waters of the Pacific Ocean: Baltimore, Md., The Johns Hopkins Press, 85 p.

Rubin, Meyer, and Berthold, S. M., 1961, U.S. Geological Survey radiocarbon dates VI: Radiocarbon, v. 3, p. 86–98.

Stearns, H. T., and Macdonald, G. A., 1946, Geology and groundwater resources of the Island of Hawaii; Hawaii Div. of Hydrography Bull. 9, 363 p.

Tsuya, Hiromichi, 1938, Geological an petrological studies of Volcano Huzi (Fuji); II. Distribution of the Aokiya-hara lava and its vent: Earthquake Research Inst. Bull., v. 16, p. 638–657.

224-352 O—66——12

SIGNIFICANT CHANGES IN VOLCANISM DURING THE CRETACEOUS IN NORTH-CENTRAL PUERTO RICO

By A. E. NELSON, Beltsville, Md.

Work done in cooperation with the Economic Development Administration of Puerto Rico

Abstract.—During Late Cretaceous time in north-central Puerto Rico the environment of deposition changed from marine to mostly subaerial. Chemical analyses show continuous variation in the composition of Cretaceous volcanic rocks. The submarine volcanic rocks are mostly basalt and andesite; most of the later subaerially deposited rocks are dacite and rhyolite.

Cretaceous lava, lava breccia, and tuff deposits, ranging in composition from basalt to rhyolite, are exposed within a 285-square-mile area in north-central Puerto Rico (fig. 1). This area, centered about 30 miles west-southwest of San Juan, is on the north flank of the main west-trending anticlinal axis of the island. Within this area abrupt facies changes and complex intertonguing relations between formations and members of formations characterize the stratigraphy of the Cretaceous rocks. Although faulting has displaced some contacts, field studies show that the stratigraphic succession is chiefly conformable.

The stratigraphic units of volcanogenic rocks discussed in this report range in age from Albion to Maestrichtian. They include the Río Orocovis Group (Nelson, in press), Pozas Formation (Berryhill, 1965), and the Mameyes and Alonso Formations (Nelson and Monroe, in press). Formations of the Río Orocovis Group and the Mameyes Formation are exposed in the eastern and southwestern parts of the report area in north-central Puerto Rico (fig. 1), where they have a total thickness of more than 5,000 meters. They contain the principal deposits of subaqueously deposited lava and basaltic tuff. The lava flows are chiefly basalt and andesite, but the basaltic lavas include some basaltic andesite, and the andesitic lavas include some dacite. The overlying rocks in the central and northern parts of the report area (fig. 1), the Pozas and Alonso Formations (Berryhill, 1965, p. 49–61; Nelson and Monroe, in press), have a stratigraphic thickness of more than 2,500 m. The Pozas and Alonso Formations include some marine-deposited andesitic lava flows in their lower parts, but in their upper part they contain subaerial pyroclastic deposits that range in chemical composition from dacite to rhyolite.

Chemical analyses of 26 samples collected from formations of the Río Orocovis Group, and from the Mameyes, Alonso, and Pozas Formations show that there is a continuous chemical variation from the older basalt lava flows to the younger rhyolitic tuffs.

GENERAL CHARACTERISTICS AND STRATIGRAPHIC RELATIONS OF CRETACEOUS FORMATIONS

Río Orocovis Group

Formations of the Río Orocovis Group consist principally of volcanic sandstone and siltstone, basalt and andesite lava, and basaltic tuff. The Río Orocovis Group has been divided into four formations, each chiefly composed of one of the main rock types, but containing small interbedded units of the other rock types common to the group. Parts of some formations are time equivalents; some intertongue laterally, and, in places, the upper part of one is interlayered with the lower part of the overlying formation. Although the Río Orocovis is mostly Late Cretaceous (Berryhill, 1965, p. 45), it probably ranges from Turonian(?) to late Santonian or early Campanian.

Rocks of the Río Orocovis are believed to be of submarine origin. The lava flows are commonly pillowed and have sedimentary interpillow material that indicates subaqueous eruption (Rittman, 1962, p. 70–73).

U.S. GEOL. SURVEY PROF. PAPER 550-D, PAGES D172-D177

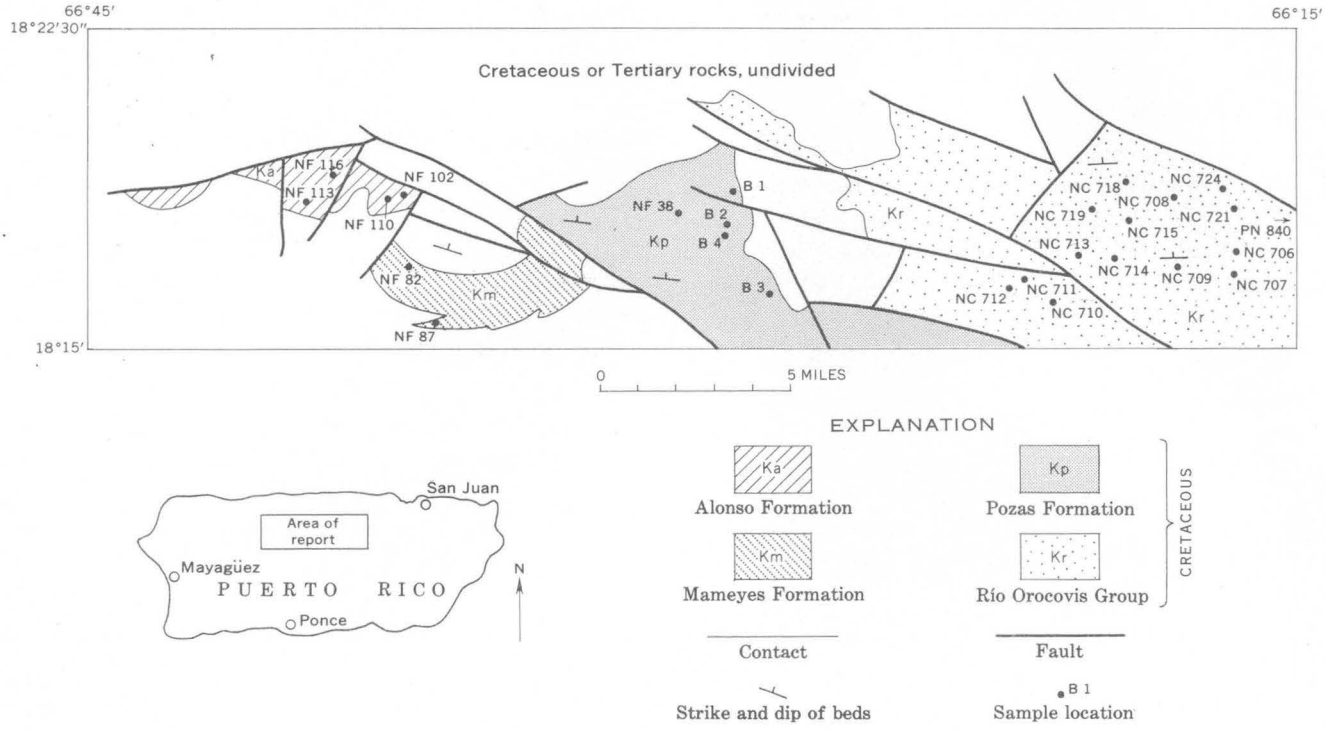

FIGURE 1.—Generalized geologic map of north-central Puerto Rico.

The basaltic tuffs are mostly massive and crudely sorted with coarser fragments near the base, but they are not well sorted and layered as are normal airborne water-laid tuffs. Although the basaltic tuffs locally contain a high percentage of pumice fragments and shards, the pumice is not unduly crushed nor the shards deformed; these tuffs lack textures characteristic of subaerially deposited welded ash flows. The basaltic tuffs in many respects resemble the aquagene tuffs described by Carlisle (1963) and probably have a similar origin. Foraminifera found in the basaltic tuffs by Berryhill (oral commun., 1961) strengthen this view. Graded volcanic sandstone and siltstone interbedded with the lava flows and basaltic tuff also suggest that these rocks were deposited in water.

Mameyes Formation

The Mameyes Formation is a sequence of andesitic lava flows containing some basalt flows and interbeds of volcanic sandstone and siltstone. It is similar in lithology to the upper part of the Río Orocovis Formation and occupies a comparable stratigraphic position, but the two formations cannot be positively correlated because they are separated by a conspicuous fault. The Mameyes Formation is Late Cretaceous in age and is also believed to be marine (Nelson and Monroe, in press).

Pozas Formation

The Pozas Formation is a heterogeneous mixture of volcanic rocks that includes volcanic breccia, conglomerate, volcanic sandstone and siltstone, reef and near-reef deposits of limestone, laharic deposits, ash flows, and some lava flows. The lavas, most of which occur in the lower part of the formation, are andesitic, and the ash flows, which occur higher in the formation, are dacitic. The formation has been assigned a Campanian to Maestrichtian age (Nelson and Monroe, in press).

Except for a subaqueous lava flow in the lower part and a shallow-water reef limestone deposit higher in the formation, most of the Pozas is subaerial (Berryhill, 1965, p. 58). Pillowed andesitic flows in the basal part of the formation are similar to lavas of the Río Orocovis Group and probably have a similar origin. Higher in the formation, however, andesite flows are massive and have a decided reddish-purple cast. This color is characteristic of the volcanic breccias, the subaerially deposited laharic deposits, and welded ash flows overlying the pillowed lava flows. It probably indicates that oxidizing conditions prevailed during the deposition of these rocks. Thus, it is suggested that early Pozas time was an important transitional period when the environment of deposition changed from submarine to subaerial. Prior to this time, most of the Cretaceous

rocks were subaqueously deposited, whereas those formed later were mostly subaerially deposited.

Alonso Formation

The Alonso Formation is similar to the Pozas Formation and contains most of the same rock types. As in the Pozas, the lavas in the Alonso are andesitic and the welded ash flows range from dacite to rhyolite in composition. The Alonso conformably overlies rocks that rest on the Mameles and occupies the same relative stratigraphic poisition as the Pozas. However, the Alonso cannot be positively correlated with the Pozas because they are in fault contact. The Alonso is Late Cretaceous in age and is believed to be mostly subaerial.

CHEMICAL RELATIONS OF THE VOLCANIC ROCKS SAMPLED

Twenty-six chemical analyses of Cretaceous volcanic rocks from north-central Puerto Rico are given in table 1. The 15 samples from the Río Orocovis Group have compositions ranging from basalt to dacite. The rocks tentatively identified as basalt have pyroxene

TABLE 1.—*Chemical analyses of volcanic*

[Samples analyzed by methods described by Shapiro and Brannock (1956, 1962).

	Río Orocovis Group											
	Basaltic tuff	Basalt	Basaltic tuff	Basalt flow breccia	Basaltic tuff	Basalt	Basalt	Basaltic tuff	Andesite	Andesite	Andesite	Dacite
Field No.	NC 706	NC 713	NC 709	NC 708	NC 707	NC 712	PN 840	NC 710	NC 721	NC 724	NC 711	NC 714
Lab No.	158712	158719	158715	158714	158713	158718	158699	158716	158726	158729	158717	158720
SiO_2	44.8	46.4	4.66	48.0	48.6	48.8	48.8	49.7	50.7	51.0	52.7	53.9
Al_2O_3	9.0	9.7	10.1	12.8	14.3	14.4	15.8	14.2	16.1	18.0	17.6	15.2
Fe_2O_3	2.3	5.4	3.6	4.0	3.0	4.4	2.7	2.8	1.6	4.8	2.6	1.9
FeO	7.6	3.3	7.1	6.3	6.8	4.6	5.4	6.4	7.4	3.9	4.7	6.3
MgO	19.7	7.2	15.0	7.9	9.4	5.4	5.3	7.5	5.3	3.9	3.8	3.3
CaO	9.8	16.1	10.7	16.0	8.6	8.3	7.9	8.6	9.5	8.0	5.0	5.2
Na_2O	.88	2.8	1.5	1.6	2.9	2.3	3.9	4.0	2.8	3.4	2.4	3.3
K_2O	.44	.95	1.0	.47	1.7	5.1	3.2	1.4	1.0	3.8	6.7	1.8
H_2O-	.46	.51	.26	.27	.30	.3	.2	.47	.87	.10	.30	.37
H_2O+	3.9	1.3	2.2	1.2	2.8	2.2	2.3	2.8	1.8	1.4	2.2	3.2
TiO_2	.55	.58	.64	.70	.82	.72	.85	.84	1.0	.88	.67	.92
P_2O_5	.19	.22	.28	.20	.47	.58	.59	.26	.26	.39	.65	.50
MnO	.17	.14	.20	.22	.19	.15	.17	.17	.20	.20	.16	.19
CO_2	.05	5.6	.05	.06	.05	2.4	2.6	.82	.16	.06	.30	3.5
Sum	100	100	99	100	100	99	100	100	99	100	100	100
Powder density by air pycnometer	3.06	----	3.06	3.14	3.01	----	3.08	2.92	2.87	2.91	2.75	2.77

NC 706. Basaltic tuff. Greenish-dark-gray tuff containing large fragments of clinopyroxene (augite(?)) in a very fine grained groundmass of crushed and partly devitrified pumice, minor microcrystalline material with faint polarization tints, and irregular patches of minute fragments of clinopyroxene and plagioclase.

NC 713. Basalt. Dark-grayish-black pillow lava containing numerous augite phenocrysts in a groundmass rich in small grains of augite with some thin laths of albite. Tiny grains of an opaque mineral, probably magnetite, are also widely dispersed. Locally, veinlets and patches of calcite are present.

NC 709. Basaltic lapilli tuff. Dark-greenish-black lapilli tuff containing fragments of basalt in matrix rich in clinopyroxene (augite(?)) crystals and fragments, partly devitrified glass, and unevenly distributed clusters of faintly birefringent material. Locally clinopyroxene is uralitized or chloritized.

NC 708. Basalt flow breccia. Dark-grayish-black flow breccia composed of fragments of clinopyroxene phenocryst basalt; aggregates of clinopyroxene and faintly crystalline material between various sized lava fragments. Locally some sericitized plagioclase is present, and, in places, patches of chlorite occur.

NC 707. Basaltic tuff. Greenish-black crystal lithic tuff rich in clinopyroxene fragments. Matrix mostly contains very fine grained dark microcrystalline material. Locally patches of fine grains of clinopyroxene and sericitized plagioclase are present. Lithic fragments are mostly very fine grained basalt.

NC 712. Basalt. Dark-greenish-gray lava containing numerous phenocrysts of clinopyroxene (augite(?)) in a fine-grained groundmass of tiny laths of albite, microcrystalline material, and grains of clinopyroxene. Magnetite and tiny grains of ilmenite(?) are widely distributed in groundmass. K-feldspar is present as irregular clusters as is calcite.

PN 840. Basalt. Dark-greenish-gray amygdaloidal lava containing clinopyroxene phenocrysts in very fine grained groundmass. Calcite occurs in amygdules. Sample collected by M. R. Pease, Jr.

NC 710. Basaltic lapilli tuff. Dark-greenish-gray clinopyroxene-rich tuff. Contains numerous fragments of fine-grained basalt lava, clinopyroxene fragments and crystals, and some sericitized calcic plagioclase. Matrix consists mostly of tiny clinopyroxene fragments and much dark, faintly crystalline patches. Locally, chlorite has formed, and veinlets and clusters of calcite are present.

NC 721. Andesite. Dark-green plagioclase (An_{54}) phenocryst lava with glomeroporphyritic texture. A few clinopyroxene phenocrysts are also present. The groundmass has an intergranular texture and contains a high percentage of clinopyroxene grains and small calcic plagioclase laths. Patches of chlorite are present.

NC 724. Andesite. Dark-gray finely vesicular plagioclase phenocryst lava. Also contains some clinopyroxene phenocrysts. Calcic plagioclase is highly sericitized and some of the clinopyroxene chloritized. The groundmass is fine grained and contains some K-feldspar and small quartz grains.

NC 711. Andesite. Dark-greenish-gray plagioclase phenocryst lava with glomeroporphyritic texture. Also contains

phenocrysts. The chemical analyses show that these rocks actually range in composition from basalt to basaltic andesite. Rocks provisionally identified as andesite in the field are plagioclase phenocryst lavas. Chemical analyses show that they range from andesite to dacite. Samples of lava breccia and pyroxene-bearing tuff have basaltic compositions.

Most of the Río Orocovis rocks are abnormally high in potassium content and have alkaline tendencies (P. H. Mattson, written commun., 1964), but some of the lava flows are spilitic (Lidiak, 1965, p. 60). According to the classifications of Poldervaart (1964), both alkali and tholeiitic basalts are present. The Río Orocovis rocks grade continuously in composition from basalt to andesite. In general, the more mafic rocks occur in the lower part of the group and the more felsic rocks in the higher part, but this is not true in all cases.

The two analyzed rocks from the Mameyes Formation have compositions similar to the intermediate andesites in the Río Orocovis Group.

The nine analyzed rocks from the Pozas and Alonso Formations range in composition from andesite to

rocks from north-central Puerto Rico

Analysts: Paul Elmore, Ivan Barlow, Samuel Botts, Gillison Chloe, Lowell Artis, H. Smith]

Rio Orocovis Group—Continued			Mameyes Formation		Alonso Formation				Pozas Formation				
Dacite	Dacite	Dacite	Dacite	Andesite	Crystal and lithic tuff	Crystal and lithic tuff	Tuff	Welded tuff	Andesite	Andesite	Dacitic andesite	Dacitic tuff	Dacitic tuff
NC 718	NC 715	NC 719	NF 87	NF 82	NF 110	NF 102	NF 116	NF 113	NF 38	B1	B4	B2	B3
158724	158721	158725	160939	160937	160943	160940	160946	160945	160947	154665	154669	154668	154662
58. 3	62. 7	64. 2	51. 6	52. 2	57. 2	58. 1	70. 9	71. 2	50. 4	54. 5	59. 5	63. 7	69. 1
17. 5	16. 0	15. 4	16. 0	17. 6	18. 8	18. 3	14. 0	14. 3	17. 2	17. 4	16. 0	16. 5	15. 7
2. 6	3. 0	1. 6	3. 5	4. 2	3. 5	2. 5	2. 8	1. 6	5. 9	6. 6	5. 5	3. 7	3. 3
2. 4	2. 2	3. 6	6. 3	4. 0	3. 6	4. 1	. 55	. 74	4. 7	. 91	1. 2	1. 0	. 26
1. 6	1. 3	2. 0	4. 2	4. 2	1. 6	3. 1	. 46	. 45	5. 3	2. 5	2. 9	1. 3	. 24
2. 3	6. 2	2. 3	6. 0	7. 1	5. 6	3. 8	1. 4	. 82	8. 7	5. 6	3. 6	2. 2	. 84
4. 4	4. 2	2. 3	4. 2	3. 0	4. 0	2. 8	4. 5	2. 4	2. 6	3. 4	2. 2	4. 2	7. 1
7. 0	1. 3	5. 8	3. 0	4. 7	1. 8	3. 6	2. 6	6. 2	1. 2	3. 8	2. 2	4. 2	2. 0
. 16	. 38	. 25	. 22	. 11	. 16	. 18	. 16	. 14	. 74				
1. 3	1. 7	1. 7	2. 1	. 86	2. 0	1. 6	. 74	. 74	1. 7	3. 0	5. 6	2. 2	1. 0
. 64	. 58	. 58	1. 2	. 78	. 78	. 87	. 62	. 35	. 97	. 66	. 74	. 74	. 64
. 40	. 20	. 20	. 96	. 72	. 60	. 43	. 18	. 05	. 28	. 44	. 40	. 22	. 17
. 16	. 14	. 14	. 22	. 16	. 12	. 14	. 08	. 08	. 17	. 21	. 18	. 15	. 10
1. 4	. 05	. 05	. 05	. 05	. 05	. 05	. 73	. 07	. 08	1. 0			
100	100	100	99	100	100	99	100	99	100	100	100	100	101
2. 66	2. 78	2. 69											

a few clinopyroxene phenocrysts. Plagioclase phenocrysts are sericitized. Groundmass is fine-grained with hyalopilitic texture. Locally, K-feldspar is present in groundmass and calcite occurs in tiny clusters and veinlets.

NC 714. Dacite. Dark-gray plagioclase (An_{30}) phenocryst pillow lava, in part vesicular. Locally, feldspars altered to sericite. The groundmass, which is fine grained and has an intersertal texture, contains K-feldspar, ilmenite, magnetite, chlorite, and calcite.

NC 718. Dacite. Dark-grayish-green plagioclase (An_{28}) phenocryst pillow lava that also contains a few clinopyroxene phenocrysts. The groundmass, with an intersertal texture, is fine grained and contains much devitrified, weakly birefringent material. Opaque mineral grains (probably magnetite) are widely dispersed.

NC 715. Dacite. Dark-green finely vesicular plagioclase (An_{35}) phenocryst pillow lava. Locally, sparse clinopyroxene phenocrysts are present. Groundmass is fine grained with an intersertal texture. Sericite, calcite, and chlorite are present.

NC 719. Dacite. Dark-gray to purple lava that contains numerous slender slightly sericitized plagioclase (An_{36}(?)) phenocrysts in fine-grained groundmass.

NF 87. Dacite. Dark-gray plagioclase (An_{6-8}) phenocryst lava with glomeroporphyritic texture. Groundmass is fine to medium grained with intergranular texture. Groundmass mostly contains thin laths of plagioclase, stubby grains of clinopyroxene, and some minor K-feldspar.

NF 82. Andesite. Light-bluish-gray plagioclase (An_{35}(?)) phenocryst lava that also contains some clinopyroxene phenocrysts. Groundmass, which has an intersertal to intergranular texture, is fine grained with numerous calcic plagioclase laths; it also contains some K-feldspar.

NF 110. Crystal and lithic tuff. Reddish tuff containing plagioclase (An_{41-48}) fragments and crystals, lava fragments, and some clinopyroxene fragments in a devitrified glassy matrix. The matrix is a dark very fine grained weakly birefringent material.

NF 102. Crystal and lithic tuff. Reddish tuff containing plagioclase (An_{42-50}) fragments and crystals, together with some lava fragments all of which are embedded in a devitrified glassy matrix. Matrix is a very dark fine-grained microcrystalline material that is weakly birefringent. Some quartz grains are present.

NF 116. Tuff. Light-brownish-pink layered tuff containing a few plagioclase (An_{38}) fragments together with a few lava fragments embedded in a devitrified glassy matrix. Matrix is dark gray and faintly microcrystalline.

NF 113. Welded tuff. Reddish-brown well-layered welded tuff containing a few calcic plagioclase fragments. The matrix is fine grained faintly birefringent and contains some quartz.

NF 38. Andesite. Reddish lava containing many short stubby plagioclase (An_{30}) phenocrysts together with a few large clinopyroxene phenocrysts. Groundmass has a hyalopilitic texture and is rich in devitrified glass and much of the microcrystalline material exhibits faint pleochroic tints. Small grains of clinopyroxene and laths of plagioclase are dispersed in the groundmass.

B 1-4. Collected by H. L. Berryhill (1965, p. 57).

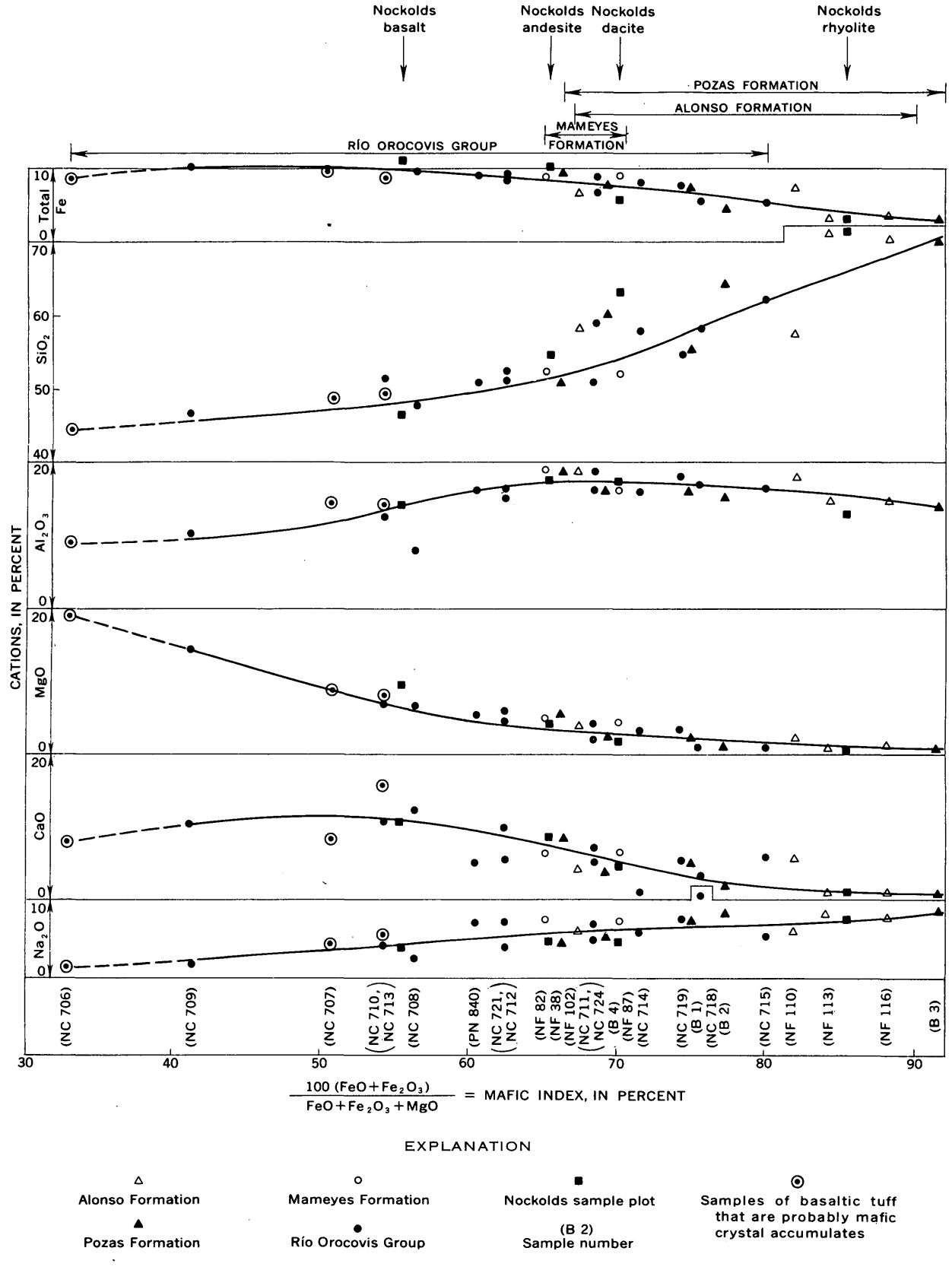

FIGURE 2.—Variation diagram of cations plotted against mafic index for volcanic rocks in north-central Puerto Rico. Numbers in parentheses at bottom of diagram are sample numbers from table 1.

rhyolite. One sample (NF 38) from the Pozas Formation is a subaerially(?) deposited andesite lava. The other samples are from subaerially deposited pyroclastic rocks that range in composition from dacite to rhyolite.

Most of the analyzed rocks contain less than 1 percent TiO_2 and would, therefore, be classed as circumoceanic by Chayes (1964, p. 1585).

Figure 2 is a variation diagram based on the analyses in table 1. Arrows at the top of the diagram indicate mafic indices of average alkalic basalt, andesite, dacite, and rhyolite from Nockolds (1954). Compositional ranges of the various stratigraphic units sampled and analysed are also shown at the top of the diagram; the circled points represent samples of basaltic tuff that are probably mafic crystal accumulates, and the variation curve is, therefore, dashed where one of these analyses extends the mafic end of the curve.

The diagram clearly shows the continuous chemical variation from the older, relatively mafic basalts of the Río Orocovis Group to the younger, rhyolitic rocks of the Alonso and Pozas Formations. The compositional range of volcanic rocks in the Río Orocovis Group is greater than the Mameyes, and both the Río Orocovis and Mameyes ranges overlap the more mafic end of the compositional ranges of the Alonso and Pozas Formations.

Figure 3 is an iron-magnesium-alkalies (FMA) diagram showing the analyses for the samples listed in table 1. In general, the FMA plot for these analyses follows the plotted curve representing fractional crystallization of calc-alkalic rocks (Hess, 1960, pl. 11).

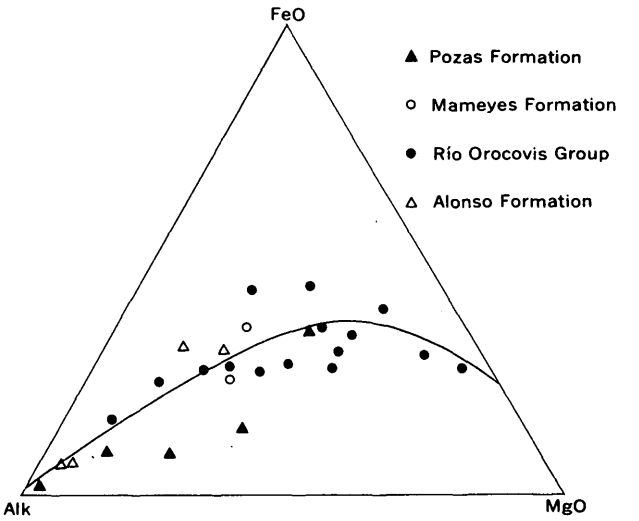

FIGURE 3.—Iron-magnesium-alkalies (FMA) diagram for volcanic rocks in north-central Puerto Rico.

CONCLUSIONS

Significant changes in environment of deposition and volcanism occurred in north-central Puerto Rico during the Cretaceous Period. The older rocks, those of the Mameyes Formation and the Río Orocovis Group, were subaqueously deposited. After eruption of the submarine lava flows in the lower part of the Pozas Formation, probably during Campanian and early Maestrichtian time, deposition was mostly subaerial.

Chemical analyses indicate continuous chemical variation from mafic to felsic volcanic rocks. Rocks of the Río Orocovis Group and Mameyes Formation, most of which are basalt or andesite, are rich in potash and have alkaline tendencies. Later rocks of the Pozas and Alonso Formations are mostly dacitic or rhyolitic and are calc-alkaline and are more felsic and silica saturated. Most of the early volcanic rocks are lavas, whereas younger rocks are chiefly pyroclastic. Additional petrologic study, however, will be needed to understand the magmatic relations between suites of volcanic rocks and to determine whether the variation is due to continuous systematic change in magma composition in a single chamber or to a change in magmatic source.

REFERENCES

Berryhill, H. L., 1965, Geology of the Ciales quadrangle, Puerto Rico: U.S. Geol. Survey Bull. 1184, 116 p.

Carlisle, Donald, 1963, Pillow breccias and their aquagene tuffs, Quadra Island, British Columbia: Jour. Geology, v. 71, no. 1, p. 48–71.

Chayes, Felix, 1964, A petrographic distinction between Cenozoic volcanics in and around the open oceans: Jour. Geophys. Research, v. 69, no. 8, p. 1573–1588.

Hess, H. H., 1960, Stillwater igneous complex, Montana: Geol. Soc. America Mem. 80, 230 p.

Lidiak, E. G., 1965, Petrology of andesitic, spilitic, and keratophyric flow rock, north-central Puerto Rico: Geol. Soc. America Bull., v. 76, no. 1, p. 57–87.

Nelson, A. E., in press, Cretaceous and Tertiary rocks in the Corozal quadrangle, Northern Puerto Rico: U.S. Geol. Survey Bull. 1244–C.

Nelson, A. E., and Monroe, W. H., in press, Geology of the Florida quadrangle, Puerto Rico: U.S. Geol. Survey Bull. 1221–C.

Nockolds, S. R., 1954, Average chemical compositions of some igneous rocks: Geol. Soc. America Bull., v. 65, no. 10, p. 1007–1032.

Poldervaart, Arie, 1964, Chemical definition of alkali basalts and tholeiites: Geol. Soc. America Bull., v. 75, no. 3, p. 229–232.

Rittman, A. L., 1962, Volcanoes and their activity: New York, John Wiley and Sons, 305 p.

Shapiro, Leonard, and Brannock, W. W., 1956, Rapid analysis of silicate rocks: U.S. Geol. Survey Bull. 1036–C, p. 19–56.

——— 1962, Rapid analysis of silicate, carbonate, and phosphate rocks: U.S. Geol. Survey Bull. 1144–A, p. A1–A56.

SOLUBILITY IMPLICATIONS OF APATITE IN SEA WATER

By CHARLES E. ROBERSON, Menlo Park, Calif.

Abstract.—Solubility studies using fluorapatite and marine phosphorite in artificial sea-water solutions confirm that the solubility of these solid phases is a function of pH. These experiments show that pK′ (—log K′) for the reaction $Ca_5(PO_4)_3F(solid)+3H_2O=5Ca^{+2}+3HPO_4^{-2}+F^{-1}+3OH^-$ is 52±1.5. The data suggest that at pH 8.2, the equilibrium value for total dissolved phosphate is about 0.2 micromoles per liter. From this it is inferred that the bulk of ocean water is near saturation with respect to fluorapatite. Therefore, deposition of phosphorite whose main component is fluorapatite can be explained on continental-shelf areas where a decrease in solubility occurs because of loss of CO_2. A value determined for the second dissociation of phosphoric acid suggests that the main phosphate species is HPO_4^{-2} and that at pH 8.1 its concentration is 100 times greater than $H_2PO_4^{-1}$.

Solubility experiments with different apatite minerals were carried out, and analytical results were used to calculate equilibrium constants for a proposed solubility reaction. These constants, corrected by other thermochemical data, are compared with values calculated from literature data. Some implications relative to the marine environment are suggested. An unsuccessful attempt was made to evaluate the solubility of fluorapatite and phosphorite using the saturometer described by Weyl (1961).

Because saturometer studies were ambiguous in determining the solubility of phosphorite in sea water, solubility experiments were conducted. In these experiments different samples of apatite and phosphorite were placed in contact with artificial sea water, and the increase in the concentration of ions upon dissolution of the apatite was measured. In solutions having pH values above about pH 4, the solubility of apatite in sea water is so low that, of the constituents making up apatite, only increases in the phosphate concentration could be analytically measured with reasonable accuracy.

Acknowledgments.—This report was prepared as partial fulfillment for a Master of Science degree at the University of California at San Diego (Roberson, 1965) under the direction of Prof. E. D. Goldberg and the financial support of the U.S. Geological Survey. In addition to review by colleagues of the Geological Survey this report was also reviewed by Prof. R. M. Pytkowicz of the University of Oregon.

PHOSPHORITE IN THE SEA

Marine phosphatic nodules were first discovered during the Challenger Expedition off the Cape of Good Hope (Sverdrup and others, 1942, p. 1032). They have now been found in many coastal regions on continental shelves and on topographic highs in the ocean.

The main constituent of phosphorite is fluorapatite (Goldschmidt, 1954, p. 465), which may be represented by the formula $Ca_{10}(PO_4)_6F_2$. The hexagonal network structure has been discussed by Altschuler and others (1958). Phosphorite contains an apatite that is probably more correctly characterized as a carbonate fluorapatite with a small deficit, relative to pure fluorapatite, of phosphate and a slight excess of F^{-1}, OH^{-1}, or both (Altschuler and others, 1958). This is designated marine apatite.

Dissolved phosphorus

Both organic and inorganic processes are at work in depositing phosphate in the sea. The assumption made in this report is that the role of biochemical processes is merely to facilitate inorganic precipitation reactions that are already thermodynamically possible.

Phosphorus, which occurs in nature only in the stable pentavalent state as orthophosphate, is found in the sea at low concentrations. The maximum concentration of soluble phosphate generally occurs at depths of 500 to 1,500 meters; it closely approaches that of the oxygen minimum (Sverdrup and others, 1942, p. 237), and is related to the high rate of decomposition of organic material.

Phosphate content in various oceans and the Mediterranean Sea ranges approximately as follows, with

the lower values occurring only in the upper few hundred meters (N. W. Rakestraw, oral commun., 1963).

	Range in phosphate (μmoles/liter)
Atlantic Ocean	0. 05–2. 5
Pacific and Indian Oceans	. 2–3. 5
Mediterranean Sea	. 02–0. 2

The bulk of the water of the oceans can be considered to be about $10^{-6.0}$ to $10^{-5.5}$ molar with respect to dissolved phosphate (Sillén, 1961, p. 567). Several workers (Dietz and others, 1942; Kramer, 1964; Sillén, 1961, p. 567) seem to think that this represents near saturation with some phosphatic solid phase or phases and that some mechanism exists to permit the attainment of saturation and precipitation in certain localized areas.

Origin of phosphorite

Kazakov (1938) was one of the first to propose a plausible mechanism for the chemical precipitation of phosphorite from the sea. Basically, his theory states that deep ocean water, which is enriched in dissolved phosphate when transported into certain environments, becomes supersaturated with respect to marine apatite.

Dietz and others (1942) attempted to evaluate the phosphate content of sea water thermodynamically in terms of saturation with tricalcium phosphate ($Ca_3(PO_4)_2$). They suggest that at a phosphate concentration of $10^{-5.98}$ molar, sea water at pH 8 is about 289 percent saturated with respect to the solid phase. There are obvious sources of error in a choice of data for such calculations and Dietz and others recognized this. However, they suggested that sea water at depths greater than a few hundred meters is saturated with respect to $Ca_3(PO_4)_2$. Emery states (1960, p. 72) that although more recent findings show that water off southern California has three times as much phosphate as Dietz and others considered, the great difference between the nature of the solid phase which is actually found in deposits and simple $Ca_3(PO_4)_2$ vitiates further refinement of calculations. Emery thinks that phosphorites result from direct precipitation as colloids in areas of strong upwelling.

Smirnov and others (1958), in studying the system $CaO–P_2O_5–H_2O$ under conditions approximating sea water, concluded that the solid phase was hydroxyapatite and that at a concentration of 0.114 milligrams/liter P_2O_5 (1.6 micromoles/liter) and pH=8.1, sea water is nearly at saturation. Sillén (1961, p. 567) thinks, from thermodynamic considerations, that deep sea water, which is $10^{-6.0}$ to $10^{-5.5}$ molar with respect to phosphate, may be in equilibrium with hydroxyapatite. Kramer (1964) concludes from thermodynamic calculations that most sea water is supersaturated with respect to hydroxyapatite and carbonate fluorapatite.

Kazakov (1938) thought that when the pH of ascending phosphate-rich water increased, $CaCO_3$ was precipitated before apatite. However, Krumbein and Garrels (1952) consider that although phosphorite has a pH-solubility relation roughly parallel to that of $CaCO_3$, the much lower solubility of phosphorite would cause the latter to precipitate at a lower pH than would $CaCO_3$. Thus, on increasing pH, phosphorite would precede $CaCO_3$ in precipitation. They (Krumbein and Garrels, 1952) conclude that the phosphorite must precipitate at a pH greater than 7.1 but less than pH 7.8, whereas calcium carbonate must precipitate above pH 7.8. Because most of the ocean water probably is near pH 7.8 they postulate that phosphorite must precipitate in unventilated basins where the pH may approach values near 7.0. This does not appear to explain how phosphorite is formed on sea mounts (Emery, 1960, p. 72), unless one concludes that the particles making up the nodules are colloidal and were precipitated at other than their deposition site.

Nature of phosphorite

Kazakov (1938) studied the system $CaO–P_2O_5–HF–H_2O$ (25°C) in solutions approximating sea water in composition. He concluded that phosphatic minerals must be crystallized exclusively in the apatite lattice.

Others appear to believe that hydroxyapatite is the stable phosphatic phase in the sea. It is inferred from the abstract of the report by Smirnov and others (1958) that they considered the solid phase in sea water to be hydroxyapatite. Sillén (1961, p. 567) suggests that hydroxyapatite is the stable calcium phosphate phase in sea water. However, in his calculations he evidently did not consider fluorapatite. Most authorities now believe that fluorapatite is the stable phosphatic phase in sea water and that hydroxyapatite is converted to fluorapatite even in low fluoride environments (see for example, Goldschmidt, 1954, p. 455–456).

The author made an estimate of the relative stability of the two phases, hydroxyapatite (HAP) and fluorapatite (FAP), using the data presented in table 1. In this table and later discussion, ΔF°_f, ΔF°_R, ΔH°_f, S°_{298} mean, respectively, standard free energy of formation, standard free energy of reaction, standard heat of formation, and entropy at 298°K (25°C).

The values of ΔF°_f shown here range widely for both FAP and HAP. Therefore, in the hope of being at least internally consistent, ΔF°_f values from the data of a single group of workers (Smirnova and others,

1962) were used. From ΔH_f° by these authors, and entropy values from Kelley and King (1961, p. 104), it is calculated that ΔF_f° values for FAP and HAP are −3,086 and −3,020 kilocalories per mole^{-1}, respectively. Entropy values for the elements are from Latimer (1952). Considering the reaction of HAP going to FAP:

$$Ca_{10}(PO_4)_6(OH)_2(\text{solid}) + 2F^{-1} = Ca_{10}(PO_4)_6F_2 + 2OH^{-1}.$$

At equilibrium

$$\frac{[OH^{-1}]^2}{[F^{-1}]^2} = \text{constant } (K),$$

where [ ] denotes molal activities. The value for ΔF_R° can be used to calculate the value of K. At 25°C

$$\Delta F_R^\circ = -1.364 \log K.$$

ΔF_R° is −9 kcal mole^{-1}, and therefore $K = 10^{6.6}$. From this

$$[OH^{-1}] = 2{,}000\ [F^{-1}],$$

and it can be seen that the activity of F^{-1} is very small relative to that of OH^{-1} when FAP and HAP are in equilibrium with solution. Accordingly, it is assumed that fluorapatite is stable relative to hydroxyapatite under the stated conditions. Presumably, hydroxyfluorapatite also would be more stable than pure hydroxyapatite.

TABLE 1.—*Standard free energy of formation* (ΔF_f°) *values at 25°C*

	ΔF_f°
Fluorapatite ($Ca_{10}(PO_4)_6F_2$)	[1] −3,090
	[2] −3,113
	[3] −3,079
	[4] −3,074
	[5] −3,086
Hydroxyapatite ($Ca_{10}(PO_4)_6(OH)_2$)	[6] −3,037
	[7] −3,026
	[8] −3,023
	[9] −3,020

[1] Calculated using a thermodynamic solubility product (K_{sp}) of $10^{-120.9}$ reported by Farr and Elmore (1962, p. 317) and ΔF_f° values reported by Latimer (1952).
[2] Calculated from enthalpy of formation value (ΔH_f°) = −3,296 kcal mole^{-1} (Jacques, 1963, p. 3820) and entropy (S_{298}°) value of 185.4 cal deg^{-1} mole^{-1} (Kelley and King, 1961, p. 104).
[3] Calculated from ΔH_f° = −3,262 kcal mole^{-1} (Gottschal, 1958) and S_{298}° = 185.4 cal deg^{-1} mole^{-1} (Kelley and King, 1961, p. 104).
[4] Calculated from my solubility data and presented for comparison (Roberson, 1965).
[5] Calculated from ΔH_f° = −3,269 kcal mole^{-1} (Smirnova and others, 1962) and S_{298}° = 185.4 cal deg^{-1} mole^{-1} (Kelley and King, 1961, p. 104).
[6] Calculated from ΔH_f° value of −3,229 kcal mole^{-1} (Jacques, 1963, p. 3820) and S_{298}° = 186.6 cal deg^{-1} mole^{-1} (Kelley and King, 1961, p. 104).
[7] Calculated $(K_{sp})^{1/2} = 10^{-57.3}$ (Bjerrum and others, 1958, p. 58) and ΔF_f° values (Latimer, 1952).
[8] Calculated using $K_{sp} = 10^{-114}$ (Kramer, 1964, p. 637).
[9] Calculated from ΔH_f° = −3,212 kcal mole^{-1} (Smirnova and others, 1962) and S_{298}° = 186.6 cal deg^{-1} mole^{-1} (Kelley and King, 1961, p. 104).

Admittedly, selection of different ΔF_f° values for FAP and HAP from different workers may show quite different results, although the free-energy values for FAP are consistently more negative than those for HAP.

Phosphorite is not a pure fluorapatite but contains a little carbonate within the apatite lattice. Moreover, phosphorite is not made up of a single phosphate mineral; it commonly contains calcite, aragonite, quartz, and feldspar. The preponderance of geologic evidence, however, supports the theoretical considerations indicating that an apatite lattice containing fluorine is stable in both marine and terrestrial environments.

Altschuler and others (1958, p. 47–49) have discussed the structure of apatites. The apatite structure is host to many substitutions by cations and anions. Hydroxide (OH^{-1}) and chloride (Cl^{-1}) are the most likely substitutes for F^{-1} in the apatite lattice, but these ions, being larger than F^{-1}, do not fit into the structure so well, hence they form less stable apatites. Many apatites, however, are nearly pure chlor-apatites, but these were formed under conditions of high temperature (M. N. A. Peterson, written commun., 1965).

SOLUBILITY CONSIDERATIONS

It was initially planned to use the saturometer (Weyl, 1961) to try to determine whether sea water is saturated with respect to marine phosphorite. It was thought that this tool might give a thermodynamic approach to the solubility problem. However, the author was unable to explain the saturometer results in terms of equilibrium or disequilibrium with respect to apatite or marine phosphorite.

The problem of measuring pH in solid-liquid mixtures has long troubled many workers (Garrels, 1960, p. 66; LaMer, 1962, p. 977; Clark, 1964; Kruyt, 1952, p. 184–186; and Zhelesnova, 1962). In the present study the results appeared explainable largely on the basis of the low solubility of apatite. Thus, the dissociation of phosphoric acid in an apatite-sea water equilibrium environment exerts less control on the pH of the solution than do slight impurities of carbon dioxide; this occurred even though considerable precautions were taken to exclude CO_2. Solubility experiments discussed later (but not discussed with respect to this aspect) supported this conclusion.

Some solubility considerations are presented below.

Solubility reaction of fluorapatite

If the reaction of fluorapatite with water is reversible, the following reaction should be valid at the pH values encountered in sea water (using half of the empirical formula for fluorapatite):

$$Ca_5(PO_4)_3F\ \text{solid} + 3H_2O = 5Ca^{+2} + 3HPO_4^{-2} + F^{-1} + 3OH^{-1}. \quad (1)$$

The mass-action equilibrium expression for equation 1 is

$$[Ca^{+2}]^5[HPO_4^{-2}]^3[F^{-1}][OH^{-1}]^3 = K. \quad (1a)$$

Using the ΔF_f° values [1] for fluorapatite reported in table 1, the equilibrium constant at room temperature ranges from 10^{-61} (using my solubility data) to 10^{-75} using the lowest value for $\Delta F_{f\,FAP}^\circ$ calculated from the literature. The attempt was made to evaluate the activity product (equation 1a) for sea water. It would have been valid to consider a reaction which involved PO_4^{-3} or $H_2PO_4^{-1}$ ions instead of HPO_4^{-2}, but it appears from other considerations (discussed later) that HPO_4^{-2} is the major phosphate species at the pH of most ocean water (around 8).

The activity of OH^{-1} can be obtained quite precisely from pH; the activity of Ca^{+2} in sea water is known with reasonable accuracy because of extensive work on the carbonate system in sea water by others (see, for example, Buch, 1951). On the other hand, to my knowledge, there has been no way to accurately evaluate the stoichiometric concentration of HPO_4^{-2}, much less its activity.[2] Complexing reactions in the case of HPO_4^{-2} and F^{-1} probably account for the "disabling" of much or most of both ions. For example, it is herein assumed that not more than 25 percent of the molar concentration of F^{-1} is uncomplexed and available to form apatite and probably less than half of the HPO_4^{-2} is uncomplexed. In view of these difficulties, an ion product [3] is used here.

The decision to write the reaction of fluorapatite with water (equation (1)) in terms of HPO_4^{-2} instead of PO_4^{-3} or $H_2PO_4^{-1}$ is based on calculations involving equations below. There are four species which might be considered: H_3PO_4, $H_2PO_4^{-1}$, HPO_4^{-2}, and PO_4^{-3}. They are all related to the hydrogen-ion concentration by the following mass-action equations which are directly derived from the three-step dissociation of phosphoric acid:

$$\frac{[H^{+1}][H_2PO_4^{-1}]}{[H_3PO_4]}=K_1=10^{-2.2}\ 25°C, \tag{3}$$

$$\frac{[H^{+1}][HPO_4^{-2}]}{[H_2PO_4^{-1}]}=K_2=10^{-7.2}\ 25°C, \tag{4}$$

and

$$\frac{[H^{+1}][PO_4^{-3}]}{[HPO_4^{-2}]}=K_3=10^{-12.2}\ 25°C. \tag{5}$$

These thermodynamic dissociation constants (25°C) are the reciprocals of the formation constants reported by Bjerrum and others (1958, p. 57, ref. 16). They are related to the apparent constants as follows:

$$K_1'=\frac{[H^{+1}](H_2PO_4^{-1})}{(H_3PO_4)}=K_1\frac{\gamma_{H_3PO_4}}{\gamma_{H_2PO_4^{-1}}}, \tag{3a}$$

$$K_2'=\frac{[H^{+1}](HPO_4^{-2})}{(H_2PO_4^{-1})}=K_2\frac{\gamma_{H_2PO_4^{-1}}}{\gamma_{HPO_4^{-2}}}, \tag{4a}$$

$$K_3'=\frac{[H^{+1}](PO_4^{-3})}{(HPO_4^{-2})}=K_3\frac{\gamma_{HPO_4^{-2}}}{\gamma_{PO_4^{-3}}}. \tag{5a}$$

From equations 3, 4, and 5 it can be confidently calculated at pH 8 that only HPO_4^{-2} and $H_2PO_4^{-1}$ are analytically important in very dilute solutions. But this assumes activity coefficients equal to unity for all species, which is not true for sea water. Because the activity coefficients of the phosphate species, in solutions having the ionic strength of sea water, are difficult to evaluate, it is desirable to work with the apparent constants K_1', K_2', and K_3' (see earlier). A value for K_2' was measured (discussed later) and found to be as a first approximation, $10^{-6.1}$. R. M. Pytkowicz (written commun., 1965) has recently made a determination of K_2' for sea water of normal salinity and found a preliminary value of $10^{-6.2}$. Because no firm values for K_1' and K_3' are available, only guesses for limiting values can be made on the basis of equations 3a and 5a. Considering the first constant, the ratio $\gamma_{H_3PO_4}/\gamma_{H_2PO_4^{-1}}$ would increase at ionic strengths up to that of sea water ($\mu=0.7$). This is because the activity coefficient for the uncharged species is probably somewhat greater than 1.0 at ionic strength 0.7 (Butler, 1964, p. 439). On the other hand, $\gamma_{H_2PO_4}$ is almost certain to be less than 1.0. Therefore, K_1' must be $>K_1$, and H_3PO_4 cannot be analytically important at the pH values that are found either in sea water or in this study.

The importance of PO_4^{-3} can be evaluated from equation 5a. The importance of complexing becomes obvious in the case of ions like HPO_4^{-2} and PO_4^{-3}; therefore it is hard to estimate a value for K_3'. The ratio $\gamma_{HPO_4^{-2}}/\gamma_{PO_4^{-3}}$ would probably increase greatly in going from infinitely dilute solutions to that of sea water, because at any given ionic strength up to at least 0.5, the activity coefficient of a trivalent ion would be lower than that of a divalent ion (Butler, 1964, p. 438). However, as a limiting case, it is estimated that the ratio $\gamma_{HPO_4^{-2}}/\gamma_{PO_4^{-3}}$ cannot be greater than about 100. Therefore, K_3' would be no larger than about 10^{-10} (probably smaller). Using this value PO_4^{-3} would be less than 2 percent of the total phosphate. This would again be

[1] Actually half of the F_f° values because it was desired to consider half of the empirical formula for fluorapatite.

[2] In this report, a tentative value for the apparent equilibrium constant is presented for the second dissociation of phosphoric acid. This should provide a fair estimate of the stoichiometric concentration of HPO_4^{-2}.

[3] More properly a "hybrid" product wherethe molal activity of OH^{-1} and the molar concentrations of all other ions are used. This approach has been commonly employed in the study of the carbon dioxide system in sea water. When such a product is a constant it has generally been called an apparent equilibrium constant (K_{eq}') as opposed to a thermodynamic constant (K_{eq}). (See, for example, Sverdrup and others, 1942, p. 204.) For reaction (1) K' is related to K as

$$(Ca^{+2})^5(HPO_4^{-2})^3(F^{-1})[OH^{-1}]^3=K'=\frac{K}{\gamma_{Ca^{+2}}^5\gamma_{HPO_4^{-2}}^3\gamma_{F^{-1}}}, \tag{2}$$

where [ ] denotes activities, ( ) denotes molarity and γion is the activity coefficient of an ion.

analytically unimportant because the total phosphate dissolved $(P)_T$ in the solutions which were at pH values between 8 and 9 in this study had values of only about 10^{-7} molar. Therefore, the only analytically important phosphate species are assumed to be HPO_4^{-2} and $H_2PO_4^{-1}$, and the following relations can be used to obtain HPO_4^{-2}:

$$K_2' = \frac{[H^{+1}](HPO_4^{-2})}{(H_2PO_4^{-1})} = K_2 \times \frac{\gamma_{H_2PO_4^{-1}}}{\gamma_{HPO_4^{-2}}}, \quad (4a)$$

and

$$(P)_T = (HPO_4^{-2}) + (H_2PO_4^{-1}), \quad (6)$$

where $(P)_T$ is the molar concentration of total dissolved phosphate. One is left with the choice of using the expression for K_2' or the one for K_2. It appears that there are no values in the literature for K_2' in sea water. There are apparently good values for $K_2(10^{-7.20})$. However, if K_2 is used, then not only the problem of finding good values for $\gamma_{H_2PO_4^{-1}}$ and $\gamma_{HPO_4^{-2}}$, but also evaluation of the amount of complexing which undoubtedly occurs in the case of ions like $H_2PO_4^{-1}$ and especially HPO_4^{-2}, become acute.

An apparent equilibrium constant (K_2') should have a built-in compensation for these difficulties. Accordingly, an approximate value was determined which is used in the calculations presented later. The determination was made as follows: A 100-milliliter-portion of artificial sea water which had been prepared free of CO_2 species and boric acid species, was adjusted to pH 3.7 with phosphoric acid. While holding the ionic strength constant (0.7) the solution was titrated with sodium hydroxide. The pH was measured with a pH meter (Radiometer PHM–4) using a glass electrode. The titration curve (fig. 1) suggests $(HPO_4^{-2})/(H_2PO_4^{-1}) = 1.0$ at pH 6.1; hence $pK_2' = 6.1 \pm 0.2$ (p denotes the negative logarithm). This is presented as a first approximation of pK_2' at 25°±0.1°C in sea water of salinity=35 parts per thousand. R. M. Pytkowicz (written commun., 1965) has suggested a preliminary value for pK_2' of 6.2 based on measurement.

On the basis of the value $pK_2' = 6.1$, the measured pH and total dissolved phosphate $(P)_T$, and relations 4a and 6,

$$\frac{[H^{+1}](HPO_4^{-2})}{(H_2PO_4^{-1})} = 10^{-6.1}, \quad (4a)$$

and

$$(P)_T = (HPO_4^{-2}) + (H_2PO_4^{-1}), \quad (6)$$

and combining, one obtains

$$(HPO_4^{-2}) = \frac{(P)_T}{1 + \frac{[H^{+1}]}{10^{-6.1}}}. \quad (4a, 6)$$

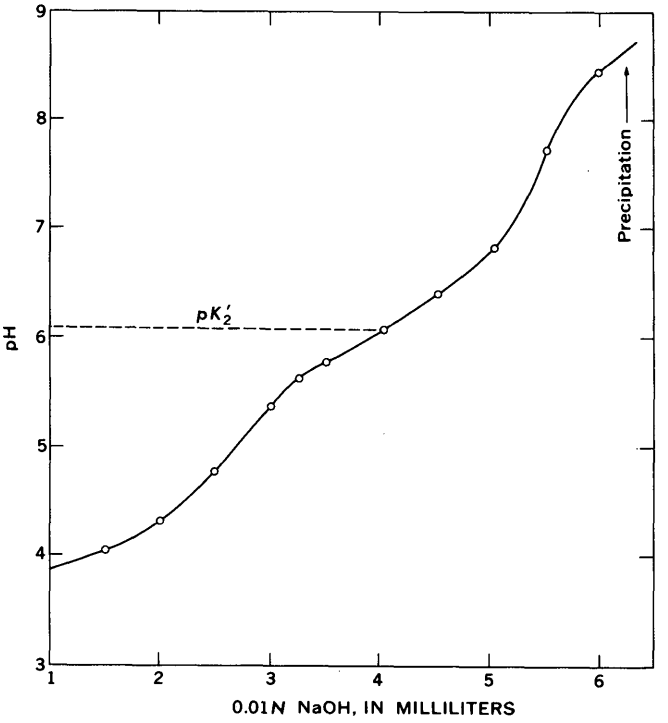

FIGURE 1.—Approximate determination of the second apparent dissociation constant for phosphoric acid in sea water (24°± 2°C, salinity 35 parts per thousand).

Solubility experiments

Data were obtained from a series of solubility experiments (table 2) for testing the constancy of $(Ca^{+2})^5(HPO_4^{-2})^3(F^{-1})[OH^{-1}]^3$, and hence the possibility of equilibrium of sea water with fluorapatite. Solutions of artificial sea water were prepared according to the formulation of Lyman and Fleming (Sverdrup and others, 1942, p. 186) except that no boric acid and bicarbonate were added. An additional amount of sodium chloride equivalent to the sodium bicarbonate was used to replace the latter. The synthetic sea water was made boric acid free and largely CO_2 free, so that the absence of these two buffer systems would permit the solubility reaction of fluorapatite and the phosphoric acid dissociation reactions to control the pH. Such control does not appear to be possible in natural sea water, owing to the much lower solubility of apatite relative to carbonate and other CO_2-dependent species. It was found that in these experiments small impurities of CO_2 appeared to be able to control the pH of the solutions.

The solutions were placed in Pyrex vessels holding 1,000 to 1,500 milliliters of solution. Glass covers containing holes for insertion of pH electrodes and a gas-washing tube were provided. Nitrogen washed with sea water to minimize evaporation of the test solution

TABLE 2.—*Data for experiments in which apatitic minerals were in contact with artificial sea water*

[Values in parentheses are assumed]

Experiment	Source of apatite	pH		Calcium (moles/liter X 10^2)		Phosphate (moles/liter X 10^6)			Fluoride (moles/liter X 10^4)		Time washed with nitrogen gas (months)
		Initial	At end of N_2 wash	Initial	Final	Total Initial	Total Final	Calc. HPO_4 (final)	Initial	Final	
1	Durango, Mexico	8. 40	8. 15	0. 9	0. 9	1	0. 1	0. 1	0. 9	0. 9	1
2	do	7. 00	7. 20	. 9	. 9	1	4. 0	3. 8	. 9	. 8	1
3	Canada	8. 30	8. 20	1. 02	1. 02	0. 0	. 22	. 22	1. 00	1. 02	2. 0
4	do	4. 48	6. 30	1. 02	1. 03	. 0	6. 0	3. 7	1. 00	1. 07	2. 0
5	Marine	8. 32	8. 60	1. 02	(1. 02)	. 7	. 10	. 1	1. 00	(1. 00)	2. 0
6	do	4. 80	8. 50	1. 02	(1. 02)	. 6	. 10	. 1	1. 00	(1. 00)	2. 0
7	do	2. 81	4. 85	1. 07	1. 20	1. 4	560	30	. 95	3. 52	. 5
8	do	3. 50	5. 85	1. 07	1. 09	. 1	100	36	. 95	1. 34	. 5

was bubbled slowly and continuously through the solutions to provide an inert atmosphere and to stir the solution. The pH of the solutions was adjusted prior to adding the solid phase and was measured periodically during the course of the experiments. Dissolved phosphate was also monitored. Calcium and usually fluoride concentrations were measured on the solutions at the beginning and end of the experiments. Total carbon dioxide was measured at the end of the runs. The experiments were carried on for periods of from 0.5 to 2 months.

In the experiments, three different apatitic phosphates were used:

(1) Marine phosphorite. (From the sea floor off southern California.) X-ray diffraction showed several percent of dolomite but detected no calcite or aragonite. Chemical analysis (B. F. d'Anglejan, written commun., 1962) shows the composition of a similar specimen to be $Ca_{10}(PO_4)_{5\cdot1}F_{1\cdot7}$ (my calculation) with the deficit in charge presumably due to other ions. Altschuler and others (1958) report a more general composition for marine phosphorite to be represented by the formula $Ca_{10}(PO_4, CO_3)_6F_{2-3}$ with some carbonate substituting for phosphate and with additional fluoride making up the deficit in charge caused by the substituting carbonate.

(2) *Apatite from Durango, Mexico.* This is a relatively pure fluorapatite, with no carbonate, and is commonly used as a standard.

(3) *Carbonate fluorapatite from Ontario, Canada.* This sample, kindly supplied by R. L. Gulbrandson (U.S. Geological Survey) is reported to contain about 1 percent carbonate supposedly substituting for phosphate. It contained no $CaCO_3$ mineral impurity by X-ray analysis.

A summary of the experimental data is shown in table 2. The data are for 25°C and salinity=35 parts per thousand. The following reaction was assumed valid:

$$Ca_5(PO_4)_3F\ (\text{solid}) + 3H_2O = 5Ca^{+2} + 3HPO_4^{-2} + F^{-1} + 3HO^{-1}. \quad (1)$$

The product (equation 2) was then calculated from the data in table 2. The values for the ion product (I.P.) are shown below (table 3).

The mean value of I.P. from our experimental data is 10^{-52}. This represents a very large difference with reference to the thermodynamic constant of 10^{-75} calculated from $1/2\Delta F^\circ_{f\,FAP}=1556$ kcal mole^{-1} (table 1, ref. 2). If we use a $1/2\Delta F^\circ_f$ value for fluorapatite of -1540 kcal deg^{-1} mole^{-1} (the largest value obtained from the literature of others (table 1, third value), then the thermodynamic K is 10^{-63}.

In one of the experiments (4, table 3) in which the ion product was 10^{-53}, comparison was made with a thermodynamic value of $K=10^{-63}$. The data necessary for comparison are shown in table 4.

Then, using the activity product (equation 1a)

$$[Ca^{+2}]^5[HPO_4^{-2}]^3[F^{-1}][OH^{-1}]^3=\text{A.P.},$$

where $[Ca^{+2}]=\gamma_{Ca^{+2}}(Ca^{+2})$ and $[HPO_4^{-2}]=\gamma_{HPO_4^{-2}}(HPO_4^{-4})$ etc., and substituting from table 3, the A.P. is found to be 10^{-61}. This is fairly good agreement with K for Equation 1a ($K=10^{-63}$) calculated using $1/2\Delta F^\circ_f$ for fluorapatite$=-1540$ kcal mole^{-1} (table 1).

These calculations, which are necessarily only approximations, may suggest near equilibrium for the phosphate dissolved in sea water. This is further supported by a comparison of sea-water values for dissolved phosphate with those obtained from a plot of

TABLE 3.—*Values for the ion product (I.P.) for three different apatitic phosphates*

Experiment	*Apatite*	(*from equation 2*) $-log[(Ca^{+2})^5(HPO_4^{-2})^3(F^{-1})[OH_4^{-1}]^3]=I.P.$
1	Durango	52. 8
2	do	51. 0
3	Canadian	51. 3
4	do	53. 0
5	Marine	51. 0
6	do	51. 1
7	do	54. 1
8	do	51. 4

total dissolved phosphate $(P)_T$ against pH. This plot is made from the solubility experiment data (see fig. 2). A plot (not shown) of calculated HPO_4^{-2} against pH showed comparable relations.

TABLE 4.—*Data for calculation of activity product (equation 1a) for fluorapatite in sea water (experiment 4)*

	Moles/liter
Ca^{+2} (measured)	1.02×10^{-2}
Ca^{+2} (uncomplexed)	$.95\times10^{-2}$
	[1] $10^{-2.02}$
HPO_4^{-2} (calculated from analytical $(P)_T$)	3.7×10^{-6}
HPO_4^{-2} (uncomplexed)	[2] 1.6×10^{-6}
	$10^{-5.80}$
F^{-1} (measured)	1.07×10^{-4}
F^{-1} (uncomplexed)	[3] $.25\times10^{-4}$
	$10^{-4.60}$
γCa^{+2}	$10^{-0.55}$
γHPO_4^{-2}	[4] $10^{-0.80}$
γF^{-1}	[5] $10^{-0.22}$
pH=6.30; $[OH^{-1}]$	$10^{-7.70}$

[1] Garrels and Thompson (1962, p. 57).
[2] Estimated, using stability constants from Bjerrum and others (1958) for the species $MgHPO_4^0$, $CaHPO_4^0$, $NaPO_4^{-3}$ and activity coefficients for Mg^{+2}, Ca^{+2}, Na^{+1}, and K^{+1}, and for the complex ions from Garrels and Thompson (1962, p. 61). This is only a first approximation, and there may be other complex ions for which no data were available.
[3] Author's estimation.
[4] Sillén (1961, p. 567).
[5] Calculated, using $-\log \gamma_i = \frac{AZ^2\sqrt{\mu}}{1+Ba^0\sqrt{\mu}}$ (Klotz, 1950, p. 329). Admittedly, this was not intended for use at high ionic strengths, but almost complete lack of data (such as mean activity coefficients for phosphate solutions) necessitated such use.

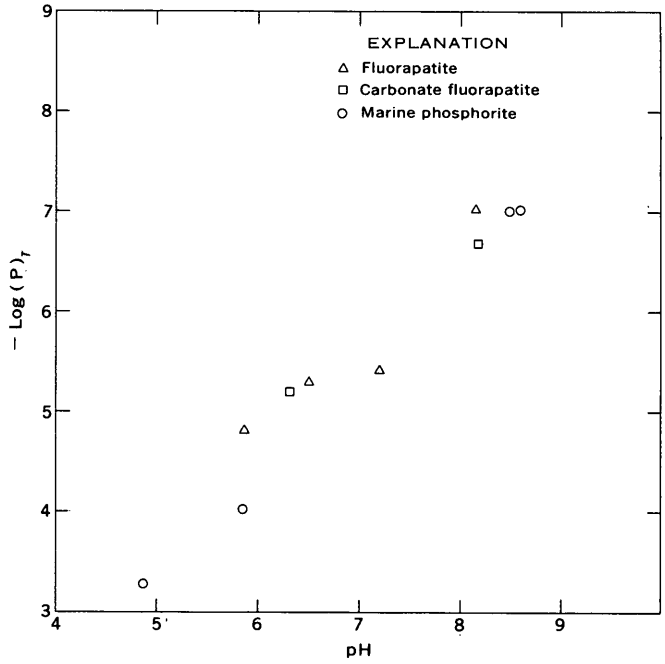

FIGURE 2.—Experimental data showing relations of total dissolved phosphate $(P)_T$ in moles/liter for artificial sea water in contact with different apatites.

CONCLUSIONS AND SUMMARY

(1) Although the difficulties involved in extrapolating laboratory results to the ocean environment are obvious, it is inferred that at pH 8.2, which approximates that of near-surface sea water, the equilibrium amount of total dissolved phosphate $(P)_T$ is about 0.2 μ moles/liter.

(2) At pH values near 7.0, which may be approached in stagnant ocean basins, the $(P)_T$ suggested is 1.8 μ moles/liter.

(3) It is estimated as a first approximation that for sea water at pH 8.0 and $HPO_4^{-2} = 3\mu$ moles/liter, more than half of the HPO_4^{-2} is complexed with Mg^{+2}, Ca^{+2}, Na^{+}, and K^{+}. Fluoride ion may be involved as MgF^{+1} complex to the extent of about 50 percent of the total fluoride and also may be complexed by other major cations.

(4) Factors of chemical complexing make it difficult to evaluate activities of ions in solubility-product calculations. Therefore, this report considers ion products for such calculations.

(5) An ion product of about 10^{-52} was obtained from solubility experiments with various samples of apatite and artificial sea water.

(6) The ion product of 10^{-53}, when corrected by allowances for activity coefficients and the amount of complexing, yields an estimate for ion activity products of 10^{-61}. This is in reasonable agreement with one value for the thermodynamic K for the reaction (10^{-63}) calculated using thermochemical data from literature for fluorapatite. The other values calculated from literature data are considerably smaller. This might be inferred to mean that traces of impurities in the fluorapatite do not greatly decrease the solubility of that mineral as suggested by Arrhenius (1963, p. 682), in terms of a solubility product.

(7) A tentative value for the apparent second dissociation constant for phosphoric acid is $10^{-6.1}$. Therefore, at pH 8.0, which is that of most sea water, only HPO_4^{-2} ion is of analytical importance.

(8) Problems suggested for study to provide working tools for further study of the phosphate system in sea water are:

(a) Determination of apparent dissociation constants for the phosphoric acid system. This report suggests a tentative value for K'_2. This value is supported by a preliminary determination by R. M. Pytkowicz (written commun., 1965). In addition, values for K'_1 and K'_3 are needed.

(b) More detailed determination of the solubility of apatite in sea water is needed.

(c) For the present, it may be easier to study the phosphate system using ion products. However, it would be very desirable to develop specific ion activity electrodes—at least for one of the

phosphate species and for F^{-1}. In lieu of this, a detailed study of complexes involved and evaluation of activity coefficients would be highly desirable.

REFERENCES

Altschuler, Z. S., Clarke, R. S., Jr., and Young, E. J., 1958, Geochemistry of uranium in apatite and phosphorite: U.S. Geol. Survey Prof. Paper 314–D, p. 45–90.

Arrhenius, G. O. S., 1963, Pelagic sediments *in* Hill, M. N., ed., The sea: New York, Interscience Pub., v. 3, 963 p.

Bjerrum, Jannik, Schwarzenbach, Gerold, and Sillén, L. G., 1958, Stability constants, pt. II, Inorganic ligands: London, The Chem. Soc. Spec. Pub. 7, 131 p.

Buch, Kurt, 1951, Das Kohlensaure gleichgewichtssystem in Meerwasser: Havsforskn Inst. Skr, Helsingf., no. 151, 18 p.

Butler, J. N., 1964, Ionic equilibrium: Reading, Mass., Addison-Wesley, 547 p.

Clark, J. S., 1964, An examination of the pH of calcareous soils: Soil Sci., v. 98, no. 3, p. 145–151.

Dietz, R. S., Emery, K. O., and Shepard, F. P., 1942, Phosphorite deposits on the sea floor off southern California: Geol. Soc. America Bull., v. 53, no. 6, p. 815–848.

Emery, K. O., 1960, The sea off southern California: New York, John Wiley and Sons, Inc., 366 p.

Farr, T. D., and Elmore, K. L., 1962, System $CaO–P_2O_5–HF–H_2O$—Thermodynamic properties: Jour. Phys. Chemistry, v. 66, no. 2, p. 315–321.

Garrels, R. M., 1960, Mineral equilibria: New York, Harper and Bros., 254 p.

Garrels, R. M., and Thompson, M. E., 1962, A chemical model for sea water at 25°C and one atmosphere total pressure: Am. Jour. Sci., v. 260, p. 57–66.

Goldschmidt, V. M. (Alex Muir, ed.), 1954, Geochemistry: Oxford, Clarendon Press, 730 p.

Gottschal, A. J., 1958, Heats of formation of hydroxy-, fluor-, and chlorapatite: South African Chem. Inst. Jour., v. 11, p. 45–52; abs. *in* Chem. Abs., 1959, v. 53, p. 11978.

Jacques, J. K., 1963, The heats of formation of fluorapatite and hydroxyapatite: Chem. Sec. Jour. [London], p. 3820–3822.

Kazakov, A. V., 1938, The phosphorite facies and the genesis of natural phosphates: Soviet Geol., v. 8, p. 33–47.

Kelley, K. K., and King, E. G., 1961, Contributions to the data on theoretical metallurgy; XIV, Entropies of the elements and inorganic compounds: U.S. Bur. Mines Bull. 592, 149 p.

Klotz, I. M., 1950, Chemical thermodynamics: Englewood Cliffs, N.J., Prentice-Hall, 369 p.

Kramer, J. R., 1964, Sea water—saturation with apatites and carbonates: Science, v. 146, p. 637–638.

Krumbein, W. C., and Garrels, R. M., 1952, Origin and classification of chemical sediments in terms of pH and oxidation-reduction potentials: Jour. Geology, v. 60, no. 1, p. 1–33.

Kruyt, H. R., 1952, Colloid science: Houston, Tex., Elsevier Press, v. 1, 389 p.

LaMer, V. K., 1962, The solubility behavior of hydroxyapatite: Jour. Phys. Chemistry, v. 66, no. 6, p. 973–978.

Latimer, W. M., 1952, Oxidation potentials: Englewood Cliffs, N.J., Prentice-Hall, 392 p.

Roberson, C. E., 1965, Solubility implications of apatite in sea water: Univ. California, San Diego, Masters thesis.

Sillén, L. G., 1961, The physical chemistry of sea water, *in* Sears, Mary, ed., Oceanography: Internat. Oceanog. Cong., New York, Am. Acad. Advancement Sci. Pub. 67, 654 p.

Smirnov, A. I., Ivnitskaya, R. B., and Zalavina, T. P., 1958, Preliminary results of a study of the $CaO–P_2O_5–H_2O$ system under conditions closely approaching natural conditions: Trudy Gosudarst. Nauch.-Issledovatel. Inst. Gorno-Khim., Syr ' ya, no. 4, p. 86–91; abs. in Chem. Abstracts, 1961, v. 55, p 15094.

Smirnova, Z. G., Illarionov, V. V., and Vol ' fkovich, S. I., 1962, Heats of formation of fluorapatite and hydroxyl apatite and α and β modifications of tricalcium phosphate: Zhur. Neorg. Khim., v. 7, p. 1779–1782.

Sverdrup, H. U., Johnson, M. W., and Fleming, R. H., 1942, The oceans: Englewood Cliffs, N.J., Prentice-Hall, 1087 p.

Weyl, P. K., 1961, The carbonate saturometer: Jour. Geology, v. 69, p. 32–44.

Zhelesnova, A. A., 1962, On the suspension effect in connection with pH determination of sea sediments [English summary]: Inst. Okeanologii, Akad. Nauk. SSSR, v. 54, p. 83–89.

PRELIMINARY RESULTS OF GEOCHEMICAL PROSPECTING IN NORTHERN MICHIGAN

By KENNETH SEGERSTROM and W. H. RAYMOND, Denver, Colo.

Work done in cooperation with the Geological Survey Division of the Michigan Department of Conservation

Abstract.—High concentration of copper, lead, and zinc were found locally in soils of Marquette County, Mich. Samples with anomalous metal concentrations were collected where the cover of surficial materials (chiefly ground moraine) is thin and contains abundant admixtures of colluvium derived from bedrock ridges. Marked bunching of anomalies showed up in three small areas north of the Dead River Storage Basin. Soils underlain by a thick cover of glacial materials (chiefly ice-contact deposits and outwash sand) did not show anomalous concentrations of the base metals. It is concluded that most base metals in these concentrations are not from distant sources, and that their migration has been largely postglacial.

Geochemical prospecting by means of soil sampling was conducted in Marquette County, Mich. (fig. 1), during the 1963 and 1964 field seasons. Over 600 samples were collected and analyzed for their content of copper, lead, and zinc.

Preliminary results have encouraged the continuance of sampling in the so-called Northern Range, just north of the Dead River Storage Basin, where the glacial cover is relatively thin; they have discouraged its continuance in the Southern Range between the Dead River and the Marquette Iron Range, where the glacial cover is much thicker. The Northern Range is rolling terrain with northwest-trending ridges of resistant lower Precambrian metamorphosed volcanic and intrusive rocks which lie on the limbs and along the crest of an anticlinorium. Narrow valleys dissect the ridges in fault zones. The main ridges of the anticlinorium are bordered to the north and south by broad synclinal valleys underlain by poorly resistant slate of middle Precambrian age. The stoss side of bedrock ridges tends to have a till cover, whereas the synclinal valleys are deeply filled with outwash sand and ice-contact deposits. The most extensive bedrock exposures are on the lee side of the ridges. The fault valleys are north trending and are floored with humus-rich alluvium and swamp deposits.

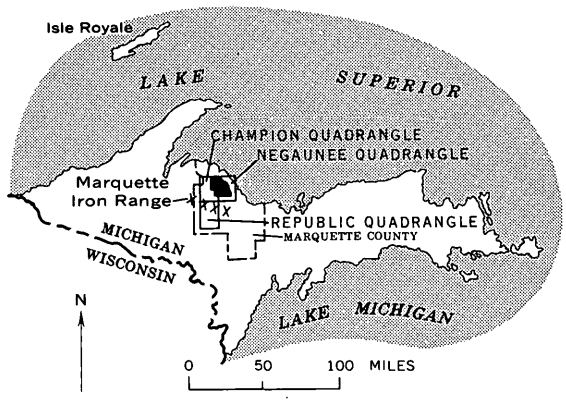

FIGURE 1.—Map of northern Michigan, showing area of report (solid pattern).

Known mineral deposits of the area (fig. 2) are limited to a zone of lower Precambrian outcrops immediately north of the Dead River Storage Basin. All the mines and prospects are on small faults or shears with quartz-carbonate-sulfide mineralization. None has produced more than a few tons of ore (lead-silver) and all have been abandoned for decades. Dump material from the workings in NE1/4 sec. 25, T. 49 N., R. 28 W., and on section line between secs. 34 and 35, T. 49 N., R. 27 W., is exceptionally rich in galena. Material from the prospect in NW1/4 sec. 33, T. 49 N., R. 27 W., is exceptionally rich in sphalerite.

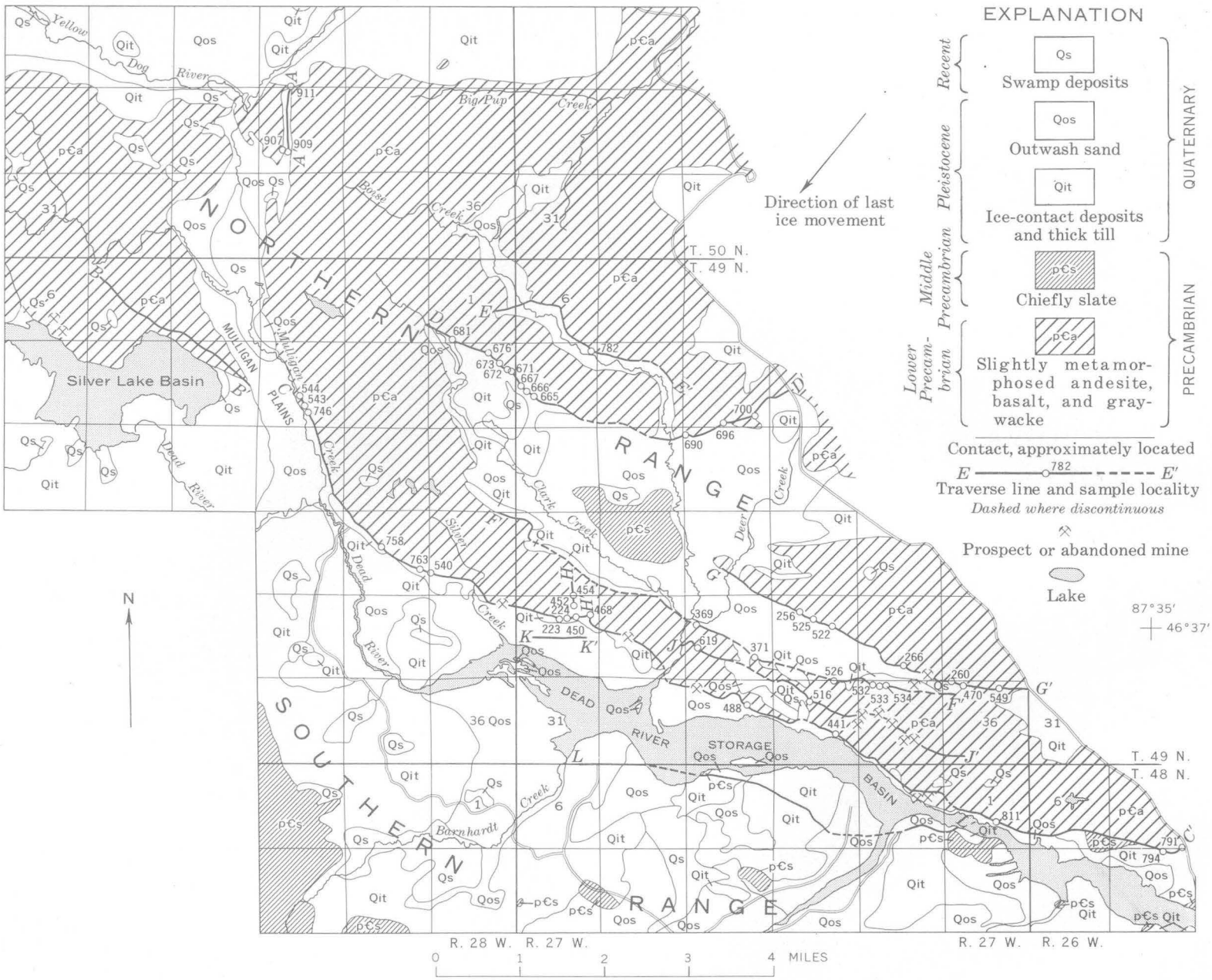

FIGURE 2.—Geologic map of parts of Negaunee and Champion quadrangles, Marquette County, Mich., showing traverse lines and samples with anomalous metal content.

COLLECTION AND ANALYSIS OF SAMPLES

In 1963 over 200 soil samples were taken at scattered localities throughout the Negaunee, Champion, and Republic quadrangles. The highest concentrations of base metals in the soils were obtained near the bases of ridges in the Northern Range and along narrow valleys that cut through the ridges (west-central part of Negaunee quadrangle and northeast part of Champion quadrangle).

In 1964 about 400 more samples were taken on 10 traverses along the ridges and narrow transverse valleys of the Northern Range. These traverses are lettered A through H, J, and K (fig. 2). Traverse L was run south of the Dead River Storage Basin. Soil samples were generally taken at intervals of approximately 500 feet and were collected where possible from the orange-brown, iron oxide-enriched B zone. However, in many localities where the soil cover was shallow, the material available for sampling was humus, rock chips, and very little else. Stream-sediment samples were taken along traverse H. These few stream-sediment samples were taken along a small brook of intermittent flow (not shown on fig. 2) and consisted of humus-rich sand. About a handful of each sample was collected.

Analyses of the samples were made in the Denver Laboratories of the U.S. Geological Survey. The dried samples were screened, and material passing through a 50-mesh screen was pulverized. The pulverized fraction was analyzed for total copper, lead, and zinc by standard geochemical prospecting methods that utilize a pyrosulfate fusion to decompose the sample (Ward and others, 1963, p. 20–25). The minimum content of metal detectable with the method was 10 parts per million for copper, and 25 ppm for lead and zinc. Twenty-one percent of all the samples contained less than 10 ppm of Cu, and 3 percent contained 100 ppm or more. Sixty percent of the samples contained less than 25 ppm of Pb, and 2 percent contained 100 ppm or more. Thirty-six percent of the samples contained less than 25 ppm of Zn, and 6 percent contained 100 ppm or more. A threshold between "background" and anomalous values was chosen at 100 ppm each for copper, lead, and zinc. Most samples that contained anomalous concentrations of one or two of the metals had only background values for the other metal or metals.

Analytical results for the samples which had an anomalous concentration of one or more metals are shown in table 1. The sample localities are shown in figure 2. Not shown are some samples with high concentrations of the base metals, but which were taken near mines and prospects, and hence may reflect contamination by dump material.

INTERPRETATION OF RESULTS

Exceptionally close bunching of anomalies is noted in NE1/4 sec. 30, T. 49 N., R. 27 W., on traverses C and H (sample Nos. 223, 224, 450, 452, 454, and 468 of table 1). Thin soil, in large part colluvial and in part derived from sandy ground moraine, was sampled in the portion of traverse C mentioned above. Immediately to the north, finely disseminated sulfides are exposed in outcrops of greenstone. A sample of sheared rock from an outcrop 240 feet northwest of sample locality 223 (fig. 2) contained 1,700 ppm of Zn,

TABLE 1.—*Results of chemical analyses of 44 soil samples and 3 stream-sediment samples that showed anomalous concentrations of copper, lead, and zinc*

[In parts per million]

Sample No.	Traverse	Cu	Pb	Zn	Sample No.	Traverse	Cu	Pb	Zn	Sample No.	Traverse	Cu	Pb	Zn
223	C–C′	60	450	100	525	G–G′	20	75	200	676	D–D′	120	200	800
224	do	900	100	150	526	F–F′	40	25	125	681	do	80	160	50
256	G–G′	110	<25	100	532	do	150	<25	75	690	do	140	1, 000	500
260	do	75	75	600	533	do	40	75	100	696	do	60	80	120
266	do	40	25	125	534	do	40	<25	300	700	do	40	80	120
369	F–F′	20	100	100	540	C–C′	75	25	250	746	C–C′	60	80	100
371	do	80	50	120	543	do	40	50	450	758	do	120	40	50
441	C–C′	20	100	150	544	do	10	200	75	763	do	160	25	50
450[1]	do	400	25	25	549	G–G′	60	350	50	782	E–E′	160	25	<25
452[1]	H–H′	200	50	100	619	J–J′	440	<25	300	791	C–C′	60	<25	120
454[1]	do	400	100	2, 500	655	D–D′	300	100	50	794	do	40	80	100
468	C–C′	450	50	250	666	do	160	40	120	811	do	120	40	50
470	G–G′	150	50	125	667	do	600	50	100	907	A–A′	300	<25	100
488	C–C′	200	50	100	671	do	80	80	100	909	do	20	<25	1, 500
516	J–J′	60	25	300	672	do	300	160	500	911	do	10	<25	1, 000
522	G–G′	20	<25	200	673	do	80	120	120					

[1] Stream sediment.

200 ppm of Pb, 60 ppm of Cu, and 0.08 ounce of Ag per ton (about 3 ppm). Traverse H is in a narrow valley which apparently follows a north-striking fault or fracture zone. Gossan float at the south end of the valley is further evidence that the area is mineralized, although no vein quartz is exposed here, and very little quartz is exposed elsewhere in sec. 30. The presence of nearby mineralized outcrops suggests that the anomalous amounts of copper, lead, and zinc in the soil are derived locally rather than by long glacial transport from a distant ore body to the northeast. The anomalous concentrations of base metal in the soil of this area could, therefore, reflect an underlying sulfide body or one located up the slope of the ridge not far to the north.

A conjugate system of north-striking and east-striking faults or fractures is immediately to the northeast of an exceptional bunching of anomalies on traverse D, in W1/2 sec. 7, T. 49 N., R. 27 W., and NE1/4 sec. 12, T. 49 N., R. 28 W. (samples 655, 666, 667, 671, 672, 673, and 676 of table 1). Little quartz or sulfides were observed in adjacent bedrock outcrops. It is possible that the anomalies reflect mineralization along the faults. However, the possibility that the metallic content of the soils was derived from reworked ground moraine, transported from far to the northeast, cannot be ruled out.

Three anomalies are closely spaced along traverse F, in the extreme northwestern part of sec. 35, T. 49 N., R. 27 W. (samples 532, 533, and 534 of table 1). The sample localities are about 60 feet above an outwash plain, to the north, and approximately at a contact between a kame terrace and the stoss flank of a ridge to the south. The ridge is mostly of greenstone with a thin veneer of ground moraine. Samples were taken of sandy glacial soil with minor admixtures of colluvium. Copper, lead, and zinc could have been glacially transported from far to the northeast, but small, abandoned lead-silver prospects on quartz veins and shear zones in the same section suggest that less distant, concealed metallic deposits may have contributed to the anomalies.

It seems probable that the anomalous concentrations of Cu, Pb, and Zn in soils of the Northern Range are in large part postglacial and reflect a local source. A reason for this supposition is that most of the anomalous samples were collected near the base of bedrock ridges and contain much colluvial material. Detailed sampling of known mineralized areas (prospects and abandoned mines shown on fig. 2) shows that anomalous halos of base metals generally do not extend more than 500 feet from the deposits, even in a downslope or downglacier direction. Therefore, some of the anomalies reported here may well reflect hitherto unknown deposits of copper, lead, zinc, and (or) silver that are only a few hundred feet distant from sample localities. If this is so, more detailed sampling or geophysical studies, or both, in and near the areas of known geochemical anomalies could lead to the discovery of such deposits.

REFERENCE

Ward, F. N., Lakin, H. W., Canney, F. C., and others, 1963, Analytical methods used in geochemical exploration by the U.S. Geological Survey: U.S. Geol. Survey Bull. 1152, 100 p.

BIOTITE, POTASSIUM-FELDSPAR, AND WHOLE-ROCK AGES OF ADAMELLITE, CLARK MOUNTAINS, WEST ANTARCTICA

By E. L. BOUDETTE,[1] R. F. MARVIN,[2] and C. E. HEDGE,[2]
[1] Washington, D.C., [2] Denver, Colo.

Work supported by the National Science Foundation

Abstract.—The Clark Mountains, West Antarctica, are underlain by metamorphosed graywacke and argillite that have been intruded by adamellite. Biotite and potassium feldspar from the adamellite gave K-Ar and Rb-Sr ages of 143±4 m.y. and 137±9 m.y., respectively, or middle Mesozoic; a Rb-Sr whole-rock age of 116±10 m.y. was also obtained. The dated rock is petrochemically comparable to undated intrusives in northwestern Marie Byrd Land, interior West Antarctica, the Eights Coast, and the Antarctic Peninsula; it is distinct from a dated rock of similar age from the Eights Coast batholith. The radiometric ages also establish a minimum age for the intruded and metamorphosed eugeosynclinal rocks which may be equivalent to the upper Paleozoic eugeosynclinal rocks of the Antarctic Peninsula.

REGIONAL SETTING AND PETROGRAPHY

The Clark Mountains in northwestern Marie Byrd Land, West Antarctica (fig. 1), are underlain by graywacke and argillite that have been regionally metamorphosed to chlorite grade. These rocks have been intruded by a coarse-grained, salmon-pink adamellite, and contact metamorphism has produced resistant hornfels which forms Mount Jones and, in part, Mount Van Valkenburg (E. L. Boudette, unpub. data[1]; McKelvey, 1960, p. A52). The intrusive contact is remarkably sharp and discordant, and it appears that there was very little assimilation of the wallrock. Minor aplite dikes genetically related to the large pluton intrude the hornfels, and lamprophyre dikes intrude both the hornfels and adjacent adamellite. As only the eastern contact of the intrusive body is exposed in the Clark Mountains, the extent and size of the pluton are not known. The adamellite is part of the granite–quartz diorite intrusive series in the southern Edsel Ford Ranges described by Warner (1945, p. 103–104, 114).

The adamellite is coarse grained, fresh to slightly weathered, and extensively jointed. Weak foliation is common, and intense brecciation occurs locally. Miarolitic cavities containing quartz and feldspar euhedra occur at Mount Atwood. Near the contact the intrusive rock becomes medium to fine grained without appreciable change in color or mineral content. Most quartz in the rock is smoky black. Iron oxide and carbonate coatings, common on joints in the hornfels, were not seen in the adamellite.

The adamellite from Mount Atwood (table 1) contains an orthoclase patch perthite with a large amount of exsolved, well-twinned albite; myrmekite occurs locally. In plane-polarized light the potassium feldspar is dusty brown. The pink color in the hand specimen is due to a partly oxidized iron component. Plagioclase altered incipiently to sericite occurs as paragenetically early coarse anhedra and as medium to fine subhedral grains associated with late quartz, myrmekite, and muscovite. The quartz is unstrained and contains abundant fluid inclusions and sparse inclusions of amphibole, apatite, sphene, and zircon. The biotite is mostly fresh, but small grains and thin marginal rims are altered to chlorite. Some biotite in contact with quartz shows minor alteration to chlorite, opaque minerals, and amphibole. Chlorite in biotite and sericitic plagioclase suggests deuteric alteration of the adamellite probably late in the crystallization period; there are no textural features suggesting postintrusive metamorphism or cataclastic deformation.

[1] *In* Traverse operations, Byrd Land traverse: Natl. Sci. Foundation, U.S. Antarctic Research Program, Status Rept., no. 13, Jan. 1960, p. 13–14 [duplicated].

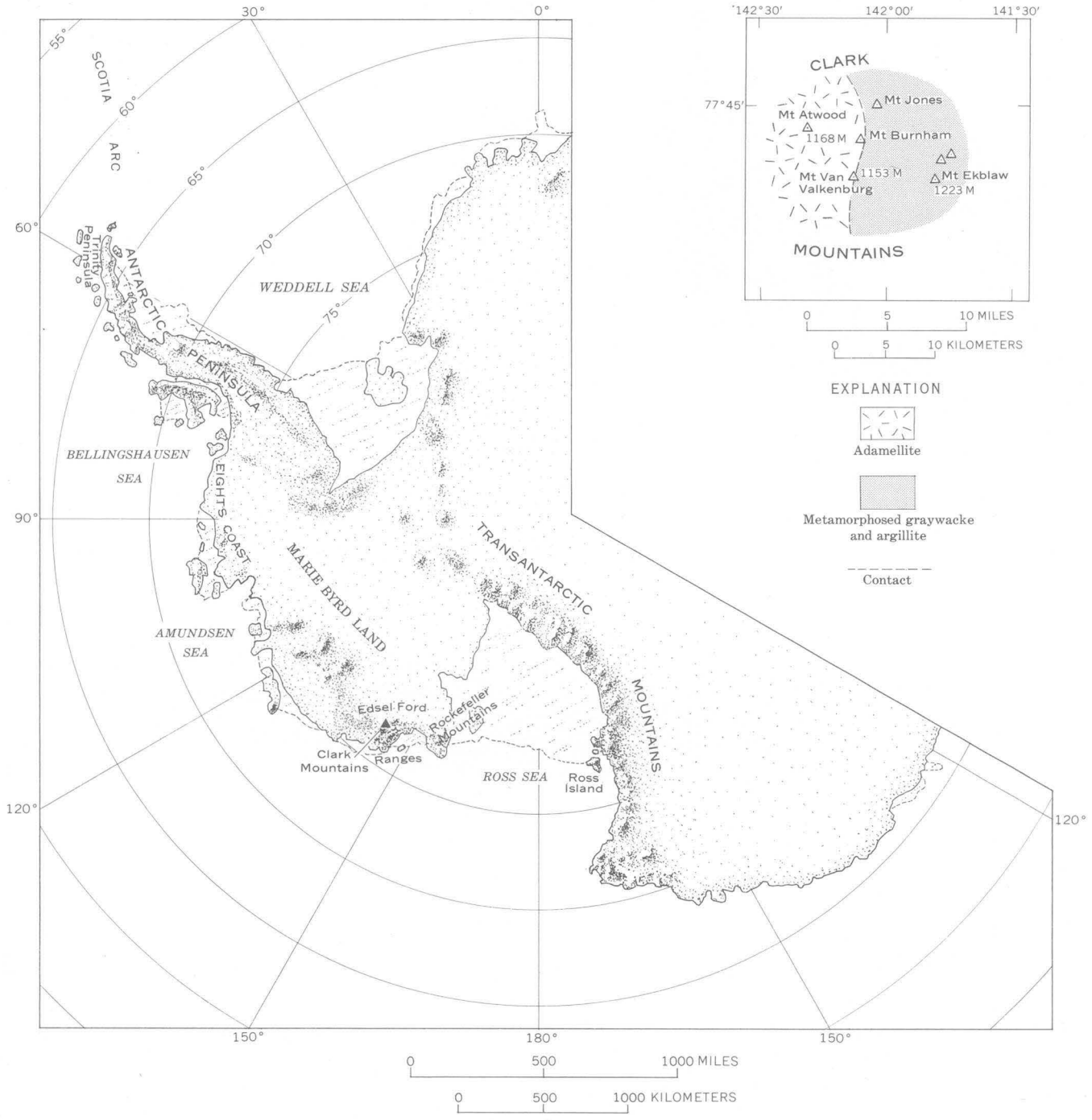

FIGURE 1.—Index map of West Antarctica, showing the location of the Edsel Ford Ranges and Clark Mountains. Inset map shows the geology of the Clark Mountains and location of Mount Atwood.

AGE DETERMINATION

Adamellite selected for age work, from Mount Atwood (fig. 1), was collected well within the pluton and away from the contact and intrusive lamprophyre dikes. Biotite and potassium-feldspar concentrates sufficient for K–Ar and Rb–Sr age work were obtained, but the sample was too small to provide enough zircon for Pb–α dating. The K–Ar age of biotite and Rb–Sr age of a whole-rock split, together with the corresponding analytical data, are listed in tables 2 and 3, respectively. The analytical procedures for the K–Ar and Rb–Sr analyses are similar to those described by Goldich and others (1961) and Zartman (1964).

These are the first ages to be reported from this re-

TABLE 1.—*Chemical analysis, CIPW norm, and mode of adamellite from Mount Atwood, Clark Mountains, West Antarctica*

[Approximate location of sample (field No. BTB-30, lab. No. 156227): lat 77°16′12″ S., long 142°18′54″ W. Tr., trace]

Chemical analysis[1]		CIPW norm		Mode[2]	
Constituent	Weight percent	Mineral	Percent	Mineral	Volume percent
SiO_2	76. 5	Quartz	37. 6	Quartz	37. 8
Al_2O_3	12. 0	Orthoclase	28. 9	Orthoclase perthite.	34. 3
Fe_2O_3	. 6	Albite	29. 3	Plagioclase[3]	25. 7
FeO	. 44	Anorthite	2. 5	Biotite	2. 1
MgO	. 11	Corundum	. 3	Muscovite	. 1
CaO	. 49	Hypersthene	. 6	Sericite	Tr.
Na_2O	3. 4	Magnetite	. 9	Chlorite	Tr.
K_2O	4. 8	Ilmenite	. 2	Magnetite-ilmenite.	Tr.
H_2O^+, H_2O^-	. 45	Total	100. 3	Apatite	Tr.
				Amphibole	Tr.
TiO_2	. 08			Sphene	Tr.
P_2O	. 02			Calcite	Tr.
MnO	. 03			Zircon	Tr.
CO_2	. 05			Myrmekite	Tr.
Total	98. 97				

[1] By methods similar to those described by Shapiro and Brannock (1956). Analysts: Paul Elmore, Ivan Barlow, Samuel Botts, and Gillison Chloe.
[2] Based on 2,402 points counted by the Chayes method.
[3] Average composition is An_6 as determined by oil-immersion method.

TABLE 2.—*Analytical data and K-Ar age of biotite from adamellite, Mount Atwood, Clark Mountains, West Antarctica*

[Analysts: R. F. Marvin, H. H. Mehnert, and Wayne Mountjoy. Approximate location of sample (field No. BTB-30): lat 77°16′12″ S., long 142°18′54″ W.]

Sample	K_{20} (percent)	K^{40} (ppm)	$*Ar^{40}$ (ppm)	$*Ar^{40}$ (percent)	$\frac{*Ar^{40}}{K^{40}}$	Age (m.y.)
523–B	6. 34 avg	6. 42	0. 0557	92	0. 00867	143±4

Symbol: *radiogenic isotope.
Decay constants: K^{40}, $\lambda_\epsilon = 0.585 \times 10^{-10}yr^{-1}$ $\lambda_\beta = 4.72 \times 10^{-10}yr^{-1}$.
Abundance: $K^{40} = 1.22 \times 10^{-4}$g/g K.
Potassium determinations, 6.34 percent and 6.35 percent K_2O, made with a Perkin-Elmer flame photometer with Li internal standard; Ar determined by isotope-dilution techniques.

TABLE 3.—*Analytical data and Rb-Sr age of K-feldspar (F) and whole rock (R) from adamellite, Mount Atwood, Clark Mountains, West Antarctica*

[Analysts: C. E. Hedge and F. G. Walthall. Approximate location of sample (field No. BTB-30): lat 77°16′12″ S., long 142°18′54″ W.]

Sample	Rb^{87} (ppm)	Normal Sr (ppm)	$*Sr^{87}$ (ppm)	$\frac{*Sr^{87}}{Rb^{87}}$	$\frac{*Sr^{87}}{\text{total } Sr^{87}}$	Age (m.y.)
523 F	126. 4	13. 75	0. 255	0. 00202	0. 212	137±9
523 R	96. 67	11. 03	. 165	. 00171	. 179	116±10

Symbol: *radiogenic isotope.
Decay constant: Rb^{87}, $\lambda_\beta = 1.47 \times 10^{-11}yr^{-1}$.
Abundance: $Rb^{87} = 0.283$ g/gRb.
Rb and Sr determined by isotope-dilution techniques.

gion and should be considered preliminary. The K–Ar age of 143±4 million years (biotite) and the Rb–Sr age of 137±9 m.y. (potassium feldspar) are in good agreement. The whole-rock Rb–Sr age of 116±10 m.y. is appreciably younger than the other two isotopic ages; this discordancy was not further investigated. With this in mind, the authors consider the adamellite to have a minimum age of 140 m.y. (Late Jurassic).

PETROCHEMICAL CORRELATION OF INTRUSIVE ROCKS IN WEST ANTARCTICA

The petrochemical correlation of intrusive rocks of West Antarctica, exclusive of the Transantarctic Mountains, is provisional in view of the few samples involved and their wide areal distribution over a terrane where there is relatively little exposed bedrock. Chemically analyzed rocks are grouped geographically herein according to four extensive regions of West Antarctica: Northwestern Marie Byrd Land, interior West Antarctica, Eights Coast, and Antarctic Peninsula. The rocks are compared normatively (fig. 2).

Wade (1937, p. 1395) hypothesized that the plutonic rocks of the southern Edsel Ford Ranges are part of the Andean mobile belt. As an alternative, Hamilton (1961) suggested that the granite–quartz diorite series of the southern Edsel Ford Ranges and similar rocks of the Rockefeller Mountains bear petrochemical and petrographic similarities to undated rocks of interior West Antarctica, and are different from the Cretaceous to lower Tertiary (Andean) granitic-gabbro suite of the Antarctic Peninsula; he inferred a Silurian to Permian age for the intrusives of northwestern Marie Byrd Land and interior West Antarctica.

Normative comparisons (fig. 2) do, indeed, indicate a remarkable similarity between the granitic rocks of northwestern Marie Byrd Land and those from interior West Antarctica. Rocks of the Andean suite from the Antarctic Peninsula, as far as known, however, plot near the same variation curves without marked contrast in tie-line trends, and it is suggested that they also are petrochemically equivalent to rocks of northwestern Marie Byrd Land and interior West Antarctica. There appears to be confusion in the assignment of rocks to the Andean suite, as two of Hamilton's (1961) samples (156230 and 156231) seem to be related petrochemically to batholithic rocks of the Eights Coast.

AGE CORRELATIONS IN WEST ANTARCTICA

The similarity in chemical and petrographic features of the Clark Mountains adamellite and of other rocks

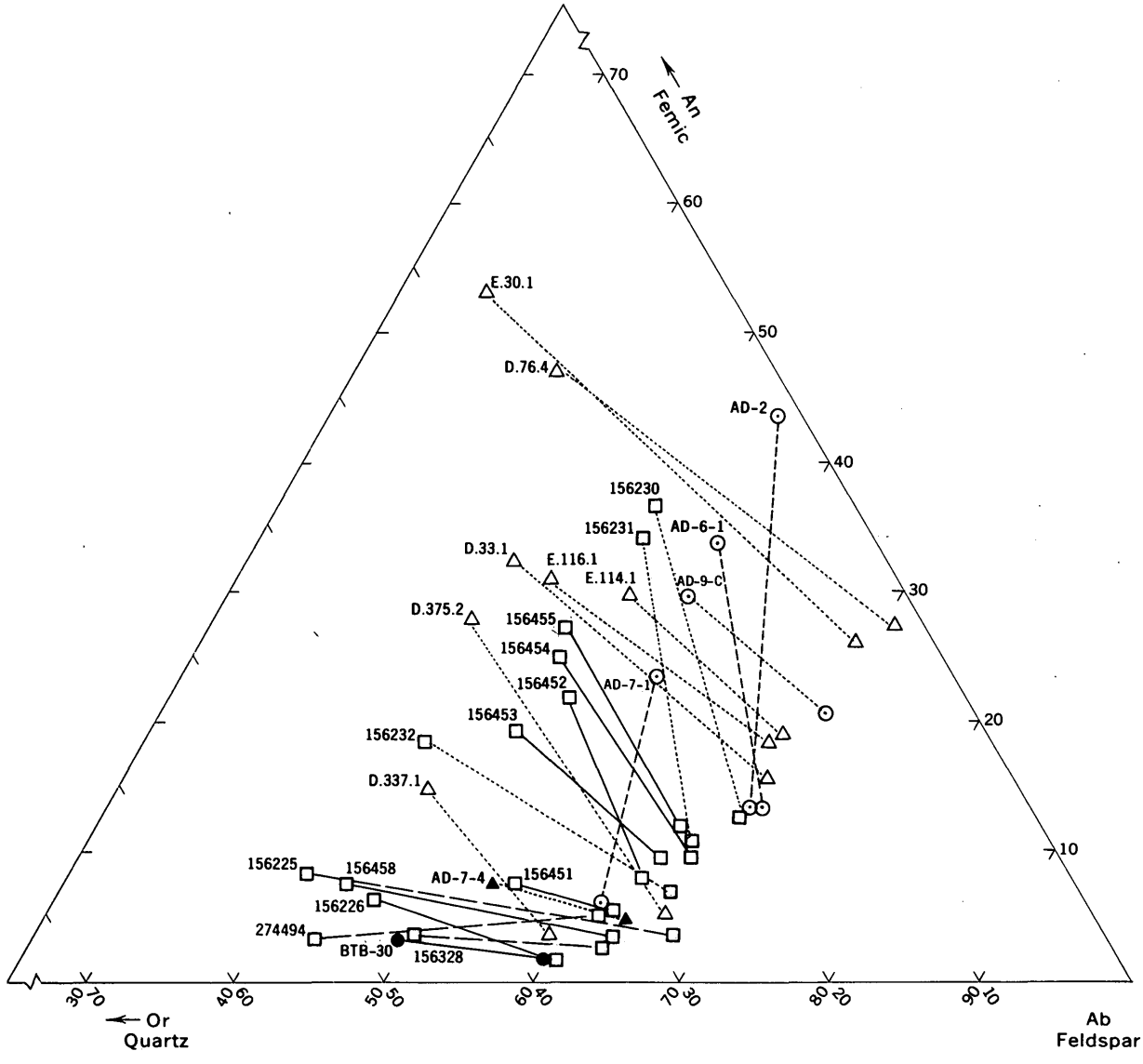

FIGURE 2.—Larsen plots showing normative comparison of rocks of the northwestern Marie Byrd Land (solid lines) with those of interior West Antarctica (long-dashed lines), the Eights Coast batholith (short-dashed lines), and those of the Andean granite-gabbro intrusive suite (dotted lines). Symbols: □, data from Hamilton (1961); ⊙, data from Drake and others (1964); △, data from Adie (1955); ▲, unpublished data (Avery Ala Drake, Jr., U.S. Geol. Survey); and ●, data from dated sample collected by Boudette. Numbers on symbols inside the triangle are sample numbers.

of northwestern Marie Byrd Land and rocks of interior West Antarctica does not necessitate their being all the same age. These rocks crop out over a linear distance of 950 kilometers, and in part, may well range from Silurian to Permian in age as has been suggested.

The data on ages of plutonic rocks in West Antarctica as well as the adjacent Scotia Arc are few. Drake and others (1964) have summarized these data to suggest five regional intrusive or metamorphic events, or both: (1) Precambrian and early Paleozoic, (2) late Carboniferous, (3) Late Triassic to Early Jurassic, (4) middle Mesozoic, and (5) Late Cretaceous to early Tertiary (Andean). A zircon concentrate from the quartz diorite at the Eights Coast composite batholith, about 1,300 km away, had a Pb–α age of 150±20 m.y. (Drake and others, 1964). Biotite in the same rock was apparently recrystallized 97±5 m.y. ago. Although the Pb–α age is comparable to the isotopic mineral ages for the Clark Mountains adamellite, it is unlikely that the rocks from the two areas are part of the same intrusive series, in view of their wide separation and petrochemical dissimilarity (fig. 2). However, a

pink granitic rock which intrudes the Eights Coast quartz diorite and is possibly chemically equivalent to granite of the Andean suite, is petrochemically similar to the Clark Mountains adamellite (Avery Ala Drake, Jr., unpub. data), and future dating may show similarity in ages. If a belt of rocks of the Andean intrusive suite (here inferred) continues through northern Marie Byrd Land from its westerly appearance at the Eights Coast (Drake and others, 1964, p. D53), a valid correlation with rocks of northwestern Marie Byrd Land may be made, assuming a range in ages of Andean suite rocks of 50 m.y. or more. If this hypothesis is correct, petrochemically comparable intrusions were emplaced in northwestern Marie Byrd Land earlier than in the Eights Coast and Antarctic Peninsula. Geologically unmapped areas along the coast are potential sources of tie-in data.

If the Clark Mountains intrusive is dated correctly, the minimum age for the intruded metasedimentary rock is 140 m.y., and this is possibly the minimum age for other metamorphosed rocks in the southern Edsel Ford Ranges. If plutonism in northwestern Marie Byrd Land occurred as an early phase of Andean orogeny in middle Mesozoic times as is here suggested, a eugeosynclinal sedimentary assemblage comparable in age to the upper Paleozoic "Trinity Peninsula Series" (Adie, 1957; 1964, p. 310-311) may be represented by the metamorphic rocks.

REFERENCES

Adie, R. J., 1955, The petrology of Graham Land. II, The Andean granite-gabbro intrusive suite: Falkland Islands Dependencies Survey Sci. Rept. 12, 39 p.

——— 1957, The petrology of Graham Land. III, Metamorphic rocks of the Trinity Peninsula Series: Falkland Islands Dependencies Survey Sci. Rept. 20, 26 p.

——— 1964, Stratigraphic correlation in West Antarctica, *in* R. J. Adie, ed., Antarctic geology: Amsterdam, North Holland Pub. Co. p. 307–313.

Drake, A. A., Jr., Stern, T. W., and Thomas, H. H., 1964, Radiometric ages of zircon and biotite in quartz diorite, Eights Coast, Antarctica, *in* Geological Survey Research 1964: U.S. Geol. Survey Prof. Paper 501–D, p. D50–D53.

Goldich, S. S., Nier, A. O. C., Baadsgaard, Haefdon, Hoffman, J. H., and Krueger, N. W., 1961, The Precambrian geology and geochronology of Minnesota: Minnesota Geol. Survey Bull. 41, 193 p.

Hamilton, Warren, 1961, Petrochemistry of probable Paleozoic granitic rocks from the Ross Sea Region, Antarctica: Art. 225 *in* U.S. Geol. Survey Prof. Paper 424–C, p. C209–C212.

McKelvey, V. E., compiler, 1960, Synopsis of geologic results: U.S. Geol. Survey Prof. Paper 400–A, 136 p.

Shapiro, Leonard, and Brannock, W. W., 1956, Rapid analysis of silicate rocks: U.S. Geol. Survey Bull. 1036–C, p. 19–56.

Wade, F. A., 1937, Petrologic and structural relations of the Edsel Ford Ranges, Marie Byrd Land, to other Antarctic Mountains: Geol. Soc. America Bull., v. 48, p. 1387–1396.

Warner, L. A., 1945, Structure and petrography of the southern Edsel Ford Ranges, Antarctica: Am. Philos. Soc. Proc., v. 89, p. 78–122.

Zartman, R. E., 1964, A geochronologic study of the Lone Grove Pluton from the Llano uplift, Texas: Jour. Petrology, v. 5, no. 3, p. 359–408.

POTASSIUM-ARGON AGES OF TERTIARY PLUTONS IN THE PRINCE WILLIAM SOUND REGION, ALASKA

By MARVIN A. LANPHERE, Menlo Park, Calif.

Abstract.—Potassium-argon ages of biotite and hornblende from four plutons in the western part of Prince William Sound, in southern Alaska, range from 34.4 to 36.6 m.y. with a mean age of 35.8 m.y. These data indicate that emplacement of the plutons occurred early in the Oligocene.

A belt of granitic intrusive rocks rims the northern margin of the Pacific Ocean basin from western Canada to southwestern Alaska. The plutons along this belt vary in tectonic setting, intrusive style, and age, though nearly all the plutons are late Mesozoic or Tertiary. A more precise chronology for these plutonic rocks is being determined at several localities, utilizing isotopic mineral ages. In the Prince William Sound region of southern Alaska, potassium-argon mineral ages indicate a well-defined middle Tertiary (early Oligocene) age for emplacement of several plutons.

GEOLOGIC SETTING

The distribution of major geologic units in the Prince William Sound region as compiled by George Plafker, of the U.S. Geological Survey, is shown on figure 1. The two major stratigraphic units, the Valdez and Orca Groups, were originally named and described by Schrader (1900; Schrader and Spencer, 1901) as the Valdez and Orca Series. The age of these units has been a subject for speculation because of the rarity of diagnostic fossils. On the basis of its apparently higher degree of metamorphism the Valdez Group generally has been considered to be older than the Orca Group. Moffit (1954) summarized the early work and available evidence from fossils, and he favored a Mesozoic, probably Late Cretaceous, age for both units. But on the basis of new fossil collections and restudy of previous collections, Plafker and MacNeil (1966) concluded that the age of the Valdez Group is Jurassic or Cretaceous and that the age of the Orca Group is early Tertiary. Subsequently, Plafker (*in* Case and others, in press) revised the age of the Valdez Group to Jurassic(?) and Cretaceous.

The lithology of the Valdez and Orca Groups has been summarized by Plafker and MacNeil (1966). The Valdez Group is composed of a monotonous sequence of graywacke, slate, argillite, and conglomerate with minor amounts of mafic igneous rock. The Orca Group can be divided into two lithologic units. The lower unit consists predominantly of mafic volcanic rocks and conglomeratic rocks which intertongue with graywacke and argillite. The upper unit of the Orca Group consists mainly of sandstone, siltstone, and argillite with minor amounts of volcanic and conglomeratic rocks. The lower, or volcanic, unit contains marine megafossils of middle or late Eocene age, and the upper, sedimentary unit contains pollen of post-Mesozoic age (Plafker and MacNeil, 1966).

Small plutons of granitic rocks intrude the Valdez Group at several localities in the western part of Prince William Sound, and one large intrusive mass cuts the Orca Group in the eastern part of the Sound. In the present report mineral ages are reported for samples from four plutons that intrude the Valdez Group, but no samples of datable material have been collected from the pluton that intrudes the Orca Group.

The analyzed samples show a wide variation in texture and composition. Samples PW–1 and PW–2 are medium-grained granodiorite, PW–8 is medium-grained quartz diorite, and PW–9 is coarse-grained quartz monzonite. In all these samples brown biotite is the most abundant mafic mineral; green hornblende is subordinate except in PW–8 where hornblende and biotite are approximately equal in abundance.

U.S. GEOL. SURVEY PROF. PAPER 550-D, PAGES D195-D198

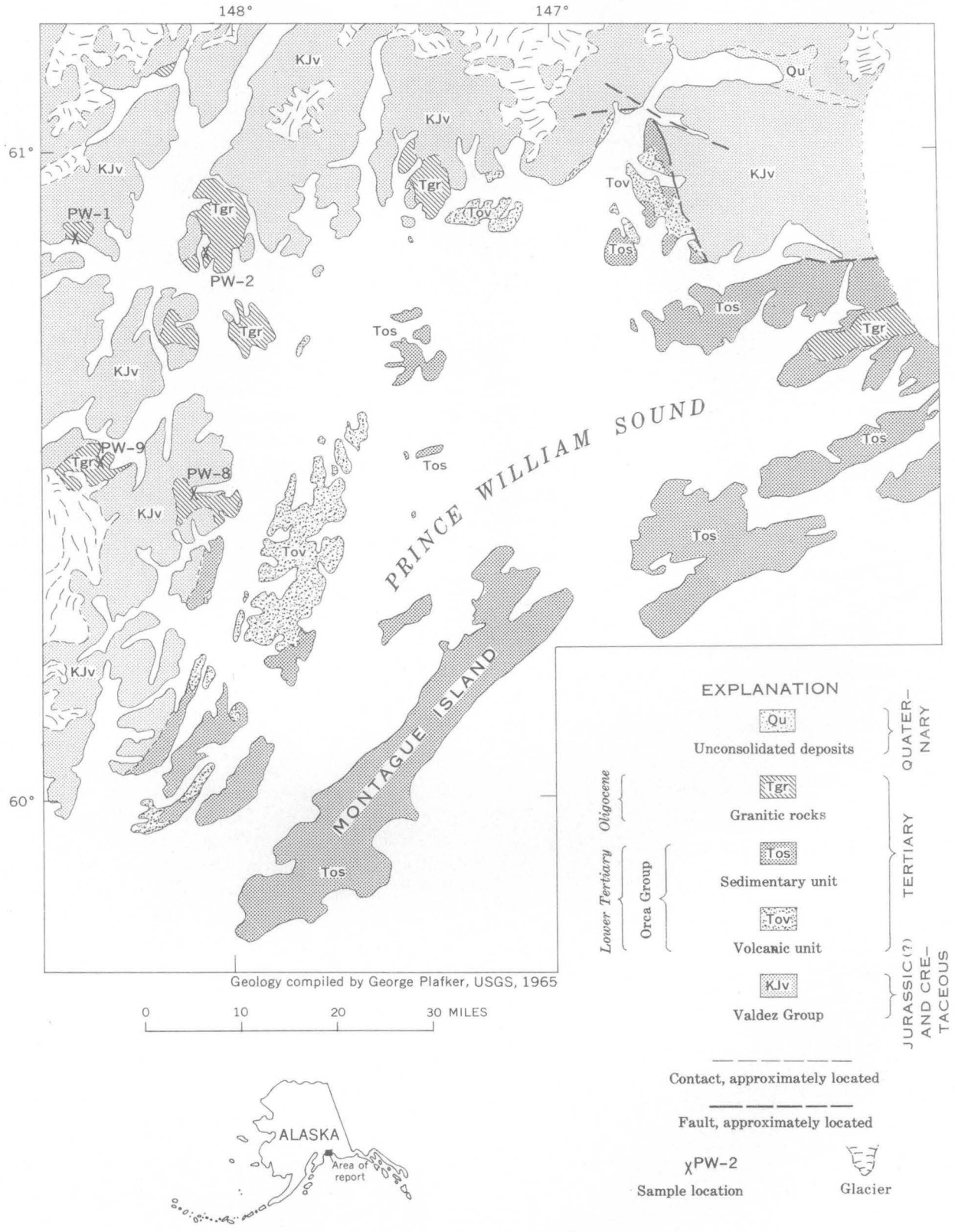

FIGURE 1.—Generalized geologic map of part of the Prince William Sound region, Alaska, showing location of dated samples.

ANALYTICAL RESULTS

The argon analyses were made using standard isotope-dilution techniques, and the potassium analyses were done by flame photometry using a lithium internal standard. The plus-or-minus value assigned to each apparent age (table 1) is the estimated standard deviation of analytical precision, exclusive of possible systematic errors introduced by an uncertainty in the value of the decay constant for electron capture of K^{40}.

The apparent ages of the analyzed minerals are in excellent agreement, and there are no significant differences in age between the four plutons. The mean value is 35.8 million years, and the total spread is 2.2 m.y. or 6.1 percent of the mean value. I estimate the standard deviation of precision (σ) in our laboratory to be approximately 3 percent. This figure is based on repetitive analyses of a homogeneous muscovite concentrate (Lanphere and Dalrymple, 1965) combined with estimates of the uncertainties in calibration of the argon tracer system and potassium standard solutions. In order to demonstrate that there is an actual difference in age among these plutons at the 95-percent confidence level, the observed difference must be greater than 2.772 σ (McIntyre, 1963) or 3.0 m.y. for the Prince William Sound data. Thus, I conclude that there is no actual difference in the age of these plutons and that they were emplaced approximately 36 m.y. ago.

DISCUSSION OF RESULTS

The inferred emplacement age of 36 m.y. for the plutons that intrude the Valdez Group is early Oligocene according to the potassium-argon time scale of Evernden and others (1964) and the Tertiary correlation chart of Wood and others (1941). The pluton in the eastern part of the Sound that intrudes the Orca Group is lithologically similar to the plutons that intrude the Valdez and may belong to the same plutonic event. The Orca Group was highly deformed before it was intruded by granitic rocks, and on the basis of stratigraphic evidence Plafker and MacNeil (1966) suggested that this episode of deformation may have culminated in the interval late Eocene to early Oligocene. If the plutons that intrude the Valdez and Orca are correlative, the potassium-argon data suggest that the episode of tectonic deformation probably was concluded by the end of the Eocene.

Early Tertiary potassium-argon ages ranging from 57 to 60 m.y. have been measured on granitic rocks of the Shumagin-Kodiak belt southwest of Prince William Sound. These ages suggest an early Eocene igneous event that is significantly older than the Oligocene plutonism in Prince William Sound. A complex Tertiary plutonic history on Baranof Island in southeastern Alaska is indicated by potassium-argon ages ranging from 24 to 48 m.y. (R. A. Loney, D. A. Brew, and M. A. Lanphere, written commun., 1966). All these data indicate that a belt of Tertiary plutonism extends for several hundred miles along the margin of the Pacific Ocean; unravelling of the detailed Tertiary plutonic history will require additional work.

TABLE 1.—*Potassium-argon ages and analytical data for Tertiary plutons in the Prince William Sound area, Alaska*

[Potassium analyses by H. C. Whitehead and L. B. Schlocker; argon analyses by M. A. Lanphere]

Field No.	Mineral	K_2O analyses (percent)	Average K_2O (percent)	Ar^{40}_{rad} (10^{-10} moles/g)	$\frac{Ar^{40}_{rad}}{Ar^{40}_{total}}$	Apparent age (millions of years)	Location
PW-1	Biotite	8. 00, 8. 05	8. 02	4. 388	0. 61	36. 6±1. 0	Seward (D–4) quadrangle; north shore of Passage Canal; lat 60°50′ N., long 148°29′ W.
PW-2	Biotite	8. 18, 8. 20	8. 19	4. 332	. 59	35. 5± . 9	Seward (D–3) quadrangle; east shore of Esther Lake; lat 60°50′ N., long 148°03′ W.
PW-8	Biotite	8. 22, 8. 31	8. 26	4. 457	. 81	36. 2±1. 0	Seward (B–3) quadangle; east shore of Eshamy Lake; lat 60°27′ N., long 148°06′30″ W.
	Hornblende	. 619, . 626	. 622	. 3194	. 48	34. 4±1. 2	
PW-9	Biotite	8. 02, 8. 03	8. 02	4. 325	. 85	36. 1± . 9	Seward (B–4) quadangle; south shore of Deep Water Bay; lat 60°29′30″ N., long 148°23′ W.

Decay constants for K^{40}: $\lambda_\epsilon = 0.585 \times 10^{-10}$ year^{-1}; $\lambda\beta = 4.72 \times 10^{-10}$ year^{-1}.
Atomic abundance of $K^{40} = 1.19 \times 10^{-4}$.

REFERENCES

Case, J. E., Barnes, D. F., Plafker, George, and Robbins, S. L., in press, Gravity survey and regional geology of Prince William Sound epicentral region, Alaska: U.S. Geol. Survey Prof. Paper 543–C.

Evernden, J. F., Savage, D. E., Curtis, G. H., and James, G. T., 1964, Potassium-argon dates and the Cenozoic mammalian chronology of North America: Am. Jour. Sci., v. 262, p. 145–198.

Lanphere, M. A., and Dalrymple, G. B., 1965, P–207—an inter-laboratory standard muscovite for argon and potassium analyses: Jour. Geophys. Research, v. 70 p. 3497–3503.

McIntyre, D. B., 1963, Precision and resolution in geochronometry, *in* Albritton, C. C., ed., The fabric of geology: Reading, Mass., Addison-Wesley Publishing Co., Inc., p. 112–134.

Moffit, F. H., 1954, Geology of the Prince William Sound region, Alaska: U.S. Geol. Survey Bull. 989–E, p. 225–310.

Plafker, George, and MacNeil, F. S., 1966, Stratigraphic significance of Tertiary fossils from the Orca Group in the Prince William Sound region, Alaska, *in* Geological Survey Research 1966: U.S. Geol. Survey Prof. Paper 550–B, p. B62–B68.

Schrader, F. C., 1900, A reconnaissance of a part of Prince William Sound and the Copper River district, Alaska, in 1898: U.S. Geol. Survey Ann. Rept. 20, pt. 7, p. 341–423.

Schrader, F. C., and Spencer, A. C., 1901, The geology and mineral resources of a portion of the Copper River district, Alaska: U.S. Geol. Survey Spec. Pub., 93 p.

Wood, H. E. and others, 1941, Nomenclature and correlation of the North American continental Tertiary: Geol. Soc. America Bull., v. 52, p. 1–48.

PRECAMBRIAN PHOSPHORITE IN THE BELT SERIES IN MONTANA

By R. A. GULBRANDSEN, Menlo Park, Calif.

Abstract.—A thin bed of phosphorite (23.5 percent P_2O_5) found in the younger part of the Precambrian Belt Series in Montana is one of only a small number of phosphorite occurrences of this age known in the world. It may contain fossils; one distinct structure observed in thin section is similar to a sponge spicule. Knowledge that phosphorites have formed in Precambrian times should provide incentive for exploration in such previously overlooked terranes, although some lines of evidence indicate that Precambrian phosphorite may be rare.

The Precambrian phosphorite discovered in Montana is one of only a few such deposits known in the world. The only other occurrence of Precambrian phosphorite in the United States is in the Ocoee Series in Tennessee, which, although known earlier, was first noted in the literature by Hamilton (1961) and described by Wedow and others (1966). The earliest descriptions of phosphorite in the Precambrian are of nodules that were found in Scotland (Peach and others, 1907) and Sweden (Hedstrom, 1930). Other references mention occurrences in China (Ho, 1942; Wang and Huo, 1945a, 1945b; and Hsieh and Chao, 1948), and Czechoslovakia (Shatskii, 1955). However, the only Precambrian phosphorite of large extent and of probable economic importance is in Russia (Mats, 1956). The present worldwide search for phosphorite has generally ignored Precambrian sedimentary terrane on the assumption that phosphorite in any significant amounts probably did not form during the Precambrian. The geochemical implications of this assumption have received little attention.

DESCRIPTION OF THE PHOSPHORITE

Phosphorite was found in a new roadcut on U.S. Route 91 just south of the Lyon Creek road overpass in Wolf Creek Canyon, about 30 miles north of Helena, Mont. (fig. 1). It occurs as a 0.25– to 1.0–inch-thick layer within an 8-inch bed of light-brownish-gray to light-green coarse siltstone. Discontinuous laminae and individual grains of phosphate occur in the siltstone both above and below the phosphorite layer. The phosphorite occurs in the central part of the Spokane Formation, a predominantly red-bed unit, of the Belt Series. The Belt Series is very slightly metamorphosed and of late Precambrian age, probably about 1 billion years old (Gulbrandsen and others, 1963).

The phosphatic rock is a medium-grained pelletal phosphorite, dark gray to black in the richer phosphatic parts and speckled light and dark in the leaner ones. The dark color probably is due to organic matter in the pellets. Quartz and plagioclase of coarse silt to very fine sand size form a matrix for the pellets, and quartz cements the entire rock.

The principal minerals of the phosphorite are carbonate fluorapatite (identified by X-ray and chemical analyses), quartz, muscovite, and plagioclase (albite or oligoclase). Minor minerals are chalcocite, zircon, chlorite, tourmaline, malachite, and biotite(?). Apatite occurs mainly as microcrystalline aggregates in pellet or other aggregate form, but clear, colorless megacrystalline apatite occurs within microcrystalline aggregates, on the edges of such aggregates, in clusters, and as disseminated small subhedra or euhedra.

The mineral composition of the pellets and other aggregate forms is varied, and the kinds and proportions of minerals reflect diverse origins of the phosphorite components, a feature common to most phosphorite. The compositions range from nearly pure apatite to rock clasts for the most part lacking apatite. The clasts are fragments of chert, mudstone, and siltstone. In the forms composed dominantly of apatite, the other minerals are considered as inclusions. Most such inclusions are very fine grained muscovite that may have crystallized contemporaneously with the apatite. Inclusions of relatively coarse muscovite, accompanied by quartz and feldspar, are likely of detrital origin.

The apatite pellets range in shape from ovular or spherical to highly irregular forms that appear to be the product of deformation of incompletely lithified

U.S. GEOL. SURVEY PROF. PAPER 550-D, PAGES D199-D202

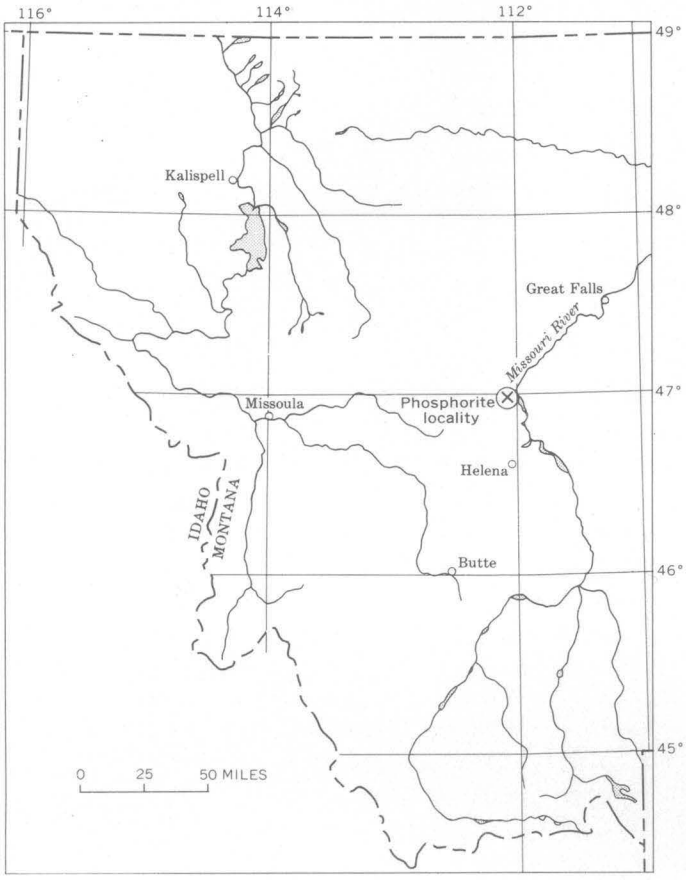

FIGURE 1.—Map of western Montana, showing phosphorite locality.

pellets during compaction of the bed. Some shapes are due to recrystallization and secondary growths of apatite along the pellet borders. Some quartz replacement along pellet borders has also modified their shape. Hemispherical forms represent broken pellets. Other microcrystalline aggregates, lacking the rounded borders of pellets, are possibly fragments of disrupted microcrystalline apatite layers that were not fully lithified when broken. Oolites are rare.

One circular grain, as seen in thin section (fig. 2), has a distinct structure that is of special interest because of its similarity to cross sections of sponge spicules in phosphorite of the Permian Phosphoria Formation. It also has the same composition as the spicules in which the inner canals have been enlarged and filled with microcrystalline apatite, and in which the outer rings are composed of quartz derived from opal. Other structures of possible organic origin are also present but are not clearly identifiable with known forms.

CHEMICAL COMPOSITION

Partial chemical and spectrographic analyses of the phosphorite are presented in table 1. Nearly all the amounts of CaO, P_2O_5, F, and CO_2 are combined in carbonate fluorapatite (plagioclase would require only a very small amount of the CaO, and malachite only a trace of the CO_2). The summation of these constituents, about 56 percent, provides an approximate estimate of the amount of apatite in the sample. Most likely the SO_3, rare earths, and part of the Na_2O are also in the apatite, although they are neither of large amount nor of special concern here. It is significant that the composition of the apatite in this Precambrian phosphorite does not appear to be particularly different from younger apatite, such as that reported in the Permian Phosphoria by the author (U.S. Geol. Survey, 1964, p. A8).

The presence of approximately 1 percent of copper in the phosphorite, however, is unusual. It is contained in chalcocite, except for a trace amount in malachite formed by alteration of chalcocite. The chalcocite is mostly in microfractures in pellets. Some of the fractures cut several pellets and must have formed after the rock was lithified but before the quartz cement was introduced. Some chalcocite is disseminated in pellets, shows no relationship to fractures, and could have formed at the same time as the pellets. If the chalcocite was confined to one period of deposition, however, it was late. The possibility that this relatively coarse grained rock had a high permeability before quartz cementation may be the reason why the copper was introduced and confined to this particular bed.

GEOLOGIC IMPLICATIONS

Although this phosphorite is neither of economic importance nor of special petrologic significance, its

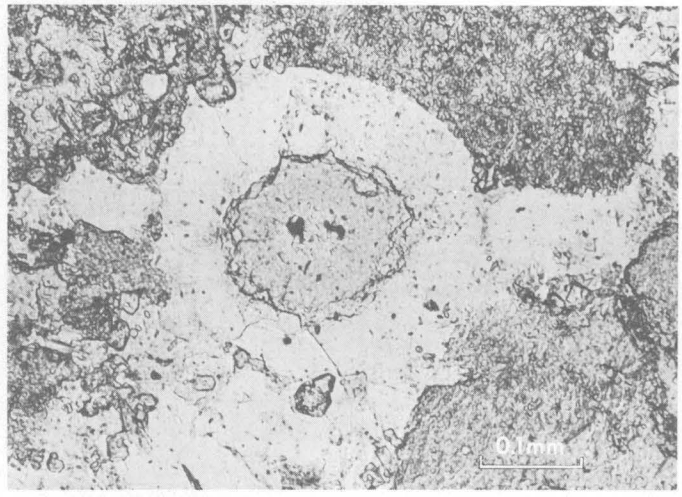

FIGURE 2.—Photomicrograph of phosphorite, showing possible organic structure. The central part of circular structure is composed of microcrystalline apatite; the outer ring is composed of quartz.

TABLE 1.—*Composition of Precambrian phosphorite from Montana*

[Analysts: L. B. Beatty, chemical analysis; Chris Heropoulos, spectrographic analysis Laboratory No. of sample, 65M–1300]

Constituent	Amount	Constituent	Amount
Partial chemical analysis, in percent by weight			
Total Fe as Fe_2O_3	0.74	MnO	0.19
CaO	30.7	CuO	1.16
Na_2O	.67	F	2.1
K_2O	1.54	CO_2	.85
TiO_2	.48	SO_3	.24
P_2O_5	22.5	Total S as S	.29
Semiquantitative spectrographic analysis [1]			
Si	>10	Ho	0.007
Al	5	La	.07
Mg	.5	Mo	.002
Ag	.002	Nd	.15
B	.003	Ni	.0015
Ba	.03	Pb	.02
Be	.0007	Pr	.02
Ce	.15	Sc	.002
Co	.0002	Sm	.05
Cr	.01	Sr	.1
Er	.015	Tm	.002
Eu	.01	V	.015
Dy	.05	Y	.2
Ga	.001	Yb	.01
Gd	.05	Zr	.03

[1] Results are reported in percent to the nearest number in the series, 1, 0.7, 0.5, 0.3, 0.2, 0.15, and 0.1, and so forth, which represent approximate midpoints of group data on a geometric scale. The assigned group for semiquantitative results will include the quantitative value about 30 percent of the time.

discovery once again focuses attention on the commonly held assumption that phosphorite is nearly absent in the Precambrian. The composition of sediments, the development of life, and the chemical evolution of sea water are basically involved in this assumption.

Geijer (1963), in comparing the phosphorus content of Precambrian and post-Precambrian sedimentary iron ores, found that post-Precambrian ores generally have about 10 times more phosphorus than the older ones, and he attributed the increase largely to the addition of hard animal parts. Nanz (1953) found that the fine-grained sedimentary rocks of post-Precambrian age have more phosphorus than older rocks, and he too suggested a relation with the development of life. To extract phosphorus from sea water at a greater rate in post-Precambrian times than earlier would require an increase in the supply of phosphorus to the seas, if a balance of the phosphorus input-output budget is assumed. Yet Gulick (1955) postulates that there may have been more phosphorus in the Precambrian seas than later, for under the reducing conditions likely to have existed in the early seas, more soluble forms of phosphorus than calcium phosphate, such as calcium phosphites or hypophosphites, may have been stable. If so, the amount of phosphorus in sea water diminished with time and the rate of phosphate deposition increased through the chemical evolution of sea water. The importance of phosphorus to practically all energy reactions in the living cell suggests to Gulick (1955) that an abundance of phosphorus in the early seas may have favored its extensive use in living matter and that adjustments to the minute amount of phosphorus in present-day sea water have been made through evolutionary processes. Although the hard parts of animals contribute to the phosphorus content of sedimentary rocks, they make up only a small part of the phosphorus in phosphorites. The role of life or organic activity, however, in creating conditions favorable for the concentration of phosphorus in phosphorites may be a major one. This concept would support the supposition of phosphorite scarcity in Precambrian times when the magnitude of life was low.

Despite evidence that supports the concept of phosphorite scarcity in Precambrian times, this scarcity may be only apparent and due in large part to insufficient exploration. Where Precambrian rocks have been metamorphosed, phosphorites may be altered in appearance and be difficult to recognize, but the apatite is not likely to be destroyed. This feature, plus the lack of previous exploration, should provide much incentive for a thorough search of Precambrian terranes for phosphorite.

REFERENCES

Geijer, Per, 1963, Some aspects of phosphorus in Precambrian sedimentation: Arkiv Mineral. Geol., v. 3, no. 9, p. 165–186.

Gulbrandsen, R. A., Goldich, S. S., and Thomas, H. H., 1963, Glauconite from the Precambrian Belt Series, Montana: Science, v. 140, no. 3565, p. 390–391.

Gulick, Addison, 1955, Phosphorus as a factor in the origin of life: Am. Scientist, v. 43, no. 3, p. 479–489.

Hamilton, Warren, 1961, Geology of the Richardson Cove and Jones Cove quadrangles, Tennessee: U.S. Geol. Survey Prof. Paper 349–A, p. A1–A55.

Hedström, H., 1930, Fosforitbollar från Visingsoserien?: Arsb. Sver. geol. Undersökn, v. 23, no. 6, p. 1–8.

Ho, C. S., 1942, Phosphate deposits of Tungshan, Chengchiang, Yunnan: China Geol. Survey. Bull. 35, p. 41–43.

Hsieh, C. Y., and Chao, C. H., 1948, Note on the phosphate deposits in China: Geol. Soc. China Bull., v. 28, no. 1–2, p. 71–74.

Mats, V. D., 1956, Geologicheskie kriterii i metody poiskov fosforitov v pozdnedokembriiskikh otlozheniiakh zapadnogo Pribaikalia [Geologic criteria and methods of prospecting for phosphorites in late Precambrian deposits of western Pribaikal] V sbornike: Materialy soveshchaniia geol. Vost. Sibiri i Daln. Vostoka po metodike geol.-semoch. i poisk. rabot. Chita, p. 410–418.

Nanz, R. H., Jr., 1953, Chemical composition of pre-Cambrian slates with notes on the geochemical evolution of lutites: Jour. Geology, v. 61, no. 1, p. 51–64.

Peach, B. N., Horne, J. Gunn, W., Clough, C. T., Hinzman, L. W.,

and Teal, J. J. H., 1907, The geological structure of the North-West Highlands of Scotland: Great Britain Geol. Survey Mem., p. 1–668.

Shatskii, N. S., 1955, Phosphorite-bearing formations and the classification of phosphorite deposits: Akad. Sci. USSR, Conf. Sedimentary Rocks, no. 2, p. 7–99.

U.S. Geological Survey, 1964, Geological Survey Research, Chapter A: U.S. Geol. Survey Prof. Paper 501–A, 367 p.

Wang, C. C., and Huo, S. C., 1945a, The phosphate deposits of Chichiaoshan, Chengkung, Yunnan: China Geol. Survey Bull. 36, p. 7–8.

——— 1945b, The phosphate deposits of Kuangching, Sungming, Yunnan: China Geol. Survey Bull. 36, p. 5–6.

Wedow, Helmuth, Jr., Carpenter, R. H., and Lehr, J. R., 1966, Phosphorite in the Precambrian Ocoee Series of the East Fork manganese district, Sevier County, Tennessee [abs.]: Geol. Soc. America, Southeastern Section Mtg., Athens, Ga., Program, p. 46.

A POTENTIAL SOURCE OF BRICK CLAY IN THE BELTSVILLE AREA, PRINCE GEORGES AND MONTGOMERY COUNTIES, MARYLAND

By C. F. WITHINGTON, Washington, D.C.

Abstract.—Bricks have been made successfully in the laboratory from silty clay that accumulates as waste material in sediment ponds of gravel-washing plants near Beltsville, Md. The composition of the clay compares favorably with the raw material now being used commercially for common brick. The laboratory brick fires light pink and hard to very hard, at temperatures of 1,900°F to 2,000°F. If further tests show that the waste material can be used commercially for making brick, it may form the basis for a new source of brick in the Beltsville area.

A potential source of clay for face brick was found during geologic mapping in the Beltsville quadrangle, Montgomery and Prince Georges Counties, Md. This raw material, silty clay from the washing of sand and gravel, at present is being wasted. Mineral resources now being exploited in the Beltsville area include sand and gravel for aggregate, and clay for brick. If the clay washed from the gravel proves suitable for commercial use in brickmaking, it may represent a substantial increase in the mineral resources of the area.

Sand and gravel, which are far more important, have been produced in the area for more than 30 years. The gravel is obtained from the Patuxent and the overlying Patapsco Formations of Cretaceous age, and from Quaternary deposits. The clay and silt in an average sample of gravel amount to about 1 percent, by weight, of the total. Thus, assuming that between 30,000 and 35,000 tons of gravel are processed daily in the Beltsville area, 300 to 350 tons of clay and silt are also being handled each day. In processing the gravel it is necessary to remove the fine material by washing. Before the 1950s the wash water, with the waste sedimentary material, was allowed to pass into the streams of the area. This waste disposal increased the sediment load of the Anacostia River and helped contribute to flooding at Bladensburg, Md., more than 4 miles south of the Beltsville area (Williams, 1942, p. 23.). Since then the gravel-plant operators have built sediment ponds in an effort to prevent stream pollution by the waste material. At present these ponds cover a total area of more than 100 acres. When a pond becomes filled with sediment, it must either be abandoned or reclaimed by removing the accumulated waste material. Use of the area of an abandoned pond for building purposes is lost because any structure built on it would be in danger of subsidence. On the other hand, disposal of the material accumulated in a pond has been difficult and expensive.

CHARACTER OF THE SEDIMENT

Eight random samples of waste sediment were collected in 1965 from 4 settling ponds for determination of physical properties: 2 samples from the pond of the Contee Sand and Gravel Co., 3 samples from the pond of W. H. McCeney Sand and Gravel Co., 1 sample from the pond (now abandoned) of the Prince Georges Sand and Gravel Co., and 2 samples from the pond of the A. H. Smith Co. (fig. 1).

The general lithology of the material in these samples was determined by performing grain-size analyses, finding Atterberg limits, and making mineralogic determinations on each of the samples collected. The grain-size distribution was determined for each sample, following the procedure of pipet analysis as described by Krumbein and Pettijohn (1938, p. 166–168). The results of these analyses (see table 1) indicate that 50 to 70 percent of the material is of clay size, averaging about 60 percent, and that most of the remainder is of silt size, though traces of fine sand were found in some samples.

Atterberg limits were also determined using a standard procedure (U.S. War Department, 1945, p. 54–57). The values of the Atterberg limits found are as follows: liquid limits, 29 to 56; plastic limits, 19 to 50; and plastic index, 5 to 25. According to the Unified Soils Classification System (U.S. Army Corps of En-

U.S. GEOL. SURVEY PROF. PAPER 550-D, PAGES D203-D208

224-352 O—66——14

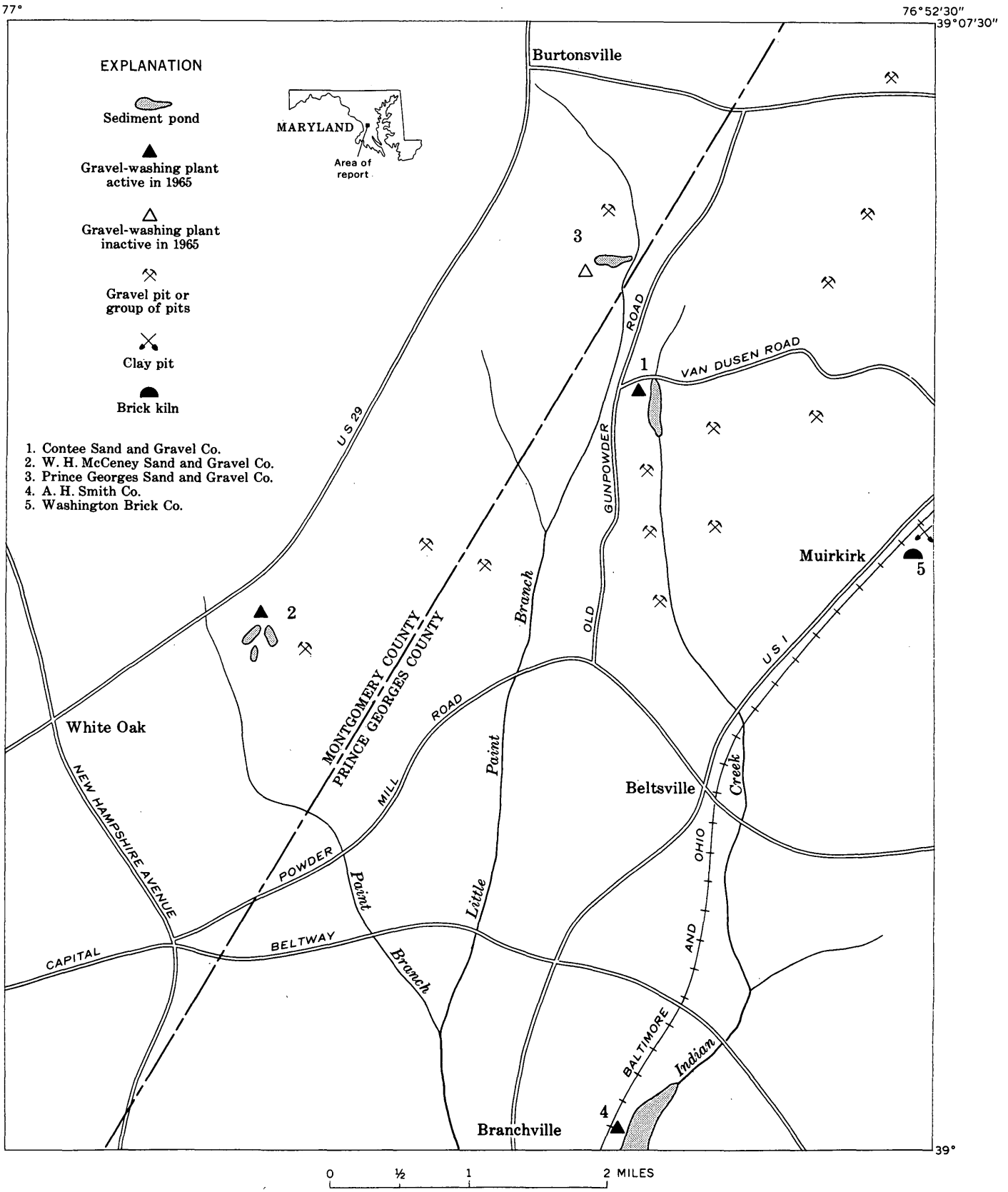

FIGURE 1.—Map of the Beltsville quadrangle, Maryland, showing location of sediment ponds.

TABLE 1.—*Texture, mineral composition, and other physical properties of unfired samples from sediment ponds of gravel-washing plants in the Beltsville area, Maryland*

Sample No.	Locality (fig. 1)	Grain-size distribution (percent of total sample, by weight)			Approximate content and proportions of clay minerals as estimated by X-ray-diffraction methods (percent)				Approximate content of other minerals as estimated by X-ray-diffraction methods (percent) [1]		Munsell color notation	Dry strength	Texture and workability	Atterberg limits [2]	Unified Soil Classification group symbols [3]
		Clay (<1/256 mm)	Silt (1/256-1/16 mm)	Sand (1/16-2 mm)	Kaolinite	Illite	Montmorillonite	Clay minerals in total sample (percent)	Mineral	Amount (percent)					
C–1	Contee Sand and Gravel Co., south side Van Dusen road; material removed from pond.	57	43	Tr.	70	25	5	50	Quartz	50	10*YR*8/4	Very good.	Smooth, fine, easy working, medium plasticity, lean.	LL–43 PL–19 PI–24	CL
C–2	Contee Sand and Gravel Co. pond; north end.	55	45	Tr.	60	30	10	50	do	50	2.5*YR*8/4	do	do	LL–30 PL–21 PI–19	CL
Mc–1	W. H. McCeney Sand and Gravel Co.; material from top of west pond.	70	30	------	70	25	5	65	do	35	10*YR*8/3	do	Smooth, fine, easy working, low plasticity, lean.	LL–47 PL–32 PI–15	ML
Mc–2	W. H. McCeney Sand and Gravel Co. pond; from gully, south side, west pond; material excavated from pond.	60	40	Tr.	60	30	10	55	do	45	10*YR*8/4	do	Smooth, fine, easy working, medium plasticity.	LL–56 PL–31 PI–25	MH
Mc–3	W. H. McCeney Sand and Gravel Co. west pond; material from top surface.	53	47	------	50	40	10	44	do	56	10*YR*8/3	do	Smooth, fine, easy working, low plasticity.	LL–35 PL–23 PI–12	ML
PG–1	Prince Georges Sand and Gravel Co.; abandoned pond.	66	32	2	70	20	10	60	do	40	2.5*YR*8/4	do	Smooth, fine, easy working, medium plasticity.	LL–55 PL–50 PI–5	MH
S–1	A. H. Smith Co. pond, ¼ mile from wash plant.	57	43	------	60	30	10	53	Quartz Feldspar	47 Tr.	2.5*YR*8/4	do	Smooth, low-medium plasticity, lean to moderately lean.	LL–29 PL–21 PI–8	CL
S–2	A. H. Smith Co. pond, near plant.	51	47	2	70	25	5	45	Quartz Feldspar	55 1	10*YR*7/3	do	Smooth, fine, easy working, medium, plasticity.	LL–53 PL–30 PI–23	MH

[1] Trace of unidentified iron minerals occurs in all samples.
[2] Symbols: LL, liquid limit; PL, plastic limit; PI, plastic index.
[3] Symbols: C, clay; M, silt; L, low plasticity; and H, high plasticity.

gineers, 1953) the material is classified as silt of low plasticity, clay of low plasticity, and silt of high plasticity (fig. 2).

The mineralogy of the clay minerals, as determined by X-ray diffraction, is characterized by 50 to 70 percent kaolinite, averaging 60 percent, with illite making up 25 to 40 percent, and montmorillonite making up 5 to 10 percent. X-ray diffraction also showed that quartz is the most abundant nonclay mineral, making up an estimated 50 to 60 percent of the total sample; traces of feldspar were found in the two samples from the A. H. Smith Co. pond. The material in general can be described as silty clay, with low to medium plasticity, that is smooth and easy working. Material such as this is suitable for making brick and for use in the impervious cores of earth dams.

LABORATORY PREPARATION OF BRICKS

Bricks were made in the laboratory under a process modified from that described by Klinefelter and Hamlin (1957, p. 53–54). Results of laboratory firing of the bricks are shown in table 2. The samples were air-dried, and then about 2 pounds of each sample was powdered so as to pass the No. 40 (0.42 mm) sieve. Although traces of sand are present in the ponds, sand-size material was virtually absent in the samples taken. Each sample was moistened until it reached a plastic state, as judged by "feel," and the wet material was placed in an airtight container for several days to allow it to attain a uniform moisture content. The material was then molded in an aluminum form, open at top and bottom, to make a brick 22 mm × 48 mm × 12 mm. Parallel marks 20 mm apart were placed on each brick to determine the percentage of shrinkage. The bricks were allowed to air-dry for about a week, after which the percentage of dry shrinkage was determined. At the time of molding of the brick, a small portion of the clay of each sample was made into balls about ¼ inch (6.35 mm) in diameter for use in the quick-fire test; they also were set aside to air-dry.

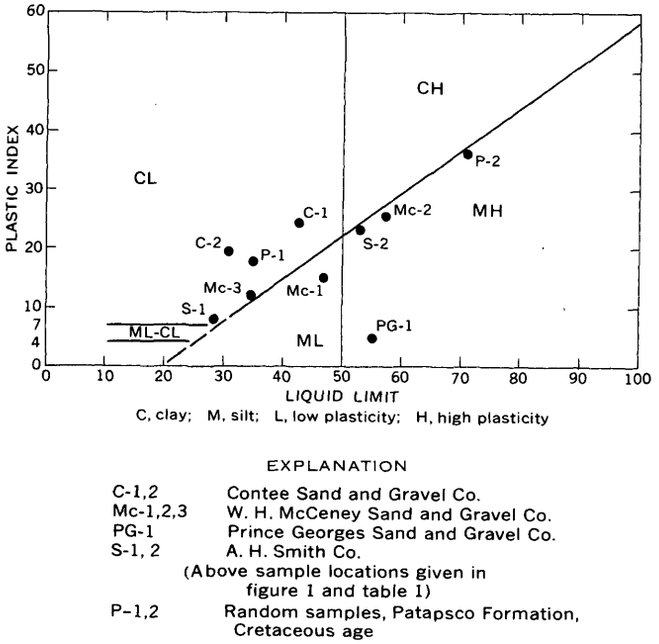

FIGURE 2.—Graph showing the Unified Soil Classification of samples from sediment ponds, Beltsville area, Maryland. Samples plotted on standard plasticity chart (U.S. Army Corps of Engineers, 1953).

The bricks were slow-fired in a kiln with a capacity of 2,400°F. Seven bricks from each sample were placed in a cold kiln, and the temperature was raised. After each increment of 100°F from 1,800°F to 2,400°F a brick of each sample was removed, and at the same time a quick-fire test was made by placing balls of clay into the oven. None of the material in the quick-fire test bloated; this indicates that the material is unsuitable for lightweight aggregate.

After each brick was removed from the kiln, the color, hardness, percentage of linear shrinkage, water absorption, and specific gravity were determined. The color determinations were made from the Munsell color chart (Munsell Color Co., 1954). The hardness was estimated using a classification based in part on work done by the U.S. Department of Agriculture.[1] The water absorption was determined from the weight of water absorbed in a partial vacuum.

The bricks fired at temperatures of 1,900°F to 2,000°F (the temperatures at which most commercial bricks are made) are weak orange-pink, hard to very hard, with a shrinkage generally of 5 percent and water absorption of 19 to 32 percent. The specific gravity averages about 1.5. At temperatures of 2,100°F to 2,300°F the bricks become reddish brown and very hard; the linear shrinkage increases to as much as 15 percent, averaging about 10 percent. Water absorption ranges from about 11 to 31 percent, decreasing at 2,300°F to about 11 to 18 percent. Specific gravity ranges from 1.34 to 2.82, becoming slightly greater at the higher temperatures. At 2,400°F the bricks darken to reddish gray, light gray, and dark gray, and become steel hard—that is, they cannot be scratched with a steel needle. Shrinkage amounts to as much as 20 percent but averages about 10 percent. Water absorption decreases to between 7.5 and 17 percent, and specific gravity decreases to between 1.4 and 2.4 percent. No tests were made above 2,400°F. Although the color of the brick is attractive, it is

[1] U.S. Department of Agriculture, Soil Conversation Service, [1963], Description of materials, chap. 1 *in* Engineering geology, sec. 8 *of* National Engineering Handbook: p. 13.

lighter than that of brick now being manufactured in the area; this could be changed by mixing color additives such as hematite with the clay.

With the exception of color, the material from the sediment ponds compares favorably with the clay now being used for brick in the Washington area. This clay is from the Patapsco Formation of Cretaceous age; it is generally reddish brown, and is sandy and silty and moderately plastic. The clay-mineral content is 50 to 80 percent kaolinite, 30 to 50 percent illite, and a few percent of a mixed-layer clay; no montmorillonite has been reported. Bricks made from the Patapsco clay by Knechtel and others (1961) are similar in most respects to those reported here. Two samples of the Patapsco Formation were tested for Atterberg limits. The liquid limit ranges from 70 to 35, the plastic limit from 34 to 18, and the plastic index from 36 to 17 (see fig. 2). This material may be classified according to the Unified Soil Classification system as clay of low plasticity or silt of high plasticity.

Further tests should be made on the sediments in the ponds to see if brick can be made commercially from them. In addition, the material should be checked by pyrometric-cone equivalent tests for suitability for high-refractory brick.

The importance of using this material for brick should not be overlooked, for the rapid urbanization of the Washington metropolitan area has diminished the available reserves of clay in the area. Thus, the use of this waste material would insure a continued inexpensive supply of brick for the metropolitan area.

TABLE 2.—*Results of ceramic tests on fired samples from sediment ponds of gravel-washing plants in the Beltsville area, Maryland*

Sample No. (see table 1 for location)	Munsell color notation	Hardness [1]	Linear shrinkage (percent)	Water absorption (percent)[2]	Specific gravity (approx.)
1,800°F					
C-1	10R8/3	Hard	5	31	1.60
C-2	2.5YR7/4	do	5	19	1.63
Mc-1	2.5YR7/4	do	5	32	1.32
Mc-2	2.5YR8/4	do	5	29	1.53
Mc-3	2.5YR8/4	do	5	24	1.68
PG-1	2.5YR6/6	do	8.7	29	1.46
S-1	2.5YR8/4	do	5	21	1.54
S-2	2.5YR8/4	do	5	26	1.52
1,900°F					
C-1	10R8/3	Hard	5	27	1.58
C-2	2.5YR7/4	do	5	20	1.61
Mc-1	2.5YR7/4	do	5	32	1.48
Mc-2	2.5YR7/4	do	5	29	1.53
Mc-3	2YR8/4	do	5	23	1.25
PG-1	2.5YR8/4	do	5.5	29	1.48
S-1	2.5YR8/4	do	5	21	1.66
S-2	2.5YR8/4	do	5	29	1.54
2,000°F					
C-1	10R8/3	Very hard.	5	25	1.70
C-2	2.5YR7/4	do	5	19	1.73
Mc-1	2.5YR7/4	do	5	30	1.58
Mc-2	2.5YR7/4	do	5	27	1.44
Mc-3	2.5YR8/4	do	5	22	1.31
PG-1	2.5YR7/6	do	5	28	1.56
S-1	2.5YR8/4	do	5	20	1.66
S-2	2.5YR8/4	do	5	24	1.56
2,100°F					
C-1	10R8/3	Very hard.	7.5	14.6	1.96
C-2	2.5YR7/4	do	5	12	1.75
Mc-1	2.5YR7/4	do	8	31	1.60
Mc-2	2.5YR7/4	do	13.25	20	1.76
Mc-3	2.5YR7/6	do	5	21	1.40
PG-1	2.5YR7/6	do	13.4	25	1.73
S-1	2.5YR7/4	do	7.5	19	1.74
S-2	2.5YR7/4	do	7.5	21	1.68
2,200°F					
C-1	10R7/3	Very hard.	10	15.7	2.5
C-2	2.5YR6/4	do	10	11	1.81
Mc-1	2.5YR6/4	do	11.25	19	1.83
Mc-2	2.5YR6/4	do	14.5	14	2.03
Mc-3	2.5YR7/2	do	6.25	21	1.34
PG-1	2.5YR6/4	do	15	15	1.69
S-1	2.5YR6/2	do	7.5	12	1.81
S-2	2.5YR6/4	do	10	18	1.77

TABLE 2.—*Results of ceramic tests on fired samples from sediment ponds of gravel-washing plants in the Beltsville area, Maryland*—Continued

Sample No. (see table 1 for location)	Munsell color notation	Hardness [1]	Linear shrinkage (percent)	Water absorption (percent)[2]	Specific gravity (approx.)
2,300°F					
C-1	7.5YR6/2	Very hard.	12.5	10.6	2.4
C-2	2.5YR5/2	do	10	14	1.84
Mc-1	2.5YR8/2	do	11.25	15	1.92
Mc-2	2.5YR5/4	do	15	11	2.10
Mc-3	2.5YR7/2	do	6.25	18	1.48
PG-1	2.5YR5/4	do	14	12	2.82
S-1	2.5YR5/2	do	7.5	13	1.83
S-2	2.5YR6/4	do	10	16	1.80
2,400°F					
C-1	10YR6/2	Steel hard.	15	7.5	2.4
C-2	2.5YR8/2	do	8	13	1.85
Mc-1	10YR8/2	do	13.75	11	2.04
Mc-2	10YR6/1	do	20	8	2.25
Mc-3	10YR8/1	do	7.5	17	1.40
PG-1	2.5YR5/2	do	17.5	10	1.92
S-1	5YR7/1	do	7.5	12	1.86
S-2	2.5YR7/2	do	10	12	1.88

[1] Determination based in part on U.S. Department of Agriculture studies (U.S. Dept. Agriculture Soil Conservation Service, 1963, Description of materials, chap. 1 *in* Engineering geology, sec. 8 *of* National Engineering Handbook: p. 13).
[2] Percentage based on weight of water absorbed.

Equally important, a commercial use for this material should help relieve a potential sediment-pollution hazard in local streams.

REFERENCES

Klinefelter, T. A., and Hamlin, H. P., 1957, Syllabus of clay testing: U.S. Bur. Mines Bull. 565, 67 p.

Knechtel, M. M., Hamlin, H. P., Hosterman, J. W., and Carroll, Dorothy, 1961, Physical properties of nonmarine Cretaceous clays in the Maryland coastal plain: Maryland Dept. Geology, Mines, and Water Resources Bull. 23, 11 p.

Krumbein, W. C., and Pettijohn, F. J., 1938, Manual of sedimentary petrography: New York, D. Appleton-Century Co., 549 p.

Munsell Color Co., Inc., 1954, Soil color chart: Baltimore, Md.

U.S. Army Corps of Engineers, 1953, The unified soil classification system: Waterways Exp. Sta., Tech. Memo. 3–357, 30 p.

U.S. War Department, 1945, Soil testing set No. 1 and expedient tests: Tech. Bull. TB5–253–1, 95 p.

Williams, M. T., 1942, A history of erosion in the Anacostia drainage basin: Washington, The Catholic Univ. of America Press, 59 p.

USE OF THE SCANNING ELECTRON MICROSCOPE IN GEOLOGIC STUDIES

By EDWARD J. DWORNIK, Washington, D.C.

Abstract.—Micrographs of several types of materials show that the advantages of the scanning electron microscope over the optical microscope are greater resolution (presently about 500 A) and great depth of field, which allow direct examination of surface features of irregular objects. The advantages over the transmission electron microscope are greater depth of field and easier sample preparation; however, the resolving power is less than that of the transmission microscope, and electron diffraction is not possible with the scanning type. For those problems in which morphology, microstructure and texture are important, the scanning electron microscope will be a useful tool in conjunction with a transmission electron microscope.

To evaluate the applicability of the scanning electron microscope to the study of various types of materials in cosmic dust investigations, several samples were examined in the microscope at the laboratory of the Pulp and Paper Research Institute of Canada. In that laboratory the instrument has been used as an adjunct tool to the conventional high-resolution electron microscope in research on paper and pulp fibers and related problems. The scanning electron microscope at the institute was described in principle by Smith and Oatley (1955) and built subsequently at Cambridge University; details of construction of the instrument are described by Smith (1959 and 1960).

In the scanning electron microscope a finely focused beam of electrons approximately 300 angstroms in diameter is accelerated by a voltage of 15 kilovolts and focused onto a sample at a 45° angle by magnetic lenses. Deflection coils sweep the beam over the area of interest in a scanning sequence, "kicking out" secondary low-energy electrons from the sample surface. These electrons are collected by a scintillation counter whose output is detected by a photomultiplier tube. The output from the photomultiplier is converted to a voltage, amplified, and used to control the brightness of a cathode-ray tube in synchronization with the primary beam scan. An image of the surface topography of the sample is presented on the screen, and is photographed with a 35-mm camera. The area scanned governs the magnification and is varied by controlling the deflection coils. The area can be varied from several square microns to several square millimeters, allowing useful magnifications from × 40,000 to × 100. A mechanical stage allows for traversing as much as a square centimeter of sample surface.

The resolution of the scanning electron microscope is limited to 500 A by the size of the focused electron beam. Theoretically it is possible to focus the beam to about 30 A, closer to the resolution of a transmission electron microscope (<10 A). Pease and Nixon (1965) have reported using a beam diameter of the order of 100 A. For many electron-microscope studies in which replicas are made the scanning electron microscope approaches the same capabilities with less difficulty in sample preparation. It is not possible to obtain electron diffraction information with the instrument.

For highly irregular surfaces the inherently great depth of field of the scanning electron microscope allows the complete depiction of the object's surface. If necessary, stereomicrographs may be prepared by changing the specimen angle slightly between exposures. The increased resolution (about 10 times greater) of the instrument over the optical microscope, together with the depth of field, gives the scanning electron microscope unique capabilities for studying etched mineral-grain surfaces, microfossils, filters, and other similar items. Although one may gain an order of magnitude in resolution over the optical microscope one must sacrifice ability to resolve color and to "see through" certain materials. Examples of scanning electron micrographs are shown in figures 1 and 2.

U.S. GEOL. SURVEY PROF. PAPER 550-D, PAGES D209-D213

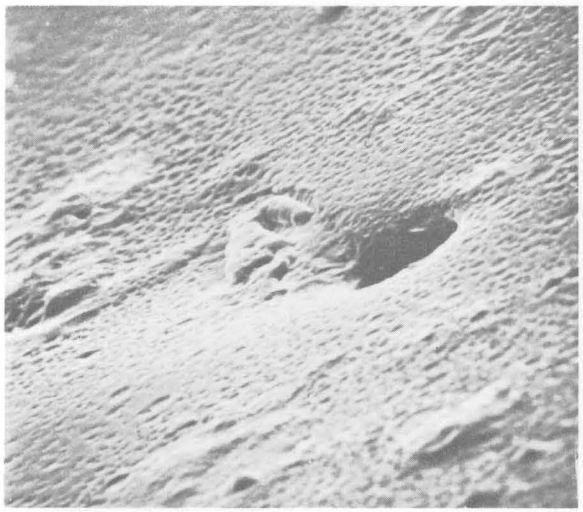

A. Tektite. ×860

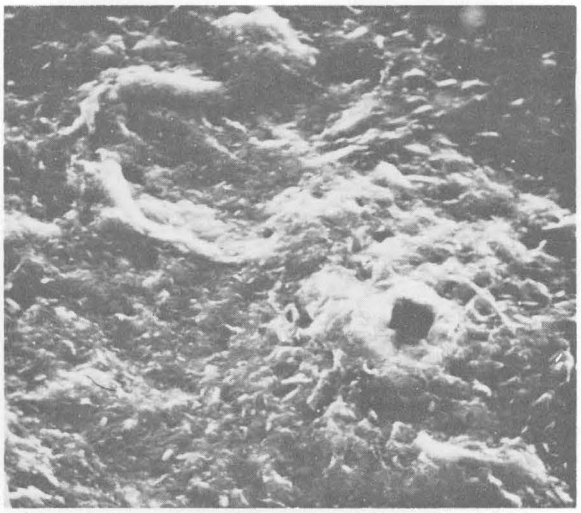

B. Obsidian. ×1170

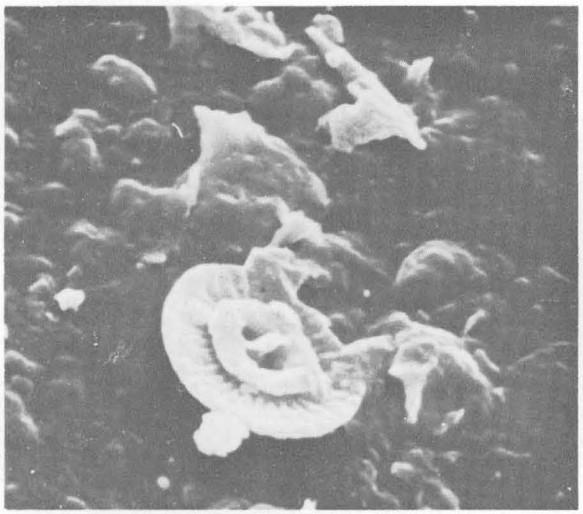

C. Coccolith. ×2730

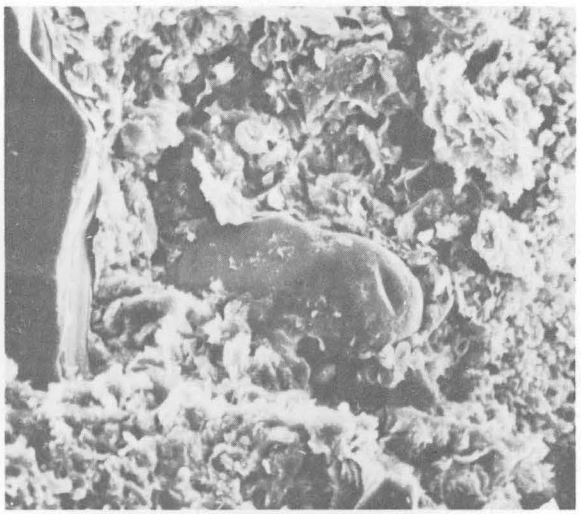

D. Glauconitic clay. ×690

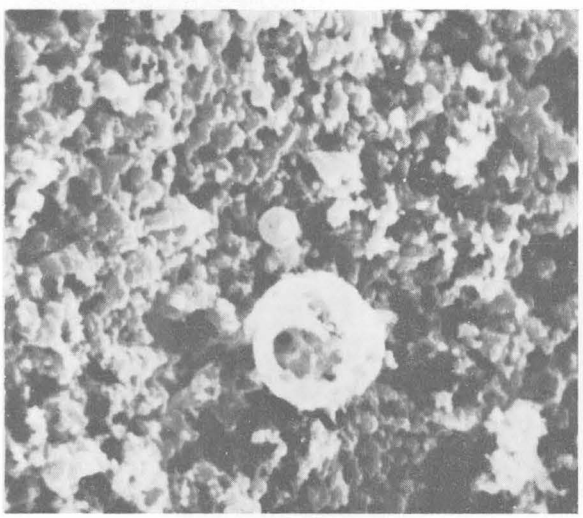

E. Airborne dust. ×4300

F. Airborne dust. ×2400

FIGURE 1.—Micrographs of a tektite, obsidian, a coccolith, glauconitic clay, and airborne dust, made with a scanning electron microscope.

A. Surface of a freshly fractured tektite, showing pock-marked character and also a void. (Specimen from E. C. T. Chao, U.S. Geol. Survey.)

B. Surface of obsidian (volcanic glass), showing a void that is almost square in cross section.

C. Coccolith from glauconitic clay, New Jersey. This type of microfossil represents an ideal subject for scanning electron microscopy. The intricate architecture is readily depicted, and study of gross number of species would be simplified by this technique. This specimen was located on a mount prepared for conventional electron microscopy.

D. Portion of a bulk sample of glauconitic clay from which the specimen in *C* was recovered. A glauconite pebble (center of picture), a book of bent mica (left edge of picture), and several coccoliths are evident in the photograph. Matrix is mostly montmorillonite. This direct observation of the bulk dry sample makes separation and suspension of constituents unnecessary and reduces the possibility of introducing artifacts that could cause difficulty in interpretation of standard electronmicrographs. Microtextural study of loosely compacted sediments is greatly facilitated. (Specimens submitted by Harold Gill, U.S. Geol. Survey.)

E. Airborne dust particles trapped on a millipore membrane filter. The hollowed-out spherules would appear solid in a transmission electron micrograph, due to absorption of the electron beam, and the true character would be lost. The particles adhering to the surface of the spherules are readily observable by this technique, but might be missed in conventional transmission microscopy. 1-micron filter pores can be seen in background.

F. Airborne angular dust particles trapped on a cotton filter fiber. Hygroscopic particles and those soluble in water or organic liquids can be prepared for the scanning electron microscope directly without suspension in distilled water.

The samples are prepared for examination simply by cementing them to the surface of an aluminum disk. The disk and sample are placed in a special holder and rotated at 200 revolutions per minute in a vacuum while a weighed amount of Au-Pd wire is evaporated onto the whirling disk from an angle of 60°. This insures that all surfaces of the sample are made electrically conducting.

The placement of the specimen in a high vacuum and the resultant desiccation may preclude the study of some materials. Also, bombardment by the electron beam can cause some difficulty in those samples that are nonconducting and (or) of hollow or skeletal nature. This latter limitation can be overcome to a great extent by evaporating the conductive metal coating onto the specimen and working with a lower accelerating potential of the electron beam.

Direct observation of nonconducting materials has been reported by Thornley (1960) and by Thornley and Cartz (1962).

Acknowledgments.—The collaboration of Messrs. Alex Rezanowich and Ian Fraser of the Pulp and Paper Research Institute of Canada in the preparation of the scanning electron micrograph is gratefully acknowledged. Thanks are also due to Mr. S. M. Chapman of the same organization for permission to

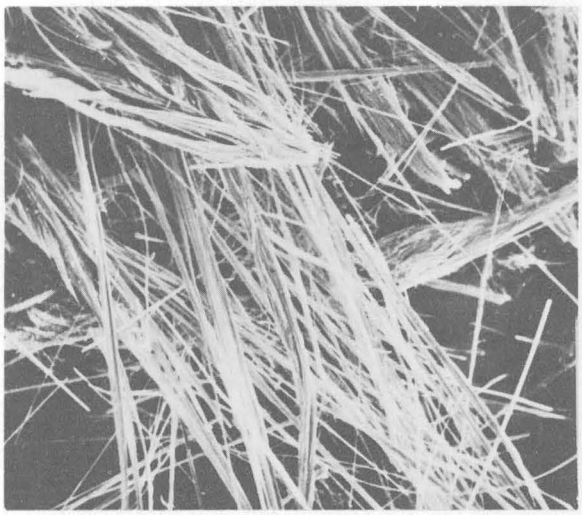

A. Hewettite. ×130

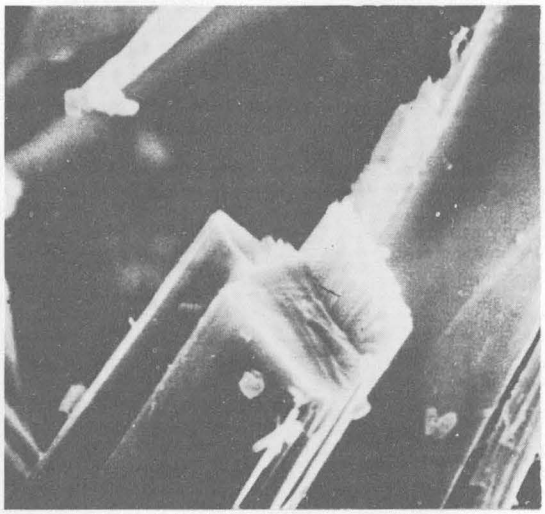

B. Serpentine. ×4500

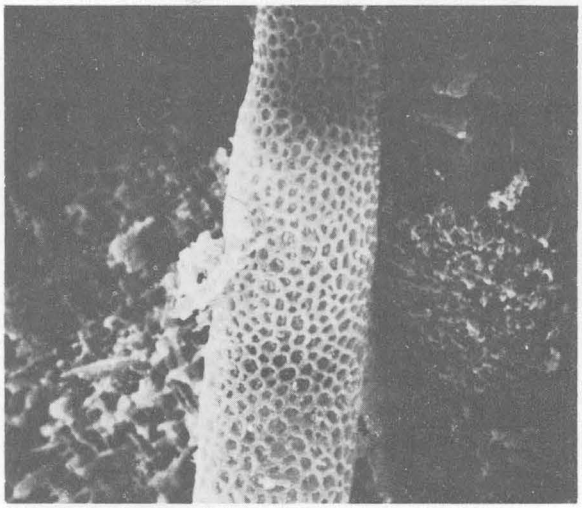

C. Alga. ×2530

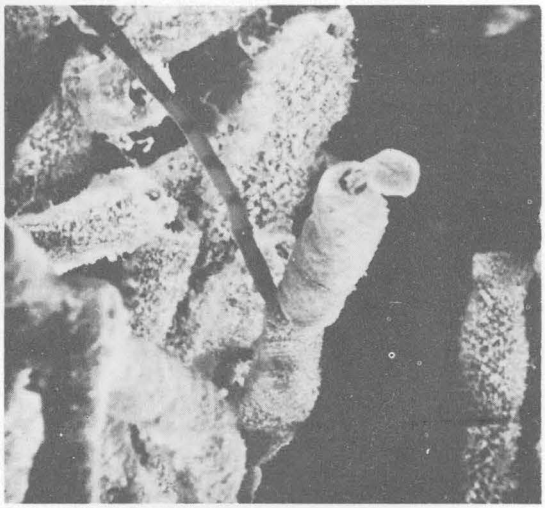

D. Calcitic tubes. ×390

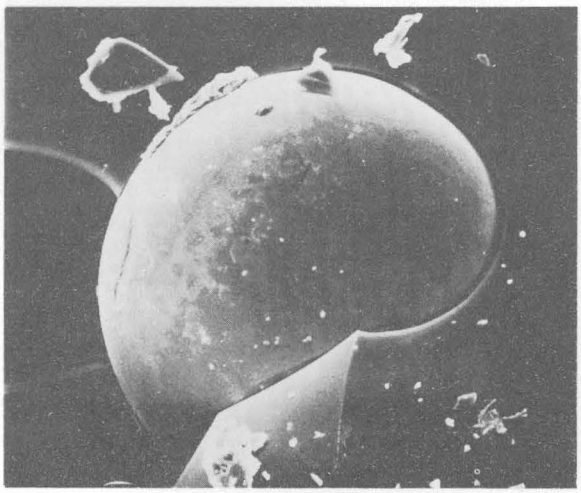

E. Metallic spherule. ×680

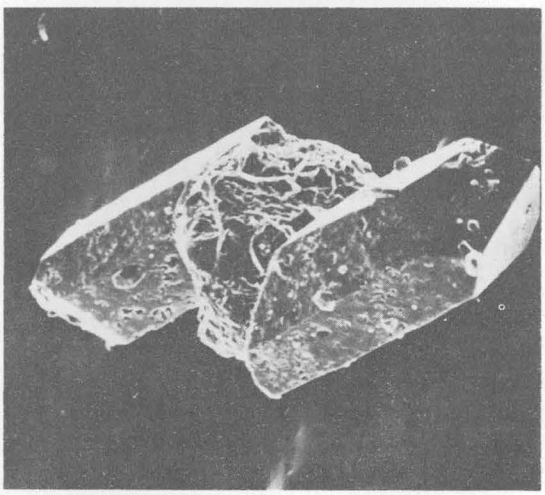

F. Quartz crystals. ×210

FIGURE 2.—Micrographs of hewettite, serpentine, algae, metallic spherule, and quartz, made with a scanning electron microscope.

A. Fibrous crystals of hewettite, a calcium vanadate. The great depth of focus of the scanning electron microscope is emphasized in this relatively low magnification photograph.

B. Termination of serpentine fiber. This three-quarters end view shows that the fiber is solid rather than tubular. Cleavage would produce lathlike particles.

C. Portion of a blue-green alga, devoid of calcareous overgrowth, showing pores which may have served as loci for secreting calcite. The skeletal character of the "wooly" calcite is seen in the background.

D. Tubes formed by calcite-secreting algae from Russel Cave, Ala. Each of the "wooly" calcite tubules surrounds an alga responsible for its secretion. (Specimen from J. T. Hack, U.S. Geol. Survey.)

E. Metallic spherule exposed on a fracture surface of a philippinite (tektite). This technique offers an excellent means for study of surface irregularities and features of metallic and other inclusions in tektites. (Specimen submitted by E. C. T. Chao, U.S. Geol. Survey.)

F. Two well-developed quartz crystals growing from a common seed. The crystals in various stages of growth were recovered by digestion of an oolitic limestone in boiling HCl and an oxidizing bleach. Information on morphologic development, etch patterns, and surface features of crystals and seeds can be obtained. Replication of these features is virtually impossible or at best is exceedingly difficult by conventional electron microscope techniques. (Specimens from L. G. Henbest, U.S. Geol. Survey.)

work at the laboratory. The help of Mr. J. A. Denson and Ralph Christian in the assembly of the photographs is also gratefully acknowledged.

REFERENCES

Pease, R. F. W., and Nixon, W. C., 1965, High resolution scanning electron microscopy: London, Jour. Sci. Inst., v. 42, p. 81–86.

Smith, K. C. A., 1959, Scanning electron microscopy in pulp and paper research: Pulp Paper Mag. Canada (tech. sect.), v. 60, p. T366–T371.

——— 1960, A versatile scanning electron microscope, *in* Houwink, A. L., and Spit, B. J., eds., Proceedings of European Regional Conference on Electron Microscopy: Delft, p. 177–180.

Smith, K. C. A., and Oatley, C. W., 1955, The scanning electron microscope and its fields of application: British Jour. Appl. Physics., v. 6, p. 391–399.

Thornley, R. F. M., 1960, Recent developments in scanning electron microscopy, *in* Houwink, A. L., and Spit, B. J., eds., Proceedings of European Regional Conference on Electron Microscopy: Delft, p. 173–176.

Thornley, R. F. M., and Cartz, L. J., 1962, Direct examination of ceramic surfaces with the scanning electronmicroscope: Am. Ceramic Soc. Jour., v. 45, p. 425–428.

APPROXIMATING STEADY LINEAR FLOW IN A CONFINED AQUIFER OF NONUNIFORM THICKNESS

By CHARLES A. APPEL, Miami, Fla.

Abstract.—Formulas are given for steady linear flow in a section of an "ideal" confined nonleaky aquifer having the shape of two or more partial wedges connected end to end in such a way that the thickness change is nowhere abrupt. The formulas are for the case where the top and bottom surfaces of each wedge intersect the horizontal at angles whose tangents are not greater than 0.2. Analysis of the formula for a partial wedge indicates that the use of the average aquifer thickness, with Darcy's law, gives estimates of flow with sufficient accuracy for most applications, where the changes in thickness are not very large.

Darcy's law probably is the most frequently used formula in the solution of problems on the linear flow of ground water. A convenient form of this law is

$$Q=\frac{Pb(h_1-h_2)}{L}, \tag{1}$$

where

Q=rate of discharge per unit of aquifer width between two parallel equipotential planes,
P=coefficient of permeability of the aquifer,
b=aquifer thickness,
h_1 and h_2=heads above an arbitrary datum at the two parallel equipotential planes, and
L=distance between the two equipotential planes.

Although the aquifer thickness in equation 1 is a constant, the equation frequently is applied to situations where the aquifer thickness is not uniform in the area under consideration. Hantush (1962, p. 714) has developed an equation for the flow in an aquifer that is shaped like part of a wedge and whose thickness changes linearly along the direction of flow. This paper extends Hantush's results to the case of flow through an aquifer that can be approximated by a series of wedges. It is shown that the permeability of such an aquifer or the flow through it can be estimated, under certain conditions, from the head gradient. The equation by Hantush for part of a wedge is compared to Darcy's law for flow through an aquifer having a thickness equal to the average thickness of a partial wedge.

FLOW THROUGH AN AQUIFER SHAPED LIKE PART OF A WEDGE

The steady-state flow per unit width of an aquifer that is shaped like part of a wedge, between two parallel equipotential planes (Hantush, 1962, eq. 10b on p. 714), is given by

$$Q'=\frac{P(h_1-h_2)}{\frac{L}{b_2-b_1}\log_e\frac{b_2}{b_1}}, \tag{2}$$

where h_1, h_2, P, and L, are as previously defined, $\log_e$ is the natural logarithm, b_1 and b_2 are aquifer thicknesses at equipotential planes 1 and 2, and Q' is the rate of flow per unit width of aquifer. The development of this equation assumes that the vertical differences in head in the aquifer are negligible, the upper and lower surfaces of the aquifer dip at angles whose tangents are not greater than 0.2, the aquifer is nonleaky and homogeneous and isotropic, and the change in aquifer thickness per unit of horizontal distance is greatest in a direction perpendicular to the equipotential planes.

In order to test the inference that flow through an aquifer shaped like part of a wedge is closely approximated by Darcy's law modified for the flow through an aquifer having a uniform thickness that is equal to the average thickness of the partial wedge, let Q' from equation 2 be expressed as

$$Q'=\left[P\left(\frac{b_1+b_2}{2}\right)\left(\frac{h_1-h_2}{L}\right)\right]C, \tag{3}$$

where

$$C=\frac{1}{\left(\frac{1}{R-1}+\frac{1}{2}\right)\log_e R},$$

and R is the ratio of the maximum to minimum thicknesses of the partial wedge.

The term within brackets in equation 3 is Darcy's law modified for the flow through an aquifer of uniform thickness that equals the average thickness of the partial wedge, and C is a correction factor which adjusts the flow rate determined by Darcy's law to the flow rate determined by equation 2.

The ratio R, where the aquifer is shaped like part of a wedge, provides a convenient index of the nonuniformity of thickness of the aquifer. Figure 1 illustrates the general form of the relation between correction factor C (equation 3) and the ratio R. Values of C for selected values of the ratio R are also given in table 1. These values show that where an aquifer is shaped like part of a wedge and the ratio of the maximum to minimum thickness is 2 or less, the error introduced by assuming that the flow rate is the same as would occur through an aquifer having a uniform thickness equal to the average thickness of the partial wedge is not more than 4 percent. Where the ratio is 6, the error is about 20 percent. As the ratio of the maximum to minimum thickness increases, so does the error in estimating the flow by the bracketed term in equation 3.

The relation between the C factor and the value R (table 1) indicates that, in many instances, use of the average thickness in estimating, by Darcy's law, the flow rate in an aquifer shaped like part of a wedge is justified because results of sufficient accuracy for practical applications are obtained.

FLOW THROUGH AN AQUIFER SHAPED LIKE A SERIES OF SEVERAL PARTIAL WEDGES

The steady-state flow through an aquifer shaped approximately like several partial wedges connected end-to-end can be determined by a generalization of equation 2. The following development assumes that the partial wedges are connected in such a way that the aquifer thickness does not change abruptly. Figure 2 shows a sectional view of part of a hypothetical aquifer that comprises a series of three partial wedges. Because a steady state is assumed, the flow through each partial wedge between equipotential planes 1 and 2 is equal. Thus, application of equation 2 to each wedge gives

$$Q' = \frac{P(h_1-h_2)}{\frac{L_1}{b_2-b_1}\log_e\frac{b_2}{b_1}} = \frac{P(h_2-h_3)}{\frac{L_2}{b_3-b_2}\log_e\frac{b_3}{b_2}} = \frac{P(h_3-h_4)}{\frac{L_3}{b_4-b_3}\log_e\frac{b_4}{b_3}}. \quad (4)$$

As the situation is shown on figure 2, only the values of h_1 and h_4 are assumed to be known. From equation 4

$$\left.\begin{aligned} \frac{Q'L_1}{P(b_2-b_1)}\log_e\frac{b_2}{b_1} &= h_1-h_2 \\ \frac{Q'L_2}{P(b_3-b_2)}\log_e\frac{b_3}{b_2} &= h_2-h_3 \\ \frac{Q'L_3}{P(b_4-b_3)}\log_e\frac{b_4}{b_3} &= h_3-h_4 \end{aligned}\right\}. \quad (5)$$

Addition of these expressions gives

$$\frac{Q'}{P}\left[\frac{L_1\log_e\frac{b_2}{b_1}}{b_2-b_1}+\frac{L_2\log_e\frac{b_3}{b_2}}{b_3-b_2}+\frac{L_3\log_e\frac{b_4}{b_3}}{b_4-b_3}\right]=h_1-h_4, \quad (6)$$

which can be rearranged as

$$Q' = \frac{P(h_1-h_4)}{\frac{L_1\log_e\frac{b_2}{b_1}}{b_2-b_1}+\frac{L_2\log_e\frac{b_3}{b_2}}{b_3-b_2}+\frac{L_3\log_e\frac{b_4}{b_3}}{b_4-b_3}}. \quad (7)$$

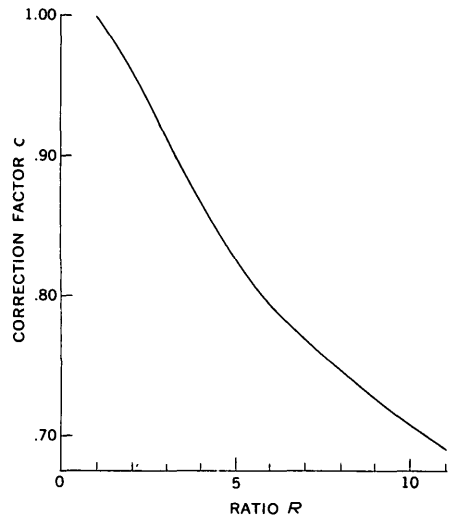

FIGURE 1.—Graph showing relationship of correction factor C (equation 3) to ratio of aquifer maximum to minimum thicknesses R in an aquifer shaped like part of a wedge.

TABLE 1.—*Values of the correction factor* C *(equation 3) for selected values of* R

R	C	R	C	R	C	R	C
1.0	1.000	1.8	0.972	3.0	0.910	5.5	0.812
1.2	.997	1.9	.967	3.25	.899	6	.798
1.3	.994	2.0	.962	3.5	.887	7	.770
1.4	.991	2.2	.952	3.75	.876	8	.748
1.5	.986	2.4	.941	4.0	.866	9	.728
1.6	.982	2.6	.930	4.5	.846	10	.711
1.7	.977	2.8	.921	5.0	.829	11	.695

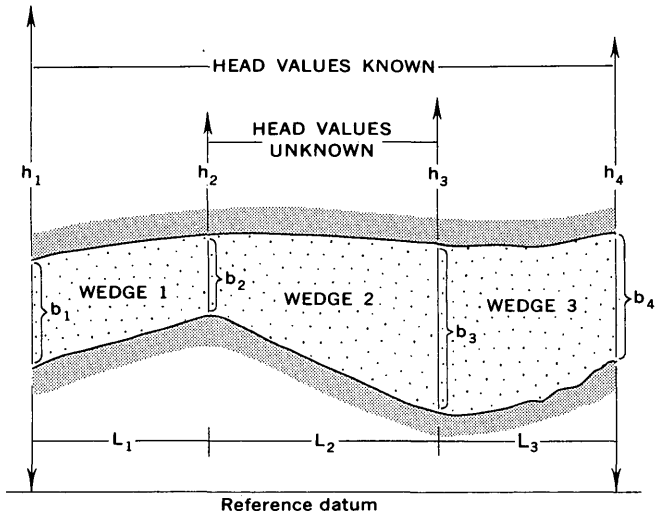

FIGURE 2.—Sectional view of part of a hypothetical aquifer, between parallel equipotential planes, and an approximation of the form of the aquifer by parts of three wedges in series.

Equation 7 is for an aquifer approximated by a series of three partial wedges. An expression for flow through a series of any number (n) of partial wedges is

$$Q' = \frac{P(h_1 - h_{n+1})}{\sum_{i=1}^{n} \frac{L_i \log_e \frac{b_{i+1}}{b_i}}{b_{i+1} - b_i}}. \qquad (8)$$

Inherent in the development of equation 8 is the assumption that the aquifer can be approximated entirely by partial wedges. If, however, the aquifer includes one or more sections of uniform thickness, the appropriate term(s) in the summation in equation 8 becomes L_i/b_i (Darcy's law).

Equations 3 and 8 can be used in a manner similar to Darcy's law. Thus they can be used to solve for the flow between two equipotential planes of known values if the permeability is known, or they can be used to solve for the permeability if the flow between two equipotential planes of known values is known.

REFERENCE

Hantush, M. S., 1962, Flow of ground water in sands of nonuniform thickness; pt. 2, Approximate theory: Jour. Geophys. Research, v. 67, no. 2, p. 711–720.

THE WHITE RIVER FORMATION AS AN AQUIFER IN SOUTHEASTERN WYOMING AND ADJACENT PARTS OF NEBRASKA AND COLORADO

By MARLIN E. LOWRY, Cheyenne, Wyo.

Work done in cooperation with the Wyoming State Engineer

Abstract.—Many large-yield water wells in southeastern Wyoming, northeastern Colorado, and southwestern Nebraska reportedly tap the White River Formation, of Oligocene age, which is predominantly siltstone. However, most of these wells probably tap overlying alluvium that is composed of pebbles derived from the White River Formation rather than the White River Formation itself. Although previous workers have suggested that various kinds of fractures are the water-conducting openings where large yields are known to be derived from the White River, the openings are thought more likely to be tubes formed by piping before the formation was buried by alluvium.

The White River Formation of Oligocene age, which consists predominantly of siltstone, has been considered to be an important aquifer in several areas in southeastern Wyoming, southwestern Nebraska, and northeastern Colorado. Several investigators (Babcock and Bjorklund, 1956; Babcock and Rapp, 1952; Babcock and Visher, 1952; Bjorklund, 1957, 1959; McLaughlin, 1948; Morris and Babcock, 1960; Rapp and others, 1957; Rapp and others, 1953; Visher and Babcock, 1953; Weist, 1964, 1965) have stated that the sources of water to the large-yield wells tapping the formation are porous zones of reworked siltstone and various kinds of fractures. The purpose of this article is to present evidence that the White River Formation has been mistakenly identified as the aquifer tapped by many wells and that openings produced by piping are more likely than fractures to account for the locally high secondary permeability in those few places where the formation does transmit large quantities of water to wells.

CHARACTER OF THE WHITE RIVER FORMATION

The White River Formation is as much as 1,000 feet thick. It unconformably overlies older rocks and is overlain disconformably by either the Arikaree Formation of Miocene age, the Ogallala Formation of Miocene and Pliocene age, or alluvium of Quaternary age. The White River Formation consists of massive, very light pinkish-gray siltstone. It is typically exposed in bluffs that have a blocky appearance because of weathering along lines of weakness. Locally a badlands topography has developed on outcrops of the formation. All Oligocene rocks are here assigned to the White River Formation. Subordinate units of the White River, the Chadron Formation (below) and Brule Formation (above), of previous authors, are not used in this report.

The White River Formation is remarkably uniform in grain size throughout the area shown in figure 1. Denson and Bergandahl (1961), who made particle-size analyses of about 100 samples from 10 measured sections, state (1961, p. C170) "In general, these rocks consist of 65 to 85 percent silt and 5 to 25 percent very fine grained sand embedded in a matrix of clay-size particles." Eight of these measured sections are within the area shown in figure 1, and two are about 20 miles north of the area. Coarse-grained channel deposits within the White River Formation in Scotts Bluff County, Nebr., are described by Wenzel and others (1946, p. 67–68), and similar deposits are known to occur elsewhere.

OCCURRENCE OF GROUND WATER

Although ground water occurs in channel deposits in the White River Formation, these deposits are excluded from consideration because they are unquestionably zones of primary permeability that are in the White River Formation, and, therefore, do not bear signifi-

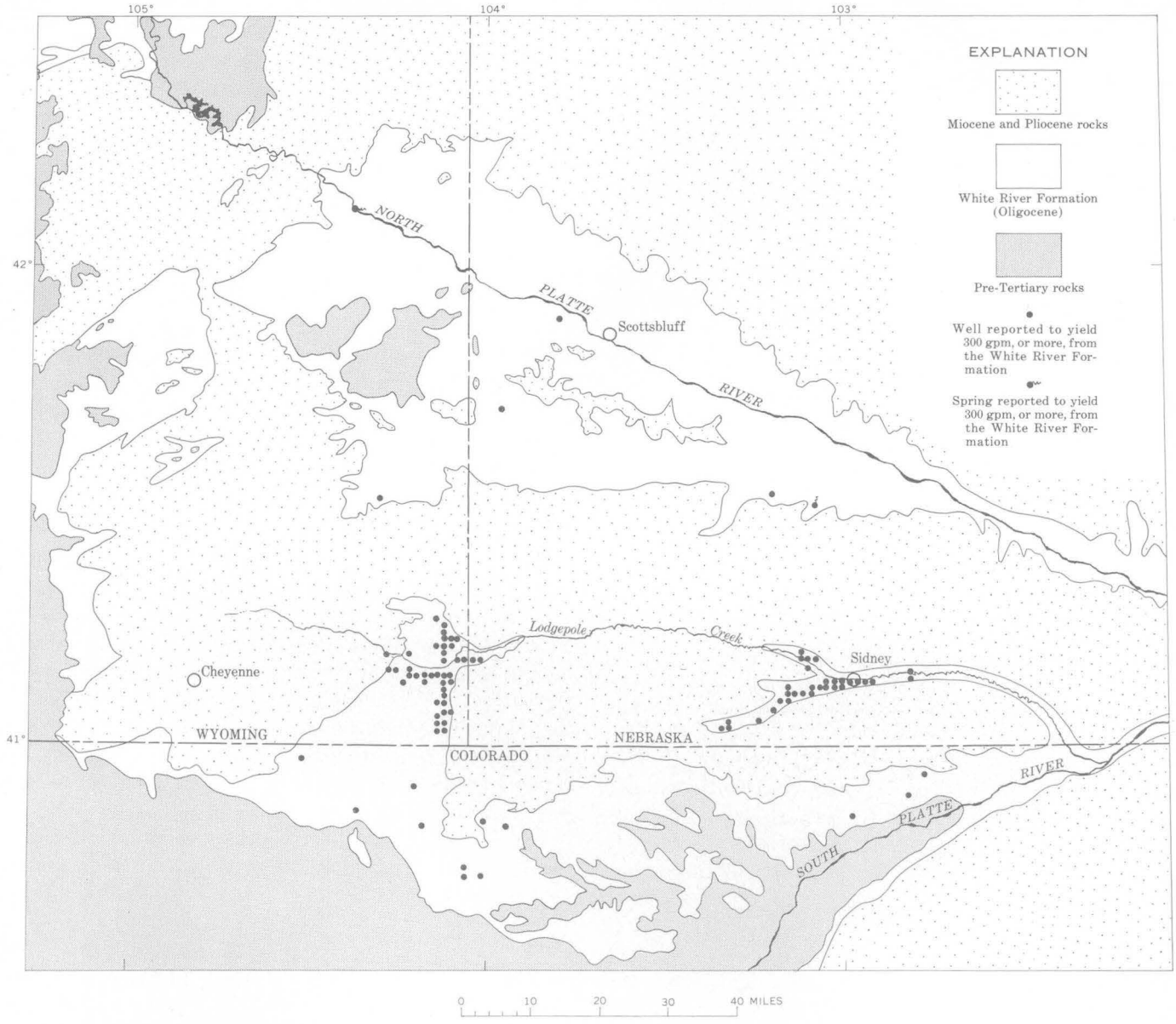

FIGURE 1.—Generalized geologic map of southeastern Wyoming and adjacent parts of Nebraska and Colorado, showing the locations of large-yield wells that reportedly tap the White River Formation. Wells known to tap gravel channels within the White River, or to tap both alluvium and the White River Formation, are excluded. Where there is more than one large-yield well in a section, only one well is shown.

cantly on the problem. Wells known to tap these deposits are not shown in figure 1. Wells tapping porous zones of reworked siltstone are shown in figure 1 because they were reported in previous publications to yield water from the White River Formation. In describing these zones, some earlier workers have stated that the permeability of the formation is increased by porous zones of reworked White River, and some state that the top part of the formation consists of rounded pebbles of reworked siltstone. The term "top," as used here, refers to an erosion surface and not to the stratigraphic top of the formation. According to McLaughlin (1948, p. 13), test drilling in the Lodgepole Creek valley, near Julesburg, Colo., showed that the so-called porous zone actually is alluvium overlying the White River Formation, and not the White River Formation. McLaughlin (1948, p. 13) stated:

> During the test drilling done by the town of Julesburg, it was found that the "porous" zone consists of moderately well rounded pebbles of reworked Brule [White River] clay, the pebbles ranging in diameter from less than half an inch to more than 2 inches. Inasmuch as the so-called "porous" zone is actually a deposit of coarse gravel that is confined to the zone

underlying the alluvium, it perhaps should be considered a part of the alluvium. The material lying above the "porous zone," although doubtless reworked, resembles so closely the Brule clay from which it was derived that it cannot readily be distinguished from it.

McLaughlin's statement that the porous zone is actually alluvium is supported both by figure 1, which shows that the large-yield wells are almost entirely restricted to valleys of major drainage, and by an observation by Bjorklund (1957, p. 13) that in the lower Lodgepole Creek valley the porous zone pinches out toward the valley sides.

Most of the large-yield wells that are reported to yield water from the White River Formation probably yield water from the alluvium. Although the porous zone has been recognized as alluvium by some workers, its inclusion with the White River, because of the difficulty in differentiating the two, has left the impression that the White River is a much better aquifer than it really is.

Several methods have been used to determine hydraulic constants for what is actually the White River Formation, and very different results have been obtained. These differences are attributed to the fact that laboratory-determined values represent primary permeability, whereas field-determined values are believed to represent secondary permeability.

According to Rapp and others (1957, p. 42), the coefficient of permeability for 7 samples of siltstone from the formation in Goshen County, Wyo., was determined in the hydrologic laboratory of the U.S. Geological Survey to range from values too small to be measured to 0.2 gallons per day per square foot. These values represent the permeability of the intergrain pores.

Using seepage methods, Wenzel and others (1946, p. 85) determined field coefficients of permeability of from 243 to 889 gpd per sq ft, for an assumed 100-ft thickness of aquifer in Scotts Bluff County, Nebr. The average coefficient of permeability from one pumping test in southern Platte County, Wyo., was reported by Morris and Babcock (1960, p. 52) to be 36 gpd per sq ft. Welder and Weeks (1965, p. 49), applying a regional method of analysis, computed coefficients of transmissibility ranging from 450 to 1,000 gpd per ft for the formation near Glendo in Platte County, Wyo.

The large differences in the results from laboratory and field methods strongly suggest that the large yields from wells tapping the White River Formation are due to secondary permeability. Furthermore, because considerably different yields have been obtained from two closely spaced wells of equal depth, it is obvious that the openings which transmit water are neither uniformly distributed nor of uniform size.

224-352 O—66——15

NATURE OF THE LARGE WATER-BEARING OPENINGS

In discussing the water-bearing properties of the White River Formation, many writers have emphasized that nearly vertical fractures are the water-conducting passages. Most reports have a statement similar to that of Babcock and Bjorklund (1956, p. 14):

In some places, nearly vertical fractures, or fissures, penetrate to unknown depths within the formation and possibly penetrate completely through it. Surface traces of these fractures, some of which are at least 1 foot wide and 1 mile long, are seen easily on aerial photographs, but they are difficult to detect and follow on the ground.

Outcrops where fractures in the White River Formation have been identified from aerial photographs (Babcock and Rapp, 1952, fig. 6; Visher and Babcock, 1953, fig. 9) show no evidence of unusual fracturing. The features that they regarded as fractures are believed, for the following reasons, to be remnants of trails: (1) the features curve around hills and through narrow passes, and do not appear to have been a factor in the development of the drainage pattern; (2) they are not seen on the best bedrock exposures, but are well developed where there is a cover of soil or colluvium; and (3) they look the same on aerial photographs as known trails such as the Cheyenne-Deadwood stagecoach trail, whereas known faults in the White River Formation in Laramie County, Wyo., are not apparent on photographs.

Trails were abundant because the area was traversed by one of the principal routes of the Texas Trail, which was a network of paths. The Texas Trail was used from about 1876 to 1896 in the northern cattle drives and, in 1887 alone, more than 13,000 animals passed near Lusk, Wyo. (Thorp, 1946, p. 133). In describing the trail, Brayer and Brayer (1952, p. 62) state "So heavily pounded by the thousands of sharp hoofs, the depression marking the main path is still clearly discernible in many places." The trail, in part, followed preexisting buffalo trails, which also are still visible in some areas.

Clastic dikes, such as those shown in figure 2, are numerous in some White River outcrops. Although the dikes cannot be seen on the high-altitude aerial photographs, they are similar in other respects (width, vertical character) to the nearly vertical fissures referred to by previous investigators. The extent to which they can be traced is limited by soil or other cover, but some can be traced for several hundred feet. The clastic material in the dikes generally has distinct vertical laminations, indicating that the material was forced in under pressure; this suggests, in turn, that open fissures do not exist. The dike material in most localities is similar in grain size to the wallrock, so

FIGURE 2.—Clastic dikes (shown by arrows) in the White River Formation, NW¼ sec. 9, T. 12 N., R. 63 W. (about 22 miles, airline, southeast of Cheyenne, fig. 1), Laramie County, Wyo.

its permeability is not greatly different from the rest of the formation.

No open vertical fissures were seen in Laramie County, Wyo., where most of the fieldwork upon which this paper is based was done. The only open fissure known to the author is one reported by Rapp and others (1957, pl. 6). This fissure, which was in an improved dirt road, was revealed when a truck tire broke through the cap of covering material. As it seems unlikely that a fissure so close to the roadbed would go unnoticed at the time of road construction, the opening probably formed after the road was constructed. Furthermore, if such fissures do exist and are conduits for water in the White River Formation, large springs should issue from fissures near stream level in the area. Fissure springs are not known to occur here, however. In describing the Goshen Hole in Goshen County, Wyo., Rapp and others(1957, p. 16) state that springs characteristically flow down the escarpment faces from the contact of the White River with the overlying Arikaree Formation. Springs in two localities are reported to yield large supplies from the White River Formation (fig. 1). Two springs in sec. 25, T. 25 N., R. 63 W. (along the North Platte River about 40 miles upstream from Scottsbluff, fig. 1), emit from openings that are principally the result of near-surface weathering. According to the owner of the land, the large yield is maintained only when a nearby irrigation canal contains water. The discharge is less than 5 gallon per minute when the canal is dry. The spring in sec. 28, T. 18 N., R. 50 W. (about 40 miles southeast of Scottsbluff, fig. 1), was not visited by the author.

As shown in figure 3, the White River Formation may be highly fractured. Although such fractures in weathered exposures appear to be quite permeable, fractures in fresh exposures, which are more representative of conditions at depth, generally are either closed or are only barely open, and so would not yield large supplies of water to wells. Moreover, there is no evidence that the large-yield wells are related to structural features such as faults, where fracturing would be more intensive.

Piping, a process by which subterranean channels or pipes are formed by the movement of water through relatively insoluble, incoherent rocks, is thought to provide a better explanation of the locally high secondary permeability of the White River Formation.

In describing piping as a geomorphic agent, Parker (1963) listed the following basic essentials for the formation of pipes: (1) Water enough to saturate some part of the soil or bedrock above base level; (2) hydraulic head to move water through a subterranean route; (3) presence of a permeable, erodible soil or bedrock above base level; and (4) an outlet for flow. Material is transported in suspension by the moving water.

Near Pine Bluffs, Wyo., where many of the large-yield wells are located, conditions suitable for piping probably existed before the alluvium was deposited. Test drilling has shown that, beneath the alluvium, there is an erosion surface on the White River Formation with a local relief of 100 feet (Rapp and others, 1953, pl. 3). Therefore, the necessary hydraulic head and outlet for flow were present. Piping is an active process in the formation, in some areas, at

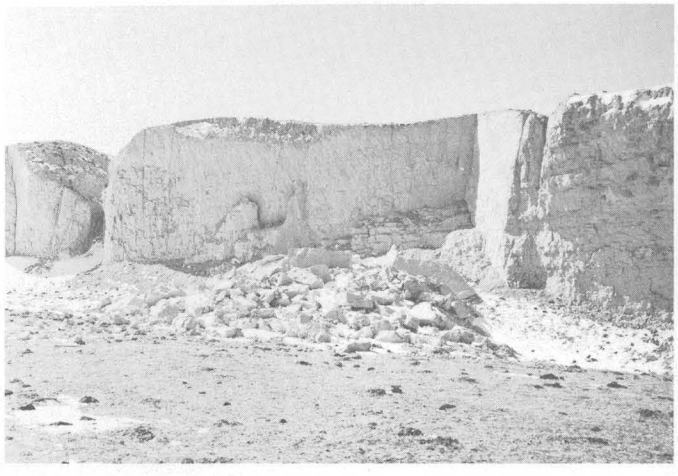

FIGURE 3.—Fractured siltstone of the White River Formation, sec. 2, T. 14 N., R. 69 W. (about 14 miles west-northwest of Cheyenne, fig. 1), Laramie County, Wyo. Fractures are much more pronounced on weathered surfaces, right and left background, than on freshly exposed surfaces, center.

present; so it is necessary to assume only that there was, at times, sufficient water to saturate some part of the formation above base level. The water table in the Pine Bluffs area is now shallow, so if pipes such as those shown in figure 4 were formed before the White River Formation was buried beneath alluvial deposits, they now would be filled with water and would yield large supplies to wells that were drilled into or through them.

Although large-yield wells tapping the White River Formation are not known to have been drilled outside the principal valleys, H. M. DeGraw, of the Nebraska Geological Survey (oral commun., Nov. 22, 1965), reports that a highly permeable zone in the White River Formation was penetrated in drilling a test hole north of Lodgepole Creek valley in Deuel County, Nebr. There the White River is overlain by the Ogallala Formation. He stated further that a surface of considerable relief was developed on the White River before the Ogallala was deposited in that area. It seems likely, therefore, that conditions suitable for the formation of pipes existed before the Ogallala was deposited, and that pipes rather than fractures account for the locally high secondary permeability of the White River Formation.

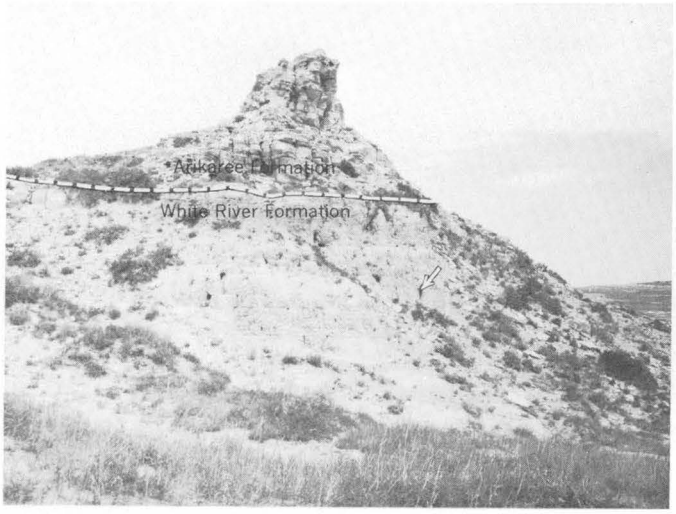

A

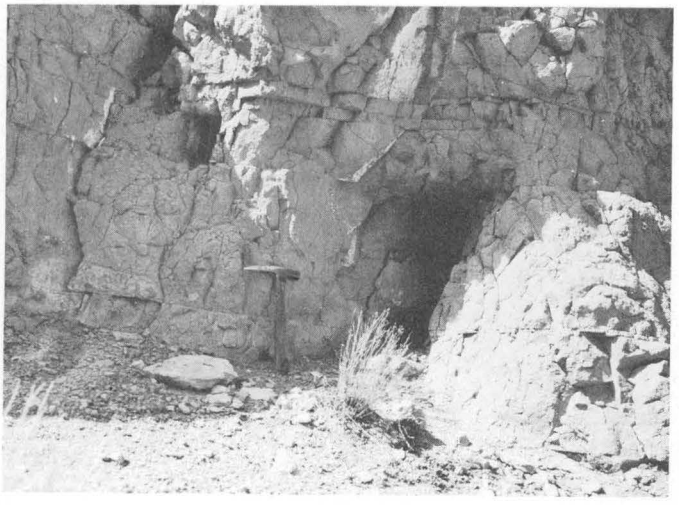

B

FIGURE 4.—*A*, Outcrop of Arikaree and White River Formations, NE¼ sec. 24, T. 18 N., R. 61 W. (about 35 miles southwest of Scottsbluff, fig. 1), Laramie County, Wyo., showing several pipes (dark spots) in the White River Formation. *B*, Closeup of pipe designated by arrow in *A*.

REFERENCES

Babcock, H. M., and Bjorklund, L. J., 1956, Ground-water geology of parts of Laramie and Albany Counties, Wyo., and Weld County, Colo., with a section on Chemical quality of the ground water, by L. R. Kister: U.S. Geol. Survey Water-Supply Paper 1367, 61 p.

Babcock, H. M., and Rapp, J. R., 1952, Reconnaissance of the geology and ground-water resources of the Horse Creek–Bear Creek area, Laramie and Goshen Counties, Wyo., with a section on the Chemical quality of the water, by W. H. Durum: U.S. Geol. Survey Circ. 162, 28 p.

Babcock, H. M., and Visher, F. N., 1952, Reconnaissance of the geology and ground-water resources of the Pumpkin Creek area, Morrill and Banner Counties, Nebr., with a section on the Chemical quality of water, by W. H. Durum: U.S. Geol. Survey Circ. 156, 30 p.

Bjorklund, L. J., 1957, Geology and ground-water resources of the lower Lodgepole Creek drainage basin, Nebraska, with a section on Chemical quality of the water, by E. R. Jochens: U.S. Geol. Survey Water-Supply Paper 1410, 76 p.

——— 1959, Geology and ground-water resources of the upper Lodgepole Creek drainage basin, Wyoming, with a section on Chemical quality of the water, by R. A. Krieger and E. R. Jochens: U.S. Geol. Survey Water-Supply Paper 1483, 40 p.

Brayer, G. M., and Brayer, H. O., 1952, American cattle trails 1540–1900: Denver, Colo., Smith-Brooks Printing Co., 128 p.

Denson, N. M., and Bergendahl, M. H., 1961, Middle and upper Tertiary rocks of southeastern Wyoming and adjoining areas: Art. 209 *in* U.S. Geol. Survey Prof. Paper 424–C, p. C168–C172.

McLaughlin, T. G., 1948, Ground water in the Julesburg area, Colorado: Colorado Water Conserv. Board Circ. 1, 20 p.

Morris, D. A., and Babcock, H. M., 1960, Geology and ground-water resources of Platte County, Wyo., with a section on Chemical quality of the water, by R. H. Langford: U.S. Geol. Survey Water-Supply Paper 1490, 195 p.

Parker, G. G., 1963, Piping, a geomorphic agent in landform development of the drylands: Berkeley, Calif., Internat. Assoc. Sci. Hydrology, Pub. 65, p. 103–113.

Rapp, J. R., Visher, F. N., and Littleton, R. T., 1957, Geology and ground-water resources of Goshen County, Wyo.: U.S. Geol. Survey Water-Supply Paper 1377, 145 p.

Rapp, J. R., Warner, D. A., and Morgan, A. M., 1953, Geology and ground-water resources of the Egbert–Pine Bluffs–

Carpenter area, Laramie County, Wyo.: U.S. Geol. Survey Water-Supply Paper 1140, 67 p.

Thorp, Russell, 1946, Early cowboy days in Wyoming, *in* The Westerners brand book 1945: Denver, Bradford Robinson Printing Co., p. 131–143.

Visher, F. N., and Babcock, H. M., 1953, Ground-water conditions in the soil and moisture conservation demonstration area near Torrington, Goshen County, Wyo., with a section on the Chemical quality of the ground water, by W. H. Durum and R. A. Krieger: U.S. Geol. Survey Circ. 238, 51 p.

Weist, W. G., Jr., 1964, Hydrogeologic data from parts of Larimer, Logan, Morgan, Sedgwick, and Weld Counties, Colo.: Colorado Water Conserv. Board Basic-Data Rept. 16, 30 p.

——— 1965, Reconnaissance of the ground-water resources in parts of Larimer, Logan, Morgan, Sedgwick, and Weld Counties, Colo.: U.S. Geol. Survey Water-Supply Paper 1809–L, 24 p.

Welder, G. E., and Weeks, E. P., 1965, Hydrologic conditions near Glendo, Platte County, Wyo.: U.S. Geol. Survey Water-Supply Paper 1791, 82 p.

Wenzel, L. K., Cady, R. C., and Waite, H. A., 1946, Geology and ground-water resources of Scotts Bluff County, Nebr.: U.S. Geol. Survey Water-Supply Paper 943, 150 p.

HYDRAULIC CORRELATION OF FRACTURE ZONES IN BURIED CRYSTALLINE ROCK AT THE SAVANNAH RIVER PLANT, NEAR AIKEN, SOUTH CAROLINA

By I. WENDELL MARINE, Aiken, S.C.

Work done in cooperation with the U.S. Atomic Energy Commission

Abstract.—Two types of open fractures characterize the upper 1,000 feet of the buried crystalline rock at the Savannah River Plant of the U.S. Atomic Energy Commission. One pervades the entire rock mass, thereby making it a single hydraulic unit; however, fractures of this type are so minute that water movement through them is exceedingly slow. The other type, restricted to definite zones, consists of larger openings that transmit water at a faster rate. Some zones containing this type of fracture can be correlated between wells by hydraulic methods.

An exploratory drilling and testing program, part of an investigation of the feasibility of storing radioactive waste in artificially excavated chambers in crystalline basement rock (Christl, 1964; Siple, 1964; Proctor and Marine, 1965), has been completed at the U.S. Atomic Energy Commission's Savannah River Plant near Aiken, S.C. (fig. 1). The Savannah River Plant is located on the Atlantic Coastal Plain about 20 miles southeast of the outcrop of the crystalline rocks at the fall line, which separates the Piedmont and Coastal Plain provinces. The crystalline rocks at the proposed storage site are buried beneath approximately 930 feet of unconsolidated to semiconsolidated sediments consisting predominantly of sand and clay.

In order to investigate the hydrologic character of the crystalline rocks, 7 wells were drilled within a circular area having a radius of 4,300 feet (fig. 2). Each well was drilled by conventional rotary methods to a point from 10 to 200 feet below the top of the crystalline rock, and then was cased and cemented as shown on figure 3. All except 2 holes (DRB 5 and 7) were then continued by coring until a total of 1,000 feet of crystalline rock had been penetrated. Holes DRB 5 and 7 were drilled an additional 200 and 245

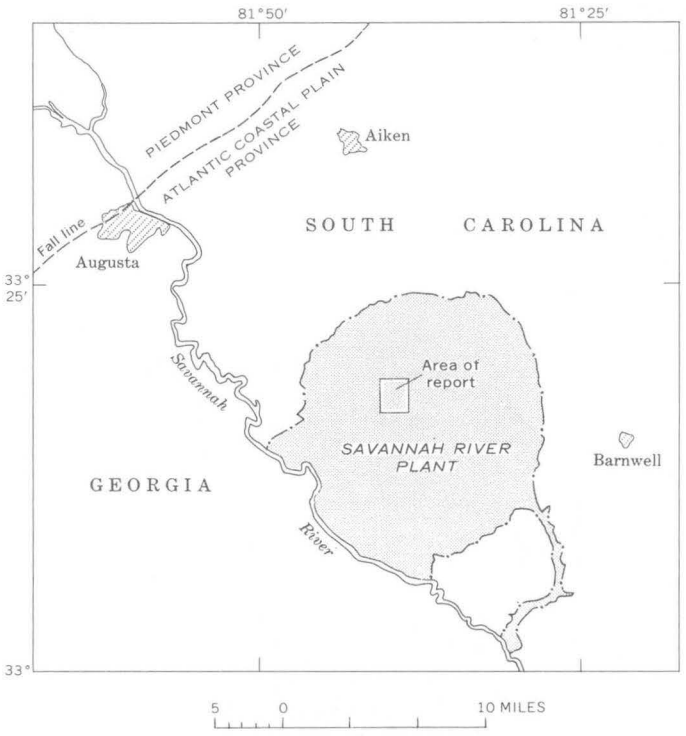

FIGURE 1.—Location of the Savannah River Plant and area of report.

feet, respectively, below the base of the cemented section before continuous coring (which also reached total depths of about 900 and 1,000 feet, respectively, below the top of the rock) was begun.

To the depths explored by drilling and coring the crystalline rock is composed predominantly of chlorite-hornblende schist and hornblende gneiss, and of lesser amounts of quartzite. Calcite occurs as fillings in

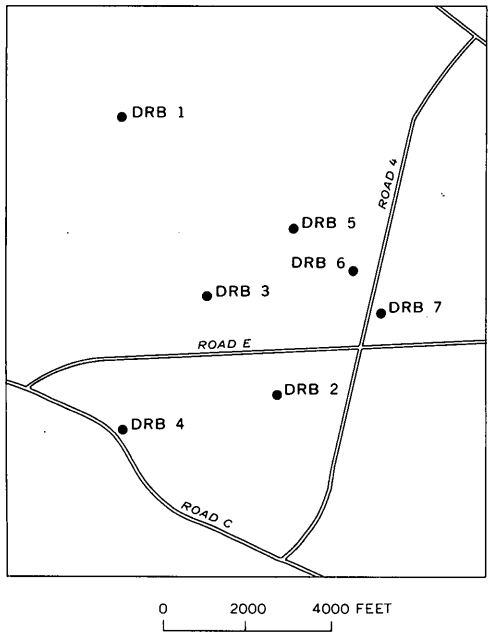

FIGURE 2.—Location of exploration wells cored into crystalline rock at the Savannah River Plant.

some fractures. The foliation or schistosity strikes northeast and has an average dip of about 55° SE. Immediately overlying the crystalline rock is a layer of saprolite or residual clay formed by subaerial weathering of the crystalline rock before deposition of the overlying sediments. The saprolite averages 50 feet in thickness and effectively separates the water that occurs in the fractured crystalline rock below from that in the sand above.

DISTRIBUTION OF THE FRACTURES

Two types of fractures were found in the upper 1,000 feet of crystalline rock. One type, which consists of openings so small that water movement through them is extremely slow, extends throughout the entire mass of crystalline rock. The other type consists of fractures open wide enough to permit transmission of water at a significantly faster rate; these fractures occur in vertically restricted but laterally extensive zones.

The water-transmitting properties of fractures present in the crystalline rock mass could not be inferred from the physical properties of the rock as determined by breaks in the core or by deflections on geophysical logs. The integrity of the cores ranged from sound rock that had to be artificially broken in order to have a convenient length of core to handle (3 or 4 feet) to core that was so broken that it crumbled when removed from the core barrel. . However, the number of fractures shown by the core has little relationship to the occurrence of water-transmitting fractures in the rock as it exists in place. The coring process and the strength of the rock account for most of the fractures as seen in the core. When tested in place for the capactiy to transmit water, some sections of rock that were represented by highly fragmented cores yielded insignificant quantities of water. Many former fractures have been healed by calcite, and it was thought possible that an abundance of these, as observed in the cores, might afford a clue to the existence of some fractures still open due to incomplete healing. This was not found to be true.

Although some open fractures are indicated by deflections on the sonic, neutron, and caliper logs, identical deflections commonly indicate differences in rock properties that are unrelated to the presence of open fractures. The only method whereby zones of open fractures in these holes could be located was measurement of the rate at which water could be injected into or removed from sections of rock that had been isolated from the remainder of the well by the inflation of rubber packers. The results of the tests on intervals for which the inflow or outflow was more than 1 gallon per minute are indicated on figure 3.

As a result of the hydraulic tests using packers, it was found that much of the mass of crystalline rock is pervaded by fractures of small magnitude that transmit water extremely slowly. These fine fractures occur at inhomogeneities in the rock (for example, along chlorite seams, at the contact of gneiss and schist, and along healed fractures). Because this system of fine fractures apparently extends through the full thickness of crystalline rock that was penetrated by the drill, there is reason to believe that at least this upper thousand feet of the crystalline rock is hydraulically connected, and consequently that the entire mass constitutes a single hydraulic unit. Thus, even where an open hole is drilled into rock cut only by fine fractures, the slow inflow of water eventually fills the hole to a level indicative of the piezometric surface in that section of rock. This water level responds to changes in pressure due to the withdrawal or injection of water at other places within the rock, but the response is both delayed and protracted compared to that in a hole open to one or more zones of larger fractures.

It is the larger fractures, in laterally extensive zones, that permit relatively rapid response to pressure changes and the transmission of significant quantities of water to or from a well or other excavation. A possible geometry of two zones of these larger fractures is shown diagramatically on figure 4. Some

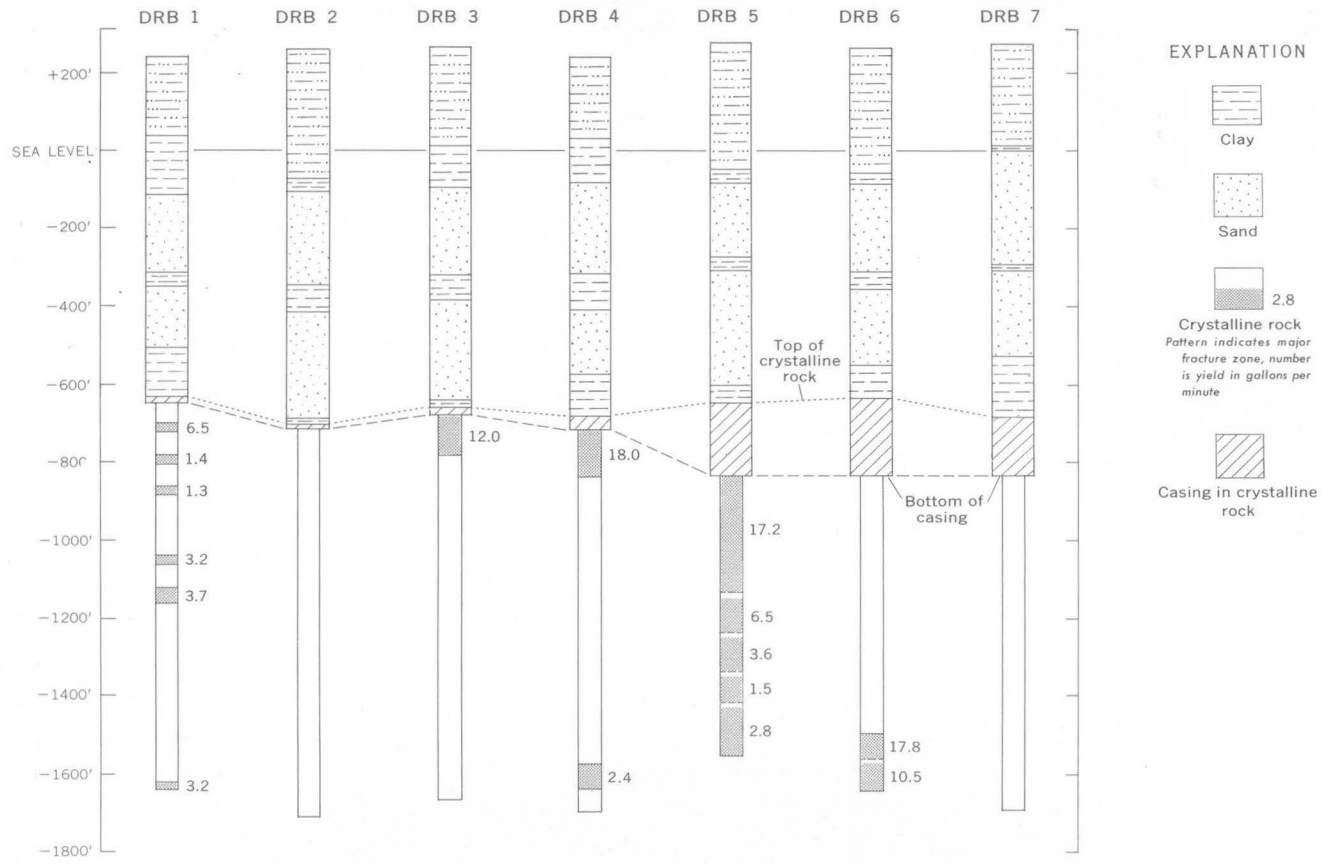

FIGURE 3.—Location and yield of fractured sections of crystalline rock that yield more than 1 gallon per minute of water.

wells penetrate sections of rock containing the larger fractures that could not be correlated into this geometry (particularly the lower parts of DRB 1 and 5).

CORRELATION OF THE FRACTURE ZONES

One of these zones of larger fractures, here termed the shallow fracture zone, is at the top of the crystalline rock just beneath the saprolite, where the rock is weathered but has not yet been reduced to clay. These fractures are believed to have resulted from unloading and weathering during the time that the crystalline rock was exposed to the atmosphere because of their widespread occurrence at the top of the rock. Fractures in this zone probably decrease in number and openness with depth. During drilling of holes 1, 3, and 4 water losses in this zone were 20 gpm or more, and parts of this interval had to be cemented so that drilling could proceed. Because coring through this zone in holes DRB 1, 3, and 4 had proved so difficult, holes DRB 5, 6, and 7 were drilled and cased below this horizon, and consequently no tests of its water-yielding capability were made at these sites. However, a single shallow-rock core made to verify rock penetration in hole DRB 6 contained a very weathered and open fracture which indicates the presence of this zone at this site. It seems likely, because other fractures are abundant at shallow depths in the rock in hole DRB 5, that this zone is present there. The zone is known to be absent at DRB 2; there is no information about its presence at DRB 7.

The other zone of larger fractures, termed the inclined fracture zone, dips at an angle of 10° or more. This zone occurs near the bottom of holes DRB 4 and 6, which are located along the strike of the schistosity. This zone probably merges with the shallow fracture zone in the vicinity of DRB 3 and 5, which are also along the strike of the schistosity. This zone is believed to be too deep to have been reached in the drilling of DRB 2 and 7. Some of the fractures in DRB 1 have hydraulic continuity with this zone, but the geometry of the connection is undetermined. The number and openness of fractures in the rock, except for those in the shallow fracture zone, seem to bear no relation to depth.

Hydraulic continuity of the inclined fracture zone is indicated by the response of the water level in DRB 6 to swabbing tests in DRB 5, as shown on figure 5. (Swabbing is a method of removing a column of water

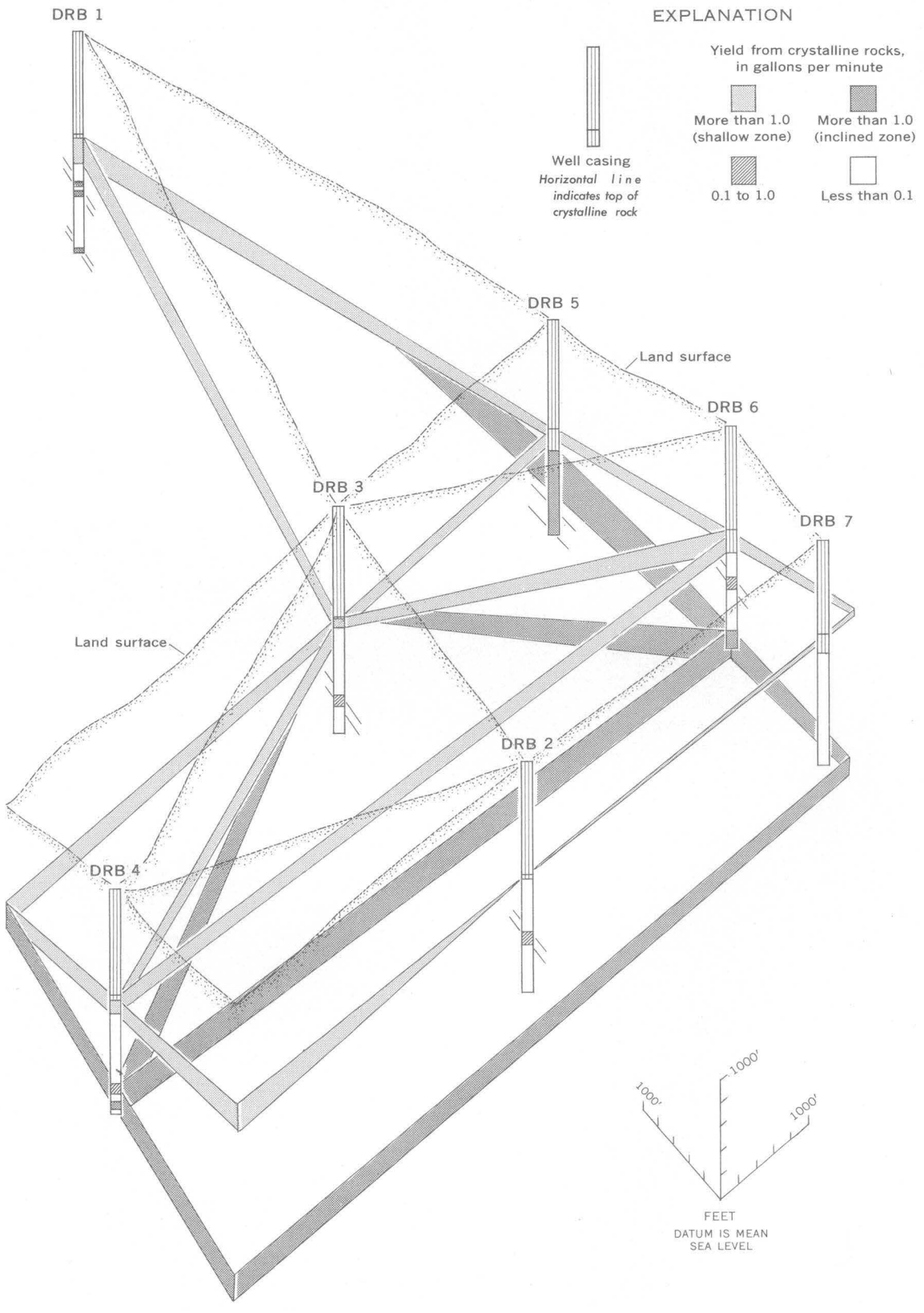

FIGURE 4.—Correlation of fracture zones inferred from swabbing, pumping, and injection tests.

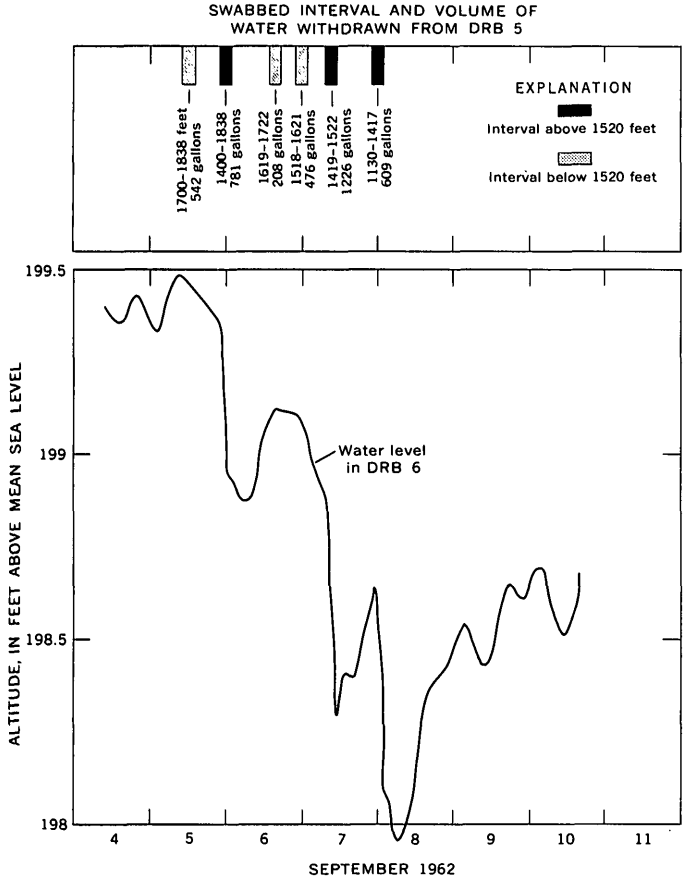

FIGURE 5.—Relation of water-levels in DRB 6 to withdrawals from packed-off intervals in DRB 5.

from drill rods or packer tubing by withdrawing an expandable rubber cup on the end of a cable.) When water was swabbed from intervals of rock above a depth of 1,520 feet below land surface, the water level in DRB 6 immediately declined, whereas swabbing from packed-off intervals of rock below this depth had no discernible effect on the water level in DRB 6. The only open fractures in DRB 6 (fig. 4) occur near the bottom part of the hole, and thus the fracture zone in the upper part of DRB 5 is correlated with that in the lower part of DRB 6.

The inclined fracture zone intersects the shallow fracture zone in the vicinity of DRB 3 and 5, and there is a hydraulic connection between the two zones. This is shown by the fact that pumping the shallow fracture zone at DRB 3 at 5 gpm for 4 days caused 13 feet of drawdown in the deep fractures at DRB 4 (inclined zone) as opposed to only 10 feet in the shallow zone. The drawdowns in these separate fracture zones could be determined independently in DRB 4 because a permanent packer and cement plug 177 feet long were installed to separate the two zones.

Hydraulic communication within the crystalline rocks apparently is better in the northwest-southeast direction than in the northeast-southwest direction. Evidence supporting this was obtained by recording the lapse of time between the start of pumping from DRB 6 and the first indication of water-level decline in other holes. DRB 6, which is open to only the inclined zone of fractures, was pumped for 31 days at a rate of 20.5 gpm. The time lapse before the start of drawdown was 8 minutes in DRB 5, 3 hours in DRB 7, and 7 hours in DRB 1, all in a northwest-southeast line; but the time lapse was 21 hours in DRB 3, 35 hours in DRB 4, and 159 hours in DRB 2, all of which are southwest of DRB 6, the pumped well.

REFERENCES

Christl, R. J., 1964, Storage of radioactive wastes in basement rock beneath the Savannah River Plant: E. I. du Pont de Nemours & Co., Savannah River Laboratory, DP–844, 106 p.

Proctor, J. F., and I. W. Marine, 1965, Geologic, hydrologic, and safety considerations in the storage of radioactive wastes in a vault excavated in crystalline rock: Nuclear Science and Engineering, v. 22, p. 350–365.

Siple, G. E., 1964, Geohydrology of storage of radioactive waste in crystalline rocks at the AEC Savannah River Plant, South Carolina, *in* Geological Survey Research 1964: U.S. Geol. Survey Prof. Paper 501–C, p. C180–C184.

EFFECT OF SAMPLING AND TESTING METHODS ON COMPUTED HYDRAULIC PROPERTIES OF GLACIAL OUTWASH AT PIKETON, OHIO

By STANLEY E. NORRIS and RICHARD E. FIDLER, Columbus, Ohio

Work done in cooperation with the U.S. Atomic Energy Commission and the Ohio Department of Natural Resources, Division of Water

Abstract.—Particle-size distribution and permeability were determined in the laboratory for samples from two adjacent test holes, one drilled with an auger and the other "bailed in" with cable-tool equipment. Discrepancies in the logs and in analytical values obtained in the laboratory for samples from the same reported depths in these holes are believed to be inherent in the drilling methods. For both sets of samples, transmissibility computed from laboratory results is far less than the value determined from a pumping test. Laboratory and pumping-test values probably are not equatable unless flow direction with respect to bedding is the same.

For years hydrologists have sought indirect methods of computing, or at least estimating, the transmissibility of sand and gravel aquifers. One way in which this attempt has been made is by measuring the permeability of small samples of the water-bearing material in the laboratory, and by using these measurements in estimating the permeability of the deposit. However, the values of permeability of many samples of disturbed and recompacted material, as determined in the laboratory, are not consistent nor realistic. The purpose of this paper is to show that differences in drilling methods by which the aquifer materials commonly are sampled may greatly affect the results obtained; and to point out that, because of differences in the direction of flow through the aquifer materials, laboratory and field techniques of determining the permeability of an aquifer may yield widely different values.

A study of the physical and hydraulic characteristics of water-bearing glacial outwash at a site (lat 39°04′42″ N., long 83°01′46″ W.) near Piketon, in southern Ohio, was made in 1963 for the U.S. Atomic Energy Commission. During the study two test holes, less than 3 feet apart, were drilled to the base of the glacial outwash, and samples were obtained at various depths for laboratory determination of grain size and permeability. One hole, 4½ inches in diameter, was bored by means of a truck-mounted, continuous-flight, power auger; the other, 12 inches in diameter, was "bailed in"—that is, a cable-tool drilling rig was used to drive the casting and alternately to bail out the sediment from within it. Detailed logs were made of the materials penetrated, and samples representing depth increments of about 5 feet were collected for sieve analysis by the Goodyear Atomic Corp., operating contractor for the Atomic Energy Commission. The samples were used for permeability determination by the U.S. Geological Survey hydrologic laboratory, Denver, Colo.

The thickness of the outwash at the test site is between 80 and 85 feet, and the depth to the water table is about 20 feet. For the most part the water-bearing materials consist of "clean" coarse sand and fine gravel interbedded with layers of "dirty" medium to coarse sand. Curves representing the particle-size distribution of both types, as determined from sieve analysis of samples from this and nine other bailed-in test holes, were presented by Norris and Fidler (1965). The curves for the two types differ significantly, in that those which represent the finer grained, "dirty" material not only lie farther to the left—in the direction of finer grain size—but also are generally steeper—reflect a narrower range of grain sizes—than the curves representing the coarser grained material.

The log of the bailed-in test hole agrees closely with the logs of the other bailed-in holes at the test site. The internal consistency of the group of logs, together with precautions taken during the drilling, convince the authors that the log of the bailed-in hole is a reasonably accurate record of the thicknesses and types of materials penetrated. Bailer loads representing each sampled interval were thoroughly mixed during collection of the samples, and heaving of the material penetrated was prevented during the bailing. On the other hand, the log of the augered hole differs from it so markedly that it is believed to be considerably less accurate. Part of the discrepancy undoubtedly relates to the way in which, in the respective methods, the samples are brought to the surface. In the augering method the material is forced to the surface, following the spiral flutes of the auger, as the auger bites deeper into the sediment; some mixing of the material moving up from any given depth interval with that in the sides of the hole probably is unavoidable. For example, the log of the bailed-in hole indicates "sand" in the interval between the depth of 28 and 48 feet, whereas the log of the augered hole indicates "gravel" and "sand and gravel" in the same interval. Similarly, the log of the bailed-in hole indicates "sand and gravel" in the interval from 48 to 58 feet, whereas the log of the augered hole indicates "sand" in the same interval. Another reason for believing that the log of the bailed-in hole is the more accurate is that the bailing-in method, unlike the augering method, requires no interpretation of depth of sample origin.

As shown in table 1, the sizes for which 60 percent and 10 percent of the particles were finer were much greater for the average of all samples from the bailed-in hole than for that from the augered hole. Similarly, the averages for the sand-zone samples were larger for the bailed-in hole than for the augered hole.

TABLE 1.—*Particle-size characteristics of samples from bailed-in and augered test holes*

	Measures of particle size (mm)		Uniformity coefficient
	60-percent-finer size, by weight	10-percent-finer size, by weight	
Average of all samples			
Bailed-in test hole	4. 58	0. 49	9. 34
Augered test hole	3. 05	. 29	10. 58
Average of samples from sand zones			
Bailed-in test hole	0. 64	0. 19	3. 32
Augered test hole	. 35	. 10	3. 50

It seems reasonable to explain this observation by concluding that the samples obtained by bailing contained a disproportionately high proportion of the larger particles and those obtained by augering a disproportionately high proportion of the finer particles.

The uniformity coefficient, which is defined as the ratio of the 60-percent-finer size to the 10-percent-finer size, indicates whether (1) the particles are chiefly of the same size or (2) there is a wide range in their diameters. Stated in another way, a small uniformity coefficient indicates a well-sorted mixture, while a large uniformity coefficient indicates a poorly sorted mixture. The data in table 1 show that the uniformity coefficients were nearly the same for the averages of all samples from both the bailed-in and augered holes, and that they were nearly the same for the averages of the samples from the sand zones only. These observations suggest that (1) the samples obtained by bailing lacked a large fraction of the smaller size particles, (2) those obtained by augering lacked a large fraction of the larger size particles, or (3) both these effects occurred. Possibly the lowering of the bailer into the hole agitated the water enough for a fairly large fraction of the finer grained particles to become suspended in the water and therefore not to be included in the sample. In augering, on the other hand, it is likely that the spiral became so clogged with the more cohesive and finer grained materials that much of the less cohesive and coarser grained material was forced aside as the auger penetrated deeper, and thus was not lifted to the surface.

The coefficients of permeability determined in the laboratory, together with the coefficients of transmissibility computed from them, are given in table 2. As would be expected because they contained proportionately less of the finer size particles, the samples from the bailed-in hole had a much higher average coefficient of permeability than the samples from the augered hole. Consequently, the coefficient of transmissibility (coefficient of permeability $\times$ thickness of material) computed from the permeability data is much greater for the bailed-in hole than for the augered hole.

The coefficient of transmissibility computed from data provided by a 9-day pumping test at the same site is 215,000 gallons per day per foot; the average coefficient of permeability computed from the coefficient of transmissibility is 3,300 gallons per day per square foot. The transmissibility value from the pumping-test data is nearly 4 times the total laboratory-determined value for samples from the bailed-in hole, and it is 47 times that for samples from the augered hole. That the value from the field test is so

TABLE 2.—*Laboratory permeability and computed transmissibility of samples from bailed-in and augered test holes*

Depth (feet) [1]	Thickness (feet)	Coefficient of permeability (gpd per sq ft) [2]	Coefficient of transmissibility (gpd per ft)
Bailed-in test hole			
28	8	3,600	28,800
33 [3]	5	100	500
38 [3]	5	320	1,600
42 [3]	4	180	720
48 [3]	6	16	96
53	5	440	2,200
58	5	1,100	5,500
63	5	1,800	9,000
68	5	330	1,650
74	6	420	2,520
77 [3]	3	480	1,440
82	5	230	1,150
Coefficient of transmissibility			55,176
Augered test hole			
23	5	5	25
28	5	30	150
33	5	57	285
38	5	150	750
43	5	540	2,700
48	5	19	95
53 [3]	5	17	85
58 [3]	5	12	60
63	5	8	40
68	5	9	45
73	5	22	110
78	5	22	110
83	5	13	65
Coefficient of transmissibility			4,520

[1] Depth to bottom of sampled interval.
[2] At 60° F.
[3] Sand zones logged by the driller.

much greater than the laboratory-determined value for samples obtained by bailing is, at first, rather surprising when it is considered that the samples tested in the laboratory probably were disproportionately low in the finer particles. Possibly the seemingly wide discrepancy stems from the difference in direction of flow with respect to orientation of the particles that constituted the tested materials. The direction of water movement through the aquifer to the pumped well in the field test is largely lateral, whereas it is vertical through the sample in the laboratory permeameter.

The relation of permeability to orientation of grains and direction of water movement has been discussed by Weeks (1964, p. D193) as follows:

> Anisotropic permeability in clastic sediments is due in part to the orientation of the constituent grains. Plate-shaped grains within the sediments tend to be oriented with their flat surfaces approximately parallel to the bedding plane. Such orientation minimizes the vertical cross-sectional area and, by increasing the tortuosity of the vertically interconnected pores, reduces the vertical permeability.

Thus, even though they seemingly differ in the wrong direction, the transmissibility values computed from the pumping-test data and from the laboratory determinations of permeability may be equally valid for the direction of flow and the particle-size distribution of the material tested. However, from the evidence obtained, there seems no way to determine which—the differences in the particle-size distribution of the tested materials, or the direction of flow through the materials with respect to orientation of the constituent particles—accounts in larger measure for the discrepancy in the transmissibility values.

In another paper, Norris and Fidler (1966) describe methods used to measure the average vertical permeability of the aquifer at Piketon. The value obtained was 365 gpd per sq ft and is believed to be of the correct order of magnitude. As might be expected, this value falls between the two average values of vertical permeability determined in the laboratory. It is not so great as the average—890 gpd per sq ft—for the samples obtained by bailing, which contained more of the coarser and less of the finer particles; and it is not so small as the average—70 gpd per sq ft—for the samples obtained by augering, which contained less of the coarser and more of the finer particles. If the particle-size distribution of the samples tested in the laboratory had been the same as that of the sediment in place, the average laboratory value would have been much closer to the value obtained by the other methods.

The reasons that are believed to account for the discrepancies between the hydraulic constants determined in the laboratory and those computed from pumping-test data may be summarized as follows: (1) The methods used to obtain the samples for laboratory testing were unsatisfactory because the distribution of particle sizes in the samples differed markedly from that of the undisturbed sediment in the field; (2) the direction of flow through the recompacted samples tested in the laboratory was normal to the bedding, whereas the direction of flow during the field test was parallel to the bedding.

REFERENCES

Norris, S. E., and Fidler, R. E., 1965, Relation of permeability to particle size in a glacial-outwash aquifer at Piketon, Ohio, *in* Geological Survey Research 1965: U.S. Geol. Survey Prof. Paper 525–D, p. D203-D206.

——— 1966, Use of type curves developed from electric analog studies of unconfined flow to determine the vertical permeability of an aquifer at Piketon, Ohio: Ground Water, v. 4, no. 3, p. 43–48.

Weeks, E. P., 1964, Field methods for determining vertical permeability and aquifer anisotropy, *in* Geological Survey Research 1964: U.S. Geol. Survey Prof. Paper 501–D, p. D193–D198.

INTERSTATE CORRELATION OF AQUIFERS, SOUTHWESTERN LOUISIANA AND SOUTHEASTERN TEXAS

By A. N. TURCAN, JR., J. B. WESSELMAN, and CHABOT KILBURN,
Baton Rouge, La., Houston, Tex., Lake Charles, La.

Abstract.—Three major aquifers—the Chicot, Evangeline, and Jasper—and two aquicludes—the Burkeville and one as yet unnamed—are recognized on an interstate basis in part of the Louisiana-Texas Gulf Coast region. These hydrologic units consist of sediments of Miocene, Pliocene, and Pleistocene ages. Wells tapping the aquifers supply about a billion gallons of water per day for industrial, agricultural, and municipal use.

The U.S. Geological Survey recently constructed an analog model of the fresh-water aquifers that underlie an area of about 20,000 square miles of the West Gulf Coastal Plain in southeastern Texas and southwestern Louisiana (fig. 1). The average total yield of the industrial, irrigation, and municipal wells in this area, now about a billion gallons per day, is likely to increase significantly. The availability of such large supplies of water is playing an important role in the economic development of this and other parts of the "booming" Gulf Coast region, and the model is expected to facilitate continuing study of this vital resource as it is further developed.

Analysis of the many geologic and hydrologic data compiled preparatory to construction of the model led to the recognition of three distinct aquifers and two aquicludes. Two of the aquifers—the Chicot and the Evangeline—had been recognized in southwestern Louisiana for some time previously, but their names had not been applied to the equivalent water-bearing strata in southeastern Texas. The third aquifer, to which a name had not previously been applied in any part of the area, is here designated the Jasper after Jasper County, Tex., which is within the area where the stratigraphic units constituting this aquifer either crop out or are near the land surface (Sellards and others, 1932, p. 741; Darton and others, 1937). The upper of the aquicludes, named the Burkeville for the town of Burkeville in Newton County, Tex., separates

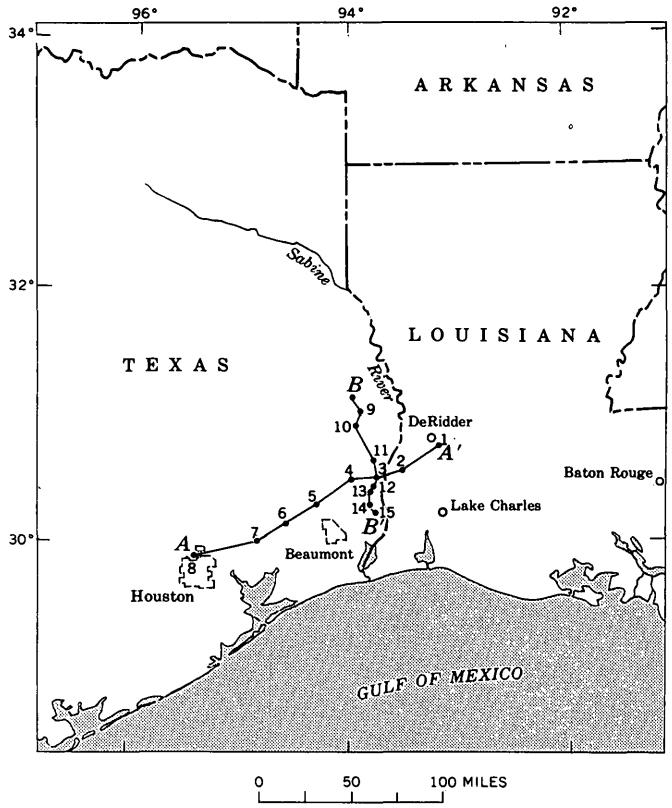

FIGURE 1.—Index map of Louisiana and eastern Texas, showing area of report and location of sections A–A' and B–B' (figs. 2 and 3).

the Jasper and Evangeline aquifers; the lower, as yet unnamed, underlies the Jasper. The relations of these 5 hydrologic units to one another and the approximate positions of the interface between the fresh and saline water in each aquifer are shown by 2 geohydrologic sections, one (fig. 2) along the strike and the other (fig. 3) along the dip of the strata. Also shown are the spontaneous potential and short-normal resistivity curves

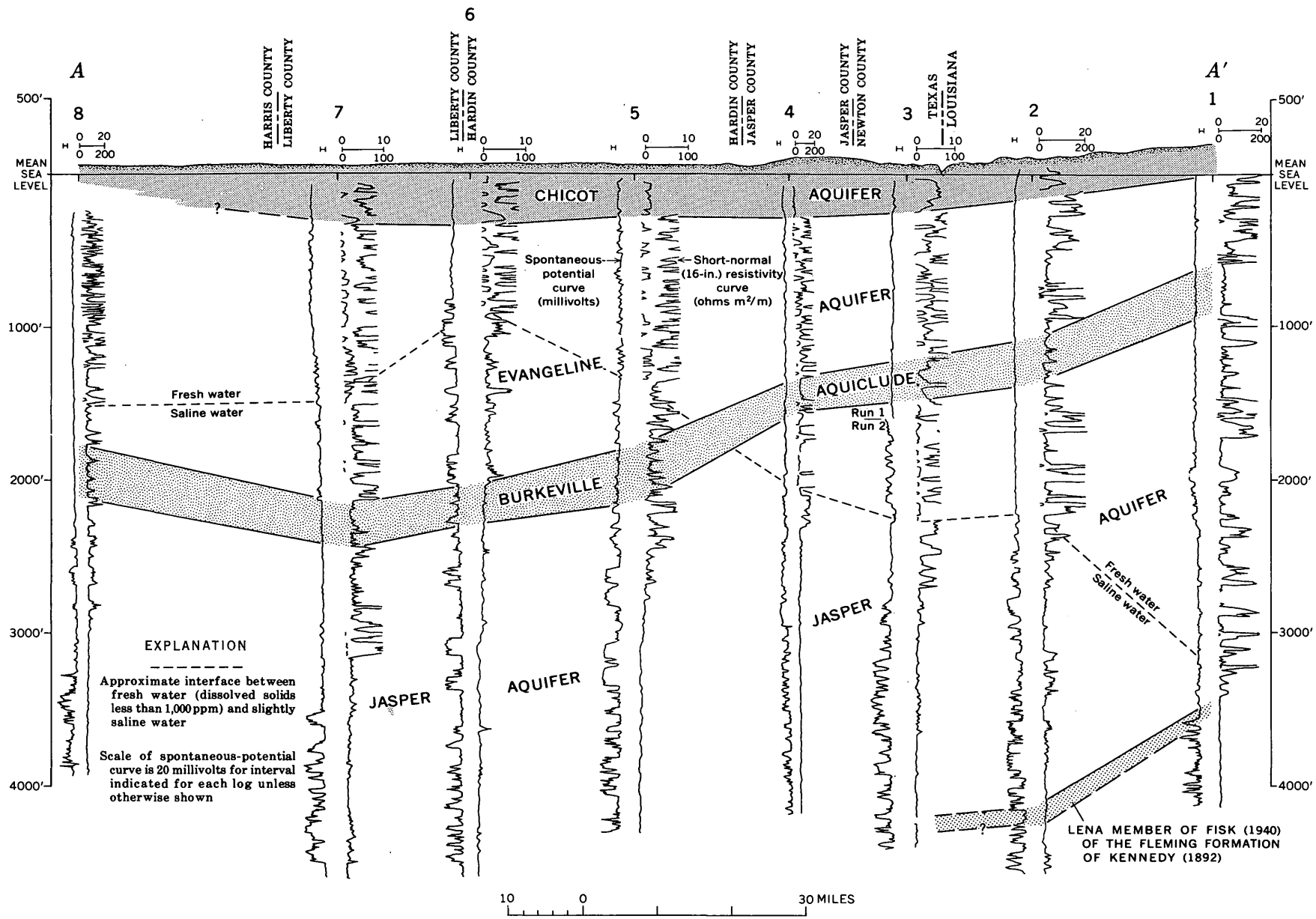

FIGURE 2.—Geohydrologic section A–A' along the strike of the strata from near Houston, Tex., to near De Ridder, La. Section based on electric logs shown for numbered wells. Location of section shown on figure 1.

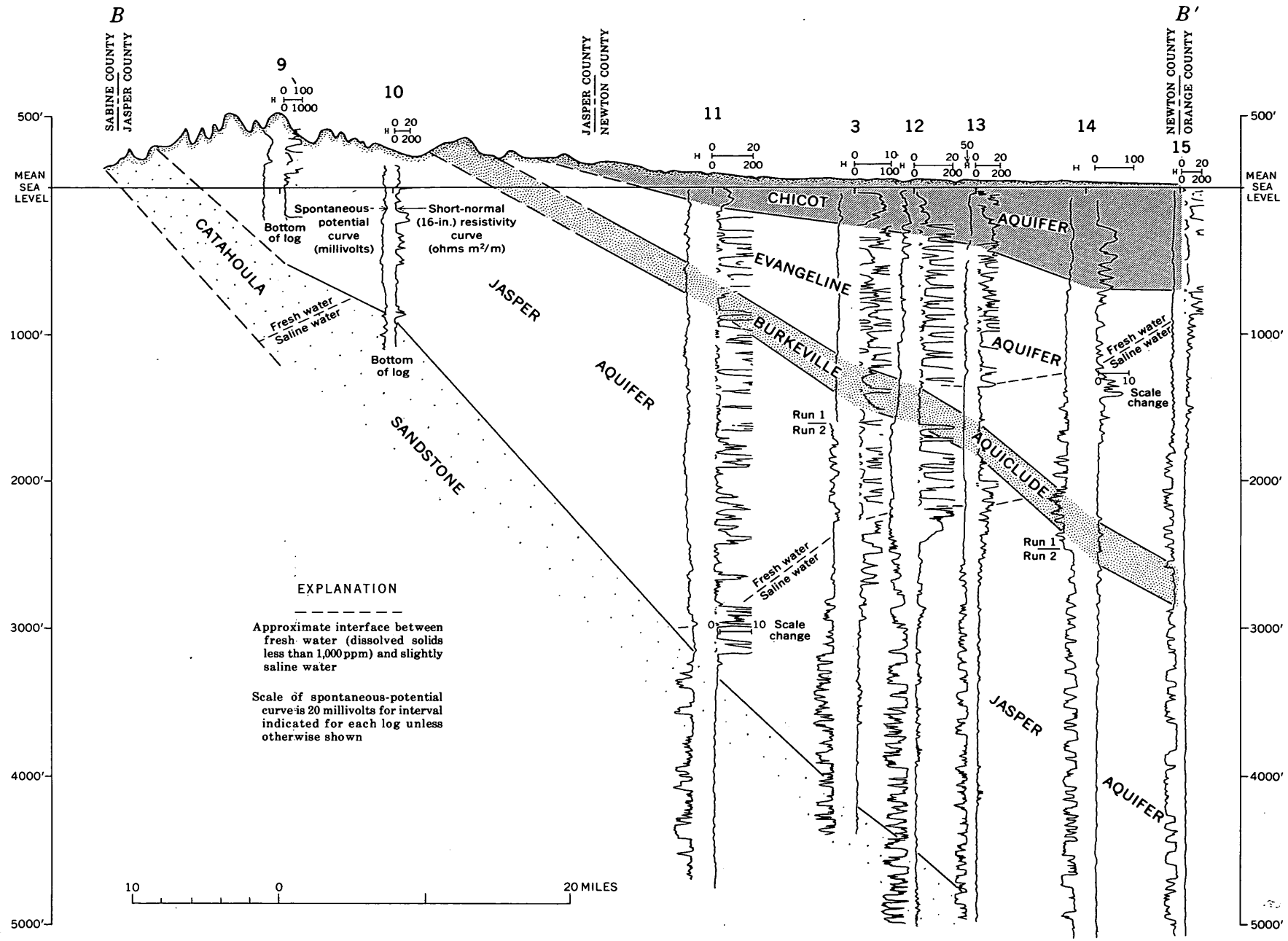

FIGURE 3.—Geohydrologic section B–B' along the dip of the strata in Jasper and Newton Counties, Tex. Section based on electric logs shown for numbered wells. Location of section shown on figure 1.

for each of the wells along the line of section. The stratigraphic and hydrologic units composing each of the aquifers and aquicludes in the two States are indicated in table 1.

TABLE 1.—*The principal aquifers and aquicludes of southwestern Louisiana and southeastern Texas, and corresponding stratigraphic and hydrologic units*

Aquifer or aquiclude	Louisiana	Texas
Chicot aquifer	Prairie, Montgomery, Bentley, and Williana Formations of Pleistocene age (Jones and others, 1956).	Beaumont Clay, Alta Loma Sand of Rose (1943), and Lissie Formation of Pleistocene age; and Willis Sand of Pliocene(?) age in eastern Texas. Alta Loma Sand of Rose (1943) in the Houston district (Wood and others, 1965).
Evangeline aquifer	Foley Formation of Pliocene age (Jones and others, 1956), or Blounts Creek Member of Fisk (1940) of the Fleming Formation of Kennedy (1892) of Miocene age.[1]	Goliad Sand of Pliocene age in eastern Texas. "Heavily pumped layer" in the Houston district (Wood and others, 1965).
Burkeville aquiclude	Castor Creek Member of Fisk (1940) of the Fleming Formation of Kennedy (1892) of Miocene age. [1]	Upper part of Lagarto Clay of Miocene(?) age in eastern Texas. Zone 2 in the Houston district (Wood and others, 1965).
Jasper aquifer	Williamson Creek, Dough Hills, and Carnahan Bayou Members of Fisk (1940) of the Fleming Formation of Kennedy (1892) of Miocene age.[1]	Lower part of Lagarto Clay of Miocene(?) age and Oakville Sandstone of Miocene age.
Unnamed aquiclude	Lena Member of Fisk (1940) of the Fleming Formation of Kennedy (1892) of Miocene age.[1]	Upper part of Catahoula Sandstone of Miocene(?) age in eastern Texas.

[1]Nomenclature involving the Fleming Formation (Kennedy, 1892; Fisk, 1940) has been accepted and used by the Louisiana Geological Survey; it does not necessarily conform to that of the U.S. Geological Survey.

The purpose of this paper is to establish names for use in interstate correlation of the hydrologic units and to characterize each in terms of the stratigraphic units composing them, their hydraulic constants, and their relative importance in the water supply of the area.

CHICOT AQUIFER

As defined by Jones (*in* Jones and others, 1956, p. 214), the Chicot aquifer (reservoir) in Louisiana includes the Prairie, Montgomery, Bentley, and Williana Formations of Pleistocene age. This aquifer is traced into southeastern Texas and includes beds recognized as the Beaumont Clay, the Alta Loma Sand of Rose (1943), the Lissie Formation, and the Willis Sand. Traced southwestward, it is correlated with the Alta Loma Sand of Rose (1943) in the Houston district. In southwestern Louisiana this aquifer is composed primarily of sand or of sand and gravel, and has a regional average coefficient of permeability of 1,500 gallons per day per square foot. The Chicot aquifer has average coefficients of permeability of about 1,400 gpd per sq ft in southeastern Texas and 500 gpd per sq ft in Harris County east of Houston (R. K. Gabrysch, oral commun., 1965). The Alta Loma Sand of Rose (1943), a part of the Chicot aquifer in Texas, was described by Wood and others (1963) as one of the most prolific aquifers of the Gulf Coast region. In Louisiana the Chicot aquifer supplies an average of 500 million gallons per day of water and is capable of providing additional large quantities. In Texas the Chicot aquifer supplies about 200 mgd.

In Louisiana the base of the Chicot aquifer is equivalent to the base of the Pleistocene beds (Jones and others, 1956), whereas in eastern Texas the Willis Sand, which is probably the base of the Chicot, is considered by the U.S. Geological Survey to be of Pliocene(?) age. According to Baker (1964, p. 21) the age assignment of the Willis has been a controversial issue for some time. Recent geologic studies in eastern Texas by Bernard and LeBlanc (*in* Bernard and others, 1962), p. 177), and recent correlations made in Jasper and Newton Counties, Tex., by Geological Survey workers, suggest that the Willis is of Pleistocene(?) age.

The geologic names assigned to sediments of the Chicot and Evangeline aquifers in the Houston district, as mapped by Wood and others (1965, fig. 3), conflict in part with those used for similar sediments farther east in Texas. Regardless of the disagreement in assignment of the geologic names and ages of the formations which comprise them, the Chicot and Evangeline aquifers were mapped as continuous hydrologic units in Louisiana and into Texas (see fig. 2).

EVANGELINE AQUIFER

Jones (*in* Jones and others, 1956, p. 205) assigned the name Evangeline to a water-bearing heterogeneous sequence of sand and clay (Foley Formation) of Pliocene age that occurs below the base of the Pleistocene sequence in southwestern Louisiana. He did not define the base of the Evangeline, partly because the

information was scanty and partly because the objectives of that study did not include mapping of the Evangeline aquifer. Rogers (*in* Rogers and Calandro, 1965, p. 33) believed that the Evangeline aquifer was hydrologically correlative with the Blounts Creek Member of Fisk (1940) of the Miocene Fleming Formation of Kennedy (1892). The fact that both Fisk (1940) and Welch (1942) previously considered the sediments immediately below the base of the Pleistocene sequence in Louisiana to be Fisk's Blounts Creek Member substantiates Rogers' correlation. Therefore, it is reasonable to conclude that, in Louisiana, the base of the Evangeline aquifer is the same as that of the Blounts Creek Member.

The Chicot and Evangeline aquifers are separated in part of the area by a clay; where a clay is not present the aquifers can be differentiated by other criteria. Normally, this separation is made on the basis of grain size. Whereas the Chicot consists chiefly of coarse sand and gravel, the Evangeline is composed of finer grained sediments. The contact between these beds is usually recognizable on electrical logs because the resistivity of the Chicot aquifer generally is higher than that of the Evangeline aquifer. The aquifers are also distinguished on the basis of differences in water quality, drill cuttings, and permeability. These criteria were used in identifying the contact of the Chicot with the Evangeline. The Evangeline aquifer was extended into Texas, where it includes sediments that are probably the Goliad Sand of Pliocene age in Jasper and Newton Counties and other parts of southeastern Texas; the Evangeline is correlated also with the "heavily pumped layer" of the Houston district, as mapped by Wood and Gabrysch (*in* Wood and others, 1965, fig. 3). (See table 1.)

Although the Evangeline aquifer is not developed to any large degree as a source of water in southwestern Louisiana, it is a potential source for moderate to large supplies of water. In southeastern Texas, especially in the Houston district and surrounding areas, this aquifer is the principal source of water and supplies an average of about 700 mgd. Jones and others (1954, p. 131) stated that the sands of the Evangeline aquifer in Louisiana have an estimated coefficient of permeability that ranges from about 250 to 1,000 gpd per sq ft. More recent observations, however, indicate that the latter value may be too high. The coefficient of permeability of the Blounts Creek Member of Fisk (1940) in Vernon Parish, La. ranges from 150 to 300 gpd per sq ft (Rogers and Calandro, 1965, p. 33), which is similar to that determined for the sands in the Evangeline aquifer in Texas. In the Houston district and eastern Texas, the average coefficient of permeability of the Evangeline is about 250 gpd per sq ft.

224-352 O—66——16

BURKEVILLE AQUICLUDE

A relatively thick and areally extensive clay below the base of the Evangeline aquifer is referred to as the Burkeville aquiclude. In southwestern Louisiana this aquiclude consists of the Castor Creek Member of Fisk (1940) of the Fleming Formation of Kennedy (1892), and in southeastern Texas it consists of the upper part of the Lagarto Clay, which is correlated with zone 2 (Wood and others, 1965, fig. 3) in the Houston area. This clay, which in some places is as thick as 300 feet, is an effective barrier to vertical movement of water. In addition to being a noticeable clay interval on electrical logs, the Burkeville aquiclude is traceable by means of the fossil gastropod *Potamides matsoni*. Rogers (*in* Rogers and Calandro, 1965, p. 8) states that Fisk's Castor Creek Member contains this fossil, and Plummer (*in* Sellards and others, 1932, p. 748) reports the fossil in the Lagarto Clay also. The presence of the fossil in both rock units—the former in Louisiana and the latter in Texas—is believed to establish the equivalency of these units.

JASPER AQUIFER

The name Jasper is proposed for the aquifer which includes the Williamson Creek, Dough Hills, and Carnahan Bayou Members of Fisk (1940) of the Fleming Formation of Kennedy (1892) in Louisiana, and the lower part of the Lagarto Clay and the Oakville Sandstone in Texas. A clay identified as the Lena Member of Fisk (1940) of the Fleming Formation in Louisiana (fig. 2) is believed to be equivalent to the upper part of the Catahoula Sandstone in Texas (fig. 3), and is an excellent marker zone for the base of the Jasper aquifer. The depth to the top of the Jasper is known throughout the area, but the depth to the bottom is known only where the aquifer contains fresh water. Although the Jasper aquifer is tapped by only a few wells in Vernon and Rapides Parishes, La., and in southeastern Texas, it is a major potential source of water. Sands of the aquifer have a coefficient of permeability that ranges generally from about 200 gpd per sq ft to 700 gpd per sq ft, and averages 500 gpd per sq ft. Additional information and widespread development of this aquifer may necessitate its subdivision into smaller hydrologic units by region or by local area.

SUMMARY

Definition and correlation of the three principal fresh-water aquifers that underline southeastern Texas and southwestern Louisiana should aid in the planning, on an interstate basis, for full development of these important sources of ground-water supplies. Although, from present evidence, the upper and lower boundaries of the aquifers seem not to coincide in all parts of the area with the boundaries of recognized stratigraphic units, closer agreement between the boundaries may be apparent after additional geologic and hydrologic data become available.

REFERENCES

Baker, E. T., Jr., 1964, Geology and ground-water resources of Hardin County, Texas: Texas Water Comm. Bull. 6406, 179 p., 8 pls., 26 figs., 11 tables.

Bernard, H. A., LeBlanc, R. J., and Major, C. F., 1962, Recent and Pleistocene geology of southeast Texas: Houston Geol. Soc., p. 175–224.

Darton, N. H., Stephenson, L. W., and Gardner, Julia (compilers), 1937, Geologic map of Texas: U.S. Geol. Survey, scale 1:500,000.

Fisk, H. N., 1940, Geology of Avoyelles and Rapides Parishes: Lousiana Dept. Conserv. Geol. Bull. 18, p. 158–175, pl. 6.

Jones, P. H., Hendricks, E. L., Irelan, Burdge, and others, 1956, Water resources of southwestern Louisiana: U.S. Geol. Survey Water-Supply Paper 1364, 460 p., 38 pls., 73 figs.

Jones, P. H., Turcan, A. N., Jr., and Skibitzke, H. E., 1954, Geology and ground-water resources of southwestern Louisiana: Louisiana Dept. Conserv. Geol. Bull. 30, p. 53–61, 128–138.

Kennedy, William, 1892, A section from Terrell, Kaufman County, to Sabine Pass on the Gulf of Mexico: Texas Geol. Survey 3d Ann. Rept., p. 45, 62.

Rogers, J. E., and Calandro, A. J., 1965, Water resources of Vernon Parish, Louisiana: Louisiana Dept. Conserv. and Louisiana Dept. Public Works Water Resources Bull. 6, 104 p.

Rose, N. A., 1943, Progress report on the ground-water resources of the Texas City area: U.S. Geol. Survey open-file report, 45 p., 3 figs.

Sellards, E. H., Adkins, W. S., Plummer, F. B., 1932, The geology of Texas, v. 1, Stratigraphy: Texas Univ. Bull. 3232, 1007 p., 54 figs., 11 pls.

Welch, R. N., 1942, Geology of Vernon Parish: Louisiana Dept. Conserv. Geol. Bull. 22, p. 3, 37, 61–62.

Wood, L. A., Gabrysch, R. K., and Marvin, Richard, 1963, Reconnaissance investigation of the ground-water resources of the Gulf Coast region, Texas: Texas Water Comm. Bull. 6305, 114 p., 15 pls., 18 figs., 14 tables.

Wood, L. A., Gabrysch, R. K., and Patten, E. P., 1965, Analog model study of ground water in the Houston district, Texas: Texas Water Comm. Bull. 6508, 103 p., 43 figs.

RECONNAISSANCE SURVEY OF GROUND-WATER QUALITY IN THE GREAT BASIN

By J. H. FETH, Menlo Park, Calif.

Abstract.—The Great Basin is noted for its areas of excessive heat, negligible precipitation, and commercially valuable brines. Nevertheless, virtually all valleys in the region produce some potable ground water. More than 80 percent of 2,731 analyses of ground water show less than 1,000 ppm of dissolved-solids, although some brines contain as much as 325,000 ppm, mostly sodium chloride. There is a wide diversity of chemical types; in the lower ranges of concentration the waters are typically of calcium or sodium bicarbonate types, whereas sodium or calcium sulfate or chloride types dominate the higher ranges. Some supplies are renewable, but in other basins all pumpage seemingly is from storage alone.

This report is a preliminary assessment of (1) the adequacy of present knowledge of the quality and quantity of ground water in the Great Basin, and (2) the probable immediate and future needs for desalination of mineralized ground water. It is part of the U.S. Geological Survey's continuing study of saline ground-water resources of the Nation.

The Great Basin, as outlined in figure 1, is a region in which all streams drain to closed lakes or playas and none drain to the sea. It includes most of Nevada, large areas in California, Utah, and Oregon, a small part of southeastern Idaho, and a thin sliver along the southwestern border of Wyoming. Its present climate ranges from arid and semiarid on the valley floors to humid in the higher mountains within and peripheral to the Great Basin. Most of the Great Basin was without exterior drainage in Pleistocene time, as it still is. Therefore, for tens of thousands of years water has been discharged from this part of the basin only by evaporation and transpiration, and no salts have been carried out of the region by streamflow.

OVERALL CHEMICAL QUALITY OF GROUND WATER

Much of the hydrologic work in the Great Basin has been of the reconnaissance type; few areas have been studied in detail. Consequently, chemical data are sparse for most of the area, and nonexistent for parts of it. Some hydrologic basins are represented by only

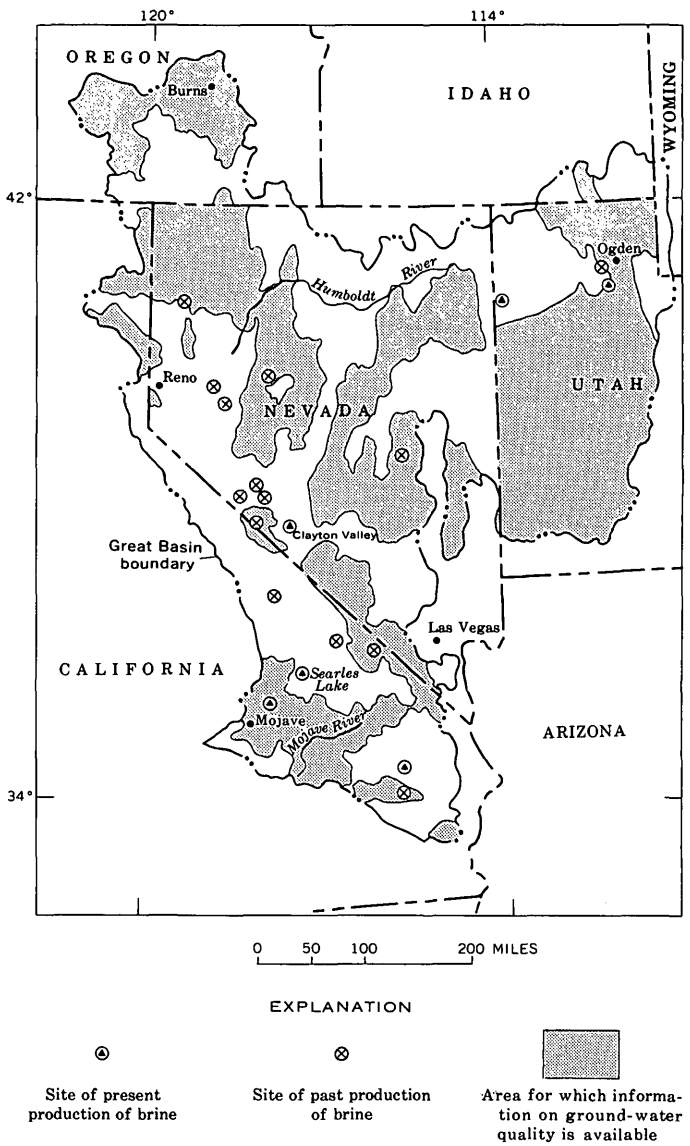

FIGURE 1.—Outline map of the Great Basin, showing areas where data are available on water quality, and sites of past and present production of salines from brines. Boundary of Great Basin, except in Wyoming, after Snyder and others (1964).

2 or 3 analyses, others by 10 or even 40; but few are represented by as many as 100. In general, the number of analyses varies with the degree of development of ground water for man's use and with the intensity of the hydrologic studies that have been made of the basins. Those areas for which at least some water-quality information is on hand are shown in figure 1. The chemical analyses are in publications and open-file reports of the U.S. Geological Survey and of the geological and water-resources agencies of the Great Basin States.

Significantly, extremely few hydrologic basins for which data are available are without one or more sources of potable ground water. According to the standards established by the U.S. Public Health Service (1962, p. 34), water having more than 500 parts per million of dissolved solids is not recommended for public supplies if water of better quality is available. It is recognized by the Public Health Service, however, that water containing more than 2,000 ppm of dissolved solids is used successfully in some places. For the Great Basin as a whole, more than 80 percent of the available analyses show water having less than 1,000 ppm of dissolved solids, and 57 percent show water having less than 500 ppm. From a tabulation, by regions, of the percentages of analyses showing concentrations in different ranges, it is evident that from region to region within the Great Basin the distribution of ground-water salinities, as so far reported, is nearly the same (table 1).

There is a wide variety of chemical water types in the region. Where dissolved-solids concentrations are less than 500 ppm. calcium magnesium bicarbonate, calcium sodium bicarbonate, or sodium bicarbonate types are commonly found. Water with mixed anions is common in ranges from 500 to 2,000 ppm of dissolved solids, and sodium bicarbonate water continues as a type to concentrations greater than 1,000 ppm but not as great as 3,000 ppm. No water of calcium bicarbonate nor calcium magnesium bicarbonate type has been reported from the Great Basin in concentrations exceeding 1,000 ppm. In the range of 2,000–10,000 ppm, sodium is the dominant cation, and sulfate and especially chloride dominate the anions. Sodium sulfate and sodium chloride types are the more common; rarely, calcium sulfate and calcium chloride types occur. With but few exceptions, water having more than 10,000 ppm is of sodium chloride character. The rare exceptions are water of calcium chloride or calcium magnesium chloride type. Distribution and chemical types of water having 1,000 ppm or more of dissolved solids have been illustrated by Feth and others (1965, sheet 2).

The potability and palatability of water are determined largely, though not entirely, by its anion content. A water with 1,000 ppm of dissolved solids, largely sodium bicarbonate, may taste a little flat, but it is potable. The same concentration of sodium chloride is hardly tolerated save by persons long accustomed to its use. To a somewhat lesser degree, the same comparison can be made between sodium bicarbonate water and calcium or sodium sulfate water. So dissolved-solids content offers a general and convenient criterion for evaluating the potability of water. It is used as a general guideline in this discussion.

In many closed-basin valleys, ground water contains small to modest concentrations of dissolved solids except beneath or closely peripheral to a perennially wet or salt-encrusted playa. In those situations there is an artesian system in which the playa is the principal area of discharge. Concentration by evaporation, and perhaps concentration by ion filtration in the subplaya muds, lead to high mineral concentrations in water beneath the playa, whereas elsewhere in the system potable water can be found. The relationships and processes controlling occurrences of this kind are still poorly known.

The data for Utah were examined critically to evaluate the bias introduced into the tabulated values by grossly uneven regional distribution of analyses. In the Great Basin part of that State, about 60 percent of the 1,018 available analyses represent the heavily populated area that extends along the west base of

TABLE 1.—*Distribution of water-quality analyses by region and by concentration ranges*

Dissolved-solids concentration (parts per million)	Southeastern California (Mojave Desert region)		Oregon and northeastern California		Nevada		Utah		Idaho		Great Basin	
	No. of analyses	Percent	No. of analyses	Percent	No. of analyses	Percent	No. of analyses	Percent	No. of analyses	Percent	No. of analyses	Percent
Less than 500	545	50.8	121	60.5	230	57.4	641	63.0	17	42.5	1,554	56.9
500–1,000	297	27.7	37	18.5	116	28.9	212	20.8	9	22.5	671	24.6
1,000–2,000	150	14.0	25	12.5	36	9.0	88	8.6	9	22.5	308	11.3
2,000–10,000	66	6.2	13	6.5	17	4.2	60	5.9	5	12.5	161	5.9
10,000–100,000	14	1.3	4	2.0	2	.5	17	1.7	0	0	37	1.3
Total	1,072	100	200	100	401	100	1,018	100	40	100	2,731	100

the Wasatch Mountains from the northeast shore of Great Salt Lake southward to Utah Lake (fig. 2).

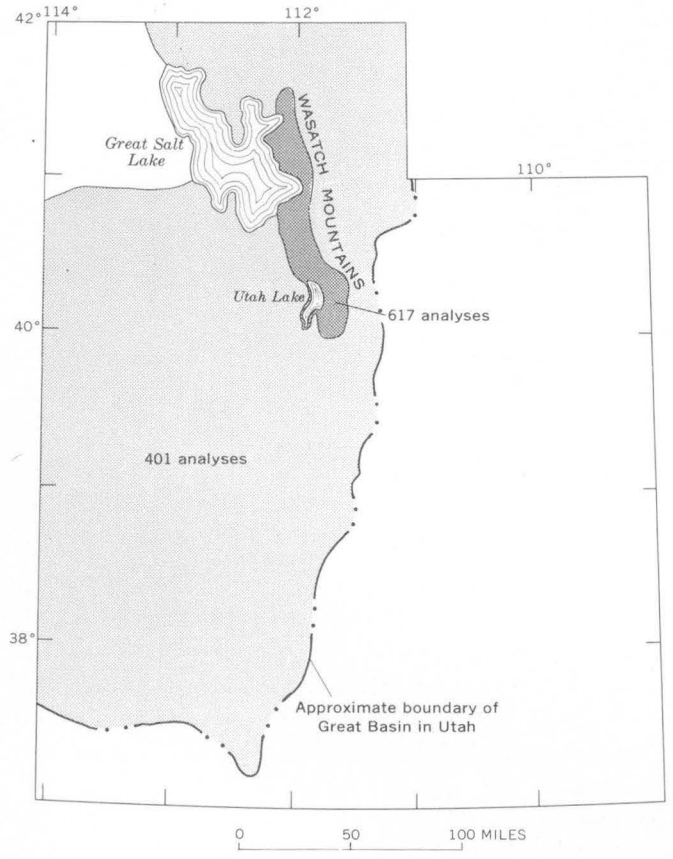

FIGURE 2.—Map showing the area along the west base of the Wasatch Mountains (heavy shading), and other areas in Utah (light shading), for which data on ground-water quality are available.

Runoff from the Wasatch Mountains is a source of abundant recharge, and the mineral content of the water is low. As might be expected, a larger percentage of ground-water samples from this part of Utah falls in the "less-than-500-ppm" range than from other areas in the State. Figure 3 shows graphically the proportions of the ground-water samples from the area at the west base of the Wasatch Mountains, from other areas in Utah, and from the State as a whole that fall within different ranges of dissolved-solids concentration. The maximum difference between the percentages in a single concentration range is 10.5 percent. Inasmuch as the maldistribution of samples from Utah presents the maximum opportunity for bias among the presently considered data, it is likely that the percentage values shown in table 1 are reasonably representative of actual conditions throughout those areas in the Great Basin for which water-quality data are available.

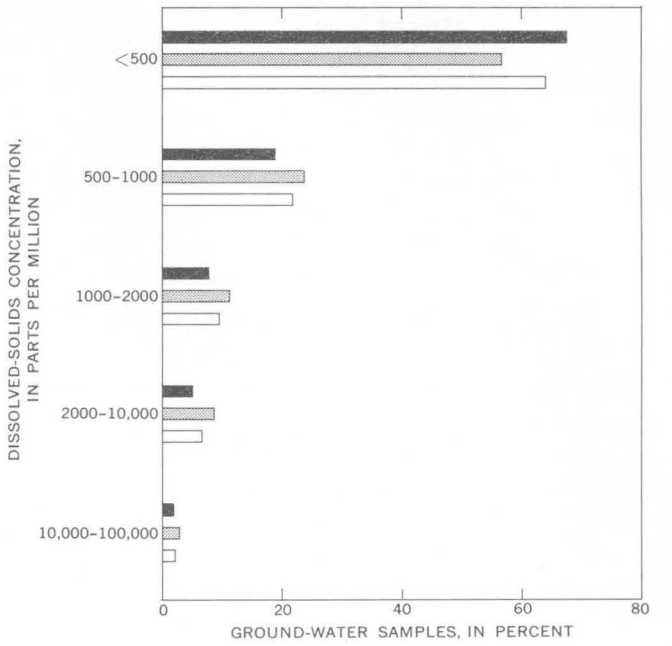

FIGURE 3.—Percentage distribution of ground-water samples from Utah in selected ranges of dissolved-solids concentration. Upper bar, area along west base of Wasatch Mountains (617 analyses); middle bar, other areas (401 analyses); lower bar, State total (1,018 analyses).

NEED FOR DESALINATION IN THE GREAT BASIN

Although the chemical quality of the ground water is surprisingly good, considered on a regional basis, desalination of moderately to highly mineralized ground water locally may play a large part in the future economy of the Great Basin. In those areas within the Great Basin where all the developed supplies of water contain more than 500 ppm of dissolved solids, and in those other areas where no potable water can be obtained, desalination may prove to be the remedy for present water-supply problems.

In much of the Great Basin the average annual recharge is less than the amount of water currently being pumped per year. In such areas the ground water used is obtained largely from nonrenewable storage, and that use is causing a decline in water levels. As this ground-water depletion continues, the hydraulic gradient will steepen, and eventually water of higher mineral content may be drawn into the potable-water aquifers in some basins. Elsewhere, supplies of potable water may approach exhaustion or their levels may be drawn down to below economic limits of pumping lift. It is likely that where saline ground water could be produced in large quantities, desalination or the importation of fresh water will become necessary if the local economy is to endure. Obviously, the relative rates and location of pumping, the amount of salvable discharge, and volumes of

potable ground water in storage will control the time when new sources of supply will become necessary in each individual basin. Meanwhile, further exploration of ground-water quality may disclose additional basins where even now potable water cannot be produced. So, locally, there may be an early demand for desalination; for the Great Basin as a whole, however, the demand seems to be some distance in the future.

RENEWABLE AND NONRENEWABLE GROUND-WATER SUPPLIES

The degree to which the ground-water resources in the valleys of the Great Basin are renewable obviously differs widely from place to place and is not easily determined. Ground-water basins adjacent to mountains that receive 30 inches or more of precipitation yearly are recharged with water of good quality in fairly copious amounts. For example, gaging-station records for the Mojave River in the period 1931–60 (U.S. Geological Survey, 1960, p. 274–279; 1963, p, 192–194), near the headwaters of the stream and at Victorville, Calif., 20 miles downstream, show an average loss in the reach between those stations of about 10,000 acre-feet per year. Even when allowance is made for losses by evapotranspiration this still leaves a residual amount of water, considerably larger than 5,000 acre-feet per year, that presumably recharges the aquifers of the upper Mojave River Valley. That recharge is reflected by the fact that in the upper Mojave River Valley, 29 wells of the 75 sampled yield water with less than 10 ppm of chloride, and by the generally low concentrations of dissolved solids in water from wells near the river. Similarly, where recharge from the Wasatch Mountains in Utah is large, 80 of 617 samples had chloride concentrations of less than 10 ppm. At those places the low chloride content of the ground water is evidence that the ground-water supply is being renewed.

Some other sources of low-chloride water are less obvious. For example, 6 of 28 samples from the Amargosa Desert, an area of very low precipitation on the border between Nevada and California, had less than 10 ppm of chloride. The overall distribution of water samples with low chloride content in the Great Basin is shown in table 2.

Eakin (1966) has summarized evidence for deep circulation of ground water in a regional carbonate-rock aquifer system that extends beneath several surface drainage basins in southeastern Nevada, and Walker and Eakin (1963, p. 15, 20–21) inferred that much of the recharge to aquifers underlying the Amargosa Desert is derived by water movement from

TABLE 2.—*Areal distribution of water samples having <10 ppm of chloride*

Area	Number of samples	Samples with <10 ppm of chloride	
		Number	Percentage
Mojave Desert region	1, 072	82	7. 6
Oregon and northern California	200	64	32
Nevada	401	64	16
Utah	1, 018	158	15. 5
Idaho	40	None	0
Total	2, 731	368	13. 3

beyond the desert boundaries through the interbasin aquifer system. Some occurrences of low-chloride water in basins where recharge from surface sources within the basin are negligible may be explained by transbasin ground-water percolation such as Eakin describes.

In other areas where low-chloride ground water occurs in the absence of obvious sources of recharge it is likely that water being pumped today originated as recharge during pluvial stages of the Pleistocene and, therefore, that the supply is not renewable. When the supply of fresh water is exhausted in such areas, unpotable water, if present, may have to be desalinized to make it suitable for use. A corollary of the concept that some of the ground water currently being used was derived from recharge during the Pleistocene Epoch is that long contact with aquifer minerals does not necessarily lead to large concentrations of dissolved-solids in the water.

OCCURRENCE OF BRINES

Concentrated brines are processed for their content of commercially useful minerals at 6 places at the present time; at 14 other places brines have been processed in the past (fig. 1). Brines pumped from wells for mineral production contain as much as 325,000 ppm of dissolved solids. The brines typically underlie playas or salt-crusted marshes in the lowest—commonly nearly central—parts of the basins in which they occur. Snyder (1962) classified several of the varied hydrologic systems present in the Great Basin, and Stone (1956) described various types of playas, including those like Searles Lake, Calif., which are occupied by bodies of crystalline salines. Most concentrated brines occur at shallow depth, and scanty data suggest that beneath at least some playas dissolved-solids concentrations decrease progressively with increasing depth. The available evidence indicates that potable water also occurs in virtually all basins where brines are known to occur, except the basin of Searles Lake (G. I. Smith,

oral commun., 1965), and perhaps that in Clayton Valley, Nev. (Dole, 1913, p. 331–332). The degree of lateral and vertical interconnection between brine aquifers and potable-water aquifers remains, however, virtually unexplored.

NEED FOR ADDITIONAL HYDROLOGIC STUDIES

Much more needs to be known regarding the hydrology of the Great Basin as a whole before the full potential of the region for water-resource development can be evaluated accurately. The rapid growth of population in the basin since World War II has made increasing demands upon available water. Development of light industry, recreation, and agriculture is continuing.

Evaluation of the renewable supplies should include determination not only of volumes of water withdrawn, but also of the fraction that is not consumptively used but is returned to the aquifers. Changes in chemical quality that result from use and reuse of the water also should be determined. The rates at which the freshwater and saline-water aquifers are replenished naturally need to be known, and possible means for augmenting the rates of replenishment should be explored. There is virtually no information on volumes of saline water available for development. The lateral and vertical relations between fresh and saline water in desert basins require study for the optimum utilization of fresh-water aquifers.

REFERENCES

Dole, R. B., 1913, Exploration of salines in Silver Peak Marsh, Nevada, *in* Contributions to economic geology, Salines: U.S. Geol. Survey Bull, 530, p. 330–345.

Eakin, T. E., in press, A regional interbasin ground-water system in the White River area, southeastern Nevada: Water Resources Research, v. 2, no. 2, p. 251–271.

Feth, J. H. and others, 1965, Preliminary map of the conterminous United States showing depth to and quality of shallowest ground water containing more than 1,000 parts per million dissolved solids: U.S. Geol. Survey Hydrol. Inv. Atlas HA–199.

Snyder, C. T., 1962, A hydrologic classification of valleys in the Great Basin, Western United States: Internat. Assoc. Sci. Hydrology, VII^{e} Annee, no. 3, p. 53–59.

Snyder, C. T., Hardman, George, and Zdenek, F. F., 1964, Pleistocene lakes in the Great Basin: U.S. Geol. Survey Misc. Geol. Inv. Map I–416.

Stone, R. O., 1956, A geologic investigation of playa lakes: Univ. Southern California, unpub. PhD. thesis, 302 p.

U.S. Geological Survey, 1960, Compilation of records of surface waters of the United States through September 1950; pt. 10, the Great Basin: U.S. Geol. Survey Water-Supply Paper 1314, 485 p.

——— 1963, Compilation of records of surface waters of the United States, October 1950 to September 1960; pt. 10, the Great Basin: U.S. Geol. Survey Water-Supply Paper 1734, 318 p., [1964].

U.S. Public Health Service, 1962, Public Health Service drinking water standards: Public Health Service Pub. 956, 61 p.

Walker, G. E., and Eakin, T. E., 1963, Geology and ground water of Amargosa Desert, Nevada-California: Nevada Dept. Conserv. Nat. Resources, Ground-water Resources, Reconn. Ser. Rept. 14, 45 p.

THE WINTER PHYTOPLANKTON, AND PHYSICAL AND CHEMICAL CHARACTERISTICS OF PRETTY LAKE, INDIANA

By ROBERT G. LIPSCOMB, Fort Wayne, Ind.

Abstract.—Wintertime data from a small lake show that after ice formed on the surface a distinct phytoplankton population developed and declined at a depth of water that suggests heterotrophy. Diatom species of the Bacillariophyceae were the dominant phytoplankton. During the peak concentration of cells *Cyclotella bodanica* Eulenstein predominated. The temperature of the lake increased by a few degrees during the ice-cover period, and the peak algal concentration was coincident with the maximum water temperature at a depth of 40 feet. Except for silica, nitrate, and pH, chemical data did not correlate with fluctuations in the phytoplankton population. By late season, quality of the deep water had been affected by winter stagnation; dissolved oxygen became deficient, pH decreased, and the decay product H_2S (hydrogen sulfide) became readily detectable.

Most standing bodies of water in the middle latitudes undergo complete mixing (overturn) in the fall. Lipscomb (1966) described some of the botanical, physical, and chemical characteristics of this phenomenon for Pretty Lake, Lagrange County, Ind. In that study it was shown that by late fall the water temperature and the concentration of dissolved oxygen were isometric in a column of water near the center of the lake, and that the phytoplankton population not only was fairly uniformly distributed throughout the column but also exhibited an appreciable increase in density that was approximately 80 percent dominated by a few species of diatoms (Bacillariophyceae).

Welch (1952, p. 259) discussed some possible causes for this kind of phytoplankton increase, such as complete aeration or at least greater aeration, and the release and circulation of decomposition products from the bottom. He concluded that overturn conditions apparently develop optimum conditions to which the diatoms respond vigorously, often becoming the chief primary producers during these times.

The formation of ice marks the beginning of another interesting phase in the annual cycle of bodies of water. Wind-induced circulation, water evaporation, and the free exchange of gases with the atmosphere do not occur under a cover of ice. The penetration of light into the water is affected largely by the quality and thickness of the ice and, to a lesser degree, by the extent of snow cover on the surface.

Ice began to form on Pretty Lake in mid-December, and an attempt to study some of the phytoplankton dynamics within the lake was initiated on December 27, when conditions were first reasonably safe to work on the ice. All data in this report pertain to a vertical column of water near the center of the lake, and all depths of water recorded for the ice period were measured from the water surface within a hole in the ice. The maximum depth of the lake is 82 feet.

THERMAL PATTERN

The first data show a downward trend in the average water temperature from the overturn conditions of December 13 (fig. 1). By January 7, however, the colder upper layer of water was beginning to warm, under the influence of increased insolation and an insulating ice cover.

Pure water has its greatest density at 4°C. This anomalous characteristic means that water warming to 4°C will sink and displace colder, less dense water beneath, producing circulation. Deep circulation doubtlessly was reduced as the water temperature in the column approached 4°C, and particularly as the water temperature between depths of about 5 and 20 feet (see curves for 2–14–64 and 3–6–64, fig. 1) rose above 4°C owing to late-season warming. The break in the water-temperature curve at a depth of about 40 feet (see curves for 2–14–64 and 3–6–64, fig. 1) rose a zone of water with a temperature slightly less than 4°C which had its lower limit near the bottom of the lake. This layer sandwiched between zones of slightly warmer water, which persisted until breakup of the

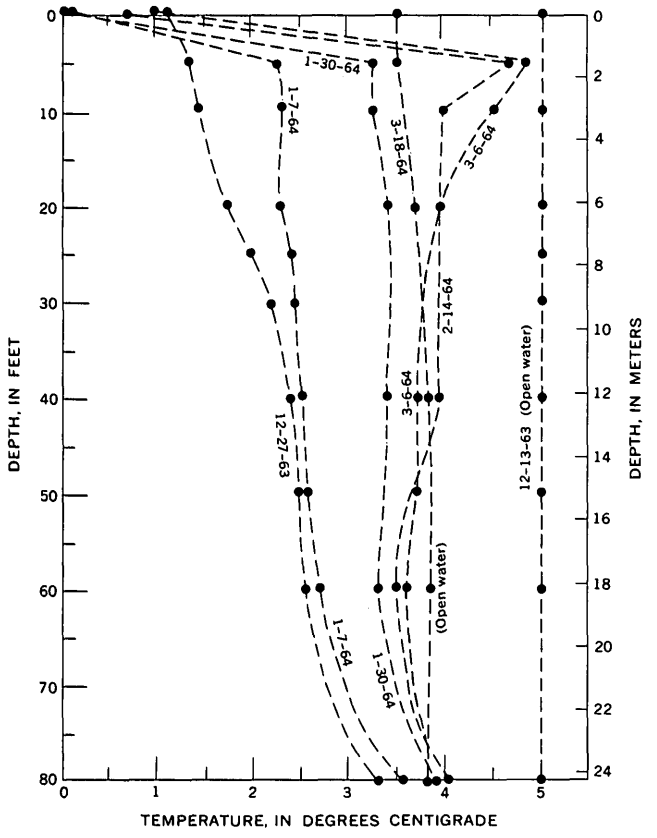

FIGURE 1.—Temperature profiles in the center of Pretty Lake, winter 1963–64.

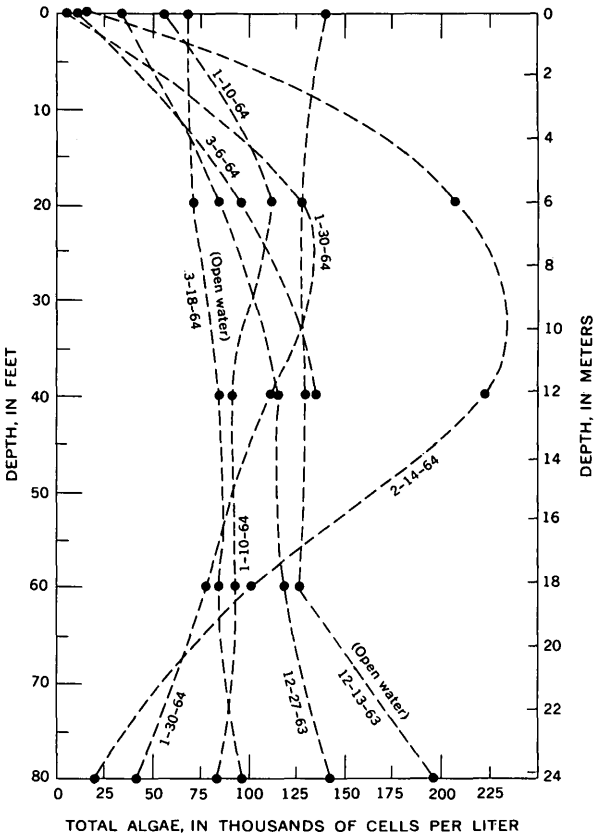

FIGURE 2.—Distribution of phytoplankton with depth at the center of Pretty Lake, winter 1963–64.

ice, probably resulted from the simultaneous increase in density, diffusion of solutes from the bottom sediments, and conduction of heat into the thin layer of bottom water (Hutchinson, 1957, p. 454).

THE PHYTOPLANKTON

Distribution

By January 10 the increasing insolation appeared to influence the phytoplankton population, which had declined from its concentration of December 13, early in the ice-cover period. Beginning at a depth of about 20 feet (curve 1-10-64, fig. 2) the concentration of cells had begun to increase, and by February 14 it reached an estimated maximum of at least 230,000 cells per liter at a depth between 35 to 40 feet. However, it seems inconceivable that an algal peak developed at this depth range, using light as a source of energy, even assuming a low-intensity requirement. Although it has been shown that light transmission through clear ice may be 96 percent of that for lake water, the presence of air bubbles in the ice greatly reduces light transmission. Moreover, light transmission may be totally obstructed by snow cover (Ruttner, 1963, p. 23). Bubble-free ice did not exist on Pretty Lake, and a partial to complete snow cover was present throughout most of the study period, especially near the end, so that the transmission of light sufficient to account for the development of the observed algal peak hardly seems plausible.

Development of the concentration of cells without light, at the depth shown in figure 2, would require another source of energy for metabolism. The cells may have changed from autotrophism (self-nourishing) to heterotrophism (nourishing from others), a kind of change Rodhe (1955) has attributed to the productivity in the "microalgae" in subarctic lakes during conditions of heavy ice cover and weak light. It is suspected, however, that had the number of samples been greater near the surface of the lake, the algal peak probably would be seen to have developed much higher, in the region of greater light intensity. In that case the data presented here would suggest that cells settled out from the shallower, better-lighted water.

Diatoms predominated in the samples. Many of the dead cells were devoid of contents. The appearance of such cells at some level in the water marked the

beginning of the deterioration of the algal peak there. As one would expect, however, the number of these cells observed was significantly less than the number of dead cells near the bottom of the lake following the development of the algal peak subsequent to the previous fall overturn (profile 12-13-63, fig. 2).

Phytoplankton population-density declined toward the end of the period of ice cover, either under the influence of light deficiency due to greater thickness (approximately 1.6 feet) or low transparency of ice, or because of a deficiency in an organic source of energy. The observed peak population, nevertheless, was simultaneous with the maximum water temperature at a depth of 40 feet during the period of ice cover.

Dominant forms

Of the four classes of algae represented in the phytoplankton, the diatoms predominated by a sizable and uniform margin (table 1). The diatoms (Bacillariophyceae) also predominated in the late fall, subsequent to the overturn (Lipscomb, 1966). Although the dominant species in both maximums were *Asterionella formosa* Hassell, *Fragilaria crotonensis* Kitton, *Cyclotella bodanica* Eulenstein, and *Melosira ambigua* (Grunow) Müeller,[1] their percentage concentrations differed as shown in table 2. Only *C. bodanica* increased in percentage concentration as the phytoplankton population developed to its maximum.

TABLE 1.—*Percentage concentration of dominant algal classes for all depths at the center of Pretty Lake, winter 1963–64.*

Classes of algae	Date					
	Dec. 27	Jan. 10	Jan. 30	Feb. 14	Mar. 6	Mar. 18
Myxophyceae	7	7	8	9	13	10
Chlorophyceae	2	2	1	----	----	----
Bacillariophyceae (diatoms)	88	89	87	81	85	87
Chrysophyceae	----	----	2	6	----	----
Others	3	2	2	4	2	3

The Myxophyceae (table 1) were represented by nearly equal concentrations of *Oscillatoria* sp. and *Aphanizomenon holsaticum* Richter (Drouet, 1959, p. 102 and 112), which increased slowly to represent about 13 percent of the total algae present prior to ice breakup. Of the remaining classes of algae (table 1), the Chlorophyceae (green algae) and the Chrysophyceae (golden-brown algae), the very small concentration of a few representative forms emphasizes their intolerance of the winter environment.

[1] Drs. Chas. W. Reimer and Ruth Patrick, Philadelphia Academy of Science, Philadelphia, Pa., identified the diatoms *Asterionella formosa* Hassell and *Melosira ambigua* (Grunow) Müeller, and verified the identification of other diatoms reported in this study.

TABLE 2.—*Percentage concentration of dominant diatom species from all depths at the center of Pretty Lake, winter 1963–64.*

Species of diatoms	Date						
	Dec. 13	Dec. 27	Jan. 10	Jan. 30	Feb. 14	Mar. 6	Mar. 18
Asterionella formosa [1]	29	23	23	18	3	----	----
Fragilaria crotonensis [1]	26	28	18	10	20	6	4
Cyclotella bodanica	18	25	32	55	54	75	72
Melosira ambigua [1]	9	7	8	4	3	2	1
Others	18	17	19	13	20	17	23

[1] Colonial forms; each colony is equated with a single cell of a noncolonial form in determination of concentration.

CHEMICAL PROPERTIES

Oxygen

Dissolved oxygen is probably the most frequently used indicator of biological activity in limnological studies. It is a byproduct of photo-synthesis, and any increase in its concentration within an ice-covered lake is attributable to winter phytoplankton productivity. The ice cover on Pretty Lake was continuous during the study period, and as a result the dissolved-oxygen distribution throughout the column (profile 1-30-64, fig. 3*A*) was typical of dimictic (circulating twice annually) lakes as described by Hutchison (1957, p. 627). Thus, winter stagnation, or the development of oxygen-free water at great depths due to biological and chemical oxidation of bottom sediments, which imports a readily detectable odor of H_2S (hydrogen sulfide), occurred during the last half of January. At most depths the concentration of dissolved oxygen progressively decreased until ice breakup. However, there was an increase near the surface (profile 3-6-64, fig. 3*A*) which is clearly correlated with the late-season warming (profile 3-6-64, fig. 1). Unfortunately, phytoplakton data are not available to explain this dissolved-oxygen increase more fully. In terms of percentage saturation the distribution of dissolved oxygen appeared as shown in figure 3*B*.

pH

The pH of natural water is closely associated with CO_2 (carbon dioxide) concentration. The uptake and release of CO_2 in plant and animal metabolism upset the equilibrium in the water, and if it were not for the presence of buffering mixtures of weak acids and their salts, such as H_2CO_3 (carbonic acid) and $Ca(HCO_3)_2$ (calcium bicarbonate), major and rapid fluctuations in pH would result (Ruttner, 1963, p. 61-72). It is important to living systems that such fluctuations do not occur.

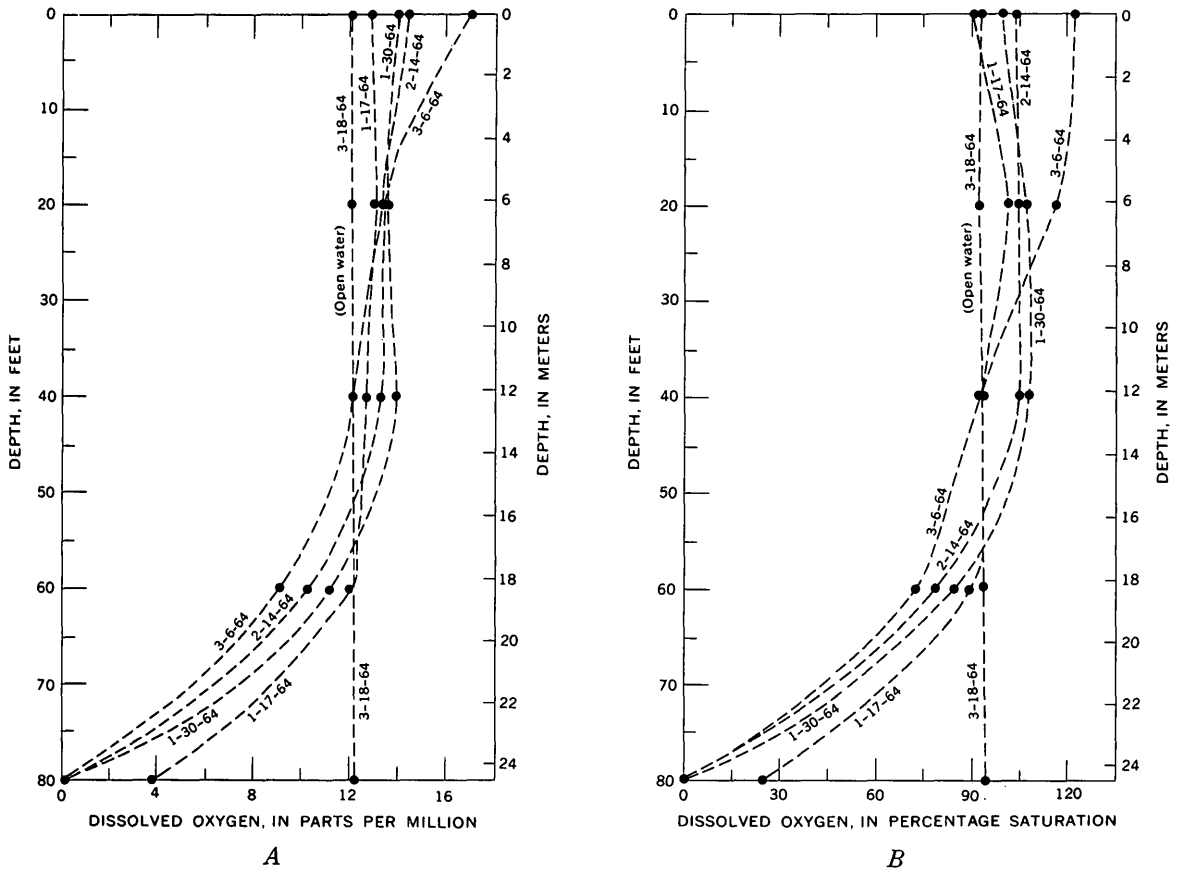

FIGURE 3.—Vertical profiles of dissolved-oxygen concentrations and percentage saturation at the center of Pretty Lake, winter 1963–64.

An inverse relation between the concentration of CO_2 and pH is illustrated by the slight increase in pH (fig. 4) during the development of the phytoplankton peak (see curve for 2-14-64, fig. 2), at a time when CO_2 would have been assimilated. Near the bottom of the lake the pH decreased progressively throughout the ice period owing to biological and chemical evolution of CO_2 (see following section). Near the surface of the lake, pH increased (that is, CO_2 decreased) during the late-season warming. These changes attributed to increase in water temperature, may also have been due in part to dilution by melting ice or to photosynthetic activity of the phytoplankton.

Calcium (total hardness and alkalinity)

The water in Pretty Lake is well buffered. The total hardness of the water, expressed as parts per million of $CaCO_3$ (calcium carbonate) (fig. 5), is believed to be due largely to the presence of $Ca(HCO_3)_2$, which with $CaCO_3$ and H_2CO_3 make up the principal buffering mixtures in Pretty Lake.

Ruttner (1963, p. 62) states that a certain surplus supply of CO_2 must remain in solution in water for $Ca(HCO_3)_2$ to be stable, and that if this equilibrium CO_2 is lost (as by CO_2 uptake in photosynthesis, or by loss of CO_2 to the atmosphere), $Ca(HCO_3)_2$ is precipitated as $CaCO_3$ and free CO_2 is released in solution to bring about a new equilibrium. Within an ice-covered lake this kind of reaction causes the deeper water to be relatively hard, and to become harder as the season progresses (fig. 5). The concentration of calcium (fig. 6) and the alkalinity (fig. 7) increase in the deep water, which has low pH, as $Ca(HCO_3)_2$ dissociates into Ca^{+2} (calcium ion) and HCO_3^{-1} (bicarbonate ion), and HCO_3^{-1} further dissociates into H^{+1} (hydrogen ion) and CO_3^{-2} (carbonate ion) (Hem, 1959, p. 71). The concentration of Ca^{+2} and the hardness decrease at lesser depths, and the pH remains fairly stable, as shown in figures 6, 5, and 4, respectively.

Silica

SiO_2 (silica) is the chief constituent in the frustules (valves) of diatoms, and it can be utilized by these forms even when it is present in the water in low concentrations (Hutchinson, 1957, p. 797). This is particularly true of planktonic species. The data in

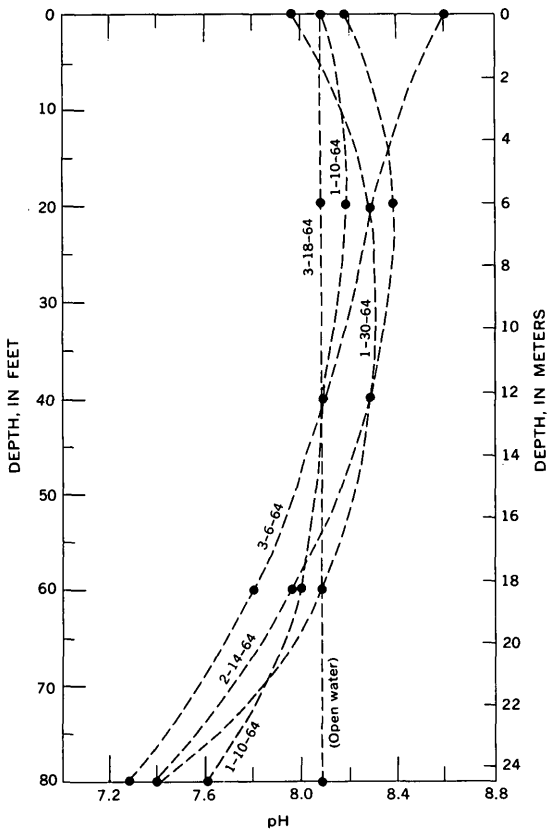

FIGURE 4.—Vertical profiles of pH at the center of Pretty Lake, winter 1963–64.

figure 8 show a decrease in the concentration of SiO_2 in the February 14 samples, coincident with the phytoplankton population peak (which was composed largely of diatoms; see fig. 2, and table 1). The data show also that the concentration of cells at the bottom of the lake decreased concurrently, while the concentration of SiO_2 increased. In addition, much of the diaton material collected was fragmentary. From these data it would seem that the diatom frustules were dissolving as they settled to the bottom of the lake. It has long been claimed by many workers that diatoms are extremely resistant to chemical breakdown in water. Large deposits of diatomaceous earth (mostly marine deposits) are known in many parts of the world to attest these claims. Welch (1952, p. 200) states that according to Conger (1941) the available evidence indicates that SiO_2 deposition by diatoms is a one-way process. Sverdrup and others (1942, p. 262) state an opposing view, that silicon removed from sea water by diatoms may return to solution after they die and that the high silicon content commonly found near the bottom is due to resolution of the settled siliceous shells. More recently Ruttner (1963, p. 93) asserted that a rise in the silicate content in the hypolimnion after a diatom maximum of late summer and autumn is noteworthy, for it indicates that silicates are released from the sediments. It is assumed that in this regard the result would be no different following a winter diatom maximum. The silicon cycle in nature is complex, and it is probable that under certain conditions each of these processes occurs.

Phosphate

Of all the elements in nature, phosphorus is most frequently thought to be one which limits life. Compounds containing phosphorus are particularly important in energy-transformation reactions, but phosphorus is usually present in natural waters in such small amounts in relation to its concentration in cells that the needs of many life forms (living systems) are not met. On the other hand, in some natural waters phosphorus is relatively abundant, and there it can act as a fertilizer for growth in the living community.

In this study the concentration of total phosphorus in the water is expressed as phosphate (fig. 9). There was little relative change in the upper levels

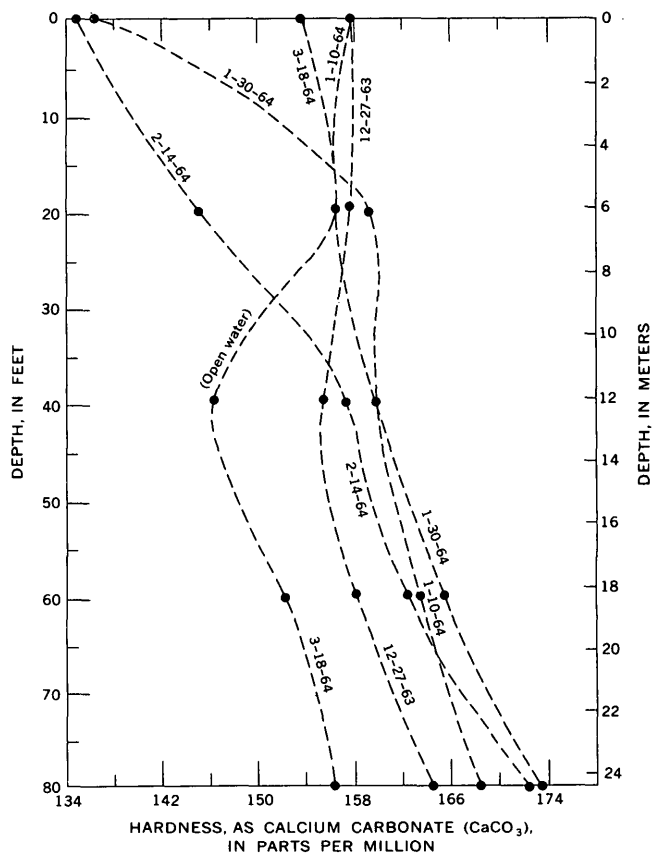

FIGURE 5.—Vertical profiles of hardness, expressed as concentration of $CaCO_3$, at the center of Pretty Lake, winter 1963–64.

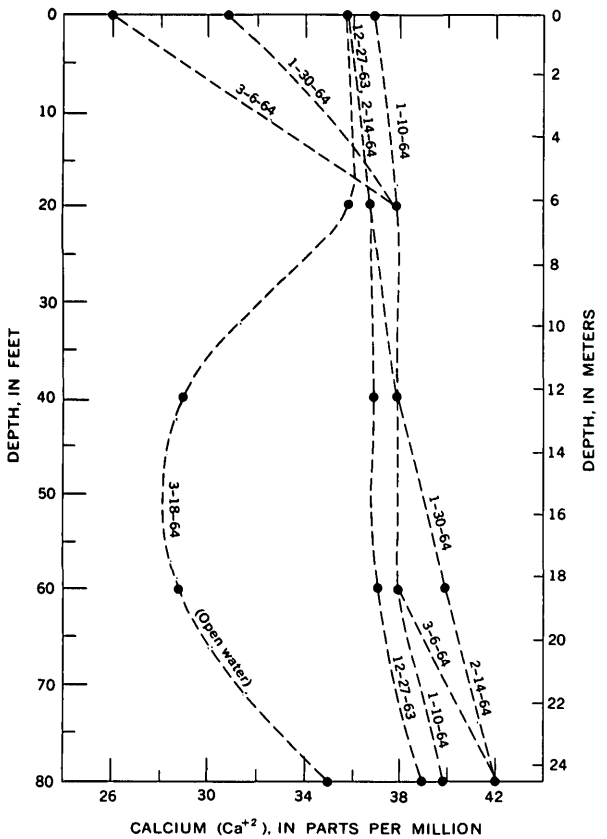

FIGURE 6.—Vertical profiles of calcium concentration at the center of Pretty Lake, winter 1963–64.

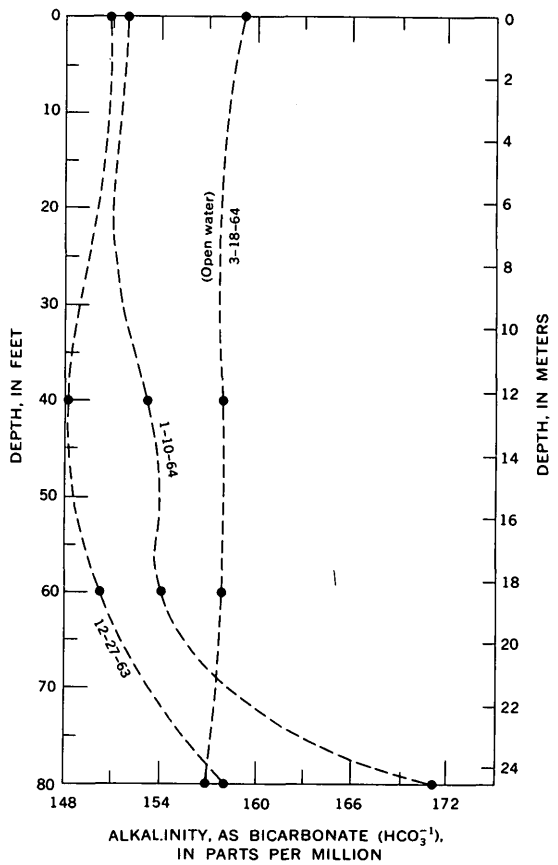

FIGURE 7.—Vertical profiles of alkalinity, expressed as concentration of HCO_3^{-1}, at the center of Pretty Lake, winter 1963–64.

of the lake during the ice period. The largest change occurred at greater depths as stagnation developed, and probably represented releases of phosphorous bound up in settling particulate matter (such as dissolving protoplasm in diatom cells) and phosphate ions from the mud surface at the bottom (Hutchinson, 1957, p. 735–737).

Nitrate

Nitrogen is an important constituent of proteins, which in turn are integral parts of the living substance protoplasm. N_2 (atmospheric nitrogen) is physiologically unavailable to most green plants, but plays an important role in energy transformation for nitrifying or nitrogen-fixing bacteria and certain blue-green algae. NH_3 (ammonia), NO_2^{-1} (nitrite), and NO_3^{-1} (nitrate) are products of nitrification and are natural sources of nitrogen for the chlorophyll-bearing plants, which include most of the algae. Conversely, the denitrifying bacteria reduce compounds of nitrogen: NO_3^{-1} is reduced to NO_2^{-1}, then (rarely to N_2) to NH_3. Through man's influence inorganic nitrate fertilizers and sewage wastes have become additional sources of NO_3^{-1}. Nitrate nitrogen is the principal form of inorganic nitrogen in natural waters.

Owing to uncertainties surrounding the sources of NO_3^{-1} and its methods of determination, it has been difficult to correlate NO_3^{-1} utilization with algal populations in limnological studies. The values presented in figure 10 probably are high as a result of NO_2^{-1} interference, which was not taken into consideration early in the course of chemical analyses of water in the Pretty Lake project. Taras (1950) states that in water with greater than 0.2 ppm of NO_2^{-1}, analyses will produce high NO_3^{-1} results that are erratic and unreproducible. After the analyses shown in figure 10 had been made, it was found that the NO_2^{-1} concentration in the water in Pretty Lake, and especially in the deep water, far exceeds this limitation; thus the concentration of NO_2^{-1} may have interfered with the NO_3^{-1} analyses. Because accuracy of determination of NO_3^{-1} is believed to be to the nearest tenth of a part per million (Hem, 1959, p. 116), analytical error in NO_3^{-1} analyses should be insignificant apart from the NO_2^{-1} interference. In view of these circumstances, only a

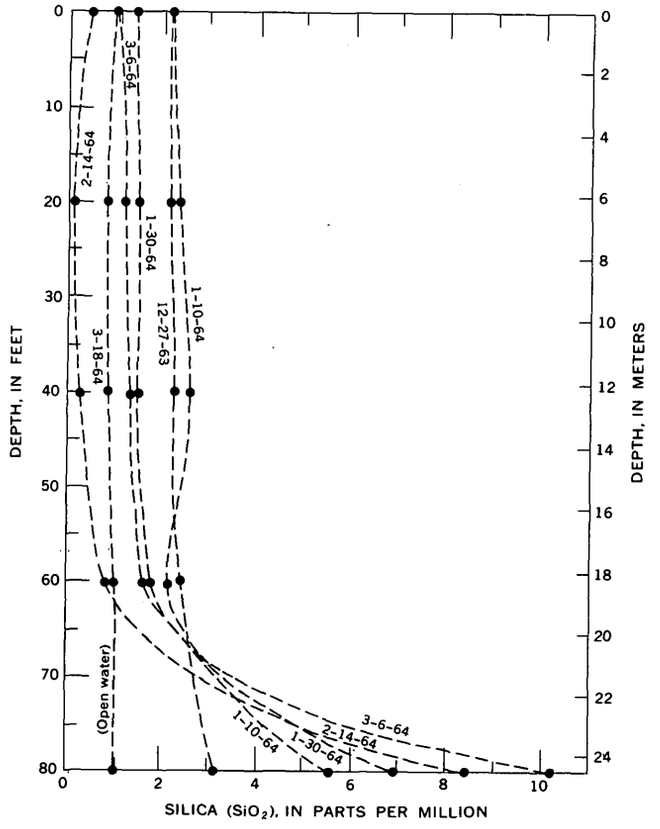

FIGURE 8.—Vertical profiles of SiO_2 (silica) concentration at the center of Pretty Lake, winter 1963–64.

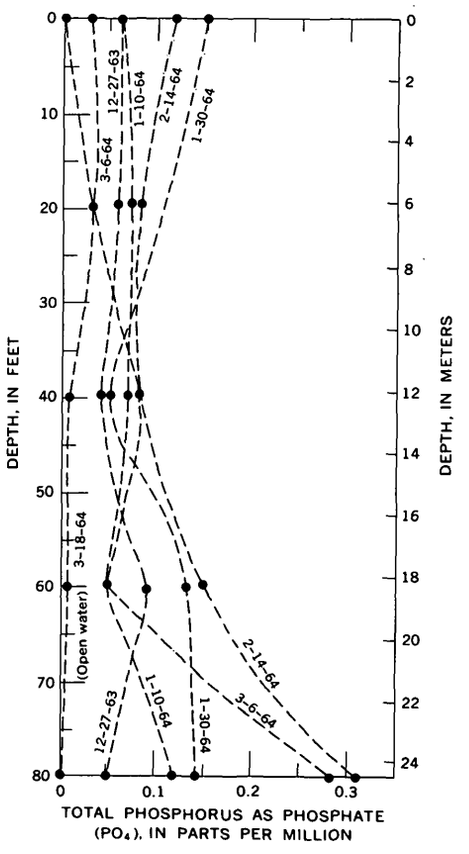

FIGURE 9.—Vertical profiles of total phosphorus, expressed as concentration of phosphate, at the center of Pretty Lake, winter 1963–64.

limited interpretation of the data presented in figure 10 will be attempted.

Early in the period when the lake was covered with ice (profile 12-27-63, fig. 10) the maximum concentration of NO_3^{-1} was found at a depth of about 40 feet, where the phytoplankton population (profile 12–27–63, fig. 2) was less than it had been at the fall overturn (profile 12–13–63, fig. 2). The lesser concentration of NO_3^{-1} at the top and at the bottom of the lake probably represents utilization by phytoplankton and by denitrifying bacteria, respectively.

By January 30, NO_3^{-1} was not detectable at or below the depth of the early maximum, while above this depth it had increased appreciably. These data are suspect if, as discussed earlier, the algal population peak developed high in the lake (see section on phytoplankton, first paragraph), for an increase in the concentration of NO_3^{-1} with diminishing depth early in the peak development would be inconsistent with increasing utilization by the algae. And, although a reduction in the concentration of NO_3^{-1} would be expected in the beginning, the deficiency shown at 40 feet can hardly explain the observed increase in the algal population concentration later at that depth. At the observed peak concentration of phytoplankton (2-14-64, fig. 2), however, NO_3^{-1} was detectable again. This was perhaps due to a stationary or beginning death phase of the algal population in which NO_3^{-1} utilization would be significantly reduced or nonexistent. A NO_3^{-1} deficiency now existed from about 60 feet to the bottom of the lake. By March 6, the concentration of phytoplankton was considerably less at 40 feet, and there had been an appreciable increase in the concentration of NO_3^{-1}.

SPRING OVERTURN

Lakes in the middle latitudes which overturn in the fall usually overturn in the spring as well. Many of these lakes are ice covered during the winter. When such lakes become ice free again in the spring they often overturn very quickly.

The ice breakup in Pretty Lake began with the melting of shore ice under relatively calm conditions. A period of warm weather preceded a brisk wind which

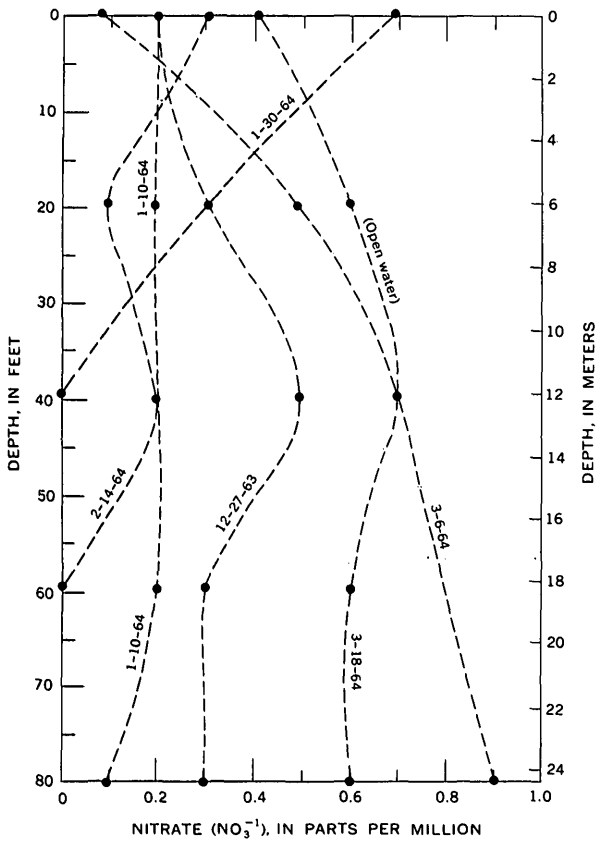

FIGURE 10.—Vertical profiles of nitrate (NO_3^{-1}) concentration at the center of Pretty Lake, winter 1963–64.

finally removed the ice on March 17. When approximately 200 feet of water was exposed around most of the lake, wind and waves obliterated the remaining ice float in about 24 hours.

On the following day, March 18, the water temperature of the newly exposed lake was almost 4° C (fig. 1), and vertical mixing was rapidly nearing completion. That spring overturn had already occurred is vividly illustrated in the isometry of most of the water properties. Only hardness (fig. 5) and Ca^{+2} (fig. 6) show stratification beginning at a depth of about 20 feet. Below this depth, dissolving carbonate minerals from the bottom probably had not yet had sufficient time to come into equilibrium with CO_2 in the circulating waters of the newly opened lake.

SUMMARY

This study shows some of the characteristics of winter phytoplankton dynamics in a deep body of fresh water in the middle latitudes. Species of diatoms were the dominant phytoplankton, and under a complete cover of ice the observed population concentration increased significantly at a depth of water which suggests heterotrophy. The population peak was coincident with the maximum water temperature at that depth late in the ice-cover period; the temperature of the water was a couple of degrees centigrade warmer than at the beginning of the period. The study has shown Pretty Lake to be an example of a dimictic lake in which winter stagnation developed late in the season. In the deep water, H_2S replaced dissolved oxygen, and the pH decreased. The development of this temporary stagnation is an important process which affects water quality in deep lakes and reservoirs when the presence of a continuous ice cover of sufficient duration results in anaerobic conditions in the bottom water. The characteristics of phytoplankton dynamics, and physical and chemical characteristics, will differ from one lake or reservoir to another, of course, depending on individual basin morphology, the weather, and many other factors.

REFERENCES

Conger, P. S., 1941, Fixation of silica by diatoms, *in* A symposium on hydrology: Madison, Wis., Univ. Wisconsin Press, p. 395–396.

Drouet, Francis, 1959 Myxophyceae, *in* Ward, H. B., and Whipple, G. C. (Edmondson, W. T., ed.) Fresh-water biology: New York, John Wiley & Sons, Inc., p. 95–114.

Hem, J. D., 1959, Study and interpretation of the chemical characteristics of natural water: U.S. Geol. Survey Water-Supply Paper 1473, 269 p.

Hutchinson, G. E., 1957, A treatise on limnology, v. 1: New York, John Wiley & Sons, Inc., 1015 p.

Lipscomb, R. G., 1966, Botanical and chemical characteristics during the fall overturn of a small eutrophic lake, Pretty Lake, Indiana, *in* Geological Survey Research, 1966: U.S. Geol. Survey Prof. Paper 550–B, p. B204–B208.

Rodhe, W., 1955, Can plankton production proceed during winter darkness in sub-arctic lakes? Internat. Ver. Limnol. Verh. Vol. 12, p. 117–122.

Ruttner, Franz, 1963, Fundamentals of limnology, 3d ed.: Toronto, University of Toronto Press, 295 p.

Sverdrup, H. U., and others, 1942, The oceans, their physics, chemistry and general biology: New York, Prentice-Hall, Inc., 1087 p.

Taras, M. J., 1950, Phenodisulfonic acid method for determining nitrate in water: Anal. Chemistry, v. 22, p. 1020–1022.

Welch, P. S., 1952, Limnology, 2d ed.: New York, McGraw-Hill, Inc., 538 p.

DISTRIBUTION OF RADIOACTIVITY IN THE ALLUVIUM OF A DISPOSAL AREA AT LOS ALAMOS, NEW MEXICO

By WILLIAM D. PURTYMUN, GEORGE L. JOHNSON,[1] and EDWARD C. JOHN, Albuquerque, N. Mex.

Work done in cooperation with the U.S. Atomic Energy Commission and the Los Alamos Scientific Laboratory

Abstract.—Fine particles in alluvial material in a disposal area for liquid radioactive wastes at Los Alamos have greater affinity for radionuclides than coarse particles; however, most of the radioactivity is in the coarse material, which is more abundant. The radioactivity in the alluvium is dispersed by waste water and storm runoff and decreases with distance from the point of effluent outfall. Most of the radionuclides are retained in the upper 3 feet of the deposits, resulting in very little change in the quality of the ground water perched in the alluvium.

Liquid industrial wastes produced at the Los Alamos Scientific Laboratory, in north-central New Mexico, contain small but undesirable amounts of radioactivity. These wastes are treated by chemical processes and by ion exchange to reduce the radioactivity to less than 10 percent of the MPC (maximum permissible concentration), as recommended by the International Committee on Radiation Protection, before discharge to a disposal area in Mortandad Canyon, about 2 miles southeast of the community of Los Alamos. The effluent, diluted by waste water and storm runoff, infiltrates a small perched ground-water body in the alluvium (Abrahams and others, 1962). Some radionuclides in the effluent become bound to particles of the alluvium, thereby reducing the amount of radioactive contamination of the perched water.

This report is based on data collected in a preliminary study to determine possible areas of further investigation of transport of radionuclides on sediment. Samples of alluvium were collected from the surface to a depth of 3 feet at the point of effluent outfall and at locations 3,500 feet and 5,800 feet downstream. The samples were air dried and mechanically separated into seven fractions ranging in particle size from silt and clay to granules. The seven fractions were analyzed for gross alpha, gamma, and beta radioactivity and for radioactive strontium. The short duration of counting ($\leqq$ 30 minutes per sample) precludes a quantitative interpretation of the data, but the data are believed to indicate qualitatively the distribution of the radionuclides within the various fractions of the alluvium samples.

PARTICLE-SIZE DISTRIBUTION

The particles constituting the alluvium were derived from weathering of the Bandelier Tuff. The granules are composed principally of tuff and pumice, and contain minor amounts of quartz and sanidine crystals. The fractions from fine to very coarse sand consist mainly of quartz and sanidine crystals and fragments with minor amounts of tuff, pumice, and mafic minerals. The silt and clay fraction is composed mainly of the clay minerals montmorillonite and illite, which are the major end products of weathering of the tuff.

A cumulative curve (fig. 1) of particle-size distribution in the alluvium near the point of effluent outfall from the treatment plant shows that 95 percent of the material, by weight, is in the size range from medium sand to granules, and that 5 percent is in the size range from clay and silt to fine sand. The largest percentage of alluvium, by weight, is very coarse sand, and the smallest percentage is fine sand.

[1] Los Alamos Scientific Laboratory of the University of California.

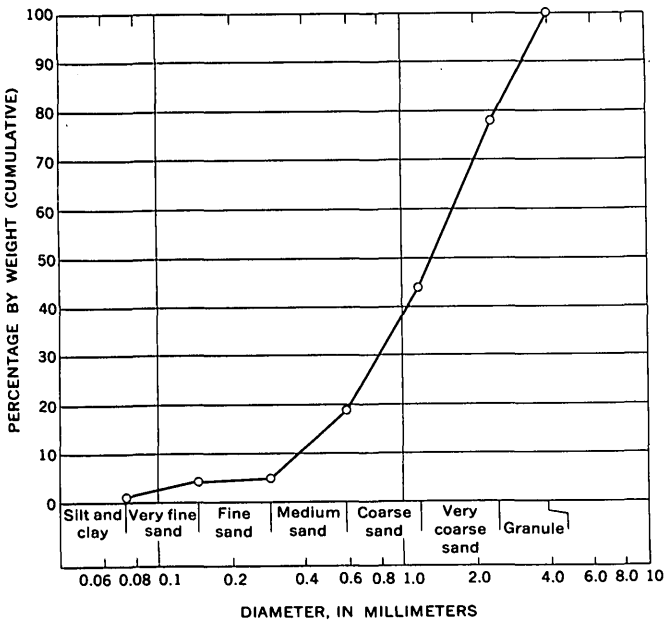

FIGURE 1.—Cumulative curve of particle-size distribution in alluvium near the point of effluent outfall from the waste-treatment plant.

RELATION OF RADIOACTIVITY TO PARTICLE SIZE AND MINERAL COMPOSITION

The distribution of the radioactivity is correlated with both the size and the mineral composition of the particles. On a unit-weight basis more radioactivity was found in the silt and clay, very fine sand, and fine sand than in the coarser fractions (table 1). The largest proportion of the radioactivity was in the silt and clay, and the proportion decreased with increasing particle size. The silt and clay, very fine sand, and fine sand are composed of clay minerals or of materials that are rapidly weathering into clays. The clay minerals montmorillonite and illite, derived from weathering of the tuff, have a relatively high ion-exchange capacity, and adsorb and retain radionuclides from the liquid wastes.

Of the larger particles, the granules have a higher concentration of gross gamma and beta radioactivity, and more radioactive strontium per unit weight than the more siliceous medium, coarse, and very coarse sand particles. This may be due to the fact that granules are primarily tuff and pumice of high microscopic porosity with large surface areas. Since the tuff and pumice are in the process of weathering, the pores contain some clay which tends to bind radionuclides.

DISTRIBUTION OF RADIOACTIVITY IN THE ALLUVIUM

A greater quantity of radionuclides was found in medium sand, coarse sand, very coarse sand, and granules than in the clay and silt, very fine sand, and fine sand. This is shown graphically in figure 2. The range from medium sand to granules makes up 95 percent of the alluvial material and, though the ability of the particles in this size range to bind radionuclides is less than that of the particles in the range from clay and silt to fine sand, the material of medium-sand to granule sizes contains more radioactvity simply because there is more of the coarse material available.

The radioactivity decreases with depth in the alluvium. Gross alpha activity decreases about 70 percent, gross gamma activity about 98 percent, and gross beta activity about 99 percent between the surface and a depth of 3 feet. Nearly all the radioactive strontium is retained within the upper foot of the alluvium.

The radioactivity also decreases with distance from the point of effluent outfall. Table 2 indicates the concentration of radioactivity at the point of outfall and at two distances downstream.

A buildup of radioactivity was expected in the alluvium near the point of effluent outfall; some radioactivity did accumulate, as noted in table 2, during the first 2 years of discharge. Primarily, dispersion of the radionuclides from the outfall area is due to flushing of alluvial particles from the area by periodic discharge

TABLE 1.—*Gross alpha, gamma, and beta radioactivity, and radioactive strontium, per unit weight of fraction*

[Analyses by the Los Alamos Scientific Laboratory, Group H-7]

Fraction	Particle diameter (millimeters)	Weight percent	Cumulative weight percent	Counts per minute per gram (dry weight)			
				Type of radioactivity			Radioactive strontium
				Gross alpha	Gross gamma	Gross beta	
Silt and clay	Less than 0. 074	1. 0	1. 0	45	128	1, 751	42
Very fine sand	0. 074– . 147	3. 5	4. 5	33	75	799	49
Fine sand	. 147– . 295	. 5	5. 0	24	61	771	27
Medium sand	. 295– . 589	13. 5	18. 5	15	33	396	23
Coarse sand	. 589–1. 17	25. 5	44. 0	8	32	414	17
Very coarse sand	1. 17 –2. 36	34. 0	78. 0	5	24	239	15
Granule	2. 36 –3. 96	22. 0	100. 0	4	35	425	31

224-352 O - 66 - 17

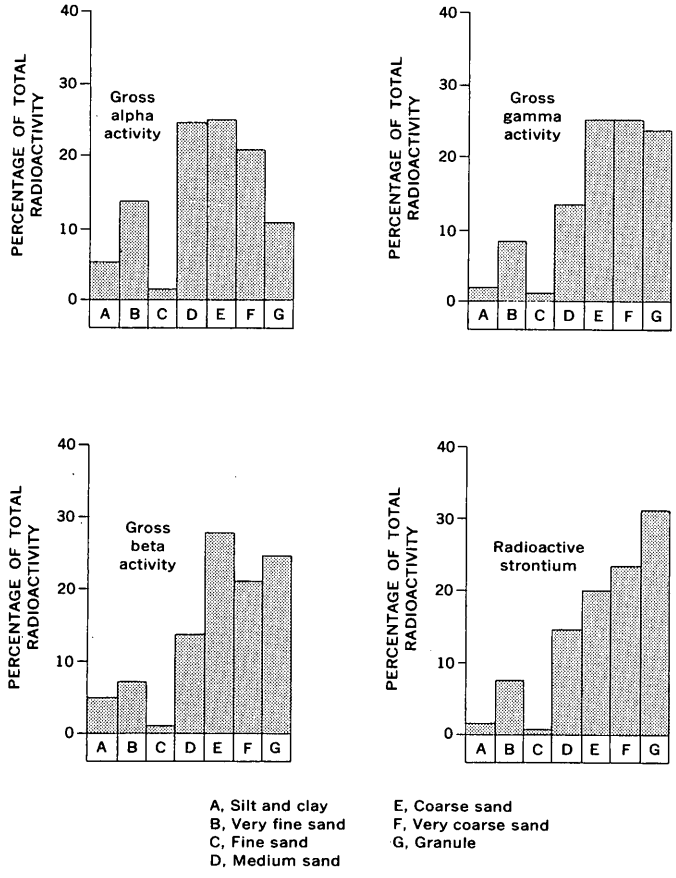

FIGURE 2.—Gross alpha, gamma, and beta activity, and radioactive strontium, in particle-size fractions of alluvium at the point of effluent outfall from the treatment plant (in percentage of 100-gram samples).

TABLE 2.—*Radioactivity of surface alluvium at the disposal area*

Type of radioactivity	Counts per minute per gram (dry weight)		
	At point of outfall	3,500 ft. from point of outfall	5,800 ft. from point of outfall
Gross alpha	9	4	2
Gross gamma	80	4	4
Gross beta	482	22	0
Radioactive strontium	25	2	4

of effluent, other waste water, and storm runoff. Radionuclides dislocated by flushing are redeposited with the translocated sediment. Radionuclides chemically dislocated are transported to an environment favorable for reprecipitation or for attachment to other alluvial materials.

The quality of the perched water in the disposal area has changed very little as disposal operations have continued. The negligible changes noted can be credited to an initial treatment of waste such that radionuclides are reduced to a level well below the MPC. Further, dilution of the treated effluent by nonradioactive waste water and storm runoff, as well as retention of radionuclides by the particles which constitute the alluvium, combine to produce a "waste stream" that is of high quality in itself. Thus, the infiltration of such a waste stream has had little effect on the quality of the perched water.

REFERENCE

Abrahams, J. H., Jr., Baltz, E. H., and Purtymun, W. D., 1962, Movement of perched ground water in alluvium near Los Alamos, New Mexico: Art. 37 *in* U.S. Geol. Survey Prof. Paper 450–B, p. B93–B94.

DESIGN AND CONSTRUCTION OF A UNIQUE INJECTION WELL ON LONG ISLAND, NEW YORK

By PHILIP COHEN and C. N. DURFOR, Mineola, N.Y.

Work done in cooperation with the Nassau County Department of Public Works

Abstract.—An injection well of unique design and construction recently completed on Long Island, N.Y., will be used in making a series of artificial-recharge experiments with highly treated sewage-plant effluent. The well, about 500 feet deep, consists of two adjacent fiberglass casings (18 inches and 4 inches in diameter) and 7 auxiliary pipes, 4 of which are made of fiberglass and 3 of polyvinyl chloride. Fiberglass was used because of its advantageous chemical and strength characteristics. A stainless-steel well screen, 62 feet long, is attached to the bottom end of each casing. Water will be injected into the aquifer through the large casing and screen, and hydraulic-head changes will be measured at several points within the well and filterpack. Geochemical reactions related to the head changes will be monitored by means of instruments in each screen.

A unique experimental injection well, designed by personnel of the U.S. Geological Survey, was completed on Long Island, N.Y., in the autumn of 1965. The well, which is in the community of Bay Park, Nassau County, will be used in a series of artificial-recharge experiments during the next several years. The experiments are designed to help evaluate the feasibility of a proposed network of "barrier" injection wells intended to retard or prevent the landward movement of salty water from the Atlantic Ocean into fresh-water aquifers that underlie Long Island. More specifically, the artificial-recharge experiments will be designed to investigate the physical and chemical factors that affect the rates at which sewage-plant effluent—treated to meet the commonly accepted standards for drinking water—can be injected into deep saturated deposits of sand and silty sand.

Clogging of the well screen, the filterpack, or the adjacent aquifer materials is a major cause of failure of injection wells. Another common cause of failure is physical or chemical deterioration of the well screen or casing (Sniegocki, 1963, p. 3). Accordingly, many of the features of the Bay Park experimental injection well were designed to study these causes of failure and, if possible, to develop methods of minimizing or preventing them.

CONSTRUCTION OF THE WELL

The major elements of the experimental well (fig. 1) are the 18-inch-diameter [1] casing and the 16-inch-diameter screen attached thereto (hereafter termed the "injection casing" and "injection screen," respectively). Other elements of the well include (a) the so-called annular-space observation well adjacent to the injection casing and screen, in the space between them and the wall of the drilled hole; (b) a deep pressure-measuring pipe which enters the injection casing just above the screen; (c) two tremie pipes extending into the filterpack which surrounds the well screens; (d) an injection pipe for water; and (e) dry wells, each 2 inches in diameter, which will accommodate the counterweights of three float-operated measuring instruments. (For clarity, the dry wells are not shown in fig. 1.)

The first step in the construction of the well was the drilling of an 8-inch-diameter test hole by the standard hydraulic-rotary method to a depth of 742 feet below land surface. Ninety cores were obtained during the drilling, and electric and gamma-ray logs were made soon after the hole was completed. On the basis of data from the cores and logs, the injection zone was selected and other details of the well design were completed. The test hole was backfilled with sand and then was reamed to a diameter of 36 inches by the reverse-rotary method to a depth of 508 feet. A plug

[1] All diameters of pipes, casings, and screens listed in this report are nominal.

U.S. GEOL. SURVEY PROF. PAPER 550-D, PAGES D253-D257

224-352 O -66 - 18

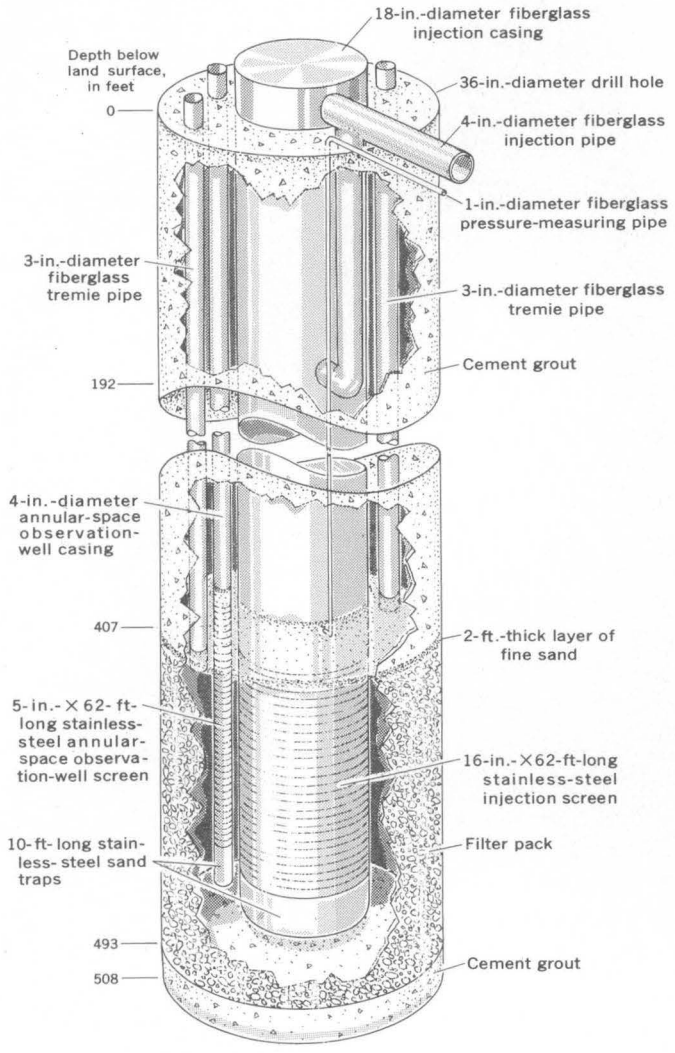

FIGURE 1.—Schematic diagram showing experimental injection well at Bay Park, Long Island, N.Y. Not to scale.

of cement grout, 15 feet thick, was emplaced in the bottom of the hole.

All casings, screens, and pipes shown in figure 1, plus pipes for the three dry wells, were lowered into the hole as a single bundle. The bundle was supported from above by a clamp attached to the 18-inch-diameter casing; the other pipes and casings were bound to the 18-inch casing with stainless-steel straps. After the bundle was in place, a filterpack consisting of very coarse sand and very fine gravel was emplaced in the annular space to a height of 11 feet above the screens. A layer of poorly sorted fine sand, 2-feet thick, was placed above the filterpack. Finally, the remainder of the hole was backfilled with cement grout.

Water will be injected through the 4-inch-diameter injection pipe into the injection casing, and thence through the injection screen into the aquifer. Valves will be installed in the 4-inch injection pipe at the land surface so that the water can be introduced into the injection casing either at land surface or at a depth of 192 feet below land surface. This arrangement will permit making a series of experiments to study the effectiveness of deep injection pipes (currently used in many injection wells) in reducing clogging. A depth of 192 feet was chosen so that the injected water can be introduced into the injection casing about 40 feet below the bowls of a turbine pump that will be installed in the well. This will avoid the possibility of turbulence associated with the flow of injected water past the pump column and bowls.

The 1-inch-diameter pressure-measuring pipe opens into the injection casing at a depth of 415 feet below land surface, or 3 feet above the top of the injection screen. At land surface the 1-inch pipe will be attached to a pressure-sensing instrument that will provide a continuous record of the changes in head in the well during the injection experiments. The pressure-measuring pipe was designed to open into the injection casing as close to the injection screen as feasible in order to measure the injection head immediately before the water moves through the screen into the filterpack and thence into the aquifer.

A portable geochemical-geophysical probe will be used in the injection screen during most of the experiments. This probe, with related equipment, will provide a continuous record of the temperature, specific conductance, dissolved oxygen, pH, and Eh of the water immediately before it moves through the screen into the filterpack. In addition, corrosion probes of the electrical-resistance type, similar to those described by Clarke (1963, p. 12–29), will be lowered into the injection screen to measure corrosion characteristics of different materials that could be used in the proposed network of injection wells.

The screen of the annular-space observation well is 5 inches in diameter, and the casing and sand trap are each 4 inches in diameter; they are the same lengths as those of the injection casing, screen, and sand trap. The screen of the annular-space observation well is roughly in the middle of the filterpack—that is, about midway between the injection screen and the wall of the drill hole. Head measurements and geochemical data, obtained from the annular-space observation well by means of a geochemical-geophysical probe identical to the one in the injection screen, will be used to study clogging, related geochemical phenomena, and accompanying head losses associated with the movement of water through the injection screen into the filterpack. If the need arises, the annular-space observation well will be used to add chemicals to the well.

The tremie pipes, each 3 inches in diameter, extend about 3 feet into the filterpack. These pipes will be used for continuous monitoring of the height of the filterpack, and, if necessary, for adding additional filterpack material to the annular space.

The 3 dry wells range in depth from 40 to 150 feet. The deepest dry well will accommodate the counterweight of a float-operated recorder that will monitor the water level in the annular-space observation well. The other 2 dry wells are for the counterweights of 2 instruments that will be used for monitoring the level of the filterpack in the tremie pipes.

A 50-horsepower turbine pump having an intake setting at 150 feet below land surface will be installed in the injection casing. The pump will be used in redeveloping the well after the injection experiments, in obtaining water samples for chemical and bacteriological analysis before and after the tests, and in studying the hydraulic effects of the recharge experiments on the well and the adjacent aquifer material—especially changes in permeability caused by clogging.

CHEMICAL AND PHYSICAL PROPERTIES OF MATERIALS USED IN THE WELL

The chemical properties of materials used in constructing the well were of special concern. On Long Island, since 1933, the drilling of industrial wells that yield more than 100,000 gallons per day has been prohibited by law unless the water is returned to the ground through "diffusion" wells or other approved structures (Johnson, 1948, p. 1160–1161). Accordingly, hundreds of recharge wells have been constructed. Many of them have failed because of chemical and biochemical reactions involving iron — that is, iron naturally in solution in the ground water, iron compounds (mainly FeS_2) in the aquifer materials, and iron in the mild-steel casings and pumps. Thus, in order to facilitate studies of corrosion, encrustation, and clogging—especially those involving the chemistry of iron—it was decided that, insofar as possible and practical, mild steel would not be used to construct and equip the experimental well.

Materials that were considered for the casings and other pipes in the well were stainless steel, vinyl-coated aluminum, mild steel coated with chemically stable liners such as epoxy resin and coal-tar enamel, polyvinyl chloride, fiberglass reinforced with epoxy or polyester resin (hereafter referred to as "fiberglass"), and asbestos cement. In addition to chemical properties, the other major factors that were considered were the strength of the material, its adaptability for use in well construction, and its cost. After considering these and other factors, the writers decided that fiberglass pipe, with watertight quick-disconnect couplings, would be the most satisfactory material for the casings and for most of the other pipes of the experimental well. Polyvinyl-chloride pipes were chosen for the dry wells.

The tensile strength of fiberglass pipe is closely related to the geometry of the fiberglass windings and is ordinarily much greater than that required in well construction. For example, the 18-inch-diameter fiberglass injection casing reportedly can withstand a pull of more than 250,000 pounds; the quick-disconnect couplings used to join the 40-foot lengths of 18-inch fiberglass pipe were designed to withstand a pull of 100,000 pounds. Similarly, the ability of the fiberglass pipe to withstand internal pressure exceeds the internal pressures anticipated during the planned experiments by more than an order of magnitude. The major element of concern regarding the strength of the fiberglass pipe, therefore, was its collapse pressure, or its ability to withstand differential external circumferential pressure.

Differential external pressure exerted on the casings by a given thickness of saturated porous deposits in which static ground-water levels are about at land surface (as is the case at the site of the experimental well) was estimated from the equation

$$P=\frac{K(Ws-Ww)h}{144},$$

where

P = differential external pressure, in pounds per square inch,
K = a dimensionless constant dependent mainly on the angle of internal friction of the material,
Ws = dry weight of the porous material, in pounds per cubic foot,
Ww = weight of water, in lb per cu ft, and
h = the height of the column of material, in feet.

The dry weight of the deposits was assumed to be 130 lb per cu ft. As a safety factor in the design of the casings and pipes, it was assumed that K would be equal to 0.50—that is, that the casings would have to withstand differential external pressure equivalent to at least half the weight of the column of saturated material. Curve 1 in figure 2 shows the differential external pressure to which the casings would be subject if the preceding assumptions are fulfilled. The curve shows that the maximum pressure on the bottom of the 18-inch casing (418 feet below land surface) that would result from the weight of the overlying saturated deposits is about 100 pounds per square inch.

If the injection screen should become severely clogged during an injection experiment, the water level in the

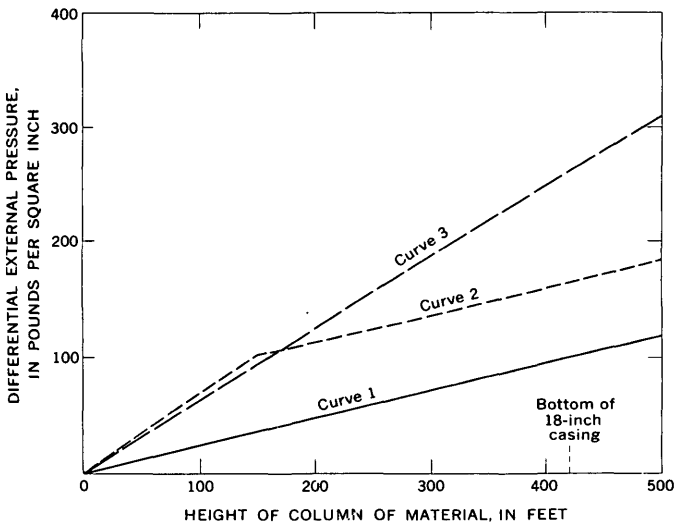

FIGURE 2.—Relation between the differential external pressures exerted on a casing and the height of a column of enclosing material. Curve 1 shows the pressure exerted by saturated sedimentary deposits. Curve 2 shows the pressure exerted by the saturated deposits plus differential hydrostatic pressure that would result if the well clogged during pumping (discharge) and the water level in the casing were drawn down to the pump intake. Curve 3 shows the pressure exerted by liquid cement grout weighing 150 lbs per cu ft.

injection casing might decline to the level of the pump intake (150 feet below land surface) during the pumping phases of the experiment. Under this condition, the difference between water levels inside and outside the casing, equivalent to a hydrostatic head of 150 feet, could cause a maximum differential external pressure on the casing wall of about 65 psi. The resulting differential pressure would increase (at a rate of about 0.43 psi per foot of depth) from zero at the land surface to about 65 psi at a depth of 150 feet and would remain constant below that depth. The sum of the differential external pressure resulting from the weight of the saturated deposits plus that resulting from pumping when the screen is severely clogged is shown as curve 2 in figure 2. The maximum differential pressure on the lowest parts of the casings and pipes from these causes would be about 160 psi.

After the annular space above the filterpack was filled with cement grout, only the lower few feet of the casings and pipes would be subjected to the pressures described in the foregoing paragraph; the remaining portions would be encased in cement and thereby would be protected. During the grouting procedure, however, the casings and pipes below a depth of 150 feet could have been subjected to an even greater pressure than that shown in curve 2 of figure 2. Before the cement hardened, the column of grout, which might weigh as much as 150 lb per cu ft, could have caused a differential pressure of about 0.6 psi per foot of column, or about 260 psi at the bottom of the casing (curve 3 of figure 2).

If the fiberglass pipe is assumed to have the physical properties of a thin-walled elastic tube, the collapse pressure (the differential external pressure at which the pipe would fail) can be computed from the equation (Roark, 1965, p. 354)

$$C=(1/4)\left(\frac{E}{1-\mu^2}\right)\left(\frac{t^3}{r^3}\right)$$

where

C=collapse pressure, in psi,
E=bulk modulus of elasticity, in pounds per square inch,
μ=Poisson's ratio,
t=wall thickness of the pipe, in inches, and
r=radius of the pipe, in inches.

The bulk modulus of elasticity of the fiberglass pipe used in the well is about 4 million psi; Poisson's ratio for the material is about 0.20.

It is apparent from the formula that the collapse pressure of the fiberglass pipe is directly proportional to the cube of the wall thickness and is inversely proportional to the cube of the radius of the pipe. Inasmuch as the cost of the fiberglass pipe is roughly proportional to the volume of fiberglass and resin, the use of pipes having the smallest possible wall thickness consistent with the collapse-pressure requirements was advantageous. Therefore, the contractor was required to pour the cement grout in two distinct phases—allowing sufficient time for the first batch to harden before adding the remainder of the cement. The casings and pipes were thereby subjected to only half the differential external pressure (about 130 psi) that would have resulted if the entire column of cement grout had been poured at one time and if the entire column had remained fluid for a finite period of time.

The wall thicknesses, computed collapse pressures, and other pertinent data regarding the fiberglass casing and pipes are summarized in table 1. The 18-inch

TABLE 1.—*Dimensions and collapse pressures of fiberglass pipes used in the Bay Park experimental injection well*

Designation of pipe	Nominal diameter (inches)	Wall thickness (inches)	Collapse pressure (psi)
Injection casing	18	0. 55	240
Annular-space observation-well casing	4	. 15	440
Injection pipe	4	. 12	220
Tremie pipes	3	. 11	405
Pressure-measuring pipe	1	[1]. 06	1, 800

[1] Standard wall thickness available from the factory.

casing was made of fiberglass reinforced with polyester resin; the other casing and pipes listed in the table were made of fiberglass reinforced with epoxy resin.

The screens of the injection well and the annular-space observation well are of the continuous wire-wrapped type and are made of type-304 stainless steel. The sand traps and the related fittings are also made of type-304 stainless steel. The slot sizes of the screens are 0.060 inch. This size was chosen in order to retain about 80 percent of the filterpack, which consists of about 71 percent very coarse sand and about 28 percent very fine gravel. The filterpack consists almost entirely of subrounded, moderately spherical particles of quartz, chert, and quartzite; it has a very high laboratory coefficient of permeability—about 18,000 gallons per day per square foot. Preliminary pumping-test data indicate that the screen and gravel pack are highly efficient and that well losses are minimal. The well had a specific capacity of 35 gallons per minute per foot of drawdown after 8 hours of pumping at a rate of 1,000 gpm. During development, the well had similar specific capacities after somewhat shorter periods of pumping at various rates ranging up to about 2,500 gpm. Even at the highest rate of pumping, the well yielded water that was virtually sediment free after only a few days of development.

Clarke (1963, p. 39) describes a successful experimental, gun-perforated small-diameter, fiberglass well, 1,000 feet in depth, in Libya. In addition, more than 400 wells equipped with 10-inch-diameter fiberglass casings and saw-slotted fiberglass screens reportedly have been completed in Pakistan during 1964–65. To the best of the writers' knowledge, however, the experimental well described in this report is the first water well constructed in the Western Hemisphere that has a fiberglass casing; and, the only water well in the world (as of 1965) that has multiple fiberglass casings and pipes, and a fiberglass casing as large as 18 inches in diameter.

Despite the fact that fiberglass presently is 2 to 4 times more expensive than mild steel, its use in experimental wells involving multiple casings and complex construction problems, and its use in special-purpose wells in highly corrosive environments, seems to be justified on the basis of the experience gained during the construction of the Bay Park injection well.

REFERENCES

Clarke, F. E., 1963, Appraisal of corrosion characteristics of western desert well waters, Egypt: U.S. Geol. Survey open-file rept., 65 p.

Johnson, A. H., 1948, Ground-water recharge on Long Island, New York: Am. Water Works Assoc. Jour., v. 47, no. 4, p. 1159–1166.

Roark, R. J., 1965, Formulas for stress and strain: New York, McGraw-Hill, 432 p.

Sniegocki, R. T., 1963, Problems in artificial recharge through wells in the Grand Prairie Region, Arkansas: U.S. Geol. Survey Water-Supply Paper 1615–F, 25 p.

FLUOROMETRIC ANALYSIS OF THE ALUMINUM ION IN NATURAL WATERS

By DONALD E. DONALDSON, Menlo Park, Calif.

Abstract.—Aluminum ions combine with Pontachrome Blue Black R (PBBR) at a pH of 4.8 to form a fluorescent complex which serves for quantitative determination of aluminum. The method is sensitive to 0.002 ppm of aluminum. Up to 8 ppm of fluoride can be tolerated. Bathophenanthroline retards the ferrous and ferric ions. The amount of dye necessary to complex the most concentrated aluminum standard was 0.50 mg per 50 ml solution. The Al-PBBR complex reaches full fluorescent development in 65 minutes. The interfering ions in the determination of aluminum by this method are Fe, Ga, Co, UO_3, Cu, Ti, and Ni.

PREVIOUS FLUOROMETRIC INVESTIGATIONS ON ALUMINUM

The fluorescence resulting from the presence of aluminum in solutions containing certain organic dyes offers promise for the quantitative determination of small concentrations of aluminum. Weissler and White (1946) reported that Pontachrome Blue Black R (PBBR) is suitable for a fluorescent reagent for the quantitative measurement of aluminum in steel, bronze, and minerals. Simons and others (1953) used the same reagent to measure parts per billion aluminum content in the surface waters of the Gulf of Mexico and the Atlantic Ocean. Will (1961) reported that the dye material, morin (2′,3,4′,5,7)-pentahydroxyflavone), was a useful reagent for the measurement of aluminum in the parts per billion range in high-purity boiler condensates. Rubins and Hagstrom (1959) reported using 8-quinolinol in the quantitative determination of aluminum in plant tissue.

The morin and PBBR dyes have both been used for determining small quantities of aluminum in natural waters. The morin reagent is more sensitive to aluminum than is PBBR; however, as is mentioned by White and Lowe (1940), the morin method requires more control over the concentration of dye, temperature, and pH than is needed for PBBR. Will (1961) reported that low concentrations of fluoride and phosphate, 5 ppb and 20 ppb, respectively, interfere in the morin method. The Pontachrome procedure was judged superior because it is less subject to fluoride and phosphate interference. Both methods are subject to interference from iron. A method of overcoming this interference for the PBBR procedure has been developed.

APPARATUS AND REAGENTS

A Turner fluorometer, model 111 was used to make the fluorometric measurements. The instrument was equipped with a general-purpose ultraviolet lamp. A Turner 1–60 +58 filter combination was used for excitation (546 millimicrons) and a Turner filter No. 23A (570 mμ) was used for fluorescence. Calibrated pyrex test tubes (12 mm × 75 mm) were used for sample cells in the instrument.

Measurements of pH were made with Beckman models N and M4C radiometer pH meters.

All glassware was washed in hot water with detergent and thoroughly rinsed with distilled water. The glassware was then treated with 1:1 reagent-grade hydrochloric acid, rinsed with distilled water, and finally with de-ionized water. Special attention to cleaning is necessary in trace constituent work to obtain consistent results.

De-ionized water. The water used to prepare all solutions was first distilled in a Barnstead still and then passed through an Amberlite MB–1 ion-exchange resin.

Aluminum stock solution. 1 milliliter = 10 micrograms of Al^{+3}. Dissolve 0.1758 grams of reagent grade $AlK(SO_4)_2 \cdot 12H_2O$ in de-ionized water containing 1–2 ml of concentrated sulfuric acid. Dilute to 1 liter.

Aluminum working solution. 1 ml = 1.0 μg of Al^{+3}. Dilute 10 ml of the aluminum stock solution of 100 ml with de-ionized water. A fresh solution was prepared prior to each analysis.

Acetic acid, 0.885*M*. Dilute 200 ml of reagent-grade glacial acetic acid to 4 liters with de-ionized water.

Ammonium acetate, 6.49*M*. Dissolve 500 g of reagent-grade ammonium acetate in 1 liter of de-ionized water.

Ethyl alcohol, 95 percent. Redistilled in an all-glass still. Undistilled ethyl alcohol contains trace contaminants which in turn fluoresce at the wavelengths employed in the analysis.

U.S. GEOL. SURVEY PROF. PAPER 550-D, PAGES D258-D261

Bathophenanthroline, 0.0015*M*. Dissolve 125 milligrams of bathophenanthroline (G. F. Smith Chemical Co., Columbus, Ohio) in 250 ml of 95-percent distilled ethyl alcohol. Store in refrigerator. The solution is stable for approximately a month under these conditions.

Pontachrome Blue Black R, 1 ml=1.00 mg. Dissolve 1.000 g of reagent-grade Pontachrome Blue Black R (E. I. DuPont de Nemours and Co., Wilmington, Del.) in 1 liter of distilled ethyl alcohol. This solution is stable for several months. As a substitute, Superchrome Blue B Extra (National Aniline Div.) was tested and found to be suitable for the procedure.

The DuPont company also manufactures Pontachrome Blue Black RM which is reportedly the same as PBBR.

ANALYTICAL PROCEDURE

1. Pipet a volume of sample containing less than 5.0 μg of Al^{+3} (25 ml maximum) into a 100-ml beaker.
2. Prepare two aluminum-free blanks from de-ionized water and sufficient standards (1.0 μg to 5.0 μg of Al^{+3}).
3. Add 5.0 ml of 0.885*M* acetic acid to each solution and heat for 2 hours just below the boiling temperature on a hotplate.
4. Cool the solutions to room temperature and add 1.0 ml of 6.49*M* ammonium acetate solution. The pH of the solutions should be between 4.6 and 4.8. If necessary, adjust the pH with 0.885*M* acetic acid.
5. Transfer each solution quantitatively into a 50-ml volumetric flask.
6. If iron is present, add 0.5 ml of 0.0015*M* bathophenanthroline. In the presence of iron, bathophenanthroline will yield a reddish color.
7. To each of the solutions add 0.5 ml of PBBR solution and bring all volumes to the 50-ml mark with de-ionized water and mix thoroughly.
8. Allow all the solutions to stand for 2 hours at room temperature. The Al-PBBR complex is stable for at least a week.
9. Measure the fluorescence intensity of each solution using the described filter system.
10. Plot fluorescence intensity readings against the aluminum concentration of standards and calculate aluminum concentrations of samples from the curve.

Typical fluorescence readings of standards are

μg Al^{+3}/50 ml	Fluorescent intensity (slit × 10)
0.0	2.0
1.0	19.0
2.0	38.0
3.0	52.0
4.0	68
5.0	86

FACTORS AFFECTING FLUORESCENCE

Analytical methods based on fluorescence excited by ultraviolet radiation are subject to interferences which may either increase or decrease the fluorescence intensity. The amounts of reagents, pH, and time of standing after addition of reagents also may influence the results. Optimum conditions for the PBBR procedure have been determined by experiments.

Fluorescence as a function of dye concentration.—Two series of samples were prepared in 50-ml volumetric flasks using constant amounts of aluminum (4.0 μg of Al^{+3}). The pH in one group was adjusted to 4.80 with ammonium acetate and acetic acid. In the other group, the pH was adjusted to 4.55. The dye concentration was varied from sample to sample, so as to give a range of 0.0 mg to 1.25 mg. After 2 hours standing, fluorescence was attained using 0.25 mg to 0.50 mg of dye at pH 4.80. At pH 4.55, maximum fluorescence was reached between 0.35 mg and 0.60 mg.

Fluorescence as a function of pH.—Twelve solutions were prepared; each solution contained an equal amount of aluminum (4.0 μg of Al^{+3}). The pH of the samples was adjusted to values ranging from 4.0 to 6.0 with varying amounts of acetic acid and ammonium acetate. The solutions were then treated with 0.5 mg of PBBR solution, made up to 50 ml, and allowed to stand 2 hours. The pH and fluorescence of each sample was then measured. Under these conditions, the optimum pH is between 4.6 and 4.8.

Fluorescence as a function of time.—Five test solutions were prepared according to the analytical procedure. The first of the test solutions contained 0.25 mg of PBBR dye, the second, 0.50 mg, the third, 0.75 mg, the fourth, 1.00 mg, and the fifth, 1.24 mg. The samples were allowed to stand 15 minutes prior to the initial reading. The time required for stability of fluorescence was approximately 50 minutes for those samples containing 0.50 mg to 0.75 mg of dye. The fluorescence of the sample containing 0.25 mg continued to increase and finally went off the scale. For concentrations of 1.0 mg to 1.25 mg of PBBR, the system stabilized at approximately 65 minutes. After these 2 solutions had stood 168 hours, the fluorescence measured was nearly the same as at 65 minutes.

The effect of interfering ions on fluorescence.—Weissler and White (1946) reported that ferric ions destroy the fluorescence produced by the Al-PBBR complex. They overcame the interference of iron as well as that of copper, nickel, chromium, and cobalt by mercury cathode electrolysis. Ishibashi and others (1957) reported that other interfering ions in the Pontachrome Blue Black R method were Fe^{+3}, Ga, Co, and vanadic acid, and that large amounts of Cu, Ti, and Ni interfere seriously. Possidoni de Albinati (1963) studied the effects of 70 different elements on the PBBR method. Among those ions creating a serious problem were Cu^{+2}, Fe^{+3}, Fe^{+2}, Co^{+2}, NO_2^{-1}, Bi^{+3}, and F^{-1}. Amounts of most of these ions that occur commonly in natural waters are too small to merit concern. However, ferrous and ferric iron may constitute serious interferences. Of the two iron species, the ferrous iron appears to have a more disturbing influence on the system. Bathophenanthroline and

TABLE 1.—*The effects of bathophenanthroline on aluminum recovery in the presence of iron*

Ratio	Bathophenanthroline 0.0015*M* (ml)	Al^{+3} added (μg)	Al^{+3} recovered (μg)
$Al^{+3}:Fe^{+3}$			
1:20	0	0. 50	0. 36
1:20	0	. 50	. 44
1:20	. 5	. 50	. 52
1:5	0	1. 00	1. 18
1:10	0	1. 00	1. 35
1:15	0	1. 00	1. 35
1:20	0	1. 00	1. 23
1:25	0	1. 00	. 80
1:30	0	1. 00	. 19
$Al^{+3}:Fe^{+2}$			
1:5	. 5	1. 00	. 98
1:10	. 5	1. 00	. 98
1:15	. 5	1. 00	. 98
1:20	. 5	1. 00	. 98
1:25	. 5	1. 00	. 95
1:30	. 5	1. 00	. 86
1:5	. 5	1. 0	. 91
1:5	. 5	1. 0	. 97
1:15	. 5	1. 0	1. 0

TABLE 2.—*Tolerance to diverse ions in the aluminum determination by PBBR*

Ion	Maximum tolerance (ppm)	Ion	Maximum tolerance (ppm)
Boron	100	Manganese	4. 0
Calcium	800	Strontium	250
Fluoride	8. 0	Sulfate	1, 000
Magnesium	200	Nitrate	40
Potassium	1, 000	Phosphate	8
Sodium	1, 000		

possibly tartaric acid can be used to decrease the interference of iron, as illustrated in table 1. The experimental data shows that bathophenanthroline will eliminate interference from iron when the ratio Fe/Al is as great as 25.

Table 2 indicates the maximum concentrations of other elements normally found in natural waters which may be tolerated in the aluminum determination by PBBR.

SOLUTIONS OF ALUMINUM HYDROXIDE POLYMER

Most procedures for determining aluminum fail when the element is present as a hydroxide polymer. To obtain the aluminum hydroxide polymer, a solution of aluminum perchlorate was treated with sodium hydroxide in an amount sufficient to give a ratio of aluminum combined to OH^{-1} of slightly over 1:3. After this material was aged for 10 days, the solution was free from any visible precipitate or turbidity. The solution at the time of preparation contained 12.4 parts per million of aluminum. The pH of the solution at the time of analysis was 6.25. To determine the amount of aluminum present, 1-ml aliquots of the aged solution were pipetted into a series of thirteen 100-ml beakers. Acetic acid, 0.6*M*, was added in varying amounts to the last 10 samples of the test group. The first three samples contained no acid, only test solution. The samples were treated with enough de-ionized water to bring all volumes to approximately 80 ml. All solutions, including those not treated with acid, were heated on a hot plate 2 hours and cooled to room temperature. The samples were transferred quantitatively to 100-ml volumetric flasks and diluted to mark with de-ionized water. Fluorometric analysis was performed on the samples to measure the aluminum present. The results in table 3 show that approximately one-sixth of the aluminum originally present was determined in the unacidified samples, but that the acid and heat treatment generally brought all or most of the aluminum to a state where it could be determined.

TABLE 3.—*The effects of varying amounts of 0.6*M *acetic acid on the aluminum hydroxide polymer*

Sample	0.6*M* acetic acid (ml)	Al^{+3} present (ppm)	Al^{+3} recovered (ppm)
1	0	12. 4	1. 8
2	0	12. 4	2. 0
3	0	12. 4	1. 8
4	10	12. 4	12. 2
5	20	12. 4	12. 4
6	30	12. 4	11. 6
7	40	12. 4	12. 4
8	5	12. 4	10. 0
9	15	12. 4	12. 4
10	25	12. 4	10. 9
11	40	12. 4	12. 4
12	60	12. 4	11. 4
13	80	12. 4	12. 8

EXPERIMENTAL RESULTS

Recovery of added aluminum by PBBR.—An experiment was performed to determine the aluminum recoverable from spiked tap water using the described analytical procedure. Eight solutions were prepared using tap water as the diluting agent. The pH of the samples prior to the addition of varying amounts of aluminum was 8.9. The first solution was analyzed to determine the amount of aluminum present. To the other 7 solutions varying amounts of aluminum were added so that a range of 0.01 ppm to 1.0 ppm of Al^{+3} existed. Fluorometric analysis indicated that

TABLE 4.—*Recovery of added aluminum by PBBR from spiked tap water*

Sample	Al^{+3} added (ppm)	Al^{+3} recovered (ppm)	Sample	Al^{+3} added (ppm)	Al^{+3} recovered (ppm)
1	0. 000	0. 006	6	0. 070	0. 072
2	. 010	. 016	7	. 100	. 102
3	. 020	. 025	8	. 150	. 161
4	. 040	. 046	9	1. 000	. 950
5	. 060	. 060			

0.006 ppm of Al^{+3} was present in the tap water initially (table 4).

Fluorometric analysis versus spectrophotometric analysis.—Three samples containing unknown amounts of aluminum were analyzed by three chemists. One chemist determined aluminum on the three unknown solutions using the Ferron procedure as described by Rainwater and Thatcher (1960, p. 97). Another chemist used Eriochrome Cyanine RC. A third chemist measured aluminum using two different fluorometric procedures, namely, the Pontachrome (PBBR) method and the morin method. The results are shown in table 5.

TABLE 5.—*Fluorometric analysis versus spectrophotometric analysis*

[Results in parts per million of Al^{+3}]

Sample	Spectrophotometric analysis	Eriochrome Cyanine RC	Fluorometric analysis	
	Ferron		PBBR	Morin
1	0. 14	0. 17	0. 16	0. 18
2	. 32	. 23	. 31	. 33
3	1. 20	1. 20	1. 21	1. 21

CONCLUSIONS

The fluorometric determination of aluminum using Pontachrome Blue Black R has proved to be a reliable and sensitive method. The minimum detectable concentration of aluminum is 0.002 ppm. The procedure is simple and rapid. Consistency in the addition of the reagents, control of pH, and time regulation have led to reproducible and accurate results.

REFERENCES

Ishibashi, M., Shigematsu, T. and Nishikawa, Y., 1957, The fluorometric determination of aluminum with Pontachrome Blue Black R: Japan Analyst, v. 6, p. 568–571.

Possidoni de Albinati, Julia Flavia, 1963, Valoracion de microcantidades de alumino [Fluorometric determination of aluminum microquantities in the presence of interferences]: Anales Asoc. Quim. Argentina, v. 51, no. 2, p. 207–222.

Rainwater, F. H., and Thatcher, L. L., 1960, Methods for collection and analysis of water samples: U.S. Geol. Survey Water-Supply Paper 1454, 301 p.

Rubins, E. J., and Hagstrom, G. R., 1959, Determination of aluminimum and iron in plant tissue: Agriculture and Food Chemistry, v. 7, p. 722–724.

Simons, L. H., Monaghan, P. H., and Taggart, M. S., 1953, Aluminum and iron in Atlantic and Gulf of Mexico surface waters: Anal. Chemistry, v. 25, pt. 1, p. 989–990.

Weissler, A. and White, C. E., 1946, Fluorometric determination of aluminum in steels, bronzes, and minerals: Indus. and Eng. Chemistry, Anal. Ed., v. 18, p. 530–534.

White, C. E., and Lowe, C. S., 1940, Determination of aluminum by photometric fluorescence measurement: Indus. and Eng. Chemistry, Anal. Ed., v. 12, p. 229–231.

Will, Fritz, 3d, 1961, Fluorometric determination of aluminum in the parts per billion range: Anal. Chemistry, v. 33, pt. 2, p. 1360–1362.

SUBJECT INDEX

[For major headings such as "Economic geology," "Geophysics," "Paleontology," see under State names or refer to table of contents]

AUTHOR INDEX